PHARMACOMETABOLOMIC STUDY OF THE HUMAN MALARIA PARASITE, *PLASMODIUM FALCIPARUM*: NEW INSIGHTS INTO PARASITE BIOLOGY AND MODE OF DRUG ACTION

Thesis is submitted in accordance with the requirements of the University of Liverpool for the degree of Doctor of Philosophy

By

MURAD ALI MUBARAKI

BSc, Med. Tech., MSc, MBPDV (with distinction)

June 2013

Dedication

To my Parents, my wife and my children

Acknowledgments

In the name of Allah, the Most Gracious, the Most Merciful. All praises and gratefulness are due to Allah who is Almighty giving me and blessing me with the mind, senses, thoughts, health, strength and time to finish this PhD. Peace and blessings of Allah be upon the last prophet, Muhammad, and on all who follow him in righteousness until the Day of Judgment. As the prophet Muhammad, peace be upon him, said, "He who is thankless to people, is thankless to Allah." I therefore gratefully acknowledge the many people who so graciously helped and supported me so as to successfully complete this thesis.

I would like to express my thankfulness to my supervisors Dr Giancarlo Biagini and Prof Steve Ward for their supervision, guidance, support and helping me polish my skills that will aid me become an excellent research scientist in the future.

I express my gratitude to the parasitology department members for providing me and offering me with all the necessary assistance whenever I need it. Special thanks to Ashley, Gemma, Paul and Eilidh for their help proof reading my thesis draft. Thanks to Miss Alison Mbeakini for helping me with the english of my thesis. Thanks to all my PhD friends in the group for making such an enjoyment environment in the lab. I am very grateful to you all.

I would like to express my sincere thankfulness and gratefulness to my beloved parents for their penitence of being away, encouragement and prayers during days and nights. Simply, there is no single word that can help me express my heartfelt to you. Thank you very much and may Allah help me to be honouring you Mammy and Daddy. Thanks are extended to my brothers and sisters for their calls, prayers and support.

I acknowledge my parents-in-law for their visits during the birth of my babies Adel and Danah. Thank you for your help while being in the UK.

I owe special thanks to my loving wife Taghreed for standing beside me throughout my PhD. She was always there for me when I need her support and help. When things went wrong with my experiments, Taghreed was always there expressing a great smile and hopeful which I can always hear it in her voice saying ‘‘Do not worry darling. May Allah help you and Almighty will replace it with much better things for you’’. Taghreed has been my inspiration and motivation for continuing to improve my knowledge and writing up this thesis. I never forget all what we have been through Taghreed. I admire and love you.

May Allah protects me and all my family from the troubled times, the hardships, trials, tribulations. May Allah gives me, my parent, my wife, my kids, my brothers and my sisters health, prosperity and goods.

Publications, Presentations and Awards

Publications:

1. Biagini, G. A., N. Fisher, A. E. Shone, **M. A. Mubaraki,** A. Srivastava, A. Hill, T. Antoine, A. J. Warman, J. Davies, C. Pidathala, R. K. Amewu, S. C. Leung, R. Sharma, P. Gibbons, D. W. Hong, B. Pacorel, A. S. Lawrenson, S. Charoensutthivarakul, L. Taylor, O. Berger, A. Mbekeani, P. A. Stocks, G. L. Nixon, J. Chadwick, J. Hemingway, M. J. Delves, R. E. Sinden, A.-M. Zeeman, C. H. M. Kocken, N. G. Berry, P. M. O'Neill, and S. A. Ward, 2012, Generation of quinolone antimalarials targeting the *Plasmodium falciparum* mitochondrial respiratory chain for the treatment and prophylaxis of malaria: Proceedings of the National Academy of Sciences of the United States of America, v. 109, p. 8298-8303.

Publications in preparation:

1. **Mubaraki MA,** Ward SA and Biagini GA. Pharmacometabolomics of *Plasmodium falciparum* mitochondrion. *In preparation*.

2. **Mubaraki MA,** Ward SA and Biagini GA. Pharmacometabolomics study of inhibitors targeting the digestive vacuole of *Plasmodium falciparum*. *In preparation*.

Presentations:

1. **Murad A Mubaraki,** Steve A Ward and Giancarlo A Biagini (2012). Metabolic Fingerprinting of *Plasmodium falciparum*. *British Society for Parasitology*. University of Strathclyde, Glasgow, UK.

2. **Murad A Mubaraki,** Steve A Ward and Giancarlo A Biagini (2011). Targeted Metabolomics of Mitochondrial and Mitochondrial-Related Metabolism in the Human Malaria Parasite *Plasmodium falciparum*. *Seventh Annual BioMalPar Conference on The Biology and Pathology of the Malaria Parasite*, EMBL Advanced Training Centre, Heidelberg, Germany.

3. **Murad A Mubaraki,** Steve A Ward and Giancarlo A Biagini (2011). Targeted Metabolomics of *Plasmodium falciparum*. *British Society for Parasitology*. University of Nottingham, Nottingham, UK.

4. **Murad A Mubaraki,** Steve A Ward and Giancarlo A Biagini (2011). Metabolomics of *Plasmodium falciparum*. The 71st Harden Conference on Metabolic Pathway Analysis. University of Chester, Chester, UK.

5. **Murad A Mubaraki,** Ashley J Warman, David Waterhouse, Giancarlo A Biagini and Steve A Ward (2010). Characterisation of Energy Metabolism of the Human Malaria Parasite, *Plasmodium falciparum. LSTM Annual Postgraduate Research Seminar Day*, Marriott Hotel, Liverpool, UK.

Awards:

1. **Distinguished Student Award (2013),** Royal Embassy of Saudi Arabia, Saudi Arabia Cultural Bureau, London, UK.

2. **Cambridge University Press and BioMed Central Prize for Best Talk (2012),** British Society for Parasitology 50th Spring Meeting, University of Strathclyde, Glasgow, UK.

3. **Best Student Researcher Prize for Poster Presentation (2011),** Liverpool School of Tropical Medicine, University of Liverpool, UK.

Table of Contents

List of Figures

Chapter 1:

Chapter 3:

Chapter 4:

Chapter 5:

Chapter 6:

Chapter 7:

List of Tables

Chapter 1:

Chapter 3:

Chapter 6:

Chapter 7:

Abbreviations

ACTs	Atemisinin-based combination therapies
AdoMet	S-adenosylemethionine
ADP	Adenosine diphosphate
AIDS	Acquired immune deficiency syndrome
AMA	Apical membrane antigen
AMP	Adenosine monophosphate
APCI	Atmospheric pressure chemical ionization
AQ	Amodiaquine
ATP	Adenosine triphosphate
ATQ	Atovaquone
AUC	Area under the curve
BCKDH	Branched chain α-ketoacid dehydrogenase complex
BK	Bongkrekic acid
BSA	Bovine serum albumin
CE	Capillary electrophoresis
CID	Collision induced dissociation
cm^2	Centimeter squared
CO_2	Carbon dioxide
CQ	Chloroquine
CTP	Cytidine triphosphate
DDP I	Dipeptidyl aminopeptidase I
DDT	Dichlorodiphenyltrichloroethane
dH_2O	Distilled water
DHAP	Dihydroxyacetone phosphate
DHFR	Dihydrofolate reductase
DHODH	Dihydroorotate dehydrogenase
DHPS	Dihydropteroate synthase
DIMS	Direct infusion mass spectrometry
DMSO	Dimethyl sulfoxide
DNA	Deoxyribonucleic acid
dTMP	deoxythymidylate
e.g.	For example
EF-G	Elongation factor G
EMP	Embden-Meyerhoff-Parnas pathway
EPM	Erythrocyte plasma membrane
ESI	Electrospray ionization
FA	Fusidic acid

FAD	Flavin adenine dinucleotide
FT-IR	Fourier transform infrared spectroscopy
g	gram
G-3-P	Glycerol-3-phosphate
G3PDH	Glycerol-3-phosphate dehydrogenase
GC	Gas chromatography
GLURP	Glutamate-rich protein
GSH	Glutathione
GSSG	Glutathione disulfide
GTP	Guanosine triphosphate
h	Hour
H_2O	Water
Hb	Hemoglobin
HEPES	4-(2-hydroxyethyl)-1-piperazineethanesulfonic acid
HESI	Heated electrospray ionisation
HGMS	High gradient magnetic separation
HILIC	Hydrophilic interaction liquid chromatography
HIV	Human immunodeficiency virus
hpi	Hours post invasion
HPLC	High performance liquid chromatography
HQC	High level of quality control
i.e.	In another word
IC_{50}	Half-maximal inhibitory concentration
IC_{90}	90% inhibitory concentration
ICR	Ion cyclotron resonance
IMP	Inosine monophosphate
iRBC	Infected red blood cell
IS	Internal Standard
ITN	Insecticide-treated bed nets
kb	Kilobase
KCN	Potassium cyanide
L	Litre
LC-MS	Liquid chromatography-mass spectrometry
LC-MS/MS	Liquid chromatography-tandem mass spectrometry
LOD	Limit of detection
LQC	Low level of quality control
M	Molar
m/z	mass-to-charge ratio
MDH	Malate dehydrogenase
MDR	Multidrug resistance

mg	miligram
min	minute
ml	milliliter
mM	Millimolar
mm	millimeter
MoA	Mode of action
MQ	Mefloquine
MQC	Medium level of quality control
MQO	Malate:quinone oxidoreductase
MRM	Multiple reactions monitoring
MS	Mass spectrometry
MSI	Metabolomics standard initiative
MSP	Merozoite surface proteins
mtETC	Mitochondrial electron transport chain
mTorr	Millitorr
MW	Molecular weight
n	Number of experiments replicates
N2	Nitrogen
NAD	nicotinamide adenine dinucleotide
NADH	reduced nicotinamide adenine dinucleotide
NADP	Nicotinamide adenine dinucleotide phosphate
NADPH	reduced Nicotinamide adenine dinucleotide phosphate
ND	Not determined
nM	Nanomolar
NMR	Nuclear magnetic resonance spectroscopy
NO	Nitric oxide
NOS	Nitric oxide synthase
NPP	New permeation pathway
O_2	Oxygen
ºC	Degrees Celsius
ODC	Ornithine decarboxylase
PBS	Phosphate buffer saline
PCA	Principal component analysis
PCR	Polymerase chain reaction
PEP	Phosphoenolpyruvate
PfCRT	*P. falciparum* chloroquine resistance transporter
PfEMP 1	*P. falciparum* erythrocyte protein 1
PfHRP-2	*P. falciparum* histidine-rich protein-2 antigen
PfLDH	*P. falciparum* lactate dehydrogenase
PfMDR 1	*P. falciparum* multidrug resistance transporter 1

PfNDH2	*P. falciparum* type II NADH:quinone oxidoreductase
PfNHE 1	*P. falciparum* Na+/H+ exchanger 1
PG	Proguanil
pH	Power of hydronium
PLS-DA	Partial least squares-discriminant analysis
pM	Picomolar
PPM	Parasite plasma membrane
ppm	Parts per million
PPP	Pentose phosphate pathway
PPQ	Piperaquine
PPS	Pentose phosphate shunt
psi	Pounds per square inch
PVM	Parasitophorous vacuole membrane
Q_0	Ubiquinone oxidation site
Q1	First quadrupole
Q2	Second quadrupole
Q3	Third quadrupole
QC	Quality control
QCDs	Quinoline-containing antimalarial drugs
QFR	Quinol-fumarate reductase
Q_i	Ubiquinone reduction site
QN	Quinine
R^2	Regression coefficients
RBC	Red blood cell
RF	Radio frequency
ROS	Reactive oxygen species
rpm	Rotations per minute
RPMI	Roswell Park Memorial Institute
rRNA	Ribosomal ribonucleic acid
RSD	Relative standard deviation
RT	Retention time
s	Second
S/N	Signal-to-noise ratio
SD	Standard deviation
SDH	Succinate dehydrogenase
SEM	Standard error of the mean
SHAM	Salicylhydroxamic
SP	Sulfadoxine-pyrimethamine
SRM	single reaction monitoring
t	time

TCA	Tricarboxylic acid
THF	Tetrahydrofolate
TOF	Time-of-flight
tRNA	Transfer RNA
TTFA	Thenoyltrifluoroacetone
TTP	Thymidine triphosphate
UDP	Uracil diphosphate
UK	United Kingdome
UMP	Uridine monophosphate
UN	Untreated
Q	Ubiquinone
QH_2	Ubiquinol
USA	United State of America
UTP	Uridine triphosphate
w/w	Weight per weight
WHO	World Health Organization
$\Delta\Psi_m$	mitochondrial membrane potential
µg	microgram
µl	Microliter
µm	Micormeter
µM	Micromolar
%	Percentage
/	per
2,3-DPG	2,3-diphosphosglycerate
2-D	Two dimension
3-D	Three dimension
5-FOA	5-Flouroorotic acid

Abstract

Malaria is a vector-borne parasitic disease spread by a bite of an infected female *Anopheles* mosquito that accounts for high morbidity and mortality, mainly in sub-Saharan Africa. Of the five species that can cause malaria in humans, *Plasmodium falciparum* is regarded the most virulent species. Antimalarial drugs, unaltered for many decades, remain the mainstay for treating *P. falciparum* infection. In addition, despite intensive research there remain significant knowledge gaps in understanding of the biology of the malaria parasite *P. falciparum*. These deficiencies hinder the ability of scientists to identify new targets for drug discovery at a time when new targets are urgently required, such as in the case of newly emerging drug resistant parasite strains. Therefore, an understanding of the biology of *P. falciparum* is helpful in identifying new drug targets. Metabolomics, defined as the comprehensive analysis of all metabolites in a biological system, offers a feasible platform for highly sensitive and specific analysis of the metabolic pathways of *P. falciparum*. This is supported by the assumption that metabolites are important players in biological systems and that resistant parasite strains may operate or alter single or multiple metabolic pathways in order to adapt to the drugs being used. Therefore, a targeted metabolomics approach was developed and validated (Chapter 3) in order to better understand the metabolic roles of mitochondria and the digestive vacuole of *P. falciparum*. Metabolite detection and quantification were conducted using a targeted LC-MS/MS metabolomics approach (Chapter 3). It was shown that metabolic activities, particularly carbohydrate metabolism, in trophozoite stage *P. falciparum*-infected RBC were remarkably higher than that of non-infected RBC (Chapter 4). This lead the study to progress further, examining the metabolic role of two components of the *P. falciparum*; the mitochondria and the digestive vacuole. A number of mitochondrial inhibitors selective for specific electron transport chain complexes and mitochondrial transporters were used to assess mitochondrial function in asexually growing trophozoite stage *P. falciparum* (Chapter 5 and 6). Despite the differing modes of action of the inhibitors, the metabolic fingerprints, which were carbamoyl-l-aspartate and dihydroorotate, from these experiments were consistent with the parasite mitochondrion playing a key role in pyrimidine biosynthesis at the point of dihydroorotate dehydrogenase (DHODH) (Chapter 5 and 6). This metabolic fingerprint, leading to parasite death, was quite distinct from fingerprints obtained from biologically distinct inhibitors such as heme-binding drugs (quinoline-containing antimalarials drugs) which primarily affected the metabolism of amino acids, perhaps in the digestive vacuole and parasite cytosol (Chapter 7). In contrast to genomic and proteomic approaches, metabolomics appears to better represent the parasites' phenotype in response to drug perturbation. Pharmacometabolomics will therefore have significant utility in understanding the biological function of parasite components; and the mode of action, efficacy and toxicity of pharmaceutical drugs.

CHAPTER 1

General Introduction

1.1. Overview

Malaria is a tropical disease of immense importance in many parts of the world. It continues to be one of the main causes of morbidity and mortality in the world particularly tropical countries (Bruce-Chwatt, 1987, Murray et al., 2012, Guerin et al., 2002). Malaria is transmitted by a bite of the infected female *Anopheles* mosquito. Malaria is caused by *Plasmodium* species parasite that lives one part of its life cycle in vertebrates (humans, animals, birds) and continues its life cycle in dipteran vectors (mosquitoes). Four major species of *Plasmodium* parasites can establish malaria in humans namely; *Plasmodium falciparum*, *Plasmodium vivax*, *Plasmodium ovale* and *Plasmodium malariae*. The monkey's parasite, *Plasmodium knowlesi*, has been recently recognized as a fifth human malaria parasite (Cox-Singh and Singh, 2008, Cox-Singh et al., 2008, White, 2008a). Despite the fact that human malaria is not considered as a zoonotic disease, *P. knowlesi* can establish a malaria disease in monkeys and humans, and can be transmitted from monkeys to humans (White, 2008a, Singh et al., 2004).

Malaria has had a greater impact on global history than any other infectious disease, impacting the outcome of wars, population travels and the development of various nations. It places a heavy economic burden on many endemic countries, contributing to the cycle of poverty and limiting economic development. In 1958, President of the United State of America Eisenhower announced in his speech for the State of the Union bold and enthusiastic plan to clear and end malaria in five years' time:

> "Another kind of work of peace is cooperation on projects of human welfare. For example, we now have it within our power to eradicate from the face of the earth that age-old scourge of mankind: malaria. We are embarking with other nations in an all-out five-year campaign to blot out this curse forever. We invite the Soviets to join with us in this great work of humanity." Eisenhower, USA President (1953 - 1961).

In 2013, fifty five years later, malaria still remains one of the deadliest infectious diseases today despite decades of enormous efforts to eradicate the disease during 1950s and 1960s. The failure of vaccine trials, the continued emergence of drug-resistant strains of *Plasmodium*, the appearance of insecticide resistance mosquitoes, global environmental changes and an ever increasing population makes the idea of malaria eradication an extremely challenging task for researchers, clinicians and politicians across the world.

1.2. Malaria as a Disease

1.2.1. Malaria in Human History: Key Discoveries

The trophozoite-derived *P. falciparum* histidine-rich protein-2 antigen (PfHRP-2) has been detected in skin, muscle, brain and lung samples from naturally desiccated Egyptian mummies dating from 3200 BC (Miller et al., 1994). The first written description of characteristic poor health, periodic fevers and enlarged spleens were documented in China, around 2700 BC (Cox, 2002, Cox, 2010). This documentation was continuing through the writings of Greek, Roman, Assyrian, Indian, Arabic and European physicians up to the nineteenth century (Cox, 2002, Cox, 2010, Sterling, 1978, Bruce-Chwatt, 1987). In the seventh century, Italians were the first who called the disease associated with swamps near Rome "mal' aria" meaning "spoiled air". With the birth of microbiology and germ theory in the end of nineteenth century, the scientific understanding of malaria began. This new way of thinking in which microorganisms caused disease led Chalres Louis Alphonse Laveran, a French army physician in Algeria (North Africa) and Nobel Prize winner in 1907, to discover the parasite causing malaria by examining the blood of infected patient who had malaria symptoms (Laveran, 1880). In 1884, Ettore Marchiafava and Angelo Celli subsequently confirmed Laveran's germ and named the protozoan observed *Plasmodium* (Smith and Sanford, 1985).

In 1894, Sir Patrick Manson, a Scottish physician and founder of tropical medicine field, postulated a theory to Sir Ronald Ross, a British physician in the Indian Medical Service and Nobel Prize winner in 1902, about the involvement of mosquitoes in malaria

transmission. In 1897, Sir Ronald Ross proved Manson's theory and made an important discovery by describing the full life cycle of *Plasmodium* inside the female mosquito (Ross, 1898). Ross's discovery into malaria was immediately followed by a series of significant works carried out by Grassi and colleagues who demonstrated conclusively the whole life cycle of *Plasmodium* in human and mosquito (Grassi, 1900). From 1945 – 1948, Shortt and Garnham contributed in decoding the mystery of injected sporozoites destination by finding out that sporozoites development and division take place in liver (pre-erythrocytic stages) prior their development in blood (erythrocytic stages) (Shortt and Garnham, 1948). The final brick was put in place when Wojciech Krotoski and his colleagues demonstrated the hyponozoite theory in *P. vivax* which can remain dormant in liver for several months after infection (Krotoski, 1985).

1.2.2. Malaria Epidemiology

Malaria is a major public health problem in over 100 malaria-endemic countries in tropical and sub-tropical regions (Figure 1.1) (WHO, 2012). It is considered one of the top three infectious disease killers, including tuberculosis and HIV/AIDS, in low income countries (WHO, 2012). It is also regarded as a disease of poverty and underdevelopment. According to WHO's latest estimates in 2011, approximately 216 million cases of malaria occur in the world and the disease kills about 655,000 people (WHO, 2012). This is translated to approximately a death from malaria every minute. However, malaria mortality rates have fallen by more than 25% globally since 2000, and by 33% in the WHO African Region (WHO, 2012). About 90% of malaria deaths occur in Africa and the majority of them are children under 5 years (Murray et al., 2012, WHO, 2012). However, the distribution of the disease varies greatly from country to country and within the countries themselves, depending on certain factors such as climate, politics, education, and economical means for the prevention of malaria transmission.

To date, there are approximately 200 species of *Plasmodium* parasites that have been described from reptiles, rodents, birds and mammals (Perkins and Austin, 2009). Of these,

only five species of *Plasmodium* parasites are known until now to cause malaria in humans. These include:

1- *P. falciparum* (Malignant Tertian Malaria): is found worldwide in tropical and subtropical areas predominantly in Africa (Snow et al., 2005). It is the most lethal *Plasmodium* species and causes the most severe form of malaria including cerebral malaria which can be fatal (Gunn, 2012). *P. falciparum* is responsible for the vast majority (around 90%) of malaria deaths and cases worldwide (WHO, 2012).

2- *P. vivax* (Benign Tertian Malaria): is the most geographically widespread species and found mostly in Asia, Latin America, and in some parts of Africa (Gunn, 2012). It is responsible for a large number of cases and increasingly being recognized as a cause of severe malaria and even death (WHO, 2012, Kochar et al., 2005). However, *P. vivax* is not found in West Africa because it can only invade erythrocyte expressing Duffy blood group antigens (Fy^a and Fy^b) which most West Africans do not have these antigens on their erythrocytes (Gunn, 2012). *P. vivax* as well as *P. ovale* has dormant liver stages (hypnozoites) that can activate and invade the blood (relapse) several months or years after the infecting mosquito bite (Gunn, 2012). In addition, *P. vivax* parasites as well as *P. ovale* parasites are only able to develop in reticulocyte (Gunn, 2012).

3- *P. ovale* (Ovale Malaria): is found mostly in Africa (especially West Africa) and the islands of the Western Pacific (Collins and Jeffery, 2005). It is biologically and morphologically very similar to *P. vivax*. However, differently from *P. vivax*, it can infect individuals who are negative for the Duffy blood group, which is the case for many residents of sub-Saharan Africa (Gunn, 2012). This explains the greater prevalence of *P. ovale* (rather than *P. vivax*) in most of Africa (Collins and Jeffery, 2005).

4- *P. malariae* (Quartan Malaria): found worldwide and it is the only human malaria parasite species that has a quartan cycle (three-day cycle) (Collins and Jeffery, 2007). Natural infections are common in chimpanzees as well as in human and latent infections can persist in them for many years if untreated (Gunn, 2012, Hayakawa et al., 2009).

5- *P. knowlesi* (Simian Malaria): is found throughout Southeast Asia as a natural pathogen of long-tailed and pig-tailed macaques (*Macaca fascicularis*) (Gunn, 2012). It has recently been shown to be a significant cause of zoonotic malaria in that region, particularly in Malaysia, as it is often mistaken for *P. malariae* but its infection consequences can be fatal (Cox-Singh and Singh, 2008, Cox-Singh et al., 2008).

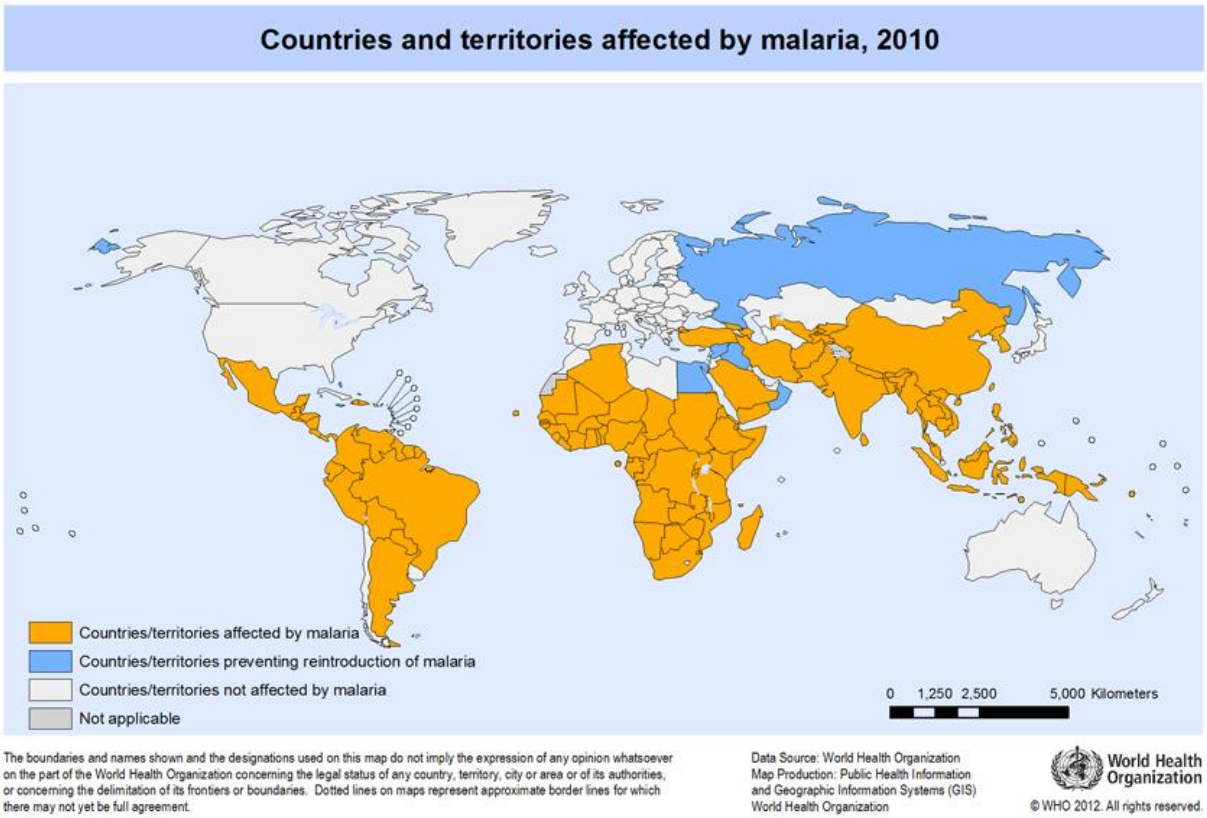

Figure 1.1. Geographical distribution of malaria.
World map shows malaria affected countries in 2010. Amber colour indicates countries affected by malaria and of high transmission. Blue indicates countries preventing reintroduction of malaria but with limited risk. White colour indicates countries that are not affected by malaria. Grey colour is not applicable to any countries. (Adapted from WHO, 2012).

1.2.3. Malaria Pathogenesis and Symptoms

Malaria pathogenesis is initiated when the parasites are released from the liver to the blood circulation. Therefore, the clinical manifestations of malarial infections are associated with the rupture of infected red blood cells (iRBC) during the blood stage of the parasites's life cycle. These drastic morphological and biochemical changes of the iRBC are central to the malaria pathogenesis (Maier et al., 2009). Thus, these modifications may results in the ability of the iRBC (primarily seen in *P. falciparum* infections) to undergo a range of adhesive interactions (cytoadherence) such as binding of iRBC with endothelial cells (sequestration), interaction of iRBC with non-infected RBC (rosetting) and other iRBC (auto-agglutination) (Miller et al., 2002).

Furthermore, the release of malaria antigens, pigment and toxins rise to a cascade of pathological events. These pathological events can range in severity from uncomplicated or mild malaria to complicated malaria or severe malaria. The clinical symptoms develop from classical symptoms of uncomplicated malaria including headache, fever, chills, sweating, and muscle pains (Laishram et al., 2012) to sometimes severely developed symptoms of complicated malaria including anemia, kidney failure, respiratory distress, cerebral malaria and often death in certain malarial patients (Warrell, 1997, Weatherall et al., 2002). These clinical manifestation of malarial infection is predominantly influenced by several factors which are (1) host age and immune status with regard to malaria and pregnancy, (2) the parasite species and its genotype and perhaps (3) the geographical, economical and social factors (Figure 1.2) (Miller et al., 2002).

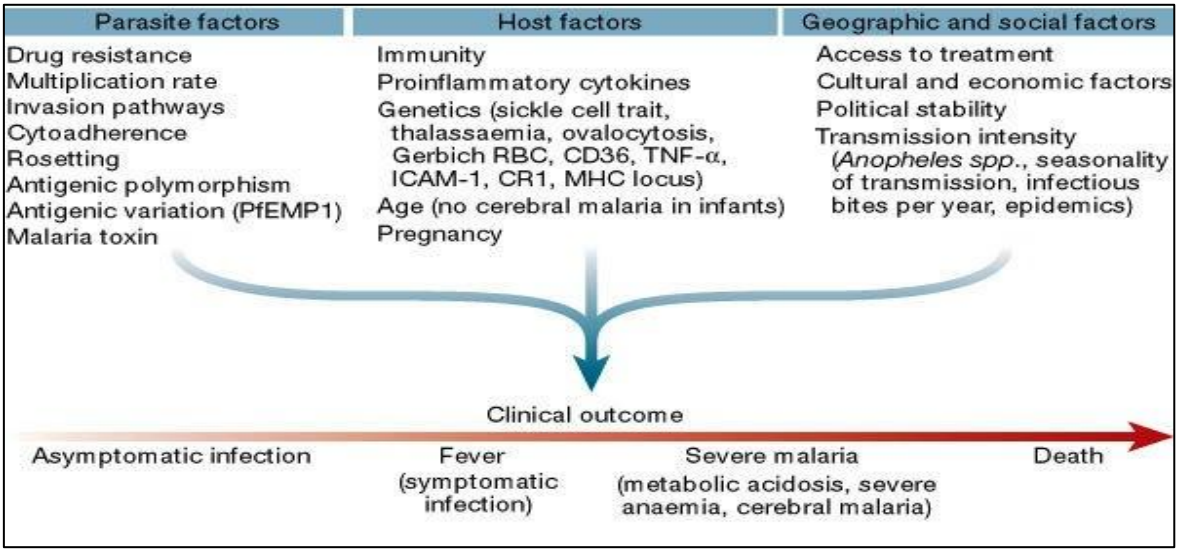

Figure 1.2. The Clinical outcome malarial infection in human.
Parasite, host, geographical and social factors determine the severity of the clinical outcome. (Adapted from Miller et al., 2002).

1.2.4. Malaria prevention and control

There are four main approaches to prevent and control malaria. These include (1) health education and primary health care, (2) malaria vaccine, (3) vector control and (4) antimalarial chemotherapy.

1.2.4.1. Health education and primary health care

Health education and primary health care is one of the important measures to control and prevent malaria. Malaria prevention and control has to be integrated into the basic health system of endemic country to improve health education and development of primary health care. The integration of this approach within antimalarial activities has been successfully test in some places (Bruce-Chwatt, 1987, Raccurt, 1997, O'Meara et al., 2009, Koram et al., 1995).

The availability of primary health care facilities in malaria-endemic areas has strong patterns in disease management through early diagnosis and prompt treatment. These facilities are also used to educate the local community in control malaria through personal protection measures. Health education helps affected people seek medical attention and it

promotes the use of insecticide-treated bed nets (Ayi et al., 2010). These methods are usually quite cheap and can provide a good first line of defence against the malaria vector. In addition, malaria has been contained quite affectively through personnel protection measures such as protective clothing, repellents and bed nets. The community protection measures has also involved in reducing the malaria transmission by the use of biological control methods such as the use of toxic agents (pyrethroids) against the mosquito vector (Kroeger et al., 1996).

1.2.4.2. Malaria Vaccines

Malaria vaccine development is a continuing area of research and unfortunately an effective and durable vaccine is not yet available. There are a number of targets that have been suggested for malaria vaccine to break the parasite life cycle. These vaccines are currently directed against three candidate stages of malaria parasite development include the pre-erythrocytic stage, erythrocytic stage and the sexual stage (Greenwood et al., 2008, Garcia-Basteiro et al., 2012).

The pre-erythrocytic stage vaccine is directed to block the sporozoite from invading or developing within the hepatocyte; hence preventing of infection (Greenwood et al., 2008, Garcia-Basteiro et al., 2012). One of the pre-erythrocytic stage vaccine candidate is RTS,S which is currently in clinical phase III trials and the final results and conclusion about its efficacy will be revealed by the end of 2014 (Mian-McCarthy et al., 2012, Garcia-Basteiro et al., 2012).

The erythrocytic stage vaccine is aimed to block merozoite invasion of RBC and inhibiting the development of schizont; therefore preventing the progression of malaria disease and eliminate or reduce the number of erythrocytic stage parasite (Greenwood et al., 2008, Girard et al., 2007). The erythrocytic stage vaccine candidates such as merozoite surface proteins 1 (MSP-1), 2 (MSP-2), 3 (MSP-3), the glutamate-rich protein (GLURP) and apical membrane antigen 1 (AMA-1) are currently in early clinical trials (Genton and Reed, 2007). Additional antigens from merozoite surface antigens such MSP-4, -5, -8, and -9, and *P. falciparum* erythrocyte protein 1 (PfEMP1) are under development as vaccine candidate (Girard et al., 2007).

The sexual stage vaccine is targeted to block human mosquito transmission by immunising against the sexual stages or gametes; thereby preventing sporozoite development in *Anopheles* mosquitoes (Garcia-Basteiro et al., 2012, Greenwood et al., 2008). Several candidates are in clinical development, including vaccines that target the Pfs25, Pvs25 and Pvs28 surface proteins, but the ISA51, an adjuvant, formulation of these vaccines turned out to be unacceptably reactogenic (Wu et al., 2008). In addition, a major challenge for this vaccine approach is proving true field efficacy (Saul, 2007).

It appears that there are still many obstacles to overcome with the main difficulties resulting from the complex nature of parasite and its life cycle. The parasite multiple stages rise the antigenic diversity and polymorphism which allow the switch of the expression of the antigenic molecules, thus the parasite is able to evade the immune response of the host(Garcia-Basteiro et al., 2012). The result is an immune response generated against a specific allelic form, which may not recognize another one. These challenges also apply equally to all potential vaccines candidate making this a very slow process with no effective vaccine likely in the near future (Garcia-Basteiro et al., 2012).

1.2.4.3. Vector Control

Since the recognition that insects transmit infectious agents and the elucidation of the parasites life cycle in their vectors, vectors have been targeted through which disease control can be successfully achieved. The objective of vector control is to reduce malaria transmission through different control strategy approaches. These include (1) using insecticides, (2) personal protective measures, (3) larval control and (4) environmental control.

Insecticides have been the most common form of vector control. The effectiveness of dichlorodiphenyltrichloroethane (DDT) against indoor resting mosquitoes led to the view that malaria could be eradicated through a combination of indoor residual spraying and disease surveillance to detect and treat any remaining diseases (Muturi et al., 2008). DDT is inexpensive and its effective use had resulted in successful malaria vector campaigns and eliminated the disease in North America, Europe and parts of Asia (Najera et al., 2011). However, DDT resistance has been reported from more than 50 species of anopheline

mosquitoes as the eradication programme for malaria vector was abandoned due to problems associated with administrative, political, logistic and financial constraints (van den Berg, 2009, Hemingway and Ranson, 2000). In addition, malaria mosquito vector has evolved resistance to another effective insecticide, synthetic pyrethroids, and there is now a need for developing new insecticide (Martinez-Torres et al., 1998).

Personal protective measures are based on insecticide impregnated materials such as bed nets and curtains. The use of insecticide-treated bed nets (ITN) can significantly reduce the child mortality, severe pregnancy associated anaemia and low birth weight infants (Muturi et al., 2008, Phillips-Howard et al., 2003, ter Kuile et al., 2003, Gosoniu et al., 2008). However, the efficacy of ITN varies with the type of insecticide, duration of use and human behaviour (Gu and Novak, 2009). Therefore, the increased resistance to most of the presently available insecticide such as deltamethrin and permethrin demands for new classes of insecticide and other alternative control measures (Phillips-Howard et al., 2003, Muturi et al., 2008).

Larval control of malaria vector is another strategy for preventive measures. Chemical and biological agents can be used to kill larvae in breading sites. Larvivorous fishes or bacterial pathogens such as *Bacillus thuringiensis israelensis* have given a new scope for novel control measures in the present resistant vector population (Walker and Lynch, 2007, Takken and Knols, 2009).

Environmental control is used to prevent breeding, nesting and feeding of malaria vectors. This can be achieved by various means such as eliminating the low spots where pools of water can be formed after rainy season, or applying locally grown plant materials to limit growth of mosquitos. In contrast, environmental changes from road, dam or pipeline construction, deforestation, agricultural and irrigation can generate new larval breeding sites. Therefore, environmental control can mostly be achieved in urban areas and require community participation and inter-sectorial collaboration.

1.2.4.4. Antimalarial Chemotherapy

Antimalarial chemotherapy has been the defensive bastions against malaria for decades especially in the absence of an effective malaria vaccine. Fundamentally, the treatment of malaria involves in killing parasites in the liver and blood circulation while providing supportive therapy to the host (Winstanley, 2000). The available antimalarial drugs fall into five broad groups according to their chemical structure and biological activities (Table 1.1) (Antoine, 2013). These include (1) quinoline-containing antimalarial drugs, (2) artemisinin-type compounds, (3) antifolates, (4) antibacterial agents and (5) hydroxynaphthoquinones. These drugs have different mode of action that interfere with the process of metabolic pathways within different subcellular organelles leading eventually to parasites death (Figure 1.3) (Greenwood et al., 2008, Biagini et al., 2003).

It has been noted that human malaria parasites have developed resistance to almost every antimalarial drug due to inadequate drug administration, level of host defence, spontaneous mutations in the parasites and pharmacokinetics and pharmacodynamics of antimalarial drugs used (White, 2004). Therefore, the use of two or three combinational antimalarial drug therapy with different modes of action and molecular targets will perhaps reduce the risk of resistance and increase the treatment efficacy (Table 1.1) (Kremsner and Krishna, 2004, White, 2004).

Table 1.1. Antimalarial drug classes, their target locations, parasite stages and their possible combinations.

Drug	Target location				Parasite stage					Combination
	C	M	DV	A	BS	LS	GS	HS	SS	
Quinoline-Containing Drugs										
Quinine			●		●		●			+ Sulfadoxine-pyrimethamine (SP); + Tetracycline; + Clindamycin; + Doxycycline
Chloroquine			●		●		●			+ Sulfadoxine-pyrimethamine (SP)
Amodiaquine			●		●		●			+ Sulfadoxine-pyrimethamine (SP)
Piperaquine			●		●					+ Dihydroartemisinin
Primaquine			●			●	●	●		
Tafenoquine			●			●	●			
Mefloquine			●		●		●			+ Sulfadoxine-pyrimethamine (Fansimef®)
Halofantrine			●		●					
Lumefantrine			●		●					+ Artemether (Coartem®, Riamet®)
Antifolates										
Pyrimethamine	●				●	●			●	+ Sulfadoxine (SP)
Sulfadoxine	●				●					+ Pyrimethamine (SP)
Proguanil	●				●	●			●	+ Atovaquone (Malarone®)
Chloroproguanil	●				●					+ Dapsone + Artesunate (Dacart®); + Dapsone (LapDap®)
Dapsone	●				●					+ Artesunate + Chloroproguanil (Dacart®); + Chloroproguanil (LapDap®)
Hydroxynapthaquinones										
Atovaquone		●			●				●	+ Proguanil (Malarone®)
Antibiotics										
Doxycycline				●	●					+ Quinine
Clindamycin				●	●					+ Quinine
Tetracycline				●	●	●				+ Quinine
Endoperoxide compounds										
Artemisinin	●	●?	●		●		●?			
Artemether	●	●?	●		●		●?			+ Lumefantrine (Coartem®, Riamet®)
Artesunate	●	●?	●		●		●?			+ Dapsone + Chloroproguanil (Dacart®); + amadioquine (ASAQ); + Mefloquine (ASMQ); + Sulfadoxine-pyrimethamine (SP)
Dihydroartemisinin	●	●?	●		●		●?			+ Piperaquine

Abbreviations: C, cytosol; M, mitochondrion; DV, digestive vacuole; A, apicoplast; BS, blood stage; LS, liver stage; GS, gametocytes stage; HS, hypnozoites stage and SS, sporozoites stage. (Adapted from Antoine, 2013)

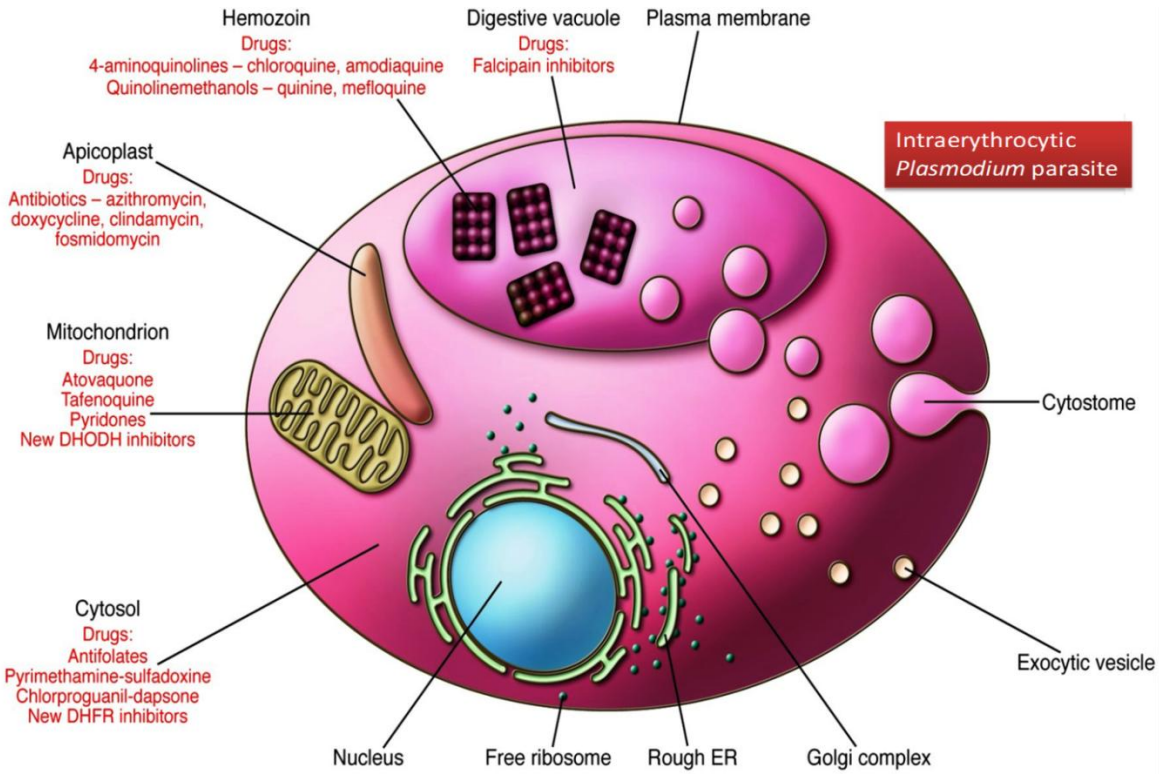

Figure 1.3. Representation of some of the major classes of antimalarial drugs targeted at specific intracellular compartments of *P. falciparum* parasite.

The 4-aminoquinolines (e.g chloroquine and amodiaquine), and the quinolinemethanols (e.g quinine and mefloquine) act inside the digestive vacuole of the parasite. The falcipain inhibitors targeted to the cysteine proteases. Antibiotics such as azithromycin, doxycycline and clindamycin act inside the apicoplast by inhibiting protein translation. Atovaquone and other selected compounds inhibit electron transport chain in the mitochondrion. The antifolate drugs act by disrupting folate biosynthesis in cytosol. The targets and sites of action of other antimalarials, including artemisinin and its derivatives, remain an area of active investigation. (Adapted from Greenwood et al., 2008).

1.2.4.4.1. Quinoline-containing antimalarial drugs

Quinoline-containing antimalarial drugs (QCDs) include some of the most common antimalarial drug families. Quinolines are aromatic nitrogen compounds characterized by a central solid-ring structure, essentially benzene fused to pyridine at two adjacent carbon atoms (Figure 1.4). However, there can be various functional groups on the main quinoline molecule that add to solubility and specificity of drug activity. The main QCDs that are used as antimalarial drugs can be divided into groups based on their chemical class. These

include (1) type-1 drugs 4-aminoquinolines (chloroquine, amodiaquine, pyronaridine, bis-quinoline piperaquine) are weak bases, deprotonated, and hydrophilic at pH 7.0, and (2) type-2 drugs aryl-amino alcohols (quinine, mefloquine, halofantrine, lumefantrine) are weaker bases and lipid soluble at neutral pH (Figure 1.4) (Olliaro, 2001, O'Neill et al., 2012). Additional QCDs include the 8-aminoquinoline, primaquine (Figure 1.4).

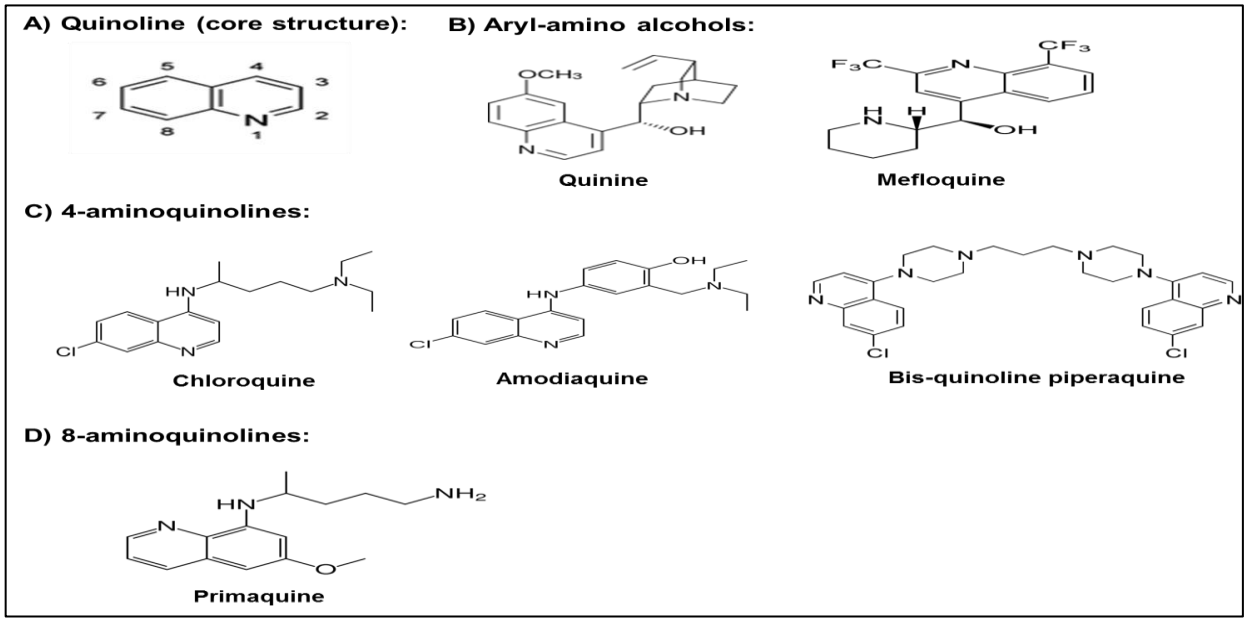

Figure 1.4. Chemical structures of some quinoline-containing antimalarial.
(A) quinoline ring core structure. (B) Aryl-amino alcohols drugs include quinine and mefloquine. (C) 4-aminoquinolines drugs include chloroquine, amodiaquine and piperaquine. (D) 8-aminoquinoline drug include primaquine.

Recognition of the therapeutic value of the 'fever bark tree' cinchona dates back to the 17th century before the parasitic nature of malaria was understood (Achan et al., 2011). It was not until 19th century when the active ingredient of the cinchona bark, quinine, was isolated and successfully synthesized to overcome the problem associated with the limited natural supplies (Seeman, 2007, Foley and Tilley, 1998, Woodward and Doering, 1944). The elucidation of quinine structure and then the identification of quinoline ring as key pharmacophore led to the development of synthetic drug families that include aryl-amino alcohol, 4-aminoquinolines and 8-aminoquinolines (Figure 1.4).

It is appropriate to start with the 4-aminoquinolines chloroquine which became available for several decades as a drug of choice for malaria treatment and prophylaxis (Muller and Hyde, 2010). The success of chloroquine has been based on its excellent clinical efficacy, limited host toxicity, ease of use and simple and cost-effective synthesis (Hyde, 2007a, Muller and Hyde, 2010, Biagini et al., 2003). Since chloroquine introduction in 1940s, it has saved countless millions of lives but its use against *P. falciparum* in now confined to limited areas of North Africa, Central America and the Caribbean region because its efficacy has decreased in the last two decades, mainly as a result of the development and the emergence of widespread of parasite resistance in every region where *P. falciparum* is prevalent such as sub-Saharan Africa (Muller and Hyde, 2010, Wellems and Plowe, 2001, O'Neill et al., 2012, Biagini et al., 2003, Payne, 1987). Therefore, the research into 4-aminoquinoline antimalarials has led to synthesis of amodiaquine (a Mannich base) and piperaquine (a bisquinoline) which have been shown to be effective against chloroquine-resistant strains of *P. falciparum* parasite (O'Neill et al., 2012, O'Neill et al., 1998, Biagini et al., 2003). In addition, a newer generation of aryl-amino alcohol quinine have been synthesised as response to the increasing problem of drug resistance. These include the development of mefloquine (a quinoline methanol), lumefantrine (also known as benflumetol) and halofantrine (a phenanthrene methanol). Nonetheless, quinine can be combined with an antibiotic (doxycycline or tetracycline) to enhance the treatment efficacy especially where some degree of quinine resistance may be present, such as in southeast Asia (Ejaz et al., 2007). In addition, 8-aminoquinolines drugs such as primaquine have been used to eradicate malaria hypnozoites from the liver as well as for malaria prophylaxis.

The exact mode of action (MoA) of QCDs is not fully understood (O'Neill et al., 2012, Muller and Hyde, 2010). However, it has been thought that QCDs, with the exception of 8-aminoquinoline primaquine (used primarily to act against hypnozoite and sexual stages infection), are thought to share a common target by interfering with the process of toxic heme polymerisation in the digestive vacuole of the asexual parasite stage although additional targets may also be involved in some cases (Figure 1.5) (Fitch, 2004, Muller and Hyde, 2010, Bray et al., 2005, O'Neill et al., 2012, Slater and Cerami, 1992). There is a

compelling evidence supporting the central role of a heme dependent mechanism in the action of 4-aminoquinoline and aryl-amino alcohol (Mungthin et al., 1998). Chloroquine is a weak base that accumulates in the parasite's acidic digestive vacuole and increase the pH and osmolality of the vesicles, leading to swelling and membrane leakiness (Krogstad and Schlesinger, 1987). Chloroquine becomes deprotonated in the digestive vacuole and trapped inside it (Olliaro, 2001). It appears that the most widely accepted theory about the MoA of chloroquine is to directly inhibit the polymerization of toxic heme molecules (produced from hemoglobin degradation) into hemazoin, and monomeric heme accumulates to levels in the digestive vacuole that kill the parasite (Slater and Cerami, 1992). However, there is a debate about chloroquine MoA which perhaps also include the interaction with the parasite DNA (Meshnick, 1990), impairment of lysosome function (Homewood et al., 1972) and inhibition of heme dependent protein synthesis (Surolia and Padmanaban, 1991). Therefore, in order to elucidate the MoA of QCDs, chapter 7 presents new insights into these drugs MoA using pharmacometabolomics approach.

The emergence of resistance to QCDs represents one of the predominant problems in malaria control. QCDs, such as chloroquine and quinine, resistance emerged in just 10 years after its introductios to all regions where malaria is endemic including Thai-Cambodian border in 1960s, Colombia-Venezuela border in 1970s and all sub-Saharan Africa in 1980s (Mita et al., 2009). Malaria parasites resistance to QCDs have been demonstrated by several studies showing that it is associated with point mutations in the transporter proteins that are located on the parasite digestive vacuole. Currently, genes associated with altered QCDs response are the *P. falciparum* chloroquine resistance transporter (*pfcrt*), the *P. falciparum* multidrug resistance transporter 1 (*pfmdr1*), and the *P. falciparum* Na^+/H^+ exchanger 1 (*pfnhe1*) (reviewed in (Petersen et al., 2011)). The involvement of *pfcrt* polymorphisms, particularly the K76T mutation, has been established for chloroquine and 4-aminoquinoline resistances (Lakshmanan et al., 2005, Fidock et al., 2000). This chloroquine resistance may acts by enabling the active efflux of diprotonated chloroquine out of the digestive vacuole and hence reducing the DV chloroquine concentration (Martin et al., 2009, Martin and Kirk, 2004). *Pfmdr1* has been associated to the altered susceptibility of malaria parasites to mefloquine, halofantrine and quinine but its

association remains unclear and other genetic factors may be involved such as *pfcrt* (Ward and Bray, 2000). *Pfmdr1* is a homolog of the multidrug resistance (MDR) transporter family, which is associated with drug resistance in mammalian tumor cells (Foote et al., 1989), that is thought to enable an increased drug efflux and decreased intracellular drug accumulation in parasite (Petersen et al., 2011). *Pfmdr1* is associated with increased malaria parasite susceptibility responses to lumefantrine, quinine, mefloquine, halofantrine and chloroquine (reviewed in (Petersen et al., 2011)). *Pfnhe1* is located in the plasma membrane and its function remains unclear but it is speculated to actively efflux protons to maintain a pH around 7.4 within the parasite (Bosia et al., 1993) . The association of *Pfnhe1* mutations with quinine resistance has been proposed but remains controversial (Okombo et al., 2010, Henry et al., 2009, Briolant et al., 2011, Andriantsoanirina et al., 2010).

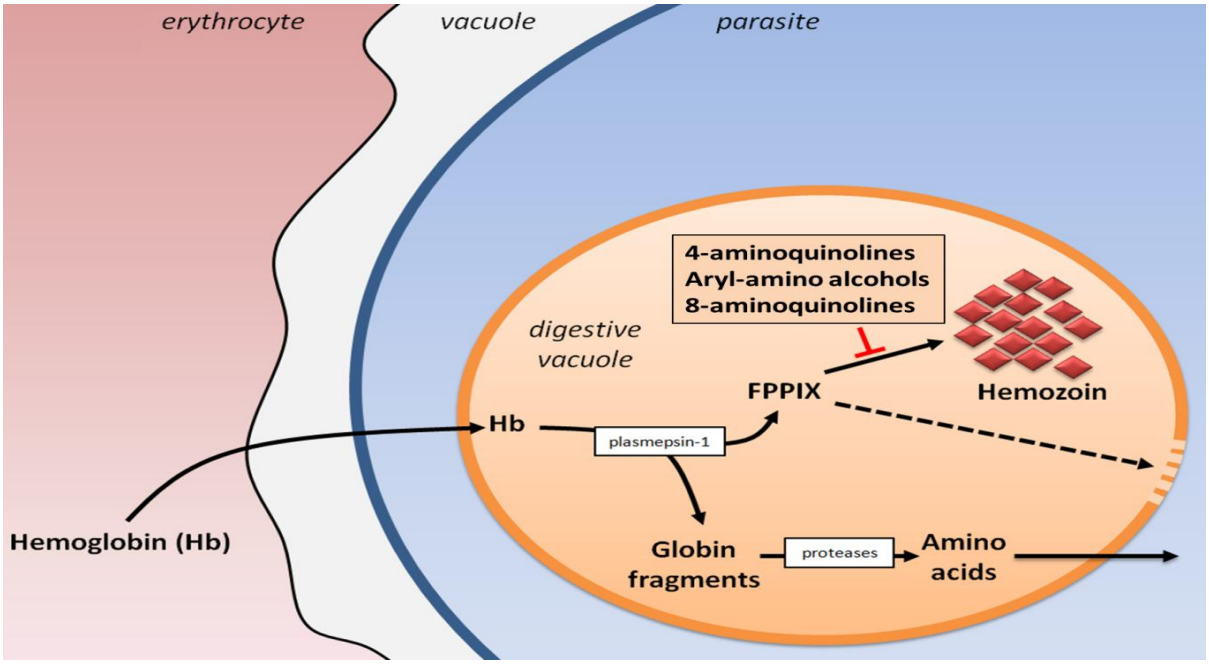

Figure 1.5. Proposed mode of action of quinoline-containing antimalarial drugs.
QCDs are thought to interfere with the process of heme polymerisation process leading to accumulation of toxic heme and eventually parasite death. (Adapted from Antoine, 2013).

1.2.4.4.2. Antifolates

Antifolates are widely used antimalarial drugs although their role in malaria control in hindered by rapid emergence of resistance under drug pressure (Plowe et al., 1998).

Antifolates are widely used in fixed-ratio combinations, most commonly sulfadoxine-pyrimethamine (SP, Fansidar^{TM}), for treatment and prophylaxis against malaria infection in chloroquine-resistant regions of Africa as well as in malaria endemic areas without supplies of Artemisinin Combination Therapy (ACT) (Gutman et al., 2012, Winstanley and Ward, 2006). There are two classes of antifolates drugs. Class I antifolates (sulfadoxine and dapsone) compete for the active site of dihydropteroate synthase (DHPS), preventing the formation of dihydropteroate (Figure 1.6) (Muller and Hyde, 2010). Class II antifolates (pyrimethamine and biguanide proguanil) inhibit parasite dihydrofolate reductase (DHFR), preventing tetrahydrofolate (necessary for biosynthesis of deoxythymidylate (dTMP), pyrimidine and polyamine) from being formed (Figure 1.6) (Olliaro, 2001). Growth of malaria parasites requires folate derivatives (folic acid or folinic acid) which are important cellular cofactors for the production of deoxythymidylate (dTMP) and thus DNA synthesis through pyrimidine pathway (Figure 1.6). The folate synthesis is essential for the malaria parasite survival which relies on *de novo* dTMP synthesis because of its incapacity to salvage pyrimidine from the exogenous medium (Hyde, 2007b). Antifolate drugs result in decreased pyrimidine synthesis, leading to reduced DNA, serine, and methionine formation and therefore they exert high activity when DNA synthesis peaks (late trophozoites) in parasites (Gregson and Plowe, 2005, Hyde, 2007b).

Unfortunately, antifolate resistance emerged rapidly after extensive administration of sulphadoxine/pyrimethamine (SP) combinations due to point mutations in both targeted enzymes (Mita et al., 2009). The quadruple mutant form of DHFR consists of three point mutations (S108N, N51I and C51R) whereas the double mutation form of *DHPS* consists of two points mutations (A437G and K540E); both enzymes mutations have been strongly associated with treatment failure (Kublin et al., 2002). *Pf*MRP1 is also proposed to affect intracellular folate homeostasis in parasites in which point mutation (K1446R) has been proposed to increase exogenous folate efflux, decrease the competition with the incoming drugs for their targets and contribute to antifolate resistance (Dahlstrom et al., 2009).

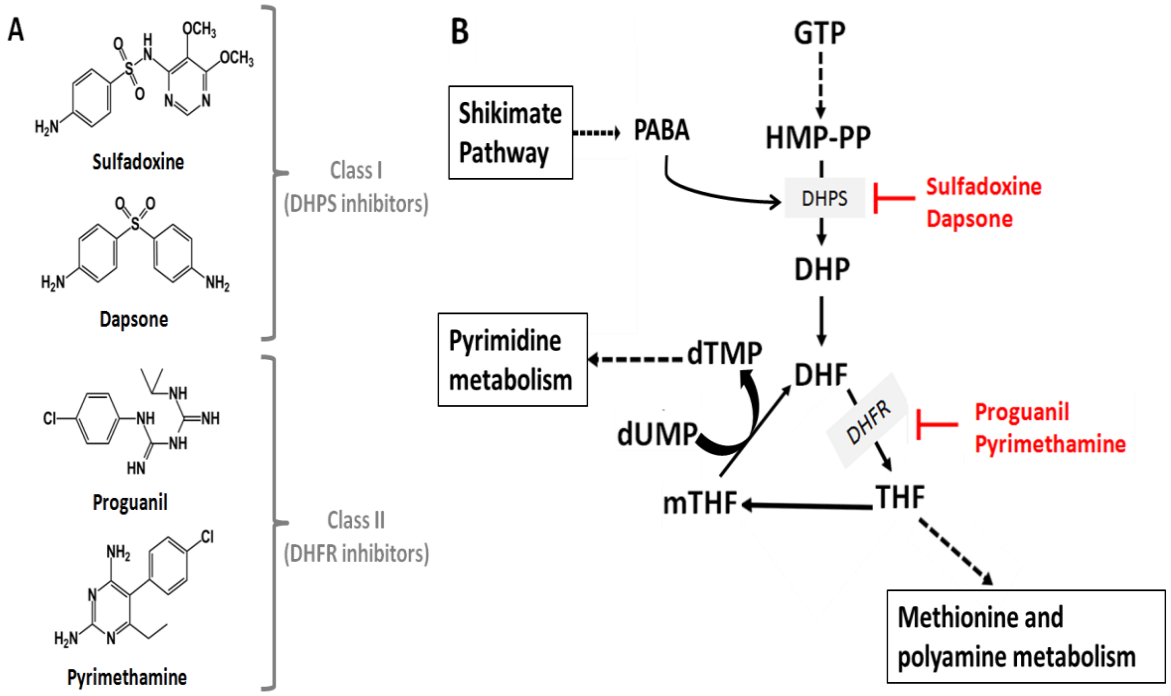

Figure 1.6. Chemical structures of antifolate drugs and their mode of action.
(A) Chemical structures of sulfadoxine, dapsone, proguanil and pyrimethamine. (B) Folate biochemical pathway in *P. falciparum* and mode of action for antifolate antimalarial drugs. Abbreviations: DHF, dihydrofolate; DHP, dihydropteroate; PABA, para-Aminobenzoic acid; THF, tetrahydrofolate; DHFR, dihydrofolate reductase; DHPS, dihydropteroate synthase; GTP, guanosine triphosphate; mTHF, methyltetrahydrofolate; dUMP, deoxy-urinidine monophosphate; HMP-PP, hydroxymethyl-pteridine-PP; dTMP, thymidine monophosphate. (Adapted from Antoine, 2013).

1.2.4.4.3. Hydroxynaphthoquinone (Atovaquone)

Atovaquone, a hydroxynaphthoquinone (2-[*trans*-4-(4'-chlorophenyl)cyclohexyl]-3 hydroxy-1.4-napthoquinone), has been developed twenty years ago and it shows activity against *Plasmodium* species (Figure 1.7 A) (Hudson et al., 1991). However, atovaquone is not very effective when used alone, as resistance to the drug develops quickly (Looareesuwan et al., 1996). Therefore, atovaquone is combined with the antifolate proguanil (forming Malarone®) which displayed synergistic effects *in vitro* and in clinical trials (Looareesuwan et al., 1999a, Canfield et al., 1995, Looareesuwan et al., 1996). The combination of atovaquone-proguanil (Malarone®) produces a near 100% curative rate but due to its costly production Malarone® is used mainly as chemoprophylaxis for travellers

visiting malaria endemic areas (Kessl et al., 2007, Looareesuwan et al., 1999b, Looareesuwan et al., 1999a).

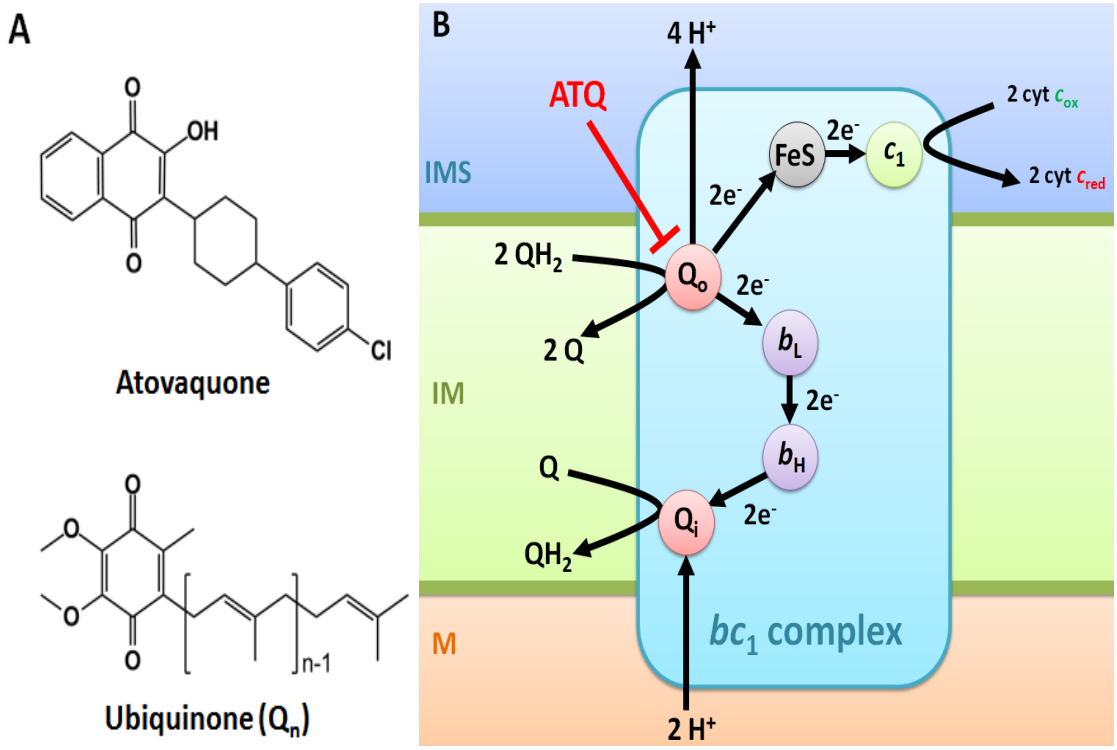

Figure 1.7. Chemical structure of atovaquone and its mode of action.
(A) Chemical structure of atovaquone and its analogue, the coenzyme ubiquinone. (B) Representation of bc_1 complex reactions and its inhibition with atovaquone (ATQ). Abbreviations: Q, ubiquinone; QH_2, ubiquinol; b_L, heme b_L binding site; b_H, heme b_H binding site; Fe-S, iron-sulfur cluster; cyt c, cytochrome c; c_1, cytochrome c binding site. (Adapted from Antoine, 2013).

Atovaquone is an inhibitor of the ubiquinol oxidation site (Q_o) of the *P. falciparum* bc_1 complex (Figure 1.7. B). The MoA of atovaquone alone and in combination with proguanil is comprehensively described in Chapters 5 and 6. In short, atovaquone inhibits the catalytic turnover of bc_1 complex, collapsing the mitochondrial membrane potential and resulting in the loss of essential mitochondrial metabolic function such as pyrimidine biosynthesis (Painter et al., 2007). Interestingly, the action of proguanil in Malarone® is not to inhibit DHFR in folate pathway (as when used by itself), but rather it lowers the effective dose needed to cause mitochondrial membrane potential collapse by atovaquone (Srivastava and Vaidya, 1999). Resistance to Malarone® has been reported in different

point mutations at the Q_o site (Musset et al., 2006, Korsinczky et al., 2000, Berry et al., 2006). Y268S, and less frequently Y268N, are the most common mutations observed, increasing the atovaquone IC_{50} by several hundred fold as compared to sensitive parasite strains (Barton et al., 2010).

1.2.4.4.4. Artemisinin-type compounds

Artemisinin (Qinghaosu; active compound) is an extract from the plant *Artemisia annua* (Chinese wormwood) that has been used as herbal remedies for the treatment of fevers in traditional Chinese medicine (White, 2008b). Artemisinin has low toxicity and high efficacy against all types of human malaria parasites including those resistant to conventional antimalarial treatment (Li et al., 1994, Krishna et al., 2008). A first generation of semi-synthetic artemisinin derivatives (known as dihydroartemisinin, artesunate and artemether) has been synthesized with higher antimalarial activity and better solubility owing to the cultivation growing demand to obtain high yields extract from *A. annua* (O'Neill and Posner, 2004). These semi-synthetic artemisinin derivatives were initially used as monotherapies and then in combination with a numerous of antimalarial drugs (refer to Table 1.1) known as artemisinin-based combination therapies (ACTs) (White, 2008b). ACTs are widely used to treat uncomplicated malaria as well as drug-resistant malaria strains with a high efficiency, rapid clearance and minimal toxicity in humans (Nosten and White, 2007, White, 2008b).

Artemisinin and its derivatives have unique trioxane ring structure with an endoperoxide bridge (C-O-O-C), lacking the nitrogen containing ring system which is found in most antimalarial drugs such as chlolorquine (Figure 1.8) (Meshnick et al., 1996). The MoA of artemisinin and its derivatives is not fully understood and still debatable (Figure 1.9) (Ding et al., 2011). The absolute requirement of the trioxane as a pharmacophore subunit of artemisinin for activity has led researchers to focus on this for the MoA studies. It has been proposed that artemisinins can exert their effect through the generation of reactive oxygen species, which can be enhanced in the presence of haem-iron that is found in parasites after hemoglobin digestion (Petersen et al., 2011). It is possible that these radicals may exert an effects by overwhelming parasite oxidative stress mechanisms (Krishna et al., 2004,

Olliaro, 2001). The trioxane pharmacophore acts as a source of hydroperoxide via the generation of an oxo-stabilised cation upon heterolysis of the peroxide bridge. This may lead to oxygenating species or hydroxyl or alkoxyl radicals which can have detrimental effects on biomolecules (Olliaro et al., 2001). Other studies found that artemisinin may acts by interference with heme detoxificatioin process in the digestive vacuole (Pandey et al., 1999) or artemisinin derivatives accumulate within neutral lipid bodies in the digestive vacuole where they damage parasite membranes after oxidation reactions (Hartwig et al., 2009). Artemisinins have also been found to inhibit mitochondrial function in *Plasmodium* parasite by interfering with the electron transport chain and by inducing reactive oxygen species leading to the loss of mitochondrial membrane potential loss, disrupting the normal function of mitochondria and eventually parasite death (Wang et al., 2010, Li et al., 2005). In addition, it has been reported that artemisinin inhibits PfATP6 (sarco/endoplasmic reticulum calcium-dependent ATPase SERCA) leading to the disruption of Ca^{2+} homeostasis in the parasite (Eckstein-Ludwig et al., 2003).

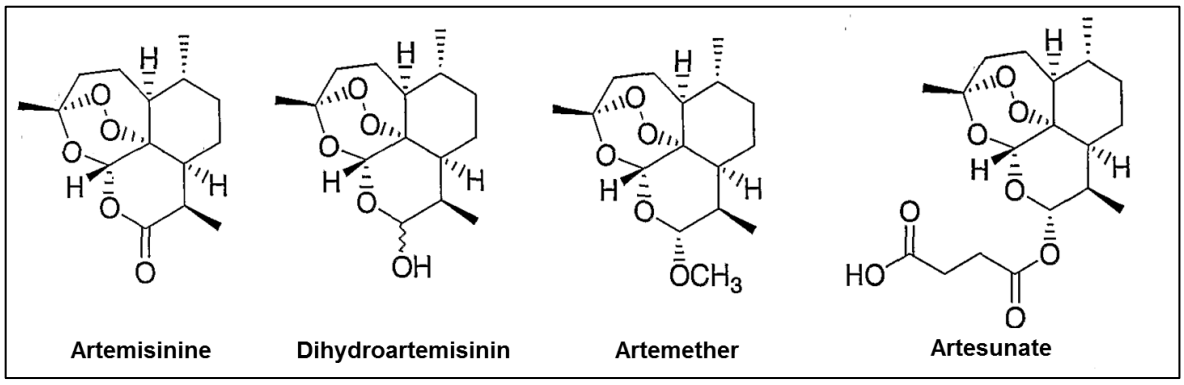

Figure 1.8. Chemical structure of artemisinin and its derivatives.

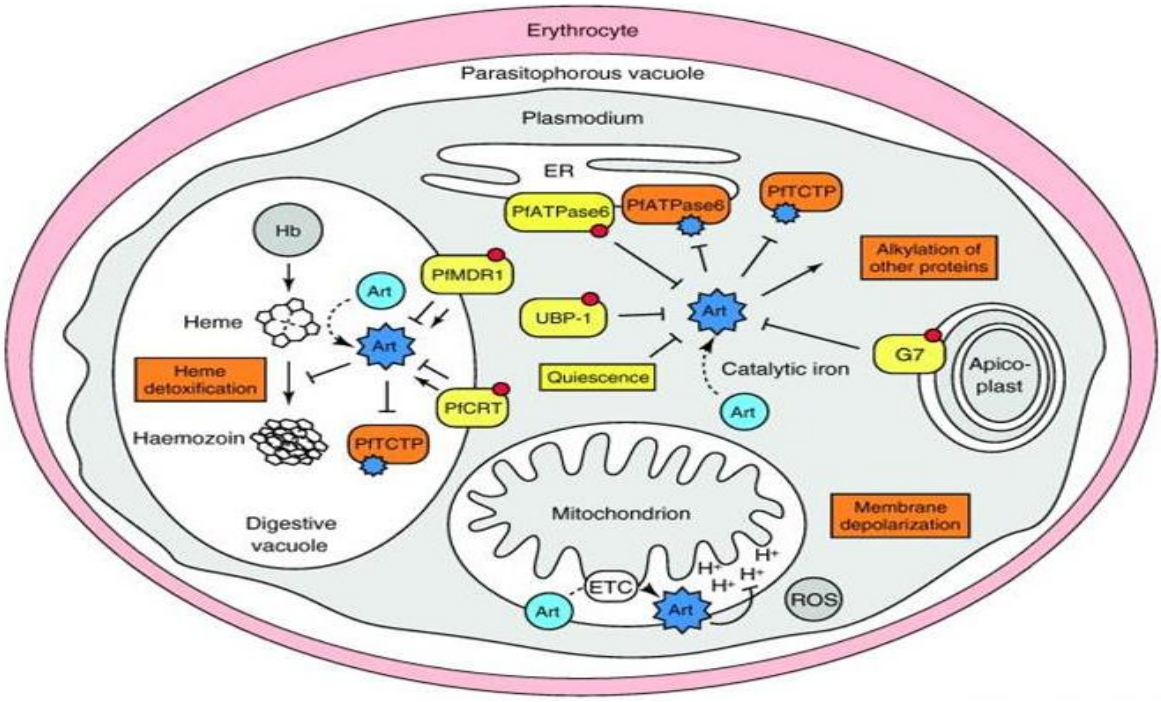

Figure 1.9. Proposed mode of action of artemisinin and resistance factors in *P. falciparum*.
It is believed that iron interacts with the peroxide bond of artemisinins (Art) resulting in active carbon centered radicals that might (i) interfere with the heme detoxification pathway; (ii) induce the alkylation of the translationally controlled tumor protein (PfTCTP) and other proteins; (iii) inhibit the sarco/endoplasmic reticulum membrane calcium ATPase 6 (PfATPase6); or (iv) interfere with *Plasmodium* mitochondrial functions through the production of reactive oxygen species (ROS). Proteins, in which mutations (red dots) have been shown to increase (arrow) or to decrease (inhibition line) *in vitro* sensitivity to Art, are indicated. Putative targets or target mechanisms are labelled in orange and putative resistance factors in yellow. (Adapted from Ding et al., 2011).

Artemisinin resistance has not been documented until 2010 on the Thai-Cambodian border (Dondorp et al., 2009). However, the direct evidence of the resistant mechanisms has not been well understood. The findings from the sequencing data did not show any correlation between artemisinin resistance and *pfcrt*, *pfmdr1* or *pfatp6* genes (Imwong et al., 2010). Interestingly, evidence from transcriptomic studies suggests that artemisinin resistance may be associated with reduced activity of basic metabolic (e.g. glycolysis and nucleotide metabolism) and cellular maturation (e.g. DNA replication) pathways in the parasites (Mok et al., 2011).

1.2.4.4.5. Antibacterial Agents

Several antibiotics have shown an antimalarial effect targeting prokaryote-like organelles such as apicoplast and mitochondria (McFadden and Roos, 1999, Lim and McFadden, 2010, Vaidya, 2004). Antibiotics exert their action by inhibiting the prokaryote-like processes in *Plasmodium* parasites such as protein synthesis and DNA/RNA replication (Dahl and Rosenthal, 2008, Johnson et al., 2011, Vaidya, 2004). Interestingly, antibiotics do not immediately kill malaria parasites, but they cause what is known as ‘‘delayed death phenotype’’ or ‘‘delayed kill effect’’ in the second erythrocytic cycle (Ramya et al., 2007). This effect equates to longer parasite clearance times and prolonged symptoms as compared with classical antimalarial (Lell and Kremsner, 2002). Therefore, antibiotics such as doxycycline and tetracycline are used in combination with quinine for non-immunes experiencing acute malaria to achieve faster acting effect by classical antimalarial drug and clearance of remaining parasites by antibiotic particularly those showing reduced sensitivity against antimalarial drug (Schlitzer, 2008).

1.3. Malaria parasite biology

Human malaria can be caused by five species of *Plasmodium* parasites, all of which undergo similar life cycles within the host although slight differences are observed. Research in recent decades has shed light on many aspects of *Plasmodium* biology, broadening understanding of how parasites interact with the host system, cause human disease. However, this fundamental area of research is essential parasite biology although there are numerous questions remain unanswered and new questions have arisen. In addition, knowledge of the detailed structure, physiology and biochemistry of the parasite can be helpful for identifying new potential antimalarial targets for the synthesis of new drugs and providing accurate immunolocalization of antigens for the design of vaccine.

1.3.1. Human malaria parasite life cycle

The human malaria parasite, *Plasmodium* species, undergoes over a dozen distinguishable stages of development as it moves from the mosquito vector to human host and back again.

One way to simplify this complex life cycle is to consider it in three distinct replicative stages include liver stage, blood stage and mosquito stage (Figure 1.10).

The liver stage of malaria begins with the bite of an infected female anopheline mosquito, when sporozoites are introduced into the human host skin together with mosquito saliva during a blood meal. Following the mosquito injection, the sporozoites rapidly make their way to liver where they invade the liver cells (hepatocytes). Over a course of 5 to 15 days, depending on the *Plasmodium* species, the sporozoites undergo a process of asexual reproduction, known as exoerythrocytic schizogony (the splitting process), that results in the production of thousands daughter parasites called merozoites (Oaks Jr, 1991). The duration of liver stage schizogony is characteristic for each species. For instance, minimum maturation time of 5 days in *P. falciparum* and 15 days *P. malariae* (Hommel, 2005). However, *P. vivax* and *P. ovale* undergo dormant phase called hypnozoites, which can persist in the liver and cause relapses by invading the blood stream months or years later (Krotoski et al., 1982, Krotoski, 1985).

The blood stage begins when the merozoites are released from the liver into the blood stream where they rapidly adhere to and invade erythrocytes to begin. Once inside the red blood cell (RBC), the parasite undergoes a 48 hours (or 72 hours for *P. malariae*) asexual blood stage reproduction known as erythrocytic schizogony. This blood stage of the *Plasmodium* life cycle consists of three distinctive developing forms of *Plasmodium* parasite including ring form, trophozoite form and schizont form. Following the merozoite invasion of RBC, it develops into a ring form over the first twelve hours post-invasion. Then, it develops into a trophozoite and remains at this stage for 14 hours. After that, the matured trophozoite is marked by multiple rounds of nuclear division resulting in the formation of schizont which is characterised by containing numerous of daughter merozoites. When the red blood cell burst, each mature schizont releases about 8-32 merozoites which are ready to invade new red blood cells and the cycle within blood stage repeats itself which is known as asexual cycle (Oaks Jr, 1991, Hommel, 2005, Cowman et al., 2012). However, some released merozoites are committed to gametocytogenesis, where they develop either into male (microgametocyte) or female (macrogametocyte) gametocytes to continue their sexual cycle in the mosquito vector. Factors that has been

shown perhaps to induce gametocytogenesis rather than schizogonic development in are hyperparasitemia, anemia and antimalarial drug treatment and it looks though the parasite sensing hostile conditions and by transforming into gametocytes they prepare to escape into new host (Hommel, 2005). Gametocytes undergo through five developing morphological stages to reach full maturity within approximately 12-14 days (Fivelman et al., 2007).

The mosquito stage begins when gametocytes are taken up during the mosquito's blood meal. Gametocytes are taken into the mosquito's midgut where they can continue their differentiation to form macrogametes and microgametes. Male microgametes are released during a process called exflagellation. Fusion of the female macrogamete with a single microgamete results in fertilization and the formation of zygote. This zygote continuously divides to develop into a motile ookinete which migrate to the wall of the mosquito's midgut, where it penetrates the peritrophic membrane, epithelium and comes to rest on the external surface of the stomach to mature and develop into an oocyst. Over a period of days (4-15 days), mature oocyst contains up to 10,000 motile sporozoites. When the occyst ruptures, the sporozoites enter the mosquito circulation and migrate to the salivary glands where they are injected into the human host when the mosquito takes the blood meal thus perpetuating the malaria life cycle (Oaks Jr, 1991, Sinden and Billingsley, 2001).

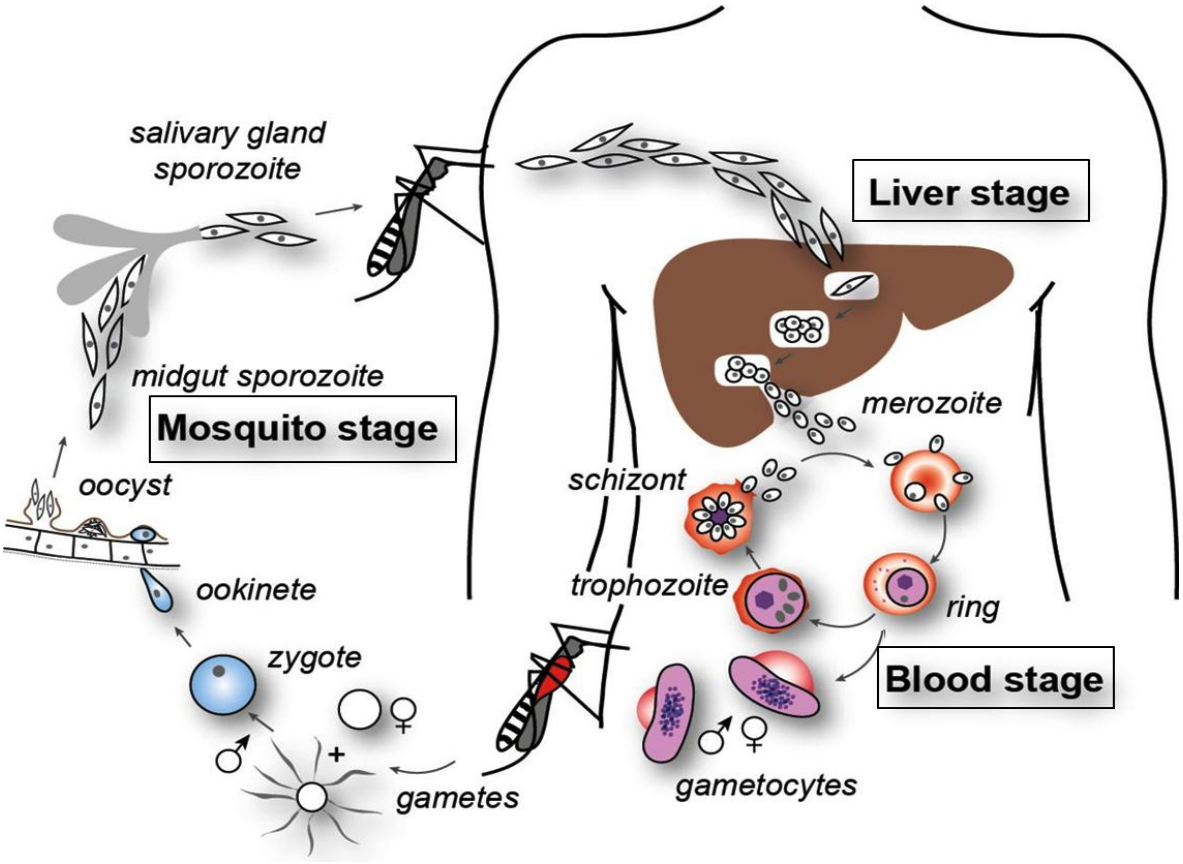

Figure 1.10. The life cycle of human malaria parasite, *P. falciparum*.
The *Anopheles* mosquito bites a human and injects sporozoite forms. These move to the liver and invade hepatocytes, in which they develop to produce exoerythrocytic merozoite forms (liver stage) that are released into the blood stream. Merozoites invade erythrocytes and grow into trophozoites and mature schizonts (blood stage). Merozoites are released that reinvade new erythrocytes. Gametocytes, formed from the asexual blood stage, are taken up by a feeding mosquito into the gut where they mature to form male and female gametes. The fertilized zygote develops to an ookinete and an oocyst and finally sporozoites that migrate to the salivary glands (mosquito stage). (Adapted from Cowman et al., 2012).

1.3.2. Structure of malaria parasite asexual blood stages

This thesis focuses on the trophozoite stage of *P. falciparum* parasite. Nonetheless, the structure of major asexual blood stages including merozoite (the invader), ring stage, trophozoite stage (feeding and highly metabolic stage) and schizont stage (the dividing stage) will be highlighted.

1.3.2.1. Merozoite

The invasive merozoite stage is immunologically important because it is briefly extracellular and hence exposed to host antibodies between leaving one RBC and invade other. It is a pear-shaped (1-2 µm) with a low flat-ended projection located at one end (Langreth et al., 1978, Bannister et al., 2000). Merozoite contains secretory vesicles, numerous ribosomes, a mitochondrion and a plastid that are located at apex whereas the nucleus is placed basally (Figure 1.11) (Bannister et al., 2000). The apical organelles containing rhoptries, micronemes, dense granules that are all membranous vesicles which discharge their contents during invasion and thus change the shape and composition of the invaded RBC membrane (Bannister et al., 2000). The secretions of rhoptries and micronemes might be essential for the attachement of merozoite to the surface of RBC leading to the formation of an invasion ditch that later develops into parasitophorous vacuole (Bannister et al., 2000). The dense granules lie separately and release their contents after invasion in order to perhaps increase the membrane area and possibly helping to facilitate the change in shape to that of a ring stage (Atkinson and Aikawa, 1990).

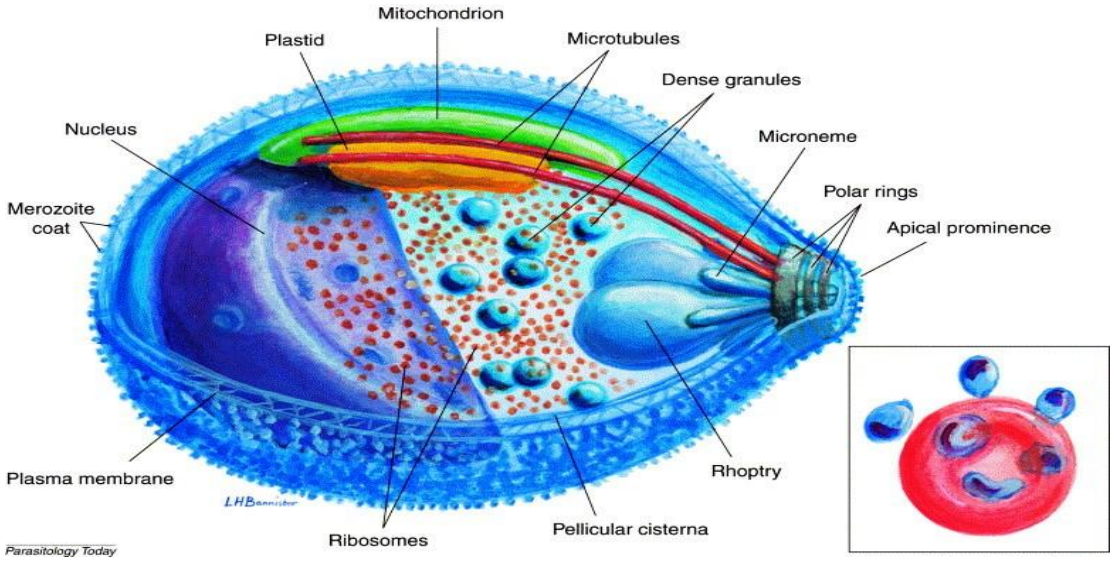

Figure 1.11. Three-dimensional organization of *P. falciparum* merozoite showing the internal structure. Inset: relative sizes of merozoites and the invaded RBC. (Adapted from Bannister et al., 2000).

1.3.2.2. Ring stage

Following merozoite invasion, it flattens into a thin discoidal, flat and cup-shaped ring form (Figure 1.12). This ring stage of the parasite is characterised by a thick circumference of cytoplasm that house the major organelles include nucleus, mitochondrion, plastid, ribosomes and endoplasmic reticulum whereas the centre of the disc is thin containing few structures (Figure 1.12) (Bannister et al., 2000). Pinocytosis is a process in which the parasite begins to feed on the surrounding RBC producing several small pigment vacuoles (Slomianny, 1990). As the ring stage develops into an early trophozoite, the cytostome appears, feeding intensifies, small pigment vacuoles fuse to form a single large central digestive vacuole and the area of the parasitophorous vacuole membrane (PVM) surrounding the parasite also increases and extends to narrow, finger-like projections that protrudes into the surrounding RBC (Elford et al., 1995, Atkinson and Aikawa, 1990). Therefore, the ring stage eventually changes the shape to a larger irregular shape trophozoite.

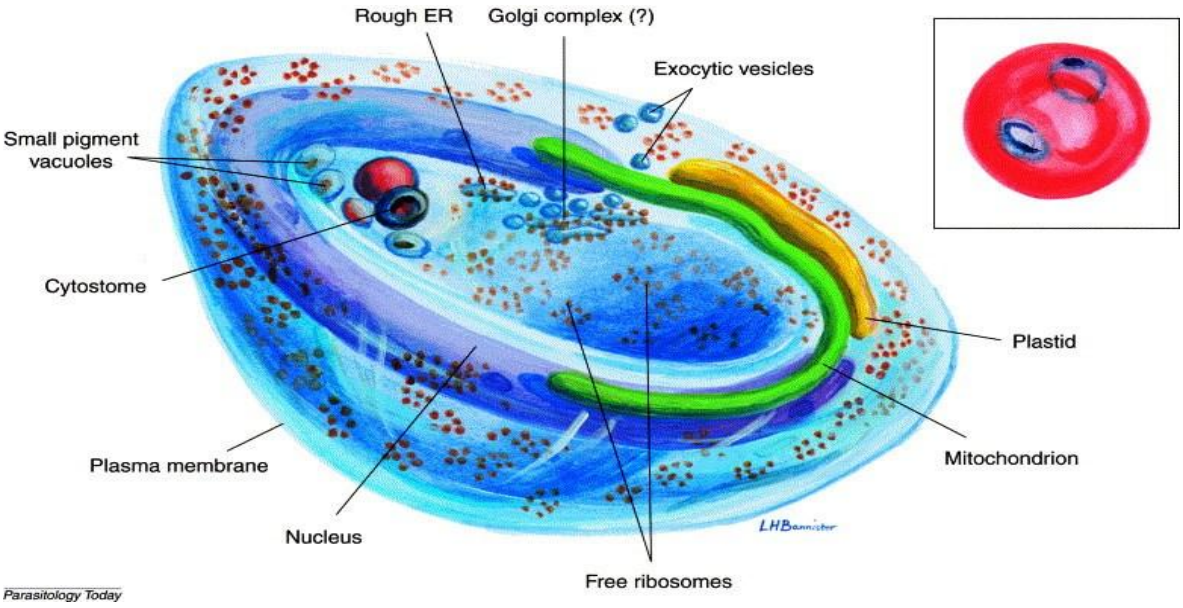

Figure 1.12. Three-dimensional organization of *P. falciparum* ring stage showing the internal structure. Inset: ring stage as seen in a Giemsa-stained film by light microscopy (Adapted from Bannister et al., 2000).

1.3.2.3. Trophozoite stage

There is no fundamental internal difference between the ring stage and trophozoite stage apart from the size and shape (Figure 1.13). Trophozoite stage feeds on the host RBC, primarily haemoglobin the predominant protein in the cell (Goldberg et al., 1990). It gradually alters RBC shape by exporting various parasite proteins into its cytoplasm and surface (Bannister et al., 2000). Several changing features are observed in the trophozoite stage. These include increasing in the numbers of free ribosomes and the enlargement of endoplasmic reticulum which denoting increased protein synthesis (Bannister et al., 2000) as well as the attachment of mitochondrion and plastid to each other which indicate perhaps metabolic interaction (van Dooren et al., 2005, Seeber and Soldati-Favre, 2010, Lim and McFadden, 2010). The PVM embraces the parasite membrane with the formation of irregular bulges and tubular invaginations. These various membranous structures correspond to the basophil-like dots seen in the Giemsa stained cytoplasm of infected RBC known as Maurer's clefts (Bannister et al., 2000).

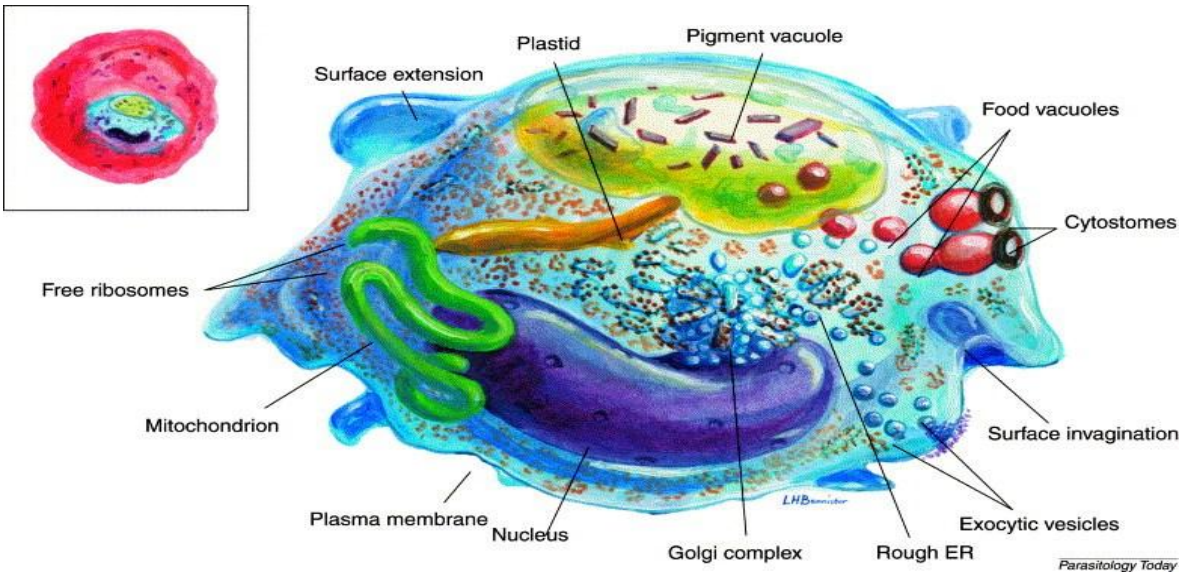

Figure 1.13. Three-dimensional organization of *P. falciparum* trophozoite stage showing the internal structure. Inset: trophozoite stage as seen in a Giemsa-stained film by light microscopy (Adapted from Bannister et al., 2000).

1.3.2.4. Schizont stage

The nuclear division of the malaria parasite takes place during the schizont stage (Figure 1.14) although synthesis of molecules that are needed for parasite multiplication such as DNA, is known to begin in the trophozoite stage (Bannister et al., 2000, White and Kilbey, 1996). RBC ingestion and parasite protein exportation at the surface of RBC continue till late in the life of schizont (Bannister et al., 2000). Numerous cytoplasmic changes occur upon the beginning of nuclear division include increasing in the multiplication of rough endoplasmic reticulum, free ribosomes, mitochondria and plastids (Bannister et al., 2000). A series of merozoites-forming foci (each with a set of rhoptreis) develop and appear spread out at systematic intervals around the circumference of the parasite (Jaikaria et al., 1993, Bannister et al., 2000). Before complete separation nucleus, mitochondrion and plastid move into each merozoite from the central area of the schizont cytoplasm (Bannister et al., 2000).

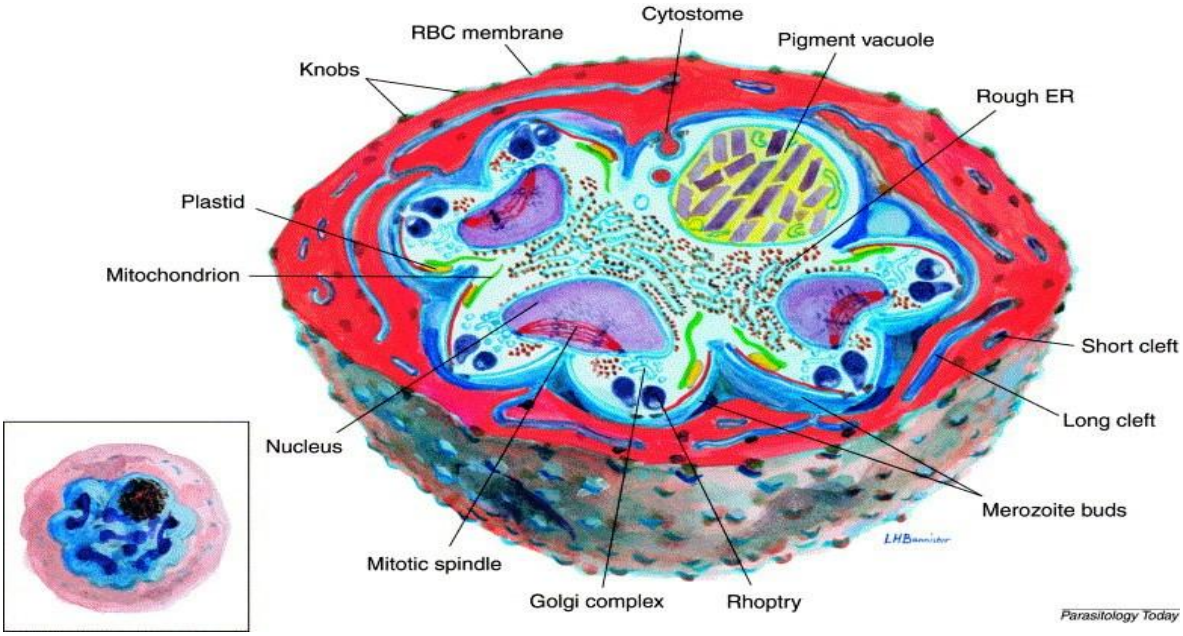

Figure 1.14. Three-dimensional organization of *P. falciparum* schizont stage showing the internal structure. Inset: schizont stage as seen in a Giemsa-stained film by light microscopy (Adapted from Bannister et al., 2000).

1.3.3. Physiology and biochemistry of malaria parasite

1.3.3.1. Feeding process and haemoglobin degradation

Feeding process in malaria parasites begins with ingestion of small portions of RBC cytosol by micropinocytosis in ring stage parasites (Slomianny, 1990). As the parasite matures (trophozoite stage), a larger volume of hemoglobin is ingested by the cytostomal system that is formed by invagination of the parasitophorous vacuolar membrane (PVM) and the parasite plasma membrane (PPM) (Slomianny, 1990). When the cytostomes ingest RBC cytosol, double membrane-delimited vesicles are formed by budding at the surface of cytostome (Slomianny, 1990, Oaks Jr, 1991). These vesicles fuse to form one large, single membrane-enclosed digestive vacuole, which is regarded as the primary site for haemoglobin degradation (Slomianny, 1990, Francis et al., 1997, Olliaro and Goldberg, 1995).

The digestive vacuole of malaria parasites is an acidic compartment with pH 5.0-5.4 (Yayon et al., 1984a). Haemoglobin represents about 95% of the dry weight of RBC and about 75% of it, is consumed by *P. falciparum* during its brief intraerythrocytic cycle (Morrison and Jeskey, 1948, Ball et al., 1948). Therefore, haemoglobin degradation is a massive and rapid catabolic process where a number of potent digestive protease enzymes involved (Goldberg, 2005). These include a group of aspartic proteases called plasmepsins, a group of cysteine proteases called falcipains, a metalloprotease called falcilysin, and at least one dipeptidylpeptidase I (Francis et al., 1997). Aminopeptidases are thought to be involved in the final peptide degradation in the cytoplasm (Kolakovich et al., 1997, Skinner-Adams et al., 2010). The action of these degradative enzymes in digestive vacuole appears to be an ordered process, requiring plasmepsins to make the initial cleavage in intact haemoglobin followed by secondary cleavages by plasmepsins and falcipains (Figure 1.15) (Goldberg et al., 1990). Falcilysin appears to recognize only short peptides generated by the upstream enzymes whereas dipeptidylpeptidases and aminopeptidases are proposed to function most efficiently in terminal degradation providing ultimately amino acid in the parasite cytosol (Goldberg et al., 1990, Goldberg, 2005, Francis et al., 1997). It has been

demonstrated that protease inhibitors exert their antimalarial activities digestive vacuole proteases and therefore merit development as antimalarial drug targets (Moura et al., 2009).

Early in the haemoglobin degradation pathway, free heme is released upon digestion of the globin chains (Francis et al., 1997). Free heme causes lethal changes to membranes and proteins and its efficient disposal is of critical importance to the malaria parasite during the proteolysis process (Bray et al., 2005). Therefore, *Plasmodium* parasite developed biocrystallization process to overcome the toxicity of heme, which crystallized into an inert pigment called hemozoin (Figure 1.15) (Egan et al., 2002, Egan, 2008). Therefore, quinoline-containing antimalarial drugs appear to function by disrupting this sequestration processs, leading to an accumulation of toxic heme products (Bray et al., 2005).

Plasmodium parasite feeds on RBC hemoglobin as an amino acids source for protein synthesis because of its limited capacity for *de novo* amino acids synthesis (Goldberg, 2005). However, *P. falciparum* can survive in medium supplying just five amino acids (methionine, cysteine, glutamine, glutamate and isoleucine) that are in limited supply or absent from hemoglobin (Divo et al., 1985a). In addition, it has been shown that amino acids from radiolabeled haemoglobin are incorporated into parasite proteins providing an evidence for the importance of RBC haemoglobin for the parasite survival (Sherman and Tanigosh.L, 1970, McCormic.Gj, 1970). Amino acids utilization for the parasite growth appears to be pivotal because parasites grown in the five amino acids supplemented medium are more sensitive to haemoglobin degradation inhibitors than those grown in full medium (Francis et al., 1994). Intriguingly, it has been noted that a significant portion of amino acids released from haemoglobin is excreted by the parasite (Zarchin et al., 1986, Krugliak et al., 2002). Therefore, it has been hypothesized that the reason behind the existence of digestive vacuole could be attributed as making room for the parasite in its host cell (Krugliak et al., 2002, Ginsburg, 1990) or to control RBC osmotic stability (Lew et al., 2003). More insights about the amino acids metabolism and the role of digestive vacuole are presented in chapters 4 and 7, respectively.

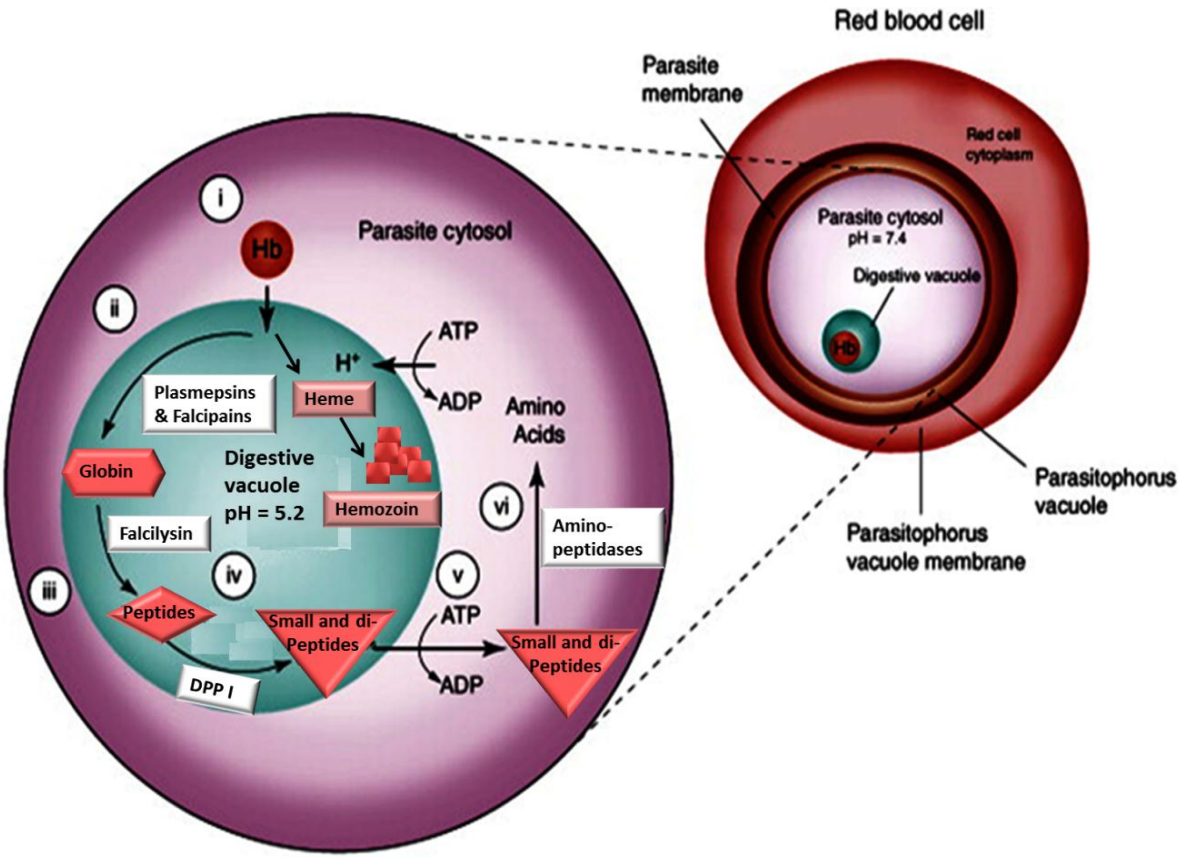

Figure 1.15. Representation of haemoglobin degradation pathway in *P. falciparum*.
Digestion of host haemoglobin (Hb) by *P. falciparum* takes place within the acidic digestive vacuole. Red cell haemoglobin is transported to the DV (i) where a number of protease enzymes, including aspartic proteases (plasmepsins I, II and IV), cysteine proteinases (falcipains 2, 2′ and 3) (ii) and a metallo-protease (falcilysin), initiate catabolism (iii). Dipeptidyl aminopeptidase I (DDP I) acts by further cleaving of generated peptides by upstream enzymes into dipeptides (iv). The small peptide fragments derived from haemoglobin degradation in the digestive vacuole are transported to the parasite cytosol (v) where they are further digested by aminopeptidases providing amino acids (vi). (Adapted with modification from Skinner-Adams et al., 2010).

1.3.3.2. Nutrient access and metabolism

The passage of nutrients from the extracellular space to the malaria parasite cytosol involves a transfer across the RBC membrane, PVM and PPM. Different mechanisms may involve in nutrients transport across these membranes including diffusion along a gradient of substrate and carrier-mediated transport (Hommel, 2005). Two groups of transporters protein involve in the nutrients transport mechanism including (i) carrier proteins that bind

solutes and then undergo conformational change to move them across a membrane and (ii) channel proteins that are essentially gated, water-filled pores (Figure 1.16) (Staines et al., 2010, Kirk, 2001). Because of the rapid growth and replication of the parasite, the normal transport processes of the RBC are not sufficient to meet the parasite demand. Therefore, the parasite, alongside other transporters, evolved a transport process known as new permeation pathway (NPP) to increase the nutrients traffic across the membranes (Kirk, 2001). Most nutrients required by the *Plasmodium* parasite originate from the extracellular space such as host plasma. These include carbon sources (e.g. glucose), purines (e.g. adenine), amino acids, anions, cations and vitamin (e.g. folate or B9) (Hommel, 2005).

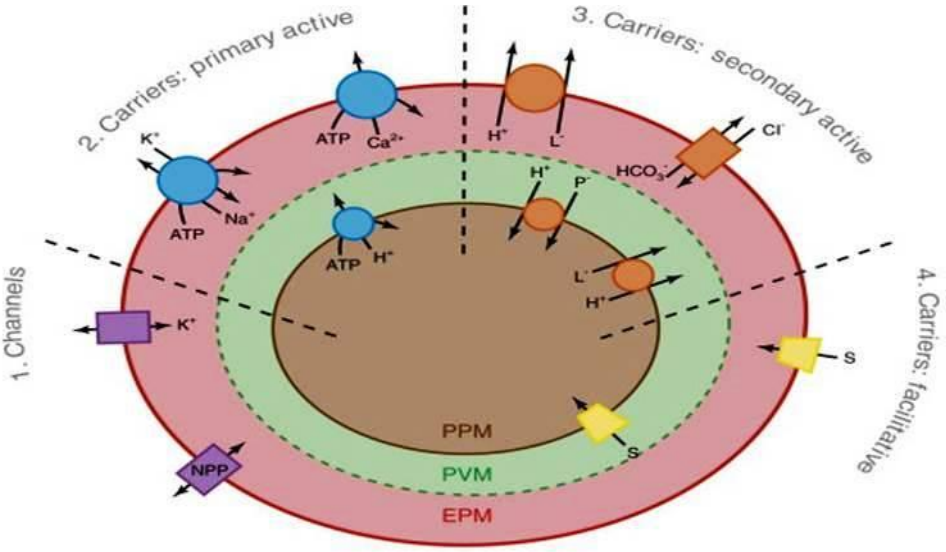

Figure 1.16. Diagram of transport protein classes and transport mechanisms of RBC and parasite transport processes in *P. falciparum*.

Illustrated are erythrocyte plasma membrane (EPM), parasitophorous vacuole membrane (PVM) and parasite plasma membrane (PPM). (1) Channels: examples are the Gardos channel (Ca^{2+}-activated K^+ channel) and the new permeability pathways (NPP) in the EPM. (2) Primary active carriers: examples are the Na^+/K^+ ATPase and the plasma membrane Ca^{2+} pump in the EPM, and a V-type H^+ pump in the PPM and the digestive food vacuole. (3) Secondary active carriers: examples are the HCO_3^-/Cl^- exchanger and the H^+-coupled monocarboxylate symporter (MCT1; which mediates the efflux of lactate (L^-) in the EPM, and H^+-coupled pantothenate (P^-) and lactate symporters in the PPM. (4) Facilitative carriers: examples are the hexose transporters GLUT1 and PfHT in the EPM and PPM, respectively (they mediate the uptake of the sugar D-glucose (S). (Adapted from Staines et al., 2010).

1.3.3.3. Energy metabolism

The intraethrythrocytic malaria parasites rely mainly on glycolysis for energy generation. Glucose from the plasma enters into the *Plasmodium* cytoplasm and is subsequently degraded to lactate via the anaerobic Embden-Meyerhoff-Parnas (EMP) pathway as summarized in Figure 1.17 (Crawford, 2003). It has been shown that *P. falciparum* has increased activity of the glycolytic enzymes and of lactate dehydrogenase as compared to RBC (Roth et al., 1988). Likewise, the specific activity of the glycolytic enzymes and lactate dehydrogenase from isolated *P. falciparum* trophozoites is higher than that from RBC (Vanderjagt et al., 1990). Most of the *P. falciparum* enzymes used for glucose fermentation during its 48 h asexual cycle development have now been characterized antigenically, enzymatically, and/or genetically (reviewed in (Lang-Unnasch and Murphy, 1998)) as well as they are encoded in the *Plasmodium* genome (Gardner et al., 2002) (Figure 1.17). In addition, *Plasmodium* parasites can also utilize alternative carbon sources such as fructose albeit at a reduced proliferation rate (Woodrow et al., 2000). Studies showed that *P. falciparum* infected RBC use 100 fold more glucose (mainly during trophozoite and schizont stages) than those non-infected (Roth et al., 1988, Roth Jr, 1990). Glucose is used in *Plasmodium* metabolic pathways for nucleic acid biosynthesis, amino acid biosynthesis, TCA cycle (tricarboxylic acid) and lipid biogenesis (Figure 1.17). It has been estimated that 60-70% of the glucose consumed by *P. falciparum* is incompletely oxidised to lactate (Jensen et al., 1983) and only a small amount of glucose is oxidised to form CO_2 (Scheibel and Pflaum, 1970). This reflects the increased flux of glucose carbon into parasite biomass (nucleic acids, lipids, proteins) required for parasite growth and replication as compared to more than 90% of glucose is converted to lactate in uninfected RBCs (Olszewski and Llinas, 2011). On the other hand, these findings may indicate the lack of a fully functional TCA as well as call into querying the role of mitochondrial electron transport chain for energy generation. Answers to this assumption are provided in the chapters 4, 5, and 6. Nonetheless, synopsis about TCA and mitochondria is highlighted below.

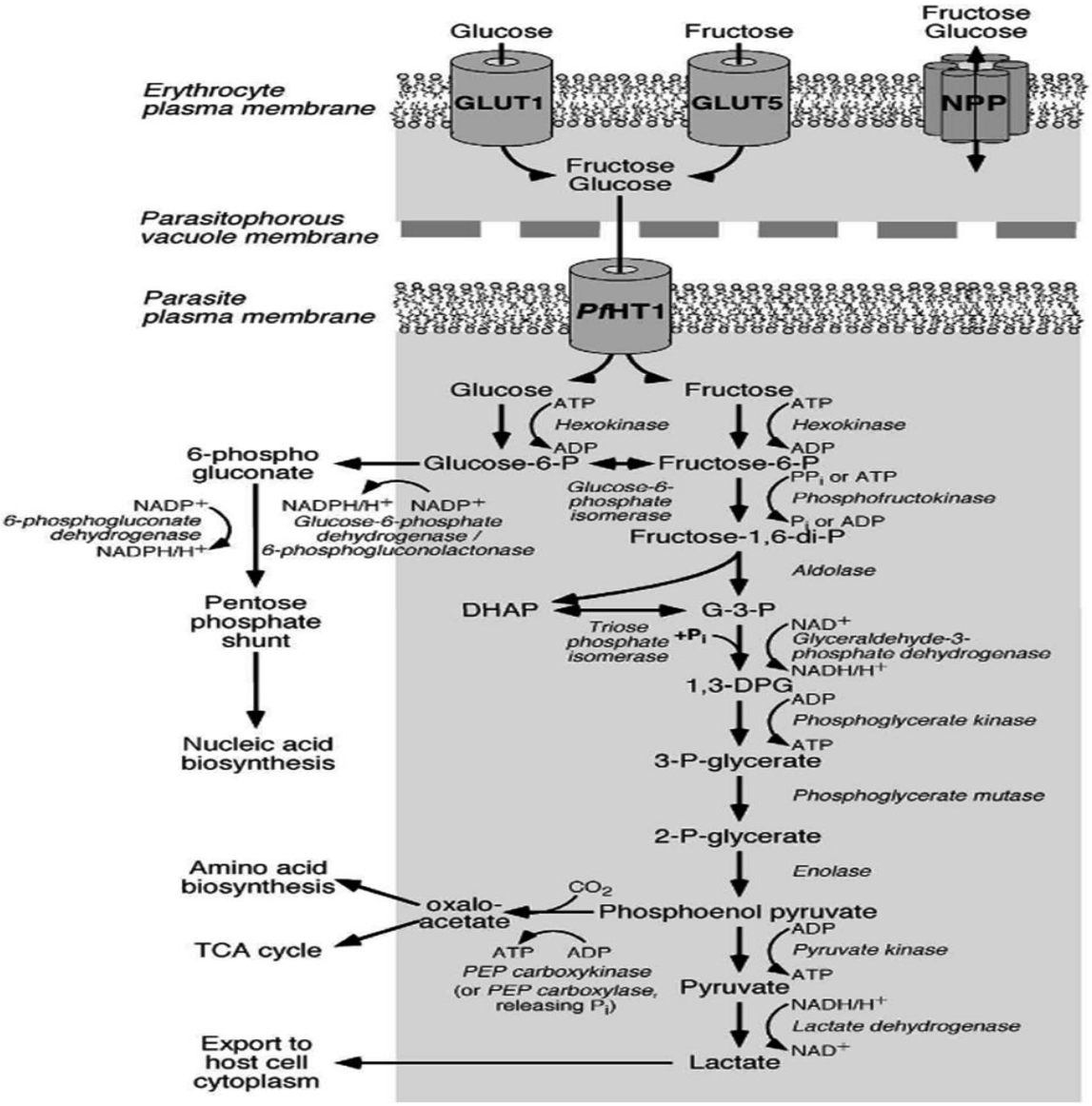

Figure 1.17: Glycolysis pathway in *P. falciparum.*

The component enzymes of the glycolysis pathways are encoded in the *Plasmodium* genome (Gardner et al., 2002). Glucose from host plasma protein is transported into the parasite via the hexose transporter located on the surface of infected RBC or via NPP transporter. Glucose is degraded via fermentation process by the parasite glycolytic enzymes producing lactate as an end product. This glycolytic pathway produces 2 ATP molecules. The oxidation of phophoenolpyruvate (PEP) produces 2 molecules of pyruvate for the production of lactate and for lipid biogenesis in the apicoplast. Branching pathways include the pentose phosphate shunt, which generates NADPH critical for oxidative stress protection, and CO_2 fixation into oxaloacetate (by the action of carboxykinases) which is then followed by transaminases action leading to generation of three amino acids (alanine, glutamate and aspartate). (Adapted from Crawford et al., 2003).

It has been reported that *P. falciparum* consumes only minimal amount oxygen (Krungkrai et al., 1999) and it prefers microaerophilic conditions of ~5% oxygen, as its growth is inhibited by normal atmospheric oxygen concentrations (Scheibel et al., 1979). These studies suggest that asexual stages of *P. falciparum* rely primarily upon glucose fermentation for their energetic requirements. This is in keeping with the study demonstrating that inhibitors of mitochondrial respiration have only a small effect on the parasite ATP pools (Fry et al., 1990). One molecule of glucose is degraded into two molecules of pyruvate via the glycolysis pathway. In eukaryotic organisms, pyruvate dehydrogenase has been recognised as an essential enzyme responsible for connecting the glycolytic pathway and TCA cycle and hence it catalyses the conversion of pyruvate to acetyl-CoA in the mitochondrial matrix. However, pyruvate dehydrogenase in malaria parasite is located only in apicoplast not in the mitochondria and thus role of pyruvate dehydrogenase is solely to produce acetyl-CoA for lipid biogenesis in apicoplast (Foth et al., 2005). In addition, the *P. falciparum* genome encodes all the necessary enzymes for TCA cycle (Gardner et al., 2002) which are actively expressed during the asexual blood life stages (Bozdech et al., 2003). Although it has been recently published that *P. falciparum* possess a branched TCA pathway rather than conventional cycle (Olszewski et al., 2011), now the authors of this paper come to the retraction of the whole article stating that TCA metabolism in blood-stage *P. falciparum* is not branched but primarily oxidative (Figure 1.18) (Olszewski et al., 2013). Human RBC has incomplete TCA cycle (Prankerd, 1955) and it was suggested Linas and Vaidya groups that the reductive flux occurs primarily in the RBCs and not in the parasite itself (Olszewski et al., 2013). Therefore, there was an excessive interference from surrounding uninfected RBCs which has led to incorrect interpretation of stating that *P. falciparum* operates reductive and oxidative pathways with 2-oxoglutarate being the entry point to feed both pathways which converge to generate malate (Olszewski et al., 2013).

However, the role of *Plasmodium* mitochondrion has not been fully understood. *Plasmodium* mitochondrion contains both conserved and unusual features. These include (1) an active electron transport chain that is thought to serve as electron disposal system to supply pyrimidine biosynthesis (Painter et al., 2007), as well as to generate the

mitochondrial membrane potential ($\Delta\Psi_m$) across the inner mitochondrial membrane that is necessary for electron transport (2) participation in iron-sulphur cluster biosynthesis and unusual hybrid haem biosynthesis pathway, with enzymes localizing in both the mitochondrion and plastid organelles (reviewed in (Vaidya and Mather, 2009, van Dooren et al., 2006)).

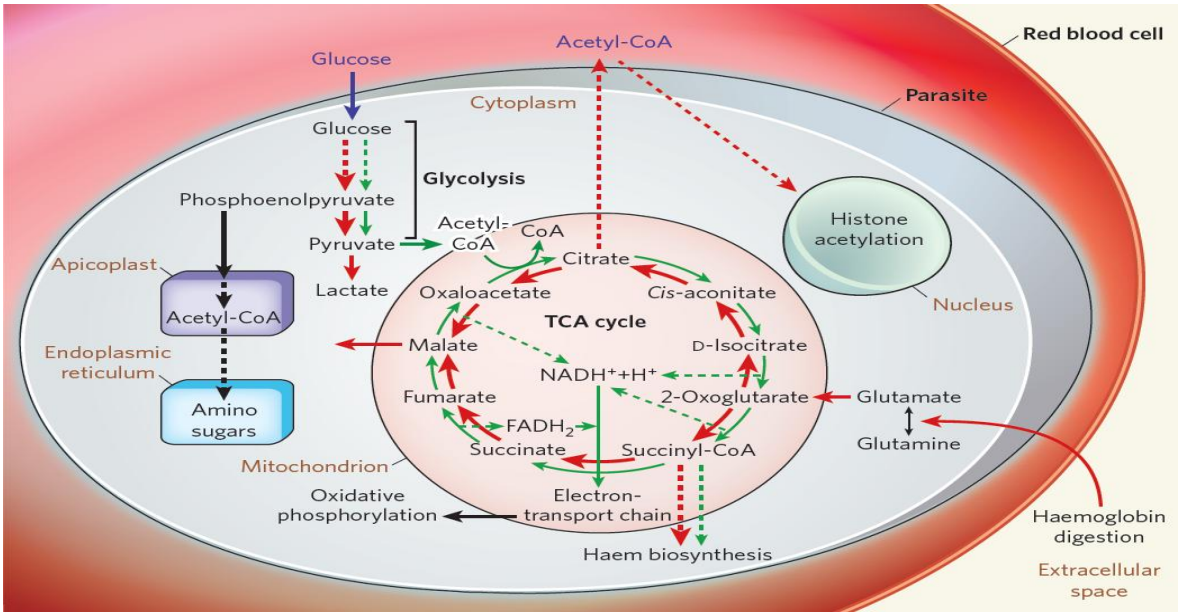

Figure 1.18. Illustration of TCA pathways in *P. falciparum*.
The classical oxidative TCA cycle used by *P. falciparum* is indicated by green arrows, and the branched pathway which was incorrectly thought to be used by *P. falciparum* is shown in red. Dashed arrows indicate multiple steps. (Adapted from Ginsburg 2010).

1.3.3.4. Nucleotide metabolism

The synthesis of nucleotides by malaria parasite necessitates the availability of purines and pyrimidines (the constituents of the nucleotides) as well as an adequate supply of ribose sugars and phosphate. The biosynthesis of purines, pyrimidines and folate as well as mitochondrial electron transport chain are intimately linked (Figure 1.19) (Olliaro and Yuthavong, 1999). Table 1.2 below summarizes the major differences between *Plasmodium* parasite and human in purines, pyrimidines and folate metabolic pathways. Blood stage *Plasmodium* parasites are incapable of *de novo* purine synthesis unlike mammalian cells and therefore they depend on salvage pathway to obtain performed host

purine precursors (hypoxanthine, adenosine, guanine) from the extracellular milieu through a number of transporters, some of which have been identified and characterized (as reviewed in (Sherman, 1979, Downie et al., 2008)). In infected RBC, the influx of purines into RBC is increased and there is evidence suggesting that the ATP generated by RBC is broken down to AMP and hypoxanthine (Reyes et al., 1982, Cassera et al., 2008). The parasite scavenges AMP and hypoxanthine from the host cytosol as a purine source and it converts hypoxanthine into inosine monophosphate (IMP), which serves as the precursor for the synthesis of all adenosine and guanosine nucleotides and deoxynucleotides (reviewed in (Downie et al., 2008, Kirk et al., 2009, Gero and Osullivan, 1990)).

In contrast, asexual stages of *Plasmodium* parasites are unable to salvage either pyrimidine bases or nucleoside and they have to synthesize pyrimidine nucleotide *de novo* whilst mammalian cells can either salvage or synthesize *de novo* pyrimidine nucleotides (Sherman, 1979, Krungkrai et al., 2003, Gero et al., 1984). The parasite has all enzymes required for the synthesis of uridine monophosphate (UMP) from glutamine, ATP and CO_2 (Gero and Osullivan, 1990). Pyrimidine biosynthesis in malaria parasite begins by fixing CO_2 into carbamoyl phosphate, which then condenses with aspartate to form carbamoyl-l-aspartate. This is subsequently converted into UMP, which serves as the precursor for all uridine, thymidine and cytidine (deoxy)-nucleotides (Rathod and Reyes, 1983, Krungkrai et al., 2003, Reyes et al., 1982). Interestingly, recent reports suggest that the only vital function of the parasite's mitochondrial electron transport chain is to serve as an electron sink for dihydroorotate dehydrogenase, an enzyme in this pathway (Painter et al., 2007). However, more insights about *P. falciparum* mitochondria and its role in pyrimidine biosynthesis are discussed in details in chapters 5 and 6.

Moreover, tetrahydrofolate (THF) is a key coenzyme in amino acid and nucleotide metabolism. In *P. falciparum*, it can be synthesized either via a *de novo* or salvage pathway (Krungkrai et al., 1989, Asawamahasakda and Yuthavong, 1993). The folate pathway is connected to the purine salvage through GTP, with GTP cyclohydrolase as the first enzyme in the *de novo* folate synthesis pathway (Figure 1.19) (Krungkrai et al., 1989). It is as well linked to the pyrimidine and amino acid biosynthesis via the dTMP synthesis

cycle and the methionine synthesis cycle, respectively (Figure 1.19) (Olliaro and Yuthavong, 1999). All the enzymes of the folate pathway have been studied in malaria parasites with particular interest on dihydrofolate reductase (DHFR) and dihydropteroate synthase (DHPS), which are the targets of two different classes of antifolates used as antimalarial drugs as previewed previously (section 1.2.4.4.2).

Table 1.2. Nucleotides metabolism in Plasmodium parasite and Humans. (Adapted from Olliaro and Yuthavong, 1999).

Pathway	*Plasmodium* parasite	Mammal
Pyrimidines	Synthesizes pyrimidines *de novo*; cannot salvage bases/nucleotides	Can either synthesize or salvage pyrimidine nucleotides
Purines	No *de novo* synthesis; relies on host-derived hypoxanthine as source of purine precursors	Can either synthesize or salvage purine nucleotides—hypoxanthine waste product
Folate cofactors	Can either synthesize or salvage folate precursors	No *de novo* synthesis; rely on external sources

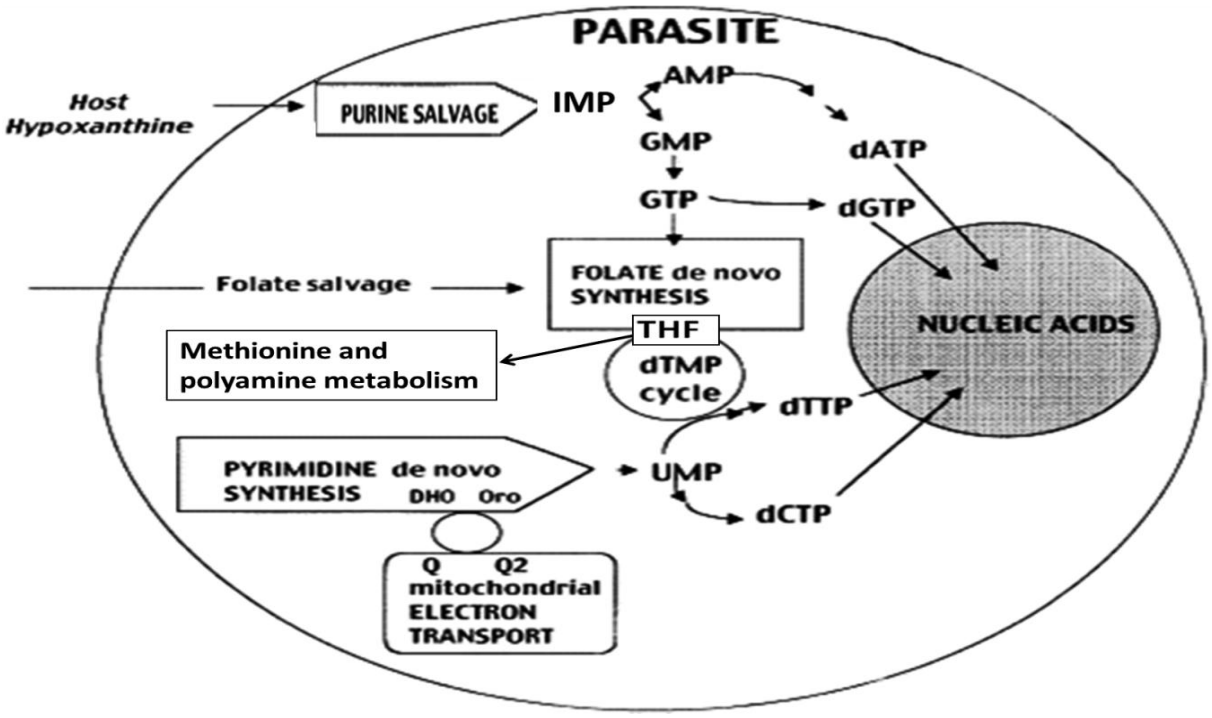

Figure 1.19. Schematic diagram shows the metabolic interconnection between purine, pyrimidine, folate synthesis pathways. (Adapted with modification from Olliaro and Yuthavong, 1999).

1.3.3.5. Protein and polyamine synthesis

During malaria parasite asexual blood stage growth, it obtains most of the amino acids required for protein synthesis and other metabolic functions from the digestion of RBC protein (primarily haemoglobin) as viewed previously (section 1.3.3.1). However, haemoglobin is not the only source for amino acids although majority (>85%) of the amino acids produced via haemoglobin degradation are excreted as waste; but rather the parasite salvage from the free amino acids pool in the plasma while some amino acids (e.g. glutamate, alanine and aspartate) are biosynthesized by the parasite itself from glucose and CO_2 (Sherman, 1977, Sherman, 1979). *Plasmodium* parasites uptake amino acids from the extracellular environment through a variety of transporters expressed to the surface of the RBC as well as via NPP (Elford et al., 1995, Ginsburg et al., 1985). These amino acids are used for protein synthesis as well as in a number of other metabolic pathways. More insights and details about amino acids metabolism are presented in chapters 4, 6 and 7. In short, glutamine and glutamate are incorporated in different metabolism such as pyrimidine biosynthesis pathway. In addition, arginine is rapidly degraded via a parasite arginase to urea and ornithine, although the parasite lacks a urea cycle (Olszewski et al., 2009). Ornithine is required precursor for polyamine synthesis. Three steps are critical for polyamine biosynthesis including (1) the decarboxylation of ornithine to putrescine via ornithine decarboxylase (ODC), (2) the formation of S-adenosylemethionine (AdoMet) from methionine and ATP, and (3) the decarboxylation of AdoMet which provides the aminopropyl groups required for the sperimidine and spermine synthesis (Assaraf et al., 1984). Methionine cycle exists to supply the substrate for methylation reactions as well as polyamine biosynthesis (Asawamahasakda and Yuthavong, 1993, Assaraf et al., 1984). Amino acids and polyamines processes are critical for the survival of blood stage malaria parasites and hence might be targeted for developing antimalarial drugs.

1.4. Metabolomics

1.4.1. Overview

Metabolomics is a post genomic research field concerned with developing analytical methods for the study of the entire repertoire of metabolites in biological systems such as cells, organs or organisms (Fiehn, 2002, Goodacre, 2005, Lakshmanan et al., 2011). This repertoire consists of many different classes of small molecules including carbohydrates, amino acids, nucleotides, antioxidants and fatty acids. These small molecules perform critical functions such as energy storage, signal transduction, maintaining cellular structure, and feedback regulation of gene expression. The identities, concentrations, and fluxes of these metabolites result from a complex interaction among gene expression, protein expression, and the environment (Figure 1.20) (Goodacre, 2005). However, the function of genes and proteins is subjected to epigenetic regulation and post-translational modifications, respectively, whilst metabolites serve as direct signatures of biochemical activity and are therefore easier to correlate with phenotype and function of cellular activities (Patti et al., 2012). This explains why metabolomics has become a powerful approach in recent years and therefore it has been applied in different areas of research. In contrast to classical biochemical approaches that often focus on single metabolite, single metabolic reaction and its kinetic properties, metabolomics involves in the collection of qualitative and quantitative data on a broad series of metabolites in order to gain an integrated understanding of the cellular response to environmental change (Kaddurah-Daouk et al., 2008, Ryan and Robards, 2006). Metabolic changes can be regarded as the ultimate consequence of environmental perturbation and therefore analyzing metabolic differences between unperturbed and perturbed systems, such as drug treated and untreated *P. falciparum* parasites, can lead to insights into the underlying biology as well as drug mode of action. This example can be used in the context of pharmacometabolomic which is the use of the techniques of metabolomics to define metabolite signals that will provide insight into mode of drug action and mechanisms responsible for parasite variations in drug response phenotypes.

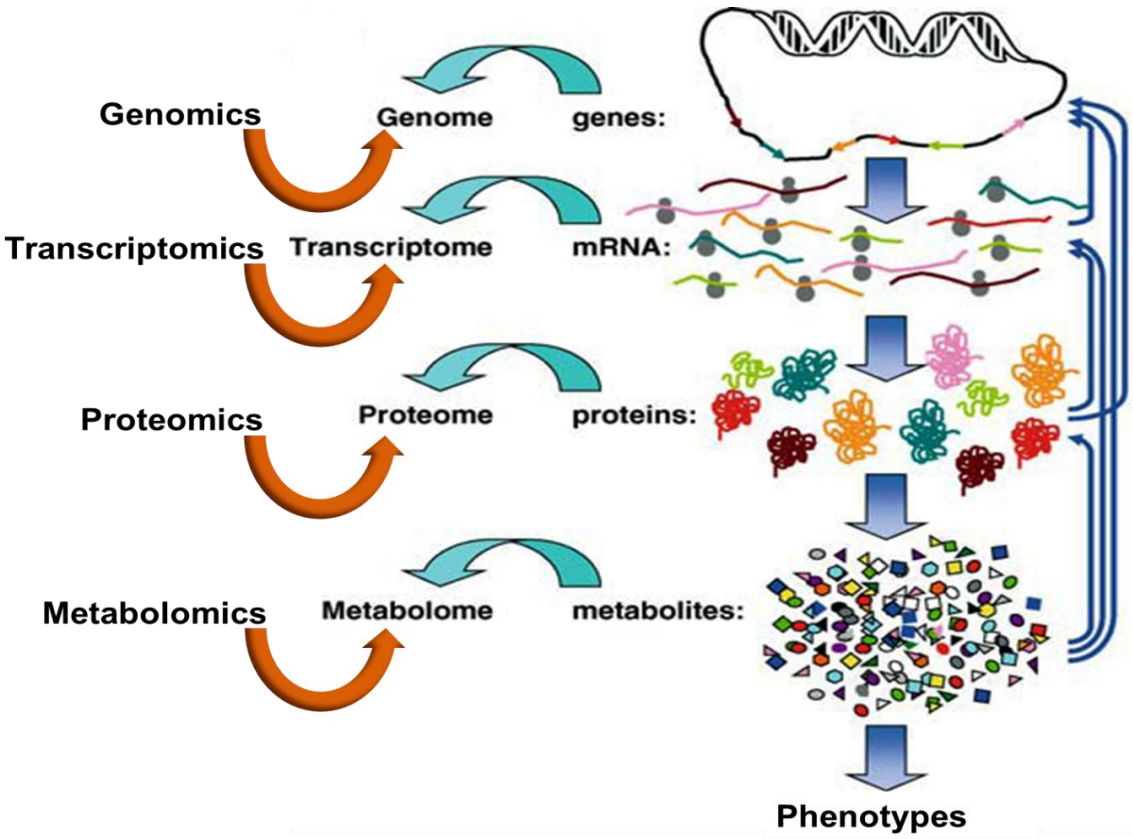

Figure 1.20. General schematic illustration of the omics organisation.
The general profiles flow from genes to transcripts to proteins to metabolites leading ultimately to cellular phenotype (function). Blue vertical arrows indicate interactions regulating the respective omic expression. (Adapted with modification from Goodacre 2005).

1.4.2. Metabolomics process workflow

A generic metabolomics workflow needs to be tailored according to sample types being studied. The metabolomics workflow is shown in (Figure 1.21) and can be described as a metabolomics pipeline. It addresses the need to have streamlines approach for sample preparation, analytical setup for data capturing and pre-processing, data analysis and knowledge assembling. Therefore, a combination of different expertises is required in multi-disciplinary teams including biologist, analytical chemists, statisticians, modellers and bioinformaticians (Dunn et al., 2011). Each phase in the metabolomics workflow has multiple choices and hence choosing the correct option for specific experiments is critical to ensure the production of robust and valid results. Therefore, it is recommended to

undertake the development and validation of each component to ensure they are fit-for-purpose (Villas-Boas et al., 2005, Dunn et al., 2011). This process of development and validation has been undertaken in chapter 3.

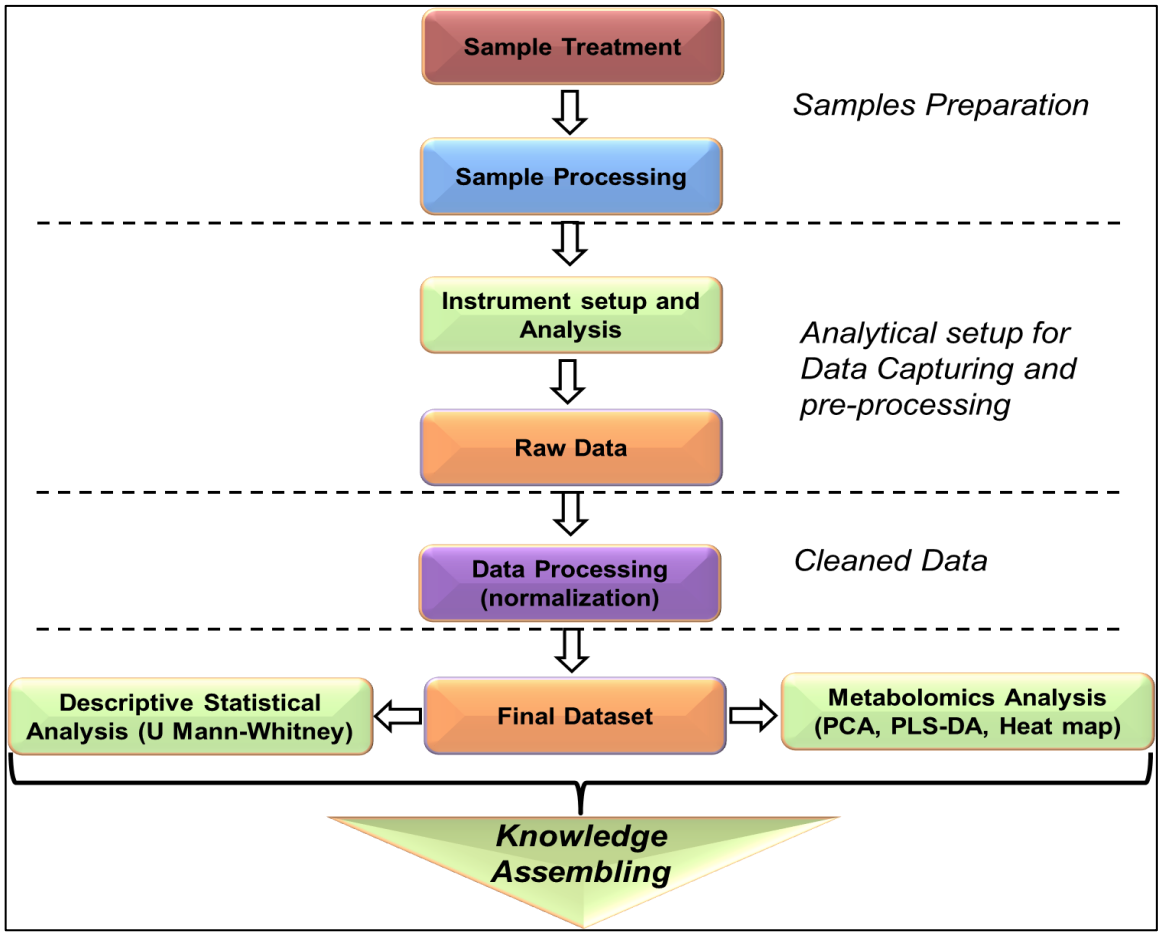

Figure 1.21. Metabolomics pipeline workflow components.

Generally, there are two types of metabolomic workflows, which can be sub-divided into targeted and untargeted approaches. Targeted metabolomics refers to an analytical method in which pre-determined set of known compounds (authentic standards) is accurately detected and quantified using appropriate internal standards (commonly, isotopes) (Figure 1.22 A) (Dudley et al., 2010). It is typically driven by a specific biochemical question or hypothesis on one or more related metabolic pathways of interest (Patti et al., 2012).

Therefore, targeted metabolomics approach is effective for measuring the effect of drugs or genetic modifications on a specific enzyme (Nicholson et al., 2002). This approach has been developed, validated and undertaken throughout this thesis to investigate the effect of drugs on a number of selected metabolic pathways in *P. falciparum* parasite as well as drug mode of action (refer to chapters 3-7).

Untargeted metabolomics refers to a method in which the aim is to get global metabolic profiling in scope through simultaneously measuring, without bias, as many metabolites as possible within a certain mass range including novel (unknown) metabolites from biological samples (Figure 1.22 B) (Patti et al., 2012, Vinayavekhin and Saghatelian, 2010). Typically, untargeted metabolomics approach is required to provide detection of 100-1000s of metabolites in a valid and robust manner which is generally applied in the pharmaceutical industry in the study of drug metabolism (Dunn et al., 2011).

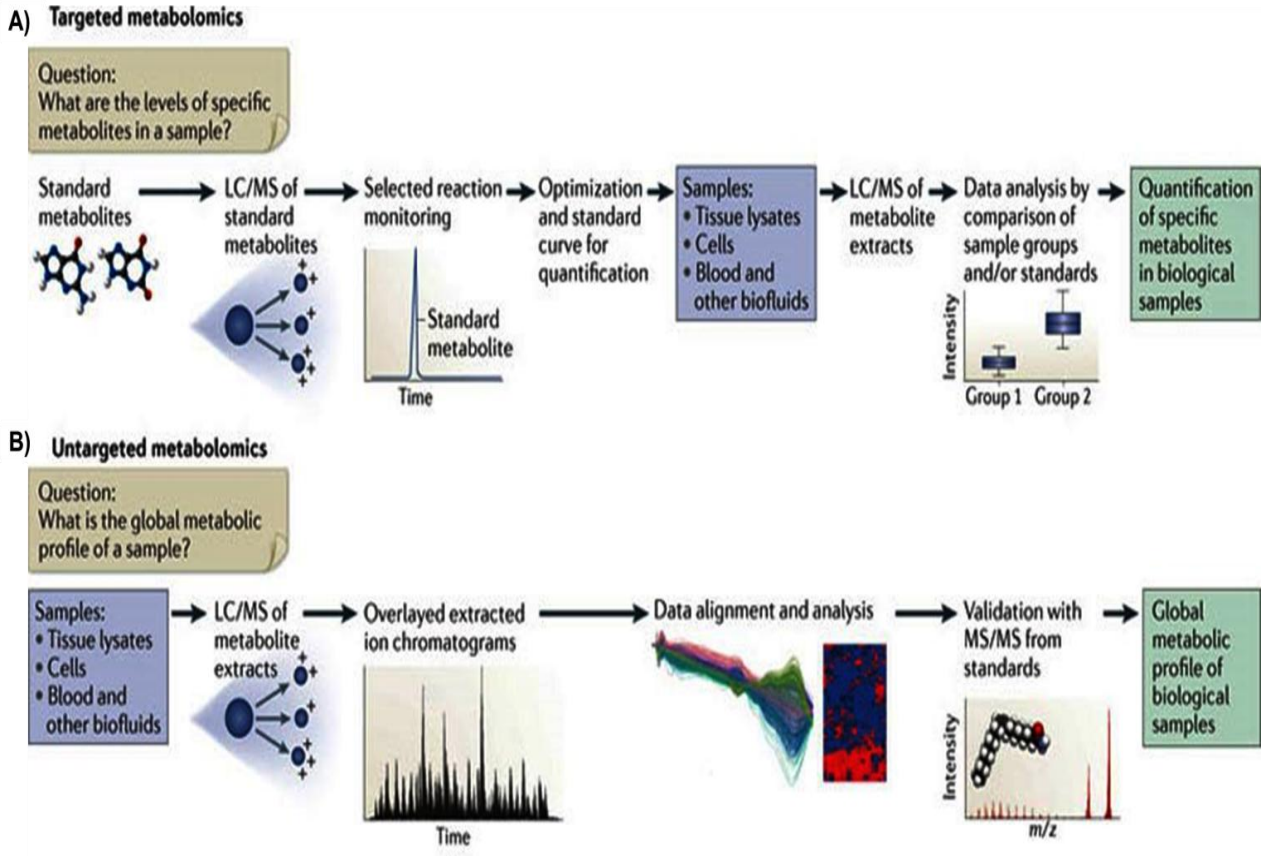

Figure 1.22. Schematic representation shows the differences between workflow of targeted and untartgetd metabolomics approaches.

A) Targeted metabolomics workflow most often uses triple quadrupole mass spectrometry. Standard compounds for the metabolites of interest are first used to set up selected reaction monitoring methods. Here, optimal instrument voltages are determined and response curves are generated for absolute quantification. Samples are then analysed based on the established standard metabolites. The data output provides quantification only of those metabolites for which standard methods have been built. B) Untargeted metabolomics workflow uses mass analyser that enables of identify both known and unknown metabolites. Samples are analysed by liquid chromatography followed by mass spectrometry (LC/MS). After data acquisition, the results are processed by using bioinformatic software to perform nonlinear retention time alignment and identify peaks that are changing between the groups of samples measured. The m/z values for the peaks of interest are searched in metabolite databases to obtain putative identifications. Putative identifications are then confirmed by comparing tandem mass spectrometry (MS/MS) data and retention time data to that of standard compounds. The untargeted workflow is global in scope and outputs data related to comprehensive cellular metabolism. (Adapted from Patti et al., 2012).

1.4.2.1. Sample preparation

Adequate methods for sample preparation are of outmost importance in metabolomics. The objective of sample preparation is to ensure that the extracted metabolites represent the metabolome in the sample. The process of sample preparation is typically divided into two steps: (1) quenching of metabolic activity and (2) extraction of metabolites into an appropriate solvent for analysis. Rapid quenching (arrest) of all biochemical processes has to be adequately preformed in the beginning of sample preparation because the metabolite levels reflect the physiologic state of the biological system particularly if it is exposed to genetic or an environmental change (Dunn et al., 2011, Villas-Boas et al., 2005). Following the quenching step, extraction step in conducted to separate the metabolites of interest from its cellular material (matrix species) (Dunn et al., 2011). However, the extraction process is often the most time-consuming step in metabolomics analysis, and it is also very challenging to avoid metabolite losses due to the large chemical diversity classes of the different metabolites containing polar (water-soluble) and non-polar (water-insoluble) metabolites as well as volatile ones (Moco et al., 2007, Besteiro et al., 2010). During the extraction of intracellular metabolites, inevitable extra variability results in a comparatively low reproducibility of any analytical method. In addition, most of the available extraction methods produce high sample dilutions that result in even lower concentrations of metabolites thus a concentration step is required using evaporation process by nitrogen stream flow (Dunn et al., 2011, Villas-Boas et al., 2005). Therefore, quenching and extraction steps should be validated for any losses or leakage of metabolites due to degradation, on-going biochemical reactions and/or sample mishandling (Villas-Boas et al., 2005, Reaves and Rabinowitz, 2011). In addition, quenching and extraction can be performed in a single step (Lakshmanan et al., 2011). It has been found that acidic acetonitrile/methanol/water (40:40:20) gave superior in extraction of many cellular metabolites of *E. coli* metabolome, including most amino acids, nucleotide and components of central carbon metabolism (Rabinowitz and Kimball, 2007). Therefore, this mixture of solvents has been used for the extraction of *P. falciparum* metabolites in this thesis.

1.4.2.2. Analytical instruments

Metabolite identification is a key step for metabolomics study. Metabolome analysis can be conducted on a variety of biological sample types and may utilize a number of different technology platforms. There are general specifications for metabolomic analytical instruments. These include (1) excellent sensitivity and resolution, (2) capability handling wide range of concentrations (from pM to mM), (3) identification and quantification of different types of molecules and (4) reproducible measurement of many samples in short analysis time (Čuperlović-Culf et al., 2010, Khoo and Al-Rubeai, 2007). The main analytical platforms used for metabolomics applications are nuclear magnetic resonance spectroscopy (NMR) and hyphenated techniques such as gas chromatography (GC), capillary electrophoresis (CE) and liquid chromatography (LC) coupled to mass spectrometry (MS). In addition, fourier transform infrared spectroscopy (FT-IR) and direct infusion mass spectrometry (DIMS) have been applied without any prior separation, except for eventual sample preparation (Figure 1.23) (Dunn and Ellis, 2005).

NMR spectroscopy functions by the application of strong magnetic fields and radio frequency (RF) pulses to the nuclei of atoms. The presence of a magnetic field causes nuclear spin for different nuclei which include ^{1}H, ^{13}C, ^{15}N and ^{31}P. Absorption of RF energy allows then the nuclei to be promoted from low-energy to high-energy spin states, and the subsequent emission of radiation during the relaxation process is detected. The NMR spectrum (chemical shift) is determined as the difference in ppm (parts per million) between the resonance frequency of the observed atom and that of a reference atom present in a reference compound. The signal intensity depends on the number of identical nuclei (Dunn and Ellis, 2005).

FT-IR is based on the principle that when the sample is interrogated with an IR beam, the functional groups within the sample will absorb the IR radiation and vibrate in one of the following ways including stretching, bending, deformation or combination vibrations. These absorptions/vibrations can then be correlated to (bio)chemical species and the

resultant IR absorption spectrum can be described as an IR fingerprint (Ellis and Goodacre, 2006).

The spectra obtained from NMR and FR-IR, are composed of the signals of many metabolites and therefore the elucidation of these complex spectra can be very complicated (Koek et al., 2011). Moreover, the limits of detection for NMR and FT-IR are much higher than for MS-based techniques, limiting the applications of NMR and FT-IR to the analysis of bulk metabolites (Koek et al., 2011, Zhang et al., 2012). Therefore, hyphenated techniques such as GC-MS, LC-MS and CE-MS, are generally favoured in metabolomics allowing identification and quantification of as many metabolites. However, none of the analytical methods will cover the full metabolome and thus parallel application of several techniques, e.g. GC-MS , LC-MS or NMR , is desirable to study the global metabolome which consists of metabolites with different polarity and molecular weight ranges (Koek et al., 2011). In addition, GC-MS is applied to the analysis of volatile organic metabolites whereas CE-MS and LC-MS is highly applicable to the analysis of a wide range of polar metabolites (Zhang et al., 2012). Although CE is very effective for hydrophilic metabolites, the buffers used for this chromatographic separation are not readily compatible with the ion source of the MS. Therefore, the development of new column chemistries such as hydrophilic interaction chromatography (HILIC) can be placed as an alternative to CE using LC/MS. Therefore, HILIC coupled to MS based metabolomics method has been undertaken in the study of this thesis aiming to investigate part of *P. falciparum* parasite metabolome.

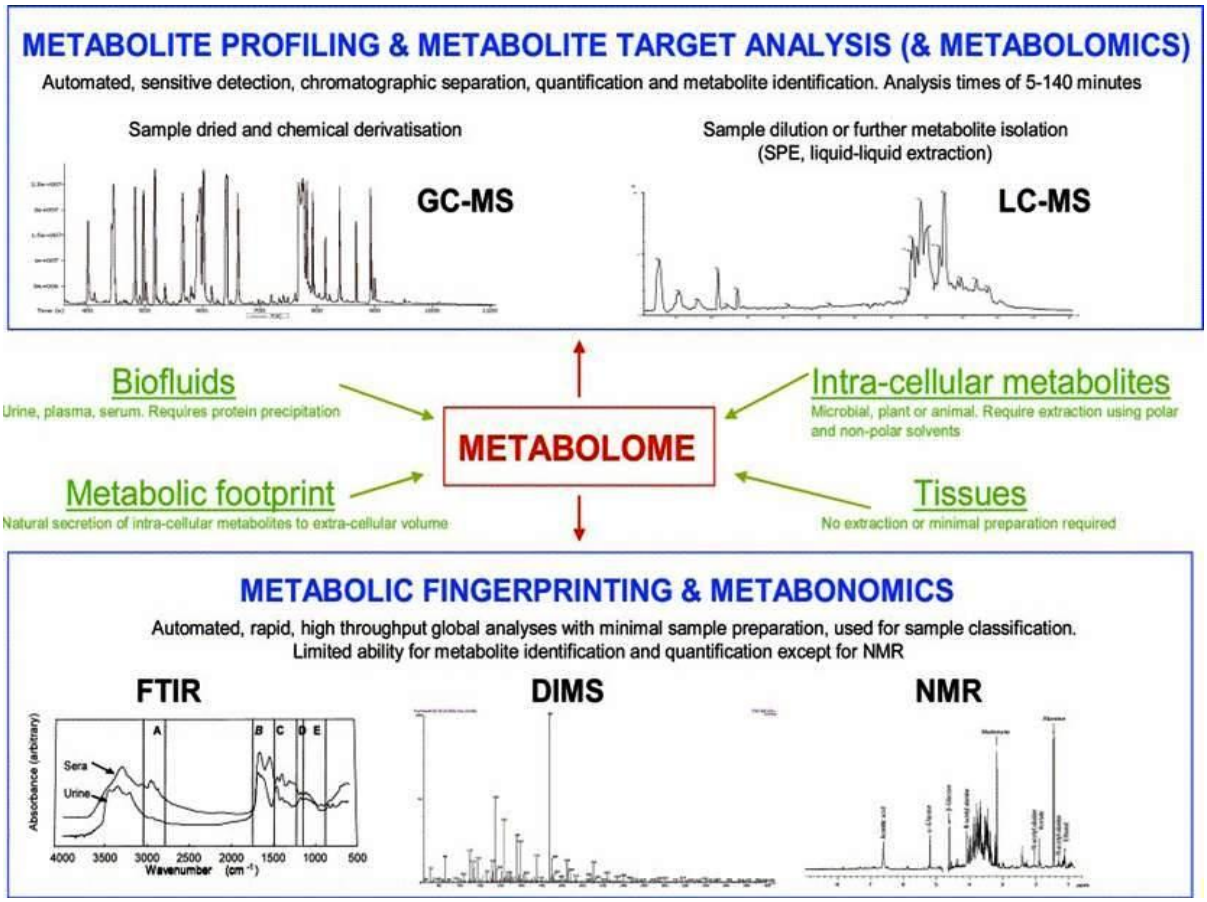

Figure 1.23. Summary of the different metabolomics-based strategies for sample preparation and sample analysis.

Mass spectrometry is focused on the measurement of an analyte mass. More precisely, it determines the mass-to-charge (*m*/*z*) ratio of electrically charged molecules. A molecule with a nominal molecular weight of 1000 and coupled to a single proton (positive ionization mode or protonation) will be detected with an *m*/*z* of 1001 [MW of molecule (1000) + H^+]. A molecule with a molecular weight of 1000 and decoupled of a single proton (negative ionization mode or deprotonation) will be detected with an *m*/*z* of 999 [MW of molecule (1000) - H^+] (El-Aneed et al., 2009, Dunn, 2011).

The role of MS in metabolomic research is constantly expanding in which it is capable of performing targeted and untargeted metabolomics analysis (Dettmer et al., 2007). There are five important requirements that need to be considered in metabolomics analysis by MS including (1) efficient metabolites extraction, (2) separation or fractionation of the analytes

by chromatography, (3) molecules ionization, (4) mass signals detection and (5) metabolite identification and quantification (Čuperlović-Culf et al., 2010). Therefore, recent advances in chromatography separation sciences, ion sources and mass analyzers have considerably improved the sensitivity, selectivity, specificity and speed of metabolite identification and quantification by MS.

A critical step in LC-MS approach is the conversion of the eluted metabolites from LC system into gas-phase ions (Rabinowitz, 2007). Generally, there are two popular ionization approaches namely electrospray ionization (ESI) and atmospheric pressure chemical ionization (APCI). Although APCI often provides better quantitative reproducibility and robustness, ESI generally offers considerably superior sensitivity particularly for water-soluble cellular metabolites. Therefore, most LC-MS approaches for cellular metabolomics employ ESI (Rabinowitz, 2007, Lu et al., 2008) which has been undertaken as an ionization source for the *P. falciparum* metabolites in this thesis.

The obtained gas-phase ions have to be directed to appropriate MS or tandem MS (MS/MS) analysers in order to generate the actual data. Major options for MS analysers include time-of-flight (TOF), ion trap and triple quadrupole MS. TOF offers high mass accuracy and the ability to identify known and unknown metabolites. Disadvantages are suboptimal sensitivity and dynamic range for known analytes. Ion traps operated in data-dependent MS/MS mode can provide spectra for both known and previously unknown analytes. If they are coupled to a high mass accuracy detector such as an ion cyclotron resonance (ICR) (Marshall et al., 1998) or orbitrap MS (Hu et al., 2005), they can provide high mass resolution product ion spectra, high sensitivity and thus they are outstanding for identification of unknown metabolites (Rabinowitz, 2007).

Triple quadrupole mass spectrometers operated in multiple reactions monitoring (MRM) mode enable quantitation of known metabolites with predetermined fragmentation patterns. At any given instant, the mass spectrometer detects only a single analyte using a selected reaction monitoring (SRM) scan: the first quadrupole (Q1) selects for the parent ion mass; the second quadrupole (Q2) conducts collision-induced dissociation (CID); and the third quadrupole (Q3) selects for the predetermined product ion mass (Figure 1.24). Each SRM

scan takes approximately 0.1 s, enabling quantitation of numerous metabolites during a single LC run. MRM scanning generally provides the best quantitative performance sensitivity and reproducibility for known analytes although it does not provide information on unknown analytes (Rabinowitz, 2007). This approach of tandem MS (MS/MS) using Triple quadrupole mass analyser has been undertaken in the study of pharmacometabolomics of *P. falciparum* in this thesis.

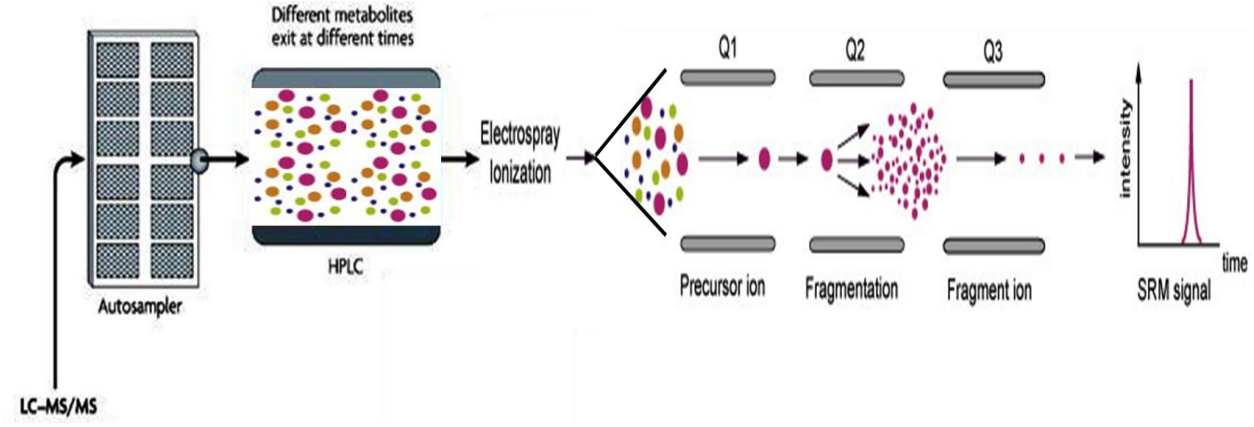

Figure 1.24. LC triple quadrupole tandem mass spectrometers use ESI as inonization source. LC-ESI-MS/MS aims to detect and quantify known cellular metabolites. Q1 is first quadrupole that selects for the precursor ion mass; Q2 is the second quadrupole that conducts collision-induced dissociation (CID) to fragment the precursor ion mass; and Q3 is the third quadrupole that selects for the predetermined fragmented ion mass.

1.4.2.3. Data analysis

Metabolomics experiment produces large volumes of data for each sample. Efficient data analysis is important in order to achieve accurate metabolite identification and quantification, which ultimately leads to generate biologically meaningful interpretations. There are a wide variety of data processing software and other tools that have been developed for data analysis in metabolomics (Katajamaa and Oresic, 2007). The mostly commonly used statistical tools for metabolomics include principal component analysis (PCA) and partial least squares discriminant analysis (PLS-DA) (Novotny et al., 2008).

PCA is a commonly used unsupervised technique. It requires no a priori knowledge of class of the sample hence, the term "unsupervised". PCA is a statistical technique that determines the most optimal linear transformation for a collection of data points in such a manner that the properties of that sample are most clearly displayed along the coordinate (i.e. principal) axes. In other words, PCA allows one to plot, visualize, and cluster multiple metabolomic data sets based on linear combinations of their shared features (Wishart, 2010). Similarly, PLS-DA uses supervised techniques to enable one to perform efficient classification and discrimination analysis of very large data sets containing a small number of samples. A variant of PLS-DA classifies the data into two blocks, one representing between-class variation and the other representing within class. Therefore, it separates the more meaningful data from the less meaningful (Xia et al., 2012, Xia et al., 2009). PCA and PLS-DA plot results are discussed in terms of component scores (the transformed variable values corresponding to a particular data point), and loadings (the weight by which each standardized original variable should be multiplied to get the component score). The Variable Influence on Projection (VIP) is a weighted sum of squares of the PLS-DA loadings taking into account the amount of explained Y-variation in each dimension. When more components are used to calculate the feature importance, the averages of the VIP scores are used (Xia et al., 2012, Xia et al., 2009). These statistical approaches have been undertaken in the data analysis of this thesis.

1.4.3. Metabolomics of malaria parasite

In the post-genomic era, metabolism of the malarial parasite has been mapped based on the current knowledge of parasite biochemistry and on pathways known to occur in other eukaryotes. Metabolomics of malaria parasite has just been started in the last recent years and only handful studies have been reported and reviewed (Lian et al., 2009, Lakshmanan et al., 2011, Olszewski and Llinas, 2011, van Brummelen et al., 2009, Kafsack and Llinas, 2010, Olszewski et al., 2011, Bulusu et al., 2011, Teng et al., 2009). However, these studies have contributed significantly in understanding of malaria parasite metabolic functions and thus they illuminate new chemotherapeutic targets for drug development, including the identification of target for drugs in current use.

Teng et al., (2009) used proton (^{1}H) NMR to identify and quantifiy more than 50 metabolites, including amino acids, nucleotides, carboxylates and other molecules, from an extract of saponin-released *P. falciparum* trophozoites (Teng et al., 2009). Lian et al., (2009) used ^{13}C NMR to study the glucose metabolism in *P. falciparum*-infected RBC, which showed that alongside the expected glucose end-products (pyruvate, alanine, lactate), glycerol and glycerol-3-phosphate were generated in the parasite suggesting the operation of a glycerol-3-phosphate shuttle in the parasite in response to growth under limited O_2 and elevated CO_2 (Lian et al., 2009). A LC-MS/MS based metabolomics was used to quantitatively measure of ~200 known metabolites of *P. falciparum* during its 48 h blood-stage developmental cycle showing that the conversion of arginine to ornithine by parasite arginase, and the potential link between parasite-induced hypoargininemia and the development of cerebral malaria (Olszewski et al., 2009). Therefore, insights into *P. falciparum* parasite biology and drugs mode of action are provided in the subsequent chapters (4-7) using pharmacometabolomics approach.

1.5. Thesis Objectives

The general objective of this thesis was to take a targeted pharmacometabolomics approach to study some selected metabolic pathways of *P. falciparum* parasites in the presence and absence of a number of antimalarial drugs and some inhibitors and to infer from these data, the drugs' mode of action. Towards this overall objective, the specific objectives are:

1. To develop and validate a targeted metabolomic platform focusing on central carbon and amino acid metabolism. This objective has been achieved successfully as described later in chapter 3.
2. To study the general differences in the metabolic profiles between uninfected human red blood cell (RBC) and those infected by *P. falciparum* (iRBC). This objective will enable the study in the subsequent chapters to focus only on *P. falciparum*-iRBC trophozoite stage in order to eliminate any bias coming from the background noise generated by RBC. This objective has been accomplished successfully as described later in chapter 4.
3. To assess the role of *P. falciparum* mitochondria and mitochondrial electron transport chain using a number of mitochondrial selected inhibitors and antimalarial drugs and show the likely mode of actions of each drug used. This work is described in chapters 5 and 6.
4. To examine the role of *P. falciparum* digestive vacuole using quinolones-containing antimalarial drugs (QCDs) and demonstrate the similarities and differences in the probable mode of action of QCDs used. This work is described in chapter 7.

CHAPTER 2

General Experimental Protocols

2.1. Introduction

The aim of this chapter was to provide information on the routine system for *Plasmodium falciparum* parasite culture and on the instrumentation of LC-MS/MS technique which has been utilized to provide the data in this thesis. This chapter will provide step-by-step methodology of the general techniques used in this thesis allowing easy reproducibility. Details of methods used in more specific instances and modification or supplements to standard methods are provided at appropriate locations within the experimental chapters.

2.2. Culture system for *P. falciparum* maintenance

The method used for culturing the *P. falciparum* parasite was adapted from (Trager and Jensen, 1976) and (Jensen and Trager, 1978). Parasite culturing was carried out using standard aseptic techniques in an Envair class II laminar flow safety cabinet. The laminar flow cabinet was thoroughly cleaned firstly with biocidal cleaner (Biocleanse Concentarte, TEKNON, UK) and then with 70% ethanol (Chemistry Department, Liverpool University, UK) before and after the parasite culturing work, to minimize contamination. All consumables used in the laminar flow cabinet were pre-sterilized unless otherwise stated. These include 75 cm^2 and 25 cm^2 Nunc™ polystyrene tissue culture flasks (Fisher Scientific, UK), 15 ml and 50 ml centrifuge tubes (UK), 2.5 ml bijou bottles (VWR, UK) and disposable cotton plugged plastic pipettes (Sterilin Limited, UK). All the solutions used for *P. falciprum* culture were prepared with distilled water (dH_2O) and sterilized through a sterile bottle top filter unit with a 0.22 μm membrane (Fisher Scientific, UK). All Glassware, 1.5 ml eppendorf tubes, 10 μl, 200 μl and 1000 μl pipette tips were sterilized by autoclaving (121 ^{0}C, 15 psi for 30 min) prior to use. Protective gloves were worn and regularly sprayed with 70% ethanol to minimize any chances of contamination. All the parasite-related centrifugations were carried out using Fisher Scientific accuSpin1 bench top centrifuge (Fisher Scientific, UK). Extra parasite culture flasks, supernatants, used pipettes, old uninfected red blood cell (RBC) and old RPMI-1640 complete culture medium were first thoroughly decontaminated in biocidal cleaner (Biocleanse Concentarte, TEKNON, UK) and then discarded in the designated waste garbage.

2.2.1. *P. falciparum* parasite strains

Two strains of *P. falciparum*, chloroquine sensitive 3D7 and transgenic 3D7-yDHOD·GFP, were used in the preliminary stages of this study (Chapter 5). However, the 3D7 strain was selected for the remaining experiments in this thesis on the basis of its robustness in continuous culture and sensitivity for various inhibitors and antimalarial drugs. The 3D7 strain was cloned from the isolate NF54 obtained from an airport worker in Amsterdam (Cowman et al., 1991).

2.2.2. Culture medium

RPMI-1640 (Roswell Park Memorial Institute) culture medium containing L-glutamine and sodium bicarbonate ($NaHCO_3$) was purchased from Sigma (Sigma, UK). Complete culture medium was prepared by adding to a 500 ml bottle of RPMI-1640 culture medium the following: 12.5 ml of pre-sterilized 1 M HEPES (4-(2-hydroxyethyl)-1-piperazine ethane sulfonic acid) (Section 2.1.2.1), 200 µl of 50 mg/ml gentamicin (Sigma, UK) (Section 2.1.2.2) and 50 ml of pooled human AB+ serum (Section 2.1.2.3). Complete culture medium was incubated at 37 °C overnight prior to use with the purpose of checking for contamination. An occurrence of contamination was characterized by a colour change in the medium from red/orange to yellow and an increase in turbidity of the medium. Complete culture medium was always prepared fresh and only used for 1 week after which the medium was discarded to avoid the effects of medium deterioration.

2.2.2.1. HEPES

HEPES (4-(2-hydroxyethyl)-1-piperazine ethane sulfonic acid) was purchased from VWR International Ltd (UK). The preparation of 1 M stock of HEPES (MW = 238.03 g) was as follows: 238.03 g of HEPES was dissolved in 700 ml of distilled water and the pH was adjusted using 5 M NaOH to 7.4 after which the solution was made up to 1 L using distilled water. This 1 M stock of HEPES was then sterilized through a sterile bottle top filter unit

with a 0.22 μm membrane (Fisher Scientific, UK), labeled, and stored at 4 °C for future use.

2.2.2.2. Gentamicin

Gentamicin 50 mg/ml was purchased from Sigma (Sigma, UK), aliquoted into 2.5 ml bijou bottles, labeled and stored at 4 °C until required.

2.2.3. Serum

Human AB+ serum was kindly donated by Ward 7Y and the Gastroenterology Unit, Royal Liverpool Hospital, Liverpool, UK. Approximately 15-20 bags of irregular volume (100-250 ml) were pooled aseptically in a previously autoclaved beaker. Human AB+ pooled serum was then aliquoted into 50 ml centrifuge tubes and stored at -20 °C until required. Prior to usage, an aliquot of 50 ml centrifuge tube containing human serum was defrosted by placing it in a water path at 37 °C for approximately 30 min. The tube was then rinsed with 70% ethanol to minimize contamination before the content was transferred aseptically into a 500 ml bottle RPMI-1640 culture medium.

2.2.4. Preparation of uninfected red blood cell

Uninfected red blood cells (RBC) used in the study was kindly donated by the North West Regional Blood Transfusion Service, Liverpool, UK. RBC was whole human O+ blood. This blood, obtained no longer than 48 h after collection, was supplied in citrate-phosphate-dextrose bags and had been tested for HIV and HBV antibodies. It was unsuitable for transfusion because of irregular bag volume. Upon receipt, the blood was aseptically aliquoted into sterile 50 ml centrifuge tubes and stored at 4 °C for only two weeks. It is important to note here that using freshly drawn blood provides better support for parasite growth.

Serum and buffy coat layer were removed prior to usage as follows: 25 ml aliquot of whole blood was centrifuged aseptically at 3000 rpm for 5 min. The serum and buffy coat layer

were carefully removed using a pre-sterilized 10 ml pipette. The remaining 10 ml of packed RBC was washed three times with RPMI-1640 incomplete culture medium supplemented with 25 mM HEPES (pH 7.4) and 20 µM gentamicin and was collected by centrifugation at 3000 rpm for 5 min. All supernatants were discarded after each wash. The washed packet erythrocytes were labeled and stored as packed cells at 4 °C for up to one week and discarded after one week, if unused.

2.2.5. Gas phase

It is well documented that prolonged parasite growth requires a gas condition with a lower O_2 concentration and a higher CO_2 concentration than atmospheric air (Scheibel et al., 1979). The gas used in this study was supplied by British Oxygen Special Gases and was composed of 3% O_2, 4% CO_2 and 93% N_2 (British Oxygen Special Gases, UK). Culture flasks were gassed aseptically inside the class II laminar flow safety cabinet as follows: the gas from the cylinder was delivered to the laminar flow safety cabinet through a length of pre-sterilized silicon rubber tubing fitted with a 0.2 µm pore size acrylic filter (Gelman Sciences Inc., UK), into a further length of pre-sterilized silicon rubber tubing terminated with another 0.2 µm acrylic filter. This terminal filter was replaced before the gassing of the culture flasks. Culture flasks were gassed individually via a pre-sterilized cotton plugged pipette fitted to the terminal acrylic filter for approximately 1 min per 75 cm^2 culture flask.

2.2.6. Cryopreservation (freezing) of parasite cultures

Parasite cultures were cryopreserved by a modified method that is similar to that of (Rowe et al., 1968, Wilson et al., 1977) in order to facilitate the rapid recovery of parasites after retrieval. This method is described below (sections 2.1.6.1 and 2.1.6.2).

2.2.6.1. Procedure of cryopreservation (freezing)

Parasite cultures of a high parasitaemia (greater than 5%), predominantly at ring stage, were transferred aseptically into sterile 50 ml centrifuge tubes and centrifuged at 2500 rpm

for 5 min. The supernatant was discarded and an equal volume of cryoprotectant solution (section 2.1.6.2) was added to the parasite culture pellet. This suspension of parasite culture pellet and cryoprotectant was allowed to equilibrate for 5 min at room temperature. Aliquots of 500 – 1000 µl of the suspension were placed into screw-capped cryotubes (Nunc, UK), labeled appropriately and then transferred into liquid nitrogen tank for storage (British Oxygen Special Gases, UK).

2.2.6.2. Preparation of cryoprotectant solution

The cryoprotectant solution was prepared as follows: 1.9 g of sodium chloride (Sigma Chemical Co, UK) was dissolved in 200 ml of distilled water to get 0.95% (w/v) physiological saline. 8.4 g of sorbitol (Sigma Chemical Co, UK) was then dissolved in the prepared saline to get 4.2% (w/v) sorbitol. Thereafter, 70 ml of glycerol (Sigma Chemical Co, UK) was added to the solution. Subsequently, the cryoprotectant solution was sterilized through a sterile bottle top filter unit with a 0.22 µm membrane (Fisher Scientific, UK), labeled, and stored at 4 °C until required.

2.2.7. Retrieval of parasite cultures

Cultures cryopreserved using the method described above was retrieved as follows: cryotubes were removed from the liquid nitrogen storage tank and allowed to defrost at room temperature or quickly thawed at 37 °C. Prior to decanting the defrosted contents of cultures into a 15 ml centrifuge tube, 70% ethanol was used to wipe the rim of the vial to minimize any chances of culture contamination. An equal volume of ice cold 3.5% (w/v) sodium chloride (Sigma Chemical Co, UK) was then added and centrifuged at 2000 rpm for 5 min. The supernatant was removed and the cell pellet was washed in an equal volume of RPMI-1640 complete culture medium, and centrifuged as before. The final supernatant was removed and the cell pellet was re-suspended in 15 ml of RPMI-1640 complete culture medium which was then made up to the desired hematocrit with washed RBC. Cell pellet suspension was then transferred to a sterile 25 cm^2 culture flask, labeled, gassed and placed in an incubator at 37 °C for 48 h.

2.2.8. Routine monitoring of culture parasitaemia

The parasitaemia of the cultures were checked regularly day by day to ensure that the parasite cultures were healthy, well synchronised (section 2.1.8.1) and within the required limits of parasitaemia (usually, 5-12%). In order to monitor the culture parasitaemia, a thin blood film from every culture flask was prepared each day by spreading a drop of cultured cells on a clean, glass microscope slide (Fisher Scientific, UK). Blood films were then fixed for 5 s in 100% methanol (Fisher Scientific, UK) and placed into a 10% Giemsa stain solution (VWR International Ltd, UK) buffered at pH 7.2 for 15-20 min. Blood films were afterwards removed, washed carefully and thoroughly under running tap water. Slides were then dried and examined under oil immersion at x1000 magnification on a light microscope (Zeiss, Germany). The parasitaemia of the culture was determined by counting the number of infected cells and expressing these as a percentage of the total number of cells counted in approximately 5-10 fields of the blood film as shown below:

Parasitaemia (%) = (number of infected red blood cells / total number of red blood cells) x 100

2.2.8.1. Synchronising parasite cultures

Sorbitol (Sigma, UK), a sugar-based alcohol, is known to have a stabilizing effect on the RBC plasma membrane (Meryman and Hornblow.M, 1968) and alter the permeability of the later stages of asexual developing parasites (Lambros and Vanderberg, 1979). The changes in the RBC compartment of the later stage parasites allow sorbitol to enter via the new permeability pathway (NPP) leading the parasites to swell due to osmotic effect and eventually lyse and die. This process allows selection of the young ring forms which are unaffected, thereby synchronising the culture.

Highly synchronous parasite cultures were used throughout this thesis. Parasite cultures were synchronised regularly by the method of Lambros and Vanderberg (1979), described above. The procedure of synchronising the parasite cultures was as follows: cultures with a high proportion of ring stage parasites were transferred aseptically to pre-sterelized

centrifuge tubes and centrifuged at 2500 rpm for 5 min at room temperature. The supernatant was removed and discarded, and the cell pellet was re-suspended in 5 ml of 5% (w/v) sorbitol (section 2.2.8.1.1). The suspension was left in the laminar flow safety cabinet to stand at room temperature for approximately 20 min, with occasional shaking of the tube, and then centrifuged as above. The supernatant was removed and discarded, and the cell pellet was washed twice in 10 ml RPMI-1640 complete culture medium and centrifuged as above. The remaining cell pellet was re-suspended in 50 ml RPMI-1640 complete culture medium for the continous culture for a minimum of 48 hours prior to use in the different experiments.

2.2.8.1.1. 5% Sorbitol Preparation

Sorbitol was purchased from Sigma (Sigma, UK). The preparation of 5% sorbitol was as follows: a 25 g of sorbitol was dissolved in 500 ml of distilled water. This prepared 5% sorbitol solution was then sterilized through a sterile bottle top filter unit with a 0.22 µm membrane (Fisher Scientific, UK), labeled, and stored at 4 °C until required.

2.2.8.2. Cultivation procedure

A modification of the method of (Trager and Jensen, 1976) and (Jensen and Trager, 1978, Jensen and Trager, 1977) was used to maintain the parasite in continuous culture in pre-sterilized plastic 75 cm² flasks (Nunc, UK). The hematocrit in the culture flasks was 2% unless otherwise stated. Cultures were initiated by seeding a red cell/RPMI-1640 complete culture medium suspension with parasitized red cells from either another culture flask (section 2.2.8.3) or parasitised cells retrieved from cryopreserved stocks (section 2.2.7). The culture flask was then gassed as described above (section 2.2.4) and placed in an incubator at 37 °C. The culture medium was changed every 48 and 24 h when the parasitaemia was less than 1.5% and higher than 2%, respectively. The procedure for this was as follows: the parasite suspension was transferred aseptically to a 50 ml centrifuge tube and centrifuged at 2500 rpm for 5 min at room temperature. The spent medium was carefully removed and discarded. Pre-warmed RPMI-1640 complete culture medium was then added to make up the volume to 15 ml and 50 ml in 25 cm² and 75 cm² culture flasks,

respectively. The culture flasks were then gassed as described above (2.2.5) and placed in an incubator at 37 °C. The parasites were sub-cultured (section 2.2.8.3) when the target parasitaemia had been reached (usually at ~10% parasitaemia).

2.2.8.3. Sub-culturing of parasites

The purpose of sub-culturing the parasites in this study is to produce a large volume of parasite pellets for metabolomics experiments described in the next experimental chapters. The process of sub-culturing was as follows: the parasitised cell suspension was centrifuged at 2500 rpm for 5 min at room temperature. The supernatant was removed and discarded. An appropriate volume of parasitised cell pellet was added to a new sterile culture flask. Fresh uninfected erythrocytes and RPMI-1640 complete culture medium were added to create the required hematocrit (usually 2%) and parasitaemia depending on size of the flask used. The culture flask was then labeled, gassed (section 2.2.5) and incubated at 37 °C. The remainder of the parasitised cells were used either in an experiment, cryopreserved (section 2.2.6) or thoroughly decontaminated and discarded (section 2.2).

2.3. Analytical system for LC-MS/MS-based targeted metabolomics

Liquid chromatography coupled to (tandem) mass spectrometry (LC-MS/MS) is defined as an analytical chemistry technique that combines the physical separation of one or more compounds before being ionized and characterized by mass-to-charge ratio (m/z) and relative abundance using MS/MS. In this section, the general materials and methods used for analytical LC-MS/MS experiments will be described.

2.3.1. LC-MS/MS instrumentation

High performance liquid chromatography (HPLC) was carried out throughout this thesis using Accela™ instruments which include the Accela Autosampler and the Accela Pump (Thermo Electron Corporation, San Jose, CA). The main function of Accela Autosampler and Accela Pump is to inject samples automatically to MS and provides the optimum performance in the flow rate ranges needed for LC and MS, respectively. The autosampler

contains a built-in column oven (5 to 95 ºC), provides tray/sample temperature control (0 to 60 ºC), and is capable of performing automated sample preparation routines. The Accela Pump is a low-pressure mixing pump with built-in solvent degassing and pulse dampening system. A TSQ Quantum Access™ Triple Stage Quadrupole MS (Thermo Electron Corporation, San Jose, CA) equipped with external electrospray ionization (ESI) source was employed for detection and analysis of metabolites. This MS provides sample ionization and mass analysis of injected samples or samples eluted from a liquid chromatography. Xcalibar software (Thermo Electron Corporation, version 2.0.7 release) was used for controlling the LC-MS/MS instrument, data acquisition and analysis.

2.3.2. Solvents and Chemicals

Water (H_2O), acetonitrile (CH_3CN) and methanol (CH_3OH) were all HPLC grade. Acetonitrile (CH_3CN) and methanol (CH_3OH) were obtained from Fischer Scientific (UK). Water (H_2O) and ammonium acetate ($C_2H_3O_2NH_4$) were purchased from VWR International Ltd (UK). Mass spectroscopy grade formic acid (CH_2O_2, ≥98%) and ammonium hydroxide (NH_4OH) were obtained from Sigma – Aldrich (UK).

2.3.3. HPLC column installation

A Luna aminopropyl column (250 mm × 2 mm with a 5 μm particle size, Phenomenex, USA) was selected for the metabolite separation throughout this study. This is because most of the metabolites that were targeted in this study were polar and therefore require hydrophilic interaction chromatography (HILIC) for effective separation of a broad range of cellular metabolites including amino acids, nucleosides, nucleotides, coenzyme A derivatives, carboxylic acids, simple sugar, and sugar phosphate (Bajad et al., 2006).

Upon receipt of the aminopropyl column, it was checked for any physical damage which may have occurred during shipping. Prior to testing the column performance and quality, it was important to equilibrate the column. Column equilibration was performed as follows: Accela Pump HPLC system was purged thoroughly with filtered and degassed mobile phase (95:5 water: acetonitrile) without buffers for 20 min. The column was then connected

to the injector corresponding to the direction of the flow label that was located on the column and the column outlet was left unattached. The pump flow rate was set at 100 µl/min and was increased to normal flow rate over 5 min. The flow was stopped when there was a free flow of solvent from the column outlet. The column outlet was thereafter wiped up and attached to the mass spectrometry detector. The column was then equilibrated by passing approximately 10-30 column volumes of mobile phase at flow rate 150 µl/min. Column volume was calculated according to the following equation:

$$V = \pi \times r^2 \times L$$

V= Column volume in ml

π= Constant factor equals to 3.14

r= Column radius in cm

L= Column length in cm

2.3.4. Mobile phase preparation

The mobile phase that was used throughout this study consisted of solvent A [20 mM ammonium acetate + 20 mM ammonium hydroxide in 95:5 water:acetonitrile (pH 9.45)] and solvent B (acetonitrile). The choice of this mobile phase was based on its appropriateness and suitability for the luna aminopropyl column as tested by the Rabinowitz lab (Bajad et al., 2006, Kimball and Rabinowitz, 2006, Rabinowitz and Kimball, 2007, Yuan et al., 2008, Lu et al., 2006).

Prior to each LC-MS/MS process, the mobile phase was freshly prepared as follows: 950 ml of HPLC grade water and 50 ml of HPLC grade acetonitrile were added in a clean glass beaker resulting in a water:acetonitrile ratio of 95:5. In the fume hood cabinet, 20 ml of 1 M ammonium acetate stock (section 2.3.4.1) and 20 ml of 1 M ammonium hydroxide stock (section 2.3.4.2) were added to the 95:5 water:acetonitile. The pH was checked and this mixture gave pH 9.45. The mobile phase was then filtered through sterile bottle top filter unit with a 0.22 µm membrane (Fisher Scientific, UK), sonicated and degassed using a sonicator (Fisher Scientific, UK) for 15 minutes.

2.3.4.1. Preparation of ammonium acetate

The preparation of 1 M stock solution of ammonium acetate ($C_2H_3O_2NH_4$) (MW = 77.08 g/mol) was as follows: 38.54 g of ammonium acetate was dissolved in 500 ml of HPLC grade water. The solution was then filtered through a sterile bottle top filter unit with a 0.22 μm membrane (Fisher Scientific, UK), labeled, and stored at 4 °C for future use.

2.3.4.2. Preparation of ammonium hydroxide

The preparation of 1 M stock solution of ammonium hydroxide (NH_4OH) (MW= 35.05 g/mol, density= 0.9 g/ml, weight percentage= 28% w/w and M= 7.190 M) was as follows: slowly 34.772 ml of 7.19 M ammonium hydroxide stock solution was added to 62.5 ml of HPLC grade water. The final volume of ammonium hydroxide solution was adjusted to 250 ml with HPLC grade water to make 1 M ammonium hydroxide stock solution. The solution was then transferred into clean glass bottle, labeled, and stored at 4 °C for future use.

2.3.5. HPLC column cleaning and storage

Appropriate HPLC column cleaning and storage conditions provide a better performance over the column lifetime. The cleaning and storage solvents consisted of HPLC grade water and acetonitrile. After analysis of samples by LC MS/MS, the luna aminopropyl column (250 mm × 2 mm with a 5 μm particle size, Phenomenex, USA) was cleaned as follows: Accela Pump HPLC lines system were purged thoroughly with filtered and degassed HPLC grade water and acetonitrile for 20 min. The column was then connected to the injector in reverse to the direction of the flow label that was located on the column and the column outlet was left unattached. The column was initially rinsed with 95% HPLC grade water, 5% ACN for about an hour then 95% ACN, 5% water overnight. The column was thereafter stored in 65% ACN, 35% water.

2.3.6. Routine mass spectrometer maintenance

To ensure the proper operation of TSQ Quantum Access™ Triple Stage Quadrupole MS, Thermo Fisher Scientific recommends daily performance of checks and cleaning of the TSQ system. This includes procedures before and after operating the TSQ system. To do this, the argon, nitrogen and system vaccum levels were checked to ensure they were up to appropriate levels prior to operating the TSQ system. Cleaning ion transfer tube, ion sweep cone, and flushing the sample transfer line, sample tube, and ESI probe were subsequently performed after operating the TSQ system. The flushing procedure was carried out by passing methanol/water (50:50) solution (section 2.3.6.1) from LC through the ESI probe for 2 h. Cleaning procedures were carried out firstly by sonicating ion transfer tube, ion sweep cone in HPLC water containing formic acid for 1 hour, then in methanol for another hour.

2.3.6.1. Preparation of methanol/water (50:50)

The preparation of methanol/water (50:50) was made as follows: a 500 ml of HPLC grade methanol and a 500 ml of HPLC grade water were added in a 1 L bottle. Sonication and degassing was thereafter carried out for 15 minutes. This cleaning solution was then placed in the reservoir area of the HPLC tanks for future use.

CHAPTER 3

Development and Validation of an Analytical Method for Targeted Metabolomics *Plasmodium falciparum*

3.1. Introduction

A key element to this thesis was the measurement of *P. falciparum* metabolites which require accurate and reliable detection and quantification. Therefore, development and validation of an analytical platform for the detection and quantification of *P. falciparum* metabolome was undertaken.

Despite intensive research in the metabolomics area in recent years, it has still proved difficult to develop a generic analytical method to detect and quantify the *P. falciparum* metabolome which includes 616 metabolites and accounts for around a thousand reactions in the compartmentalized metabolic network (Plata et al., 2010). These metabolites consist of a wide variety of compound classes with different physical and chemical properties and are present at varying dynamic ranges of concentration (Weckwerth, 2003, Xiayan and Legido-Quigley, 2008, Koek et al., 2011, Goodacre, 2005). The chemical diversity and complexity of the metabolome make it extremely challenging to profile all of the metabolome simultaneously. Furthermore, the characteristics of the metabolite molecular structure are influenced not just by its milieu but also its interactions with other molecule structures leading to ion suppression or enhancement (Cubbon et al., 2010).

Depending on the kind of metabolites to be extracted, metabolomic methods require the development of tailor-made strategies for sample preparation, metabolite extraction and separation, and ultimately data analysis (Lakshmanan et al., 2011). Therefore, to successfully develop a method, there are few steps that have to be considered. First, the scientific question in the area must be identified and addressed. Secondly, reviewing the scientific literature and selecting the metabolites of interest. Thirdly, optimization of the sensitivity and selectivity for liquid chromatography coupled to tandem mass spectrometry detection (LC-MS/MS). This includes choosing the right HPLC column for metabolite separation, selecting the best ionization mode (APCI or ESI), optimization of mass spectrometry (MS) configuration, and tuning the ion path. When an LC-MS/MS method is successfully developed and validated, sample preparation and metabolite extraction is then optimized.

Although metabolomics in malaria is still in its infancy, there are a number of robust analytical techniques that have been developed and reported to achieve an efficient and all-encompassing metabolomic analysis (Kafsack and Llinás, 2010, Plata et al., 2010, Cassera et al., 2011, Lakshmanan et al., 2011, Olszewski and Llinás, 2011, Teng et al., 2009, Bulusu et al., 2011, Jayaraman et al., 2012, Mehta et al., 2006, Olszewski et al., 2009, van Brummelen et al., 2009, Besteiro et al., 2010, Olszewski et al., 2011, Lian et al., 2009). In addition, there are different approaches including metabolic profiling and metabolic fingerprinting to detect and investigate the metabolome in various fields of research (Fiehn, 2002).

Advanced MS analysis can identify hundreds to thousands of metabolites, providing a new and extremely powerful tool for studying cell system biology and a drugs mode of action (Reaves and Rabinowitz, 2011, Tiziani et al., 2009). However, it is important to note that due to the diversity in physical and chemical structures of the metabolites, a prior knowledge of the types of molecules to be explored will dictate the protocols to be used. Targeted metabolomics as described early (Chapter 1) aims to detect and quantify a predefined set of metabolites, typically dozens or hundreds of known compounds, based on metabolite-specific signals (Lu et al., 2008). In particular, in targeted metabolomics approaches, using triplequadrupole MS, a precursor ion and a fragment of the precursor ion, producing a molecular weight and structure-specific measurement for a single metabolite (referred to as transition), are used for the sensitive and accurate determination of the compound concentration over a wide dynamic range which eventually results in a single reaction monitoring (SRM) (Rabinowitz, 2007). Each SRM scan takes approximately 0.1 s which enable the detection and quantitation of numerous metabolites during a single LC-MS/MS run (Rabinowitz, 2007). Simultaneous analysis of multiple transitions results in multiple reaction monitoring (MRM), where the collision energy and product ion mass-to-charge ratio (*m/z*) are pre-optimized for each metabolite of interest to give the best signal intensity (Lu et al., 2008). Therefore, the development of a targeted metabolomic approach was undertaken to profile a number of related metabolites for *P. falciparum* mitochondrion and digestive vacuole. In addition, in order to ensure that the developed method is reliable for metabolite detection and quantification analysis, adequate

analytical method validation was conducted. In general, analytical method validation includes studies on selectivity and carryover, metabolite recovery and stability, linearity and sensitivity (limit of detection, LOD), and performance reproducibility.

3.2. Materials and Methods

3.2.1. Solvents and Chemicals

Solvents and chemicals used for LC-MS/MS were of HPLC grade as described previously unless otherwise stated (chapter 2, section 2.3.2).

3.2.2. Targeted metabolomics method development

Electrospray ionization mode (ESI) was selected for targeted metabolomics method in this thesis owing to the fact that most of the metabolites of interest targeted were polar. In addition, although heated ESI (HESI) provided enhanced sensitivity compared with the unheated ESI, HESI had increased noise in most cases and increase metabolite decomposition due to the heat effect in the ESI probe. Therefore, unheatd ESI was preferred over heated ESI (HESI) in this thesis.

3.2.2.1. Preparation of primary stock solution standards for ion path tuning

An appropriate amount (> 1 mg) of metabolite standard (Appendix I, Table 1) was weighed out from their solid powder and then dissolved in an appropriate solvent to give 1 mg/ml of primary stock solutions and stored at -80 ºC until required. Freshly prepared 10 µg/ml working (Appendix I, Table 1) stocks were then prepared from 1 mg/ml stock solutions and used for tuning the ion path.

3.2.2.2. Ion path tuning

Freshly prepared 10 µg/ml metabolite working stocks (section 3.2.2.1) were injected directly into the MS to determine if the metabolite of interest could be detected. It was sometimes necessary to vary the concentration of metabolite being injected, as well as to modify the mode of ESI ionization (positive or negative). Once it was certain that the metabolite can be detected, MS configurations were subsequently optimized as described (section 3.2.2.3).

3.2.2.3. Mass spectrometry configurations optimization

Like ion path tuning, optimizing the MS configurations involves direct infusion of the metabolite of interest into the MS/MS, without going through liquid chromatography. When optimizing the source parameters, it was sometimes necessary to run as much mobile solvent into the MS/MS system as would be expected when chromatography is developed. The goal of optimizing the mass spectrometry configurations was to increase the sensitivity of the analysis. This was performed through series modifications of different configurations including voltage, nitrogen gas flow, collision argon gas and temperatures.

Therefore, a TSQ Quantum Access™ Triple Stage Quadrupole mass spectrometer (Thermo Electron Corporation) equipped with electrospray ionization (ESI) was employed for the metabolite detection and analysis of metabolites. ESI spray voltage was 4000 V and 5500 V for positive and negative modes, respectively. Nitrogen was used as sheath gas at 30 psi and as the auxiliary gas at 10 psi. Argon was used as the collision gas at 1.5 mTorr. The capillary temperature was 320 °C and 270 °C for positive and negative modes, respectively. Scan time for each single reaction monitoring (SRM) event transition was 0.1 s with a scan width of 1 m/z. The instrument control, data acquisition, and data analysis were achieved applying the Xcalibar software (Thermo Electron Corporation, version 2.0.7 release), which also controlled the chromatography system.

3.2.2.4. Chromatographic separation optimization

Once the source parameters were optimized, chromatography was then optimized. This involved using the appropriate chromatography column selection for separation. Hydrophilic interaction chromatography (HILIC) [Luna aminopropyl column (250 mm × 2 mm with a 5 μm particle size, Phenomenex, USA)] was selected on the bases that most metabolites of interest targeted in this thesis were polar and had been tested before (Bajad et al., 2006). In addition, appropriate flow rate and mobile phase gradient were adjusted for optimal resolution and detection.

Therefore, chromatographic separation was achieved using a Luna aminopropyl column (250 mm × 2 mm with a 5 μm particle size, Phenomenex, USA) connected to a security guard packed with double-cartridge (4 mm × 2 mm, Phenomenex, USA) to maximize contaminant removal and extend the half-life of the HPLC column. This HILIC column (described in chapter 2) was employed for the metabolites separation using an Accela Autosampler HPLC system (Thermo Fisher Scientific). The mobile phase consisted of solvent A [(20 mM ammonium acetate + 20 mM ammonium hydroxide) in 95:5 water:acetonitrile (pH 9.45)] and solvent B (acetonitrile) which was prepared as described beforehand (chapter 2, section 2.3.4). The chromatographic gradients were as follows: t = 0, 15% A; t = 15 min, 100% A; t = 33 min, 100% A; t = 35 min, 15% A; t = 45 min, 15% A. Injection volume, flow rate, column temperature and autosampler temperature were set at 20 μL, 150 μL/min, 15 °C and 15 °C, respectively. The injection needle was washed with one volume of methanol/water (50:50) solution between injections to eliminate the problem of carryover between samples.

3.2.2.5. Extraction optimization

Metabolite extraction formed part of sample preparation and involved testing many different solvents and methods of extraction to yield the best recovery. The purpose of an extraction was to extract the metabolites of interest from any interfering components (e.g. cellular matrix) and to concentrate them for detection. Extraction method must yield a good recovery of the metabolites with minimum to zero matrix effect (Rabinowitz and Kimball, 2007). Different extraction solvents were test by Rabinowitz and his colleague and they found that mixtures of acidic 0.1 M formic acid containing acetonitrile/methanol/water (40:40:20) gave superior yields for cellular metabolites in addition to providing a protection for redox and nucleotide phosphate compounds (Rabinowitz and Kimball, 2007, Yuan et al., 2008). Therefore, acidic acetonitrile/methanol/water (40:40:20 + 0.1 M formic acid) spiked with 200 μM of each internal standards namely β-alanine and DL-arabinose (section 3.2.2.5.1) for positive and negative modes, respectively, was used in this thesis as the quenching solvent and without internal standards as the extraction solvent.

3.2.2.5.1. Quenching and Extraction Solution

The quenching solution used to carry out the LC-MS/MS metabolomic experiments was acidic acetonitrile/methanol/water (40:40:20 + 0.1 M formic acid) solvent system spiked with 200 µM of each internal standards namely β-alanine and DL-arabinose for positive and negative modes, respectively. The addition of formic acid to a final concentration of 0.1 M provides additional protection of nucleotide triphosphates against degradation. The extraction solution used to carry out the metabolites extraction was acetonitrile/methanol/water (40:40:20) solvent system. This extraction solvent was neither acidic nor spiked with internal standards and was used only to extract the metabolites in a manner so as to yield as much as possible of metabolites in the supernatant and discarding the cell debris.

3.2.3. Targeted metabolomics method validation

3.2.3.1. Preparation of primary stock solution standards for calibration curve standards and quality control (QC)

Primary stock solutions were prepared in the appropriate solvent at specific (mM) concentration for each metabolite as indicated in Appendix (I, Table 2). From these stocks of primary solutions, a standard mixture of metabolites was prepared by adding 100 ul of each metabolite primary stock. Aliquots of this standard mixture were used for calibration standards, authentic quality control (QC) standards and spiking into parasite cell extracts for the recovery method. The calibration curve was obtained by analyzing the standard mixture of metabolite solution at sixteen concentrations. Standard levels were prepared by serially diluting the standard mixture solution in HPLC water as follows: 1:1, 1:2, 1:4, 1:8, 1:16, 1:32, 1:64, 1:128, 1:256, 1:512, 1:1024, 1:2048, 1:4096, 1:8192, 1:16384 and 1:32768, as indicated in appendix (I, Table 3) which show the corresponding concentration (µM) at each standard level for each metabolite. These concentrations were presented in molarity unit and were varied from metabolite to metabolite depending on molecular

weight. Calibration curves were constructed by plotting the area ratio of the metabolite standard (AUC of metabolite divided by AUC of internal standard) against its concentration. Linear regression was used to fit the calibration curve and the linearity for each metabolite was evaluated from it. Three levels of authentic QC standard were prepared, high, medium and low in order to evaluate the accuracy of the calibration curve. High quality control (HQC) represents the standard mixture at initial concentration (i.e. the standards mixture that was prepared by adding 100 µl of primary stock) (Appendix1, Table 4). Medium quality control (MQC) represents the HQC diluted by 1:10. Low quality control (LQC) represents the HQC diluted by 1:100 (Appendix1, Table 4).

3.2.3.2. Selectivity

The selectivity for the developed targeted metabolomics method was evaluated in the following parameters: consistency in the retention time for each metabolite chromatographic separation and a specific detection for the precursor ion and its corresponding product ion using the MRM scan. Therefore, authentic metabolite mixture standards and blank samples (e.g. methanol) were prepared and examined using the developed metabolomics method.

3.2.3.3. Carryover test

Carryover tests were conducted by injecting a series of methanol blanks directly following the highest concentration of standards and between the metabolomics experiment for the *P. falciparum* parasite.

3.2.3.4. Recovery (%)

The recovery of the metabolites was evaluated from cellular extracts of *P. falciparum* parasite as follows: metabolite mixtures of the standard solution were spiked with cell extracts of *P. falciparum* parasite prior to lyophilisation at the level 1 concentration indicated in (Appendix I, Table 3) and extracted and prepared as described later (Chapter 4, sections 4.2.2 and 4.2.3.1). The response, area under the curve (AUC), of the metabolites in the cell extract was divided by the corresponding metabolites standard solutions at the same concentration and expressed as percentage. In addition, the recovery of internal

standards β-alanine and DL-arabinose was carried out at concentration of 200 µM. Typically, a metabolite recovery of 70% - 120% was considered satisfactory (Koek et al., 2011, Koek et al., 2006).

3.2.3.5. Stability studies

The stability studies were conducted on the purified metabolites as follows: a mixture of metabolite standard solution at level 1 concentration indicated in (Appendix I, Table 3) was prepared and divided into four aliquots. One analysed immediately three times. Others were stored separately at 4 ºC, -20 ºC and -80 ºC. These samples were analysed in triplicate after a month to evaluate the metabolites stability during the period of a month. Normalized signals, corresponding to the AUC of the metabolite signal divided by AUC of the internal standard signal, were compared for the various storage conditions to the actual normalized signal value. The metabolite was considered stable at a specified temperature if the normalized signal after the corresponding storage had an RSD of less than 15%.

3.2.3.6. Reproducibility studies

The mixture of metabolite standard solution at level 1 concentration indicated in (Appendix I, Table 3) was plunged into the quenching solvent, acetonitrile/methanol/water (40:40:20 + 0.1 M formic acid) spiked with 200 µM of internal standards β-alanine and DL-arabinose, and then extracted and prepared as described later (Chapter 4, sections 4.2.2 and 4.2.3.1) for the sample preparation. Afterwards, it was divided into three aliquots and stored at -80 ºC. The first sample was analysed three times on Day 1. The remaining two samples were analysed on Days 2 and 3, three times in each case. The method was considered reproducible if the RSD was less than 15%

3.2.3.7. Linearity, LOD, and calibration curve accuracy

The linearity was determined for this targeted metabolomics method by generating a standard calibration curve for each metabolite. Calibration curves were generated by plotting the area ratio (AUC of the metabolite divided by the AUC of internal standard) against concentration (µM). Linear regression was then used to find the straight line that best fits the data points. This curve fitting was performed using Xcalibar

software (Thermo Electron Corporation, version 2.0.7 release). Goodness of fit for the standard calibration curves were determined by the R^2 value calculated from the software, an R^2 better than 0.98 was considered acceptable. The limit of detection (LOD) for each metabolite was evaluated by determining the lowest concentration of metabolite level that has signal-to-noise ratio (S/N) > 3. Three levels of QCs (low, medium and high; *n*=3 at each level) were prepared and used to determine the accuracy the calibration curve generated. The accuracy of 100% ± 20% (80-120%) was considered satisfactory. The accuracy of the analytical method describes how close the mean of test results obtained by the method are to the nominal concentration of the metabolite. Accuracy was calculated by the following equation and expressed as a percentage:

Accuracy (%) = (mean observed concentration/nominal concentration) x 100

3.3.Results

3.3.1. Selectivity

Two types of sample, including the authentic mixture of metabolite standards and methanol as the blank sample, were processed equally using the metabolomics method to evaluate the sensitivity of the method in terms of retention time and accurately distinguishing the metabolites precursor ion and their product ions based on the MRM scan. The chromatogram peak findings showed that the LC-MS/MS of the standard mixture was able to distinguish between different metabolite peaks based on their retention time and MRM scan as shown in the example of dihydroorotate chromatogram (Figure 3.1). The remaining metabolite chromatograms are shown in the Appendix (II, Figures 1 – 58). On the other hand, LC-MS/MS of methanol showed noisy chromatogram peaks suggesting that this metabolomics method was very selective (Figure 3.2). Tables 3.1 and 3.2 summarize all the metabolites targeted in positive and negative ionization modes, respectively, the following LC-MS/MS parameters: metabolite precursor ion and its product ion, collision induced dissociation (CID) and expected retention time (RT).

3.3.2. Carryover test

A critical issue for the LC-MS/MS metabolomics method is the tendency of metabolites to get absorbed by the HPLC column packing materials, resulting in a memory effect. However, the analysis of the present method showed no detectable carryover effect was obtained when a series of methanol blanks were injected immediately after the highest calibration standard and between the different sets of metabolomic experiments for *P. falciparum* parasite.

A)

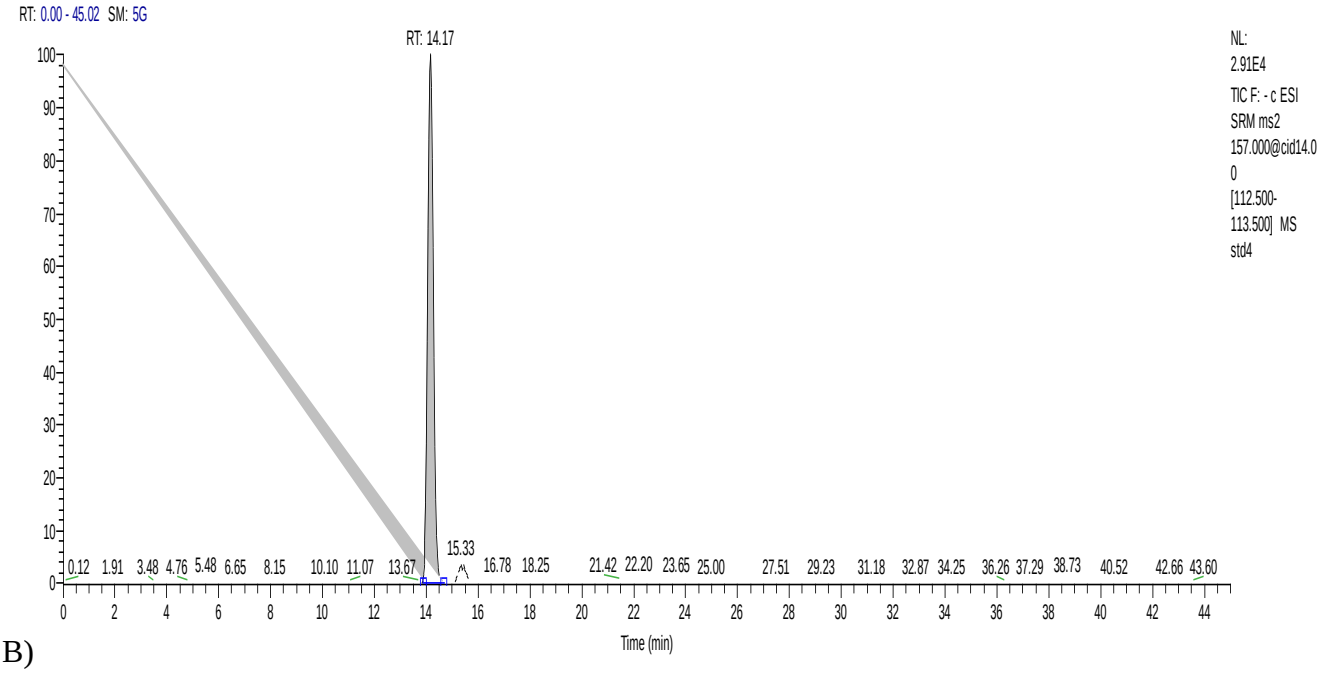

B)

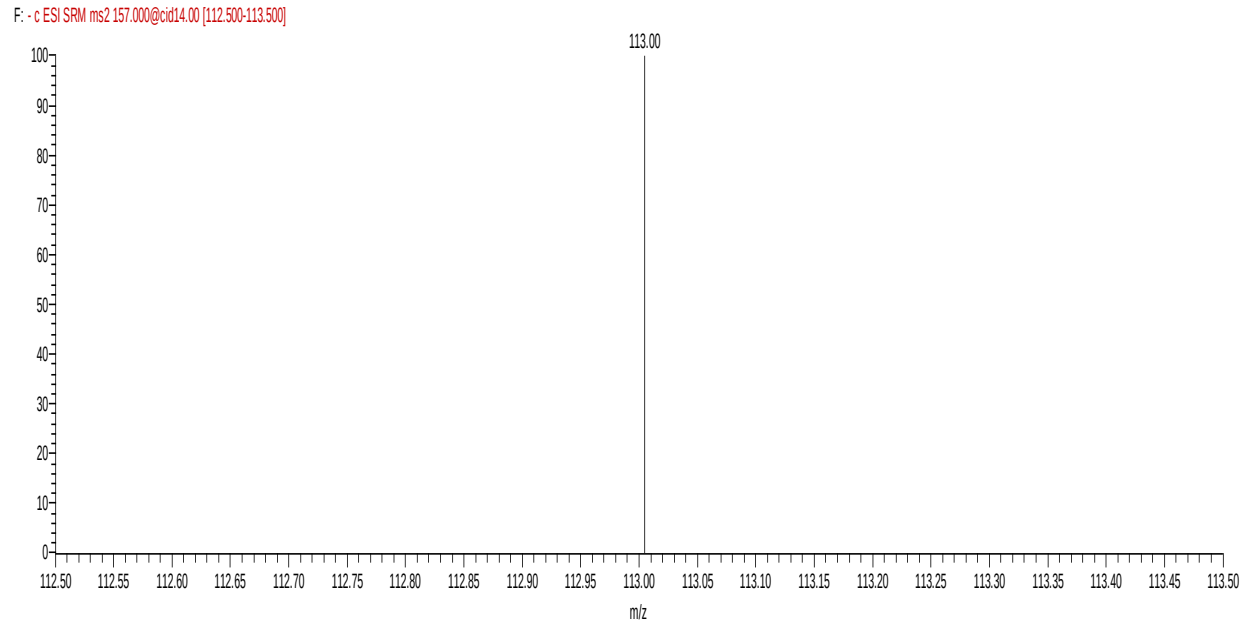

Figure 3.1: LC-MS/MS chromatogram of dihydroorotate.

A) Chromatographic separation of dihydroorotate peak shows retention time (RT) at ~14min. B) SRM scan of ionized dihydroorotate shows the detection of its product ion at mass-to-charge (m/z) of 113.

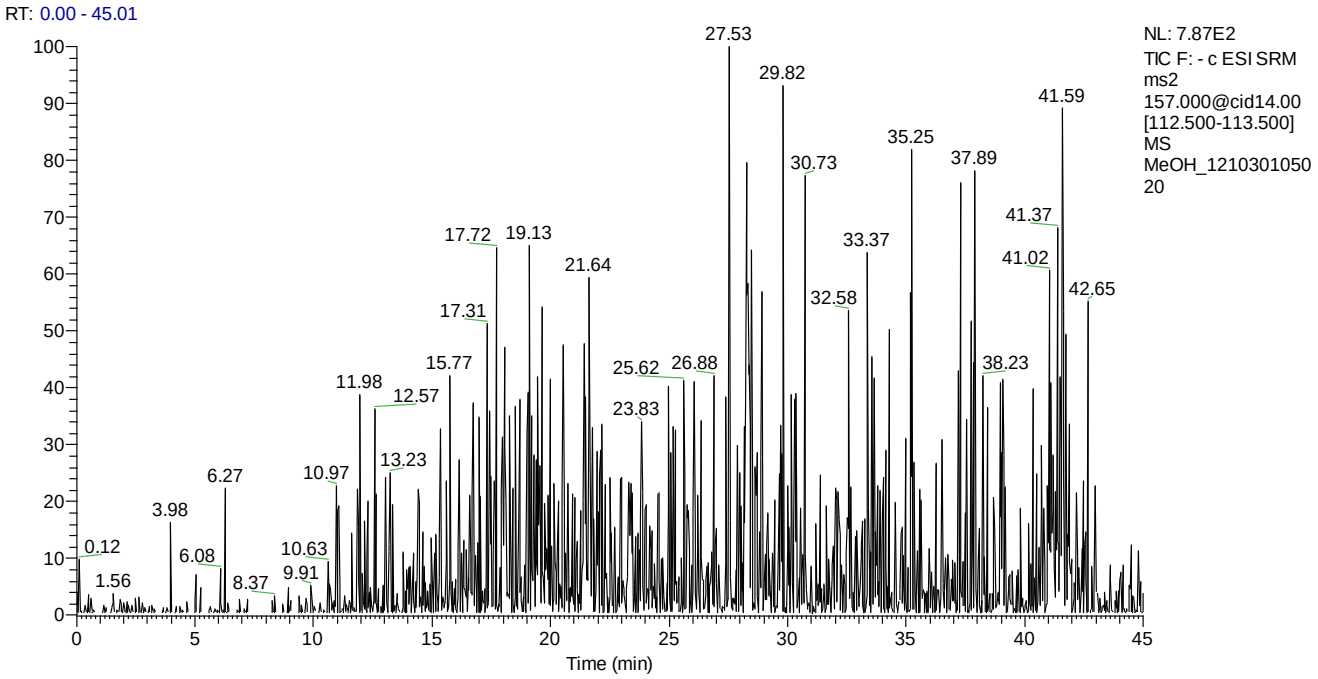

Figure 3.2: LC-MS/MS chromatogram of methanol blank.
Dihydroorotate SRM setting was selected here to evaluate the selectivity of the present LC-MS/MS method. The chromatogram shows noisy peaks and dihydroorotate peak is not observed.

Table 3.1: LC-MS/MS parameters for metabolites detected in positive ESI mode (protonation, Molecule + H^+)

Metabolite	MW (g/mol)	Precursor mass	CID	Product mass	RT (min)
Alanine	89.09	90.1	14	44.1	12.8
B-alanine	89.09	90.3	5	71.8	12.5
Serine	105.09	106	10	60	13.1
Proline	115.13	116	11	70	12.4
Valine	117.15	118	11	55	12.1
Threonine	119.12	120	11	74	13.3
Cysteine	121.16	122	21	59	26.1
(iso)-leucine	131.17	132	11	86	11.4
Asparagine	132.12	133	17	74	13.4
Ornithine	132.19	133	15	70	14.4
Aspartate	133.1	134	15	74	16.4
Glutamine	146.14	147	15	84	13.1
Lysine	146.19	147	16	84	14.4
Glutamate	147.13	148	15	84	16.5
Methionine	149.21	150	10	133	12
Histidine	155.15	156	12	110	13.6
Phenylalanine	165.19	166	28	103	11.6
Arginine	174.2	175	14	60	13.7
Citrulline	175.19	176	12	159	12.9
Carbamoyl-l-aspartate	176.12	177	17	74	21.5
Tyrosine	181.19	182	26	77	13
Tryptophan	204.23	205	16	146	11.9
GSH	307.32	308	19	162	19.7
UMP	324.18	325	12	97	22.3
AMP	347.22	348	21	136	22.8
UDP	404.16	405	19	97	23.1
ADP	427.20	428	31	136	23.5
TTP	482.16	483	25	81	27.3
CTP	483.15	484	21	112	25.1
UTP	484.14	485	30	97	27.7
ATP	507.18	508	37	136	25.5
GTP	523.18	524	37	152	27.8
GSSG	612.63	613	33	231	22
NAD	663.43	664	30	428	16.5
NADH	664.43	666	26	514	27.1
NADP	744.41	744	48	136	22.9
NADPH	745.41	746	16	729	31.9
FAD	785.55	786	24	348	22.9
Acetyl-CoA	809.57	810	28	303	24
Propionyl-CoA	823.60	824	33	317	24.2
Succinyl-CoA	867.60	868	38	361	25

Abbreviations: MW, Molecular Weight; CID, Collision Induced Dissociation; RT, retention time.

Table 3.2: LC-MS/MS parameter for metabolites detected in negative ESI mode (deprotonation, Molecule – H^+)

Metabolite	MW (g/mol)	Precursor mass	CID	Product mass	RT (min)
Lactate	90.08	89	11	43	14
Fumarate	116.07	115	11	71	25.5
Succinate	118.09	117	16	73	21.5
Oxaloacetate	132.07	131	12	87	24.2
Malate	134.09	133	12	115	21.6
Hypoxanthine	136.12	135	16	92	13.4
PABA	137.14	136	16	92	13.1
Carbamyl phosphate	141.02	140	38	79	25.7
2-Oxoglutarate	146.11	145	11	101	26.6
DL-arabinose	150.13	149.1	7	130.6	10.8
Orotate	156.10	155	13	111	15.3
Dihydroorotate	158.11	157	14	113	14.1
PEP	168.04	167	20	79	23.3
DHAP	170.06	169	43	79	29
G-3-P	172.07	171	13	79	21.8
Glucose	180.16	179	18	59	11.7
(iso)-citrate	192.12	191	18	111	23.3

Abbreviations: MW, Molecular Weight; CID, Collision Induced Dissociation; RT, retention time.

3.3.3. Recovery studies

Recovery studies were conducted for all 58 metabolites targeted in this metabolomics method including the internal standards. The area under the curve (AUC) for metabolites spiked with cellular extract of *P. falciparum* was divided by the AUC for the corresponding authentic metabolite standard and then expressed as a percentage. The results showed that ~85% of the metabolites including internal standards that were targeted in this method had a satisfactory recovery (70% - 120%) (Figure 3.3). This highlighted that the present method yields a good recovery for most of the metabolites targeted in this study. Nonetheless, in the presence of parasite matrix or any cell matrix, the influence of molecule adsorption to the analytical system results in recovery differences (high or low) for some metabolites due to many factors such as ion suppression (Annesley, 2003, Koek et al., 2006, Koek et al., 2011). Therefore, it is important to note here that proper cleaning and maintenance of the analytical system greatly enhances the quality of data output. Table 3.3 summarizes the recovery (%) for all the metabolites targeted in the method of this chapter.

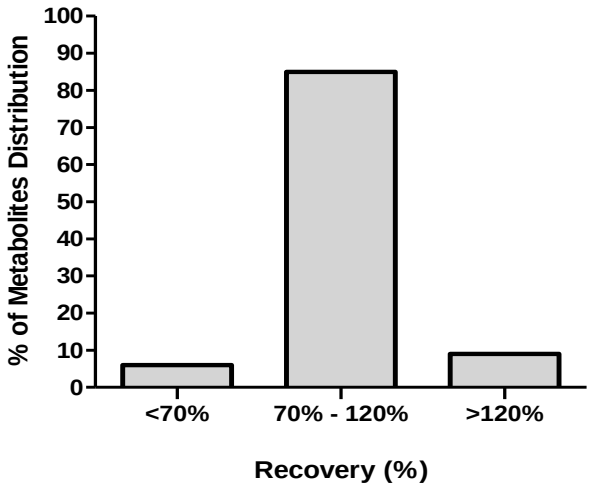

Figure 3.3: Histogram of the distribution of recovery (%) for all 58 metabolites investigated. The recovery range of 70% - 120% was considered satisfactory. Histogram showed that ~85% of the metabolites had a satisfactory recovery between 70% and 120%. The remaining 15% of the metabolites had unsatisfactory recovery in which the recovery was either high (>120%) or low (<70%).

Table 3.3: Recovery (%) of authentic metabolite standards spiked to *P. falciparum* cellular extracts

Metabolite	Recovery (%)	Metabolite	Recovery (%)
TTP	18	**Carbamoyl-l-aspartate**	100
GTP	32	**GSH**	100
PABA	43	**AMP**	101
Cysteine	44	**Glutamine**	102
ATP	77	**Oxaloacetate**	102
Threonine	85	**NADPH**	102
Ornithine	89	**UMP**	102
2-Oxoglutarate	92	**Arginine**	103
Citrulline	92	**Malate**	103
Valine	93	**Succinate**	103
G-3-P	94	**NADP**	103
Hypoxanthine	94	**Dihydroorotate**	104
Proline	95	**Histidine**	104
GSSG	95	**Acetyl-CoA**	106
Lysine	96	**Lactate**	107
NAD	96	**Phenylalanine**	107
Asparagine	97	**DL-arabinose (IS)***	107
Glutamate	97	**Carbamyl phosphate**	109
Methionine	97	**Tryptophan**	109
β-alanine (IS)*	97	**Propionyl-CoA**	111
Alanine	98	**CTP**	111
Orotate	98	**PEP**	112
FAD	98	**NADH**	113
(iso)-leucine	99	**Glucose**	118
DHAP	99	**ADP**	121
Fumarate	99	**Serine**	124
Tyrosine	99	**UDP**	126
(iso)-citrate	99	**UTP**	135
Aspartate	100	**Succinyl-CoA**	180

*IS, Internal Standard

3.3.4. Stability studies

The metabolites targeted in the metabolomics method were investigated in terms of their storage stability over a one month period. Different storage temperatures including 4 ºC, -20 ºC and -80 ºC were evaluated for each metabolite by comparing the metabolites normalized signal to that of the corresponding actual value. The relative standard deviation was then calculated from the triplicate LC-MS/MS runs for each storage temperature. The results showed that ~88% of the metabolites were stable and had an RSD less than 15% under a -80 ºC storage temperature (Figure 3.4). In addition, ~70% and ~51% of the metabolites were stable and had an RSD less than 15% under -20 ºC and 4 ºC storage temperatures, respectively (Figure 3.4). On the other hand, ~12%, ~30% and ~49% of the metabolites were unstable and had an RSD greater than 15% under -80 ºC, -20 ºC and 4 ºC storage temperatures, respectively (Figure 3.4). These results indicate that -80 ºC storage temperature had the least effect on changing metabolite stability (i.e. it is the optimal condition for keeping the metabolites). Table 3.4 summarizes the %RSD for each metabolite under the different storage temperatures.

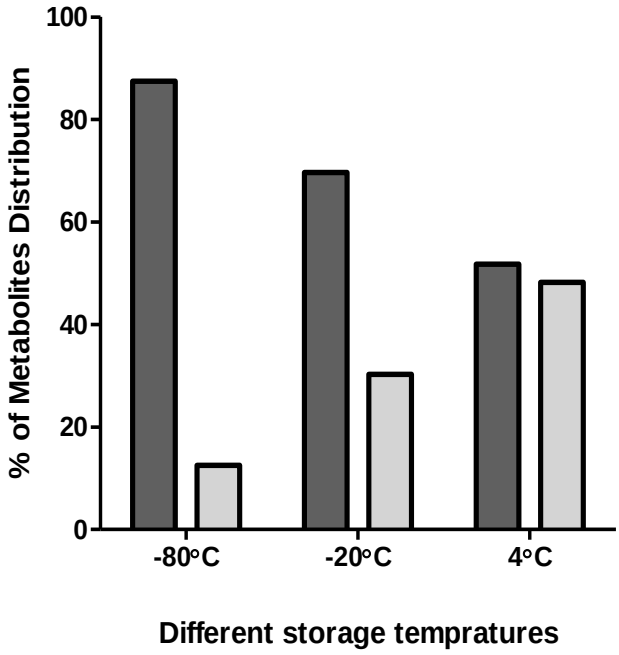

Figure 3.4: Histogram of the distribution of different storage temperatures for stable and unstable metabolites.

Stability was determined for all metabolites targeted in the present method. Stable (dark grey bar) and unstable (light grey bar) represent the percentage of metabolite distribution in -80ºC, -20ºC and 4ºC storage temperatures. %RSD was calculated for each metabolite and a metabolite is considered stable at the indicated temperature if RSD is less than 15%.

Table 3.4: Stability of the authentic metabolite standards. Metabolite is considered stable at indicated temperature if RSD is less than 15%

Metabolite	Storage Temperature		
	-80°C (% RSD)	-20°C (% RSD)	4°C (% RSD)
Tryptophan	1	5	4
Lysine	1	10	8
Succinyl-CoA	1	25	45
Arginine	2	2	10
Citrulline	2	3	7
Histidine	2	12	13
Phenylalanine	2	1	14
Methionine	3	7	14
Ornithine	3	4	12
UMP	3	5	5
NAD	3	7	18
Threonine	3	12	14
ATP	3	30	55
Carbamoyl-l-aspartate	4	7	9
Tyrosine	4	2	2
GSSG	4	4	16
Glutamate	4	8	18
TTP	4	6	49
Glutamine	6	9	11
Alanine	7	5	12
Serine	7	12	13
UDP	8	11	18
Valine	9	12	14
Asparagine	9	13	13
UTP	9	16	20
Aspartate	10	12	20
FAD	11	13	15
Proline	12	13	15
AMP	13	17	17
NADP	14	16	18
Propionyl-CoA	14	27	25
Acetyl-CoA	14	17	22
ADP	14	14	19
(iso)-leucine	14	17	22
CTP	14	16	18
NADPH	16	18	42
NADH	17	19	20
Cysteine	24	47	105
GSH	40	57	71
GTP	103	105	106

Table 3.4: (*Continued*)

Metabolite	Storage Temperature		
	-80°C (% RSD)	-20°C (% RSD)	4°C (% RSD)
Glycerol-3-phosphate	1	1	5
Orotate	1	2	11
Lactate	1	9	13
Succinate	1	3	5
(iso)-citrate	3	9	37
Dihydroorotate	3	4	8
PABA	4	6	9
Malate	5	6	12
Glucose	5	9	13
Fumarate	7	8	11
2-Oxoglutarate	7	9	13
Hypoxanthine	12	13	18
Oxaloacetate	13	12	42
PEP	13	16	21
DHAP	16	20	26
Carbamoyl phosphate	33	39	71

3.3.5. Reproducibility studies

The reproducibility of the method for metabolite mixtures, containing all 58 metabolites including internal standards at a specified concentration, was evaluated by measuring the RSD between LC-MS/MS runs, both within and between days. Intra-day reproducibility was determined by performing three repeat runs of LC-MS/MS on Day1. The analysis of Intra-day reproducibility showed that the RSD was less than 15% for ~90% of the metabolites selected for the method (Figure 3.5). In contrast, inter-day reproducibility was determined by conducting nine repeat runs of the LC-MS/MS including the intra-day data. The analysis of inter-day reproducibility showed that the RSD was less than 15% for ~75% of the metabolites targeted in the method (Figure 3.5). Nonetheless, an RSD of less than 25% was found for ~16% of the metabolites that have been analysed for inter-day reproducibility including acetyl-CoA, ADP, cysteine, GSH, NADH, NADP, NADPH, oxaloacetate and propionyl-CoA (Table 3.5). Therefore, this highlights that the effect seen in the %RSD for inter-day reproducibility was perhaps due to a stability factor for the some of the metabolites. Overall, the analysis and findings described signifying that this developed metabolomics method is reproducible.

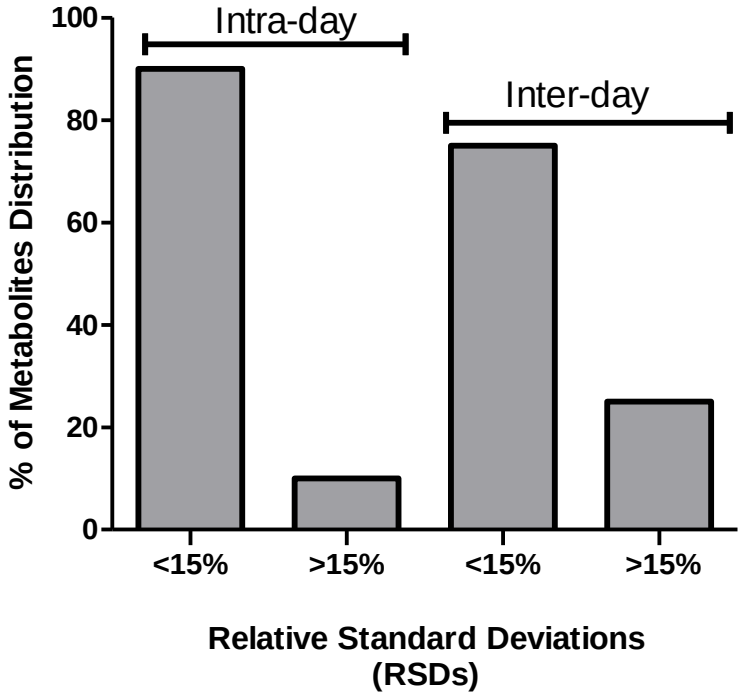

Figure 3.5: Histogram of the distribution of relative standard deviation (RSD) for metabolites investigated in intra-day and inter-day reproducibility studies.

Histogram showed that that ~90% and ~75% of the metabolites had an RSD of less than 15% in intra-day and inter-day reproducibility studies, respectively. In contrast, ~10% and ~25% of the metabolites had an RSD of greater than 15% in intra-day and inter-day reproducibility studies, respectively.

Table 3.5: Intra-day and inter-day reproducibility studies for authentic metabolite standards

Metabolite	Intra-day %RSD (n=3)	Inter-day %RSD (n=9)	Metabolite	Intra-day %RSD (n=3)	Inter-day %RSD (n=9)
(iso)-citrate	13	12	**Hypoxanthine**	12	14
(iso)-leucine	4	8	**Lactate**	10	14
2-Oxoglutarate	14	14	**Lysine**	11	15
Acetyl-CoA	2	22	**Malate**	6	14
ADP	2	16	**Methionine**	2	2
Alanine	1	9	**NAD**	4	12
AMP	1	15	**NADH**	2	16
Arginine	2	13	**NADP**	1	16
Asparagine	4	8	**NADPH**	3	18
Aspartate	3	14	**Ornithine**	2	9
ATP	135	151	**Orotate**	9	12
Carbamoyl phosphate	8	15	**Oxaloacetate**	13	21
Carbamoyl-l-aspartate	3	15	**PABA**	11	15
Citrulline	2	3	**PEP**	15	13
CTP	88	82	**Phenylalanine**	3	9
Cysteine	11	22	**Proline**	4	14
Glucose	14	11	**Propionyl-CoA**	1	21
DHAP	12	14	**Serine**	6	8
Dihydroorotate	13	9	**Succinate**	10	14
FAD	1	15	**Succinyl-CoA**	87	88
Fumarate	11	13	**Threonine**	4	12
G-3-P	13	11	**Tryptophan**	2	13
Glutamate	5	12	**TTP**	86	80
Glutamine	1	10	**Tyrosine**	3	5
GSH	13	16	**UDP**	4	15
GSSG	4	15	**UMP**	2	15
GTP	90	201	**UTP**	87	78
Histidine	2	6	**Valine**	3	11

3.3.6. Linearity, LOD and calibration curve accuracy

Standard calibration curves were generated over sixteen serially diluted concentration points for each metabolite. One example of a standard calibration curve for dihydroorotate is shown in Figure 3.6. The remaining standard calibration curves for other metabolites are shown in Appendix (II, Figures 59 – 76). Signal saturation was observed for several metabolite points at higher concentrations resulting in a non-linear calibration curve. Therefore, points with signal saturation were omitted from linearity analysis as shown in the dihydroorotate standard calibration curve (Figure 3.6). The standard calibration curves for all metabolite standards were satisfactory with regression coefficients R^2 better than 0.98 of area ratio against metabolite concentration, signifying that the method is linear for all the metabolites (Table 3.6) (Appendix II, Figures 59 – 77). Three levels of authentic QC standards (high, medium and low) were prepared (section 3.2.3.1) and used to evaluate the calibration curve accuracy. The results showed that the accuracy of metabolite standard calibration curves determined by LQC was satisfactory (80-120%) for ~91% of the calibration curves. The accuracy of the metabolites standard calibration curve determined by MQC and HQC was also satisfactory (80-120%) accounting for ~99% of the calibration curves (Figure 3.8).

The linearity range for each metabolite was also determined with the lower limit always being the limit of detection (LOD) (Table 3.6). The results of linearity range and LOD for each metabolite are summarized in Table 3.6. The distribution of LOD among all metabolites was shown in (Figure 3.7). Over 65% and 15% of the metabolites targeted in this method showed a LOD of 1-50 nM and 51-100 nM, respectively, indicating the sensitivity of the present method (Figure 3.7).

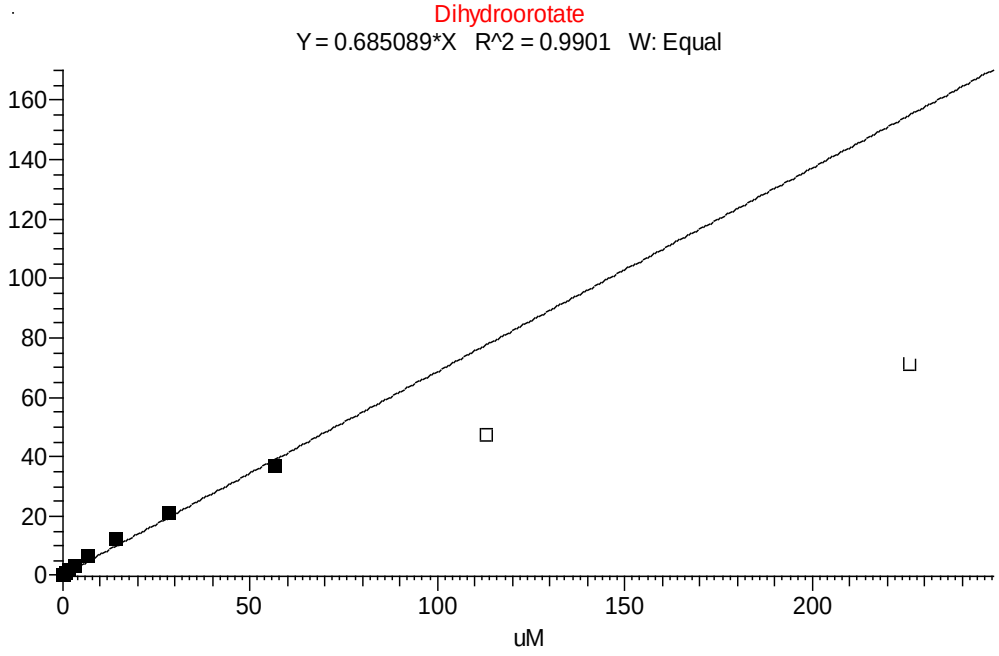

Figure 3.6: Standard calibration curve for dihydroorotate showed $R^2 > 0.99$.
The line of best fit the calibration curve was generated using equal weighted linear regression as the mathematical model of best fit. Dihydroorotate concentration in experimental parasite samples was calculated from the resulting area ratio and the regression equation of the calibration curve.

Table 3.6: Regression coefficients R^2, linearity range and limit of detection (LOD) for metabolites targeted in LC-MS/MS method

Metabolite	R^2	Linear Range (uM)	LOD (nM)	Metabolite	R^2	Linear Range (uM)	LOD (nM)
Propionyl-CoA	0.99	0.003 – 108.41	3	**AMP**	0.99	0.025 – 102.86	25
Tryptophan	0.98	0.005 – 174.87	5	**NAD**	0.99	0.026 – 53.83	26
Phenylalanine	0.99	0.006 – 216.2	6	**UMP**	0.98	0.026 – 110.17	26
Glucose	0.99	0.006 – 198.25	6	**GSH**	0.98	0.028 – 116.21	28
Citrulline	0.99	0.006 – 203.86	6	**GSSG**	0.98	0.028 – 58.3	28
Tyrosine	0.99	0.006 – 197.11	6	**2-Oxoglutarate**	0.99	0.029 – 244.45	29
G-3-P	0.99	0.006 – 207.55	6	**Valine**	0.99	0.037 – 304.86	37
(iso)-citrate	0.99	0.006 – 93	6	**UDP**	0.99	0.042 – 88.37	42
Methionine	0.99	0.007 – 239.36	7	**NADP**	0.99	0.047 – 48.04	47
Histidine	0.98	0.007 – 230.19	7	**Succinyl-CoA**	0.98	0.049 – 102.91	49
Dihydroorotate	0.99	0.007 – 56.47	7	**Hypoxanthine**	0.99	0.063 – 262.61	63
Lysine	0.99	0.007 – 244.3	7	**GTP**	0.99	0.066 – 68.26	66
Orotate	0.98	0.007 – 57.2	7	**CTP**	0.99	0.072 – 73.92	72
Glutamate	0.99	0.007 – 242.74	7	**UTP**	0.98	0.072 – 73.77	72
Acetyl-CoA	0.99	0.007 – 220.58	7	**Proline**	0.99	0.074 – 310.21	74
Ornithine	0.99	0.008 – 270.24	8	**Alanine**	0.99	0.096 – 400.87	96
Aspartate	0.99	0.008 – 268.32	8	**NADPH**	0.99	0.096 – 47.9	96
Malate	0.99	0.008 – 266.35	8	**Carbamoyl-l-aspartate**	0.99	0.097 – 202.78	97
Succinate	0.99	0.009 – 302.44	9	**NADH**	0.99	0.107 – 53.67	107
FAD	0.99	0.011 – 45.46	11	**PEP**	0.99	0.206 – 212.53	206
Glutamine	0.99	0.015 – 244.38	15	**TTP**	0.99	0.578 – 74.07	578
(iso)-leucine	0.98	0.016 – 272.27	16	**Fumarate**	0.98	0.615 – 307.69	615
Asparagine	0.98	0.016 – 270.32	16	**Serine**	0.99	0.68 – 339.84	680
ATP	0.98	0.017 – 70.42	17	**DHAP**	0.99	0.84 – 420.17	840
Threonine	0.99	0.018 – 299.82	18	**Cysteine**	0.98	1.179 – 589.73	1179
ADP	0.99	0.020 – 83.6	20	**Oxaloacetate**	0.98	5.4 – 2704.14	5400
Lactate	0.99	0.024 – 793.03	24	**Carbamoyl phosphate**	0.98	7.59 – 3799.39	7590
Arginine	0.99	0.025 – 205.02	25	**PABA**	0.98	8.151 – 260.42	8151

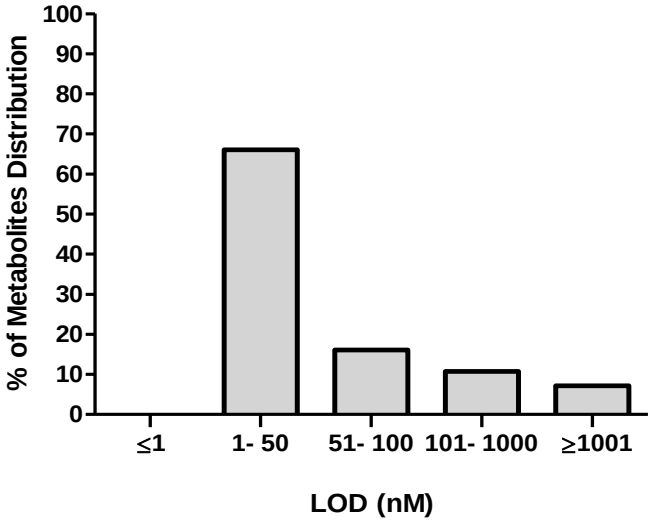

Figure 3.7: Histogram of the distribution of limit of detection (LOD) for the metabolites investigated.

Histogram shows that ~65% and ~15% of metabolites targeted in the present LC-MS/MS method have their LOD between 1-50nM and 51-100nM, respectively. The remaining ~15% of the targeted metabolites have their LOD greater than 101nM reaching sometimes up to uM and mM concentrations depending on each individual metabolite.

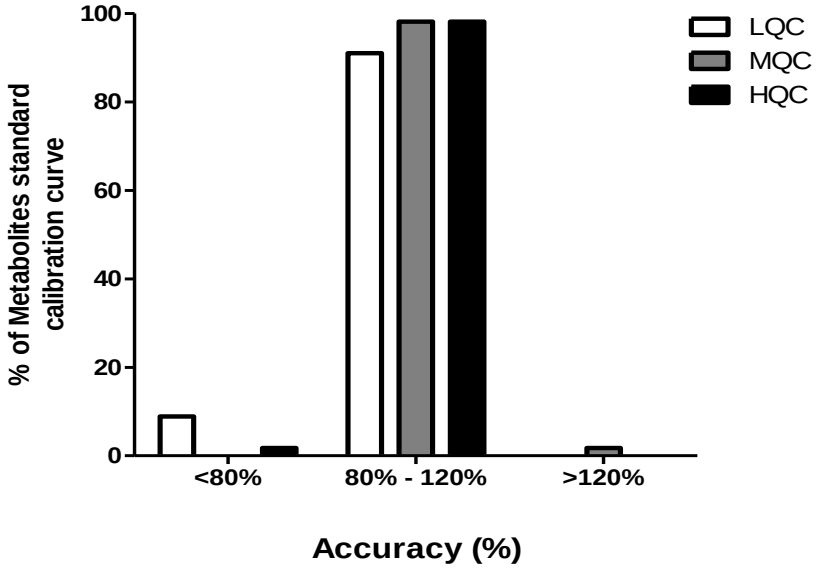

Figure 3.8: Histogram of the distribution of standard curve accuracy (%) as determined by three levels of QC (low, medium and high).

The histogram shows that ~91% of the metabolite standard calibration curves obtained a satisfactory accuracy between 80-120% for LQC. ~99% of metabolite standard calibration curves obtained a satisfactory accuracy between 80-120% for both MQC and HQC.

Table 3.7: Accuracy of standard calibration curves of LC-MS/MS targeted metabolomics as determined by three levels (low, medium and high) of authentic QCs

Metabolite	LQC				MQC				HQC			
	Nominal Conc. (uM)	Mean conc. (uM)	±SD	Accuracy (%)	Nominal Conc. (uM)	Mean conc. (uM)	±SD	Accuracy (%)	Nominal Conc. (uM)	Mean conc.	±SD	Accuracy (%)
Alanine	4.01	3.20	0.40	81.88	40.09	35.78	1.62	89.24	400.9	353.30	14.88	88.13
Asparagine	2.7	3.04	0.15	112.63	27.03	31.54	1.93	116.67	270.3	270.95	31.29	100.23
Aspartate	2.68	3.18	0.01	118.82	26.83	31.12	1.40	115.98	268.3	221.94	31.90	82.71
Glutamine	2.44	2.29	0.23	93.73	24.44	24.68	3.24	100.98	244.4	227.26	27.91	92.99
Glutamate	2.43	2.18	0.16	89.52	24.27	20.33	0.83	83.78	242.7	202.44	4.68	83.40
Arginine	2.05	2.25	0.18	109.90	20.5	21.57	2.21	105.24	205	173.90	25.50	84.82
Proline	3.1	2.73	0.32	88.03	31.02	25.62	0.81	82.61	310.2	284.64	15.03	91.76
Serine	3.4	3.51	0.43	103.32	33.98	39.63	1.22	116.62	339.8	309.98	20.88	91.21
Valine	3.05	2.91	0.43	95.41	30.49	29.12	3.66	95.50	304.9	252.91	4.90	82.96
Threonine	3	3.20	0.14	106.51	29.98	33.89	0.70	113.03	299.8	277.37	16.70	92.51
Cysteine	5.9	ND	ND	ND	58.97	49.95	3.57	84.70	589.7	613.47	65.31	104.03
(iso)-leucine	2.72	2.77	0.34	101.79	27.23	24.98	0.19	91.73	272.3	229.64	19.44	84.34
Lysine	2.44	2.00	0.18	81.82	24.43	26.96	0.09	110.35	244.3	203.32	3.30	83.22
Methionine	2.39	1.98	0.02	82.96	23.94	21.00	2.51	87.73	239.4	191.67	0.26	80.08
Histidine	2.3	2.68	0.04	116.72	23.02	26.20	1.22	113.80	230.2	210.38	15.38	91.39
Phenylalanine	2.16	2.22	0.06	102.72	21.62	21.62	0.75	100.00	216.2	195.32	6.77	90.34
Tryptophan	1.75	1.56	0.14	89.29	17.49	16.07	0.39	91.88	174.9	163.00	20.69	93.21
Tyrosine	1.97	1.46	0.16	73.97	19.71	23.25	1.32	117.97	197.1	173.81	13.53	88.18
Ornithine	2.7	2.84	0.27	105.06	27.02	25.46	2.56	94.23	270.2	258.95	56.61	95.82
Citrulline	2.04	2.01	0.25	98.30	20.39	23.13	2.52	113.46	203.9	210.17	19.19	103.09
NAD	0.54	0.48	0.05	88.23	5.38	4.91	0.12	91.27	53.8	51.97	7.46	96.55
NADH	0.54	0.47	0.04	86.17	5.37	5.03	0.19	93.74	53.7	46.42	1.56	86.48

Table 3.7: (*Continued*)

Metabolite	LQC				MQC				HQC			
	Nominal Conc. (uM)	Mean conc. (uM)	±SD	Accuracy (%)	Nominal Conc. (uM)	Mean conc. (uM)	±SD	Accuracy (%)	Nominal Conc. (uM)	Mean conc.	±SD	Accuracy (%)
GSH	1.16	1.09	0.14	94.30	11.62	10.17	0.79	87.56	116.2	121.86	17.42	104.86
GSSG	0.58	0.48	0.01	82.87	5.83	5.58	0.17	95.78	58.3	60.28	9.52	103.39
NADP	0.48	0.39	0.03	81.13	4.8	3.90	0.05	81.21	48	38.77	4.56	80.70
NADPH	0.48	0.44	0.06	90.76	4.79	4.12	0.20	85.99	47.9	40.54	4.61	84.61
FAD	0.45	0.44	0.06	98.75	4.55	4.14	0.25	90.92	45.5	42.41	7.64	93.28
UMP	1.1	1.07	0.04	97.68	11.02	9.58	0.51	86.94	110.2	92.50	4.99	83.96
UDP	0.88	0.82	0.19	93.38	8.84	7.70	2.26	87.05	88.4	80.96	6.35	91.61
UTP	0.74	0.57	0.08	76.41	7.38	6.92	1.02	93.83	73.8	65.51	3.93	88.80
CTP	0.74	0.67	0.27	90.67	7.39	6.20	0.71	83.94	73.9	68.09	8.49	92.12
TTP	0.74	0.63	0.13	85.25	7.41	6.15	0.80	82.98	74.1	68.16	3.01	92.02
AMP	1.03	1.03	0.08	100.33	10.29	10.16	1.19	98.75	102.9	104.64	9.10	101.73
ADP	0.84	0.75	0.17	88.96	8.36	7.01	0.42	83.88	83.6	76.17	4.17	91.12
ATP	0.7	0.60	0.00	85.30	7.04	5.93	0.26	84.18	70.4	70.99	10.48	100.80
GTP	0.68	0.70	0.29	103.00	6.83	6.83	2.31	100.00	68.3	80.11	22.26	117.37
Carbamoyl-l-Aspartate	2.03	1.95	0.25	96.01	20.28	20.36	2.97	100.39	202.8	186.70	8.52	92.07
Acetyl-CoA	2.21	1.96	0.09	88.60	22.06	20.77	1.23	94.14	220.6	193.72	4.27	87.75
Succinyl-CoA	1.03	ND	ND	ND	10.29	12.53	5.10	121.73	102.9	100.09	17.72	97.26
Propionyl-CoA	1.08	0.96	0.05	88.97	10.84	8.90	0.34	82.13	108.4	101.39	6.50	93.53
Glucose	1.98	1.76	0.42	89.00	19.82	17.97	2.16	90.67	198.2	180.81	4.17	91.20
Fumarate	3.08	3.26	0.39	105.95	30.77	29.69	7.84	96.48	307.7	317.85	39.39	103.30
Succinate	3.02	3.26	0.86	107.96	30.24	28.52	6.09	94.32	302.4	304.06	8.83	100.54
Malate	2.66	2.30	0.08	86.47	26.64	30.73	4.40	115.36	266.4	291.07	56.37	109.28

Table 3.7: (*Continued*)

Metabolite	LQC				MQC				HQC			
	Nominal Conc. (uM)	Mean conc. (uM)	±SD	Accuracy (%)	Nominal Conc. (uM)	Mean conc. (uM)	±SD	Accuracy (%)	Nominal Conc. (uM)	Mean conc.	±SD	Accuracy (%)
2-Oxoglutarate	2.44	2.75	0.13	112.80	24.45	26.27	1.53	107.45	244.5	271.48	9.60	111.06
(iso)-Citrate	1.86	1.56	0.62	83.92	18.6	20.32	3.46	109.23	186	162.90	38.95	87.58
PEP	2.13	2.51	0.04	118.03	21.25	20.07	4.50	94.44	212.5	198.17	12.47	93.24
PABA	2.6	1.89	1.19	72.55	26.04	26.22	1.70	100.69	260.4	286.21	30.46	109.90
G-3-P	2.08	2.21	0.31	106.25	20.76	24.05	2.23	115.86	207.6	213.59	16.52	102.91
Hypoxanthine	2.63	2.43	0.38	92.30	26.26	26.87	3.36	102.31	262.6	308.55	111.09	117.49
Orotate	2.29	2.08	0.50	90.65	22.88	21.69	2.88	94.79	228.8	225.95	43.81	98.75
Dihydroorotate	2.26	2.23	0.16	98.61	22.59	24.45	2.03	108.23	225.9	185.08	10.21	81.94
Lactate	7.93	9.20	1.69	115.98	79.3	70.83	4.81	89.32	793	705.64	81.44	88.98
DHAP	4.20	4.70	1.56	111.90	42.02	34.73	15.96	82.64	420.20	494.80	20.91	117.76
Oxaloacetate	27.04	27.51	4.47	101.74	270.42	238.00	49.55	88.01	2704.20	2521.45	624.88	93.24
Carbamyl-P	37.99	31.01	4.75	81.62	379.94	312.38	60.53	82.22	3799.40	2858.47	397.91	75.23

Abbreviations: ND, Not Determined.

3.4. Discussion

The main objective in this metabolomics approach was to determine the differences between the complete or part of the parasite cell metabolome. Although non-targeted metabolomics approaches have resulted in new insights into the functioning of biological systems, development of a sensitive, quantitative and reproducible comprehensive method is extremely challenging (De Vos et al., 2007). Therefore, a targeted metabolomics approach was selected for the study of *P. falciparum* in this thesis. The primary challenge in developing this analytical targeted metabolomics approach was balancing a comprehensive coverage of *P. falciparum* metabolome with high sensitivity and reliable quantification. Thus, an extensive method optimization and validation was required in order to determine the differences in the metabolites between parasite samples that have been collected hourly as described in the subsequent chapters. Triple-quadrupole LC-MS/MS was showed here to be used for the detection and quantification of numerous known metabolites in parallel by scanning repeatedly through different SRM events. This LC-MS/MS analytical method was successfully developed for targeted metabolomics enabling the effective detection and relative quantification of a broad range of 56 metabolites that account for ~10% of the *P. falciparum* metabolome. These metabolites are associated with several different metabolic pathways including glycolysis, TCA cycle, pyrimidine biosynthesis, purine salvage, amino acids metabolism and bioenergetics/redox couples. This targeted metabolomics approach was in accordance and similar to previous metabolomic approaches in terms of performance and reliability (Bajad et al., 2006, Rabinowitz and Kimball, 2007, Lu et al., 2008, Lu et al., 2006). The analytical performance of the present method was validated for selectivity, carryover, metabolite recovery, metabolite stability, reproducibility, linearity and limit of detection (LOD).

The method was found to have a high selectivity that enables a sensitive and specific detection for the pre-determined metabolite. This was showed by the presence of no interference or carryover peaks from other endogenous metabolites as was observed at the retention time for dihydroorotate in the blank sample. Therefore, the present LC-MS/MS method advantageously ensured the identification of each metabolite not only based on the metabolite's molecular weight or precursor mass but also on its retention time and fragmentation properties. In addition, an external and internal calibration

standard was used for reliable quantification of the metabolites. Calibration curves for all metabolites targeted in this study were fitted by linear regression with R^2 values better than 0.98 for all metabolites representing satisfactory standard calibration linearity. The accuracy of the calibration curves was determined by three levels of QC (high, medium and low) and it showed that a majority (~91% for LQC and ~99% for MQC and HQC) of metabolites obtained a satisfactory standard calibration curve with accuracy between 80-120%. The LOD of each metabolite was determined and it was found that the current method was very sensitive detecting more than 75% of the targeted metabolites in the nanomolar range, specifically, a range between 1–100 nM. The recovery (%) was determined for all metabolites including the internal standards. Satisfactory recovery (70% - 120%) was effectively achieved for most (~85%) of the metabolites targeted including the internal standards. Few (~15%) of the targeted metabolites did not display a satisfactory recovery due to either ion suppression or enhancement as observed in low and high recoveries, respectively. In addition, the present method of performance reproducibility was investigated given generally a respectable RSD of less than 15% for most of the metabolites being investigated both intra- and inter- days. With regard to metabolite stability, it was noted that different storage temperatures had a considerable effect on metabolite stability. Therefore, it was observed that the appropriate storage temperature for less than a month period is -80 ºC which led to more than ~88% of the metabolites being stable. Unstable metabolites, including NADPH, NADH, cysteine, GSH, DHAP and carbamoyl phosphate were prepared from fresh solid stocks for every LC-MS/MS run and all the parasite samples need to be processed analytically in a period of less than a month. Overall, the validation showed that the LC-MS/MS targeted metabolomics had high selectivity, sensitivity, satisfactory recovery, efficient performance reproducibility and excellent linearity values for all metabolites.

In regards to the limitations of this chapter, although this developed method had an efficient chromatographic separation for all the metabolites, the total running time of 45.0 min per sample is considered long particularly for large batches of samples. This might have had an effect on some metabolite sample stability. In addition, QC samples were prepared from authentic metabolite standards for the purpose of checking the accuracy of the calibration curve. However, it should be noted that QC samples prepared from the cell extract will give a better idea about the influence of matrix

interferences with the different levels of QC (Koek et al., 2006, Koek et al., 2011). In addition, the internal standards (IS) for positive and negative mode were chromatographically eluted during the first ~13.0 min of the running time. Nonetheless, it is important to include more than one IS for each ionization mode that can be eluted in the beginning, middle and end of the chromatograph running time. In addition, for a highly sensitive quantitative analytical approach, the most suitable IS is the isotope-labelled form of each metabolite as it behaves identically to the metabolite in the sample preparation, separation and ionization processes (Bennett et al., 2008). However, isotope-labelled metabolites are very expensive and are not available for all metabolites. In addition, one major drawback of the present method was the inability of the LC-MS/MS approach to distinguish between metabolite isomers such as citrate and leucine because it is mainly based on an MRM scan. Therefore, citrate and leucine were written in this thesis as (iso)-citrate and (iso)-leucine. It is therefore recommended that future studies should be carried using a mass spectrometer that can deliver a high-resolution accurate mass detection such as the "Exactive" Orbitrap mass spectrometry (Lu et al., 2010).

Moreover, this LC-MS/MS method seems to be robust and generally applicable to samples from various biological sources as a PhD colleague was using the same approach for investigation into the *Mycobacterium tuberculosis* (MTB) metabolome. It was also shown that this method can be expanded for more metabolites than those that were targeted as seen in the metabolomics of MTB (personal communication). This method appears also a promising tool for investigating the *P. falciparum* metabolome and the drug mode of actions as will be demonstrated in the subsequent chapters.

CHAPTER 4

Targeted Metabolomics of *Plasmodium falciparum* Infected and Uninfected Red Blood Cells

4.1. Introduction

The main objective of this chapter was to investigate the general metabolic profiles between uninfected human red blood cell (RBC) and those infected by *P. falciparum* (iRBC) using the developed LC-MS/MS targeted metabolomics approach described previously (Chapter 3).

It is well known that the primary physiological function of human RBC is the carriage of oxygen (O_2) and carbon dioxide (CO_2) between the lungs and tissues of the body, as well as maintaining homeostasis by pH buffering (Surgenor, 1974). One of the known features of human RBC is that it is non-nucleated, and therefore has evolved specific metabolic functions for its survival during its three to fourth month life span (Surgenor, 1974, Walsh, 1998). This survival of RBC uses several metabolic pathways in order to maintain its haemoglobin, biconcave shape and the electrolyte concentrations (Prankerd, 1955). These pathways are involved in the production of the necessary cofactors such as ATP, NADPH, and NADH by energy and redox metabolisms thus maintaining RBC osmotic balance, electro-neutrality and fighting oxidative stresses (Joshi and Palsson, 1989, Wiback and Palsson, 2002, Bossi and Giardina, 1996). There are four known basic metabolic pathways of RBC metabolism namely; anaerobic glycolysis, the pentose phosphate shunt (PPS), adenosine nucleotide metabolism and the Rapoport-Leubering shunt (Wiback and Palsson, 2002, Walsh, 1998). The absence of a mitochondria in mature human RBC means that energy in the form of ATP is generated exclusively from anaerobic glycolysis (Schweiger, 1962). This suggests that glucose must always be freely available for the synthesis of ATP (Prankerd, 1955). The other two important cofactors that come from this glycolytic pathway are NADH and 2,3-diphosphosglycerate (2,3-DPG). NADH is an essential cofactor for the enzyme methemoglobin reductase, which maintains heme iron in the ferrous (Fe^{2+}) state, which is a reaction necessary for the ligation of molecular oxygen by the haemoglobin molecule (Zerez et al., 1990). In addition, mature human RBC contain a considerable large amount (~5.0 mM) of 2,3-DPG, the function of which is believed to regulate the oxygen affinity of haemoglobin, generated through the Rapoport-Leubering shunt (Nikinmaa, 1990). Moreover, mature human RBC's which lose their nucleus and other organelles during development make these cells unable to synthesize RNA, protein, lipid, and purines (Bishop, 1964). Walsh et al., (1998) wrote that 10% of the carbon flow could be diverted to the PPS pathway producing two important metabolites;

NADPH for maintaining intercellular store of GSH, an oxidative damage protector, synthesized from the amino acids cysteine, glutamate and glycine, and ribulose 5-phosphate (R5P) for linking the pathway with nucleotide metabolism. Furthermore, nucleotide metabolism acts primarily to regenerate intracellular store of ATP which go through a normal turnover into adenosine and inosine (Walsh, 1998). However, human RBC do not synthesize adenosine de novo but rather takes it up from plasma and synthesizes AMP, ADP and ATP (Walsh, 1998). In general, it appears that RBC's metabolism has been comprehensively examined and this has made it possible to be simulated by virtual methods using comprehensive kinetic models (Joshi and Palsson, 1989, Jamshidi et al., 2001).

In stark contrast to uninfected RBC glucose consumption rate (~5 µmol glucose/24 h/10^9 RBCs), *P. falciparum*-iRBC is shown to rely on anaerobic glycolysis but with an estimation of 50-100 times increase in the glucose consumption rate particularly at *P. falciparum's* active stages to include trophozoite and schizont, both of which are metabolically demanding (Roth Jr, 1990). Metabolic changes that occur in RBC upon *Plasmodium* parasite invasion drastically diverge the metabolic requirements of the combined *Plasmodium*/RBC system which necessities finding energy source for growth and proliferation every 48 h (Roth, 1987, Sherman, 1979, Olszewski and Llinas, 2011). Within this time frame, parasite growth increases significantly in size and numbers during the asexual stages which demand the system to synthesize enough RNA, protein, and DNA for 12-24 new progeny (merozoites) which are subsequently released and reinvade fresh RBC (Moulder, 1948). *P. falciparum* also make major alterations to RBC to allow the direct influx and efflux of specific metabolites (e.g. glucose) using new permeability pathways (NPPs) (Kirk et al., 2005). In addition, for protein synthesis, *P. falciparum* relies principally on amino acids generated from haemoglobin degradation in the acidic digestive vacuole as well as through uptake from the extracellular space (Francis et al., 1997, Gardner et al., 2002). Furthermore, the production of energy in *Plasmodium* is a result of the glucose fermentation process consequentially leading to the accumulation and secretion of lactate and pyruvate despite the parasite having mitochondria (Sherman, 1998, Roth et al., 1988). This calls into questioning the role of the parasite mitochondrion in energy metabolism. The role of mitochondrial metabolism is examined further in the subsequent chapters (5 and 6). Similarly, there are some unresolved questions concerning apicoplast metabolism.

Ralph *et al* 2004 described the apicoplast, as a plastid-like organelle, that plays a role in fatty acid, heme, and isoprenoid biosynthesis (Ralph et al., 2004). This discovery has led to several drug discovery projects targeting plastid metabolism, however the precise role in *P. falciparum's* survival is still debated (Lim and McFadden, 2010).

The above mentioned overview shows the metabolic functions between *P. falciparum* and it's host's RBC, indicating the metabolic complexity in the parasite in comparison to the RBC. Therefore, understanding the biological differences in metabolism between both invader and host is essential for drug development as it reveals mode of action (MoA). Metabolomics offers an attractive platform for the study and understanding of the biology of *P. falciparum*-iRBC as well as RBC. The usefulness and application of this approach in malaria research was explained in depth previously (Chapter 1). Generally, metabolomics technologies and strategies (Kell, 2004, Kell, 2006, Goodacre et al., 2004, Moco et al., 2007) have iteratively improved the present understanding of systems biology of numerous model organisms. These include Archeae (Trauger et al., 2008), bacteria (Rabinowitz, 2007), yeast (Brauer et al., 2006), plants (Fiehn, 2006, Lisec et al., 2008, Beale and Sussman, 2011), insect (Pedersen et al., 2008, Kamleh et al., 2008) rodent(Sun et al., 2007), and human cell culture (Khoo and Al-Rubeai, 2007). Kirk's group was able to determine the intracellular concentrations of a range of metabolites using NMR metabolomics in saponin-permeabilized mature trophozite stage of *P.falciparum* (Teng et al., 2009). Recently, Llinas's laboratory was the first to apply metabolomics approach in 48 h developmental cycle of *P. falciparum*. This demonstrated the general variation of metabolite levels by the parasite, with numerous metabolite levels changing in each phase of the developmental cycle (Olszewski et al., 2009). On this basis, the study of this chapter was carried out primarily to determine and investigate the general metabolomics modulation of *P. falciparum*-iRBC compared to that of RBC. Therefore, this study was conducted on enriched culture of trophozoite-staged *P. falciparum*-iRBC because of its high metabolic rate in limited time (i.e. incubation time of 7 h).

4.2. Materials and Methods

4.2.1. High Gradient Magnetic separation (HGMS) for trophozoite-stage parasites enrichment

HGMS offers a means to concentrate trophozoites, schizonts and gametocytes of *P. falciparum* from suspensions, by virtue of the para-magnetic properties of these later stages. Throughout the metabolomic experiments described in this thesis, the enrichment of trophozoite-iRBC parasites was carried out using a VarioMACS™ separation unit (Miltenyi Biotec, UK), that is separating the trophozoite-stage iRBC of the parasite from early rings and uninfected RBC. However, an RBC experiment in this chapter also went through the magnetic separation unit in order to limit any variation in experiments between RBC as a control and iRBC.

The VarioMACS™ column matrix creates a high-gradient magnetic field, which attracts the iron in the trophozoite haemozoin (Ribaut et al., 2008). Poorly, but successful HGMS of late-stage iRBC from malaria parasite cultures was first described in 1981 (Paul et al., 1981). Recently, the commercially polymer coated HGMS columns have demonstrated to provide a better improved purified late-stage malaria parasite (Trang et al., 2004, Ribaut et al., 2008). However, it has been noted that sorbitol-pretreatment of the malaria parasite cultures was essential prior to carry out the HGMS procedure (Ahn et al., 2008). Therefore for the purpose of this work, the parasite cultures were synchronized with sorbitol as described earlier (chapter 2 section 2.2.7.1) for at least two cycles before purifying using the VarioMACS™ column.

The enrichment of trophozoite-stage *P. falciparum* parasites was carried out as follows: VarioMACS™ separation unit was place inside a class II Enviar laminar flow cabinet which was decontaminated with 70% ethanol. VarioMACS™ column was then sterilized by washing once with 100% ethanol. The column was then placed between the pole magnet and equilibrated for 5 min. Afterwards, the column was pre-equilibrated and filled with PBG buffer solution (1x phosphate-buffered saline (PBS), 4% w/v bovine serum albumin (BSA), 20 mM Glucose) (section 4.2.1.1) by gently pushing the PBG buffer solution through the syringe to the column in upright position to evacuate air by upward displacement. A 20 G/1-inch injection needle was thereafter connected to the stopcock subsequently after removing remaining air bubbles by gentle

finger tapping. After opening the stopcock, PBG buffer solution was then allowed to flow through the column in downward displacement.

Each metabolomic experiment replicate consisted of 15 - 20 flasks (~750 - 1000 ml) of synchronized parasite culture. Each parasite culture flask was contained 8-10% parasitaemia, >98% trophozoite-stage, which was harvested at 2500 rpm for 5 min at room temperature. The pelleted cells from each culture flask were suspended in 10 ml of PBG buffer solution. This suspension of cells was then applied on the top of the column. Without interrupting the flow or letting the column to dry, the column was rinsed with 50 ml of PBG buffer solution until the effluent was clear (no longer contained red blood cells). After this, the stopcock was closed and the column was removed from the magnet. The needle was removed from the stopcock and the column was flushed with 10-15 ml of PBG buffer solution to elute the trophozoite-stage parasites until the eluate was clear (no longer contained trophozoite). The eluate contained isolated trophozoite-staged parasite was collected in 50 ml centrifuge tube. This process was repeated again for next 14 parasite culture flasks. The pooled eluate was thereafter centrifuged at 2000 rpm for 5 min, washed twice with RPMI-1640 culture media before starting the haemocytometer counting (section 4.2.2) and the metabolomics time points experiment (section 4.2.3).

The ultimate step in enrichment procedure was to clean the column as follows: the column was washed three times with each of the following solutions namely PBG buffer solution, 1% (v/v) Tween 20 (section 4.2.1.2) and distilled water respectively. These washes were followed by a final wash with 100% ethanol. The column was then dried on a vacuum pump for one hour and covered with parafilm ready for next usage.

4.2.1.1. PBG buffer solution preparation

The PBG (1x Phosphate-buffered saline, 4% Bovine serum albumin (BSA), 20 mM Glucose) buffer solution was prepared as follows: a tablet of phosphate-buffered saline (Sigma-aldrich, UK) was dissolved in 200ml of distilled water to get 1x (w/v) physiological saline.4 g of BSA (Sigma-aldrich, UK) was then dissolved in the prepared saline to get 4 % (w/v) BSA. Thereafter, 720.6 mg of glucose (Sigma-aldrich, UK) was added to the above solution and stirred all together. Subsequently, the PBG buffer

solution was sterilized through a sterile bottle top filter unit with a 0.22 μm membrane (Fisher Scientific, UK), labeled, and stored at 4 ^{0}C until required.

4.2.1.2. 1% (v/v) Tween 20 preparation

Tween 20 was purchased from Sigma (Sigma, UK). The preparation of 1% Tween 20 was as follows: 1 ml of Tween 20 was dissolved in 100 ml of distilled water. This prepared 1% (v/v) Tween 20 solution was then labeled, and stored at room temperature until required.

4.2.2. Haemocytometer counting for infected and uninfected red blood cells

A haemocytometer (Bright-Line™ Hemacytometer, Sigma-Aldrich, UK), was used to count the parasite cells. However, the enriched trophozoite-stage parasite and packed RBC were very concentrated and presented in high numbers which made it difficult to count. A 1:50 serial dilution was thus carried out in RPMI-1640 culture media. Haemocytometer is unique in that it has a thick base and uses a special cover-glass which is thick enough to stay flat under the pull of surface tension from the solution in the counting chamber. After the haemocytometer was assembled with its cover-glass, a 15 μl of serially diluted parasites solution was loaded into the loading notch of the haemocytometer (Figure 4.1A). The haemocytometer was set on the light microscope (Zeiss, Germany) ready for counting the parasites. The parasite counting was carried out initially at x10 magnification power to determine the grid and squares area (Figure 4.1B) and then under x40 magnification power to count all the parasites in five random squares (Figure 4.1C). The counted parasites were then averaged and multiplied by 5. This was to calculate the number of parasites in 25 squares. If a 1:50 dilution was used, then the outcome of calculated parasites was multiplied by 50 (dilution factor) and finally multiplied by 10^4. This total gave number of parasites per ml. The equation to carry out the parasites calculation was as follows:

The number of parasites/ml= average of parasites count in five square x number of square counted x dilution factor x 10^4

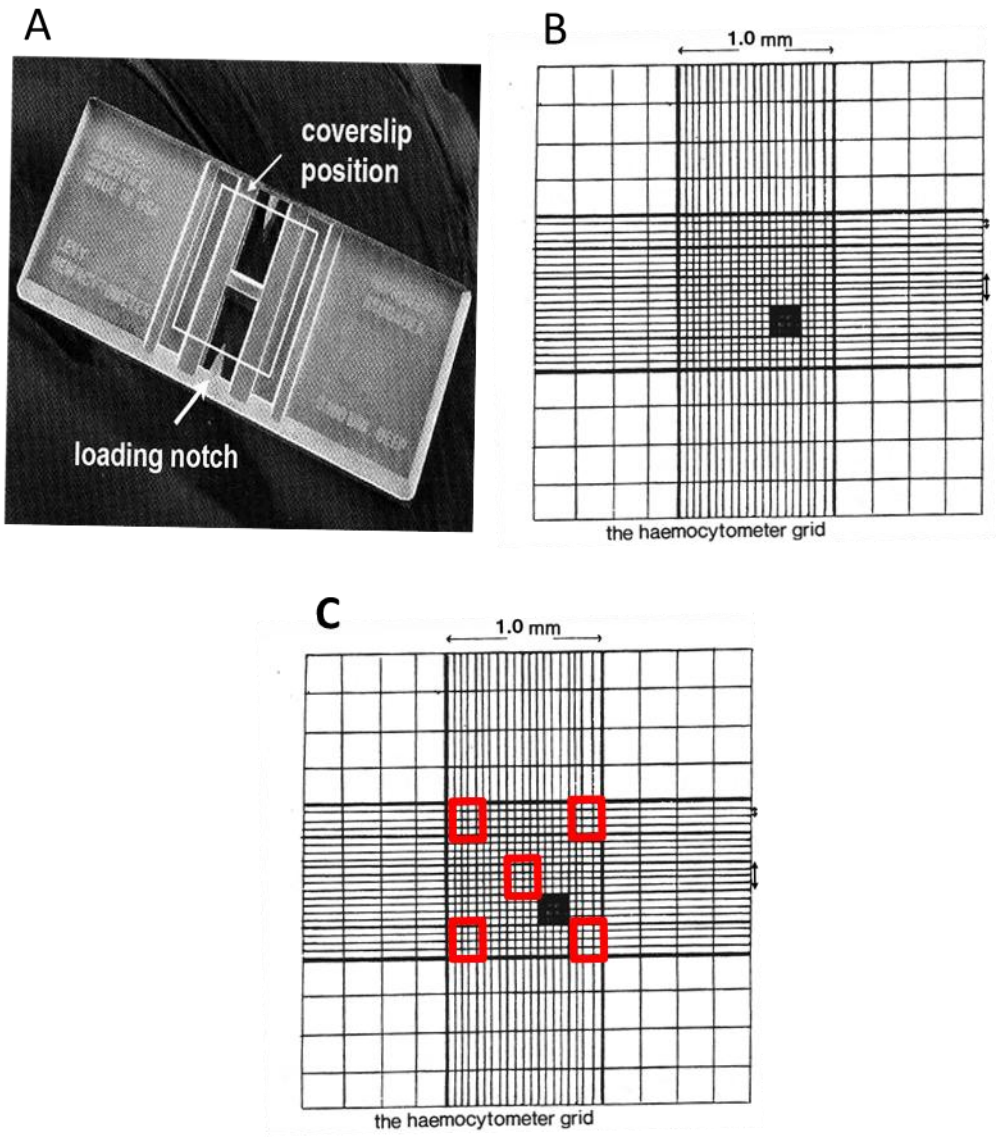

Figure 4.1: Haemocytometer chamber counting.
(A) Haemocytometer showing the loading notch and coverslip position, (B) Haemocytometer gridlines showing under light microscope four corner squares and a middle square, (C) Haemocytometer gridlines showing the five random squares marked in red in the middle square.

4.2.3. Metabolism quenching and metabolite extraction for RBC and iRBC

Briefly at this stage, the enriched trophozoite-stage iRBC and RBC were subjected to a metabolomics experiment where they were incubated in culture media at 37 °C. Subsequently, iRBC and RBC were removed in a time related manner for quenching metabolism and initiating extraction. Metabolites were then extracted, ready for the next stage of LC-MS/MS analysis (section 4.2.4).

The metabolomics experimental protocol that was carried out throughout this thesis, with minor modification in each experimental chapter; was as follows: The enriched trophozoite-stage iRBC and RBC were incubated with RPMI-1640 culture media (R8758, glutamine, and sodium bicarbonate) supplemented with 10% pooled human serum, 25 mM HEPES (pH 7.4) (VWR), 40 μM hypoxanthine (Sigma), and 20 μM gentamicin sulfate (Sigma) at 37 °C under 3% O_2/4% CO_2 in N_2 for 7 h time points course. At predetermined time intervals, one volume of incubated iRBC and RBC (~1 × 10^8 parasites/mL) was directly collected at *t*= 0 h interval for metabolically quenching into three volumes of -20 ºC quenching solvent system [acidic acetonitrile/methanol/water (40:40:20 + 0.1 M formic acid) spiked with internal standards] (chapter 3, section 3.2.2.5). After quenching, the sample was kept at -80 ºC for overnight. The sample was then centrifuged at 4500 rpm for 20 min with a rotor at 4 ºC. The supernatant was carefully transferred into a new tube and kept in ice whereas the cell debris was washed twice with three volumes of extraction solvent system [acetonitrile/methanol/water (40:40:20)] (chapter 3, section 3.2.2.5). All the supernatants for each individual sample were thereafter collected and pooled together into each corresponding sample tube. Afterwards, metabolites extracted sample was concentrated under N_2 gas flow in the fume hood by using the samples concentrator system (Techne sample concentrator, Bibby Scientific Ltd, UK) until the sample was totally dry. The sample was then kept at -80 °C ready for LC-MS/MS analysis.

4.2.4. LC-MS/MS instrumentation

Briefly at this stage, sample preparation including trophozoite-stage iRBC and RBC samples, external standards, authentic QCs, and blanks was carried out in this section aimed at LC-MS/MS. In addition, the chromatographic gradient conditions and mass

spectrometry configurations were set up as described previously in the developed method for LC-MS/MS targeted metabolomics (chapter 3).

4.2.4.1. Samples preparation

The parasite sample preparation was carried out as follows: dried sample was taken out from -80 °C freezer and resuspended in one volume of freshly prepared mobile phase [(20 mM ammonium acetate + 20 mM ammonium hydroxide) in 95:5 water:acetonitrile (pH 9.45)] (chapter 2, section 2.3.4). The resuspended sample was then transferred into an eppendorf tube and spun at high speed (17000 rpm) for 30 min at 4 °C. The supernatant was filtered using phenex-RC filters 0.2 µm into chromacol LC-MS/MS vial. The preparation of external standards, authentic QCs, and blanks was freshly carried out for each metabolomics experiment as described beforehand (chapter 3, section 3.2.3.1).

4.2.4.2. Chromatographic separation

Chromatographic separation was conducted as described earlier (chapter 3, section 3.2.2.4).

.

4.2.4.3. Mass spectrometry configuration

The configuration of mass spectrometry was set up for positive and negative modes as described previously (chapter 3, section 3.2.2.3).

4.2.5. Data treatment and analysis

The independent biological replicates from both RBC and trophozoite-stage iRBC were analyzed and the metabolite concentration was averaged at each time point. Metabolite concentration levels were quantified by applying standard curve using the known concentration of standards for each of the 34 selected reaction monitoring (SRM) because the remaining metabolites mentioned in Chapter 3 were below the limit of detection (LOD) where S/N was below than 3. The signal for each metabolite was defined as the area under the curve (AUC) of the integrated peak. Each metabolite signal was normalized to the signal of the internal standard DL-arabinose (negative mode) or β-alanine (positive mode) in the same sample. All data were expressed as the

normalized levels of metabolite in the sample at a particular time point to the number of cell counted in each experiment. In order to limit the variation in the metabolite concentrations for samples collected at time zero, fold change ratio was determined against time zero as follows: comparative metabolites fold change ratio represents the mean value for each time point in the sample divided by the mean value for the same sample collected at time zero. Data was further refined and plotted with GraphPad Prism 5.0 (GraphPad Software Inc.). The mean of fold change ratio for biological replicates was combined in a dataset file and imported into MetaboAnalyst web-based software (http://www.metaboanalyst.ca) (Xia et al., 2012, Xia et al., 2009), $\log_2$ transformed and analyzed by different metabolomics analysis tools described below.

Principal component analysis (PCA), an unsupervised method, is a type of clustering analysis that reduces the dimensionality and attempts to describe the data in as few components as possible (refer for details in definition to chapter 1, section 1.4.2.3) (Xia et al., 2009, Xia et al., 2012). With PCA, large quantities of data can be displayed graphically in a manner that makes it easy to analyze and recognize metabolic variations between different groups. This is in contrast to partial least square-discriminant analysis (PLS-DA), which is a supervised technique used to detect patterns in the data allowing for the prediction of class (or experimental condition) of the data set (refer for details in definition to chapter 1, section 1.4.2.3) (Xia et al., 2009, Xia et al., 2012). The distinction here is the ability of PLS-DA to classify the data based on a known variable such as time points, or survival.

Generally, the $\log_2$ normalized dataset was subjected to the analysis of PCA and PLS-DA and viewed as two and three dimensional score plots which followed thereafter by generating the loading plots. Metabolome profile analysis was then carried out based on a colouration method and visualized as a heat map.

4.3. Results

Metabolomics experiments were conducted on enriched trophozoite-stage iRBC and RBC as a control. The 56 metabolites targeted for this study were selected on the basis that they were the predominant metabolites involved in the core metabolism of the parasite as well as RBC. These metabolites are associated in the metabolic pathways including glycolysis, TCA cycle, pyrimidine de novo synthesis, purine salvage, amino acids metabolism and bioenergetics/redox couples. However, only 34 metabolites were detected and quantified using the metabolomics approach described previously (chapter 3) whilst the remaining 22 metabolites were below LOD. The dynamic changes of metabolites from purified RBC and trophozoite stage of iRBC were monitored in a time related manner. The quantified 34 metabolites for each iRBC and RBC were included in one dataset. This dataset represented the mean of biological replicates for each group and presented as fold change ratio that was normalized by the corresponding sample for each group collected at time zero. The following findings were obtained from the metabolomics analysis of the dataset using metabolanalyst web-based software (http://www.metaboanalyst.ca) (Xia et al., 2009, Xia et al., 2012) and the plotted line-graphs data were performed with GraphPad Prism 5.0 (GraphPad Software Inc.).

4.3.1. Metabolomics analysis of iRBC and RBC

Principal component analysis (PCA) and partial least squares-discriminant analysis (PLS-DA) was performed on the $\log_2$ transformed dataset using metabolanalyst web-based software (http://www.metaboanalyst.ca).

4.3.1.1. PCA and PLS-DA

The 2-D and 3-D score plots from PCA showed distinct separation between iRBC and RBC reflecting the occurrence of essential differences in the metabolites generated (Figure 4.4 A and B). A corresponding loading plot indicated that the separation observed on PCA clustering was mainly based in the generation of pyrimidine intermediates including carbamyol-l-aspartate, dihydroorotate and orotate (Figure 4.4 C).

Moreover, further discriminate analysis was used to indicate any further differences between RBC and iRBC. The 2-D and 3-D score plots from PLS-DA showed the same findings obtained for PCA. There was an evident clustering segregation between the clusters of RBC and iRBC in 2-D and 3-D PLS-DA score plots (Figure 4.5 A and B). In addition, the findings obtained for the corresponding loading plot for PLS-DA were similar to that obtained for PCA. PLS-DA loading plot indicated that the separation observed on 2-D and 3-D clustering was mainly based on the generation of pyrimidine intermediates including carbamyol-l-aspartate, dihydroorotate and orotate (Figure 4.5 C). Similarly, Variable Influence on Projection (VIP) score was used in metabolomics analyses to further enhance the major metabolites differences between RBC and iRBC. VIP scores were calculated based on the variability explained in PLS-DA. Metabolites with VIP score > 1 were considered the most important metabolites responsible for the differentiation between RBC and iRBC. VIP scores showed that the most significant metabolites with score > 1 were orotate, DHAP, dihydroorotate, carbamoyl-l-aspartate and PEP (Figure 4.6). However, although lactate had a borderline VIP score, it indicates that differences between RBC and iRBC were also centred in glycolysis and pyrimidine pathway (Figure 4.6). Further observations will be described in the biochemical time-dependent results (section 4.2.3)

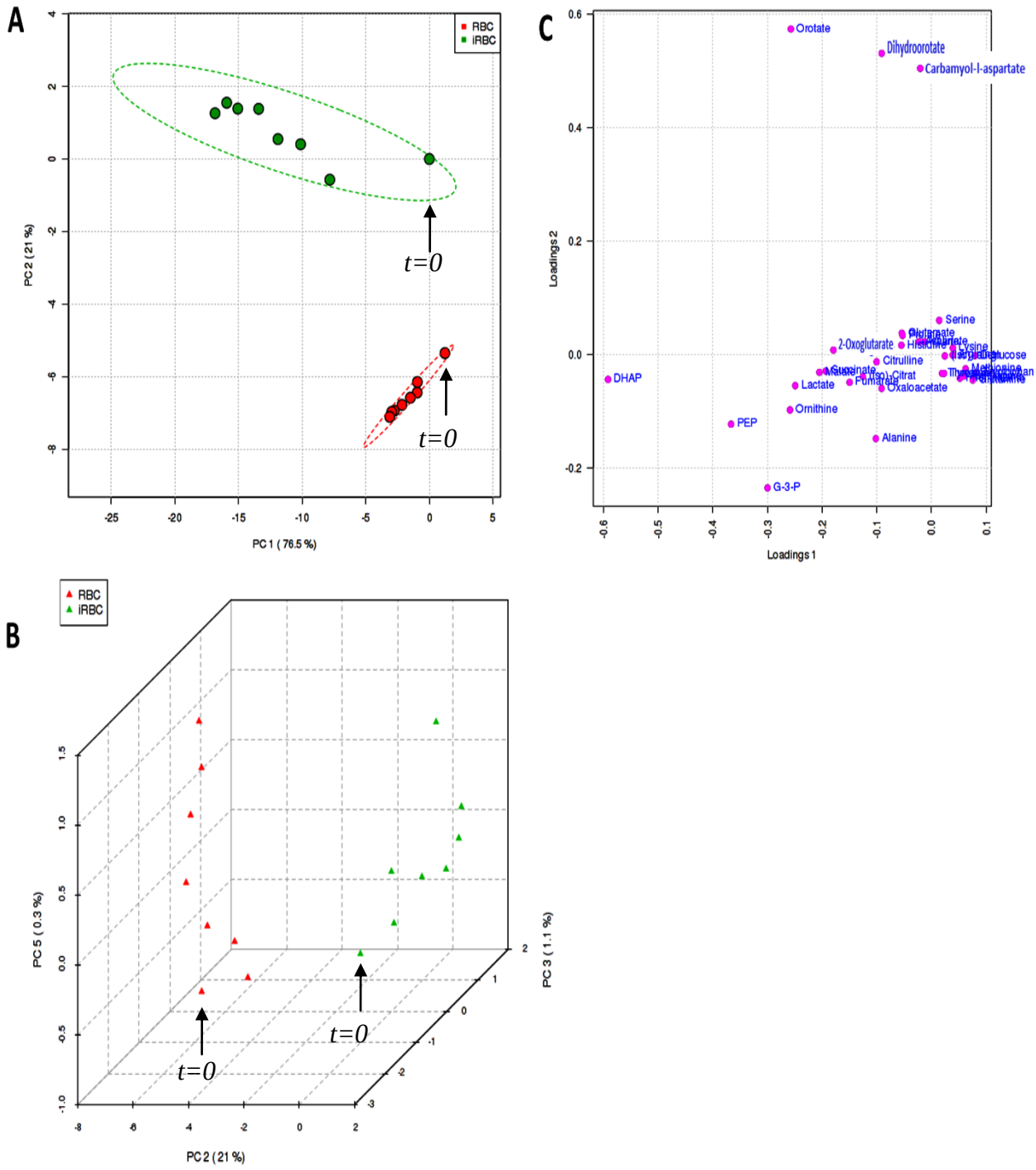

Figure 4.4: PCA score and loading plots for RBC and iRBC.

A) 2-D score plot shows divergence of two main clusters. One cluster includes the clustering of RBC (red circle) and the other cluster includes the clustering of iRBC by *P. falciparum* (green circle). Line boundary for each group represented a 95% confidence limit from each group centre. B) 3-D score plot shows the divergence of two main clusters. One cluster includes the clustering of RBC (red triangle) and the other cluster includes the clustering of iRBC by *P. falciparum* (green triangle). C) RBC and iRBC metabolites loading plot discriminate between various time points for the corresponding score plots (panel A and B) and reveals that the presence of metabolic fingerprints in carbamoyl-l-aspartate, dihydroorotate and orotate. Black arrow indicates the time zero (*t*=0) for RBC and iRBC in Panel A and B.

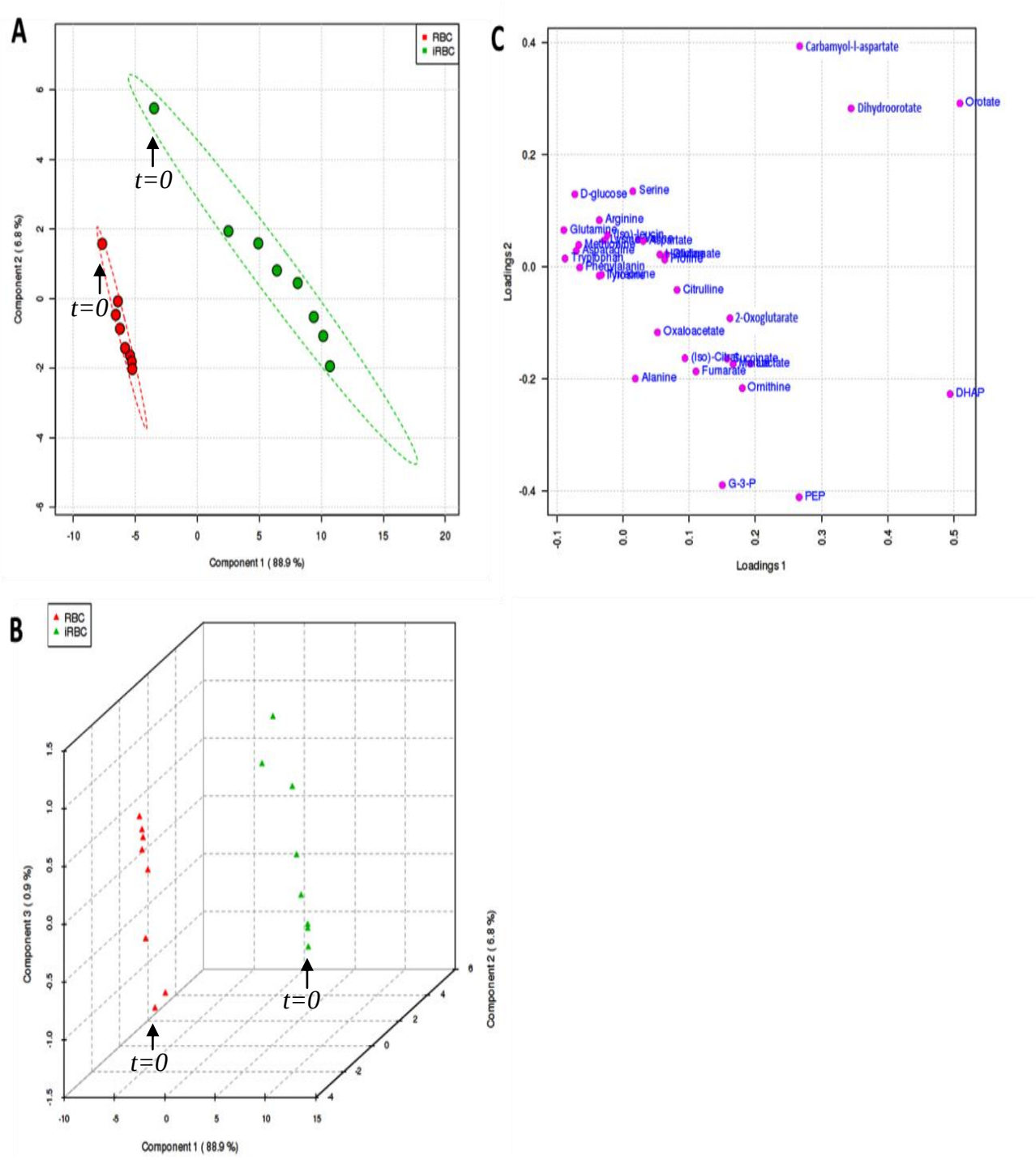

Figure 4.5: PLS-DA score and loading plots for RBC and iRBC.

A) 2-D score plot shows divergence of two main clusters. One cluster includes the clustering of RBC (red circle) and the other cluster includes the clustering of iRBC by *P. falciparum* (green circle). Line boundary for each group represented a 95% confidence limit from each group centre. B) 3-D score plot shows the divergence of two main clusters. One cluster includes the clustering of RBC (red triangle) and the other cluster includes the clustering of iRBC by *P. falciparum* (green triangle). C) RBC and iRBC metabolites loading plot discriminate between various time points for the corresponding score plots (panel A and B) and reveals that the presence of metabolic fingerprints in carbamoyl-l-aspartate, dihydroorotate and orotate. Black arrow indicates the time zero (*t*=0) for RBC and iRBC in Panel A and B.

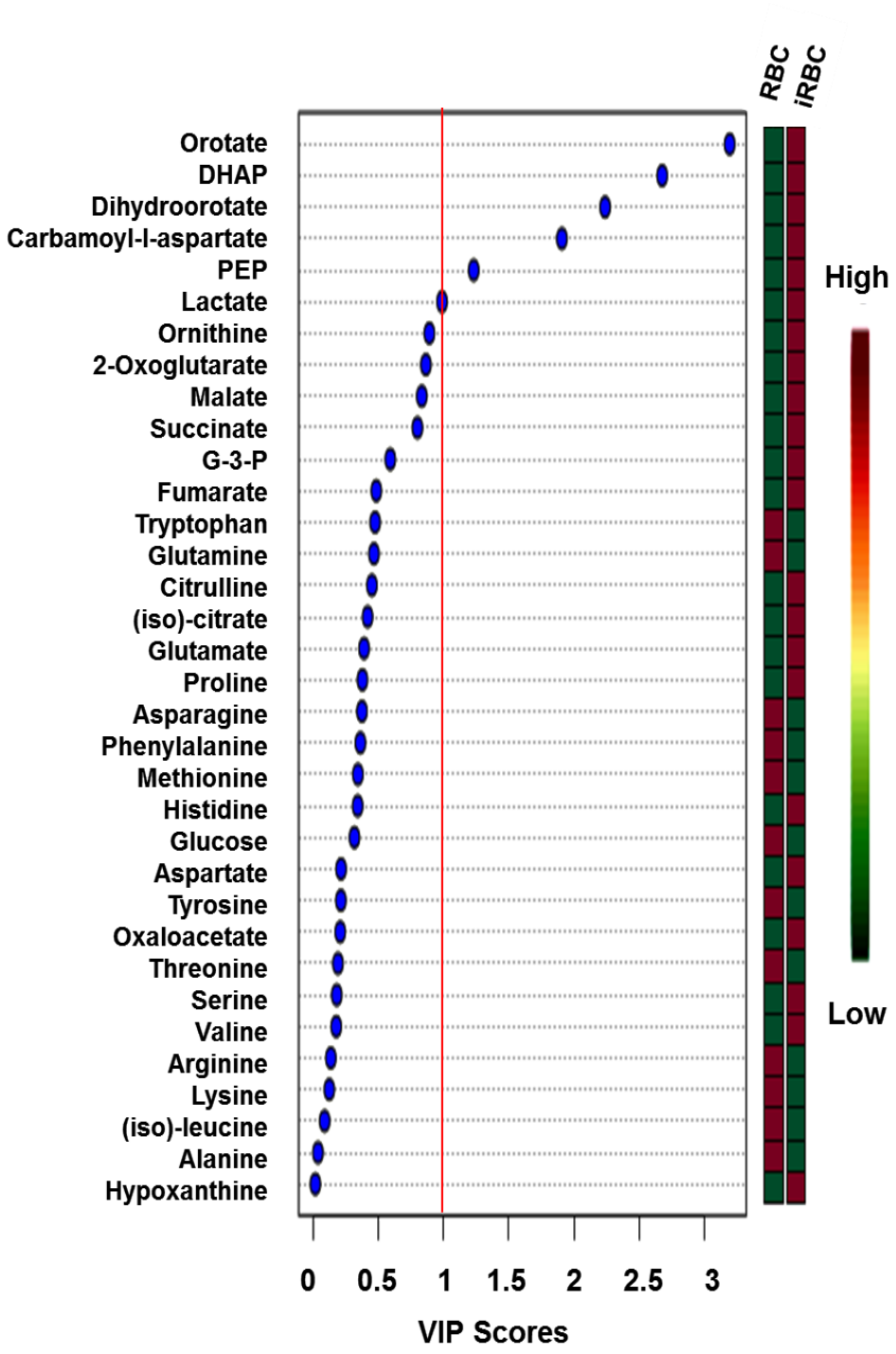

Figure 4.6: Variable Influence on Projection (VIP) score plot for RBC and iRBC.
Metabolite with VIP score > 1 was considered the most important metabolite responsible for the differentiation among RBC and iRBC. The coloured boxes on the right indicate the relative ratios of the corresponding metabolite in each group under study. Colour scale shows the colours gradient for the VIP score with dark red and dark green being the colours for high and low changed metabolites, respectively. VIP score plot shows that the most important metabolites responsible for differentiation were orotate, DHAP, dihydroorotate, carbamoyl-l-aspartate and PEP. Lactate was having borderline VIP score around 1.

4.3.1.2. Heat map for iRBC and RBC metabolome profiling

The similarity and closest measures for the log_2 transformed dataset of this chapter were analysed by metaboanalyst web-based software and presented as a heat map for visual aids.

Heat map showed visually in a colouration method the relative difference of the dynamic changes of RBC and iRBC by *P. falciparum* (Figure 4.7). It was remarkably obvious that the metabolomic profiles of iRBC showed the occurrence of production trends in the intermediates of pyrimidine, purine, glycolysis, TCA pathways and some amino acids (Figure 4.7). An iRBC showed the incidence of consumption trends in glucose as well as some amino acids including asparagine, glutamine, arginine, serine, valine, (iso)-leucine, lysine, methionine, tryptophan, tyrosine and threonine (Figure 4.7). In contrast, the metabolomics profile of RBC showed no obvious production trends in the intermediates of pyrimidine, purine, glycolysis, TCA pathways and some amino acids except alanine (Figure 4.7). In addition, there was the presence of either low or no consumption in glucose as well as some amino acids including asparagine, glutamine, arginine, serine, valine, (iso)-leucine, lysine, methionine, tryptophan, tyrosine and threonine (Figure 4.7). Moreover, the heat map presented in (Figure 4.7) summarized the relative metabolites fold changes ratio in RBC and iRBC. Major and evident metabolite changes were highlighted as mentioned above. However, detailed and specific explanation is presented as time-dependent graphs in the next section (4.3.2).

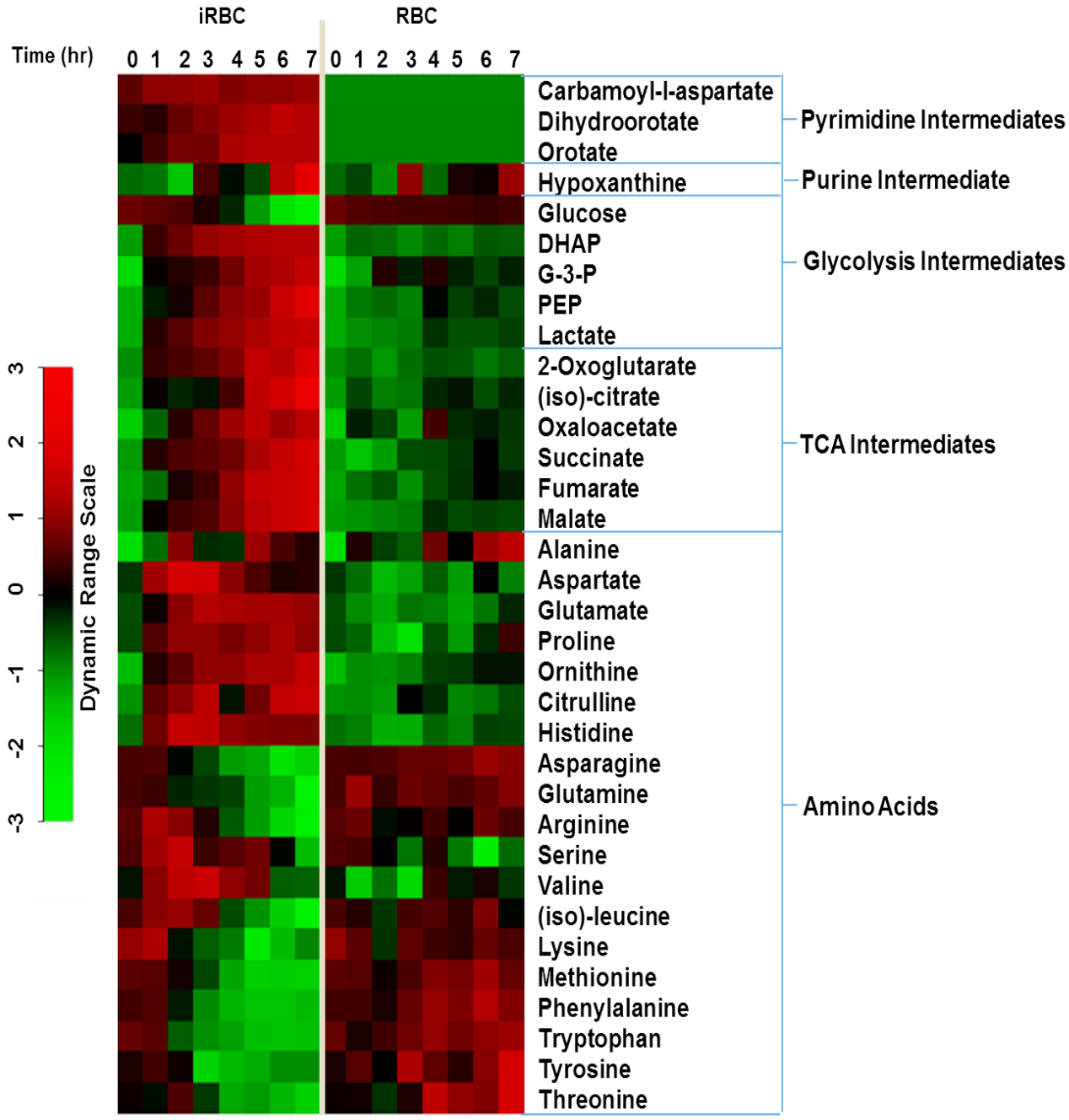

Figure 4.7: Heat map representation of RBC and iRBC dynamics metabolome.
Heat map shows dynamic changes of 34 metabolites in RBC and iRBC. Average values at each time-point obtained, using uninfected RBC and enriched trophozoite-staged *P.falciparum*-iRBC from three independent biological replicates, were divided by the corresponding average values derived from samples harvested at time (0hr) to generate the corresponding ratios. Ratios were $\log_2$ transformed and plotted on a colour dynamic range scale. Rows correspond to metabolites measured by LC-MS/MS. Columns correspond to the time course from 0hr to 7hr for each of the two blocks. Green and red colours represent decreases and increases, respectively. Black colour indicates the baseline. Abbreviations: DHAP, dihydroxyaceton phosphate; G-3-P, glycerol-3-phosphate; PEP, phosphoenol pyruvate.

4.3.2. Biochemical time-dependent of metabolites profile in RBC and iRBC

The findings described in the previous metabolomics analysis section (section 4.3.1) were basically used to distinguish the general metabolomics modulation between RBC and iRBC by *P. falciparum*. In this section, average concentration values at each time-point obtained using RBC and enriched trophozoite-stage *P. falciparum*-iRBC from independent biological replicates were divided by the corresponding average values derived from samples collected at time zero to generate the corresponding fold change ratio. Time-dependent graphs for RBC and iRBC were plotted using GraphPad Prism 5.0 (GraphPad Software Inc.).

The glucose utilization in iRBC was notably double that of RBC at 7 hr timepoint (Figure 4.8 A). Consequently, the production of dihydroxyaceton phosphate (DHAP), glycerol-l-phosphate (G-3-P), phosphoenol pyruvate (PEP) and lactate was remarkably higher in iRBC than those of RBC by at least 15 fold at 7 hr timepoint (Figure 4.8 B, C, D and E).

Tricarboxylic Acid (TCA) intermediates were detected in iRBC and RBC. These include 2-oxoglutarate, (iso)-citrate, oxaloacetate, succinate, fumarate and malate. The levels of these TCA intermediates were considerably higher in iRBC than those in RBC by at least 1 fold at 7 hr timepoint (Figure 4.9 A, B, C, D, E and F).

The amino acid trends were different in RBC and iRBC. Specifically, iRBC showed a substantial utilization of glutamine and asparagine compared to RBC by at least 0.5 fold at 7 hr timepoint (Figure 4.10 A and C). In addition, there was a variable increase trend in the production of glutamate, aspartate, alanine and histidine in iRBC compared to RBC during the 7 hr time point incubation time (Figure 4.10 B, D, E and F). Moreover, iRBC demonstrated an increase in the generation of proline, ornithine and citrulline compared to RBC (Figure 4.11 B, C and D). An iRBC showed an increase in the utilization of arginine, methionine and lysine as compared to RBC during at least the last three hours of incubation (Figure 4.11 A, E and F). Furthermore, there was an obvious trends in the utilization of (iso)-leucine, threonine, phenylalanine, tryptophan and tyrosine in iRBC compared to RBC by at least 0.5 fold at 7 hr time point (Figure

4.12 A, C, E, F and G). There were no obvious changes observed in valine and serine levels between RBC and iRBC (Figure 4.12 B and D).

Pyrimidine intermediates were detected in iRBC but not in RBC. Carbamoyl-l-asparate was utilized whilst dihydroorotate and orotate were produced in iRBC (Figure 4.13 A, B and C). There was no significant change noted in the production of purine intermediate, hypoxanthine, between RBC and iRBC except at the last two hours of incubation when hypoxanthine started to upsurge (Figure 4.13 D).

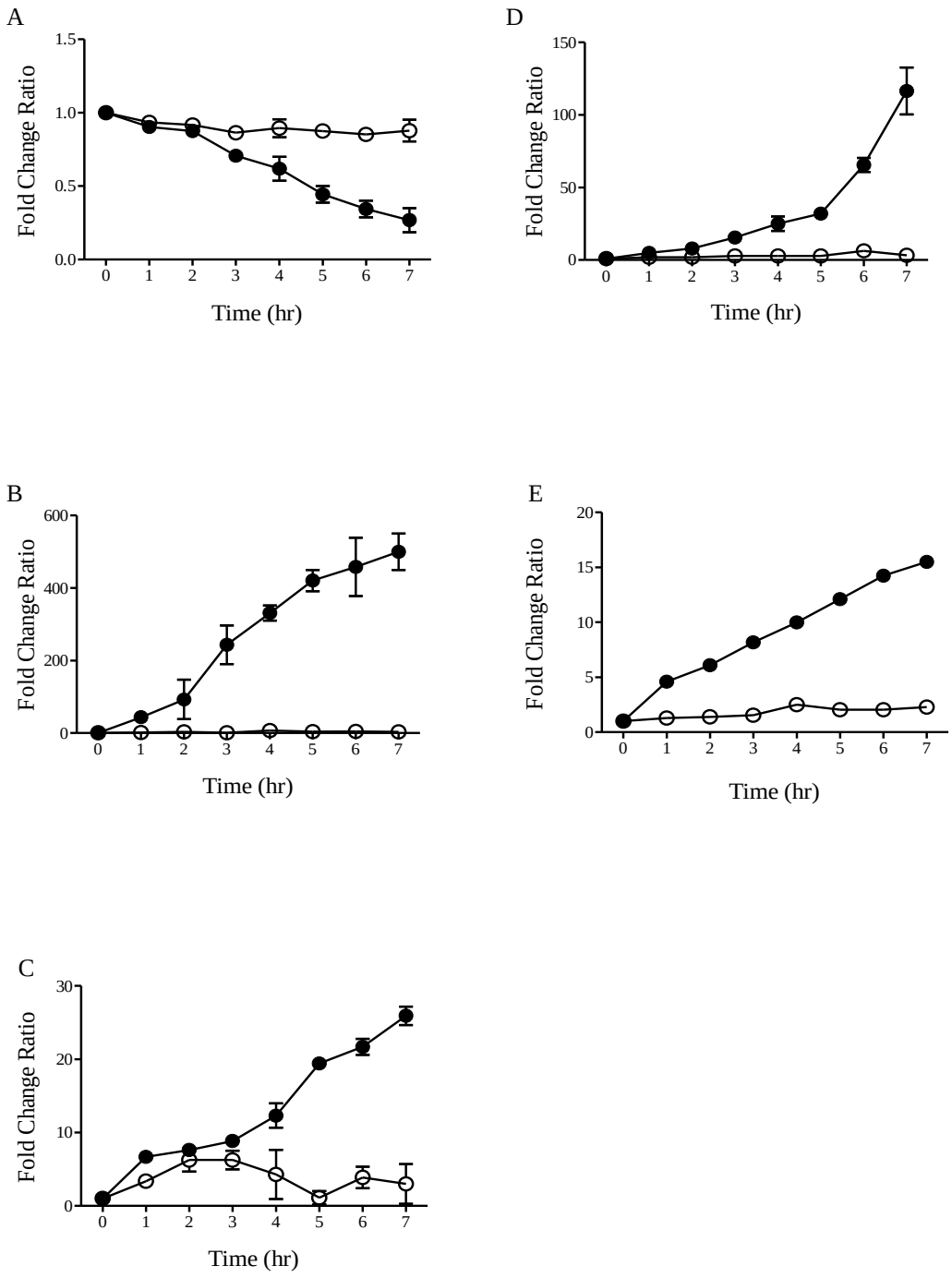

Figure 4.8: Time-dependent curves of anaerobic glycolysis intermediates in RBC and iRBC.

Anaerobic glycolysis intermediates level including (A) glucose, (B) DHAP (C) G-3-P (D) PEP and (E) Lactate were determined in RBC (open circle) and trophozoite-stage *P. falciparum*-iRBC (closed circle) by LC-MS/MS. Time-dependent curve of (A) glucose showed notable increase in its consumption in iRBC compared to RBC. As a result, remarkable production of glycolysis intermediates including (B) DHAP (C) G-3-P (D) PEP and (E) Lactate were observed in iRBC as compared to RBC. The points represent the mean ± SEM of at least duplicate independent experiments.

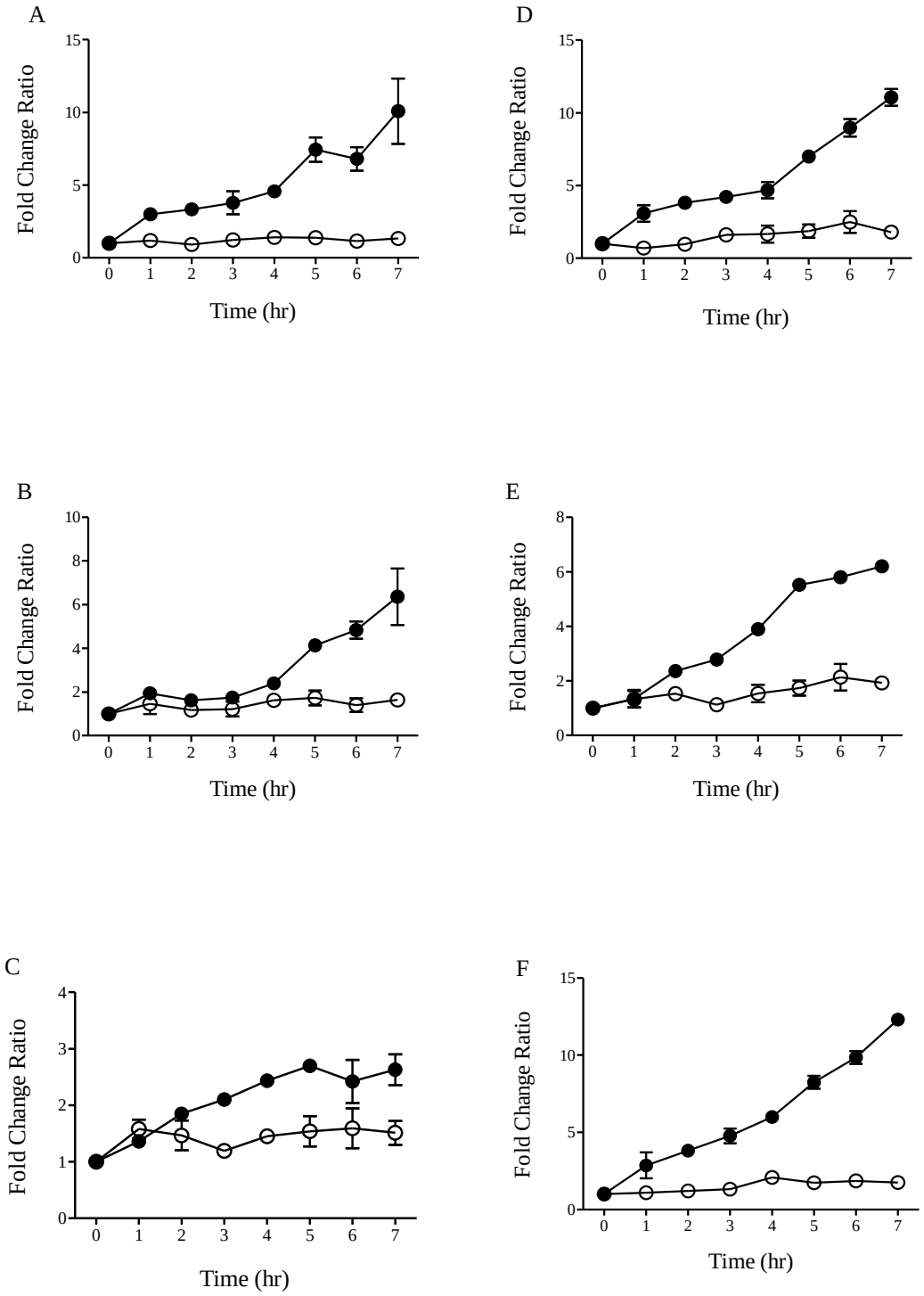

Figure 4.9: Time-dependent curves of TCA intermediates in RBC and iRBC.
TCA intermediates level including (A) 2-oxoglutarate, (B) (iso)-citrate (C) oxaloacetate (D) succinate, (E) fumarate and (F) malate were determined in RBC (open circle) and trophozoite-stage *P. falciparum*-iRBC (closed circle) by LC-MS/MS. Data showed the existence and prominent increase of all TCA intermediates targeted in iRBC compared to RBC. The points represent the mean ± SEM of at least duplicate independent experiments.

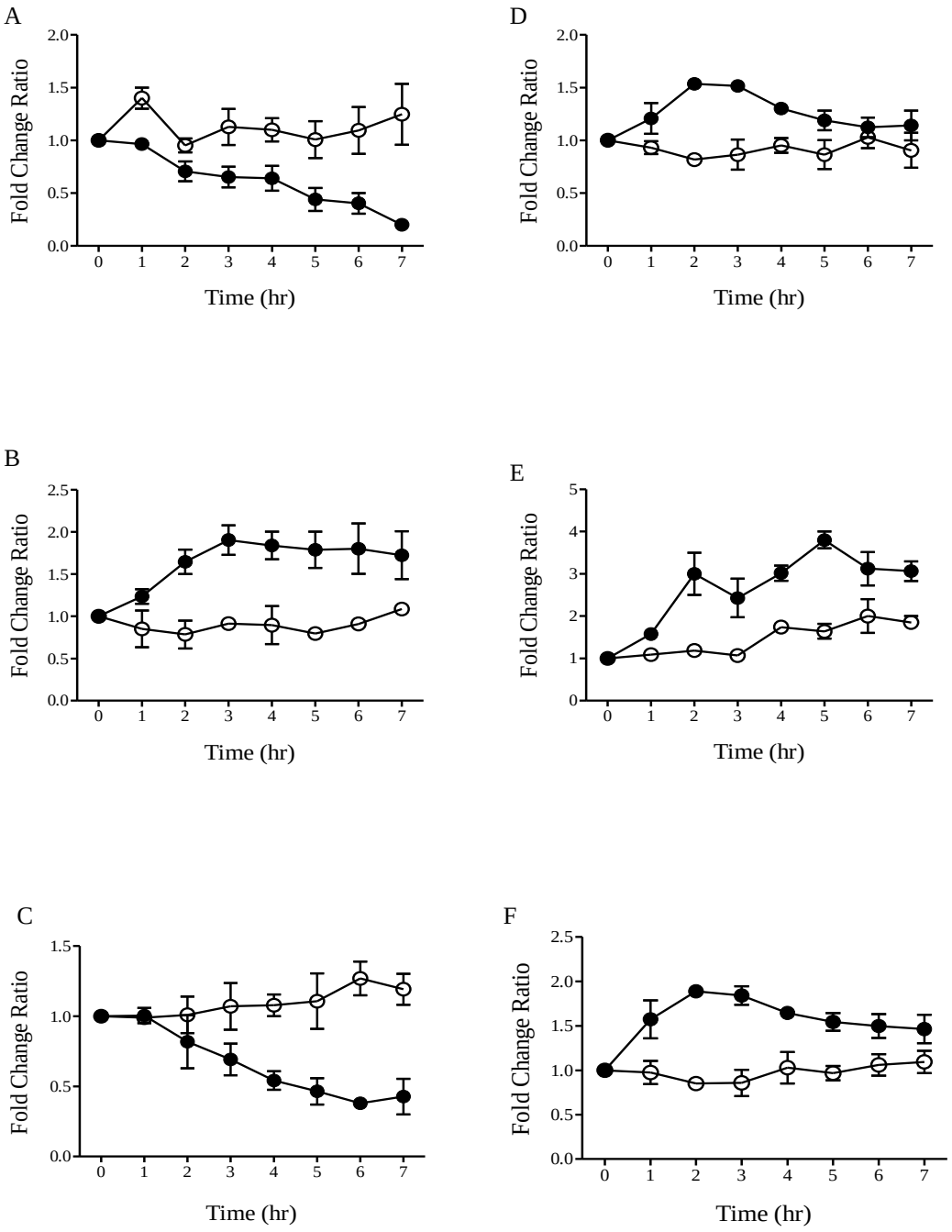

Figure 4.10: Time-dependent curves of amino acids in RBC and iRBC.
Amino acids level of (A) glutamine, (B) glutamate, (C) asparagine, (D) aspartate, (E) alanine and (F) histidine that were determined in RBC (open circle) and trophozoite-stage *P. falciparum*-iRBC (closed circle) by LC-MS/MS. Data showed an increase in the production of (B) glutamate, (D) aspartate, (E) alanine and (F) histidine in iRBC compared to RBC. In addition, iRBC showed an increase in the utilization of (A) glutamine and (C) asparagine compared to RBC. The points represent the mean ± SEM of at least duplicate independent experiments.

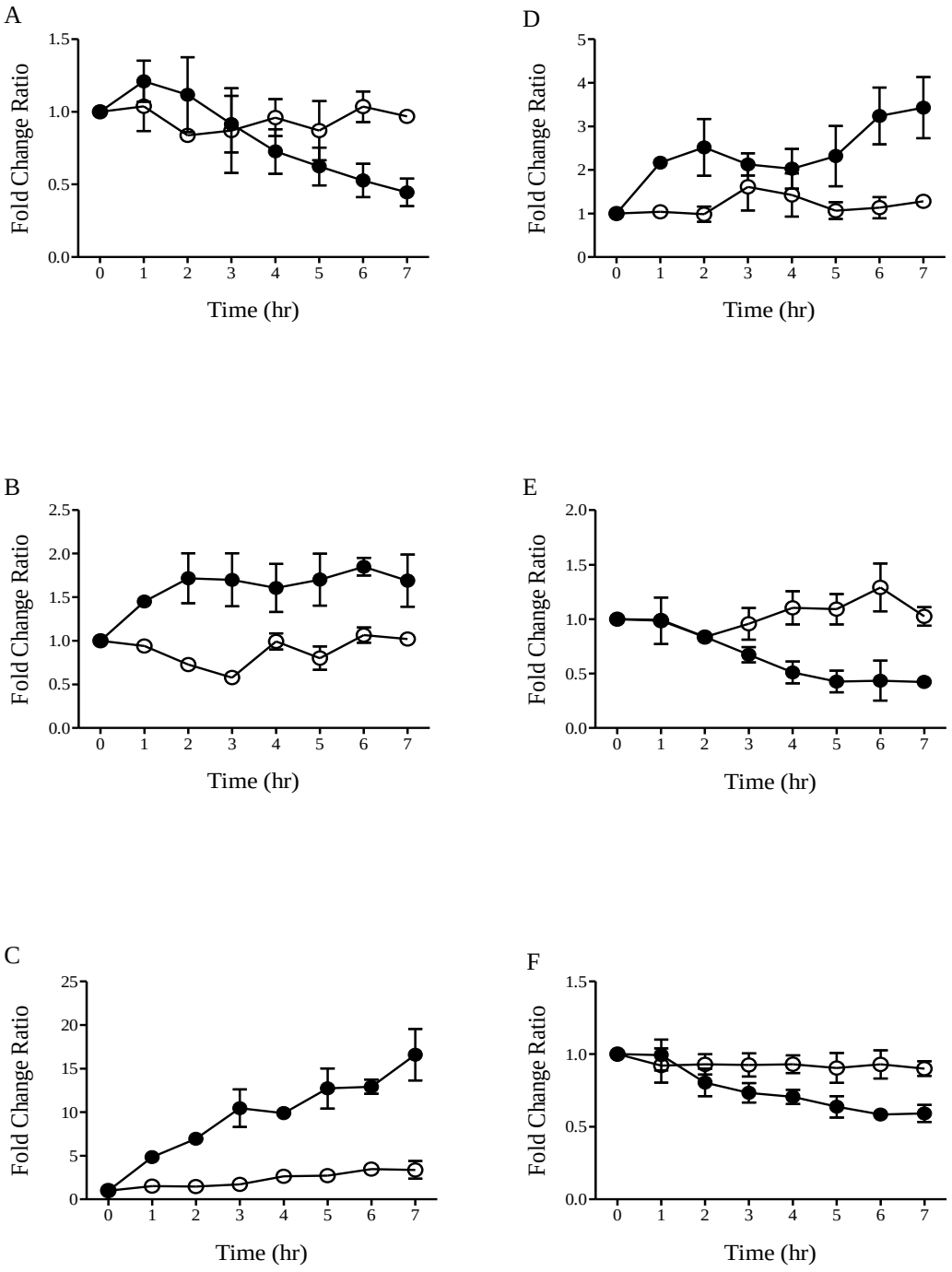

Figure 4.11: Time-dependent curves of amino acids in RBC and iRBC.
Amino acids level including (A) arginine, (B) proline, (C) ornithine, (D) citrulline, (E) methionine and (F) lysine were determined in RBC (open circle) and trophozoite-stage *P. falciparum*-iRBC (closed circle) by LC-MS/MS. Data showed increase in the production of (B) proline, (C) ornithine and (D) citrulline in iRBC compared to RBC. In addition, iRBC showed an increase in the utilization of (A) arginine, (E) methionine and (F) lysine as compared to RBC. The points represent the mean ± SEM of at least duplicate independent experiments.

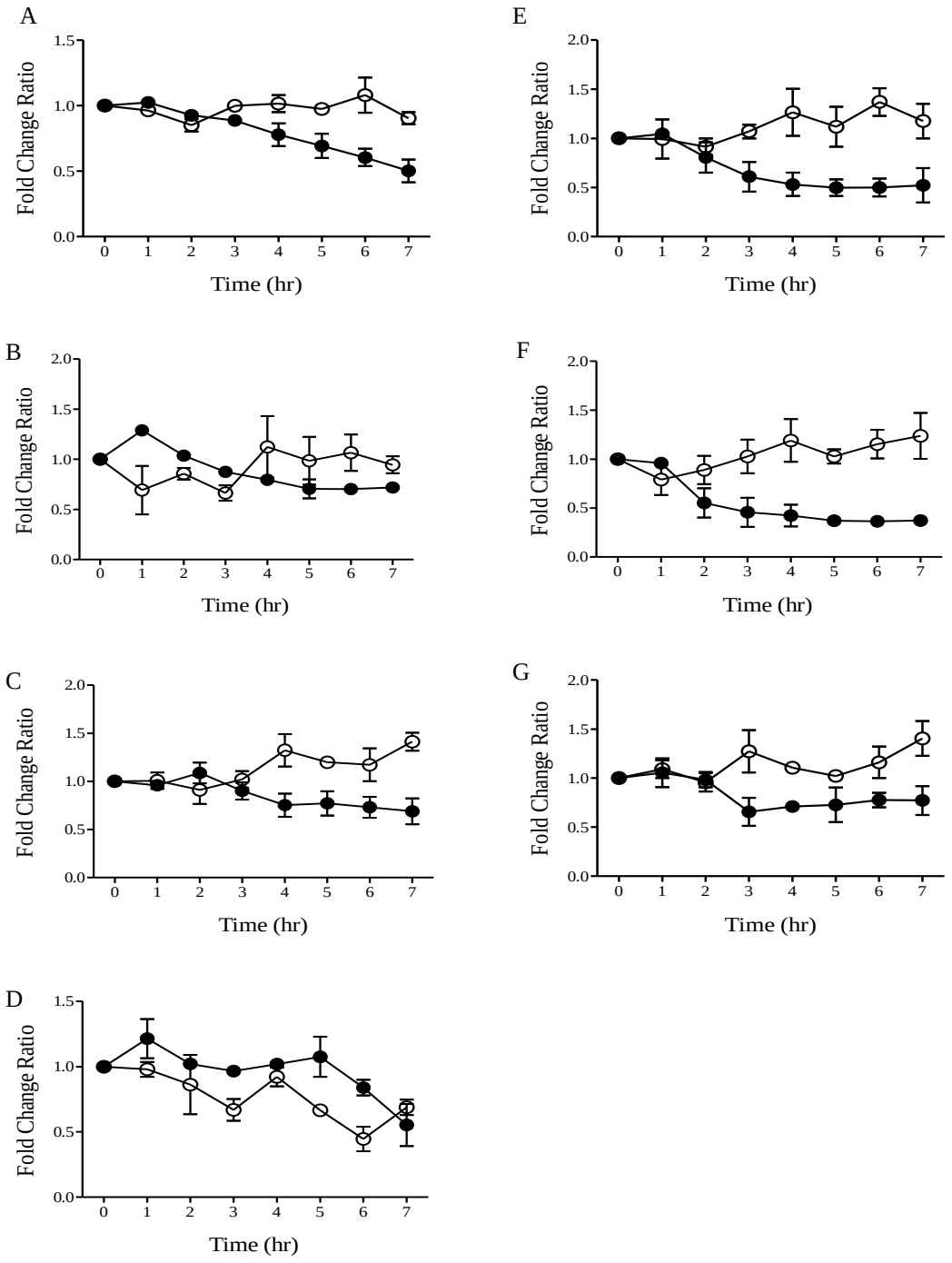

Figure 4.12: Time-dependent curves of amino acids in RBC and iRBC.
Amino acids level including (A) (iso)-leucine, (B) valine, (C) threonine, (D) serine, (E) phenylalanine, (F) tryptophan and (G) tyrosine were determined in RBC (open circle) and trophozoite-stage *P. falciparum*-iRBC (closed circle) by LC-MS/MS. Data showed an utilization trends of (A) (iso)-leucine, (C) threonine, (E) phenylalanine, (F) tryptophan and (G) tyrosine in iRBC compared to RBC. There was no obvious differences observed in (B) valine and (D) serine levels between RBC and iRBC. The points represent the mean ± SEM of at least duplicate independent experiments.

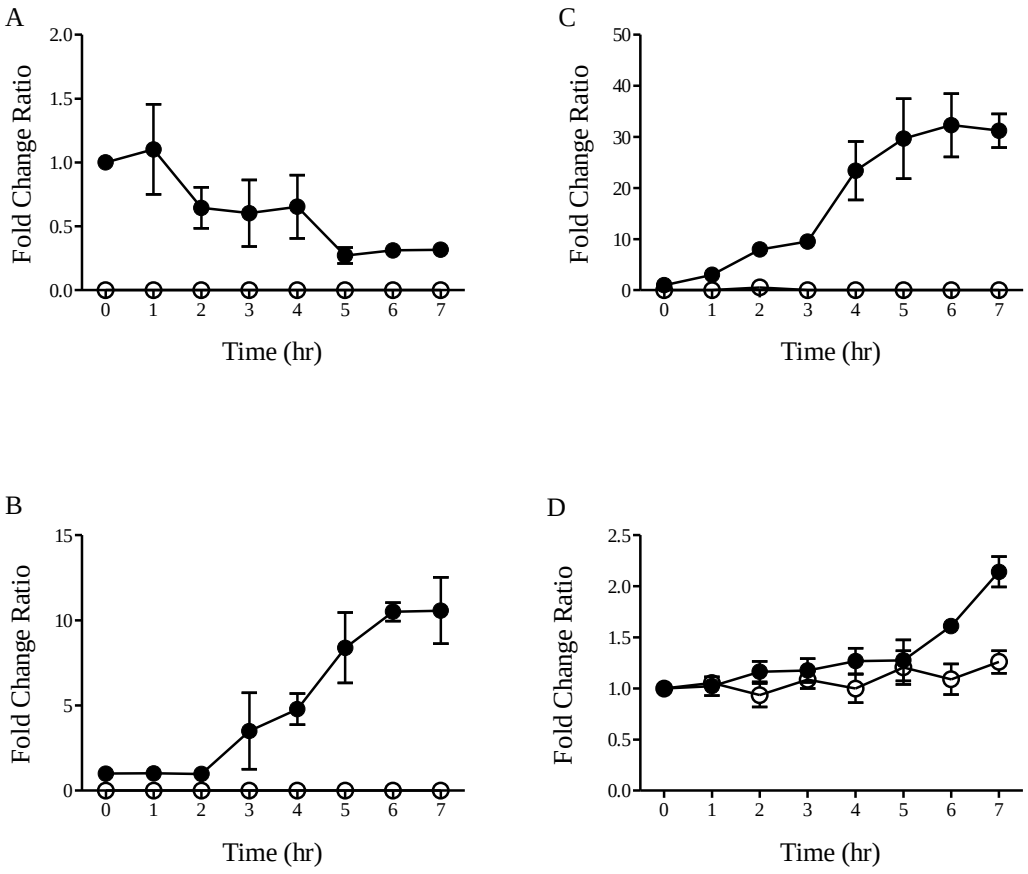

Figure 4.13: Time-dependent curves of pyrimidine and purine intermediates in RBC and iRBC.

Pyrimidne intermediates level including (A) carbamoyl-l-aspartate, (B) dihydroorotate and (C) orotate; and purine intermediate level including (D) hypoxanthine were determined in RBC (open circle) and trophozoite-stage *P. falciparum*-iRBC (closed circle) by LC-MS/MS. Data showed the existence and an increase in the utilization of (C) carbamoyl-l-aspartate alongside an increase production of (E) dihydroorotate and (F) orotate in iRBC as compared to RBC. There were no changes in (D) hypoxanthine level between RBC and iRBC expect at the last two hours of incubation. The points represent the mean ± SEM of at least duplicate independent experiments.

4.4. Discussion

The metabolomics studies in this chapter and the subsequent chapters (5, 6 and 7) were carried out in accordance with the Metabolomics Standards Initiative (MSI) guidelines for the in vitro biology/microbiology context http://msi-workgroups.sourceforge.net/.

The metabolomics analysis PCA and PLS-DA demonstrated the occurrence of distinct clustering separation between RBC and iRBC by *P. falciparum* suggesting the differences and perhaps uniqueness of overall metabolism in RBC and iRBC. In addition, loading plots for PCA and PLS-DA revealed the major metabolites that could be attributed to the separation seen in PCA and PLS-DA. These include carbamoyl-l-aspartate, dihydroorotate and orotate. Therefore, it appears that the major difference between RBC and iRBC is in the existence of pyrimidine intermediates. This was further strengthened by VIP score showing that pyrimidine intermediates, carbamoyl-l-aspartate, dihydroorotate and orotate had VIP score > 1 indicating that they were the prominent metabolites differentiating RBC and iRBC. This is consistent with what has been clearly established about RBC in that it does not synthesize pyrimidine (Tax et al., 1979) and iRBC by *P. falciparum* synthesizes pyrimidine *de novo* (Walsh and Sherman, 1968a, Walsh and Sherman, 1968b, Gutteridge and Trigg, 1970, Gutteridge et al., 1979, Gero et al., 1984, Gero and Osullivan, 1990). In addition, the biochemical time-dependent profile of orotate biosynthesis showed this by the constant conversion of carbamoyl-l-aspartate to dihydroorotate which is then catalysed to orotate. This demonstrates the demand required for DNA and RNA synthesis during the transition stage from trophozoite to schizont. This demonstration is in agreement with a transcriptomic study of *P. falciparum* cycle showing that pyrimidine and purine enzymes transcript peak at approximately 18-22 hpi (hour post-invasion) (Bozdech et al., 2003). Additionally, only hypoxanthine as purine intermediate was detected by the LC-MS/MS while the remaining purine intermediates were below LOD. It has been noted that RBC could be an important source of purines for the synthesis of *Plasmodium* nucleic acid (Bungener, 1967). RBC contains relatively high concentration of purines that its metabolism acts primarily to regenerate intracellular stores of ATP (Walsh, 1998, Sherman, 1979). This ATP undergoes normal turnover to adenosine and inosine (Walsh, 1998). When RBCs are deteriorated due to age or upon invasion by *Plasmodium*, ATP is catalysed through sequential biochemical reactions leading to significant amounts of hypoxanthine (Sherman, 1979, Bishop, 1960, Bishop, 1961).

This explains what was observed in the biochemical time-dependent findings that there were no changes in the hypoxanthine levels between iRBC and RBC except in the last two hours of the time course. This is due to the extra requirements of parasite during the transition stage from trophozoite to schizont to salvage hypoxanthine for DNA and RNA synthesis in purine metabolism.

Furthermore, it is well documented that mature human RBCs do not consume oxygen and do not have mitochondria (Schweiger, 1962). Instead, RBCs carry out anaerobic glycolysis to meet their energy needs (Prankerd, 1955, Bishop, 1964). It was noted from this chapter that both RBC and iRBC carried out fermentation of glucose leading to lactate as the major end-product. However, it was observed from the biochemical time-dependent findings that iRBC by *P. falciparum* consumed more glucose than that of RBC. It has been reported that *P. falciparum*-iRBC consumed glucose up to 100 times as compared to RBC (Roth Jr, 1990). The upsurge of glucose consumption observed in the findings of iRBC in this chapter resulted in an increase in the generation of expected major end-products including lactate, glycerol-3-phosphate (G-3-P) and alanine. This findings is consistent with results obtained showing that NMR analysis of *P. falciparum* parasite incubated in ^{13}C-glucose-supplemented media enabled the detection of five major end-products including pyruvate, lactate, alanine, G-3-P and glycerol (Lian et al., 2009). However, pyruvate and glycerol could not be detected by the present LC-MS/MS-based system because of their poor ionization potential. Therefore, it could be suggested here that a combinatorial approach (NMR and LC-MS/MS) is critical to attaining the most comprehensive analysis of small metabolites in a biological sample. Additionally, it appears from the results presented here that the proportional increase of G-3-P over time indicates that *P. falciparum* possess a G-3-P shuttle which converts dihydroxyacetone phosphate (DHAP) to G-3-P by a cytosolic glycerol-3-phosphate dehydrogenase (G3PDH) leading to reoxidation of cytosolic NADH, a glycolysis by-product (Lian et al., 2009, Danne et al., 2013). G-3-P is then converted to DHAP in the mitochondria by a membrane bound mitochondrial G3PDH which contributing to the generation of reduced form of ubiquinone in the mitochondrial respiratory chain (Danne et al., 2013). Therefore, it could be supposed here that the G-3-P shuttle functions as link between glycolysis and mitochondrial respiratory chain.

Moreover, carbon dioxide (CO_2) fixation has been studied in *P. falciparum* (Blum and Ginsburg, 1984), *P. knowlesi* (Sherman and Ting, 1968) and *P. lophurae* (Sherman and Ting, 1966) demonstrating that radiolabeled CO_2 was fixed into three major amino acids namely alanine, aspartate and glutamate probably through concerted enzymatic action of carboxykinases followed by transaminases. This was supported by the findings in biochemical time-dependent experiments demonstrating that there was a distinguished increase in the production of alanine, glutamate and aspartate in *P. falciparum*-iRBC when compared to RBC. However, it has been found recently that fumarate is converted to aspartate then incorporated into proteins and nucleic acid synthesis of *P. falciparum* (Bulusu et al., 2011, Jayaraman et al., 2012). This finding is interesting because it explains why aspartate level in *P. falciparum*-iRBC increased at the first few hours of the time course and then decreased in the last few hours of the incubation owing to the high need for DNA and RNA synthesis during the transition stage from trophozoite to schizont. In addition, iRBC showed significant utilization for asparagine compared to RBC suggesting, perhaps a similar demand in nucleic acid synthesis as noted in the production of aspartate. Furthermore, the notable increase observed in the production of alanine and histidine is consistent with the recent metabolomics study showing that alanine and histidine were increased significantly in trophozoite stage indicating the initiation of hemoglobin digestion (Olszewski et al., 2009). Nevertheless, it has been noted that alanine and histidine were also significantly accumulated in the extracellular media suggesting that the parasite only incorporates a fraction of the haemoglobin-derived amino acids into protein while it excreting the excess as waste (Olszewski et al., 2009). Therefore, it might be that the amino acids produced through CO_2 fixation are not readily incorporated into proteins because these amino acids, which have been generated through transamination reactions, can interact with pathways contributing perhaps in energy metabolism to serve as a fuel source. In addition, some amino acids might also serve as precursors or components in other metabolic pathways such as aspartate, which involves in pyrimidine and purine metabolism.

In contrast, a metabolomic studies conducted recently on human RBC has shown that there are three possible pathways contributing to the *de novo* synthesis of glutamate via alanine aminotransferase, aspartate aminotransferase and glutamine aminohydrolase (Ellinger et al., 2011). Additionally, it has been shown that glucose consumption by RBC is devoted to *de novo* alanine production (Ellinger et al., 2011, Lewis et al., 2009).

On the other hand, it has been found that there are few stages of TCA cycle in human RBC and this cycle is incompletely represented in RBC (Prankerd, 1955). Human RBC has been shown to possess high activities of malate dehydrogenase and fumarase (Shrago, 1965, Quastel, 1931). Although TCA intermediates including 2-oxoglutarate, (iso)-citrate, oxaloacetate, succinate, fumarate and malate were detected in RBC, their levels were noticeably lower than that of iRBC. This gives two indications; one is that RBC possesses the enzymes required for generating these TCA intermediates but not necessarily a functional TCA cycle because of a lack of mitochondria in human RBC. The other indication is that *P. falciparum*-iRBC has functional TCA cycle represented by the high production in TCA intermediates as compared to RBC. Both indications are correct and they are consistent with the recent retracted article of ‘‘branched TCA metabolism in *P. falciparum*’’ from Llinas’s group (Olszewski et al., 2013). In other words, it was thought that *P. falciparum* operates bifurcated TCA cycle with part of it being oxidative and the other part being reductive, and this cycle is largely disconnected from glycolysis (Olszewski et al., 2011). However, this is not valid any longer because Llinas and his co-worker stated in their retraction that the reductive flux, which was thought to be occurred in the parasite, was due to an excessive interference from the RBC (Olszewski et al., 2013). This explains why some of TCA intermediates were seen in RBC experiments of this chapter. In addition, it has therefore been confirmed that *P. falciparum* operates an oxidative TCA cycle (Olszewski et al., 2013). Moreover, it has been postulated that the main metabolic functions of the TCA cycle in the malaria parasite is the production of succinyl-CoA for haem biosynthesis (Ginsburg, 2010). However, because *P. falciparum* cannot convert citrate to acetyl-CoA, RBC possess the appropriate enzyme (ATPdependent citrate lyase) for this conversion resulting in generation of acetyl-CoA that is shuttled back to the parasite (Ginsburg, 2010).

Moreover, the role of human RBC in amino acids metabolism remains obscure. It has been thought that RBC neither utilize amino acids for protein synthesis nor having the capacity for the degradation (Harris, 1979). Nonetheless, RBC has been shown to have a dynamic role that involves in the compartmentation of amino acids between RBC and plasma in addition to perhaps transporting amino acids between tissues (Aoki et al., 1976, Pozefsky et al., 1969). The data showed that RBC might participate in the production of ornithine suggesting the ability of RBC to convert arginine to ornithine. This data is in agreement with the studies conducted on intact human RBC showing the

functionality of arginase in converting arginine to ornithine (Williams and Phang, 1982). Also, it has been reported that although RBC contributes to the production of ornithine, it is unlikely it has a significant role in urea formation because of the absence of urea-cycles enzymes such as ornithine carbamoyltransferase (Williams and Phang, 1982). Therefore, it has been suggested that ornithine is secreted by the RBC and then converted by the peripheral tissues to proline, a critical constituent of proteins in peripheral tissues such as collagen (Phang et al., 1975, Smith and Phang, 1978). Recently, it has been shown that RBC can synthesis nitric oxide (NO) using arginine as a substrate (Ulker et al., 2009, Kleinbongard et al., 2006). In contrast to RBC, the results demonstrated that *P. falciparum*-iRBC utilized arginine as a precursor for ornithine and citrulline synthesis. The results showed a notable increase in the utilization of arginine in iRBC as compared to RBC. As a result, there was an increase in the production of ornithine and citrulline levels in iRBC as compared to RBC. This is in agreement with a recent metabolomics observation demonstrating that incubating *P .falciparum*-iRBC in culture media supplemented with uniformly $^{13}C^{15}N$-labeled L-arginine resulted in depleting arginine to almost undetectable level which is coinciding in the generation of fully labelled ornithine and citrulline (Olszewski et al., 2009). Therefore, the results obtained in this chapter for arginine utilization and ornithine and citrulline production suggest the existence of urea cycle in *P. falciaprum* parasite. However, it has not been predicted in the *P. falciparum* genome that it is encoding nitric oxide synthase (NOS) or arginine deiminase for catalysing arginine to citrulline (Gardner et al., 2002). Conversely, previous biochemical study conducted on *P. falciparum*-iRBC showed that the parasite exhibit a high NOS for the synthesis of NO measured as citrulline and nitrate production (Ghigo et al., 1995). Therefore, it appears that the parasite has two pathways for catalysing arginine. One pathway is through arginase yielding ornithine, an important precursor for polyamines as well as proline. The other one is producing NO through the oxidation of arginine to citrulline. In addition, the significant formation of proline in iRBC indicates the involvement of ornithine aminotransferase in the ultimate production of proline from ornithine.

Moreover, the data of iRBC showed an evident trends of the utilization of several amino acids including methionine, lysine, (iso)-leucine, threonine, phenylalanine, tryptophan and tyrosine compared to RBC. It has been noted that human haemoglobin is a poor source of methionine, glutamine, glutamate, cysteine and contains no (iso)-leucine

(Francis et al., 1997). In addition, it has been previously found that *P. falciparum*-iRBC can be maintained only when the culture media is provided with the five amino acids, including cysteine, glutamine, glutamate, methionine and (iso)-leucine, that are lacking or present in insignificant amount in the haemoglobin (Divo et al., 1985a). Therefore, this explains the parasite need for exogenously acquisition of several amino acids particularly (iso)-leucine. Consistent with a previous report (Liu et al., 2006), it has been shown that the trophozoite stage of *P. falciparum* can grow and develop in a medium containing a single amino acid, (iso)-leucine. Moreover, as in agreement with the previous study, it has been reported that new permeability pathway (NPP) is induced at the trophozoite stage of *P. falciparum* in order to increase the permeability of several amino acids including valine, serine, threonine, (iso)-leucine (Ginsburg et al., 1985). In addition, the high utilization observed in the iRBC for (iso)-leucine is also consistent with observation of Kirk's lab showing that the rate of transport of (iso)-leucine into mature trophozoite stage of *P. falciparum*-iRBC is increased to ~5-fold than that of RBC (Martin and Kirk, 2007).

Overall, it appears that the metabolomics approach revealed that *P. falciparum*-iRBC modulates and alters the metabolism of the host RBC by exploiting to its own end. In addition, the aforementioned discussion of the results suggests that *P. falciparum*-iRBC parasite developed an extremely specialized metabolic system wherein the main source of cellular ATP in asexual stages of the parasite comes from anaerobic glycolysis and the mitochondria appears to play a minimal biochemical metabolic role in the parasite. Therefore, recent advances in metabolomics research expand further the current understanding of parasite biology as well as the malaria disease status. Furthermore, metabolomic studies are a highly useful approach in determining the metabolic differences between phenotypically divergent strains and in revealing the mode of action for poorly characterized antimalarial drugs and inhibitors. Moreover, integrated approaches of concurrent transcriptomic, proteomic and metabolomic profiles will allow investigating of the interconnections between enzyme expression, protein and metabolite levels. Likewise, the data of this chapter as well as the metabolomics platform will provide a powerful tool to a further investigation of important metabolic pathways and elucidate *P. falciparum* metabolome response to physiologically relevant perturbations such as drug exposures. Therefore, in order to get a holistic view about the biology of *P. falciparum* parasite, a pharmacomatabolomics approach has been

undertaken in the subsequent chapters to investigate the role of two essential organelles namely; mitochondria and digestive vacuole.

With regards to the limitation of this chapter, although the metabolomics platform used in this chapter was optimized (refer to chapter 3) to a higher sensitivity than that of used for the next chapter (5), the detection of bioenergetics/redox couples, UMP, UDP, UTP, TTP, CTP, and GTP was under the limit of detection in the parasite samples as well as RBC. This is could be explained as the presence of inadequate parasite materials. In addition, it has been noted that core metabolites intermediate and cofactors are required to be biosynthesized by the organism itself making these metabolites present in low levels, often more than 10,000-fold less than the most abundant metabolites (Reaves and Rabinowitz, 2011, Bennett et al., 2009). Moreover, the use of HGMS in metabolomics studies for *P. falciparum* is hampered by limited column capacity, inconsistent separation purities and high costs.

CHAPTER 5

Pharmacometabolomics Study of *Plasmodium falciparum* Mitochondria: I

5.1. Introduction

Having developed a metabolomics platform for analysis of core *P. falciparum* metabolism, in this chapter, the interplay of the parasite mitochondrion with core metabolism was investigated. This work was aided by the availability of transgenic strains resistant to atovaquone and in house ETC-specific inhibitors.

The role of *P. falciparum* mitochondria has long been a matter of dispute due to the fact that malaria parasites rely on glucose fermentation for their ATP production (Roth et al., 1988, Roth Jr, 1990). There is also evidence that malaria parasite is microaerophilic growing in low O_2 tension and elevated CO_2 (Oaks Jr, 1991, Scheibel et al., 1979). The importance of mitochondrial function to parasite growth and viability is uncertain because it has been thought that parasite mitochondria lack a functional Krebs cycle (TCA cycle) and other mitochondrial enzymes albeit there is an indication for the presence of a rudimentary ETC (Homewood et al., 1972, Blum and Ginsburg, 1984, Scheibel and Miller, 1969, Sherman, 1979). Malaria parasites possess a single acristae mitochondrion during their asexual blood cycle (Slomianny and Prensier, 1986, Divo et al., 1985b) which undergoes distinct morphologies at different asexual and sexual stages (van Dooren et al., 2005) (Figure 5.1). The *Plasmodium* mitochondrion carries the smallest sequenced mitochondrial genome to date (6-kb in length) which encodes only three mitochondrial proteins, including cytochrome *b*, cytochrome *c* oxidase subunit I and cytochrome *c* oxidase subunit III; in addition to fragmented rRNA genes (Aldritt et al., 1989, Vaidya et al., 1989, Johnson et al., 2011, Feagin et al., 1997, Feagin, 1992). Therefore, the *Plasmodium* mitochondrion must import from the cytosol the majority of proteins and tRNA to serve the physiological functions of protein synthesis and also for the upkeep of its separate genetic system (Vaidya and Mather, 2009, Vaidya and Mather, 2005). However, the metabolic role of *Plasmodium* mitochondria has been a longstanding conundrum as it is thought to lack a functional TCA cycle and the main source of energy for these parasites is glycolysis (Sherman, 1979, Bryant et al., 1964, Scheibel and Pflaum, 1970). However, genomic studies have revealed the presence of the genes necessary for a functional TCA cycle in *Plasmodium* and metabolite profiling has identified TCA intermediates, providing direct evidence of an active mitochondrion (Teng et al., 2009, Gardner et al., 2002, Olszewski et al., 2009). In addition, the findings observed in chapter (4) confirm this by representing a prominent production increase in the TCA intermediates in *P. falciparum*-iRBC. This

is also supported by further metabolomics investigation that has recently been retracted that *P. falciparum* parasite operates an oxidative TCA cycle (Olszewski et al., 2013).

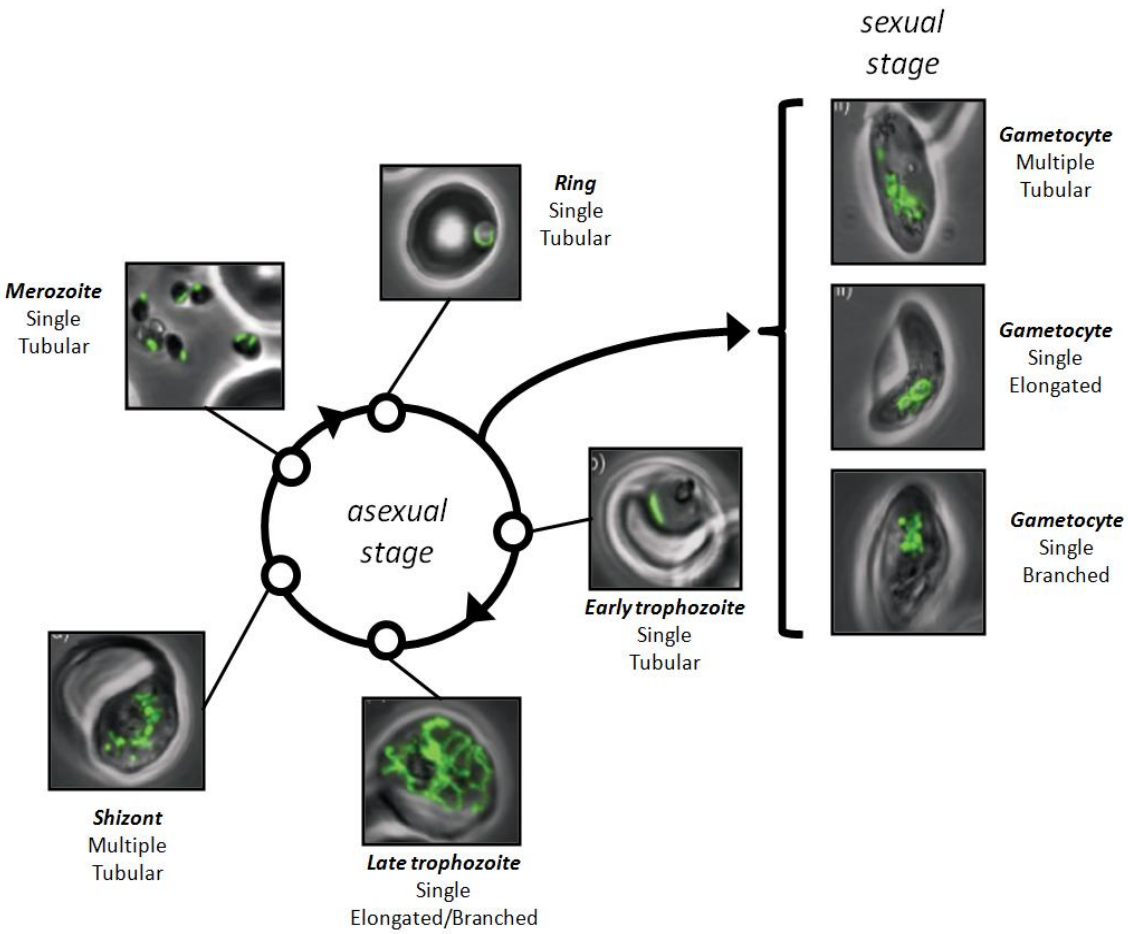

Figure 5.1: *Plasmodium falciparum* mitochondrial morphology during asexual and sexual parasite stages.

Development of the mitochondrion during the different stages of asexual cycle including ring, trophozoite, schizont and merozoite stages. The mitochondrion is typically small and tubular in appearance during the early stages of asexual cycle but by mid schizogony, it becomes highly branched in its appearance after which the mitochondrion divides late in schizogony and a single mitochondrion segregates into each daughter merozoite. In contrast, there are several forms of mitochondria during the sexual stages of *Plasmodium falciparum* including the following forms: single, branched, and as a cluster of mitochondrial lobes towards the centre of the cell. (Adapted from Van Dooren et al., 2006)

Additionally, perhaps because the RBC host loses its ability to synthesize pyrimidines *de novo*, *Plasmodium* parasites cannot salvage pyrimidines and therefore it is dependent on *de novo* pyrimidine biosynthesis (Hyde, 2007b, Cassera et al., 2011).

A number of early observations suggested that the malaria parasite mitochondrion is involved in this pyrimidine biosynthesis and the dihydroorotate dehydrogenase (DHODH) enzyme, which carries out the fourth sequential step in this pathway, appears to be present in the mitochondrial electron transport chain (mtETC) and it is sensitive to a variety of mtETC inhibitors (Gutteridge et al., 1979, Gero et al., 1984, Gero et al., 1981a, Gero et al., 1981b, Prapunwattana et al., 1988, Ittarat et al., 1994, Scott et al., 1986, Heikkila et al., 2006, Heikkila et al., 2007). Therefore, it has been hypothesized that one of the vital roles of the *Plasmodium* parasite mitochondrion is to catalyze the oxidation of dihydrooroate to orotate for pyrimidine biosynthesis through the activity of DHODH (Figure 5.2). Several lines of evidence support this assumption wherein atovaquone, a specific bc_1 complex inhibitor of the respiratory chain (Fry and Pudney, 1992), had shown a secondary effect on DHODH resulting in the increase of carbamoyl-l-aspartate and a reduction in UTP, CTP, and dTTP (Hammond et al., 1985, Seymour et al., 1994, Seymour et al., 1997). A more recent study also confirmed this involvement between mitochondrial function and pyrimidine biosynthesis by the generation of an atovaquone-resistant phenotype in a transgenic *P. falciparum* parasite expressing ubiquinone-independent yeast DHODH (Painter et al., 2007). In addition, a further link between mitochondrial functions and purine pathway has been shown by the treatment of free-parasites with atovaquone which resulted in the inhibition of the conversion of fumarate to aspartate (Jayaraman et al., 2012, Bulusu et al., 2011).

It was also noted that *P. falciparum* favours living in the low oxygen tension environment of the host cell (Scheibel et al., 1979). Nonetheless, *Plasmodium* parasites have a functional mitochondrial respiratory chain and an oxygen-requiring system that is essential for parasite development and survival. Consistent with this, the rate of oxygen consumption of *P. falciparum* and *P. yoelii yoelii* free parasites was affected by mtETC selective inhibitors demonstrating the functionality of mtETC during the asexual and sexual stages of the parasite (Krungkrai et al., 2000, Uyemura et al., 2004, Krungkrai et al., 1999) – although it is not clear from these studies whether the inhibition of O_2-consumption was specific or a result of parasite death.

In stark contrast to mammalian mitochondrial respiratory chain, the *Plasmodium* respiratory chain contains five different dehydrogenases including type II NADH dehydrogenase (PfNDH2 or rotenone-insensitive complex I), succinate:quinone oxidoreductase (SDH or complex II), malate:quinone oxidoreductase (MQO),

dihydroorotate dehydrogenase (DHODH) and glycerol-3-phosphate dehydrogenase (G3PDH) (Figure. 5.2). Each dehydrogenase potentially donates electrons to the ETC via redox reactions involving the oxidation of reducing-equivalent substrates coupled to the reduction of coenzyme ubiquinone (Q) to ubiquinol (QH_2). The redox pair ubiquinone/ubiquinol can then shuttle back and forth in the bi-layer of the mitochondrial inner membrane creating what is called the Q-cycle. The downstream re-oxidation reaction for ubiquinol (QH_2) is then carried out by ubiquinol:cytochrome *c* oxidoreductase (cytochrome bc_1 or complex III) resulting in the transfer of electrons from ubiquinol to a reduced form of cytochrome *c,* which is then oxidized by a cytochrome *c* oxidase (Complex IV) resulting in the vectorial translocation of protons (H^+) from the matrix, generating a transmembrane electrochemical potential ($\Delta\Psi_m$) and molecular oxygen to yield water (Fisher et al., 2009) (Figure 5.2). The transmembrane proton gradient is operated by an ATP synthase (complex V) to synthesize ATP although its contribution to the cellular ATP pool is believed to be minimal (Fry et al., 1990) (Figure. 5.2).

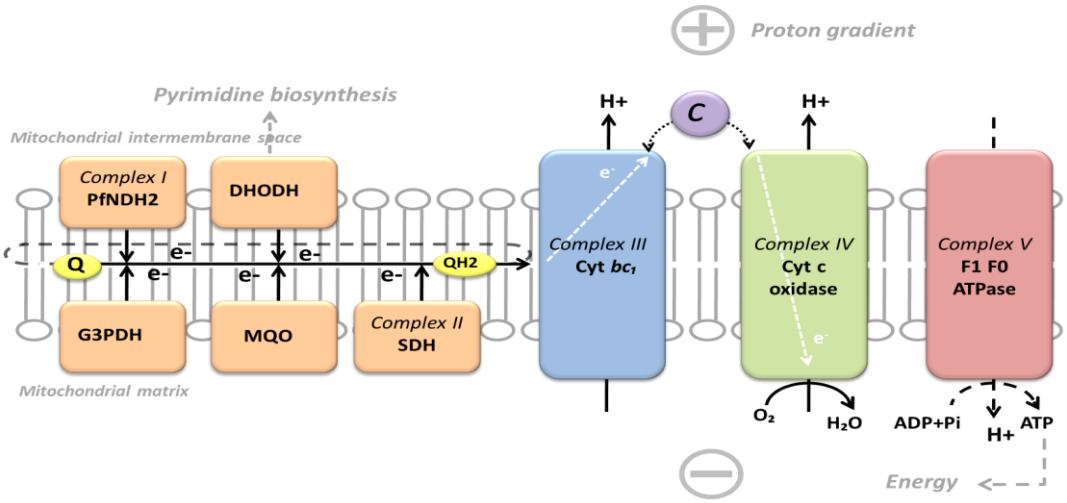

Figure 5.2: Schematic drawing of the mitochondrial electron transport chain of *Plasmodium falciparum*.

The chain consists of Complex I (PfNDH-type II NADH: quinone oxidoreductase), DHODH (dihydroorotate dehydrogenase), G3PDH (glycerol-3-phosphate dehydrogenase), MQO (malate quinone oxidoreductase), Complex II (succinate dehydrogenase), Complex III (cytochrome bc_1 complex), Cyt c (cytochrome c), Complex IV (cytochrome *c* oxidase) and Complex V (F_1F_0ATPase). Electrons are generated by mitochondrial dehydrogenases and passed to ubiquinone (Q). Re-oxidation of QH_2 releases 2 H^+ to mitochondrial intermembrane space and passes electrons to bc_1 complex. The electrons are continuously passed to cytochrome c. Finally, the cytochrome c uses the electrons and H^+ to reduce O_2 to H_2O. The *Plasmodium* genome lacks F_0 the subunit (subunits a and b) which is essential for ATP generation. Fisher et al., (2007) described the presence of a proton leak via the *Plasmodium* F_1F_0 respiratory chain to enable the maintenance of high transmembrane proton potential ($\Delta\Psi_m$).

Since DHODH is known to be critical for growth of the parasites, it has been studied extensively as a target for drug development in the last decade (Baldwin et al., 2002, Heikkilä et al., 2007, Davies et al., 2009, Baldwin et al., 2005, Patel et al., 2008). DHODH, one of the mtETC dehydrogenases, is known to be a critical key enzyme in the pyimidine biosynthesis pathway, which is essential in the parasites because they cannot salvage pyrimidines. A study undertaken by (Painter et al., 2007) showed that transgenic *P. falciparum* parasites expressing yeast DHODH (non-ubiquinone dependent) can independently synthesize the pyrimidine precursors in the presence of mtETC inhibitors such as atovaquone (Painter et al., 2007). Therefore, it has been concluded that the major specific role of the mtETC in blood stages of *P. falciparum* parasites is to solely serve as an electron disposal system for DHODH and pyrimidine synthesis and hence DHODH is the only dehydrogenase in the mtETC viable as a chemotherapeutic target (Painter et al., 2007, Vaidya et al., 2008) (Figure. 5.3).

On the other hand, it has been reported and reviewed that *P. falciparum* type II NADH dehydrogenase (PfNDH2 or rotenone-insensitive complex I) has been a promising subject for the development of a chemotherapeutic drug because PfNDH2 is missing the conventional large multisubunits of complex I that are found in most mammalian mitochondria and also it is not directly involved in proton pumping (Fisher et al., 2009, Dong et al., 2009, Biagini et al., 2006, Fisher et al., 2007). Therefore, it has been demonstrated that PfNDH2 inhibition resulted in the collapse of $\Delta\Psi_m$ by starving the bc_1 of the reduced form of ubiquinone (Biagini et al., 2006). Fry and Beesley (1991) showed previously that NADH-dependent respiration contributes ~50% of the ubiquinol flux to the bc_1 complex at maximal capacity compared to only 1% by DHODH (Fry and Beesley, 1991).

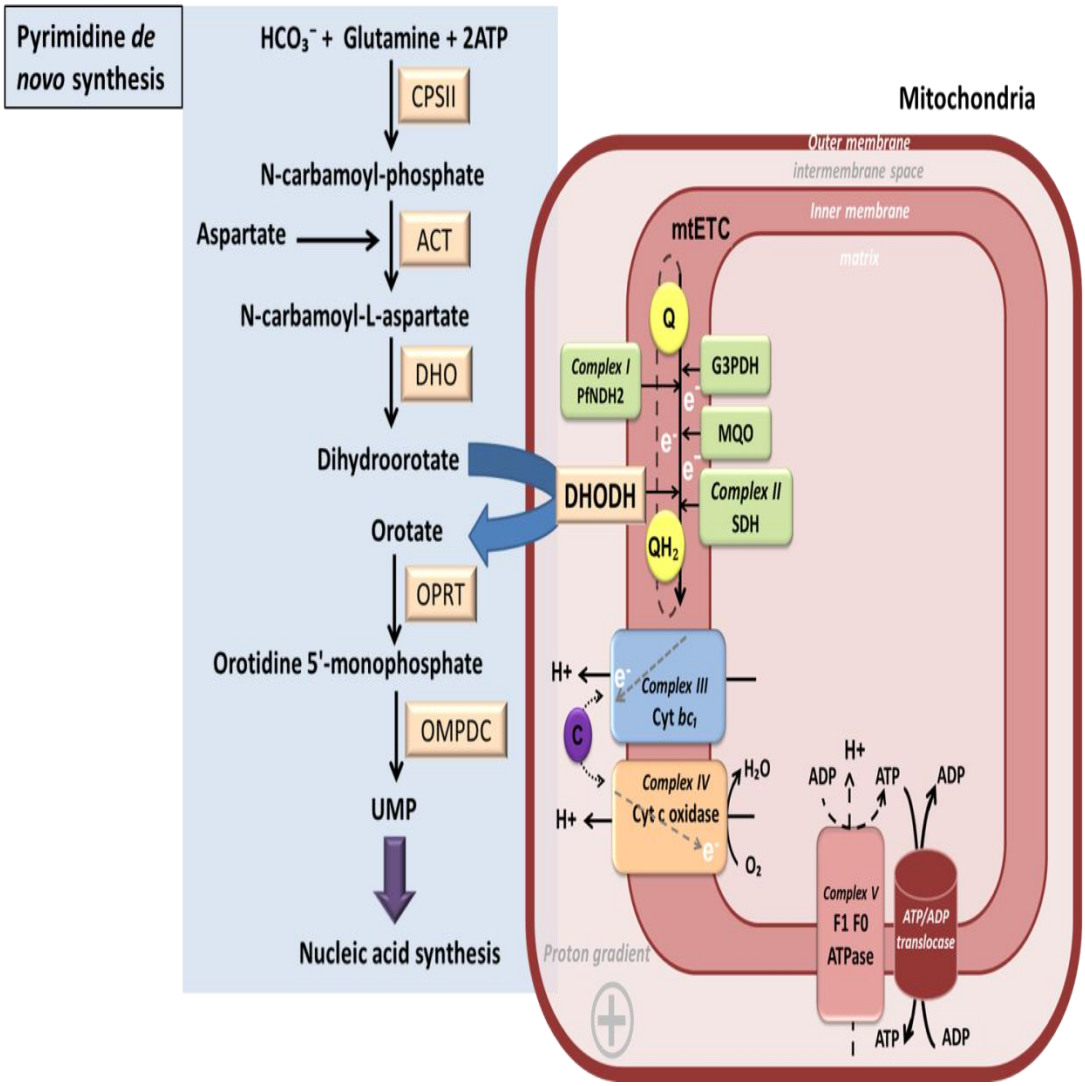

Figure 5.3: Schematic metabolic pathway of pyrimidine *de novo* synthesis and mitochondrial electron transport chain in *Plasmodium falciparum*.

The diagram depicts that pyrimidine *de novo* synthesis is linked to the mitochondrial electron transport chain (mtETC) through dihydrooroate dehydrogenase enzyme. Enzymes involved in the *de novo* pyrimidine biosynthesis are indicated in orange-coloured boxes. Abbreviations: CPSII, Carbomoyl phosphate synthatase II; ACT, Aspartate carbamoyl transferase; DHO, Dihydroorotase; DHODH, Dihydroorotate dehydrogenase; OPRT, Orotate phosphoribosyltransferase; OMPDC, Orotidine 5'-monophosphate decarboxylase.

In this regard, it seems from the aforementioned description of *P. falciparum* mitochondria and ETC that there are gaps and disagreement in understanding the metabolic role of this organelle which includes the function of certain components of the respiratory chain in the ETC and their link to other mitochondrial-related metabolism (e.g. pyrimidine biosynthesis). Therefore, the aim of this chapter was to determine whether using atovaquone (Figure 5.4A) as a proof-of-concept inhibitor to

perturb bc_1 complex of mtETC in both sensitive and transgenic *P. falciparum* strains will result in the generation of the same metabolic fingerprints. Similarly, if the findings between sensitive and transgenic parasite strains were distinct, then a new lead compound (CK-2-68) (Figure 5.4B), that has been shown to have dual-target mode of action (MoA) effects on PfNDH2 and bc_1 complex in nanomolar concentration (Pidathala et al., 2012), will be used in this study to confirm the findings of atovaquone.

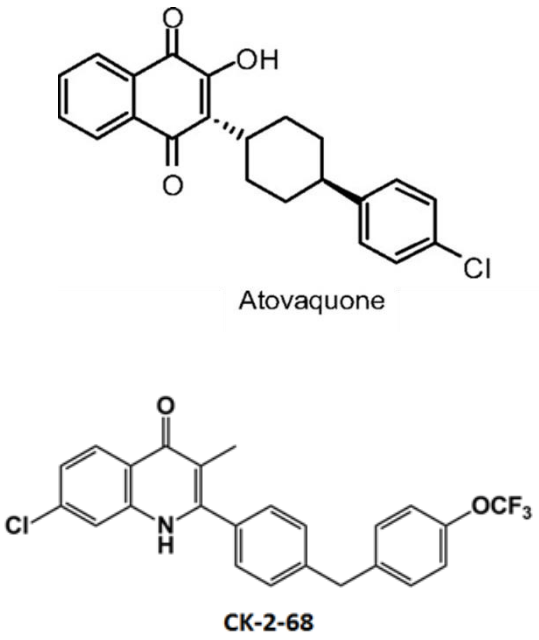

Figure 5.4: Chemical Structure of (A) Atovaquone and (B) CK-2-68.

To investigate this hypothesis, pharmacometabolomics approach was undertaken to examine the metabolic differences between sensitive and transgenic parasite strains upon drug addition.

5.2. Materials and Methods

5.2.1. Parasite culture

P. falciparum sensitive 3D7 and transgenic 3D7-yDHOD·GFP strains were maintained in synchronous cultures at 2% hematocrit as described previously (Trager and Jensen, 1976). A transgenic derivative of parental strain *P. falciparum* 3D7, 3D7-yDHODH·GFP, containing yeast DHODH gene was generated through electroporation of purified pHHyDHOD–GFP plasmid into ring stages of *P. falciparum* using a BioRad GenePulser (BioRad, UK) and was prepared by Dr. David Johnson, (Parasitology Department, Liverpool School of Tropical Medicine, UK). Purified pHHyDHOD·GFP plasmid was generously provided by Professor Akhil Vaidya (Drexel University College of Medicine, Philadelphia, USA). This plasmid contains a human dihydrofolate reductase gene as a WR99210-selectable marker (Painter et al., 2007). The transgenic parasites were grown and maintained in complete RPMI-1640 culture medium containing 2.5 nM of WR99210 (section 5.2.1.1) for the purpose of selectivity. Routine parasite culture system was thereafter followed as described in chapter 2 section 2.2.

5.2.1.1. Preparation of WR99210-selectable marker

WR99210, antifolate inhibitor, was purchased from Sigma-Aldrich (UK). The preparation of 10 mM stock of WR99210 (MW = 394.68 g/mol) was as follows: 3.9468 mg of WR99210 was dissolved in 1 ml of DMSO. This 10 mM stock of WR99210 was further diluted to 250 uM stock after which it was labeled, and stored at -20 ^{0}C for future use.

5.2.2. High-Gradient Magnetic separation (HGMS) for trophozoite-stage parasite enrichment

HGMS was conducted for trophozoite-stage *P. flaciparum* parasites as described previously (chapter 4, section 4.2.1).

5.2.3. Haemocytometer for parasite counting

Haemocytometer counting for the purified *P. falciparum* trophozoite-stage parasites was carried out as described previously (chapter 4, section 4.2.2).

5.2.4. Parasite cell metabolism quenching and metabolite extraction

Briefly at this stage, the purified trophozoite-stage parasites (section 5.2.2) were subjected to a metabolomics experiment where they were incubated in culture media at 37 °C. Subsequently, the parasites were exposed to a sub-lethal concentration (IC_{90}) of perspective drugs. Afterwards, the parasites were removed and metabolically quenched in a time related manner. Metabolites were then extracted to be ready for the next stage of LC-MS/MS analysis (section 5.2.5).

This metabolomics experimental protocol was carried out throughout this thesis, however, with minor modification in each experimental chapter. The enriched trophozoite-stage parasites (section 5.2. 2) were incubated with RPMI-1640 culture media (R8758, glutamine, and sodium bicarbonate) supplemented with 10% pooled human serum, 25 mM HEPES (pH 7.4) (VWR), 40 μM hypoxanthine (Sigma), and 20 μM gentamicin sulfate (Sigma) at 37 °C under 3% O_2/4% CO_2 in N_2 (described in chapter 2 sections 2.2.2 and 2.2.4) for a 7 hour time course. At predetermined time intervals, one volume of enriched-culture (~1 × 10^8 parasites/mL) was directly collected at *t*= 0 h and *t*= 0.5 h intervals for metabolic quenching into three volumes of -20 ºC quenching solvent system [acidic acetonitrile/methanol/water (40:40:20 + 0.1M formic acid) spiked with internal standards] (section 5.2.2.1) (Rabinowitz and Kimball, 2007). The IC_{90} concentrations of drugs was choosen for this chapter and the subsequent chapters because the IC_{50} from the preliminary data did not show any effect on the purified parasites. This is may be due to the highly parasitaemia (~95%) present for the experiment. The IC_{90} concentrations of atovaquone (2.5 nM) and CK-2-68 (50 nM) (section 5.2.4.1) were then added at *t*= 1 h time point for corresponding drug-treated enriched-cultures. DMSO was added to untreated controls in an equivalent amount to that of the drug added. After quenching, the sample was kept at -80 ºC overnight. The sample was then centrifuged at 4500 rpm for 20 min with a pre-cooled rotor at 4 ºC. The supernatant was carefully transferred into a new tube and kept on ice whereas the cell debris was washed twice with three volumes of extraction solvent system [acetonitrile/methanol/water (40:40:20)] (chapter 3, section 3.2.2.5.1). All the supernatants for each individual sample were thereafter collected and pooled together into the corresponding sample tube. Afterwards, the extracted metabolite sample was concentrated under N_2 gas flow in the fume hood by using the sample concentrator

system (Techne sample concentrator, Bibby Scientific Ltd, UK) until the sample was completely dry. The sample was then kept at -80 °C ready for LC-MS/MS analysis.

5.2.4.1. Solvent and Drug Preparation

All the solvents used to carry out the LC-MS/MS metabolomics experiments were HPLC grade as described in Chapter 2 unless otherwise stated. The solvents used for drug preparation depend on the solubility of the perspective drug. In this chapter, two drugs were used, namely atovaquone (MW = 366.84 g/mol) and CK-2-68 (MW = 443.85 g/mol) which were weighed from solid powders to an appropriate amount in a previously autoclaved eppendorf tube. Stocks of 10 mM were prepared for atovaquone and CK-2-68 as follows: 3.66 mg of atovaqoune and 4.44 mg of CK-2-68 were dissolved in a 1 ml of dimethyl sulfoxide (DMSO, Sigma, UK). Both drug stocks were then labeled and stored at -20 ºC for no longer than a month. Final dilutions were performed with RPMI-1640 culture media and freshly made prior to commencing metabolomics experiment studies.

5.2.5. LC-MS/MS instrumentation

Briefly at this stage, sample preparation including parasite samples, external standards, authentic QCs, and blanks was carried out in this section aimed at LC-MS/MS. In addition, the chromatographic gradient condition and mass spectrometry tuning was initially set up for this chapter. Final improved LC-MS/MS platform is described in chapter 3 and was used throughout this thesis.

5.2.5.1. Sample preparation

The parasite sample preparation was carried out as follows: dried sample was taken out from -80 °C freezer and resuspended in one volume of freshly prepared mobile phase [(20 mM ammonium acetate + 20 mM ammonium hydroxide) in 95:5 water:acetonitrile (pH 9.45)] (Chapter 2, section 2.3.4). The resuspended sample was then transferred into an eppendorf tube and spun at high speed for 30 min at 4 °C. The supernatant was thereafter filtered using phenex-RC membrane filters (0.2 µm pore size, Phenomenex, USA) into a chromacol LC-MS/MS vial (Chromacol, Thermo Fisher Scientific Inc.,

UK). The preparation of external standards, authentic QCs and blank was freshly carried out for each metabolomics experiment as described previously (chapter 3).

5.2.5.2. Chromatographic separation

Chromatographic separation was achieved using Luna aminopropyl column (250 mm × 2 mm with a 5 μm particle size, Phenomenex, USA) connected to security guard packed with double-cartridge (4 mm × 2 mm, Phenomenex, USA) to maximize contaminant removal and extend the half-life of the HPLC column. HILIC column (described in chapter 2 and 3) was employed for the metabolite separation using an Accela Autosampler HPLC system (Thermo Fisher Scientific). The mobile phase consisted of solvent A [(20 mM ammonium acetate + 20 mM ammonium hydroxide) in 95:5 water:acetonitrile (pH 9.45)] and solvent B (acetonitrile). The chromatographic gradients were as follows: t = 0, 15% A; t = 7 min, 100% A; t = 14 min, 100% A; t = 16min, 15% A; t = 35 min, 15% A. Injection volume, flow rate, column temperature and autosampler temperature were set at 20 μL, 150 μL/min, 15 °C and 15 °C, respectively. The injection needle was washed with one volume of methanol/water (50:50) solution between injections to eliminate the problem of carryover between samples.

5.2.5.3. Mass spectrometry configuration

A TSQ Quantum Access™ Triple Stage Quadrupole mass spectrometer (Thermo Electron Corporation) equipped with electrospray ionization (ESI) was employed for the detection and analysis of metabolites. ESI spray voltage was 3,200 V. Nitrogen was used as sheath gas at 50 psi and as the auxiliary gas at 10 psi, and argon as the collision gas at 1.5 mTorr, with the capillary temperature at 320 °C. Scan time for each single reaction monitoring (SRM) event transition was 0.1 s with a scan width of 1 m/z. The instrument control, data acquisition, and data analysis were achieved by applying the Xcalibar software (Thermo Electron Corporation, version 2.0.7 release), which also controlled the chromatography system.

5.2.6. Data treatment and analysis

The independent biological replicates from both drug-treated and untreated controls were analyzed and the metabolite concentration was averaged at each time point. Metabolite concentration levels were quantified by applying a standard calibration

curve using standards of known concentration for each of the 23 selected reaction monitoring (SRM). However, the remaining metabolites described in Chapter 3 were below the limit of detection in the parasite samples for the method of this chapter. The signal for each metabolite was defined as the area under the curve (AUC) of the integrated peak. Each metabolite signal was normalized to the signal of the internal standard DL-arabinose (negative mode) or β-alanine (positive mode) in the same sample. All data were expressed as the normalized levels of a metabolite in the sample at any one time point to the number of purified trophozoite-stage parasites in untreated and drug-treated experiments. The metabolite concentrations in drug-treated parasites were divided by their corresponding concentration in the untreated control to present the untreated controls as a baseline. This ratio was combined in a dataset file and imported into MetaboAnalyst web-based software (http://www.metaboanalyst.ca) (Xia et al., 2012, Xia et al., 2009), $\log_2$ transformed and analyzed by the different metabolomics analysis tools described previously (Chapter 4, section 4.2.5).

5.3. Results

Part of the findings obtained in this chapter was published in (Biagini et al., 2012). The metabolomics experiments carried out were conducted on two strains namely *P. falciparum* sensitive 3D7 and transgenic *P. falciparum* 3D7-yDHOD·GFP. Both strains were exposed equally to a sub-lethal concentration of atovaquone (2.5 nM, IC_{50} 0.8 ± 0.1) after 1 h of incubation. Untreated parasite controls were exposed to equivalent DMSO concentrations to the drug treated experiments. In addition, the *P. falciparum* 3D7 sensitive strain was also exposed to a sub-lethal concentration of CK-2-68 (50 nM, IC_{50} 31 ± 3).

The 23 metabolites targeted for this study were selected on the basis that they were the predominant metabolites involved in mitochondrial and related metabolism. These metabolites were associated with metabolic pathways including glycolysis, TCA cycle, pyrimidine biosynthesis, purine salvage, and amino acid metabolism. The dynamic changes of metabolites from purified parasites were monitored in a time related manner and the subsequent metabolite detection and comparative quantification were carried out using the LC-MS/MS targeted metabolomics approach. The quantified 23 metabolites for each drug-treated and untreated group were included in one dataset. This dataset represented the ratio of normalized concentration of drug-treated/untreated parasites. The following findings were obtained from the metabolomics analysis of the dataset using metabolanalyst web-based software.

5.3.1. Metabolomics analysis of *P. falciparum* parasites

5.3.1.1. PCA and PLS-DA

The 2-D score plot from PCA of normalized dataset revealed separate clusters of *P. falciparum* sensitive 3D7 and transgenic 3D7-yDHOD·GFP strains, reflecting essential differences in the metabolites generated. It reveals cluster overlap between atovaquone and CK-2-68 treated parasites, indicating commonalities in the mode of action (MoA) effect on the targeted metabolites (Figure 5.5 A). The 3-D score PCA plot was created to further examine the interrelation between atovaquone, CK-2-68 treated sensitive parasites and atovaquone-treated transgenic parasites. The 3-D score PCA plot demonstrated distinct separation among sensitive and transgenic treated parasite groups but not clear discrimination between atovaquone treated and CK-2-68 treated sensitive

parasites (Figure 5.5 B). A corresponding loading plot indicated that the divergence observed on PCA clustering was mainly based on differences in the relative amounts of carbamyol-l-aspartate and dihydroorotate, upstream intermediates of the pyrimidine biosynthesis pathway (Figure 5.5 C).

The supervised clustering method PLS-DA was carried out to improve any occurrence of poor separation obtained within the PCA model for the atovaquone treated, CK-2-68 treated sensitive parasites; and atovaquone-treated transgenic parasite. Yet again, a distinct clustering separation was observed in the 2-D PLS-DA between atovaquone treated and CK-2-68 treated sensitive parasites; and atovaquone-treated transgenic parasite (Figure 5.6 A). Interestingly, a clear divergence and separation was demonstrated in the 3-D PLS-DA among the three groups in the dataset: atovaquone treated, CK-2-68 treated sensitive parasites and atovaquone-treated transgenic parasite (Figure 5.6 B). A resultant loading plot showed that the distinguished divergence on PLS-DA clustering was consistent with that observed in the PCA loading plot which indicated carbamyol-l-aspartate and dihydroorotate as metabolic fingerprints (Figure 5.6 C).

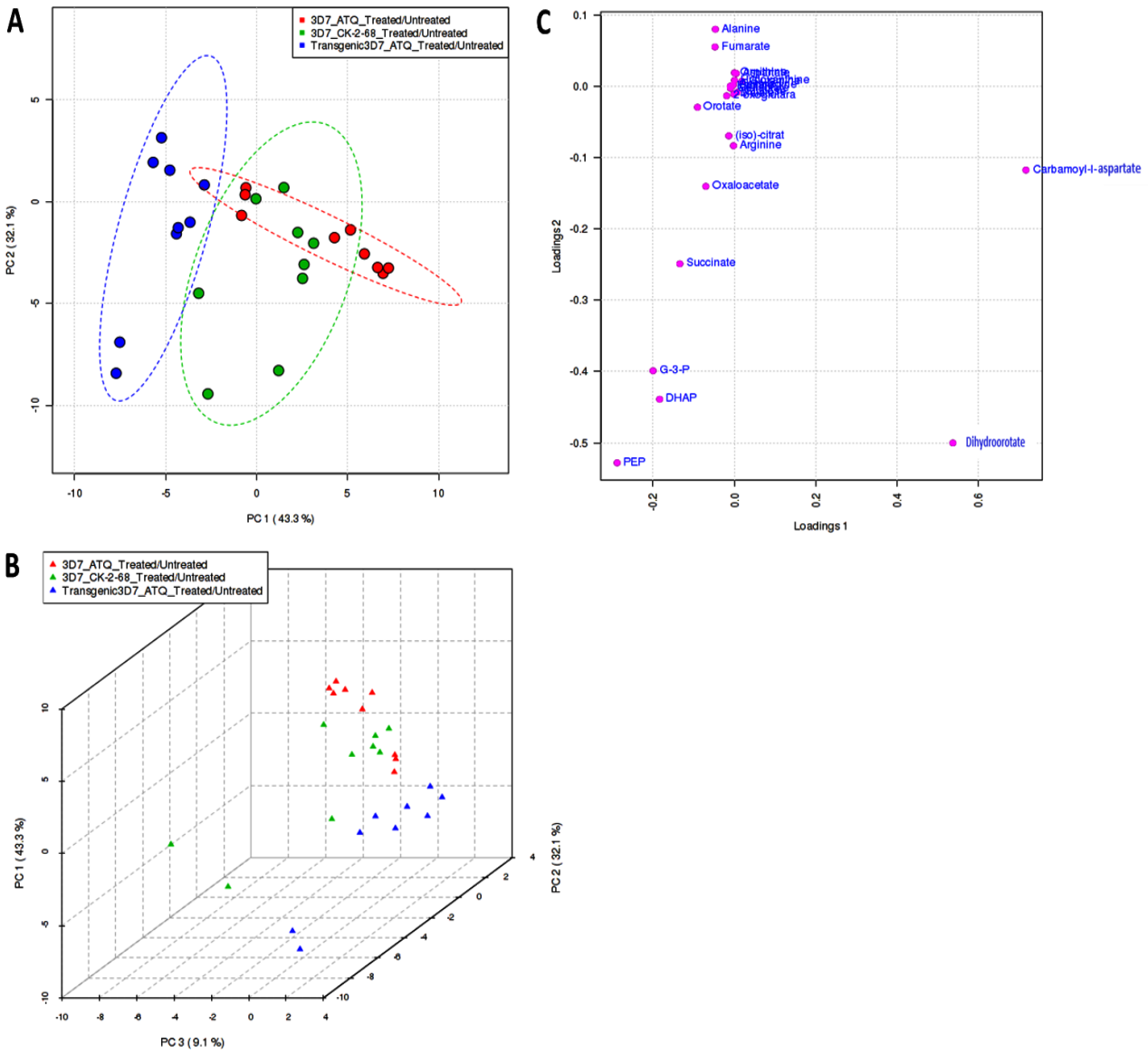

Figure 5.5: PCA score and loading plots for *P. falciparum* 3D7 sensitive and transgenic strains treated with atovaquone and CK-2-68.

A) 2-D score plot shows the clustering of *P. falciparum* 3D7 sensitive strain treated with atovaquone (ATQ) (red circle) and CK-2-68 (green circle); and the clustering of *P. falciparum* 3D7 transgenic strain treated with atovaquone (ATQ) (blue circle). Line boundary for each group represented a 95% confidence limit from each treatment centre. B) 3-D score plot shows the clustering of *P. falciparum* 3D7 sensitive strain treated with atovaquone (ATQ) (red triangle) and CK-2-68 (green triangle); and the clustering of *P. falciparum* 3D7 transgenic strain treated with atovaquone (ATQ) (blue triangle). Panels A and B show distinctive separation of the transgenic strain from the sensitive strain. C) *P. falciparum* metabolites loading plot discriminate between various time points for the corresponding score plots (panel A and B) and reveal the metabolic fingerprints in carbamoyl-l-aspartate and dihydroorotate.

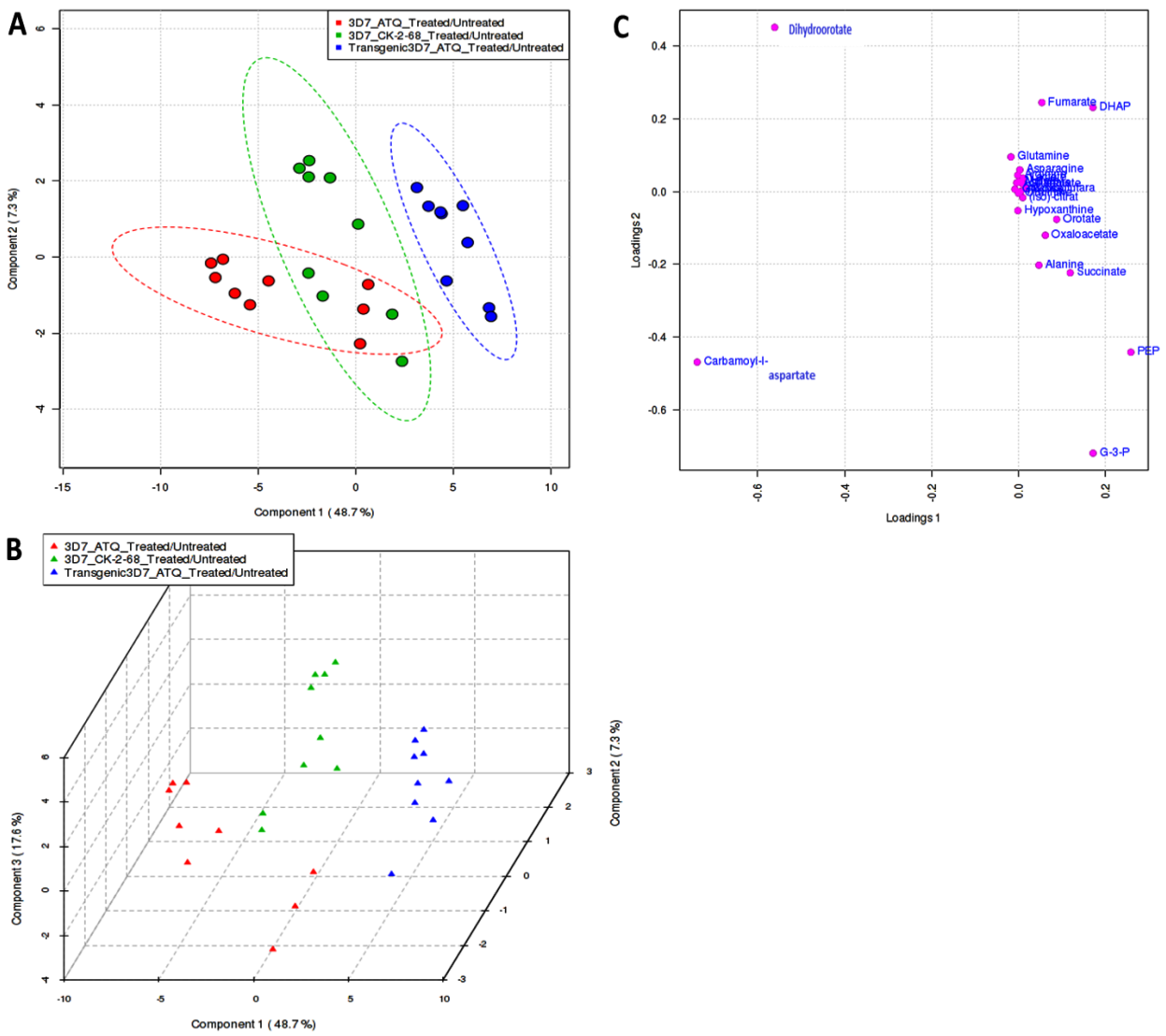

Figure 5.6: PLS-DA score and loading plots for *Plasmodium falciparum* 3D7 sensitive and transgenic strains treated with atovaquone and CK-2-68.

A) 2-D score plot shows the clustering of *P. falciparum* 3D7 sensitive strain treated with atovaquone (ATQ) (red circle) and CK-2-68 (green circle); and the clustering of *P. falciparum* 3D7 transgenic strain treated with atovaquone (ATQ) (blue circle). Line boundary for each group represented a 95% confidence limit from each treatment centre. B) 3-D score plot shows the clustering of *P. falciparum* 3D7 sensitive strain treated with atovaquone (ATQ) (red triangle) and CK-2-68 (green triangle); and the clustering of *P. falciparum* 3D7 transgenic strain treated with atovaquone (ATQ) (blue triangle). Panels A and B show distinctive separation of the transgenic strain from the sensitive strain in addition to clear segregation between atovaquone-treated and CK-2-68-treated *P. falciparum* 3D7 sensitive strain parasites. C) *P. falciparum* metabolites loading plot discriminate between various time points for the corresponding score plots (panel A and B) and reveal the metabolic fingerprints in carbamoyl-l-aspartate and dihydroorotate.

5.1.1.1. Heat map for *P. falciparum* metabolome profiling

The ratio of drug-treated/untreated dataset among all the three groups, atovaquone, CK-2-68 treated sensitive parasites and atovaquone-treated transgenic parasite, were analysed by metaboanalyst web-based software and presented as a heat map for visual aids.

The heat map highlights visually, by the use of colour, the relative difference among atovaquone, CK-2-68 treated sensitive parasites and atovaquone-treated transgenic parasites (Figure 5.7). It is visibly evident that the metabolomic profiles presented by heat map show that carbamoyl-l-aspartate and dihydroorotate in atovaquone-treated and CK-2-68-treated sensitive parasites display very similar increasing trends (Figure 5.7). However, it appears that DHAP, G-3-P and PEP profiles were different in atovaquone treated than that of CK-2-68 treated parasites. On the other hand, the trends observed in the profiles of carbamoyl-l-aspartate and dihydroorotate for atovaquone-treated transgenic parasites were entirely opposite to those seen in atovaquone-treated and CK-2-68-treated sensitive parasites (Figure 5.7). There were no other clear metabolomic profile trends observed in other metabolites selected for this experiment.

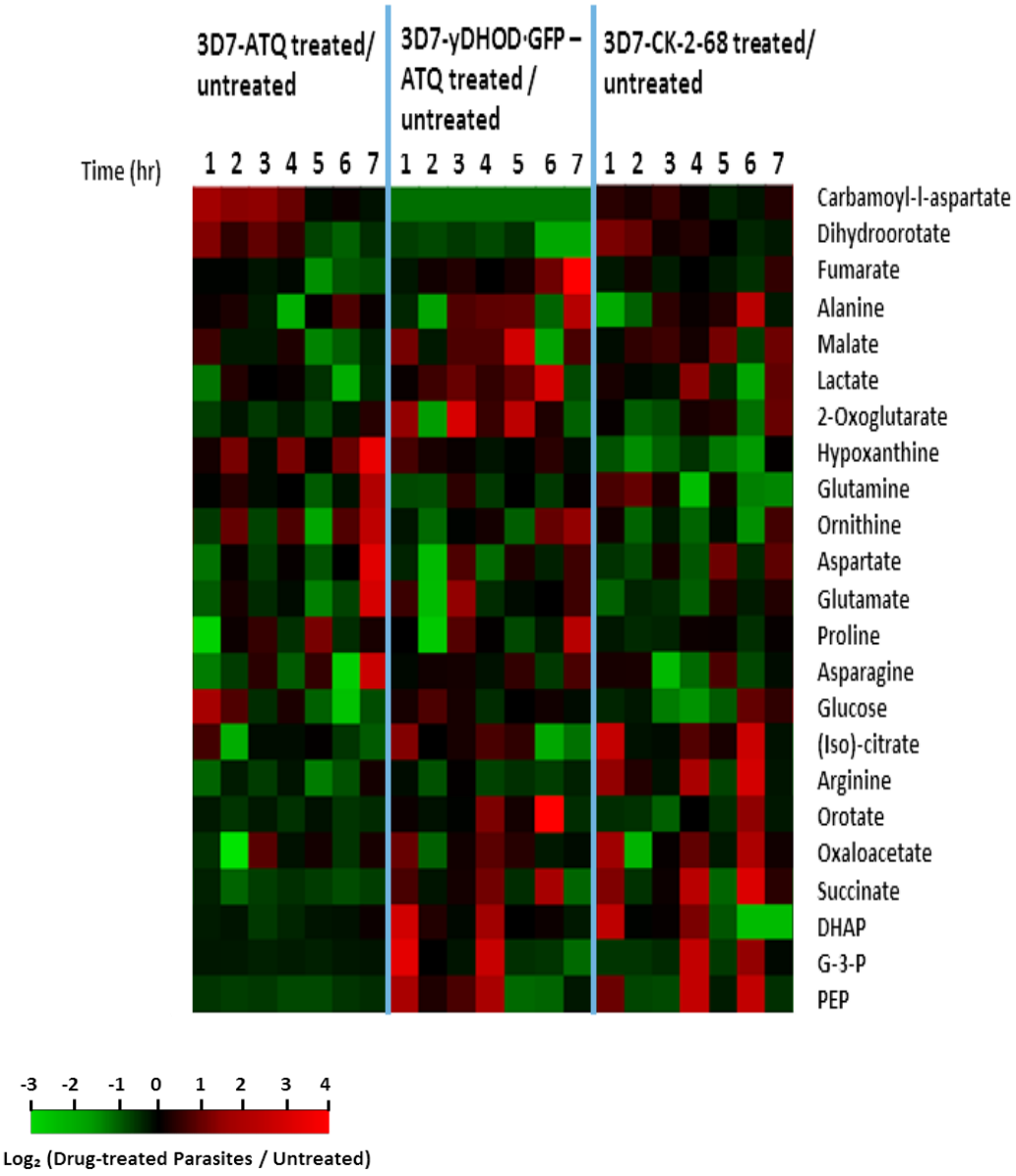

Figure 5.7: Heat map of metabolome dynamics following the addition of drug at time 1hr (50 nM CK -2–68 or 2.5 nM atovaquone) to *P. falciparum* 3D7 and 3D7-yDHODH·GFP parasites.

Fold changes are relative to untreated controls. Metabolite levels during the drug exposure course of atovaquone and CK-2-68 were normalized by purified parasite cell volume and expressed relative to the levels measured in the untreated controls. Ratios were $\log_2$ transformed and plotted on a colour scale. Rows correspond to metabolites measured by LC-MS/MS. Columns correspond to hours post drug exposure for each of the three metabolomics experiments time courses. Green and red colours represent the $\log_2$ ratio of drug-treated/untreated decreases and increases, respectively. Black colour indicates the baseline. Values are averages of triplicate independent biological experiments. Abbreviations: DHAP, dihydroxyaceton phosphate; G-3-P, glycerol-3-phosphate; PEP, phosphoenol pyruvate.

5.1.2. Biochemical time-dependent metabolic fingerprinting in *P. falciparum*

It was clear from the findings noted in loading plots of PCA and PLS-DA in addition to the results seen in the heat map that the metabolic fingerprints of *P. falciparum* mitochondria were carbamoyl-l-aspartate and dihydroorotate. The time course for the *P. falciparum* untreated controls and atovaquone and CK-2-68 treated parasite strains was carried out for 7 h and assayed metabolically. The comparative concentrations of metabolic fingerprints observed in the findings of metabolomics analysis were plotted using time-line graphs (Excel-microsoft office, 2010) and published as (Biagini et al., 2012).

The results showed that there was a notable accumulation in the amounts of carbamoyl-l-aspartate and dihydroorotate following atovaquone and CK-2-68 addition to *P. falciparum* sensitive 3D7 strain (Figure 5.8). Conversely, there were no changes in carbamoyl-l-aspartate and dihydroorotate levels in atovaquone-treated transgenic 3D7-yDHODH·GFP parasites (Figure 5.8). In addition, all the untreated parasite controls showed no variations in the concentration of carbamoyl-l-aspartate and dihydroorotate.

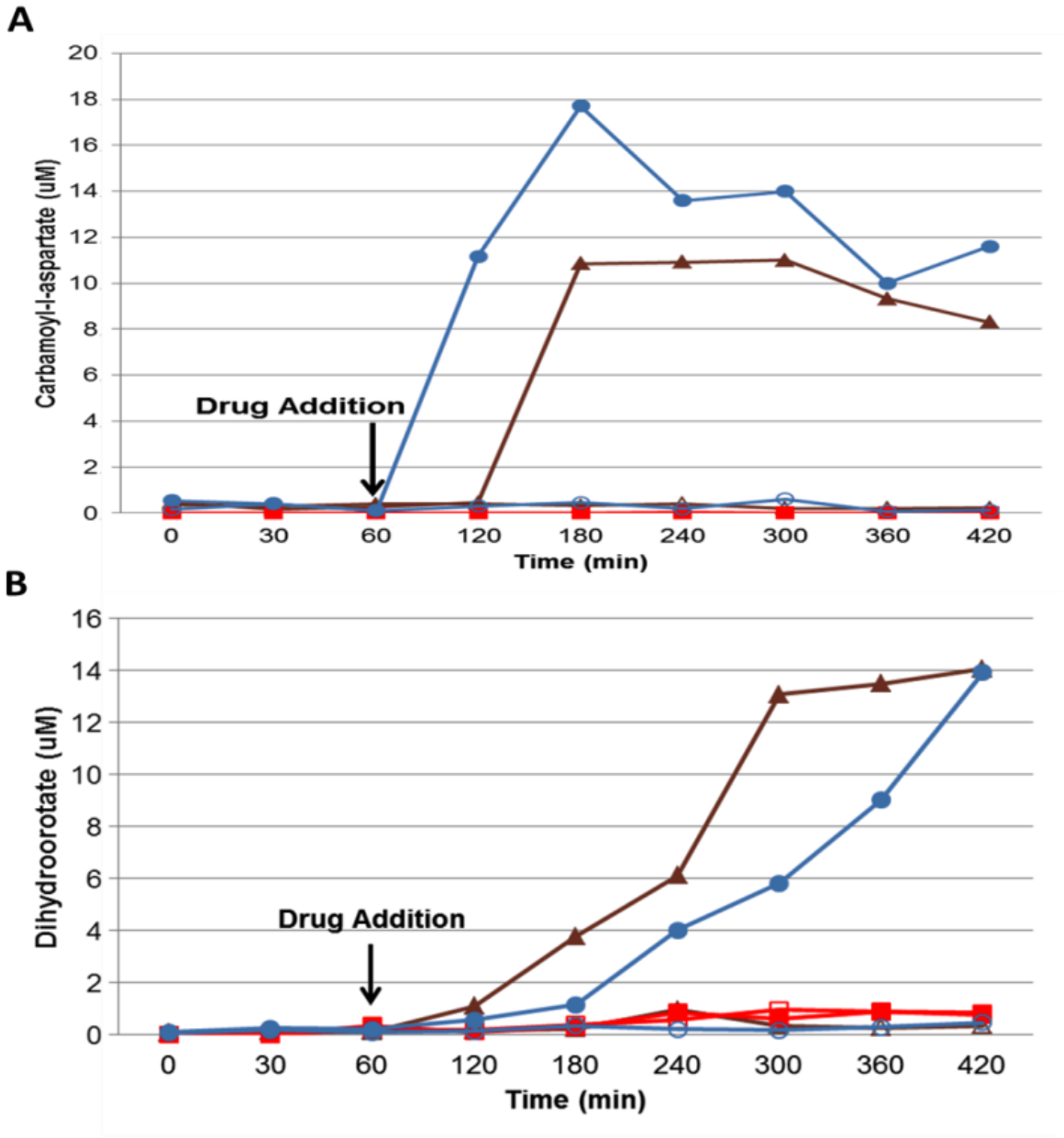

Figure 5.8: Time-dependent curves of (A) carbamoyl-l-aspartate and (B) dihydroorotate in drug-treated and untreated sensitive and transgenic strains of *P. falciparum* parasites.

A) Carbamoyl-l-aspartate B) Dihydroorotate concentration levels were determined in 3D7 untreated parasites (open brown triangle), atovaquone-treated 3D7 (closed brown triangle), untreated 3D7-yDHODH·GFP transgenic parasites (open red square), atovaquone-treated 3D7-yDHODH·GFP transgenic parasites (closed red square), 3D7 untreated parasites (open blue circle) and CK-2-68-treated 3D7 (closed blue circle).

5.4. Discussion

The metabolic function of *P. falciparum* mitochondria has long been thought to be minimal because of the existence of anaerobic glycolysis in malaria parasites as they require low O_2 and high CO_2 for growth and they have acristae mitochondria (Scheibel and Miller, 1969, Sherman, 1979, Slomianny and Prensier, 1986). However, the seminal discovery of DHODH in malaria parasites showed that it was intimately connected to the ETC at the ubiquinone level (Gutteridge et al., 1979). A study carried out by Hammond el al (1985) showed that *P. falciparum* treated with atovaquone resulted in the inhibition of pyrimidine *de novo* synthesis (Hammond et al., 1985). The malaria parasite mitochondrion has been validated as a drug target after the discovery of atovaquone which target the mtETC at the level of the bc_1 complex (Fry and Pudney, 1992). Therefore, the findings described in this chapter show that the two metabolic fingerprints, carbamoyl-l-aspartate and dihydrooroate, generated following atovaquone addition to a sensitive strain of *P. falciparum*, resulted from the collapse in the $\Delta\Psi_m$ leading to the indirect effect of atovaquone by disrupting DHODH. This is direct biochemical evidence for the site and MoA of atovaquone. In addition, the metabolic fingerprint findings for the atovaquone treated sensitive *P. falciparum* strain was consistent with the results observed previously when investigating the cytotoxicity effects of atovaquone on pyrimidine biosynthesis (Seymour et al., 1997, Seymour et al., 1994, Hammond et al., 1985). This highlighted the significant linkage between mtETC and pyrimidine biosynthesis to the DHODH enzyme.

Painter *el at.*, (2007) carried out a transfection study to generate a transgenic *P. falciparum* strain expressing cytosolic yeast DHODH which is independent of mtETC (Painter et al., 2007). The transgenic *P. falciparum* strain was shown to be completely resistant to mtETC inhibitors (Painter et al., 2007). A metabolomics study was conducted on this transgenic 3D7-yDHOD·GFP *P. falciparum* strain to examine the main metabolic differences between the sensitive and transgenic strains of *P. falciparum* upon atovaquone addition. Remarkably, both dimensions (2-D and 3-D) of PCA and PLS-DA analysis revealed a distinct segregation between sensitive and transgenic *P. falciparum* parasite strains treated with atovaquone, indicating the occurrence of a significant metabolic fingerprint producing this divergence of the strains. This divergence was examined further by loading plot to indicate the major metabolic fingerprints in both strains. Loading plots of PCA and PLS-DA indicated that

the major metabolic fingerprints were carbamoyl-l-aspartate and dihydroorotate signifying the metabolic link between pyrimidine biosynthesis and mtETC. In addition, the pyrimidine biosynthesis in the transgenic *P. falciparum* strain was not affected by the addition of atovaquone because of the presence of an alternative route of synthesis for orotate. Therefore, this cytosolic bypass provided by yDHODH was adequate to serve the critical step in pyrimidine *de novo* biosynthesis allowing the parasite to be independent of the mtETC. This was supported by conducting heat map analysis which showed clearly the clustering and metabolomics profiles of the parasites, demonstrating a distinct phenotypic signature between sensitive and transgenic parasites which occurred mainly in the upstream intermediates of the pyrimidine biosynthesis pathway.

Painter et al (2007) and Vaidya et al (2008) concluded from their work on transgenic *P. falciparum* expressing yeast DHODH that the only dehydrogenase component of the mtETC with potential as a drug target is DHODH (Painter et al., 2007, Vaidya et al., 2008). Therefore, atovaquone was used as a proof-of-concept antimalarial drug that is known to specifically target the bc_1 complex in the mtETC and the findings show essential differences between sensitive and transgenic *P. falciparum* strains following atovaquone addition. An in-house lead compound, CK-2-68, that has been shown to have dual-target MoA effects on PfNDH2 and bc_1 complex in nanomolar concentration (Pidathala et al., 2012) was used in this metabolomics study to confirm the findings of atovaquone. The 2-D of both the PCA and the PLS-DA findings showed that CK-2-68-treated and atovaquone-treated sensitive *P. falciparum* were grouped closely together (line boundary for each group represented a 95% confidence limit from each treatment centre) suggesting the commonalities in the MoA between atovaquone and CK-2-68. Further PCA and PLS-DA analysis was presented in 3-D plots which showed the noticeable aggregation of time points following the addition of CK-2-68 and atovaquone and each group was separated from each other. This shows the differences in the mode of action of each drug confirming that CK-2-68 targets a component in the mtETC other than bc_1 which is PfNDH2 (Pidathala et al., 2012, Biagini et al., 2012). However, loading plots showed that the major metabolic fingerprints for CK-2-68 and atovaquone were carbamyol-l-aspartate and dihydroorotate. Nonetheless, the relative differences in the fumarate, succinate, DHAP, G-3-P and PEP profiles between CK-2-68-treated and atovaquone-treated sensitive *P. falciparum* seems to be the cause for the divergence between both drugs. This suggests that atovaquone and CK-2-68 have

perhaps different indirect MoAs on glycolysis metabolism and some of the TCA intermediates. Furthermore, the biochemical time course for the generated metabolic fingerprints showed an accumulation in carbamoyl-l-aspartate and dihydroorotate following CK-2-68 and atovaquone addition to the sensitive parasite strain compared to the atovaquone-treated transgenic parasite strain and untreated controls.

Overall, this pharmacometabolomics approach demonstrated the evidence that *P. falciparum* mitochondrion is tightly linked to the pyrimidine biosynthesis pathway through a critical step centralized in one of the mtETC dehydrogenase components, DHODH. The findings of this chapter which presented a systemic perturbation of mitochondria by atovaquone and CK-2-68 aroused questions about the role of other mtETC components in pyrimidine biosynthesis. Therefore, the next chapter (6) will investigate further this link by targeting different mtETC components.

The major limitation of this chapter was in analyzing the bioenergetics\redox couples, pyruvate, UMP, UDP, UTP, dCTP, CTP, GTP, carbamyol phosphate as they were below the limit of detection.

CHAPTER 6

Pharmacometabolomics Study of *Plasmodium falciparum* Mitochondria: II

6.1. Introduction

The aim of this chapter is to further explore the findings obtained in the preceding chapter (5). The metabolic role of the *P. falciparum* mitochondria under the influence of number of selective mitochondrial inhibitors is investigated and the mode of actions (MoAs) of these inhibitors are highlighted.

The malaria parasite mitochondrion is a vital organelle comprising several essential enzymes. These enzymes were found to be important in sustaining a functional TCA cycle and in maintaining the membrane potential of the electron transport chain ($\Delta\Psi_m$) (Gardner et al., 2002, Krungkrai, 2004, Olszewski et al., 2013). The mitochondrial respiratory chain consists of five dehydrogenases which generate reduced coenzyme Q (CoQ). CoQ in turn is re-oxidized by bc_1 complex to feed the electron transport chain (Vaidya and Mather, 2005). Among these dehydrogenases is DHODH which appears, from the preliminary findings in chapter 5, to form a tight link between the pyrimidine biosynthesis pathway and mtETC (Figure 6.1). Therefore, it is likely this link is essential for the development and survival of asexual stages of malaria parasites as they cannot salvage pyrimidine (Gutteridge et al., 1979).

Malaria parasites harbour DHODH type II. This enzyme is a mitochondrial membrane associated protein which catalyzes the oxidation of dihydroorotate to orotate and couples the pyrimidine biosynthesis to the respiratory chain by reducing the coenzyme ubiquinone (CoQ) to ubiquinol (Figure 6.1) (Krungkrai, 1995, Malmquist et al., 2008). It has been postulated that the major function of the *P. falciparum* respiratory chain is to regenerate CoQ required as an electron acceptor for DHODH and to maintain $\Delta\Psi_m$ (Malmquist et al., 2008, Painter et al., 2007, Vaidya et al., 2008). Consistent with this, the inhibition of pyrimidine biosynthesis at DHODH level is suggested, from the observations obtained in Chapter 5, to be an indirect MoA of atovaquone. Atovaquone causes the loss of $\Delta\Psi_m$ (and thus DHODH activity) via inhibition of the bc_1 complex, eventually leading to parasite death (Figure 6.2). In addition, the metabolomics findings in Chapter 5 shows transgenic *P. falciparum* expressing cytosolic yeast DHODH became resistant to bc_1 inhibitor (atovaquone) by synthesizing pyrimidine precursors independently to the mtETC. This is in accordance with a study by Painter et al. (2007) and highlights the essential role of PfDHODH which has become an

attractive potential drug target for the development of novel antimalarials (Phillips et al., 2008, Heikkilä et al., 2007, Baldwin et al., 2005, Patel et al., 2008). However, this raises several questions as to whether the inhibition of mitochondria with a number of selective inhibitors will lead to the same metabolic effect observed previously at the level of DHODH.

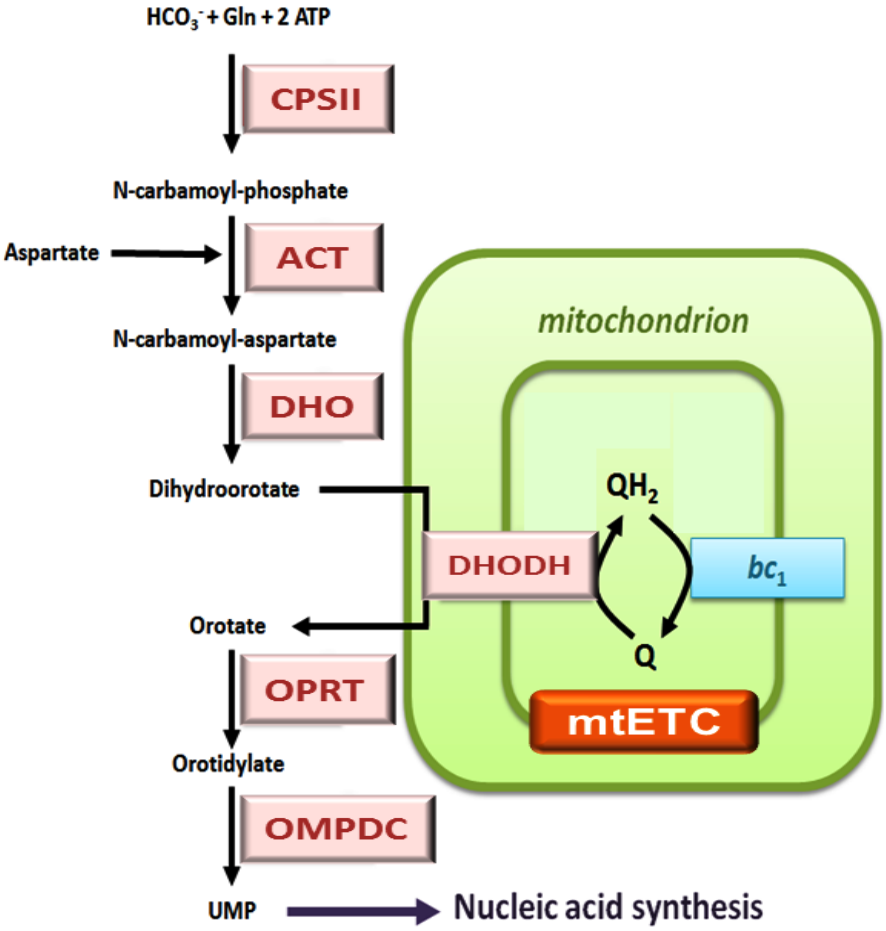

Figure 6.1: Schematic representation of the contribution of mitochondrial electron transport chain in the pyrimidine biosynthesis pathway in *P. falciparum*.

Enzymes involved in the *de novo* pyrimidine biosynthesis pathway are in pink boxes in red type. Abbreviations: CPSII, Carbomoyl phosphate synthatase II; ACT, Aspartate carbamoyl transferase; DHO, Dihydroorotase; DHODH, Dihydroorotate dehydrogenase; OPRT, Orotate phosphoribosyltransferase; OMPDC, Orotidine 5'-monophosphate decarboxylase; UMP, Uridine monophosphate.

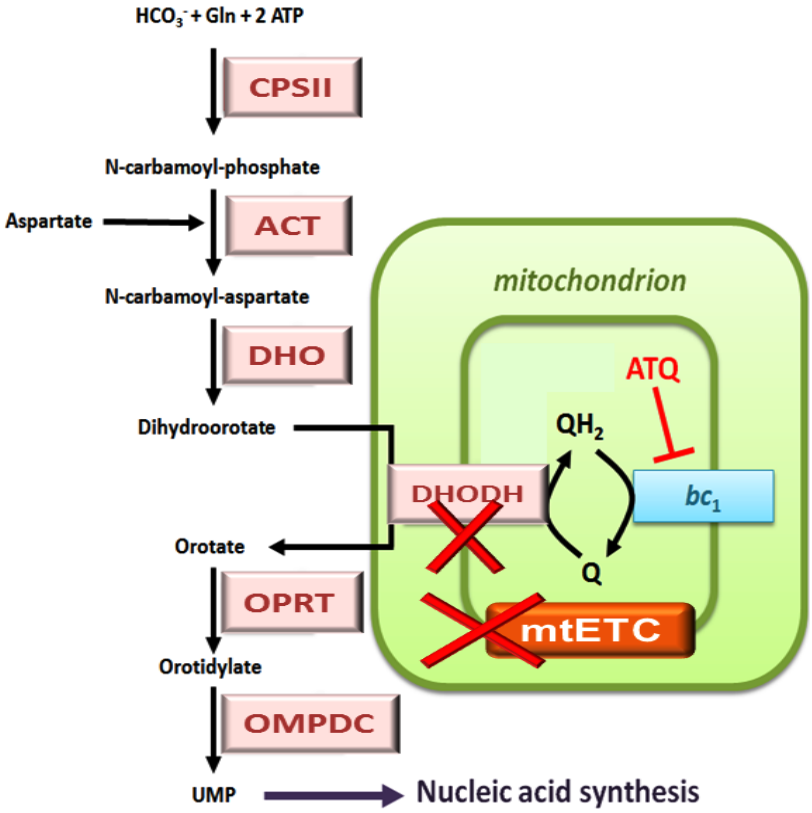

Figure 6.2: Schematic representation of the indirect effect of atovaquone on pyrimidine biosynthesis pathway in *P. falciparum*.

Atovaquone (ATQ) targets bc_1 complex in the mitochondrial electron transport chain (mtETC) leading to the depolarization of mitochondrial membrane potential (ψ_m) and eventually parasite death.

A handful of studies reported the indirect metabolic effect of atovaquone on pyrimdine biosynthesis and all of them were consistent in showing disruption of the pathway at the point of DHODH (Seymour et al., 1997, Seymour et al., 1994, Hammond et al., 1985). In addition, polarographic studies showed that the rate of mitochondrial oxygen consumption in *P. falciparum* was inhibited to various degrees by inhibitors that target each component of respiratory chain complexes I-IV in addition to targeting DHODH by 5-fluoroorotic acid (Krungkrai et al., 1999). In contrast, there is no study that shows the contribution of mtETC dehydrogenases and complexes I-IV on mitochondrial related metabolism (e.g. pyrimidine biosynthesis). In addition, Vaidya and his coworkers insist that DHODH is the only valid drug target in the mitochondria of *P. falciparum* (Painter et al., 2007, Vaidya et al., 2008). Conversely, both Biagini and Mozote propose that there are multiple drug targets within the *P. falciparum*

mitochondria (Biagini et al., 2006, Fisher et al., 2007, Biagini et al., 2008, Fisher et al., 2008, Monzote and Gille, 2010, Biagini et al., 2012). In this regards, there is a gap in the current knowledge about the role of mtETC dehydrogenases and complexes I-IV in *P. falciparum* mitochondrial related metabolism.

P. falciparum was shown to express an ADP/ATP transporter that is located in the inner mitochondrial membrane (Hatin et al., 1992). Bongkrekic acid was shown to specifically inhibit the adenine nucleotide translocase (ADP/ATP translocase) of the mitochondria (Henderson and Lardy, 1970). Whether this mitochondrial transporter is vital to the *P. falciparum* mitochondrial related metabolism is yet to be explored in this study. In addition, fusidic acid (a potent inhibitor of the translation component of elongation factor G which leads to the arresting of mitochondrial protein synthesis) has been suggested to have antimalarial activity but not as active as the known therapeutic antimalarial agents (e.g. chloroquine) (Black et al., 1985). Recently, fusidic acid was shown to specifically target *P. falciparum* mitochondria by arresting the parasite development. This confirmed reports using protein-reporter fusion which suggest that elongation factor G is a component of *P. falciparum* parasite mitochondria (Johnson et al., 2011). In addition, *P. falciparum* mitochondria rely on importing protein and tRNA for protein synthesis because mitochondrial genome lacks many genes typically found on the genome of other organisms including tRNA genes and subunits of NADH dehydrogenase (van Dooren et al., 2006). Therefore, the role of *P. falciparum* mitochondrial protein machinery synthesis in the mitochondria and mitochondrial related metabolism remains obscure.

In this chapter, biologically selective inhibitors for specific electron transport chain complexes I-IV, mitochondrial ADP/ATP transporter and mitochondrial machinery protein synthesis were used to perturb metabolic pathways generating fingerprints of metabolite concentrations and fluxes in a time-related manner. Specifically, the inhibitors used were atovaquone, atovaquone-proguanil, CK-2-68, 5-fluoroorotic acid, potassium cyanide, thenoyltrifluoroacetone, bongkrekic acid and fusidic acid. Tables 6.1 and 6.2 summarize the inhibitors used in this chapter and their proposed MoA as well as their IC_{90} values which were obtained from in-house laboratory data and used to carry out the pharmacometabolomic experiments of this chapter. Metabolite detection

and quantitation were conducted using LC-MS/MS targeted metabolomics approach as described previously (Chapter 3).

Table 6.1: Drugs used and their proposed mode of action

Compound	Proposed Mode of Action
Atovaquone	Inhibits complex III (bc_1)
Atovaquone-Proguanil	Inhibits complex III (bc_1) and sensitize $\Delta\Psi_m$
CK-2-68	Inhibits alternative complex I (PfNDH2) and complex III (bc_1)
Proguanil	Inhibits dihydrofolate reductase via its metabolite cycloguanil
5-Flouroorotic acid	Inhibits DHODH
Thenoyltrifluoroacetone	Inhibits complex II (succinate dehydrogenase)
Potassium Cyanide	Inhibits complex IV
Bongkrekic acid	Inhibits ADP/ATP mitochondrial transpoter
Fusidic acid	Inhibits elongation factor G in the mitochondrial protein synthesis machinery

Abbreviations: $\Delta\Psi_m$ mitochondrial membrane potential; DHODH, Dihydroorotate Dehydrogenase

6.2. Materials and Methods

6.2.1. High-Gradient Magnetic separation (HGMS) for trophozoite-stage parasites enrichment

The parasite cultures followed by high gradient magnetic separation (HGMS) were conducted for trophozoite-stage *P. flaciparum* parasites as described previously (chapter 4, section 4.2.1).

.

6.2.2. Haemocytometer for parasite counting

Haemocytometer counting for the purified *P. falciparum* trophozoite-stage parasites was carried out as described previously (chapter 4, section 4.2.2).

6.2.3. Parasite cells metabolism quenching and metabolites extraction

Briefly at this stage, the purified trophozoite-stage parasites (section 6.2.1) were subjected to a metabolomics experiment where they were incubated in culture media at 37 °C and subsequently exposed to drug pressure. After this the parasites were removed and metabolically quenched in a time related manner and finally the metabolites extracted to be ready for the next stage of LC-MS/MS analysis (section 6.2.4). This metabolomic experiment was conducted as described earlier (chapter 4 section 4.2.3) with the exception of the addition of drug in the study of this chapter. The IC_{90} concentrations of atovaquone (2.5 nM), atovaquone-proguanil combination (2.5 nM + 1 uM), CK-2-68 (50 nM), 5-flouroorotic acid (15 nM), bongkrekic acid (5 uM), potassium cyanide (1 mM), thenoyltrifluoroacetone (10 uM), proguanil (70 uM) and fusidic acid (200 uM) were added at 1 h time point for each set of the experiments (*n*= at least two independent replicates for each drug used) (Table 6.1). Untreated parasite controls were prepared in at least two independent biological experiments. The parasite metabolites sampling, quenching, extraction, drying and storing were performed as described beforehand (chapter 4, section 4.2.3)

6.2.3.1. Solvents and Drugs Preparation

All the solvents used to carry out the LC-MS/MS metabolomics experiments were HPLC grade as described in Chapter 2 unless otherwise stated. The solvents used for

drug preparation were different and depended on the solubility of the drug. 10mM stocks were prepared for the drugs listed in Table 6.2. These were labeled and stored at -20 ºC for no longer than a month. Final dilutions were performed with RPMI-1640 culture media which was freshly made prior to the experiment.

Table 6.2: Drugs used and their IC_{90} values.

Drugs	MW (g/mol)	IC_{90} 3D7 *P.falciparum* (nM)*	Solvent	Source
ATQ	366.83	2.5	DMSO	Sigma Aldrich
CK-2-68	443.85	50	DMSO	Prof.O'Neill, Chemistry Department, Liverpool University
PG	290.19	70×10^3	DMSO	Sigma Aldrich
5-FOA	174.09	15	DMSO	Sigma Aldrich
TTFA	222.18	10×10^3	DMSO	Sigma Aldrich
KCN	65.12	1×10^6	H_2O	Sigma Aldrich
BK	486.60	5×10^3	DMSO	Sigma Aldrich
FA	516.71	200×10^3	DMSO	Sigma Aldrich

Abbreviations: ATQ, Atovaquone; PG, Proguanil; 5FOA, 5-flouroorotic acid; TTFA, Thenoyltrifluoroacetone; KCN, Potassium Cyanide; BK, Bongkrekic acid; FA, Fusidic acid; MW, Molecular Weight. *IC_{90} values were obtained from in-house laboratory data.

6.2.4. LC-MS/MS instrumentation

Sample preparation including parasite samples, external standards, authentic QCs sample, and blanks were carried out in this section aimed at LC-MS/MS. In addition, chromatographic conditions and mass spectrometry configurations were set up ready for the samples processing.

6.2.4.1. Samples preparation

The parasite sample preparation was carried out as described previously (chapter 4, section 4.2.4.1). The preparation of external standards, authentic QC samples and blanks were freshly carried out for each metabolomics experiment as described previously (chapter 3, section 3.2.3.1).

6.2.4.2. Chromatographic separation

Chromatographic separation was conducted as described earlier (chapter 3, section 3.2.2.4).

6.2.4.3. Mass spectrometry configuration

The configuration of mass spectrometry was set up for positive and negative modes as described previously (chapter 3, section 3.2.2.3).

6.2.5. Data treatment and analysis

Metabolomics data of the biological replicates from all drugs treated parasites and untreated controls were analyzed as described previously (chapter 4 section 4.2.5).

6.3. Results

The metabolomics experiments carried out in this chapter were conducted only on the *P. falciparum* 3D7 strain. This strain was selected because of its robustness in continuous culture and sensitivity to various inhibitors and antimalarial drugs. Sets of metabolomic experiments were conducted on purified trophozoite-stage *P. falciparum*. After one hour of incubation, the enriched trophozoite-stage *P. falciparum* parasites were exposed to a sub-lethal concentration of one of the following inhibiotrs: atovaquone (2.5 nM), atovaquone-proguanil (2.5 nM + 1 µM), CK-2-68 (50 nM), 5-fluoroorotic acid (15 nM), potassium cyanide (1 mM), bongkrekic acid (5 µM), thenoyltrifluoroacetone (10 µM), proguanil (70 µM) and fusidic acid (200 µM). Nothing was added to the untreated parasite controls.

The 56 metabolites targeted for this study were selected on the basis that they are predominant metabolites in the mitochondria and mitochondrial related metabolism. These metabolites are associated with metabolic pathways including glycolysis, TCA cycle, pyrimidine biosynthesis, purine salvage, amino acids metabolism and bioenergetics/redox couples. However, only 34 metabolites were detected and quantified using the metabolomics approach described in chapter (3) whilst the remaining 22 metabolites were below the limit of detection. The dynamic changes of metabolites from purified parasites were monitored in a time related manner. The quantified 34 metabolites for each drug-treated and untreated group were included in one dataset. This dataset represented the mean of the biological replicates for each group and presented as fold change ratio that was normalized by the corresponding sample for each group collected at time zero. The following findings were obtained from the metabolomics analysis of the dataset using metabolanalyst web-based software (http://www.metaboanalyst.ca) (Xia et al., 2009, Xia et al., 2012) and the plotted line-graphs data were performed with GraphPad Prism 5.0 (GraphPad Software Inc.).

6.3.1. Metobolomics analysis of *P. falciparum* parasites

Multivariate statistical analysis using principal component analysis (PCA) and partial least squares-discriminant analysis (PLS-DA) was performed on the $\log_2$ transformed

dataset (http://www.metaboanalyst.ca) generated by LC-MS/MS and normalized at time zero.

6.3.1.1. PCA and PLS-DA

The 2-D score plot from PCA and PLS-DA of normalized dataset revealed divergence between *P. falciparum* parasites treated with atovaquone, atovaquone-proguanil, CK-2-68, 5-fluoroorotic acid, potassium cyanide and bongkrekic acid; and those treated with thenoyltrifluoroacetone, proguanil, and fusidic acid as well as untreated parasites controls (Figure 6.4A). This indicates the important differences in the inhibitors MoAs resulted in discrete separation by the different metabolites generated. In addition, the 2-D score plot from PCA and PLS-DA showed that time course points of parasites treated with atovaquone, atovaquone-proguanil, CK-2-68, 5-fluoroorotic acid, potassium cyanide and bongkrekic acid were clustered very closely to each other suggesting the similarity in the MoA of these inhibitors on the parasite mitochondria (Figure 6.4A and 6.5A). In contrast, time course points of untreated parasites and parasites treated with proguanil, thenoyltrifluoroacetone and fusidic acid were also clustered near each other suggesting either these drugs had no specific MoA effect on mitochondria or the MoA effect was not strong as the separated groups mentioned above. Further analysis was carried out using the 3-D of PCA and PLS-DA to observe a better clustering and positioning. The 3-D of PCA showed that the parasites treated with inhibitors that specifically target the different components of mtETC and ADP/ATP transporter were clustered almost together (Figure 6.4B). On the other hand, untreated parasites were grouped together with parasites treated with proguanil (Figure 6.4B). Parasites treated with fusidic acid were distinctly clustered almost separately from other treatments and untreated control indicating the specific MoA effect on different mitochondrial target other than respiratory chain (Figure 6.4B). In contrast, the 3-D of PLS-DA showed distinctively four major clusters indicting the incidence of specific discrimination between the different inhibitors treated parasites as well as untreated control parasites (Figure 6.5B). Specifically, the 3-D of PLS-DA demonstrated that CK-2-68, cyanide and bongkrekic acid treated parasites were aggregated adjacently to each other although these inhibitors have different MoAs and also different specific targets including PfNDH2/bc_1, complex IV and ADP/ATP translocase transporter, respectively. Conversely, parasites treated with atovaquone, atovaquone-proguanil and 5-fluoroorotic

acid were shown to be grouped nearby each other although 5-fluoroorotic acid specifically targets DHODH while atovaquone does not, suggesting the commonalities in the overall MoAs of the drugs effect either directly or indirectly (Figure 6.5B). On the other hand, two more clusters were observed in the 3-D PLS-DA plot and both of them were distinctively separated from each other. This includes one cluster of untreated parasite controls and parasites treated with thenoyltrifluoroacetone, and in the other cluster parasites treated with fusidic acid and proguanil (Figure 6.5B). Overall, it was clearly noted in the 3-D PLS-DA plot that parasites treated with atovaquone, atovaquone-proguanil, CK-2-68, 5-fluoroorotic acid, potassium cyanide and bongkrekic acid were clustered in one side of the plot and untreated parasites control alongside parasites treated with thenoyltrifluoroacetone, proguanil, and fusidic acid were clustered in the opposite side (Figure 6.5B).

The corresponding loading plots for PCA and PLSDA revealed that carbamoyl-l-aspartate and dihydroorotate were the major metabolic fingerprints which accounted for the aforementioned differences in the clustering of different inhibitor treated parasites alongside the untreated parasite control (Figure 6.4C and 6.5C). Similarly, Variable Influence on Projection (VIP) score was used in metabolomics analysis to further enhance the major metabolites differences among all treatments and controls. VIP scores were calculated using the variability explained in PLS-DA. Metabolites with VIP score > 1 were considered the most important metabolites responsible for the differentiation of the parasites exposed to different inhibitors (Figure 6.6). VIP score showed that the most significant metabolites with score > 1 were DHAP, orotate, alanine, fumarate, carbamoyl-l-aspartate and dihydroorotate (Figure 6.6). However, carbamyol-l-aspartate and dihydroorotate were the merely metabolites with VIP score exceeding 3 whilst DHAP, orotate, alanine, fumarate had just borderline VIP score < 1.5 suggesting that carbamoyl-l-aspartate and dihydroorotate were the prominent metabolic fingerprints (Figure 6.6).

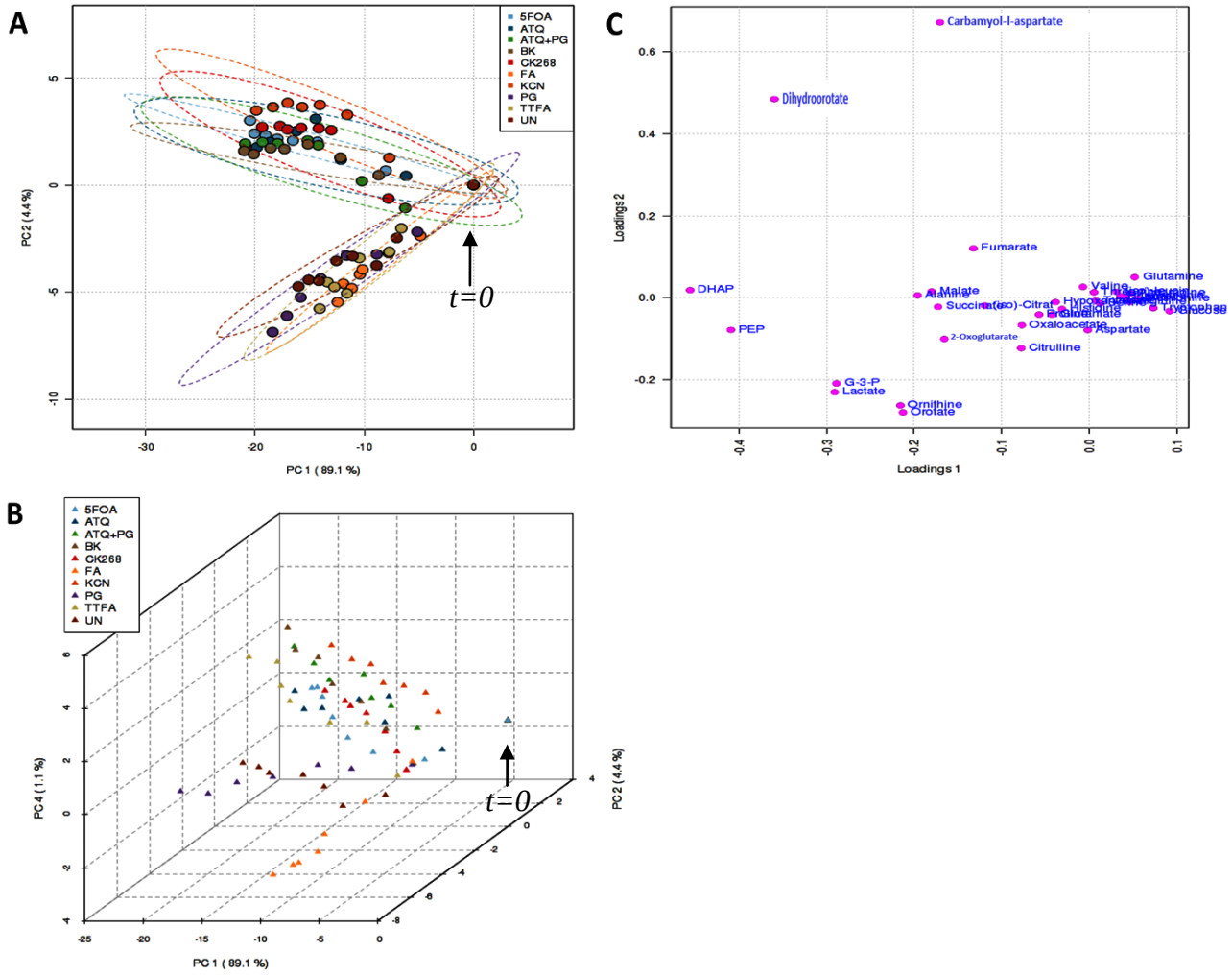

Figure 6.4: PCA score and loading plots for *P. falciparum* 3D7 upon exposure to different drugs and inhibitors.

A) 2-D score plot shows divergence of two main clusters. One cluster includes the *P. falciparum* treated with 5-flouroorotic acid (5-FOA, light blue circle), atovaquone (ATQ, dark blue circle), atovaquone-proguanil (ATQ+PG, green circle), bongkrekic acid (BK, light brown circle), CK-2-68 (red circle) and potassium cyanide (KCN, dark amber circle). The other cluster includes the untreated *P. falciparum* control (UN, dark brown circle) and *P. falciparum* treated with fusidic acid (FA, light amber circle), proguanil (PG, purple circle), thenoyltrifluoroacetone (TTFA, beige circle). Line boundary for each group represented a 95% confidence limit from each treatment centre. B) 3-D score plot shows the divergence of three main clusters. One cluster includes the clustering of *P. falciparum* treated with 5-flouroorotic acid (5-FOA, light blue triangle), atovaquone (ATQ, dark blue triangle), atovaquone-proguanil (ATQ+PG, green triangle), bongkrekic acid (BK, light brown triangle), CK-2-68 (red triangle), potassium cyanide (KCN, dark amber triangle) and thenoyltrifluoroacetone (TTFA, beige triangle). Second cluster includes the clustering of untreated *P. falciaprum* control (UN, dark brown triangle) and *P. falciparum* treated with proguanil (PG, purple triangle). Third cluster includes the clustering of *P. falciparum* treated with fusidic acid (FA, light amber triangle). C) *P. falciparum* metabolites loading plot discriminate between various time points for the corresponding score plots (panel A and B) and reveals the major metabolic fingerprints in carbamoyl-l-aspartate and dihydroorotate. Black arrow indicates the time zero (t=0) for untreated control and other drugs treatment that are all confined in the same position of 2-D and 3-D score plots.

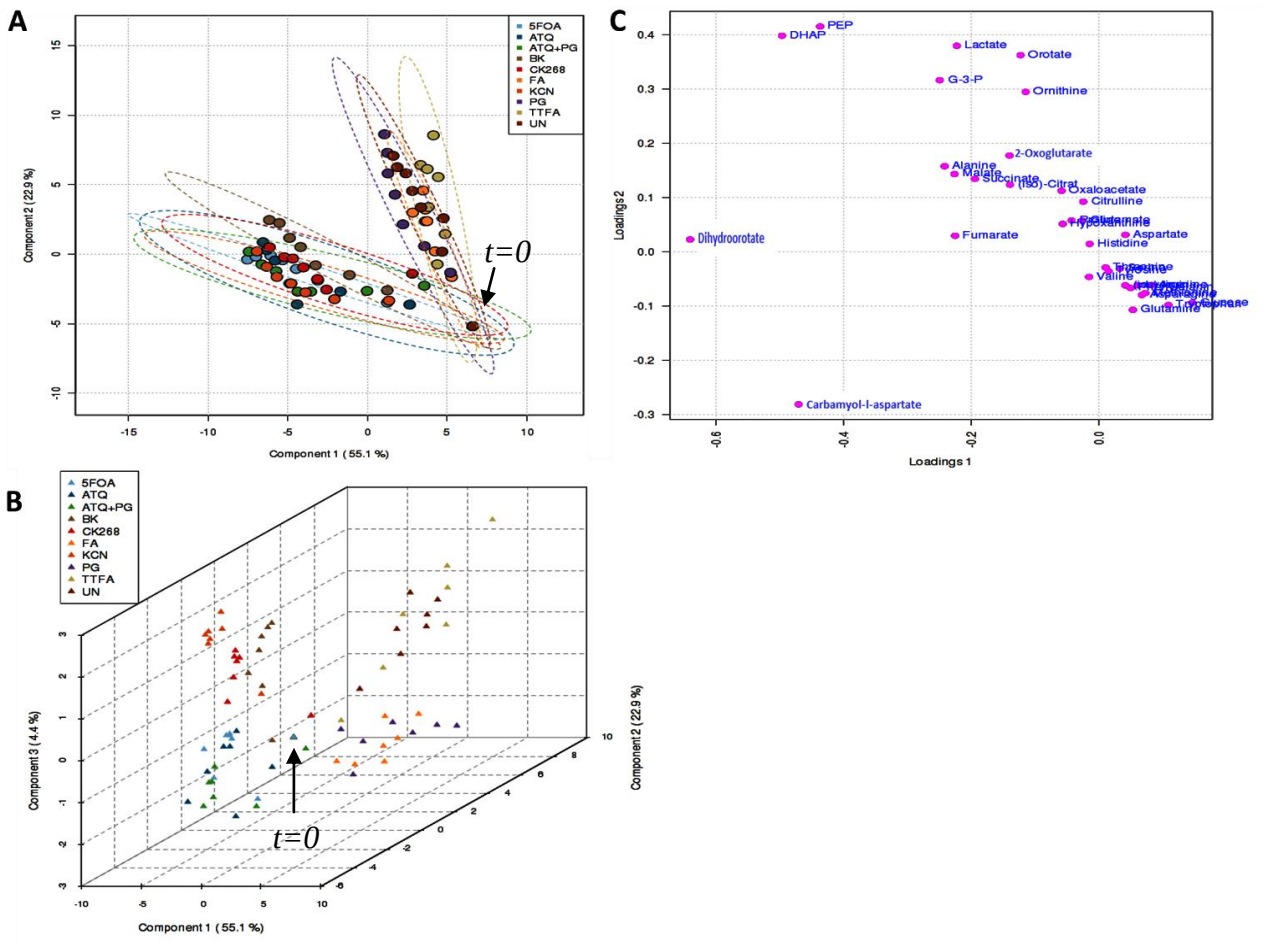

Figure 6.5: PLS-DA score and loading plots for *P. falciparum* 3D7 upon exposure to different drugs and inhibitors.

A) 2-D score plot shows divergence of two main clusters. One cluster includes the clustering of *P. falciparum* treated with 5-flouroorotic acid (5-FOA, light blue circle), atovaquone (ATQ, dark blue circle), atovaquone-proguanil (ATQ+PG, green circle), bongkrekic acid (BK, light brown circle), CK-2-68 (red circle) and potassium cyanide (KCN, dark amber circle). The other cluster includes the clustering of untreated *P. falciparum* control (UN, dark brown circle) and *P. falciparum* treated with fusidic acid (FA, light amber circle), proguanil (PG, purple circle), thenoyltrifluoroacetone (TTFA, beige circle). Line boundary for each group represented a 95% confidence limit from each treatment centre. B) 3-D score plot shows the divergence and discrimination of four main clusters. First cluster includes the clustering of untreated *P. falciaprum* control (UN, dark brown triangle) and *P. falciparum* treated with thenoyltrifluoroacetone (TTFA, beige triangle). Second cluster includes the clustering of *P. falciparum* treated with proguanil (PG, purple triangle) and fusidic acid (FA, light amber triangle). Third cluster includes the clustering of *P. falciparum* treated with 5-flouroorotic acid (5-FOA, light blue triangle), atovaquone (ATQ, dark blue triangle) and atovaquone-proguanil (ATQ+PG, green triangle). Fourth cluster includes the clustering of *P. falciparum* treated with bongkrekic acid (BK, light brown triangle), CK-2-68 (red triangle) and potassium cyanide (KCN, dark amber triangle). C) *P. falciparum* metabolites loading plot discriminate between various time points for the corresponding score plots (panel A and B) and reveals the major metabolic fingerprints in carbamoyl-l-aspartate and dihydroorotate. Black arrow indicates the time zero (*t*=0) for untreated control and other drugs treatment that are all confined in the same position of 2-D and 3-D score plots.

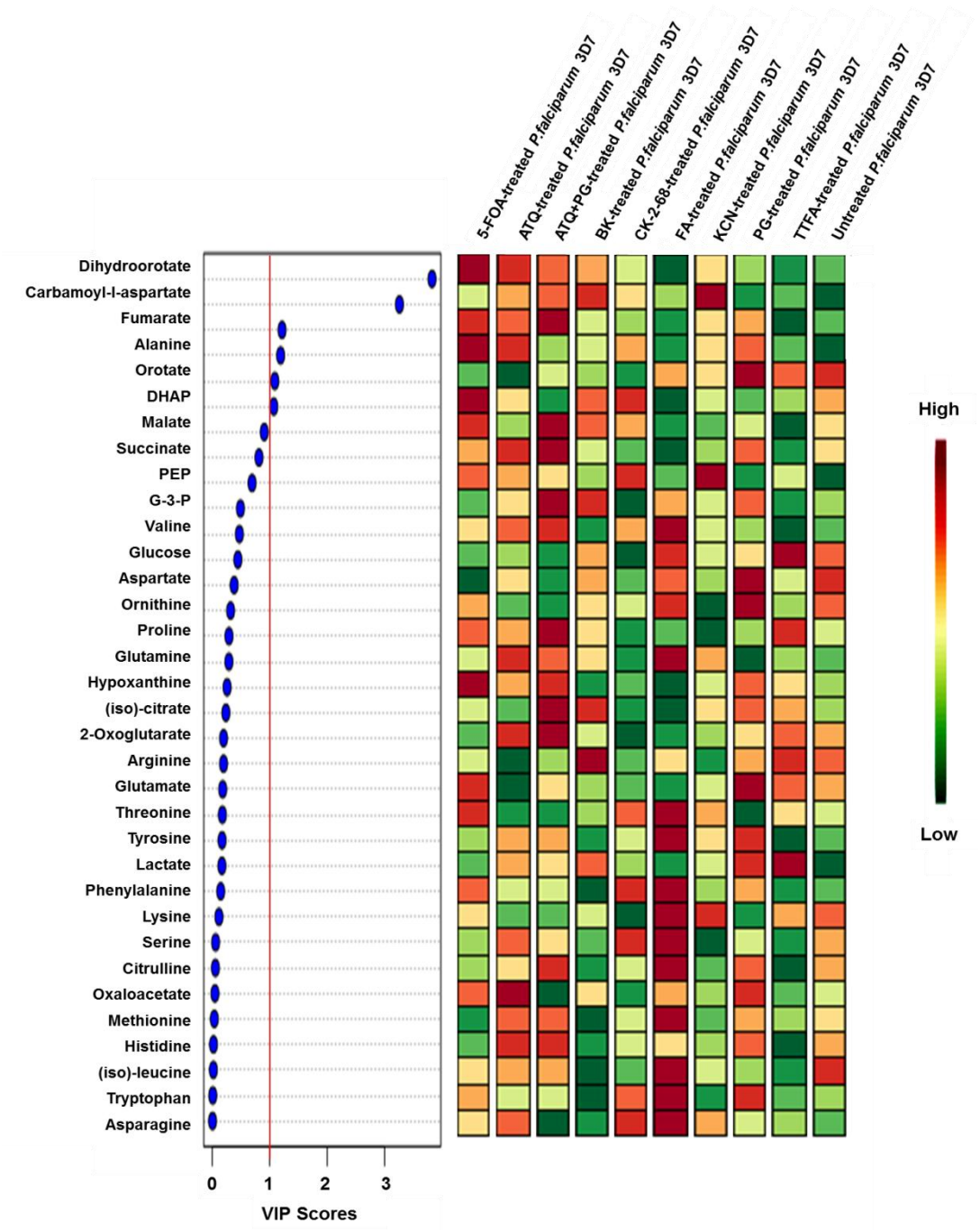

Figure 6.6: Variable Influence on Projection (VIP) score plot for *Plasmodium falciparum* 3D7 upon exposure to different drugs and inhibitors.

Metabolite with VIP score > 1 was considered the most important metabolite responsible for the differentiation among the different drugs and inhibitors used to treated *P. falciparum* parasites. The coloured boxes on the right indicate the relative ratios of the corresponding metabolite in each group under study. Colour scale shows the colours gradient for the VIP score with dark red and dark green being the colours for high and low changed metabolites, respectively. VIP score plot shows that the most important metabolites responsible for differentiation were dihydroorotate and carbamoyl-l-aspartate. Fumarate, alanine, orotate and DHAP had borderline VIP score around 1.

6.3.1.2. Heat map for *P. falciparum* metabolome profiling

The heat map visually demonstrates the relative difference of the dynamic changes of the *P. falciparum* metabolome upon exposure to different drugs and inhibitors including atovaquone, atovaquone-proguanil, CK-2-68, 5-flouroorotic acid, potassium cyanide, bongkrekic acid, thenoyltrifluoroacetone, proguanil and fusidic acid (Figure 6.7). It is visibly evident from the heat map that increasing trends in carbamoyl-l-aspartate and dihydroorotate occurs in *P. falciparum* parasites treated with mtETC selective drugs including atovaquone, atovaquone-proguanil, CK-2-68, 5-flouroorotic acid and potassium cyanide in addition to ADP/ATP translocase inhibitor, bongkrekic acid (Figure 6.7). In contrast, the trends observed in the profiles of carbamoyl-l-aspartate and dihydroorotate in the untreated control *P. falciparum* and *P. falciparum* parasites treated with thenoyltrifluoroacetone, proguanil and fusidic acid were entirely opposite to that of seen in aforementioned mtETC drugs and inhibitors (Figure 6.7).

Interestingly, *P. falciparum* parasites treated with fusidic acid showed markedly cumulative changes in amino acids including glutamine, serine, asparagine, lysine, phenylalanine, tryptophan, tyrosine, threonine, valine, alanine, ornithine, citrulline and methionine (Figure 6.7). On the other hand, glutamate dynamic levels were noticeably diminished upon treating the parasite with fusidic acid (Figure 6.7). In addition, *P. falciparum* parasites treated with fusidic acid prominently showed a reduction in the dynamic levels of TCA intermediates including 2-oxoglutarate, (iso)-citrate, fumarate, succinate and malate (Figure 6.7).

Moreover, the heat map presented in (Figure 6.7) summarized the relative fold changes ratio in *P. falciparum* following the addition of different drugs and inhibitors. Major and evident metabolite changes were highlighted in the aforementioned paragraphs. Detailed and specific explanations are presented as time-dependent graphs in the next section (6.3.2).

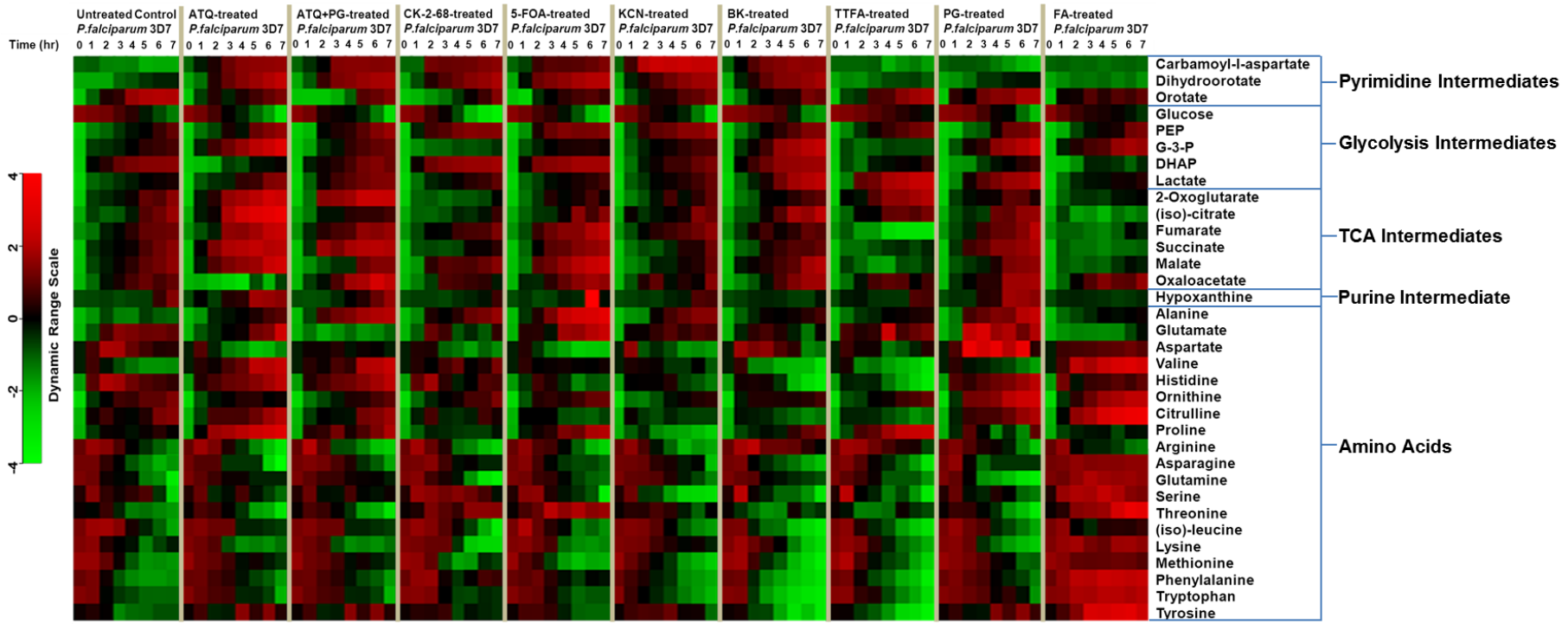

Figure 6.7: Heat map representation of *P.falciparum* 3D7 dynamics metabolome.

Heat map shows a dynamic changes of 34 metabolites in untreated *P. falciparum* control and *P. falciparum* parasites treated after one hour of incubation with atovaquone (ATQ), atovaquone-proguanil (ATQ+PG), CK-2-68, 5-flouroorotic acid (5-FOA), potassium cyanide (KCN), bongkrekic acid (BK), thenoyltrifluoroacetone (TTFA), proguanil (PG) and fusidic acid (FA). Average values at each time-point obtained using purified trophozoite-staged from three independent biological replicates were divided by the corresponding average values derived from parasites harvested at time (0 hr) to generate the corresponding ratios. Ratios were $\log_2$ transformed and plotted on a colour dynamic range scale. Rows correspond to metabolites measured by LC-MS/MS. Columns correspond to the time course from 0hr to 7hr for each of the ten blocks. Green and red colours represent decreases and increases, respectively. Black colour indicates the baseline. Abbreviations: DHAP, dihydroxyaceton phosphate; G-3-P, glycerol-3-phosphate; PEP, phosphoenol pyruvate.

6.3.2. Biochemical time–dependent of metabolites profile in *P. falciparum* parasite

The findings described previously in the analysis section (section 6.3.1) were used to distinguish the MoAs of the drugs and inhibitors used to perturb the biological system of *P. falciparum*. Average concentration values at each time-point were obtained using purified trophozoite-stages from three biological replicates. These were divided by the corresponding average values derived from parasites collected prior to the addition of the respective drug to generate the corresponding fold change ratio. Time-dependent graphs for *P. falciparum* untreated control and *P. falciparum* treated with the addition of atovaquone, atovaquone-proguanil, CK-2-68, 5-flouroorotic acid, potassium cyanide, bongkrekic acid, thenoyltrifluoroacetone, proguanil and fusidic acid were plotted using GraphPad Prism 5.0 (GraphPad Software Inc.).

It is clear that glucose level was notably utilized in untreated *P. falciparum* and *P. falciparum* treated with atovaquone, atovaquone-proguanil, CK-2-68, 5-flouroorotic acid, potassium cyanide, bongkrekic acid, thenoyltrifluoroacetone, proguanil and fusidic during the 7 hours incubation time (Figure 6.8 A, B, C, D, E, F, G, H and I). The production of phosphoenol pyruvate (PEP) among all drug treatments was higher than that of the untreated by at least 50 fold at 7 hr time point (Figure 6.11 A, B, C, D, E, F, G, H and I). Lactate production was also higher among all drug treatments except fusidic acid than that of untreated parasites by at least 15 fold at 7 hr timepoint (Figure 6.12 A, B, C, D, E, F, G, H and I). In addition, the level of dihydroxyaceton phosphate (DHAP) was noticeably decreased upon treating the parasite with atovaquone, atovaquone-proguanil, potassium cyanide, thenoyltrifluoroacetone, proguanil and fusidic acid by at least 200 fold at 7 hr timepoint compared to untreated (Figure 6.9 A, B, E, G, H and I). In contrast, there was a slight upsurge in the level of DHAP in parasites treated with CK-2-68, 5-fluoroorotic acid and bongkrekic acid (Figure 6.9 C, D and F). The level of glycerol-3-phosphate (G-3-P) was increased by more than 10 fold at 7 hr timepoint in parasites treated with atovaquone, atovaquone-proguanil, bongkrekic acid, proguanil and fusidic acid as compared to untreated parasites (Figure 6.10 A, B, F, H and I). G-3-P was notably decreased by more than 20 fold in parasite treated with thenoyltrifluoroacetone as compared to untreated parasites (Figure 6.10 G). There were no obvious changes in the G-3-P levels between untreated parasites and parasites treated with CK-2-68, 5-fluoroorotic acid and potassium cyanide (Figure 6.10 C, D and E).

The mitochondrial selective drugs and inhibitors, including atovaquone, atovaquone-proguanil, CK-2-68, 5-flouroorotic acid, potassium cyanide, bongkrekic acid, thenoyltrifluoroacetone and fusidic acid showed different patterns in the Tricarboxylic Acid (TCA) intermediates compared to untreated. Specifically, *P. falciaprum* parasites treated with atovaquone and atovaquone-proguanil showed a notable increase in the levels of 2-oxoglutarate and succinate as compared to untreated parasites (Figure 6.13 & 6.15 A and B). An evident increase of (iso)-citrate, fumarate and malate was observed in parasites following the addition of atovaquone-proguanil (Figure 6.14, 6.16 & 6.18, B) but no clear changes were noted in the levels of fumarate, oxaloacetate and malate in parasites treated with atovaquone (Figure 6.16, 6.17 & 6.18 A). As expected, there were not any changes observed in the TCA intermediates in parasite treated with proguanil (Figures 6.13, 6.14, 6.15, 6.16, 6.17 & 6.18, H). CK-2-68 treated parasites showed marked reduction in the levels of 2-oxoglutarate and succinate (Figure 6.13 and 6.15, C) but there were no changes seen in the levels of (iso)-citrate, fumarate, oxaloacetate and malate (Figures 6.14, 6.16, 6.17 & 6.18, C). There were not any obvious alterations noted in TCA intermediates in parasites treated with 5-flouroorotic acid, potassium cyanide, bongkrekic acid (Figures 6.13, 6.14, 6.15, 6.16, 6.17 & 6.18, D, E and F). However, parasite treated with thenoyltrifluoroacetone showed a clear reduction in the levels of succinate, fumarate and malate by at least 5 fold at 7 hr time point (Figures 6.15, 6.16 & 6.18, G) but not in 2-oxoglutarate, (iso)-citrate and oxaloacetate (Figures 6.13, 6.14 & 6.17, G). Surprisingly, parasites treated with fusidic acid showed a marked reduction in 2-oxoglutarate, (iso)-citrate, succinate, fumarate and malate by at least 5 fold at 7 hr time point as compared to untreated parasites (Figure 6.13, 6.14, 6.15, 6.16 & 6.18, I). In contrast, there was not any apparent change observed in oxaloacetate level following the addition of fusidic acid (Figure 6.17 I).

With the exception of thenoyltrifluoroacetone, *P. falciaprum* treated with mtETC selective inhibitors including atovaquone, atovaquone-proguanil, CK-2-68, 5-flouroorotic acid and potassium cyanide showed a distinguished accumulation of carbamoyl-l-aspartate and dihydroorotate and a subsequent reduction in orotate (Figure 6.19, 6.20 & 6.21, A, B, C, D and E). In addition, *P. falciaprum* treated with bongkrekic acid showed a notable increase in carbamoyl-l-aspartate and dihydroorotate and a clear reduction in orotate (Figure 6.19, 6.20 & 6.21, F). There were no changes

observed in the levels of carbamoyl-l-aspartate, dihydroorotate and orotate upon treating *P. falciaprum* parasites with of thenoyltrifluoroacetone, proguanil and fusidic acid compared to untreated (Figure 6.19, 6.20 & 6.21, G, H and I).

The trend in amino acids varied upon the addition of mitochondrial selective drugs and inhibitors of *P. falciparum* parasites in particular fusidic acid. With the exception of fusidic acid, *P. falciparum* parasites treated with atovaquone, atovaquone-proguanil, CK-2-68, 5-flouroorotic acid, potassium cyanide, bongkrekic acid, thenoyltrifluoroacetone and proguanil showed no obvious changes in the levels of glutamine, glutamate, arginine, proline, ornithine, citrulline, serine, asparagine, lysine, methionine, histidine, phenylalanine, tryptophan, threonine and (iso)-leucine (Figures 6.23, 6.24, 6.25, 6.26, 6.27, 6.28, 6.29, 6.30, 6.32, 6.33, 6.34, 6.35, 6.36, 6.38 & 6.39; A, B, C, D, E, F, G and H). In contrast, there was a notable increase in the level of alanine in *P. falciparum* treated with all mitochondrial selective drugs and inhibitors mentioned above as well as in parasite treated with proguanil (Figure 6.22, A, B, C, D, E, F, G and H). Aspartate levels in *P. falciparum* treated with aforementioned selective mtETC inhibitors were notably lower than that of untreated control parasite (Figure 6.31, A, B, C, D, E and G). On the other hand, *P. falciparum* parasites treated with bongkrekic acid, proguanil and fusidic acid showed no obvious changes in aspartate levels compared to untreated controls (Figure 6.31, F, H and I). There was a slight increase in tyrosine and a noticeable accumulation of valine in *P. falciparum* treated with atovaquone, atovaquone-proguanil and CK-2-68 (Figure 6.37 & 6.40, A, B and C).

As stated above, most of the changes in the amino acid trends were observed in *P. falciparum* treated with fusidic acid. There was a distinguished accumulation in glutamine, ornithine, citrulline, phenylalanine, tryptophan, tyrosine, threonine and valine following fusidic acid addition to the *P. falciparum* parasites (Figure 6.23, 6.27, 6.28, 6.35, 6.36, 6.37, 6.38 & 6.40, I). Moreover, there were a notable invariable changes observed in the levels of serine, asparagine, lysine and methionine (Figure 6.29, 6.30, 6.32 & 6.33, I). *P. falciparum* treated with fusidic acid showed no changes in the levels of arginine, proline, histidine and (iso)-leucine compared to untreated (Figure 6.25, 6.26, 6.34 & 6.39, I).

P. falciparum parasites treated with atovaquone, atovaquone-proguanil, CK-2-68, 5-flouroorotic acid, potassium cyanide, bongkrekic acid, thenoyltrifluoroacetone, proguanil and fusidic acid showed no obvious changes in the level of hypoxanthine compared to untreated parasite control (Figure 6.41, A, B, C, D, E, F, G, H and I) .

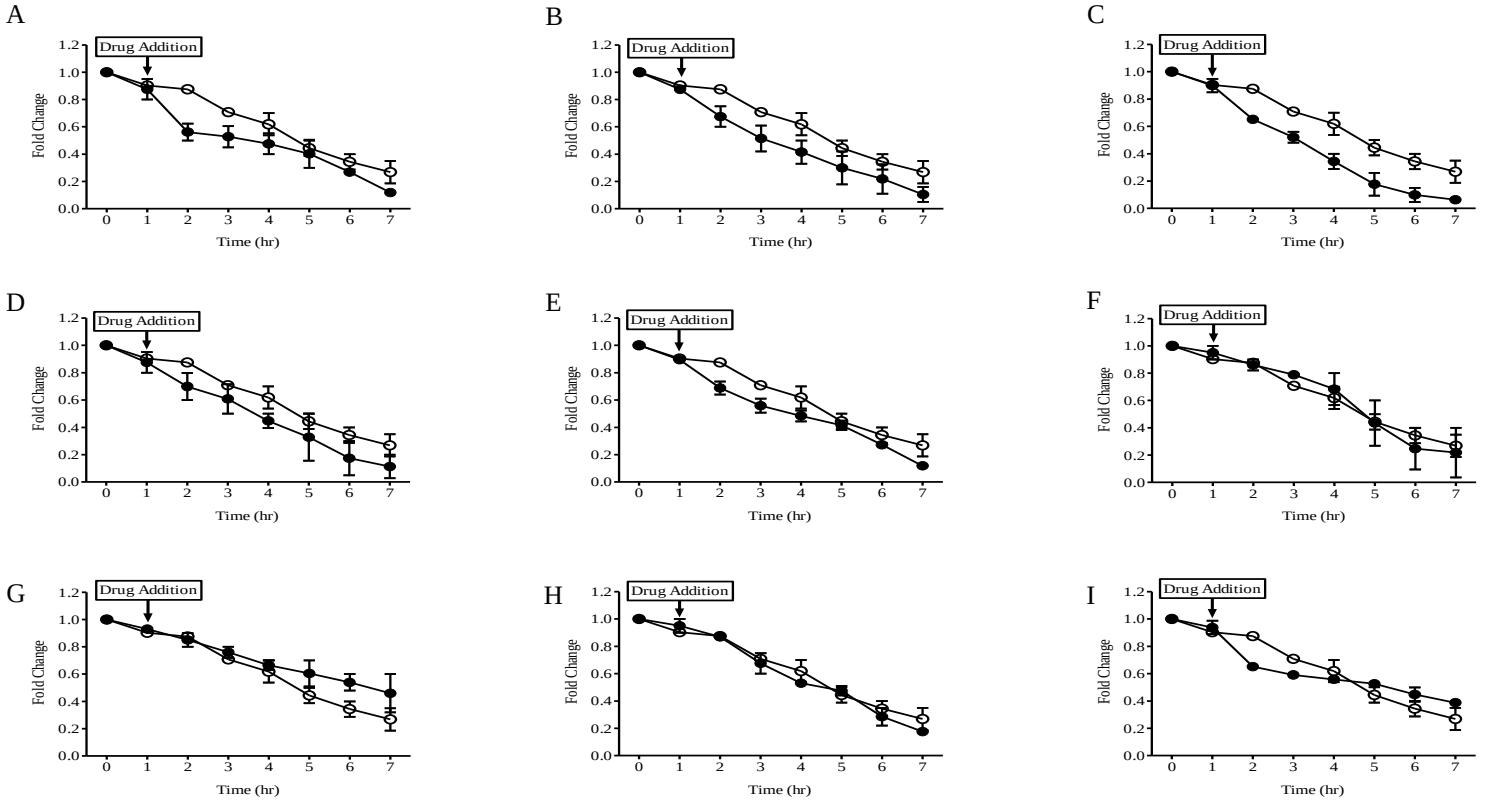

Figure 6.8: Glucose metabolism in drug-treated and untreated *P. falciparum* 3D7 parasites over time.
Glucose levels were determined in untreated (open circle) and drug-treated (closed circle) *P.falciparum* trophozoite-staged parasites by LC-MS/MS. The following drugs were added to the parasites after one hour of incubation (A) 2.5 nM atovaquone, (B) 2.5 nM atovaquone + 1 µM proguanil, (C) 50 nM CK-2-68, (D) 15 nM 5-fluoroorotic acid, (E) 1 mM potassium cyanide, (F) 5 µM bongkrekic acid, (G) 10 µM thenoyltrifluoroacetone, (H) 70 µM proguanil and (I) 200 µM fusidic acid. Data showed clearly the utilization of glucose in drugs treated and untreated parasites. The points represent the mean ± SEM of at least duplicate independent experiments.

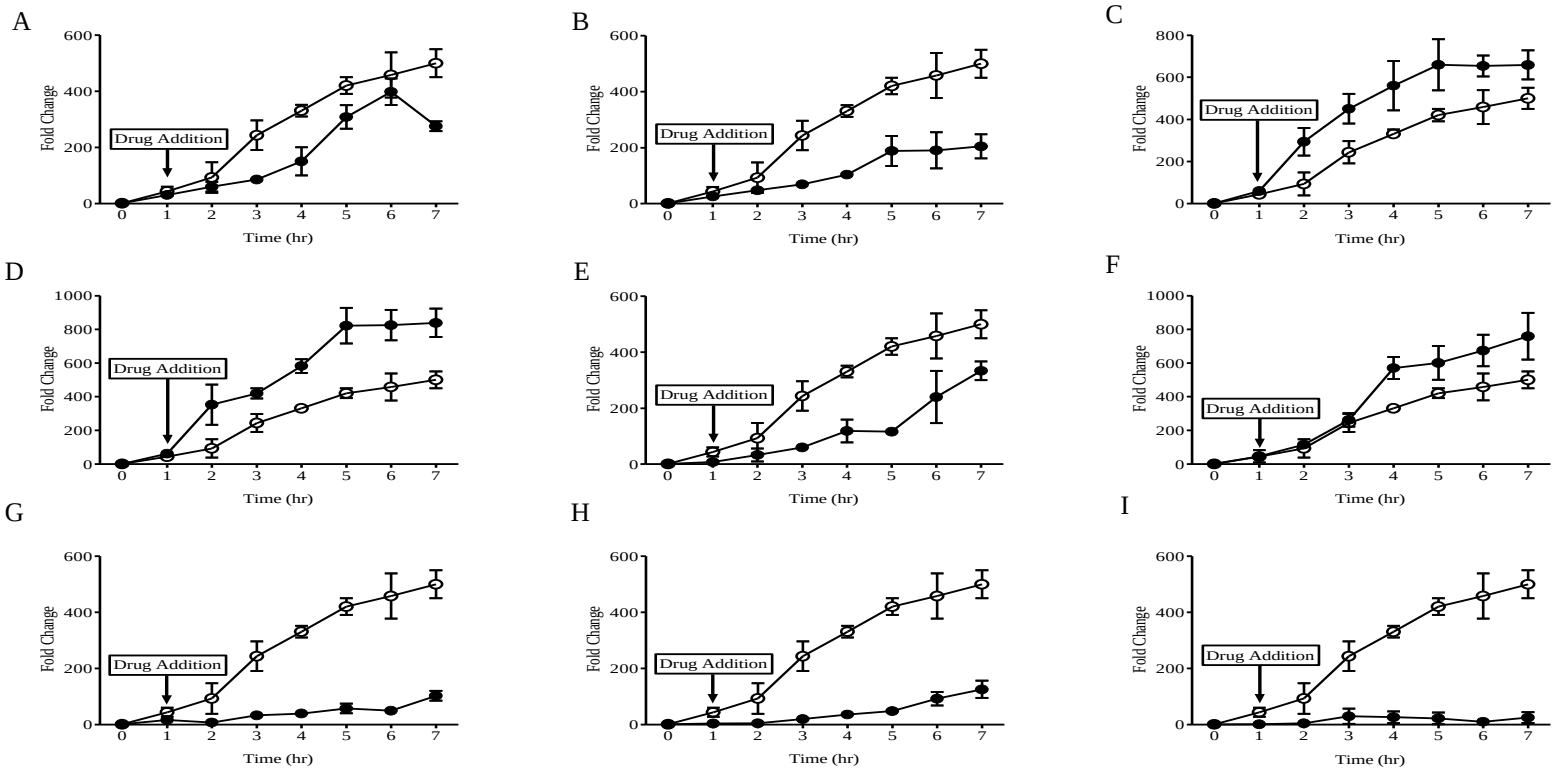

Figure 6.9: Time-dependent curves of dihydroxyaceton phosphate (DHAP) in drug-treated and untreated *P. falciparum* 3D7 parasites.
DHAP levels were measured in untreated (open circle) and drug-treated (closed circle) *P.falciparum* trophozoite-staged parasites by LC-MS/MS. Data showed clear reduction of DHAP after one hour of incubation in parasites treated with (A) 2.5 nM atovaquone, (B) 2.5 nM atovaquone + 1 µM proguanil, (E) 1 mM potassium cyanide, (G) 10 µM thenoyltrifluoroacetone, (H) 70 µM proguanil and (I) 200 µM fusidic acid. On the other hand, there was a slight increase in the level of DHAP after one hour of incubation in parasites treated with (C) 50 nM CK-2-68, (D) 15 nM 5-fluoroorotic acid, and (F) 5 µM bongkrekic acid. The points represent the mean ± SEM of at least duplicate independent experiments.

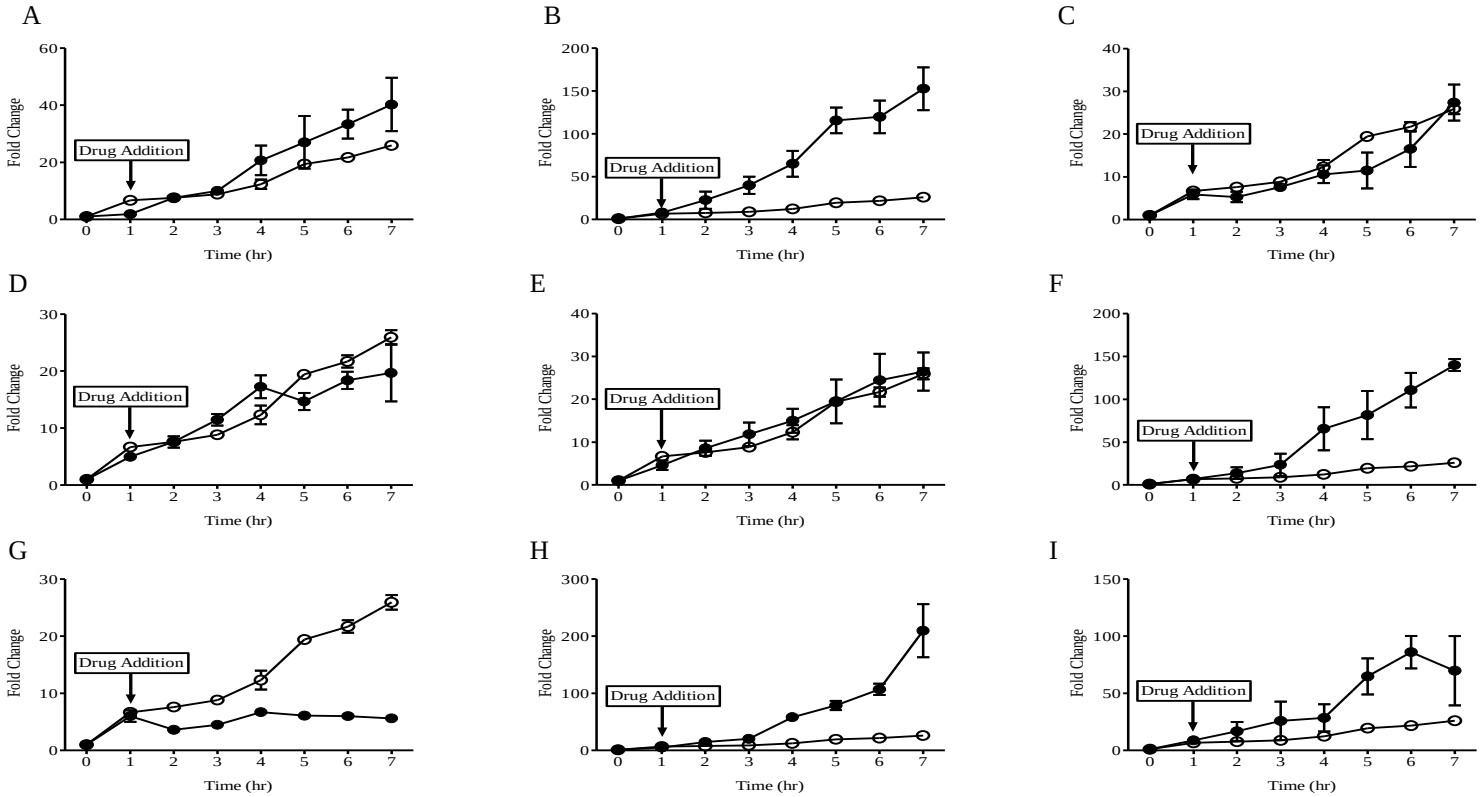

Figure 6.10: Time-dependent curves of glycerol-3-phosphate (G-3-P) in drug-treated and untreated *P. falciparum* 3D7 parasites.
G-3-P levels were determined in untreated (open circle) and drug-treated (closed circle) *P.falciparum* trophozoite-staged parasites by LC-MS/MS. Data showed an increase in the G-3-P level after one hour of incubation in parasites treated with (A) 2.5 nM atovaquone, (B) 2.5 nM atovaquone + 1 µM proguanil, (F) 5 µM bongkrekic acid, (H) 70 µM proguanil and (I) 200 µM fusidic acid. On the other hand, parasites treated with (G) 10 µM thenoyltrifluoroacetone showed a notable reduction in G-3-P level. There were no differences in parasites treated with (C) 50 nM CK-2-68, (D) 15 nM 5-fluoroorotic acid, (E) 1 mM potassium cyanide as compared to untreated parasites. The points represent the mean ± SEM of at least duplicate independent experiments.

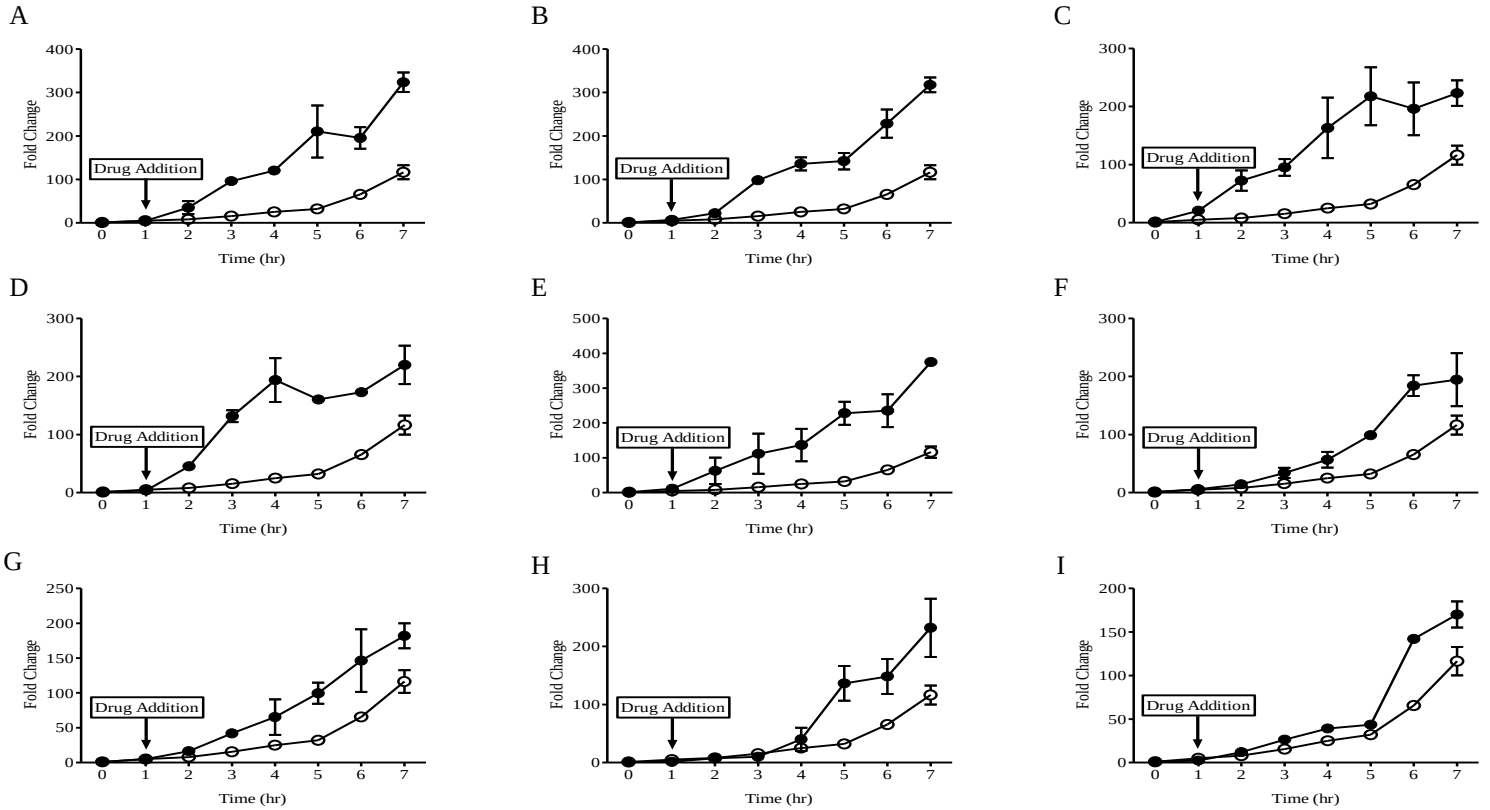

Figure 6.11: Time-dependent curves of phosphoenol pyruvate (PEP) in drug-treated and untreated *P. falciparum* 3D7 parasites.
PEP levels were determined in untreated (open circle) and drug-treated (closed circle) *P.falciparum* trophozoite-staged parasites by LC-MS/MS. Data showed a noticeable increase in PEP levels after one hour of incubation in parasites treated with (A) 2.5 nM atovaquone, (B) 2.5 nM atovaquone + 1 µM proguanil, (C) 50 nM CK-2-68, (D) 15 nM 5-fluoroorotic acid and (E) 1 mM potassium cyanide, (F) 5 µM bongkrekic acid, (G) 10 µM thenoyltrifluoroacetone, (H) 70 µM proguanil and (I) 200 µM fusidic acid. The points represent the mean ± SEM of at least duplicate independent experiments.

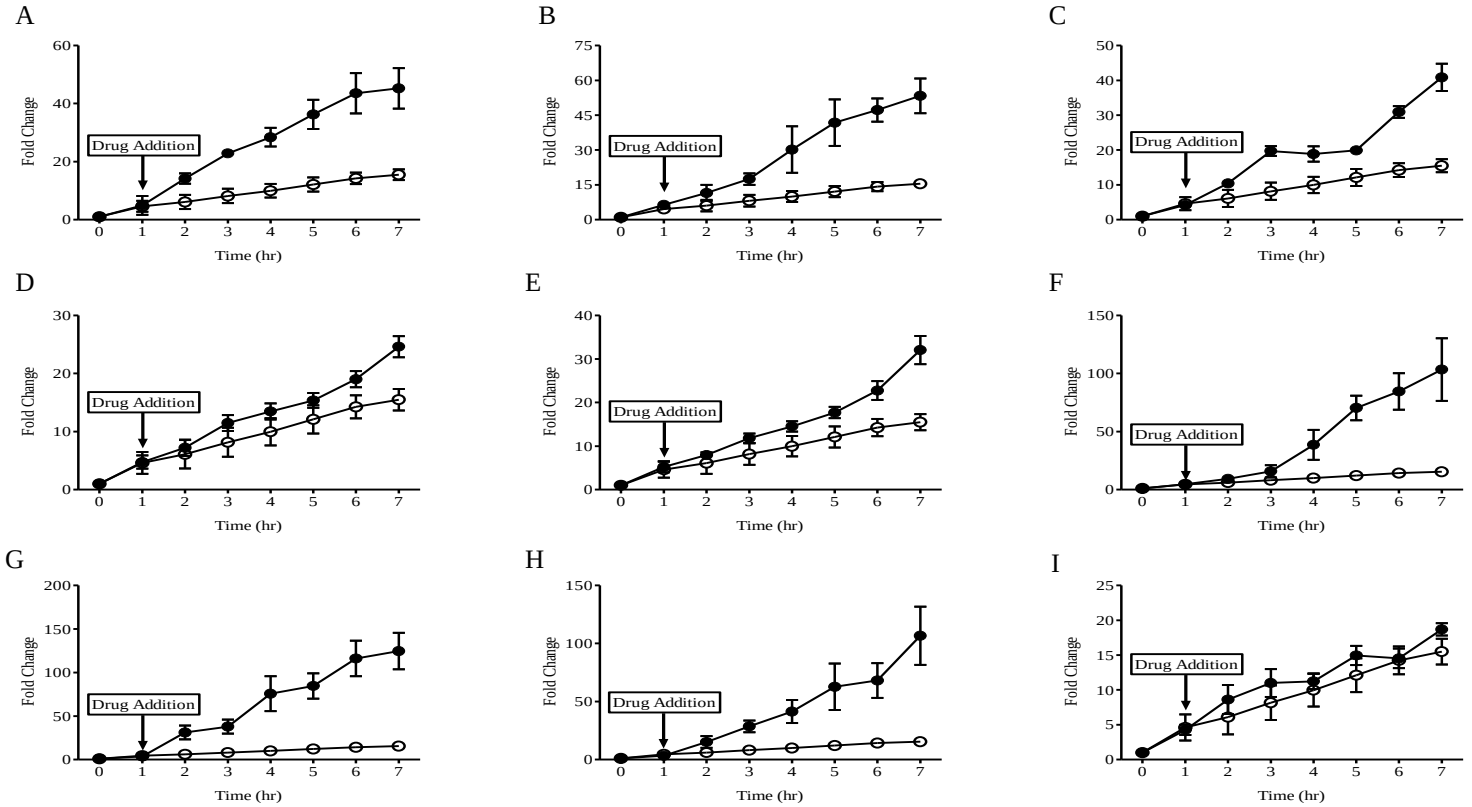

Figure 6.12: Time-dependent curves of lactate production in drug-treated and untreated *P. falciparum* 3D7 parasites.
Lactate levels were measured in untreated (open circle) and drug-treated (closed circle) *P.falciparum* trophozoite-staged parasites by LC-MS/MS. Data showed a notable increase in production of lactate after one hour of incubation in parasites treated with (A) 2.5 nM atovaquone, (B) 2.5 nM atovaquone + 1 µM proguanil, (C) 50 nM CK-2-68, (D) 15 nM 5-fluoroorotic acid, (E) 1 mM potassium cyanide, (F) 5 µM bongkrekic acid, (G) 10 µM thenoyltrifluoroacetone and (H) 70 µM proguanil. Parasites treated with (I) 200 µM fusidic acid showed no differences compared to untreated parasites. The points represent the mean ± SEM of at least duplicate independent experiments.

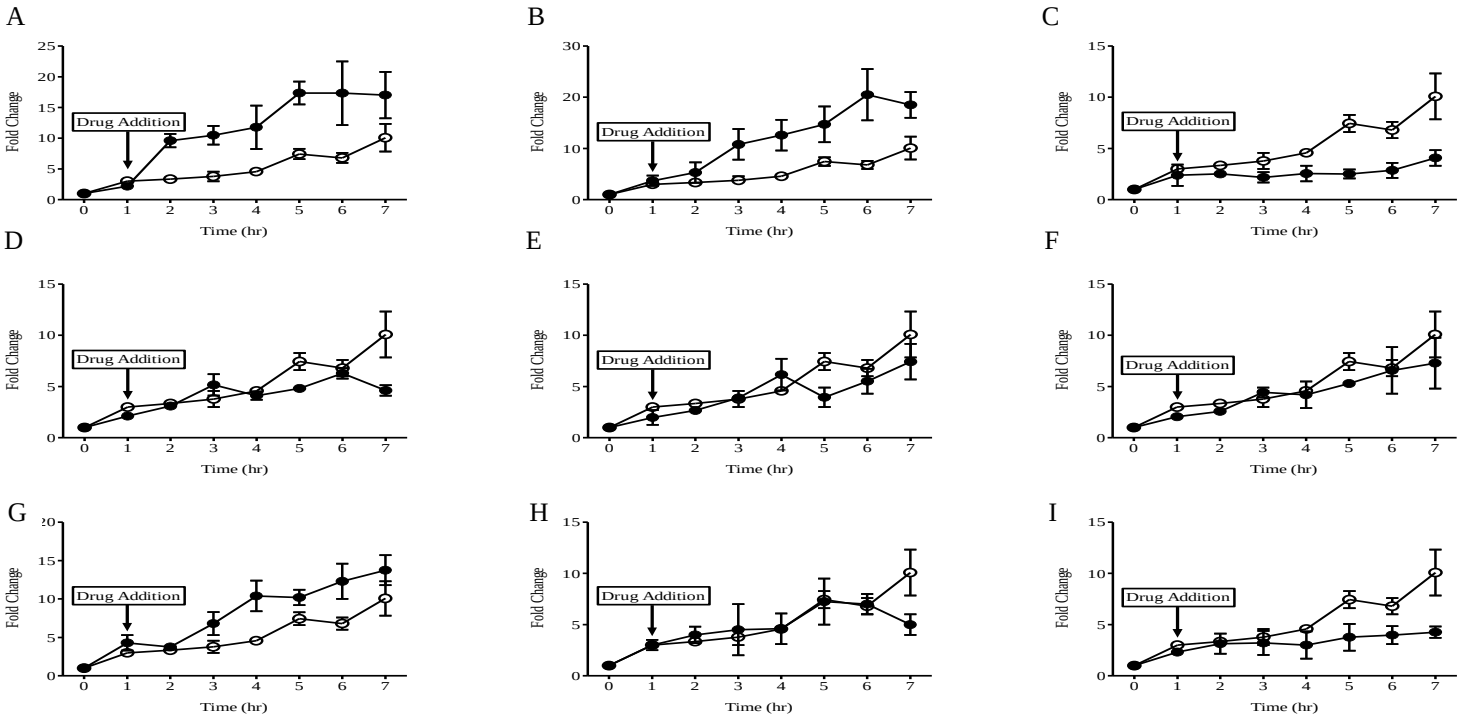

Figure 6.13: Time-dependent curves of 2-oxoglutarate in drug-treated and untreated *P. falciparum* 3D7 parasites.

2-oxoglutarate levels were determined in untreated (opened circle) and drug-treated (closed circle) *P.falciparum* trophozoite-staged parasites by LC-MS/MS. The following drugs were added to the parasites after one hour of incubation (A) 2.5 nM atovaquone, (B) 2.5 nM atovaquone + 1 µM proguanil, (C) 50 nM CK-2-68, (D) 15 nM 5-fluoroorotic acid, (E) 1 mM potassium cyanide, (F) 5 µM bongkrekic acid, (G) 10 µM thenoyltrifluoroacetone, (H) 70 µM proguanil and (I) 200 µM fusidic acid. Data showed that parasites treated with (A) 2.5 nM atovaquone and (B) 2.5 nM atovaquone + 1 µM proguanil had a notable increase of 2-oxoglutarate whereas that of treated with (C) 50 nM CK-2-68 and (I) 200 µM fusidic acid showed a distinguished reduction. The points represent the mean ± SEM of at least duplicate independent experiments. There were no clear changes observed in others drugs-treated parasites.

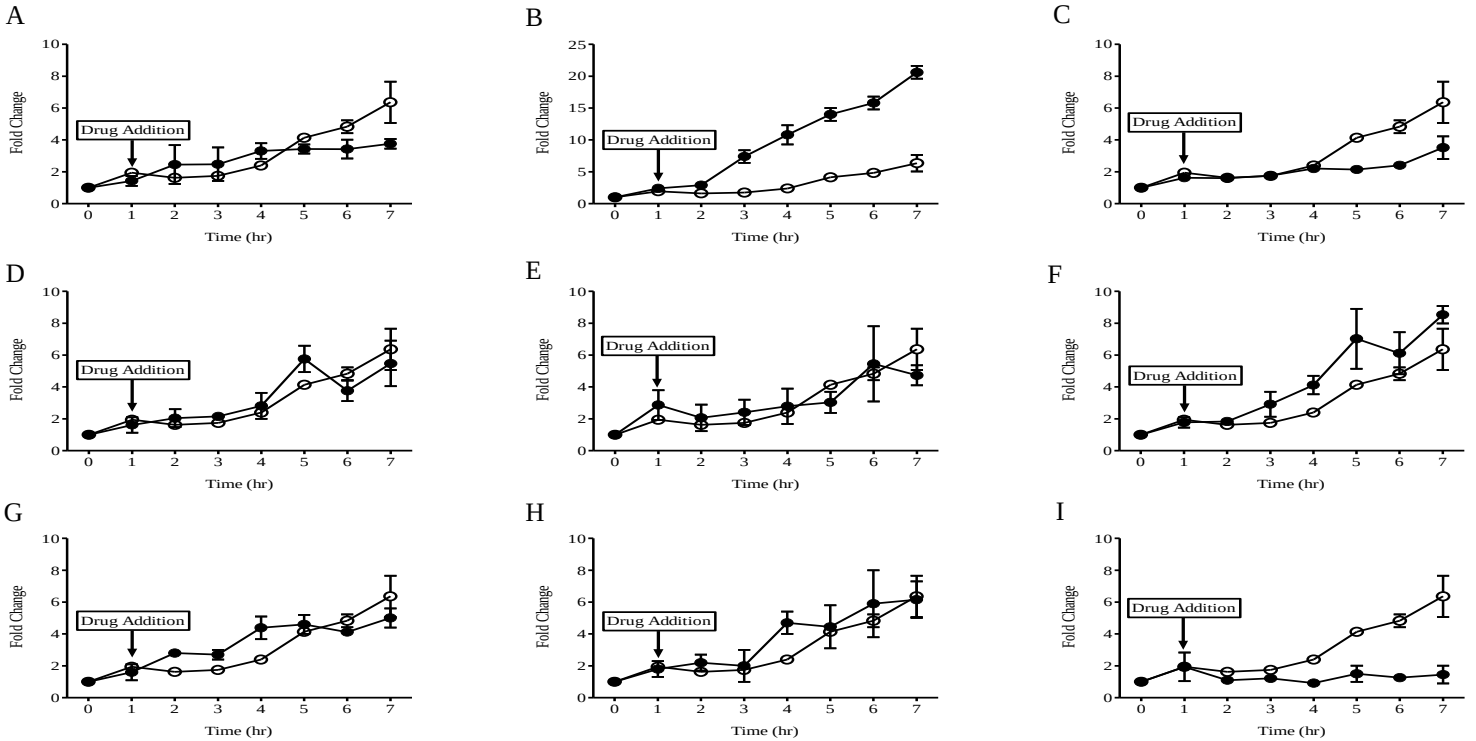

Figure 6.14:. Time-dependent curves of (iso)-citrate in drug-treated and untreated *P. falciparum* 3D7 parasites.

The (iso)-citrate levels were determined in untreated (opened circle) and drug-treated (closed circle) *P.falciparum* trophozoite-staged parasites by LC-MS/MS. The following drugs were added to the parasites after one hour of incubation (A) 2.5 nM atovaquone, (B) 2.5 nM atovaquone + 1 µM proguanil, (C) 50 nM CK-2-68, (D) 15 nM 5-fluoroorotic acid, (E) 1 mM potassium cyanide, (F) 5 µM bongkrekic acid, (G) 10 µM thenoyltrifluoroacetone, (H) 70 µM proguanil and (I) 200 µM fusidic acid. Data showed that parasites treated with (B) 2.5 nM atovaquone + 1 µM proguanil had a substantial increase of (iso)-citrate while that of treated with (I) 200 µM fusidic acid showed a notable decrease. There were no changes observed in others drugs-treated parasites. The points represent the mean ± SEM of at least duplicate independent experiments.

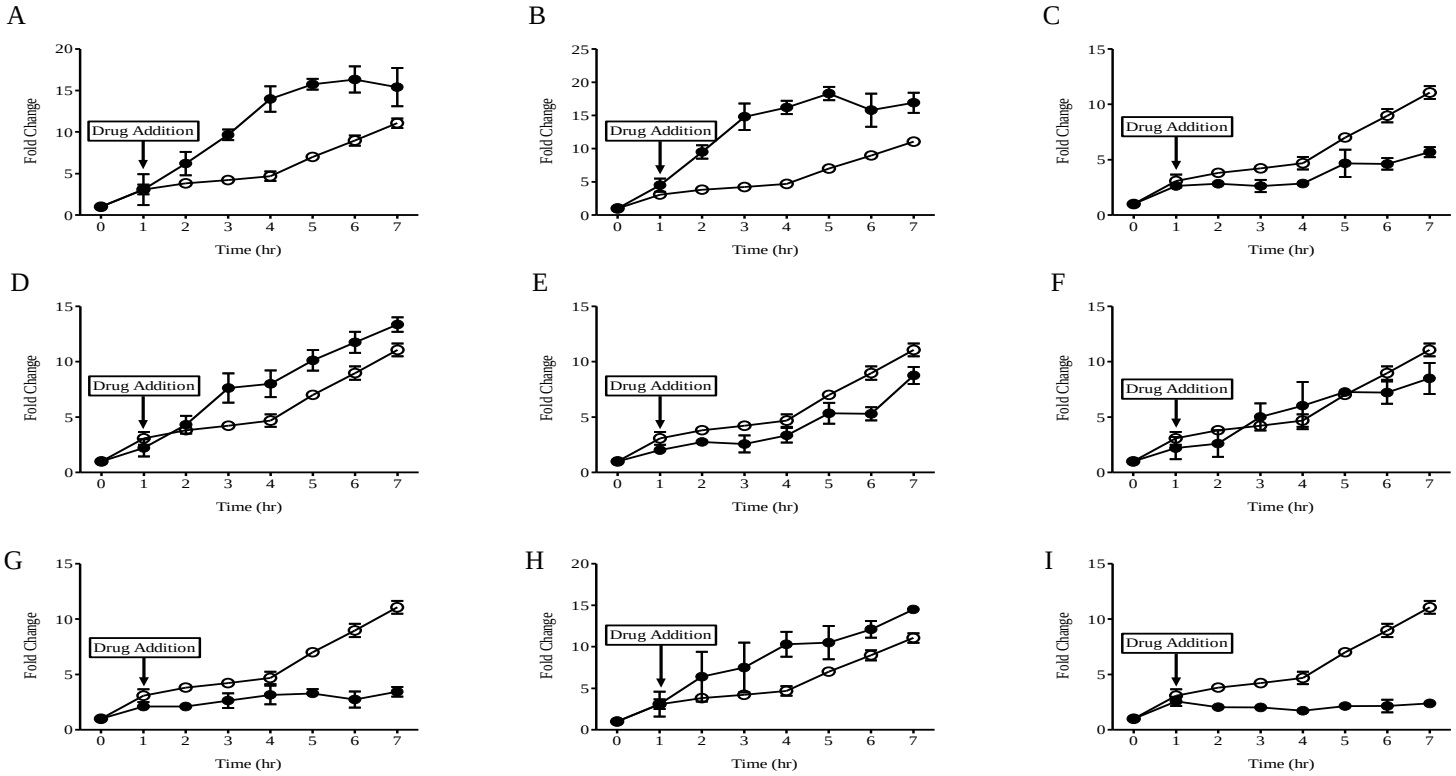

Figure 6.15: Time-dependent curves of succinate in drug-treated and untreated *P. falciparum* 3D7 parasites.
Succinate levels were determined in untreated (open circle) and drug-treated (closed circle) *P.falciparum* trophozoite-staged parasites by LC-MS/MS. The following drugs were added to the parasites after one hour of incubation (A) 2.5nM atovaquone, (B) 2.5 nM atovaquone + 1 µM proguanil, (C) 50 nM CK-2-68, (D) 15 nM 5-fluoroorotic acid, (E) 1 mM potassium cyanide, (F) 5 µM bongkrekic acid, (G) 10 µM thenoyltrifluoroacetone, (H) 70 µM proguanil and (I) 200 µM fusidic acid. Data showed a distinguished increase of succinate in parasites treated with (A) 2.5nM atovaquone, (B) 2.5 nM atovaquone + 1 µM proguanil whereas parasites treated with (C) 50 nM CK-2-68, (G) 10 µM thenoyltrifluoroacetone and (I) 200 µM fusidic acid showed a notable reduction. The points represent the mean ± SEM of at least duplicate independent experiments.

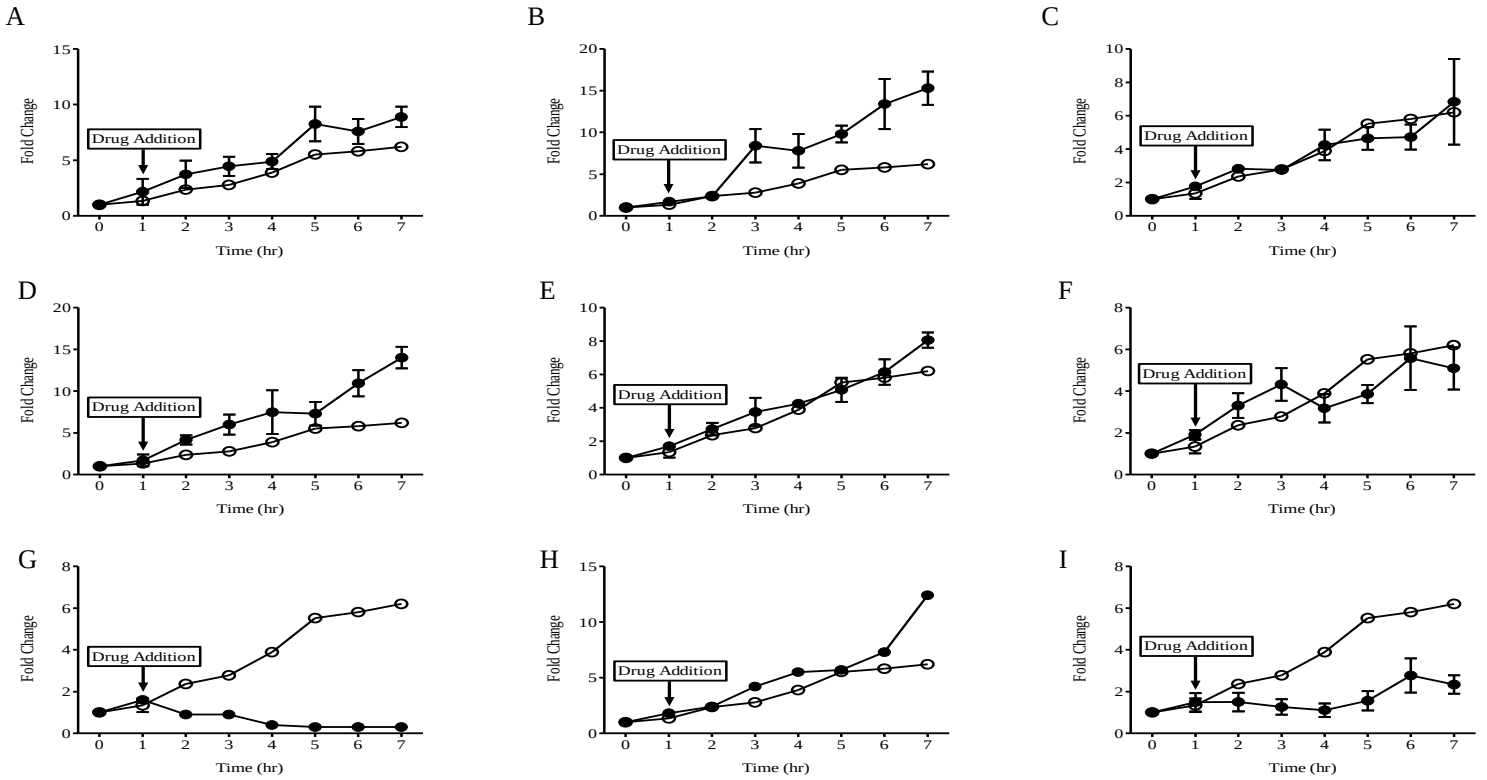

Figure 6.16: Time-dependent curves of fumarate in drug-treated and untreated *P. falciparum* 3D7 parasites.

Fumarate levels were determined in untreated (open circle) and drug-treated (closed circle) *P. falciparum* trophozoite-staged parasites by LC-MS/MS. The following drugs were added to the parasites after one hour of incubation (A) 2.5 nM atovaquone, (B) 2.5 nM atovaquone + 1 µM proguanil, (C) 50 nM CK-2-68, (D) 15 nM 5-fluoroorotic acid, (E) 1mM potassium cyanide, (F) 5 µM bongkrekic acid, (G) 10 µM thenoyltrifluoroacetone, (H) 70 µM proguanil and (I) 200 µM fusidic acid. Data showed a notable increase of fumarate in parasites treated with (B) 2.5 nM atovaquone + 1 µM proguanil whereas it showed an evident reduction of fumarate in parasites treated with (G) 10 µM thenoyltrifluoroacetone and (I) 200 µM fusidic acid. There were no clear changes observed in others drugs-treated parasites. The points represent the mean ± SEM of at least duplicate independent experiments.

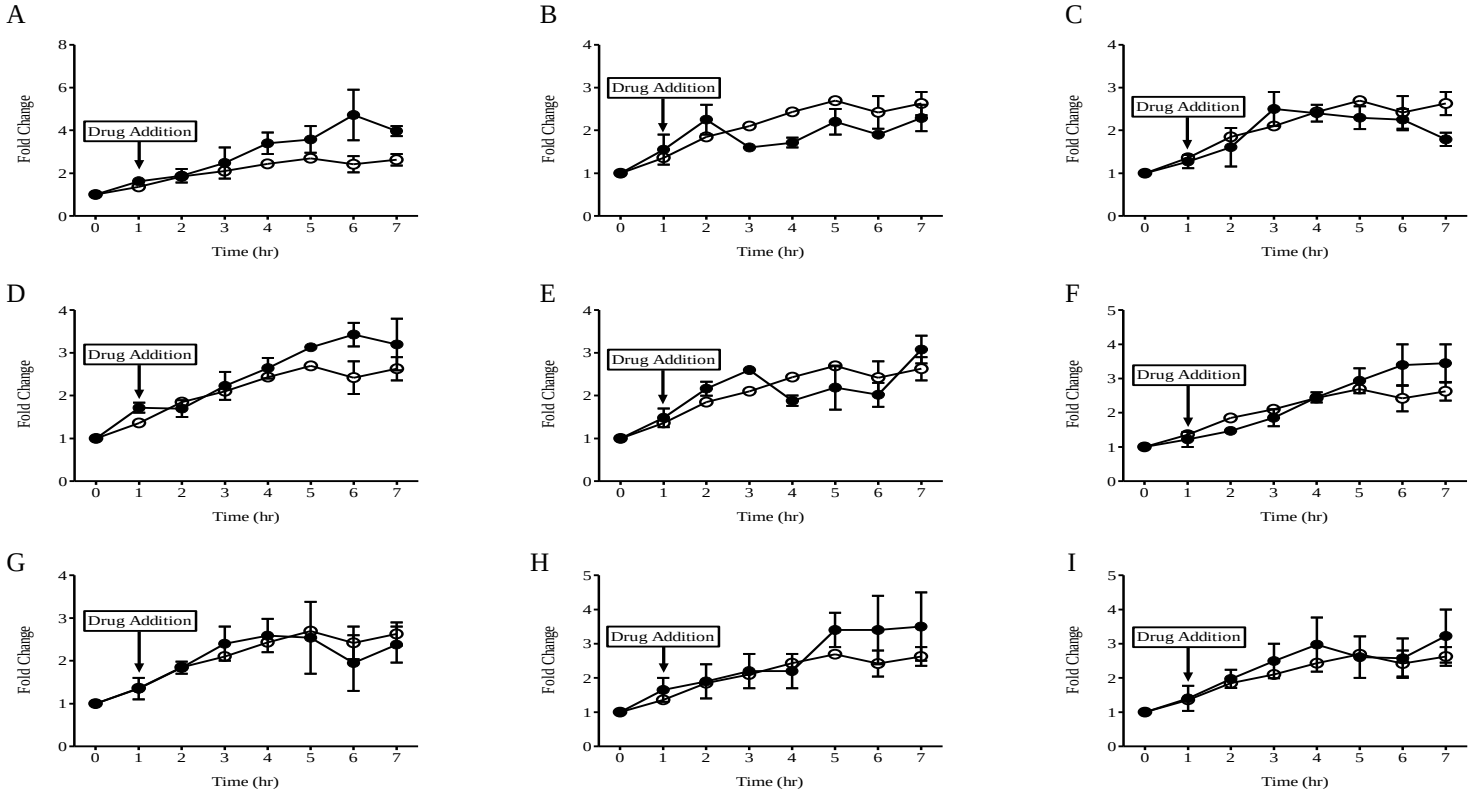

Figure 6.17: Time-dependent curves of oxaloacetate levels in drug-treated and untreated *P. falciparum* 3D7 parasites.
Oxaloacetate levels were determined in untreated (open circle) and drug-treated (closed circle) *P.falciparum* trophozoite-staged parasites by LC-MS/MS. The following drugs were added to the parasites after one hour of incubation (A) 2.5 nM atovaquone, (B) 2.5 nM atovaquone + 1 µM proguanil, (C) 50 nM CK-2-68, (D) 15 nM 5-fluoroorotic acid, (E) 1 mM potassium cyanide, (F) 5 µM bongkrekic acid, (G) 10 µM thenoyltrifluoroacetone, (H) 70 µM proguanil and (I) 200 µM fusidic acid. There were no changes observed between drugs-treated and untreated parasites. The points represent the mean ± SEM of at least duplicate independent experiments.

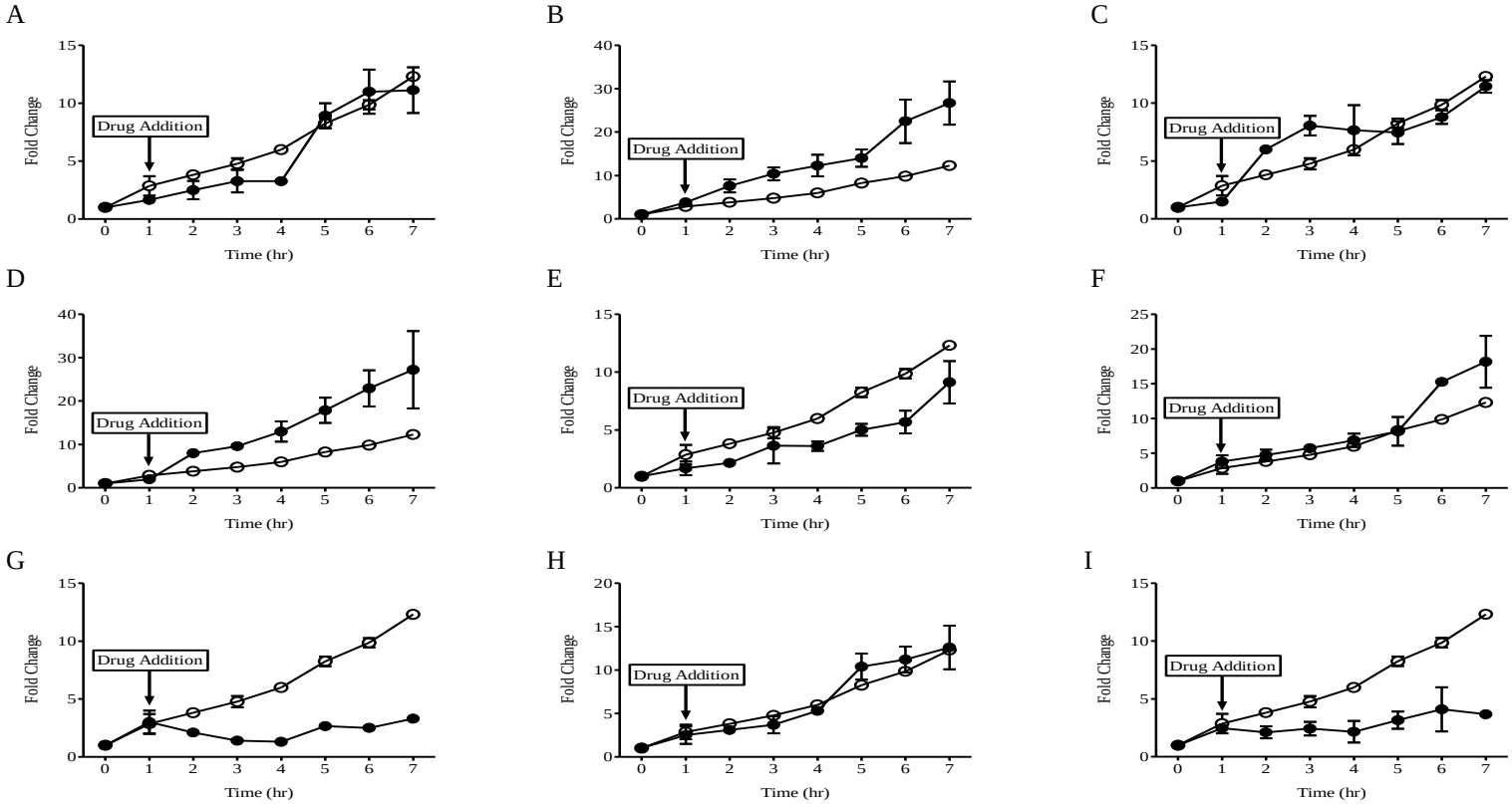

Figure 6.18: Time-dependent curves of malate production in drug-treated and untreated *P. falciparum* 3D7 parasites.
Malate levels were measured in untreated (open circle) and drug-treated (closed circle) *P. falciparum* trophozoite-staged parasites by LC-MS/MS. There were no differences in malate levels after one hour of incubation in parasites treated with (A) 2.5 nM atovaquone, (C) 50 nM CK-2-68, (D) 15 nM 5-fluoroorotic acid, (E) 1 mM potassium cyanide, (F) 5 µM bongkrekic acid, and (H) 70 µM proguanil. Conversely, data showed a slight increase of malate in parasites treated with (B) 2.5 nM atovaquone + 1 µM proguanil while there was an evident reduction in malate levels in parasites treated with (G) 10 µM thenoyltrifluoroacetone and (I) 200 µM fusidic acid. The points represent the mean ± SEM of at least duplicate independent experiments.

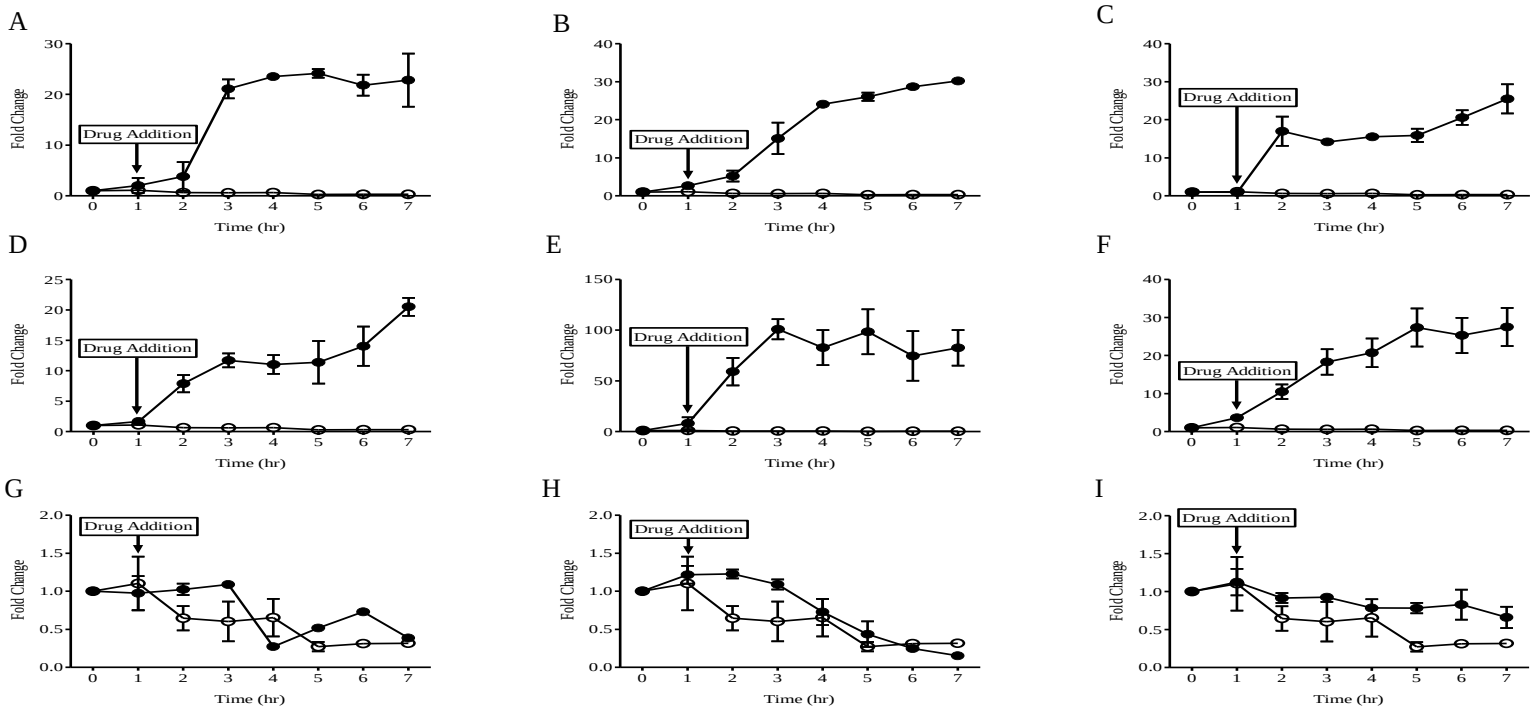

Figure 6.19: Time-dependent curves of carbamoyl-L-aspartate in drug-treated and untreated *P. falciparum* 3D7 parasites.
Carbamoyl-L-aspartate levels were determined in untreated (open circle) and drug-treated (closed circle) *P.falciparum* trophozoite-staged parasites by LC-MS/MS. The following drugs were added to the parasites after one hour of incubation (A) 2.5 nM atovaquone, (B) 2.5 nM atovaquone + 1 µM proguanil, (C) 50 nM CK-2-68, (D) 15 nM 5-fluoroorotic acid, (E) 1 mM potassium cyanide, (F) 5 µM bongkrekic acid, (G) 10 µM thenoyltrifluoroacetone, (H) 70 µM proguanil and (I) 200 µM fusidic acid. Data showed a distinguished accumulation of carbamoyl-L-aspartate in parasites treated with (A) 2.5 nM atovaquone and (B) 2.5 nM atovaquone + 1 µM proguanil, (C) 50 nM CK-2-68, (D) 15 nM 5-fluoroorotic acid, (E) 1 mM potassium cyanide and (F) 5 µM bongkrekic acid. There were no changes observed in parasites treated with (G) 10 µM thenoyltrifluoroacetone, (H) 70 µM proguanil and (I) 200 µM fusidic acid. The points represent the mean ± SEM of at least duplicate independent experiments.

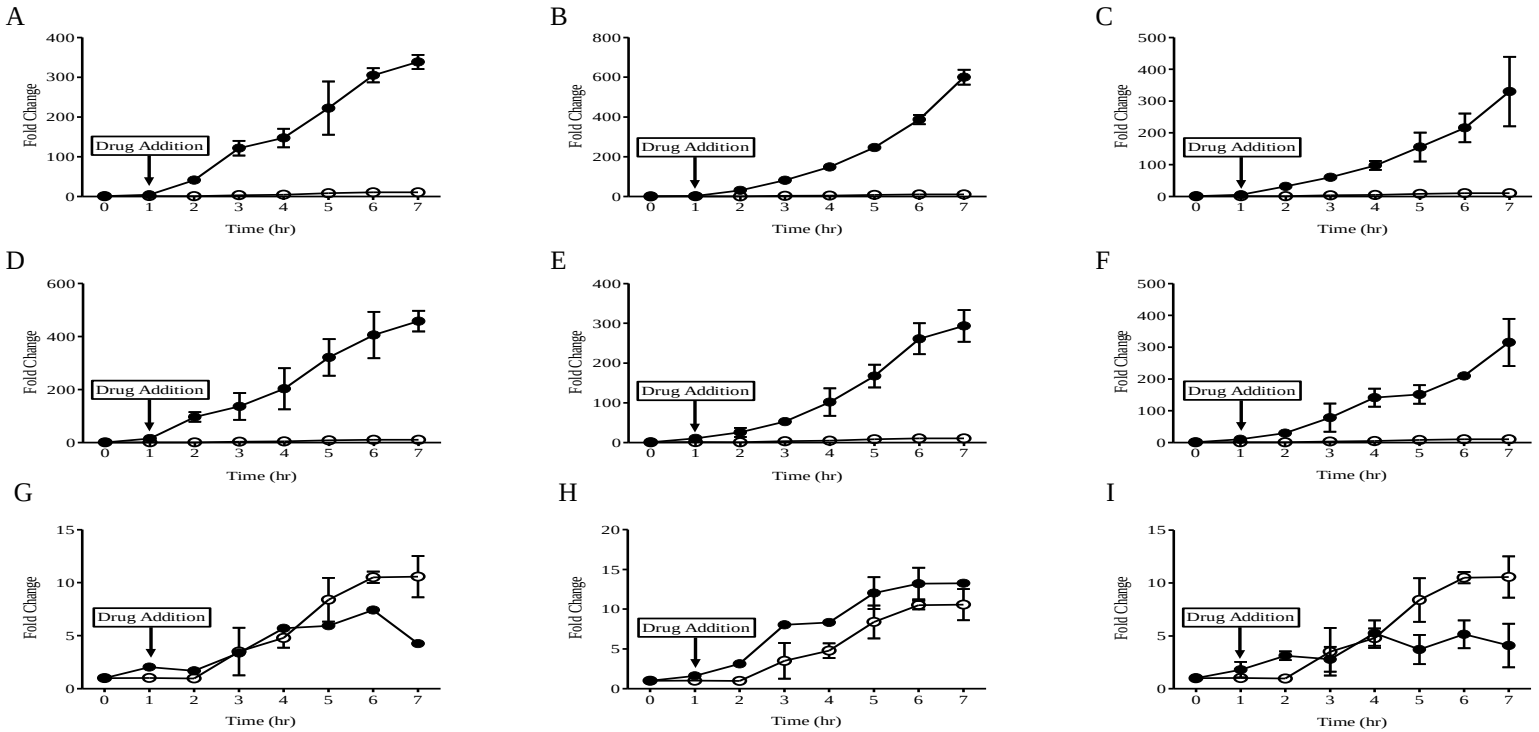

Figure 6.20: Time-dependent curves of dihydroorotate in drug-treated and untreated *P. falciparum* 3D7 parasites.

Dihydroorotate levels were determined in untreated (open circle) and drug-treated (closed circle) *P.falciparum* trophozoite-staged parasites by LC-MS/MS. The following drugs were added to the parasites after one hour of incubation (A) 2.5 nM atovaquone, (B) 2.5 nM atovaquone + 1 µM proguanil, (C) 50 nM CK-2-68, (D) 15 nM 5-fluoroorotic acid, (E) 1 mM potassium cyanide, (F) 5 µM bongkrekic acid, (G) 10 µM thenoyltrifluoroacetone, (H) 70 µM proguanil and (I) 200µM fusidic acid. Data showed a notable accumulation of dihydroorotate in parasites treated with (A) 2.5nM atovaquone and (B) 2.5 nM atovaquone + 1 µM proguanil, (C) 50 nM CK-2-68, (D) 15 nM 5-fluoroorotic acid, (E) 1 mM potassium cyanide and (F) 5 µM bongkrekic acid. There were no changes observed in parasites treated with (G) 10 µM thenoyltrifluoroacetone, (H) 70 µM proguanil and (I) 200 µM fusidic acid. The points represent the mean ± SEM of at least duplicate independent experiments.

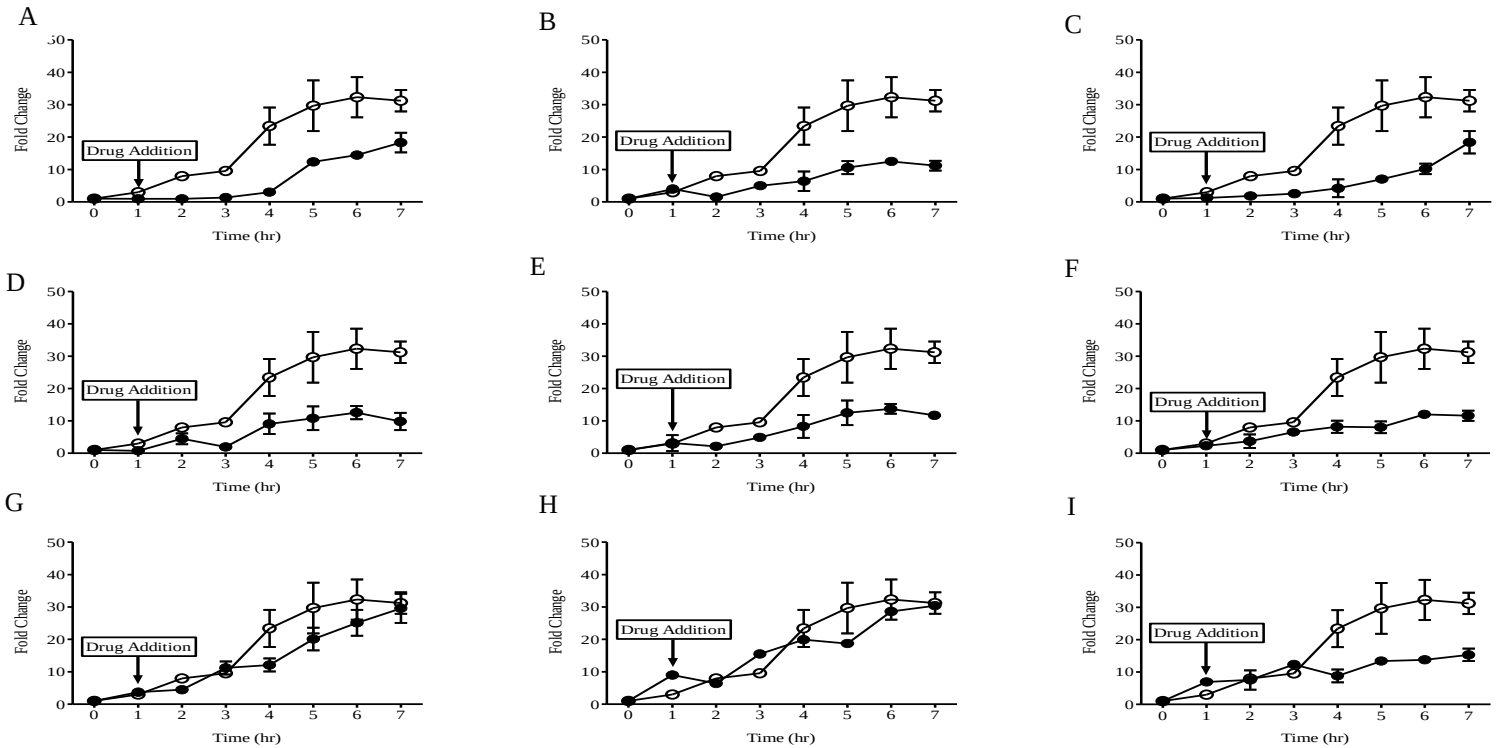

Figure 6.21: Time-dependent curves of orotate in drug-treated and untreated *P. falciparum* 3D7 parasites.

Orotate levels were determined in untreated (opened circle) and drug-treated (closed circle) *P.falciparum* trophozoite-staged parasites by LC-MS/MS. The following drugs were added to the parasites after one hour of incubation (A) 2.5 nM atovaquone, (B) 2.5 nM atovaquone + 1 µM proguanil, (C) 50 nM CK-2-68, (D) 15 nM 5-fluoroorotic acid, (E) 1 mM potassium cyanide, (F) 5 µM bongkrekic acid, (G) 10 µM thenoyltrifluoroacetone, (H) 70 µM proguanil and (I) 200µM fusidic acid. Data showed an evident reduction of orotate in parasites treated with (A) 2.5 nM atovaquone, (B) 2.5 nM atovaquone + 1 µM proguanil, (C) 50 nM CK-2-68, (D) 15 nM 5-fluoroorotic acid, (E) 1 mM potassium cyanide and (F) 5 µM bongkrekic acid. There were no changes observed in others drugs-treated parasites. The points represent the mean ± SEM of at least duplicate independent experiments.

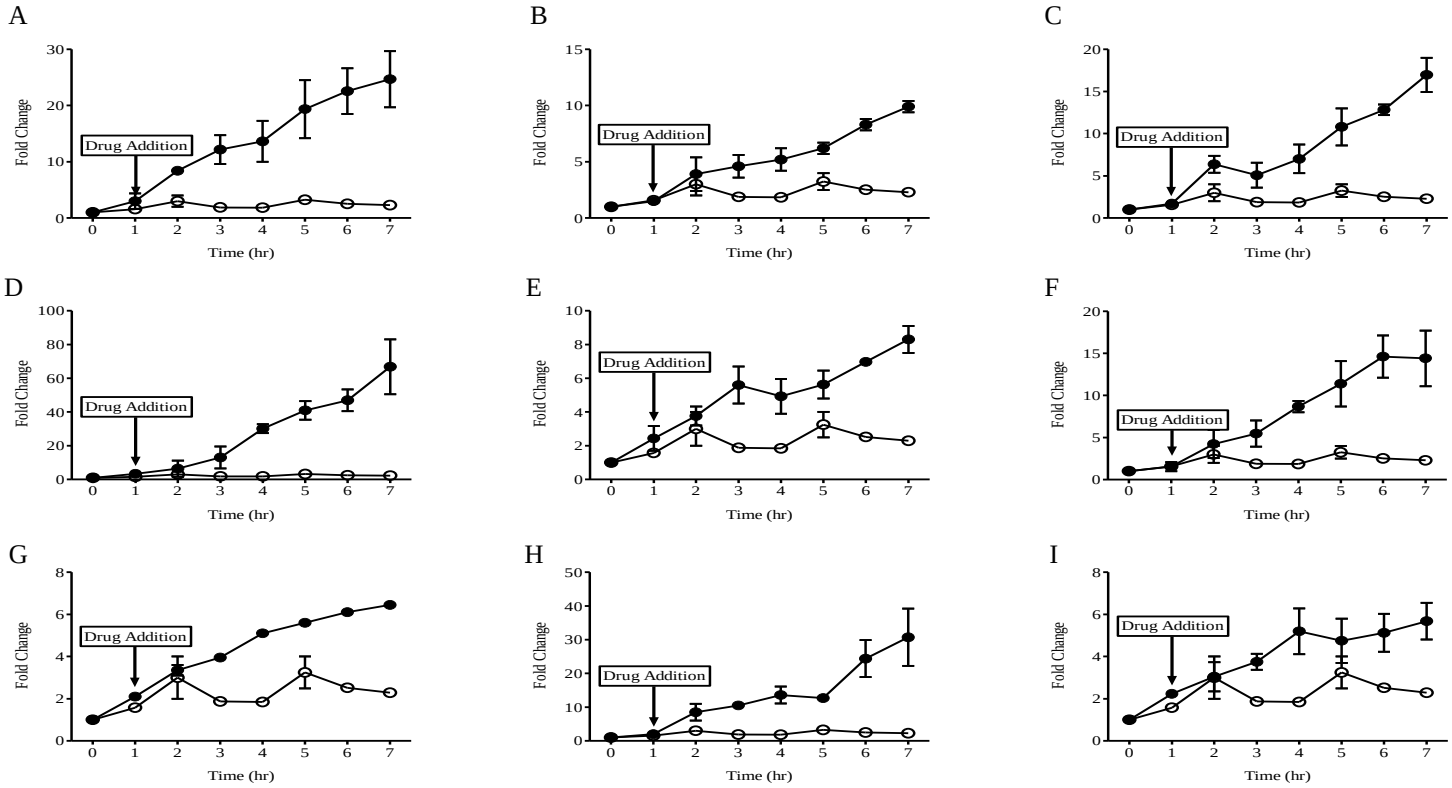

Figure 6.22: Time-dependent curves of alanine accumulation in drug-treated *P. falciparum* 3D7 parasites.
Alanine levels were determined in untreated (open circle) and drug-treated (closed circle) *P.falciparum* trophozoite-staged parasites by LC-MS/MS. Data showed a distinguished accumulation of alanine after one hour of incubation in parasites treated with (A) 2.5 nM atovaquone, (B) 2.5 nM atovaquone + 1 µM proguanil, (C) 50 nM CK-2-68, (D) 15 nM 5-fluoroorotic acid, (E) 1 mM potassium cyanide, (F) 5 µM bongkrekic acid, (G) 10 µM thenoyltrifluoroacetone, (H) 70 µM proguanil and (I) 200 µM fusidic acid. Data represent the mean ± SEM of at least duplicate independent experiments.

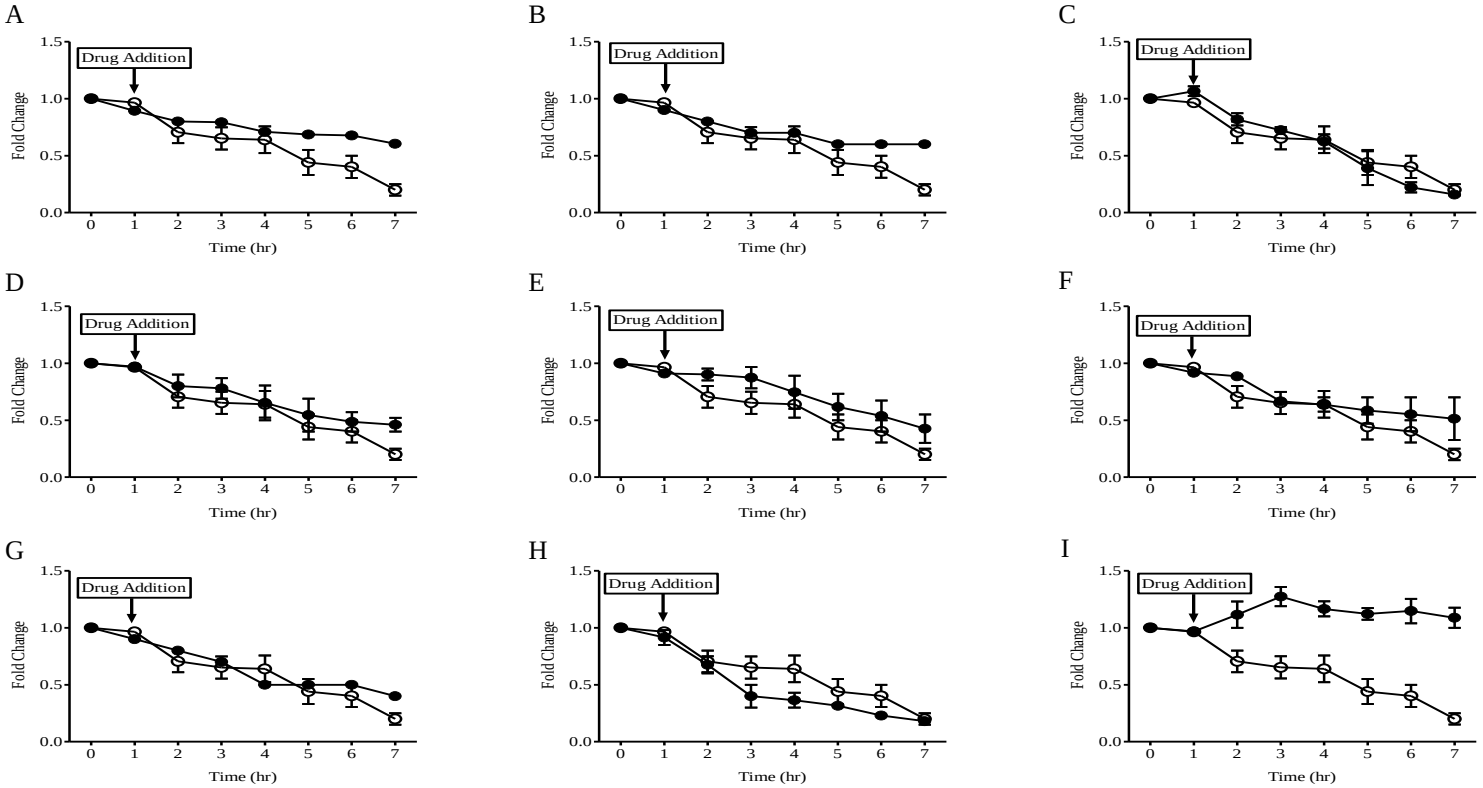

Figure 6.23: Time-dependent curves of glutamine in drug-treated and untreated *P. falciparum* 3D7 parasites.
Glutamine levels were determined in untreated (open circle) and drug-treated (closed circle) *P.falciparum* trophozoite-staged parasites by LC-MS/MS. There were no changes observed after one hour of incubation in parasites treated with (A) 2.5 nM atovaquone, (B) 2.5 nM atovaquone + 1µM proguanil, (C) 50 nM CK-2-68, (D) 15 nM 5-fluoroorotic acid, (E) 1 mM potassium cyanide, (F) 5 µM bongkrekic acid, (G) 10 µM thenoyltrifluoroacetone and (H) 70 µM proguanil. Data showed a notable accumulation of glutamine in parasites treated with (I) 200 µM fusidic acid. Data represent the mean ± SEM of at least duplicate independent experiments.

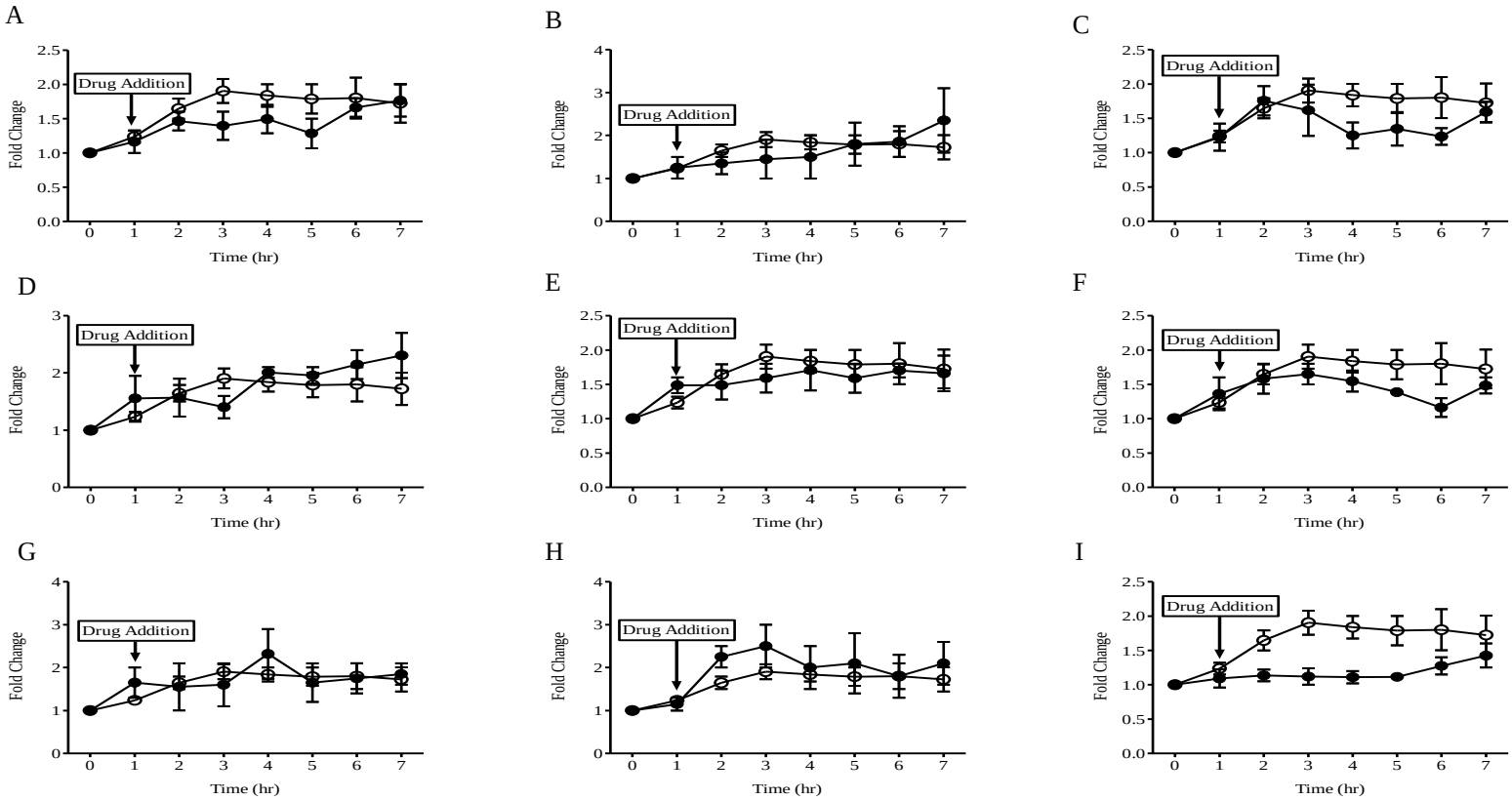

Figure 6.24: Time-dependent curves of glutamate in drug-treated and untreated *P. falciparum* 3D7 parasites.
Glutamate levels were determined in untreated (open circle) and drug-treated (closed circle) *P.falciparum* trophozoite-staged parasites by LC-MS/MS. Notable invariable changes were observed in glutamate after one hour of incubation in parasites treated with (I) 200 µM fusidic acid. There were no changes observed in parasites treated with (A) 2.5 nM atovaquone, (B) 2.5 nM atovaquone + 1 µM proguanil, (C) 50 nM CK-2-68, (D) 15 nM 5-fluoroorotic acid, (E) 1 mM potassium cyanide, (F) 5 µM bongkrekic acid, (G) 10 µM thenoyltrifluoroacetone and (H) 70 µM proguanil. Data represent the mean ± SEM of at least duplicate independent experiments.

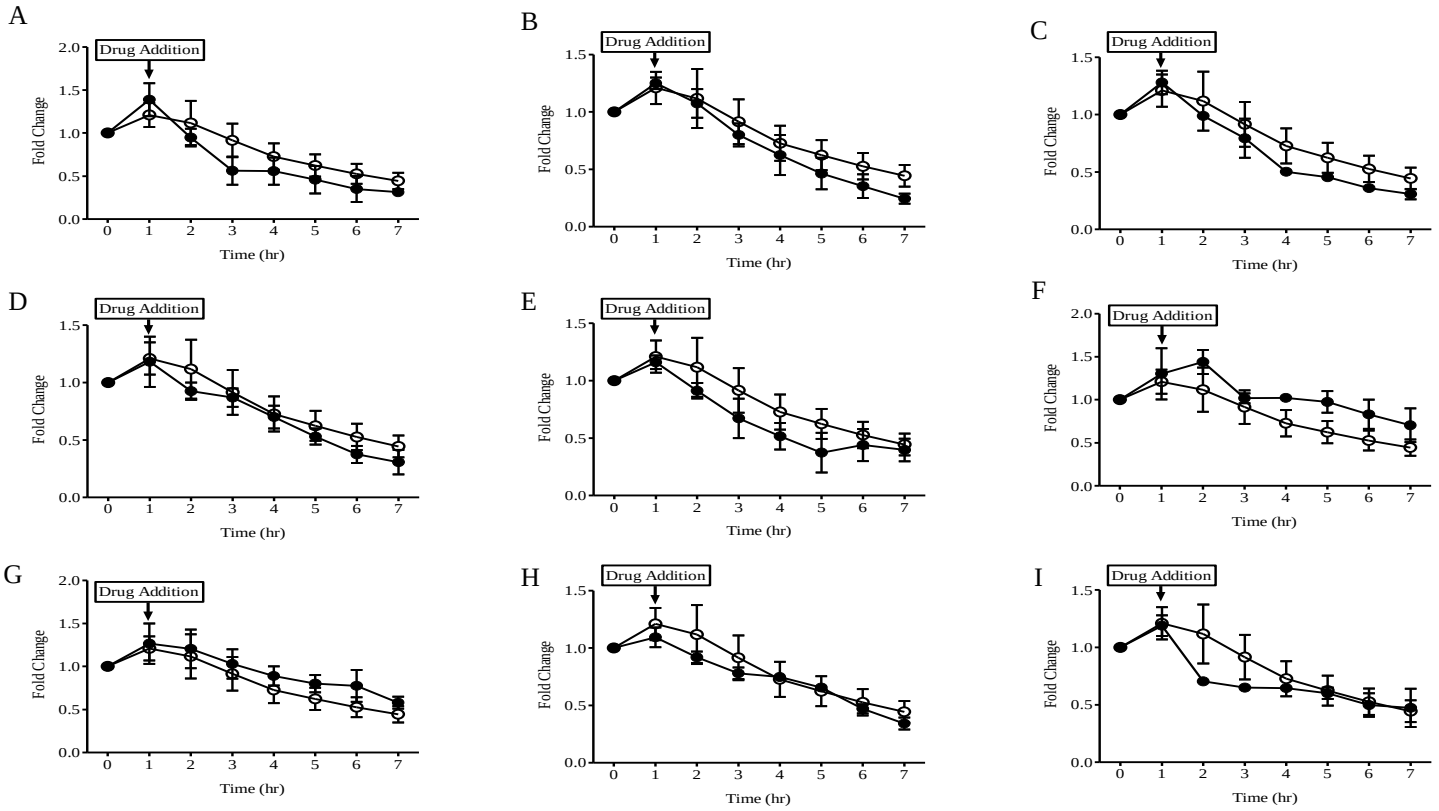

Figure 6.25: Time-dependent curves of arginie degradation in drug-treated and untreated *P. falciparum* 3D7 parasites.
Arginine degradation levels were measured in untreated (open circle) and drug-treated (closed circle) *P.falciparum* trophozoite-staged parasites by LC-MS/MS. The following drugs were added to the parasites after one hour of incubation (A) 2.5 nM atovaquone, (B) 2.5 nM atovaquone + 1 µM proguanil, (C) 50 nM CK-2-68, (D) 15 nM 5-fluoroorotic acid, (E) 1 mM potassium cyanide, (F) 5 µM bongkrekic acid, (G) 10 µM thenoyltrifluoroacetone, (H) 70 µM proguanil and (I) 200 µM fusidic acid. There were no changes between drugs-treated and untreated parasites. The points represent the mean ± SEM of at least duplicate independent experiments.

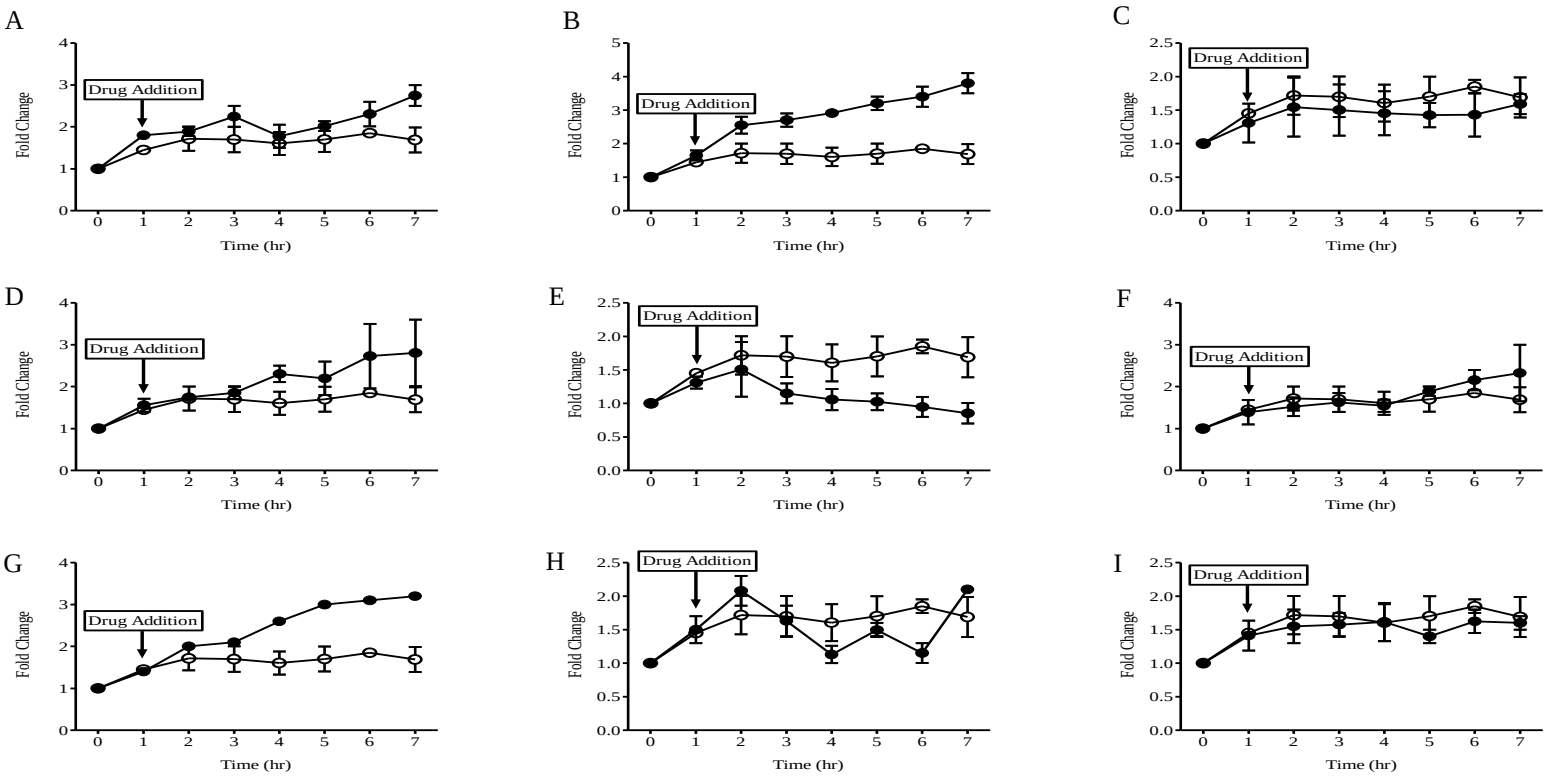

Figure 6.26: Time-dependent curves of proline in drug-treated and untreated *P. falciparum* 3D7 parasites.
Proline levels were determined in untreated (open circle) and drug-treated (closed circle) *P.falciparum* trophozoite-staged parasites by LC-MS/MS. The following drugs were added to the parasites after one hour of incubation (A) 2.5 nM atovaquone, (B) 2.5 nM atovaquone + 1 µM proguanil, (C) 50 nM CK-2-68, (D) 15 nM 5-fluoroorotic acid, (E) 1 mM potassium cyanide, (F) 5 µM bongkrekic acid, (G) 10 µM thenoyltrifluoroacetone, (H) 70 µM proguanil and (I) 200 µM fusidic acid. There were no changes observed between drugs-treated and untreated parasites. The points represent the mean ± SEM of at least duplicate independent experiments.

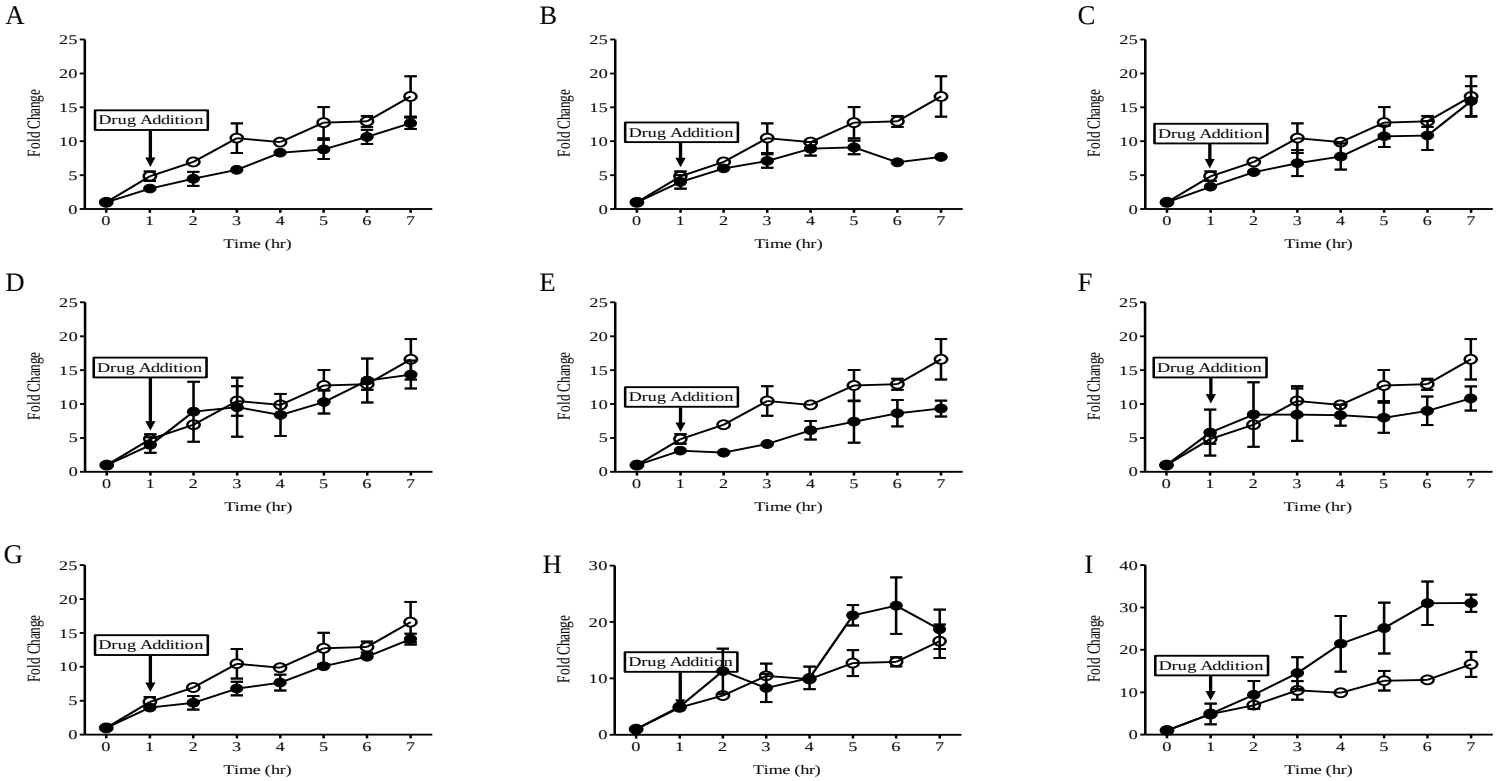

Figure 6.27: Time-dependent curves of ornithine production in drug-treated and untreated *P. falciparum* 3D7 parasites.
Ornithine levels were determined in untreated (open circle) and drug-treated (closed circle) *P.falciparum* trophozoite-staged parasites by LC-MS/MS. The following drugs were added to the parasites after one hour of incubation (A) 2.5 nM atovaquone, (B) 2.5 nM atovaquone + 1 µM proguanil, (C) 50 nM CK-2-68, (D) 15 nM 5-fluoroorotic acid, (E) 1 mM potassium cyanide, (F) 5 µM bongkrekic acid, (G) 10 µM thenoyltrifluoroacetone, (H) 70 µM proguanil and (I) 200 µM fusidic acid. Data showed a marked increase in ornithine level in parasite treated with (I) 200 µM fusidic acid. There were no changes observed between other drugs-treated and untreated parasites. The points represent the mean ± SEM of at least duplicate independent experiments.

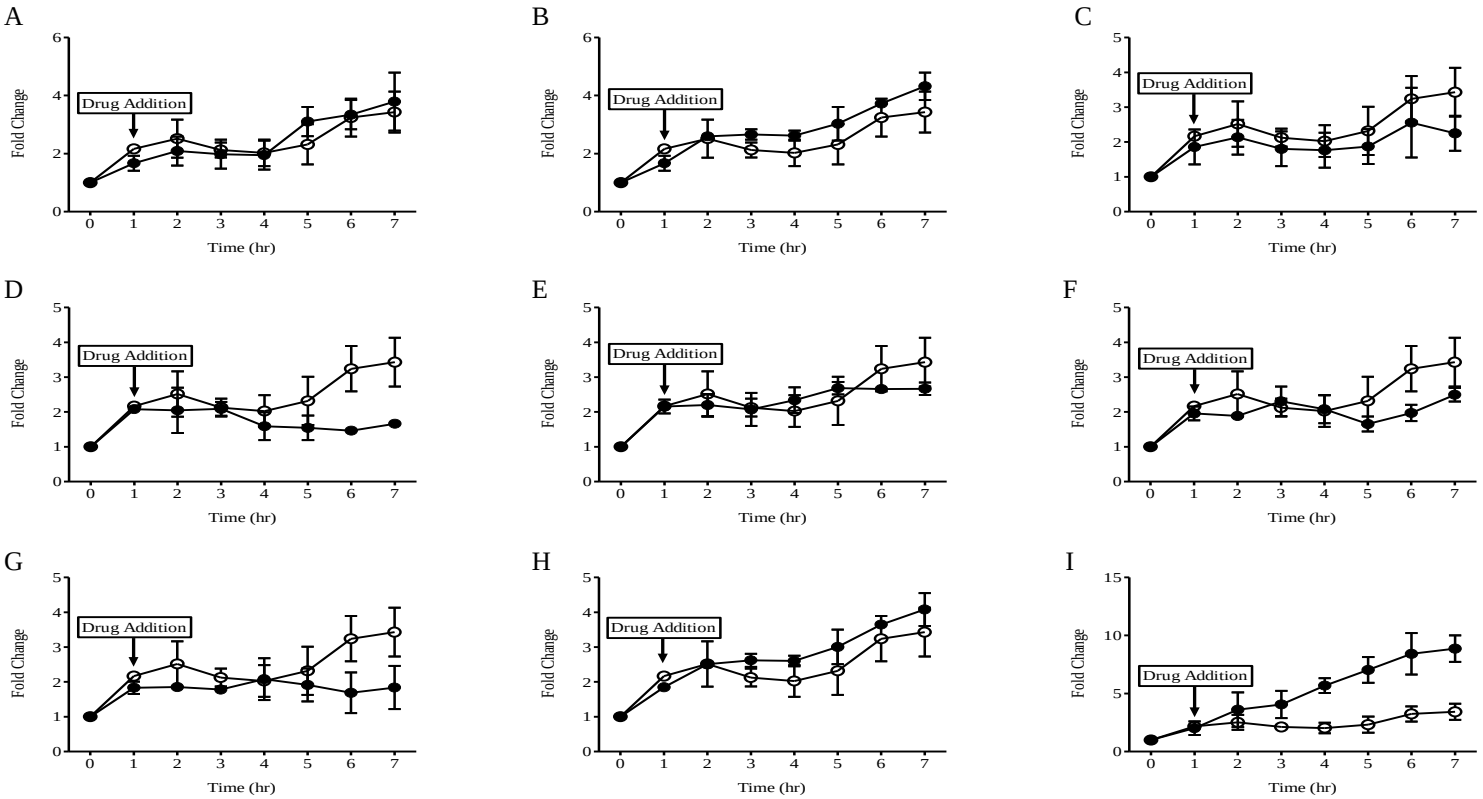

Figure 6.28: Time-dependent curves of citrulline in drug-treated and untreated *P. falciparum* 3D7 parasites.
Citrulline levels were determined in untreated (open circle) and drug-treated (closed circle) *P.falciparum* trophozoite-staged parasites by LC-MS/MS. The following drugs were added to the parasites after one hour of incubation (A) 2.5 nM atovaquone, (B) 2.5 nM atovaquone + 1 µM proguanil, (C) 50 nM CK-2-68, (D) 15 nM 5-fluoroorotic acid, (E) 1 mM potassium cyanide, (F) 5 µM bongkrekic acid, (G) 10 µM thenoyltrifluoroacetone, (H) 70 µM proguanil and (I) 200 µM fusidic acid. Data showed an evident accumulation of citrulline in parasites treated with (I) 200 µM fusidic acid. There were no changes observed between other drugs-treated and untreated parasites. Data represent the mean ± SEM of at least duplicate independent experiments.

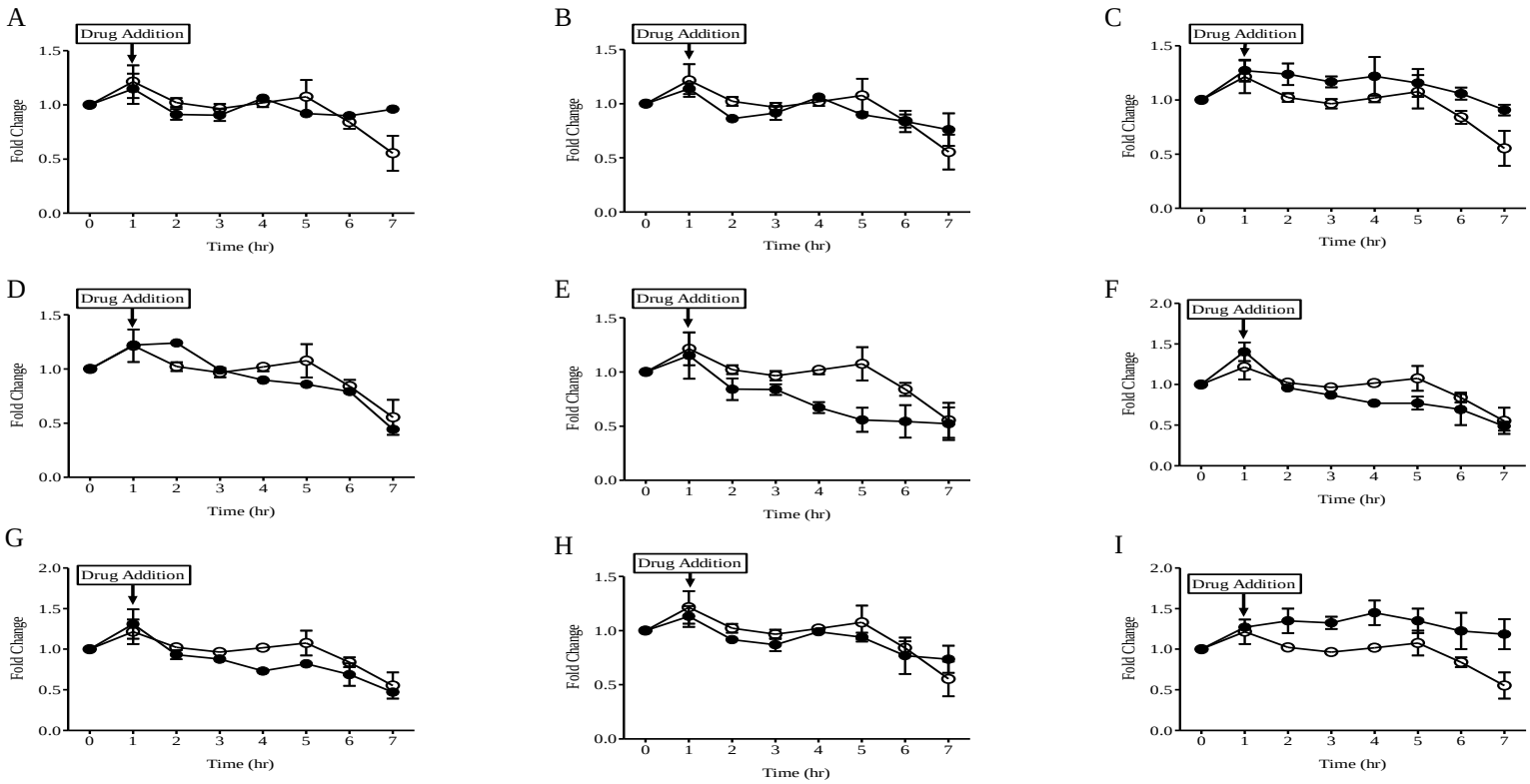

Figure 6.29: Time-dependent curves of serine in drug-treated and untreated *P. falciparum* 3D7 parasites.

Serine levels were determined in untreated (open circle) and drug-treated (closed circle) *P.falciparum* trophozoite-staged parasites by LC-MS/MS. The following drugs were added to the parasites after one hour of incubation (A) 2.5 nM atovaquone, (B) 2.5 nM atovaquone + 1 µM proguanil, (C) 50 nM CK-2-68, (D) 15 nM 5-fluoroorotic acid, (E) 1 mM potassium cyanide, (F) 5 µM bongkrekic acid, (G) 10 µM thenoyltrifluoroacetone, (H) 70 µM proguanil and (I) 200 µM fusidic acid. Data showed notable invariable changes of serine in parasites treated with (I) 200 µM fusidic acid. There were no changes among other drugs-treated parasites as compared to untreated parasites. The points represent the mean ± SEM of at least duplicate independent experiments.

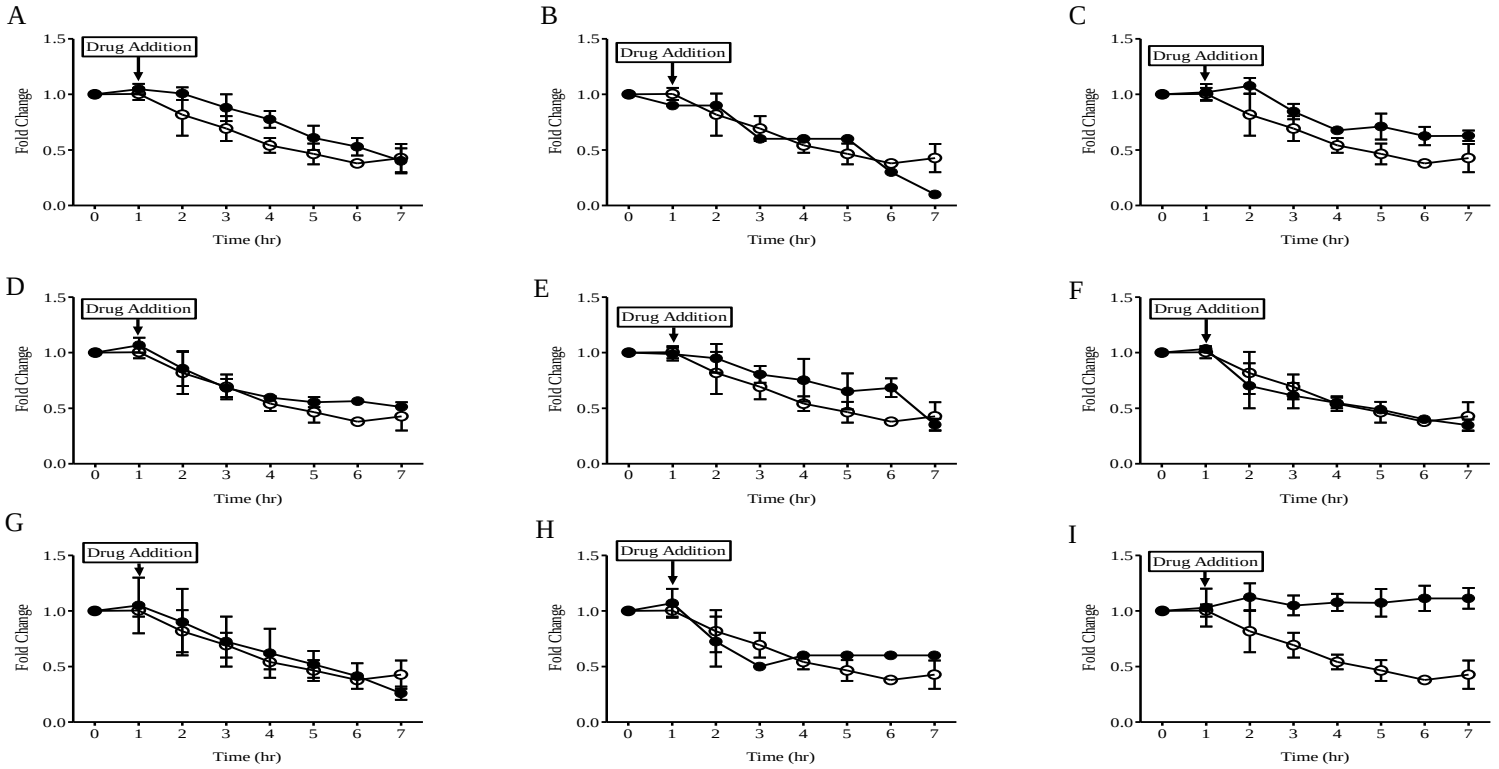

Figure 6.30: Time-dependent curves of asparagine in drug-treated and untreated *P. falciparum* 3D7 parasites.
Asparagine levels were determined in untreated (open circle) and drug-treated (closed circle) *P.falciparum* trophozoite-staged parasites by LC-MS/MS. The following drugs were added to the parasites after one hour of incubation (A) 2.5 nM atovaquone, (B) 2.5 nM atovaquone + 1 µM proguanil, (C) 50 nM CK-2-68, (D) 15 nM 5-fluoroorotic acid, (E) 1 mM potassium cyanide, (F) 5 µM bongkrekic acid, (G) 10 µM thenoyltrifluoroacetone, (H) 70 µM proguanil and (I) 200 µM fusidic acid. Data showed distinguished invariable changes of asparagine in parasites treated with (I) 200 µM fusidic acid. There were no changes observed among other drugs-treated parasites as compared to untreated parasites. The points represent the mean ± SEM of at least duplicate independent experiments.

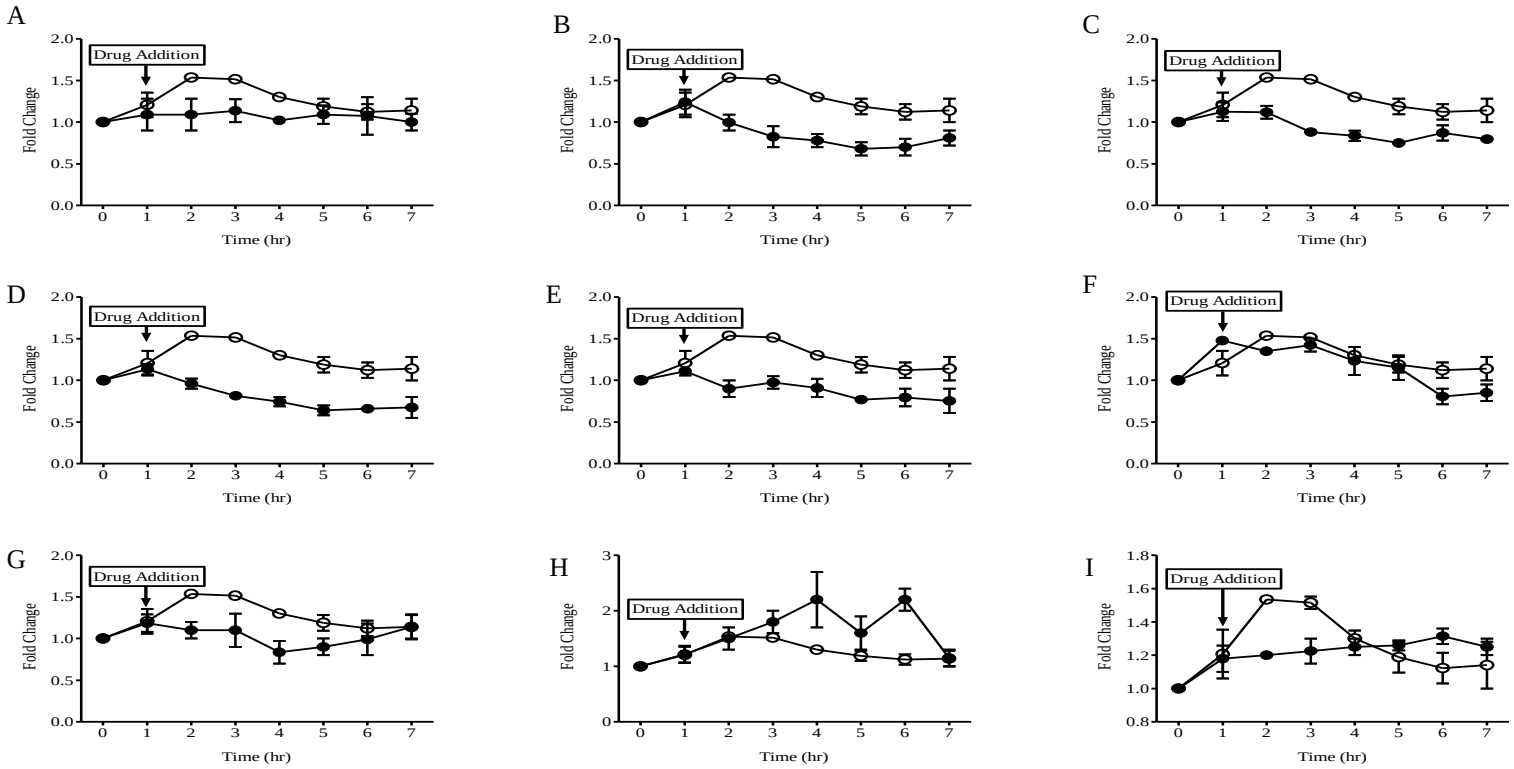

Figure 6.31: Time-dependent curves of aspartate in drug-treated and untreated *P. falciparum* 3D7 parasites.
Aspartate levels were determined in untreated (opened circle) and drug-treated (closed circle) *P.falciparum* trophozoite-staged parasites by LC-MS/MS. The following drugs were added to the parasites after one hour of incubation (A) 2.5 nM atovaquone, (B) 2.5 nM atovaquone + 1 µM proguanil, (C) 50 nM CK-2-68, (D) 15 nM 5-fluoroorotic acid, (E) 1 mM potassium cyanide, (F) 5 µM bongkrekic acid, (G) 10 µM thenoyltrifluoroacetone, (H) 70 µM proguanil and (I) 200 µM fusidic acid. Data showed a slight reduction in the level of asparate in parasites treated with (A) 2.5 nM atovaquone, (B) 2.5 nM atovaquone + 1 µM proguanil, (C) 50 nM CK-2-68, (D) 15 nM 5-fluoroorotic acid and (E) 1 mM potassium cyanide. There were no changes between drugs-treated and untreated parasites. The points represent the mean ± SEM of at least duplicate independent experiments.

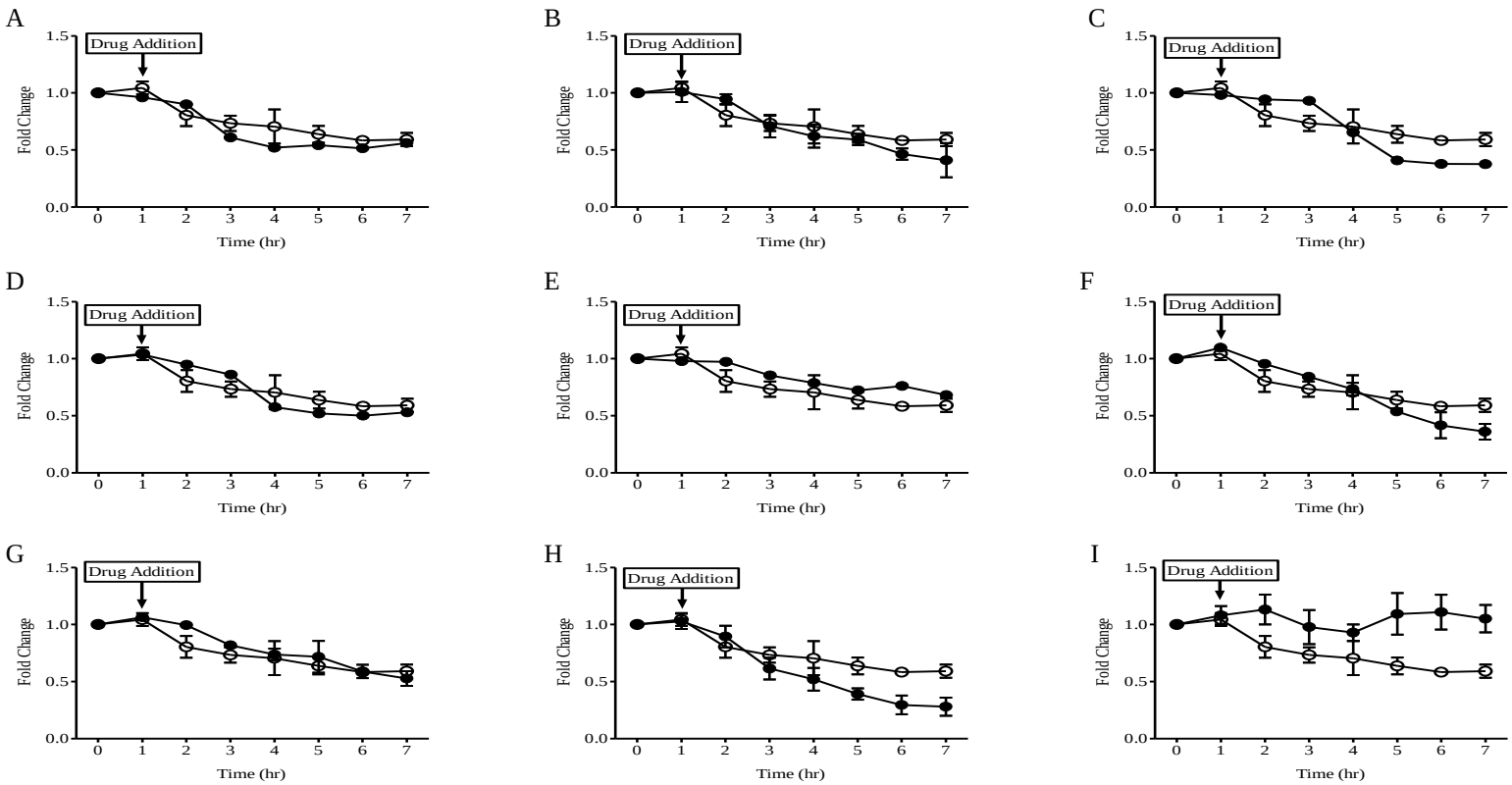

Figure 6.32: Time-dependent curves of lysine degradation in drug-treated and untreated *P. falciparum* 3D7 parasites.
Lysine degredation levels were determined in untreated (open circle) and drug-treated (closed circle) *P.falciparum* trophozoite-staged parasites by LC-MS/MS. The following drugs were added to the parasites after one hour of incubation (A) 2.5 nM atovaquone, (B) 2.5 nM atovaquone + 1 µM proguanil, (C) 50 nM CK-2-68, (D) 15 nM 5-fluoroorotic acid, (E) 1 mM potassium cyanide, (F) 5 µM bongkrekic acid, (G) 10 µM thenoyltrifluoroacetone, (H) 70 µM proguanil and (I) 200 µM fusidic acid. Data showed notable invariable changes of lysine in parasites treated with (I) 200uM fusidic acid. There were no changes between drugs-treated and untreated parasites. Data represent the mean ± SEM of at least duplicate independent experiments.

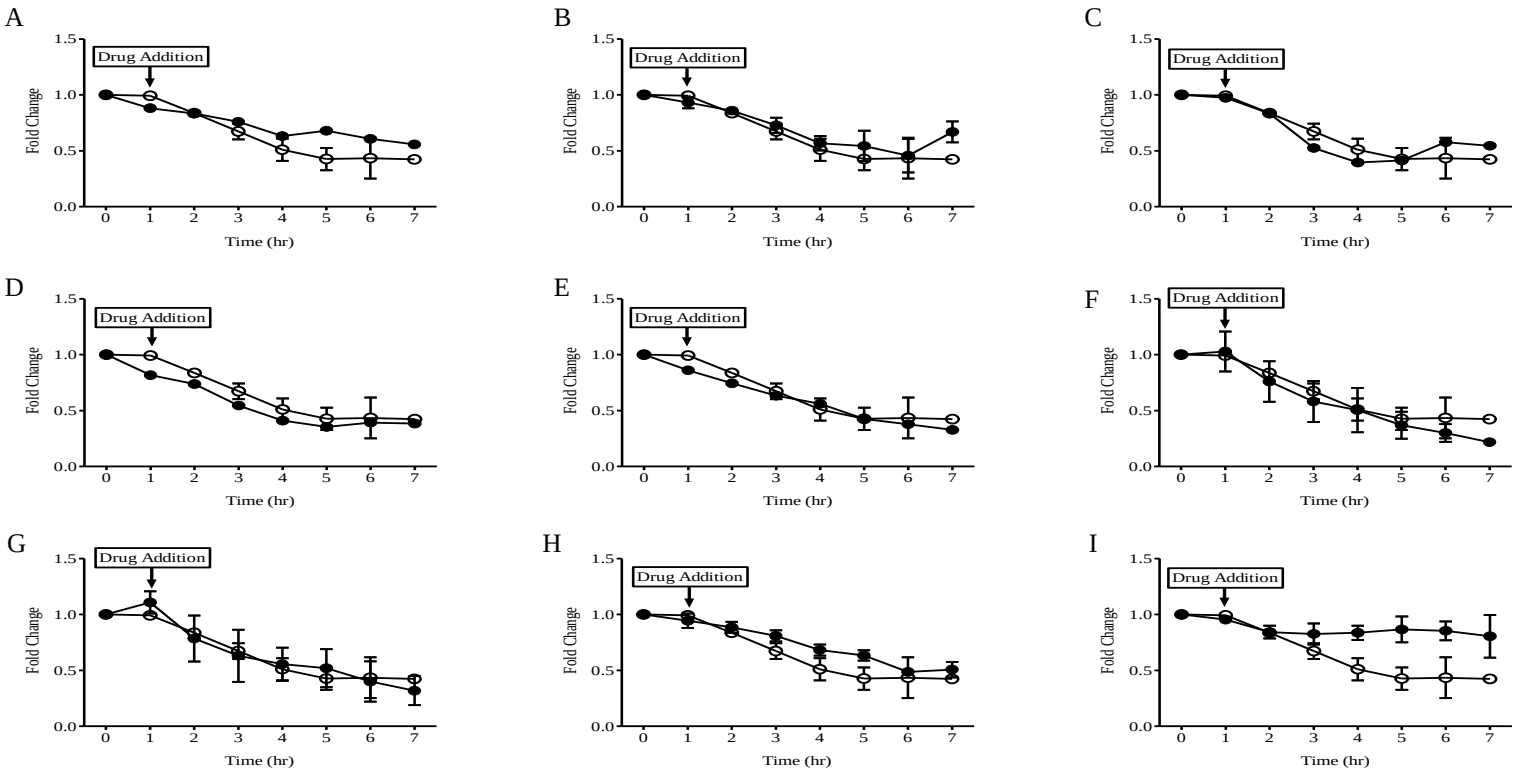

Figure 6.33: Time-dependent curves of methionine in drug-treated and untreated *P. falciparum* 3D7 parasites.
Methionine levels were determined in untreated (open circle) and drug-treated (closed circle) *P.falciparum* trophozoite-staged parasites by LC-MS/MS. The following drugs were added to the parasites after one hour of incubation (A) 2.5 nM atovaquone, (B) 2.5 nM atovaquone + 1 µM proguanil, (C) 50 nM CK-2-68, (D) 15 nM 5-fluoroorotic acid, (E) 1 mM potassium cyanide, (F) 5 µM bongkrekic acid, (G) 10 µM thenoyltrifluoroacetone, (H) 70 µM proguanil and (I) 200 µM fusidic acid. Data showed notable invariable changes in the methionine level in parasites treated with (I) 200 µM fusidic acid. There were no changes observed between others drugs-treated and untreated parasites. The points represent the mean ± SEM of at least duplicate independent experiments.

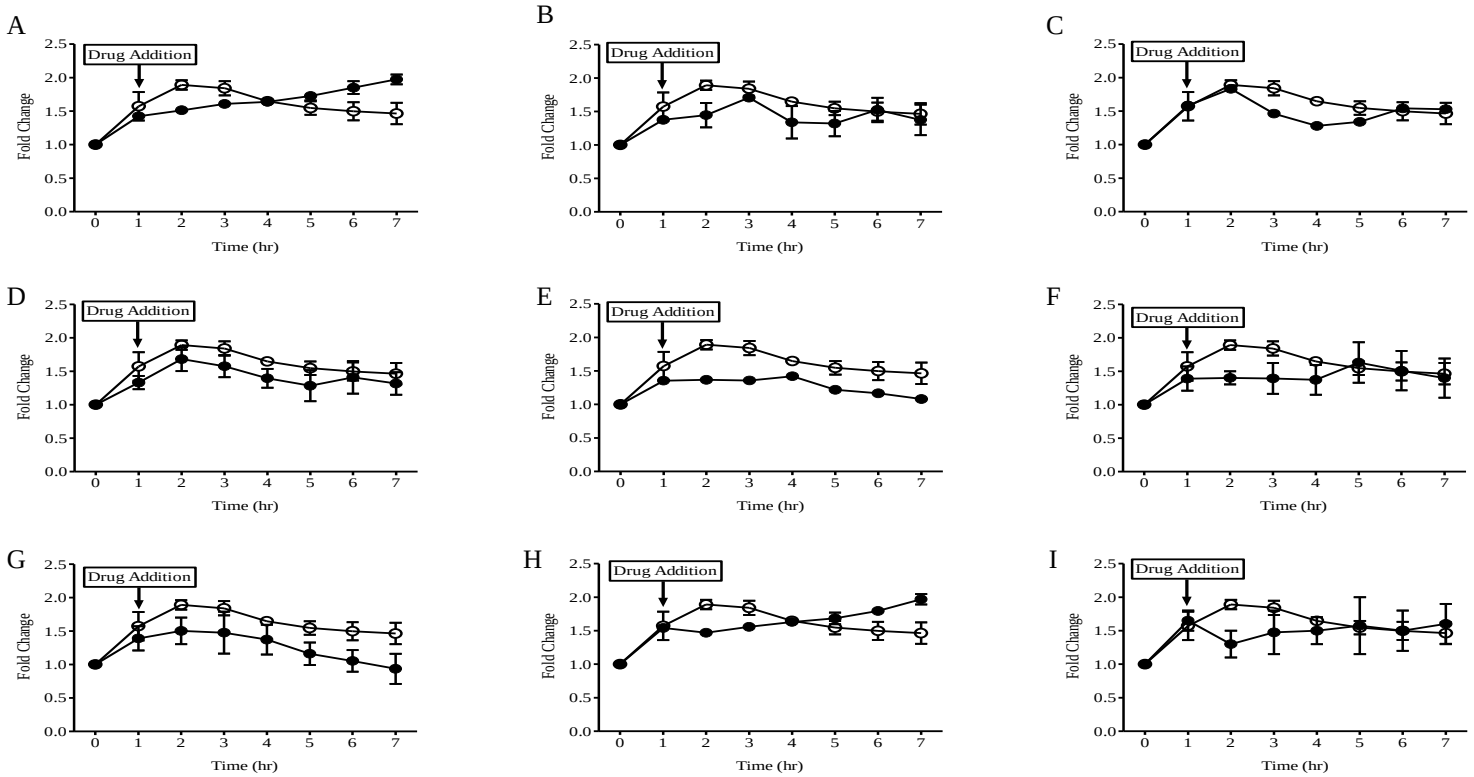

Figure 6.34: Time-dependent curves of histidine in drug-treated and untreated *P. falciparum* 3D7 parasites.
Histidine levels were determined in untreated (open circle) and drug-treated (closed circle) *P.falciparum* trophozoite-staged parasites by LC-MS/MS. The following drugs were added to the parasites after one hour of incubation (A) 2.5 nM atovaquone, (B) 2.5 nM atovaquone + 1 µM proguanil, (C) 50 nM CK-2-68, (D) 15 nM 5-fluoroorotic acid, (E) 1 mM potassium cyanide, (F) 5 µM bongkrekic acid, (G) 10 µM thenoyltrifluoroacetone, (H) 70 µM proguanil and (I) 200 µM fusidic acid. There were no changes observed between drugs-treated and untreated parasites. The points represent the mean ± SEM of at least duplicate independent experiments.

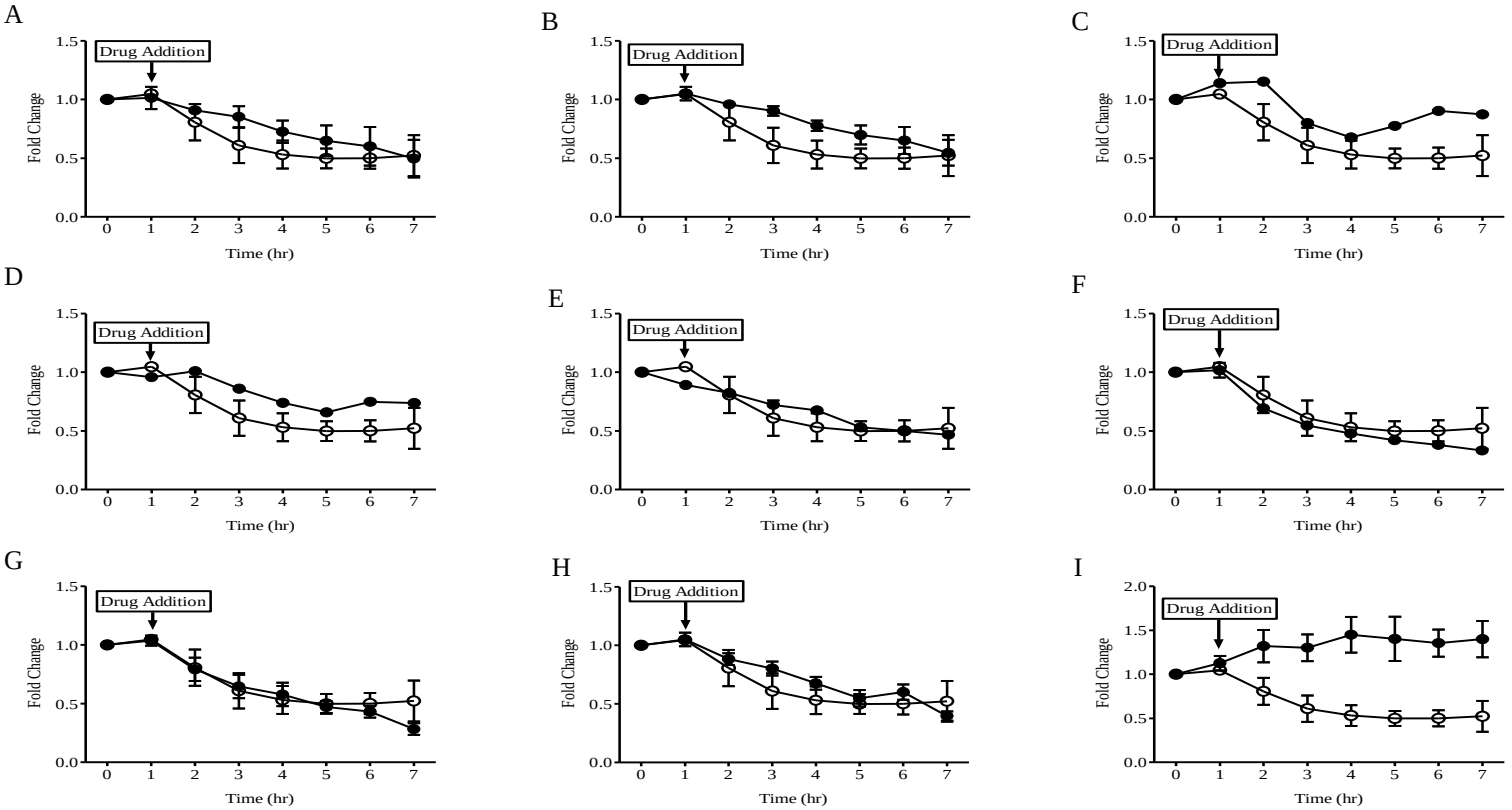

Figure 6.35: Time-dependent curves of phenylalanine in drug-treated and untreated *P. falciparum* 3D7 parasites.
Phenylalanine levels were determined in untreated (open circle) and drug-treated (closed circle) *P.falciparum* trophozoite-staged parasites by LC-MS/MS. The following drugs were added to the parasites after one hour of incubation (A) 2.5 nM atovaquone, (B) 2.5 nM atovaquone + 1 µM proguanil, (C) 50 nM CK-2-68, (D) 15 nM 5-fluoroorotic acid, (E) 1 mM potassium cyanide, (F) 5 µM bongkrekic acid, (G) 10 µM thenoyltrifluoroacetone, (H) 70 µM proguanil and (I) 200 µM fusidic acid. Phenylalanine was slightly accumulated after one hour of incubation in parasites treated with (I) 200 µM fusidic acid. There were no changes observed between others drugs-treated and untreated parasites. Data represent the mean ± SEM of at least duplicate independent experiments.

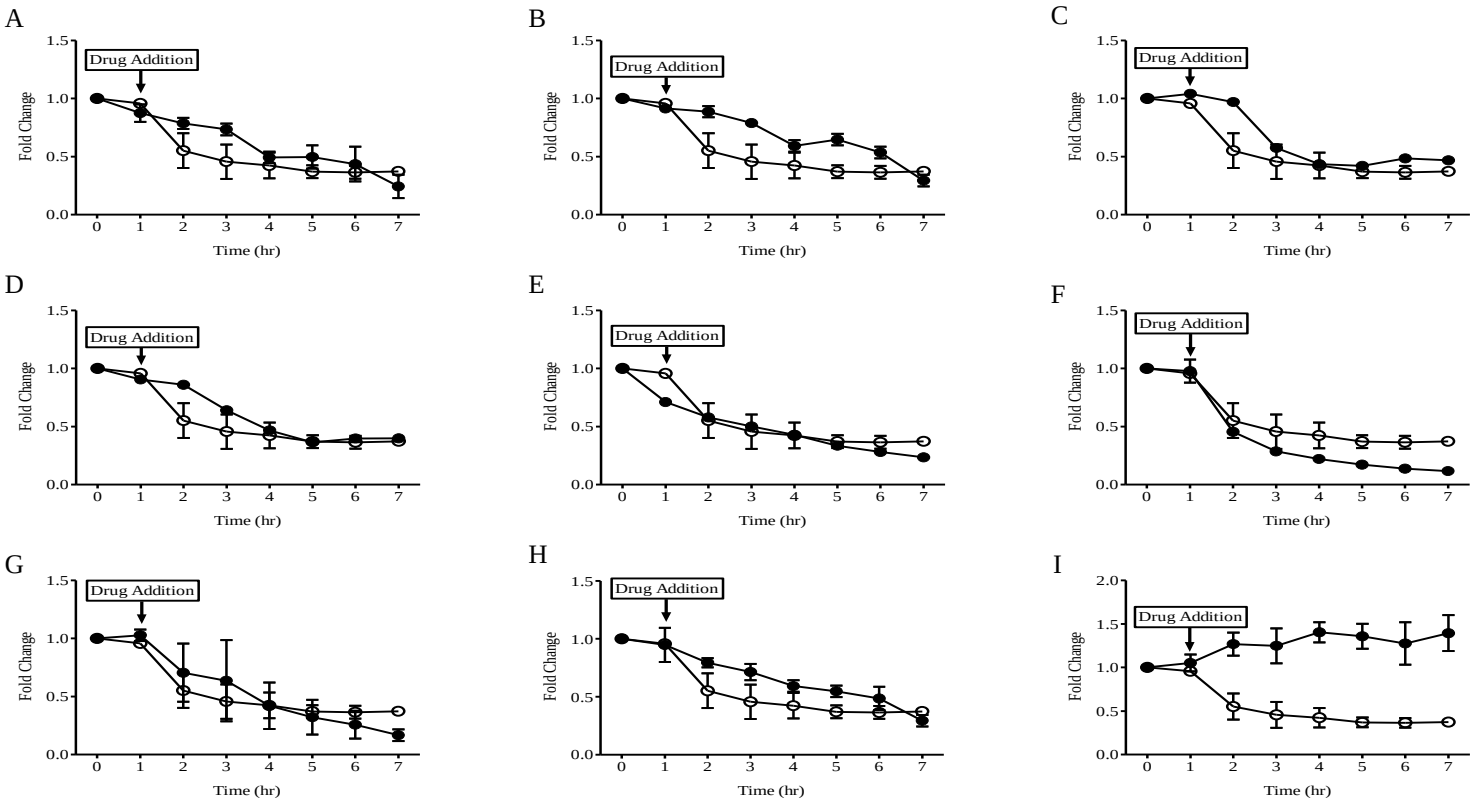

Figure 6.36: Time-dependent curves of tryptophan in drug-treated and untreated *P. falciparum* 3D7 parasites.
Tryptophan levels were determined in untreated (open circle) and drug-treated (closed circle) *P.falciparum* trophozoite-staged parasites by LC-MS/MS. The following drugs were added to the parasites after one hour of incubation (A) 2.5 nM atovaquone, (B) 2.5 nM atovaquone + 1 µM proguanil, (C) 50 nM CK-2-68, (D) 15 nM 5-fluoroorotic acid, (E) 1 mM potassium cyanide, (F) 5 µM bongkrekic acid, (G) 10 µM thenoyltrifluoroacetone, (H) 70 µM proguanil and (I) 200 µM fusidic acid. Tryptophan was slightly accumulated after one hour of incubation in parasites treated with (I) 200 µM fusidic acid. There were no changes observed between others drugs-treated and untreated parasites. Data represent the mean ± SEM of at least duplicate independent experiments.

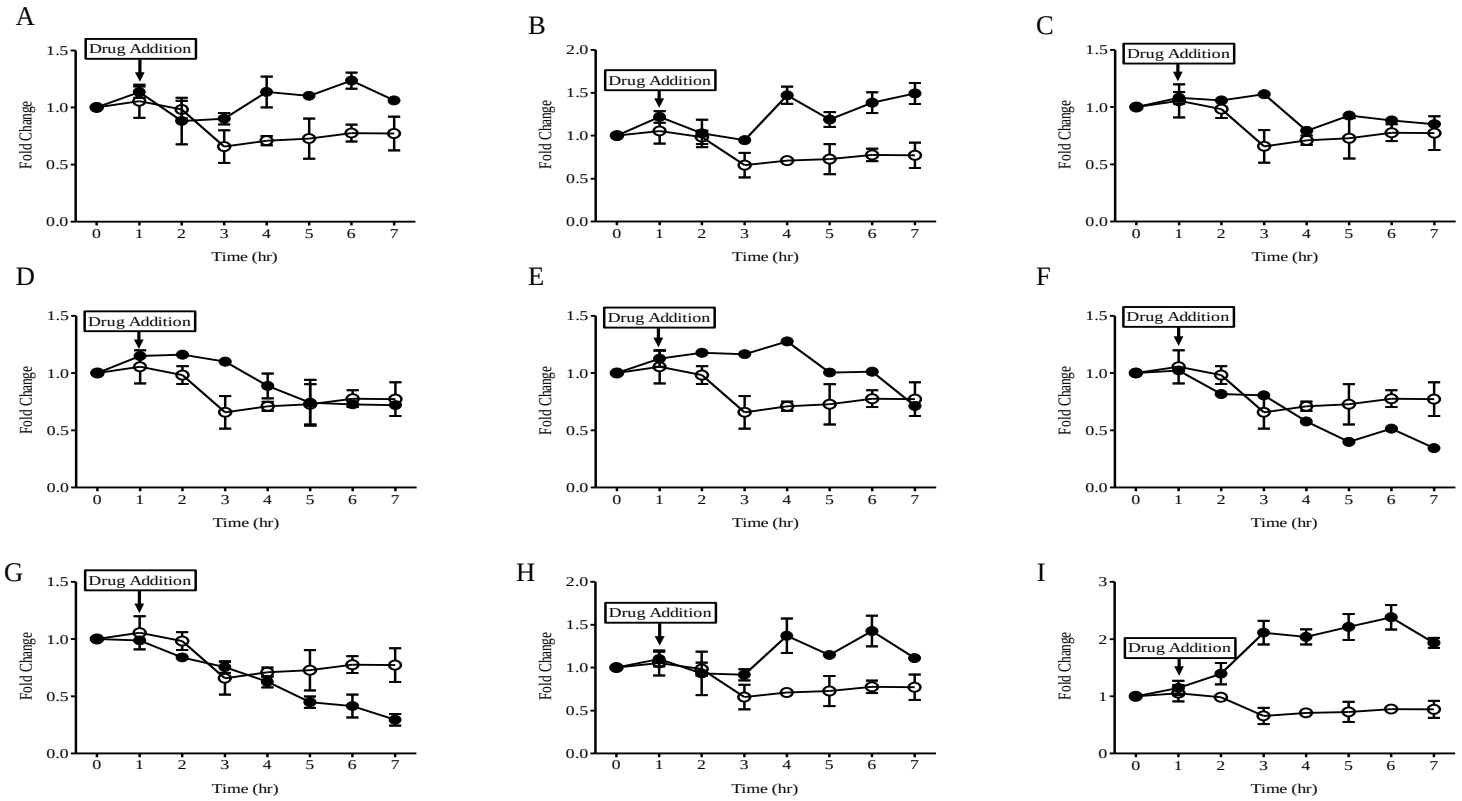

Figure 6.37: Time-dependent curves of tyrosine in drug-treated and untreated *P. falciparum* 3D7 parasites.
Tyrosine levels were determined in untreated (open circle) and drug-treated (closed circle) *P.falciparum* trophozoite-staged parasites by LC-MS/MS. The following drugs were added to the parasites after one hour of incubation (A) 2.5 nM atovaquone, (B) 2.5 nM atovaquone + 1 µM proguanil, (C) 50 nM CK-2-68, (D) 15 nM 5-fluoroorotic acid, (E) 1 mM potassium cyanide, (F) 5 µM bongkrekic acid, (G) 10 µM thenoyltrifluoroacetone, (H) 70 µM proguanil and (I) 200 µM fusidic acid. There was an evident accumulation of tyrosine after one hour of incubation in parasites treated with (I) 200 µM fusidic acid. There were no changes observed between others drugs-treated and untreated parasites. Data represent the mean ± SEM of at least duplicate independent experiments.

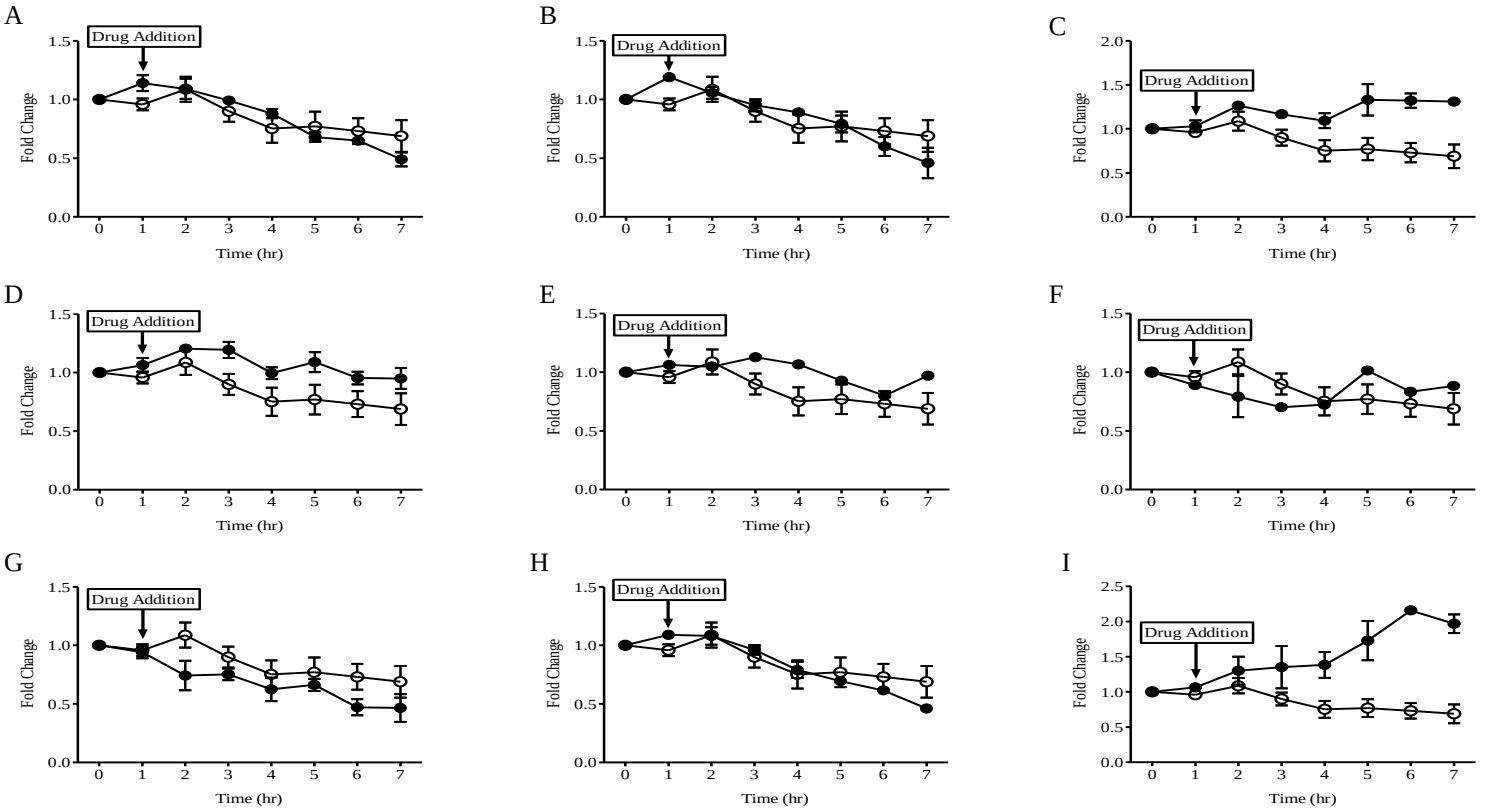

Figure 6.38: Time-dependent curves of threonine in drug-treated and untreated *P. falciparum* 3D7 parasites.
Threonine levels were determined in untreated (open circle) and drug-treated (closed circle) *P.falciparum* trophozoite-staged parasites by LC-MS/MS. The following drugs were added to the parasites after one hour of incubation (A) 2.5 nM atovaquone, (B) 2.5 nM atovaquone + 1 µM proguanil, (C) 50 nM CK-2-68, (D) 15 nM 5-fluoroorotic acid, (E) 1 mM potassium cyanide, (F) 5 µM bongkrekic acid, (G) 10 µM thenoyltrifluoroacetone, (H) 70 µM proguanil and (I) 200 µM fusidic acid. There was a notable accumulation of threonine after one hour of incubation in parasites treated with (I) 200 µM fusidic acid. There were no changes observed between others drugs-treated and untreated parasites. Data represent the mean ± SEM of at least duplicate independent experiments.

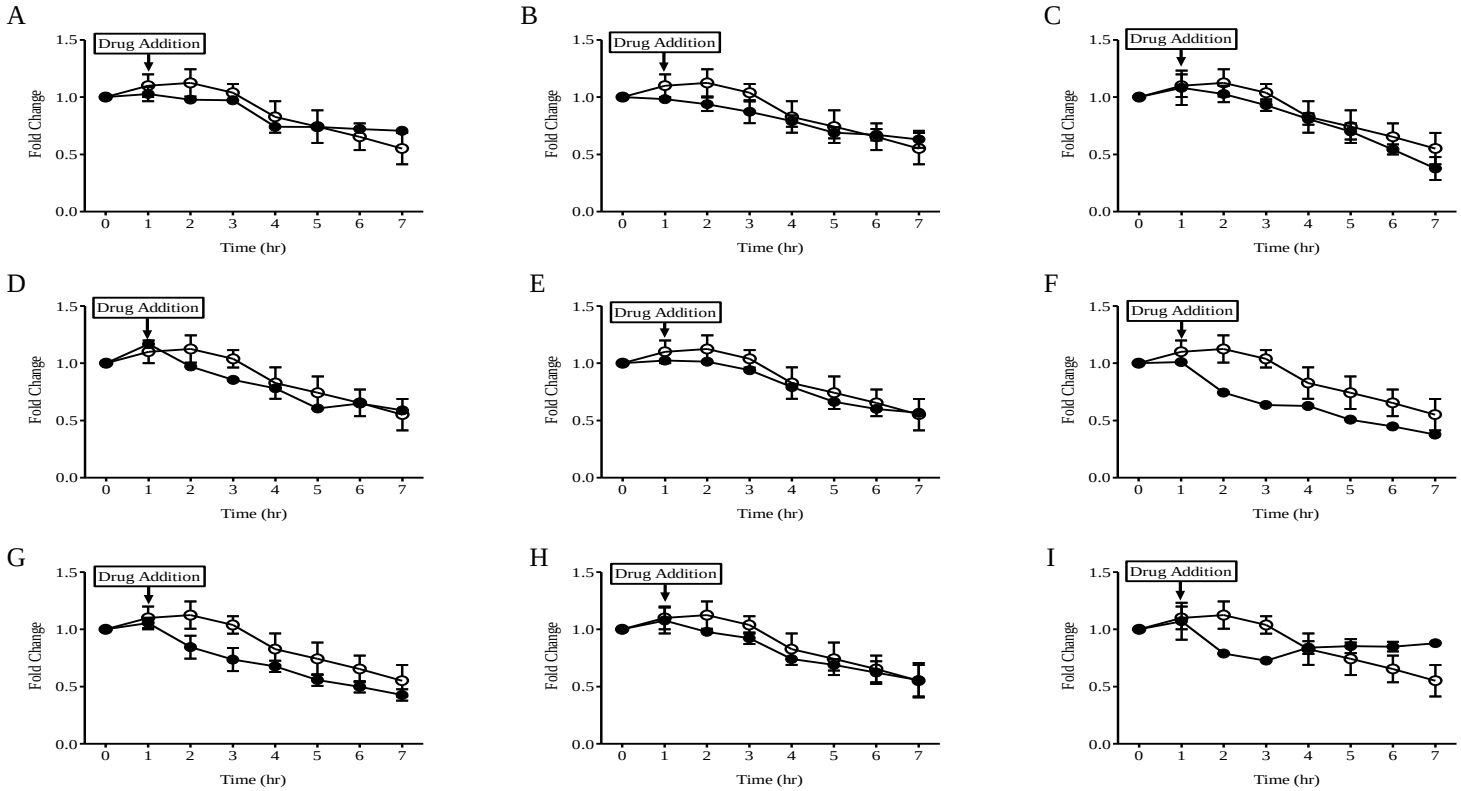

Figure 6.39: Time-dependent curves of (iso)-leucine in drug-treated and untreated *P. falciparum* 3D7 parasites.
The (iso)-leucine levels were determined in untreated (open circle) and drug-treated (closed circle) *P.falciparum* trophozoite-staged parasites by LC-MS/MS. The following drugs were added to the parasites after one hour of incubation (A) 2.5 nM atovaquone, (B) 2.5 nM atovaquone + 1 µM proguanil, (C) 50 nM CK-2-68, (D) 15 nM 5-fluoroorotic acid, (E) 1 mM potassium cyanide, (F) 5 µM bongkrekic acid, (G) 10 µM thenoyltrifluoroacetone, (H) 70 µM proguanil and (I) 200 µM fusidic acid. There were no changes observed between drugs-treated and untreated parasites. The points represent the mean ± SEM of at least duplicate independent experiments.

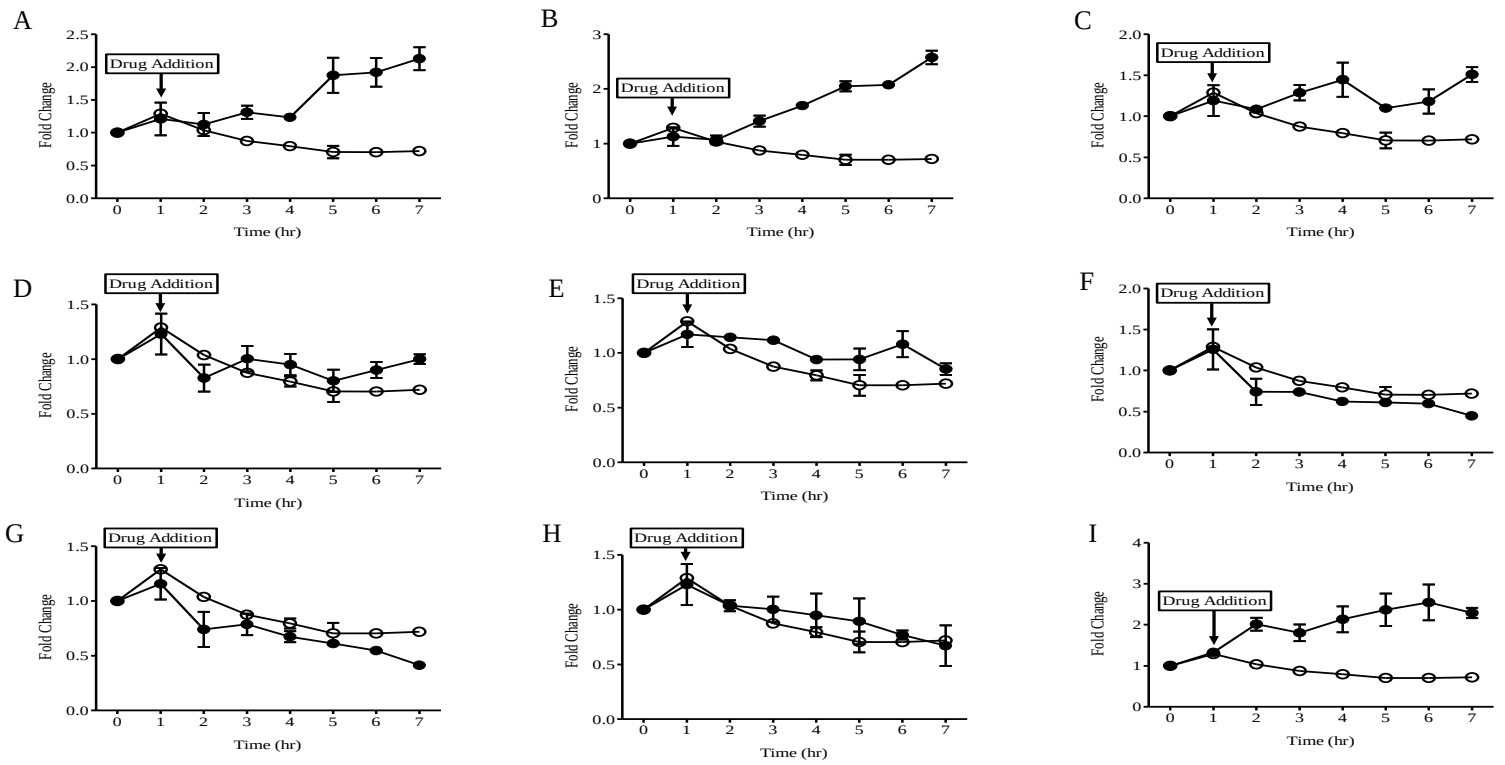

Figure 6.40: Time-dependent curves of valine in drug-treated and untreated *P. falciparum* 3D7 parasites.
Valine levels were determined in untreated (opened circle) and drug-treated (closed circle) *P.falciparum* trophozoite-staged parasites by LC-MS/MS. The following drugs were added to the parasites after one hour of incubation (A) 2.5 nM atovaquone, (B) 2.5 nM atovaquone + 1 µM proguanil, (C) 50 nM CK-2-68, (D) 15 nM 5-fluoroorotic acid, (E) 1 mM potassium cyanide, (F) 5 µM bongkrekic acid, (G) 10 µM thenoyltrifluoroacetone, (H) 70 µM proguanil and (I) 200µM fusidic acid. Data showed a distinguished accumulation of valine in parasites treated with (A) 2.5 nM atovaquone, (B) 2.5 nM atovaquone + 1 µM proguanil, (C) 50 nM CK-2-68 and (I) 200 µM fusidic acid. There were no changes observed between others drugs-treated and untreated parasites. Data represent the mean ± SEM of at least duplicate independent experiments.

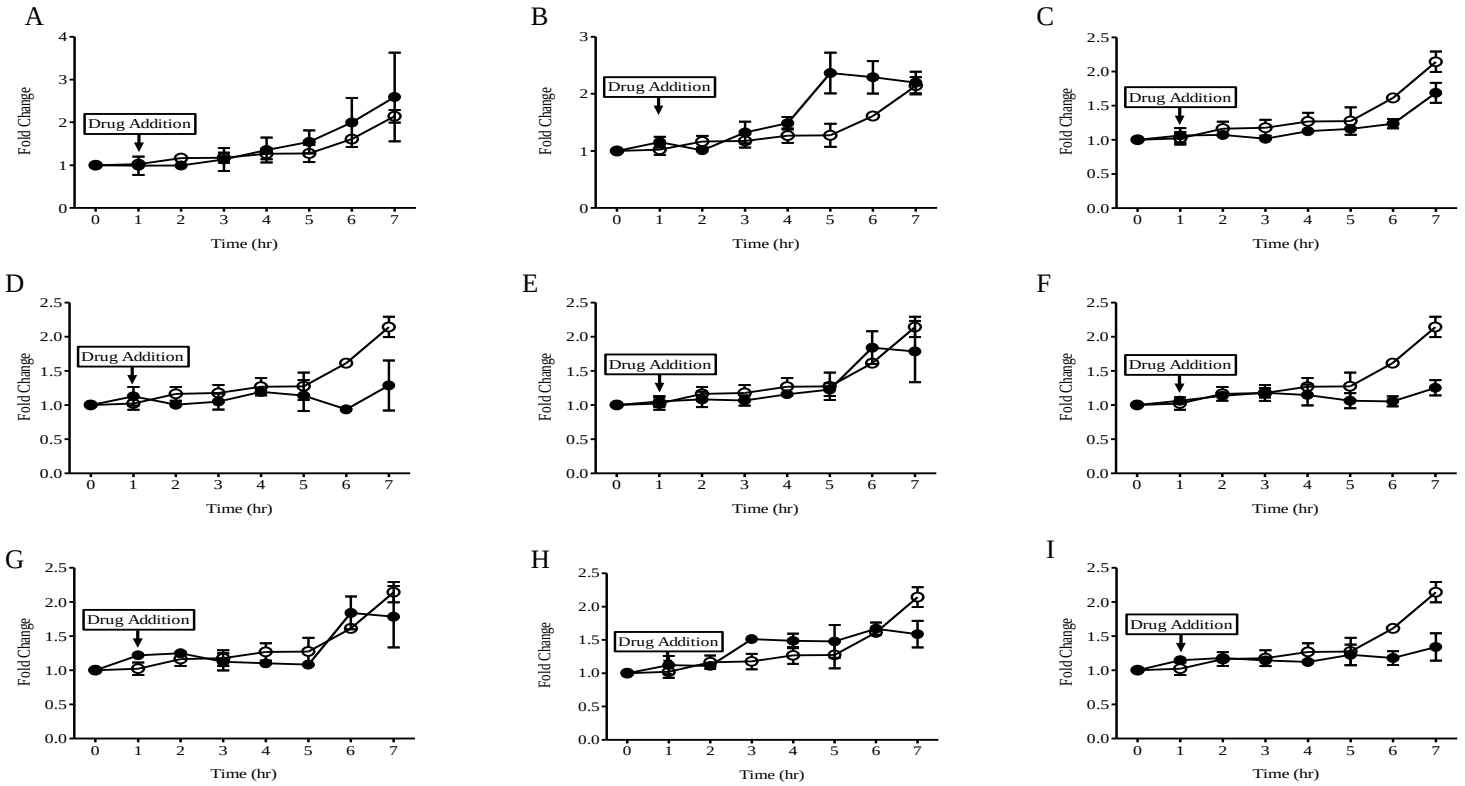

Figure 6.41: Time-dependent curves of hypoxanthine in drug-treated and untreated *P. falciparum* 3D7 parasites.
Hypoxanthine levels were determined in untreated (opened circle) and drug-treated (closed circle) *P.falciparum* trophozoite-staged parasites by LC-MS/MS. The following drugs were added to the parasites after one hour of incubation (A) 2.5 nM atovaquone, (B) 2.5 nM atovaquone + 1 µM proguanil, (C) 50 nM CK-2-68, (D) 15 nM 5-fluoroorotic acid, (E) 1 mM potassium cyanide, (F) 5 µM bongkrekic acid, (G) 10 µM thenoyltrifluoroacetone, (H) 70 µM proguanil and (I) 200µM fusidic acid. There were no changes observed between drugs-treated and untreated parasites. The points represent the mean ± SEM of at least duplicate independent experiments.

6.4. Discussion

The aims and hypotheses of this chapter were to dissect the role of mtETC components on the basis of the findings of the previous chapter (chapter 5) and to investigate whether the *P. falciparum* mitochondria can be regarded as containing multiple drug targets. It was markedly noted from the analysis of PCA and PLS-DA that the selective mitochondrial inhibitors and some antimalarial drugs used to specifically perturb *P. falciparum* mitochondria in trophozoite-stage have different MoAs.

In this regards, *P. falciparum* parasites treated with mtETC selective drugs and inhibitors including atovaquone, atovaquone-proguanil, CK-2-68, 5-flouroorotic acid, potassium cyanide, and thenoyltrifluoroacetone showed similar MoA in PCA analysis. Nevertheless, further discriminate analysis (PLS-DA) demonstrated different divergence clusters. This suggests strongly that these mtETC selective drugs and inhibitors act upon different components of *P. falciparum* mtETC. With the exception of thenoyltrifluoroacetone, *P. falciparum* parasites treated with selective inhibitors for the mtETC components including atovaquone, atovaquone-proguanil, CK-2-68, 5-fluoroorotic acid and potassium cyanide generate prominent metabolic fingerprints in the upstream pyrimidine biosynthesis pathway including carbamoyl-l-aspartate and dihydroorotate. Despite the fact that the MoA of atovaquone, atovaquone-proguanil, CK-2-28 and potassium cyanide is not directly linked to the dihydrooroate dehydrogenase (DHODH), the metabolic fingerprint findings from metabolomic experiments was in accordance with the parasite mitochondrion playing a key role in pyrimidine biosynthesis. Therefore, shutdown of the mtETC completely arrests crucial metabolic pathways within the parasite leading to parasite death. Consistent with these findings, previous studies reported that the inhibition of the mtETC in malaria parasite at cytochrome bc_1 (complex III) by atovaquone results in the accumulation of carbamoyl-l-aspartate and dihydroorotate and a reduction in UTP, CTP, and dTTP (Hammond et al., 1985, Seymour et al., 1994). Although UTP, CTP and TTP were included in the list of the targeted metabolomics analytical platform (Chapter 3); they were under the limit of detection in the parasite materials. This means there is a necessity for either an increase in adequate parasite material or a more sensitive method of detection. The reduction in orotate levels following the addition of atovaquone confirms the previous hypothesis that atovaquone has an effect on pyrimidine

intermediates (Hudson et al., 1991). Moreover, the accumulation of valine observed upon the addition of atovaquone, atovaquone-proguanil and CK-2-68 indicates that these drugs had an indirect MoA effect on the branched chain α-ketoacid dehydrogenase complex (BCKDH) that is located in the mitochondria (Gunther et al., 2005, Seeber et al., 2008, Storm and Mueller, 2012). Atovaquone is known to be a competitive inhibitor of ubiquinone binding to *Plasmodium* mitochondrial bc_1 (Fry and Pudney, 1992). Although atovaquone acts by inhibiting electron transfer in the bc_1 complex (complex III) and thereby collapsing the $\Delta\Psi_m$ (Srivastava et al., 1997, Biagini et al., 2006), its disruption of pyrimidine *de novo* biosynthesis would indicate the involvement of atovaquone (a ubiquinone (CoQ) analoge) in the reaction of DHODH. Consequently, it is conceivable that the depolarization effect of atovaquone on $\Delta\Psi_m$ results in the disturbance of vital metabolic pathway, pyrimidine biosynthesis, by the indirect inhibition of DHODH. Unsurprisingly, the effect of an atovaquone-progaunil combination on the levels of carbamyol-l-aspartate and dihydroorotate accumulation was higher than the effect produced by atovaquone alone suggesting the role of progaunil in potentiating and enhancing atovaquone's effect when they used in combination is correct. This also indicates a secondary MoA for proguanil. However, this observation was not the case when parasites treated only with proguanil. As shown in PCA and PLS-DA, the clustering of parasites treated with proguanil was entirely separated from parasites treated with atovaquone-proguanil. The biguanide proguanil by its self does not have any effect on either the $\Delta\Psi_m$ or dihydrofolate reductase (DHFR), a critical enzyme in folate pathway, but rather it becomes metabolized and converted to cycloguanil, a potent inhibitor of dihydrofolate reductase (DHFR) in folate biosynthesis (Carrington et al., 1951, Crowther and Levi, 1953, Canfield et al., 1995). Moreover, there was no clear metabolic fingerprint indication of proguanil addition although *P. falciparum* parasites were exposed to high levels of proguanil (70 µM). In contrast, exposing *P. falciparum* parasites to 1 µM proguanil in combination with sub-lethal concentration of atovaquone resulted in strong biochemical evidence of mitochondrial membrane depolarization as made evident by the two pyrimidine metabolic fingerprints discussed above. This suggests that proguanil has no direct MoA on the $\Delta\Psi_m$ but rather acts to sensitize the parasite $\Delta\Psi_m$ to depolarization by atovaquone without disturbing the mtETC (Srivastava and Vaidya, 1999). Furthermore, it was found that progunail had a small effect on *P. falciparum* parasites' oxygen consumption in polarographic assays when used alone or in combination with atovaquone or salicylhydroxamic (SHAM),

suggesting that proguanil potentiate atovaquone by indirect inhibition of the branched respiratory pathway including a cytochrome chain and an alternative terminal oxidase (Murphy et al., 1997, Murphy and Lang-Unnasch, 1999).

A 5-fluoroorotic acid, an orotate analog, has potent activity (IC_{50} in nM range) against both human and mouse malaria parasites *in vitro* and *in vivo*, respectively (Rathod et al., 1989, Queen et al., 1990, Gomez and Rathod, 1990). Malaria parasites were treated with nanomolar concentration of 5-fluoroorotic acid as a proof-of-concept for potency and if successful, to confirm biochemically the metabolic link between mitochondria and pyrimidine biosynthesis. As expected, the findings showed clearly a notable increase in carbamoyl-l-aspartate and dihydroorotate and a reduction in orotate. However, the findings of the metabolic effects of 5-fluoroorotic acid are inconsistent with the results observed by earlier studies which showed that 5-fluoroorotic acid incorporated in a significant accumulation of 5-fluoro-UMP, 5-fluoro-UDP and 5-fluoro-UTP but not of a pyrimidine intermediates suggesting that the accumulated 5-fluoro-UTP acts as a potent inhibitor on carbamoyl phosphate synthase leading to hampering the pyrimidine biosynthesis pathway at its' first step (Seymour et al., 1994, Seymour et al., 1997). Conversely, a biochemical pharmacology study performed on orotate analogs showed that 5-fluoroorotic acid was the most effective inhibitor for dihydrooroate orotase and dihydrooroate dehydrogenase leading to a 50% inhibition in *P. falciparum* growth at 10 nM (Krungkrai et al., 1992). Therefore, the results obtained for *P. falciparum* parasites treated with 5-fluoroorotic acid suggesting that this inhibitor acts upon DHODH component of the mtETC leading to the observed accumulation in the upstream pyrimidine intermediates, carbamoyl-l-aspartate and dihydroorotate, which are in keeping with the findings of Krungkrai and his colleagues (Krungkrai et al., 1992).

The results obtained for CK-2-68, a bisaryl quinolones type compound that is synthesized in-house and displayed potency in the nanomolar range against *P. falciparum* parasites (Pidathala et al., 2012), showed a parallel MoA of atovaquone and atovaquone-proguanil having its effect on the DHODH choke point (Biagini et al., 2012). It was pointed out in the literature that *Plasmodium* parasites lack the canonical proton motive NADH dehydrogenase (Complex I) but instead it harbors a bacterial-like type II NADH:ubiquinone oxidoreductase, *P. falciparum* NDH2 (Fisher et al., 2007). CK-2-68 was shown to have dual-targeting MoA (PfNDH2/bc_1) effect on *P. falciparum*

respiratory chain (Biagini et al., 2012, Pidathala et al., 2012). The development of PfNDH2/bc_1 dual-acting lead antimalarial compound (CK-2-68) was evidenced by a rapid and selective depolarization of the parasite $\Delta\Psi_m$. This leads to the disruption of pyrimidine biosynthesis, organelle dysfunction and eventually parasite death (Biagini et al., 2012). Moreover, the findings of PLS-DA clustering showed that the *P. falciparum* parasites treated with atovaquone, arovaquone-progaunil and 5-flouroorotic acid was in one cluster and that of *P. falciparum* parasites treated with CK-2-68, potassium cyanide and bongkrekic acid was in another cluster. The metabolites caused this divergence were clearly detected in the VIP score for each drug treatment and they had different profiles following the addition of each drug. These metabolites include fumarate, alanine, orotate and DHAP in addition to the major metabolic fingerprints which are carbamoyl-l-aspartate and dihydroorotate. However, it appears that fumarate is the only metabolite that had different profile in parasites treated with atovaquone, arovaquone-progaunil and 5-flouroorotic acid from those treated with CK-2-68, potassium cyanide and bongkrekic acid. This suggests that the *P. falciapurm* mitochondria houses a number of drug targets. Moreover, potassium cyanide is known to specifically and selectively inhibit cytochrome c oxidase (complex IV) (Way, 1984). It is conceivable that the detrimental effect of cyanide on the $\Delta\Psi_m$ may produce the same pyrimidine metabolic fingerprint observed with the other mtETC inhibitors. Thenoyltrifluoroacetone is known to specifically inhibit succinate dehydrogenase (complex II) (Sun et al., 2005). Thenoyltrifluoroacetone treated parasites occupied an entirely unique position from other mtETC inhibitors in the 3-D of PLS-DA suggesting the weak role of complex II in the mtETC of *P. falciparum*. However, a suppression and rescue study carried out on complex II of *P. falciparum* showed that the disruption of complex II caused growth retardation of the intra-erythrocytic forms and was rescued by addition of succinate but not fumarate suggesting that complex II in malaria parasites functions as a quinol-fumarate reductase (QFR) to produce succinate from fumarate (Tanaka et al., 2012).

Remarkably, the findings for bongkrekic acid treated parasites showed that it also had an indirect effect on DHODH resulting in a significant accumulation of carbamoyl-l-aspartate and dihydrooroate even though it targets ADP/ATP transporter in the mitochondria. Therefore, this result confirms a role for the ATP synthase complex

(complex V). However, the exact role of ATP synthase complex in parasite remains unclear although there is some evidence suggesting the essentiality of this complex to the survival of malaria parasites and that it is perhaps a valid drug target (Nina et al., 2011, Basco and Lebras, 1994). Moreover, bongkrekic acid treated parasites initially clustered with mtETC selective drugs and inhibitors in PCA and were differentiated further in PLS-DA to be clustered only with CK-2-68 and potassium cyanide treated parasites. This indicates that bongkrekic acid had a commonality in the MoA with CK-2-68 and potassium cyanide. Overall, this highlights that mitochondrial inhibition with a range of independent electron transport inhibitors results consistently in a specific and significant accumulation of two pyrimidine intermediates, carbamoyl-l-aspartate and dihydroorotate.

Fusidic acid is an antibiotic that is known to inhibit the elongation factor G (EF-G), a GTPase critical to the translocation step of protein synthesis, in the mitochondrial machinery protein synthesis. This leads to a disruption in the protein synthesis, organelle malfunction and eventually parasite death (Black et al., 1985, Johnson et al., 2011). Unexpectedly, the findings showed that upon treating the parasites with fusidic acid, there was no effect in the upstream pyrimidine intermediates indicating that $\Delta\Psi_m$ was not affected as it is observed with other mitochondrial inhibitors (e.g. atovaquone). This was clearly shown in the metabolomics analysis (PCA and PLS-DA) in that the clustering of *P. falciparum* parasite treated with fusidic acid was entirely segregated from those of mtETC inhibitors and ADP/ATP transporter inhibitors suggesting that fusidic acid had a different MoA. Nonetheless, the findings demonstrated a notable reduction in TCA intermediates including succinate, fumarate, malate, (iso)-citrate and 2-oxoglutarate when parasites were treated with fusidic acid. This suggests an indirect or secondary MoA in the intermediary fluxes of mitochondrial TCA intermediates. In addition, the MoA of fusidic acid in this study was also extended to affect a number of amino acids as it appeared in the accumulation of glutamine, ornithine, citrulline, phenylalanine, tryptophan, tyrosine, threonine and valine. Fusidic acid acted indirectly to hamper the degradation of serine, asparagine, methionine and lysine showing notable invariable changes compared to untreated control. Several lines of evidence pointed out that exposing malaria parasite to known mitochondrial protein synthesis inhibitors (e.g. tetracycline and chloramphenicol) results in a reduction of amino acids incorporation into protein synthesis (Geary and Jensen, 1983, Blum et al., 1984, Ginsburg et al.,

1986). It is likely that the effect of fusidic acid on a number of amino acids up-take, including glutamine, serine, asparagine, lysine, phenylalanine, tryptophan, tyrosine, threonine, and valine, was caused by a direct disruption in the mitochondrial protein synthetic machinery resulting in the inhibition of EF-G. Specifically, fusidic acid binds to EF-G on the ribosome and prevents the EF-G:GDP complex from leaving the ribosome leading it to obstruct the amino acid translocation to the growing polypeptide chain and effectively stalling protein synthesis by steric inhibition (Besier et al., 2003). The results obtained in this chapter for fusidic acid are in agreement with the view that it acts by inhibiting protein synthesis as reported in an early study which demonstrated that the incorporation of tyrosine, lysine, phenylalanine and alanine into protein was inhibited upon fusidic acid addition in cell-free systems from *Escherichia coli* (Vazquez, 1966). Furthermore, the result obtained for (iso)-leucine showed that after three hours of fusidic acid exposure, the parasite's up-take level was altered from decrease to a steady state suggesting that fusidic acid is active against late trophozoite and possibly schizont parasite stages. This finding is consistent with the results obtained by (Blum et al., 1984) showing that exposing the ring-staged of *P. falciparum* parasite to chloramphenicol (mitochondrial protein synthesis inhibitor) resulted in the inhibition of [^{3}H] iso-leucine incorporation into protein after 21 h indicating that chloramphenicol is a stage-specific inhibitor. On the other hand, the effect seen on alanine, glutamate, ornithine, citrulline was possibly an indirect MoA effect of fusidic acid resulting from the perturbation of the mitochondrial metabolism (e.g. alanine as an end-product from glysolysis pathway). Overall, there is clear pharmacometabolomics evidence that the *P. falciaprum* mitochondria carries out protein synthesis although the *P. falciaprum* mitochondria genome only encodes a fragmented rRNA molecules. Therefore, it appears that mitochondria import all proteins and tRNAs needed for translation of mitochondrial-encoded transcripts, and it is unclear if its fragmented rRNA is functional (Jackson et al., 2011). This view is supported by the MoA of fusidic acid showing that the large effect occurred towards the end points of the time course indicating that the synthesis of the parasite's mitochondrial protein machinery is active in the transition stage between trophozoite and schizont.

Interestingly, it was noted in the metabolomic experiments carried out in this chapter that glucose was dramatically utilized in drug-treated *P. falciparum* parasites leading to a notable elevation in as phosphoenol pyruvate (PEP) and lactate as compared to the

untreated. This could be explained as the effect of drug pressure on the perturbation of the *P. falciparum* parasites metabolic system biology. However, the effect on the rate of glucose utilization and lactate production depends on the MoA of the drug. For instance, *P. falciparum* parasites treated with atovaquone alone was demonstrated to take up glucose and produce lactate at a relatively lower rate than that of the parasites treated with atovaquone-proguanil and/or CK-2-68. Overall, the finding that *P. falciparum* parasites are voracious glucose consumers is consistent with the earlier studies and investigations of *Plasmodium* biochemistry wherein glucose was demonstrated to be an essential nutrient for survival, growth and reproduction (Bass and Johns, 1912, Hegner and MacDougall, 1926, Johns, 1931). In addition, (Sherman, 1979) noted that biochemical experiments carried out on a variety of malaria species to investigate the glucose utilization revealed lactate as a major end product of glucose catabolism together with a variety of other organic acids such as pyruvate, acetate, formate, succinate, aspartate, glutamate, alanine and CO_2. However, metabolites like pyruvate, acetate and formate could not be detected in the metabolomics analytical platform of this thesis due to the fact that they were not properly eluted and poorly ionized by LC-MS/MS. Nonetheless, lactate, succinate, aspartate, glutamate and alanine were detected using this metabolomics analytical platform and showed an increase trend over time in untreated *P. falciparum* parasites. These findings are parallel to the early reported studies on different species of malaria parasites (Bowman et al., 1960, Bowman et al., 1961, Bryant et al., 1964, Nagaraja.K, 1968). Overall, it was clearly shown that *P. falciparum* displayed different glucose metabolism phenotypes when exposing to antimalarial drugs and inhibitors.

To conclude, for a number of ETC components, their inhibitions results in a convergence in terms of the cellular response leading to parasite death. However, for other ETC components there appears to be a distinct cellular response suggesting multiple roles for the mitochondrion in the cell. With regards to the limitation of this chapter, the analytical limitation is similar to what has been discussed previously (chapter 4, section 4.4). This includes the under limit of detection of bioenergetics/redox couples, UMP, UDP, UTP, TTP, CTP, and GTP in the parasite samples. With regards to future experiments, it can be generally stated that *P. falciparum* mitochondria is a valid drug target (e.g. Malarone™) and according to the findings of this chapter it is still considered susceptible target for many drugs that act specifically on different

mitochondrial targets (e.g. transporters, protein synthesis machinery and mtETC components). Therefore, it could be suggested that future experiments could be carried out in the same means using specific drugs and inhibitors. For example, using antibiotics such as chloramphenicol and cycloheximide will enhance the current understanding of mitochondrial machinery protein synthesis. In addition, atractyloside, specific mitochondrial ADP/ATP transporter inhibitor, can be used to further confirm the existence of oxidative phosphorylation in *P. falciparum* mitochondria.

CHAPTER 7

Pharmacometabolomics Study of Inhibitors Targeting the Digestive Vacuole of *Plasmodium falciparum*

7.1. Introduction

The aim of this chapter was to investigate the *P. falciparum* cellular metabolite response following sub-lethal exposure to digestive vacuole-targeting quinoline-containing antimalarial drugs (QCDs); chloroquine, amodiaquine, piperaquine, quinine and mefloquine. The analytical approach for this work has been described previously in Chapter 3.

As mentioned previously in the general introduction (Chapter 1), there are three sources available to the parasite in which it can acquires the amino acids necessary to carry out various metabolic functions. These include; (i) biosynthesis of amino acid from carbon sources, (ii) uptake of preformed free amino acids and (iii) proteolysis of haemoglobin with the release of amino acids. The trophozoite stage of *P. falciparum* ingests and degrades the host RBC haemoglobin in the digestive vacuole (Tilley et al., 2011). The *Plasmodium* parasite has a limited capacity for the de novo synthesis of amino acid (Sherman, 1979). Therefore, it appears that haemoglobin digestion is essential for the survival of the parasite. Haemoglobin degradation is capable of providing all essential amino acids with the exception of (iso)-leucine, which is absent in human haemoglobin, and a limited supply of cysteine, methionine, glutamate and glutamine (Francis et al., 1997, Divo et al., 1985a). In addition, The *Plasmodiun* digestive vacuole is a complex organelle that is evolutionally well adapted to haemoglobin metabolism. The digestive vacuole of *Plasmodium* is believed to be the site of haemoglobin degradation, detoxification of oxygen radicals, acidification, generation of free iron and drugs accumulation (Olliaro and Goldberg, 1995). The process of haemoglobin degradation releases globin and heme (Francis et al., 1997). Haemoglobin degradation in malaria parasite appears to be an ordered process (Goldberg et al., 1990). This degradation process is preceded by endocytosis of the host haemoglobin which is then transported to an acidic digestive vacuole where a concerted action of groups of aspartic and cysteine protease enzymes and a metalloprotease break down haemoglobin initially into large peptide and later into small peptides (Bray et al., 2005). Consequently, the small peptide is then transported to the parasite cytosol where it is hydrolysed by aminopeptidase to derive amino acids that are incorporated into protein synthesis (Kolakovich et al., 1997, Rosenthal, 1998). Moreover, heme (reactive free toxic substance to the parasite) crystallization into hemozoin (an inert crystalline substance) is a parasite-specific

process that enables the detoxification of heme following its generation upon haemoglobin digestion in the digestive vacuole (Olliaro and Goldberg, 1995, Francis et al., 1997, Egan et al., 2002, Fitch et al., 1982). This crystallization process represents both an essential and a unique pharmacological drug target in malaria parasite (Kurosawa et al., 2000).

The MoA of QCD is still not properly understood, with several knowledge gaps pertaining to the exact pharmacodynamics mechanisms leading to parasite death (Ginsburg and Krugliak, 1992). Nonetheless, it has generally been supposed that QCD interfere with haemoglobin digestion (Foley and Tilley, 1998) by preventing the process of heme sequestration into a non-toxic hemozoin (Muller and Hyde, 2010, Fitch, 2004). However, QCDs can be classified on the basis of the drug chemical structure leading perhaps to distinct MoA for each drug class. In other word, QCDs class comprise most of the common antimalarial drugs that include (1) type-1 drugs 4-aminoquinolines including chloroquine, amodiaquine and piperaquine; and (2) type-2 drugs aryl-amino alcohols including quinine, mefloquine, quinidine and halofantrine (O'Neill et al., 2012, Olliaro, 2001). The two groups differ in that type-1 drugs are weak bases, deprotonated and hydrophilic at neutral pH whereas type-2 drugs are weaker bases and lipid soluble at neutral pH (Olliaro, 2001).

Chloroquine and other QCDs such as amodiaquine, piperaquine, quinine and mefloquine have been mainstays of malaria chemotherapy for decades (Biagini et al., 2003). Chloroquine is the most widely studied aminoquinoline however its MoA is still a matter of some controversy. The proposed MoAs of chloroquine include the effects on parasite DNA and RNA synthesis (Meshnick, 1990, Cohen and Yielding, 1965), the inhibition of digestive vacuole lysosomal phospholipases (Ginsburg and Geary, 1987), the inhibition of digestive vacuole proteases (Vancer Jagt et al., 1986), the inhibition of protein synthesis (Surolia and Padmanaban, 1991) and the inhibition of hemozoin formation by blocking heme polymerase enzyme leading to the accumulation of toxic heme which is lethal to the parasite (Slater and Cerami, 1992). However, the latter seems to be the most widely accepted hypothesis not only for chloroquine but also for other members of quinoline-containing antimalarial drugs. Although QCD members are thought to act in a similar way to chloroquine in that they all bind to heme (Foley and Tilley, 1998, Sullivan, 2002, Mungthin et al., 1998), their effects on the feeding process

appears to be subtly different. For instance, 4-aminoquinoline drugs, including chloroquine, amodiaquine and piperaquine, cause an accumulation of undigested haemoglobin in the parasite (Yayon et al., 1984b) whereas aryl-amino alcohol drugs, including quinine and mefloquine do not (Famin and Ginsburg, 2002). Therefore, it has been proposed that 4-aminoquinoline drugs inhibit the digestion of the haemoglobin whereas aryl-amino alcohol drugs inhibit the ingestion of the host cell haemoglobin perhaps by interfering with the endocytosis process (Bray et al., 2005).

Given the described debate surrounding the MoA of QCDs, in this chapter, a pharmacometabolomic approach has been used to determine whether parasite exposure to sub-lethal concentrations of the described set of antimalarials results in a convergent or divergent metabolite fingerprint. The results are then discussed in the context of the various hypotheses supporting the MoA of the drugs.

7.2. Materials and Methods

7.2.1. High-Gradient Magnetic separation (HGMS) for trophozoite-stage parasites enrichment

The parasite cultures followed by high gradient magnetic separation (HGMS) were conducted for trophozoite-stage *P. flaciparum* parasites as described previously (chapter 4, section 4.2.1).

7.2.2. Haemocytometer for parasite counting

Haemocytometer counting for the purified *P. falciparum* trophozoite-stage parasites was carried out as described previously (chapter 4, section 4.2.2).

7.2.3. Parasite cells metabolism quenching and metabolites extraction

Briefly at this stage, the purified trophozoite-stage parasites (section 7.2.1) were subjected to a metabolomics experiment wherewith they were incubated in culture media at 37 °C and subsequently exposed to a drug pressure. Thereafter, the parasites were removed and metabolically quenched in a time related manner. The metabolites were then extracted to be ready for the next stage of LC-MS/MS analysis (section 7.2.4). This metabolomics experiment was conducted as described earlier (chapter 4 section 4.2.3) with the exception of drugs addition in the study of this chapter. The IC_{90} concentrations of chloroquine (50 nM), amodiaquine (50 nM), piperaquine (80 nM), quinine (100 nM) and mefloquine (50 nM) were added at 1 h time point for each set of the experiments (*n*= at least two independent replicates for each drug used). Untreated parasite controls were prepared in at least two independent biological experiments. The parasite metabolites sampling, quenching, extraction, drying and storing were performed as described beforehand (chapter 4, section 4.2.3)

7.2.3.1. Solvents and Drugs Preparation

All the solvents used to carry out the LC-MS/MS metabolomics experiments were HPLC grade as described in Chapter 2 unless otherwise stated. The solvents used for drug preparation were of different depending on the solubility of the perspective drug. A 10 mM stocks were prepared for the drugs listed in (Table 7.1) , labeled and stored at

-20 ºC for no longer than a month. Final dilutions were performed with RPMI-1640 culture media and freshly made prior to commencing metabolomics experiment studies.

Table 7.1: Drugs used and their IC_{90} values.

Drugs	MW (g/mol)	IC_{90} 3D7 *P. falciparum* (nM)*	Solvent	Source
CQ	319.872	50	H_2O	Sigma Aldrich
AQ	355.861	50	DMSO	Sigma Aldrich
PPQ	535.51	80	DMSO	Sigma Aldrich
QN	324.417	100	DMSO	Sigma Aldrich
MQ	378.312	50	DMSO	Sigma Aldrich

Abbreviations: CQ, Chloroquine; AQ, Amodiaquine; PPQ, Piperaquine; QN, Quinine; MQ, Mefloquine; MW, Molecular Weight. *IC_{90} values were obtained from in-house laboratory data.

7.2.4. LC-MS/MS instrumentation

Samples preparation including parasite samples, external standards, authentic QCs sample, and blanks were carried out in this section aimed at LC-MS/MS. In addition, chromatographic conditions and mass spectrometry configurations were set up ready for the samples processing.

7.2.4.1. Samples preparation

The parasite sample preparation was carried out described previously (chapter 4, section 4.2.4.1). The preparation of external standards authentic QCs sample and blank were freshly carried out for each metabolomics experiment as described previously (chapter 3, section 3.2.3.1).

7.2.4.2. Chromatographic separation

Chromatographic separation was conducted as described earlier (chapter 3, section 3.2.2.4).

7.2.4.3. Mass spectrometry configuration

The configuration of mass spectrometry was set up for positive and negative modes as described previously (chapter 3, section 3.2.2.3).

7.2.5. Data treatment and analysis

Metabolomics data of the biological replicates from all drugs treated parasites and untreated controls were analyzed as described previously (chapter 4 section 4.2.5).

7.3. Results

7.3.1. Metobolomics analysis of *P. falciparum* parasites

Multivariate statistical analysis using principal component analysis (PCA) and partial least squares-discriminant analysis (PLS-DA) was performed on the log_2 transformed dataset (http://www.metaboanalyst.ca) generated by LC-MS/MS and normalized at time zero.

7.3.1.1. PCA and PLS-DA

The 2-D score plot from PCA revealed distinct divergence between *P. falciparum* parasites treated with quinoline-containing antimalarial drugs (QCDs) including amodiaquine, chloroquine, mefloquine, piperaquine and quinine; and untreated parasites controls (Figure 7.1 A). This indicates the commonality in the MoAs of QCDs resulted in clustering in on direction of the 2-D PCA plot. In addition, the 3-D score plot from PCA showed a better representation and positioning of the points in which it demonstaes the presence of three separated clusters (Figure 7.1 B). These include (1) the clustering of *P. falciparum* parasites treated with chloroquine, (2) the clustering of *P. falciparum* parasites treated with amodiaquine, piperaquine, quinine and mefloquine, and (3) the clustering of untreated *P. falciparum* parasites controls (Figure 7.1 B).

Therefore, further discriminate analysis was carried out to examine the differences between QCD members. The findings showed that 2-D and 3-D score plot from PLS-DA revealed five distinctive separation clusters (Figure 7.2 A and B). These include (1) the clustering of *P. falciparum* parasites treated with amodiaquine, (2) the clustering of *P. falciparum* parasites treated with chloroquine, (3) the clustering of *P. falciparum* parasites treated with piperaquine and mefloquine, (4) the clustering of *P. falciparum* parasites treated with quinine and (5) the clustering of untreated *P. falciparum* parasites controls (Figure 7.2 A and B). In addition, it appears from the 3-D PLS-DA plot that the time course points of parasites treated with chloroquine and amodaiquine were clustered towards one direction side whereas that of treated with quinine was clustered in another direction (Figure 7.2 B). This suggests that the MoA of QCDs are different and it might be drug class-related.

The corresponding loading plots for PCA and PLSDA were not very informative to indicate the major metabolic fingerprints accounted for the aforementioned differences in the clustering among different members of QCD treated parasites alongside the untreated parasites control (Figure 7.1 and 7.2, C). However, Variable Influence on Projection (VIP) score was used in metabolomics analysis to further enhance the major metabolites differences among different members of QCD treatments and untreated control. VIP score was calculated based on the variability explained in PLS-DA. Metabolites with VIP score > 1 were considered the most important metabolites responsible for the differentiation of the parasites exposed to different members of quinoline-containing antimalarial drug. VIP score showed that the most significant metabolites with score > 1 were alanine, asparagine, glutamine, lysine, orotate, DHAP and citrulline (Figure 7.3). In addition, succinate, G-3-P and phenyalanine had a borderline VIP score close to 1 (Figure 7.3). However, alanine, asparagine and glutamine were the merely metabolites with VIP score exceeding 2 whilst lysine, orotate, DHAP and citrulline had just borderline VIP score < 1.5 (Figure 7.3). This suggests that alanine, asparagine and glutamine were the prominent metabolic fingerprints.

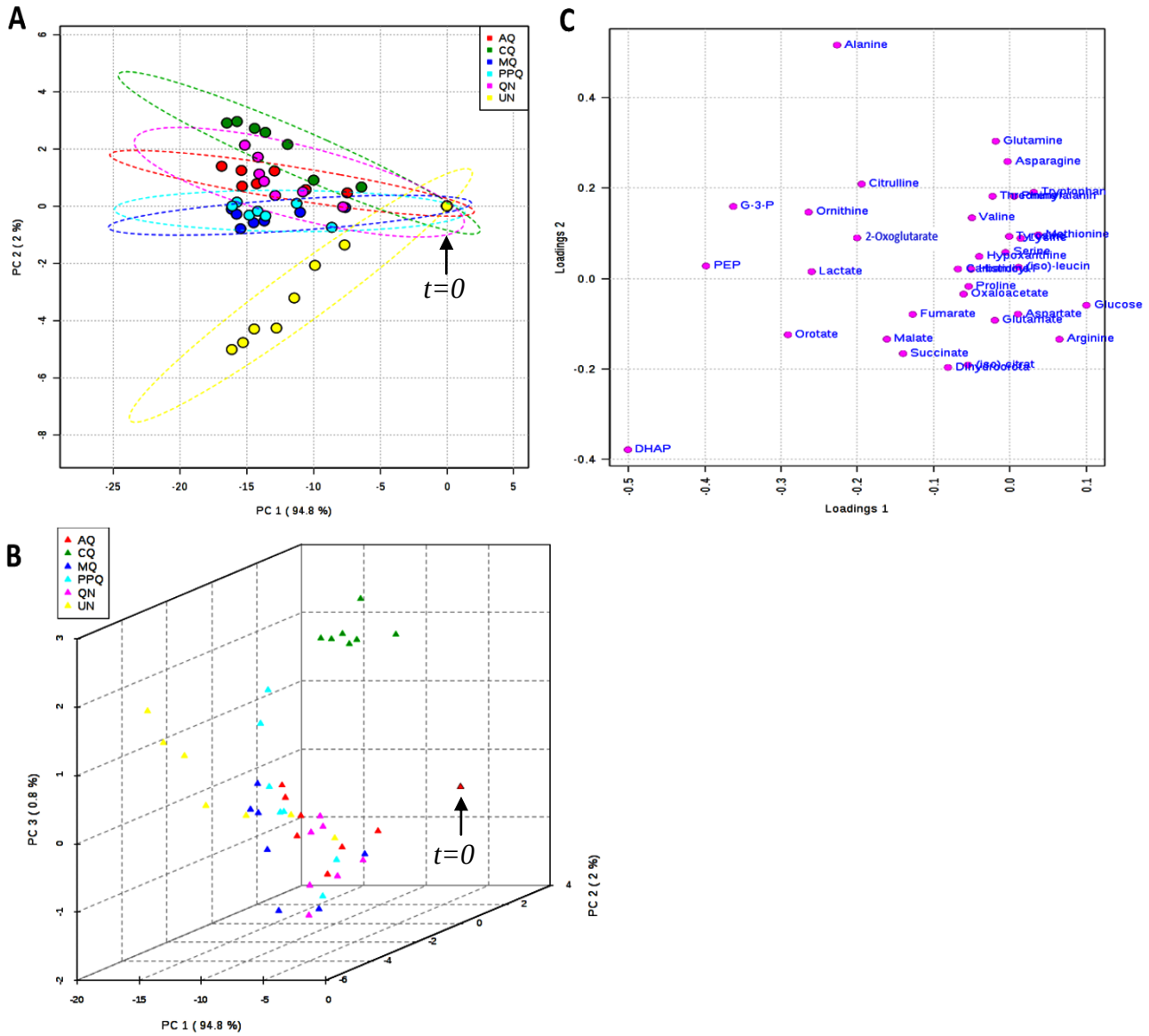

Figure 7.1: PCA score and loading plots for *P. falciparum* 3D7 upon exposure to quinoline-containing antimalarial drugs (QCDs).

A) 2-D score plot shows divergence of two main clusters. One cluster includes the clustering of *P. falciparum* treated with QCDs including amodiaquine acid (AQ, red circle), chloroquine (CQ, green circle), mefloquine (MQ, blue circle), piperaquine (PPQ, turquoise circle), quinine (QN, pink circle). The other cluster includes the clustering of untreated *P. falciparum* control (UN, yellow circle). Line boundary for each group represents a 95% confidence limit from each treatment centre. B) 3-D score plot shows the divergence of three main clusters. One cluster includes the clustering of *P. falciparum* treated with chloroquine (CQ, green triangle). Second cluster includes the clustering of untreated *P. falciaprum* control (UN, yellow triangle). Third cluster includes the clustering of *P. falciparum* treated with mefloquine (MQ, blue triangle), piperaquine (PPQ, turquoise triangle) and quinine (QN, pink triangle). C) *P. falciparum* metabolites loading plot discriminate between various time points for the corresponding score plots (panel A and B) but it was not informative. Black arrow indicates the time zero (*t*=0) for untreated control and other drugs treatment that are all confined in the same position of 2-D and 3-D score plots.

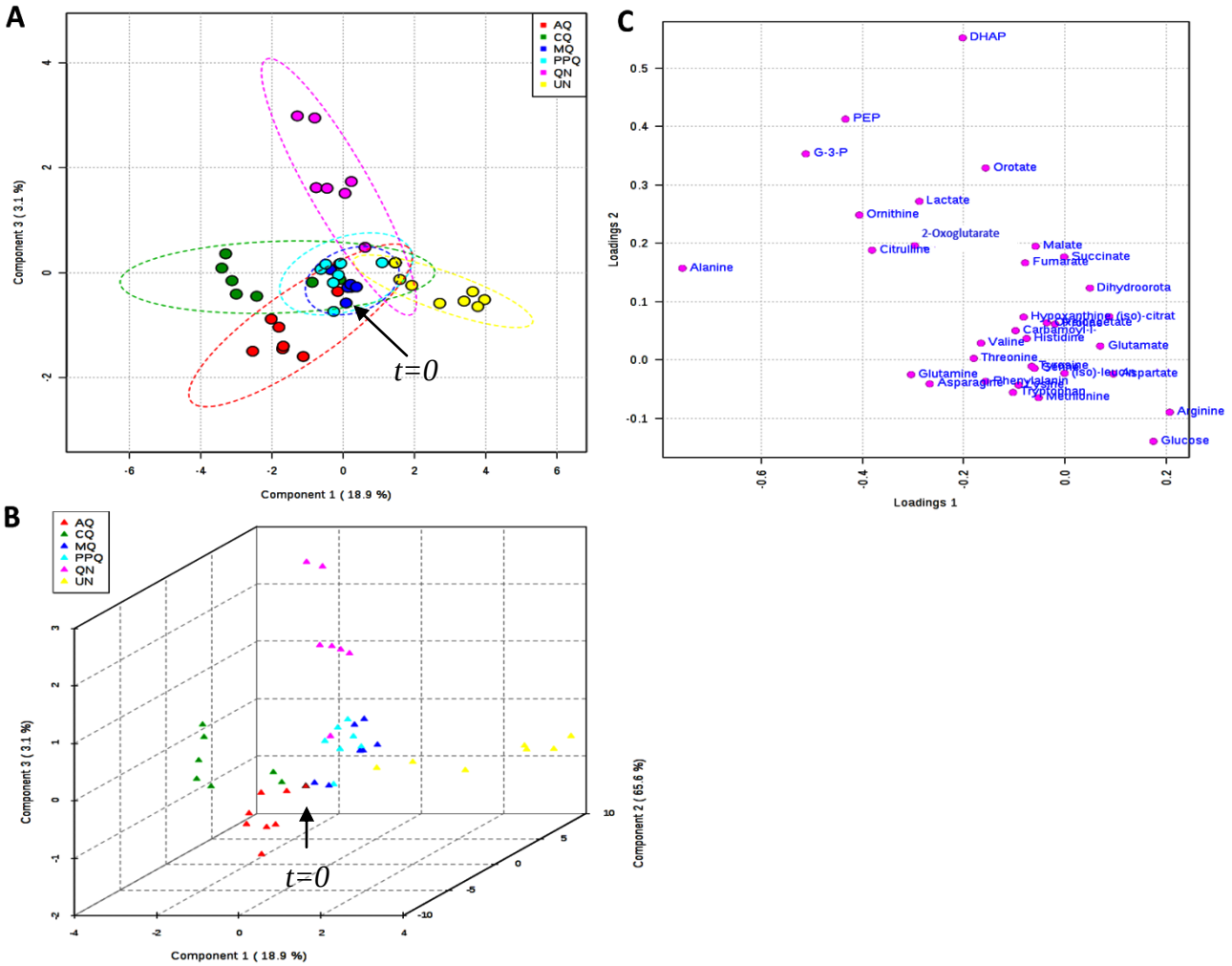

Figure 7.2: PLS-DA score and loading plots for *Plasmodium falciparum* 3D7 upon exposure to quinoline-containing antimalarial drugs (QCDs).

A) 2-D score plot shows divergence of five main clusters. First cluster includes the clustering of *P. falciparum* treated with amodiaquine (AQ, red circle). Second cluster includes the clustering of *P. falciparum* treated with chloroquine (CQ, green circle). Third cluster includes the clustering of *P. falciparum* treated with quinine (QN, pink circle). Fourth cluster includes the clustering of *P. falciparum* treated with mefloquine (MQ, blue circle) and piperaquine (PPQ, turquoise circle). Fifth cluster includes the clustering of untreated *P.falciparum* control (UN, yellow circle). Line boundary for each group represents a 95% confidence limit from each treatment centre. B) 3-D score plot shows the divergence and discrimination of five main clusters. First cluster includes the clustering of *P. falciparum* treated with amodiaquine (AQ, red triangle). Second cluster includes the clustering of *P. falciparum* treated with chloroquine (CQ, green triangle). Third cluster includes the clustering of *P. falciparum* treated with quinine (QN, pink triangle). Fourth cluster includes the clustering of *P. falciparum* treated with mefloquine (MQ, blue triangle) and piperaquine (PPQ, turquoise triangle). Fifth cluster includes the clustering of untreated *P. falciparum* control (UN, yellow triangle). C) *P. falciparum* metabolites loading plot discriminate between various time points for the corresponding score plots (panel A and B) but it was not informative. Black arrow indicates the time zero (*t*=0) for untreated control and other drugs treatment that are all confined in the same position of 2-D and 3-D score plots.

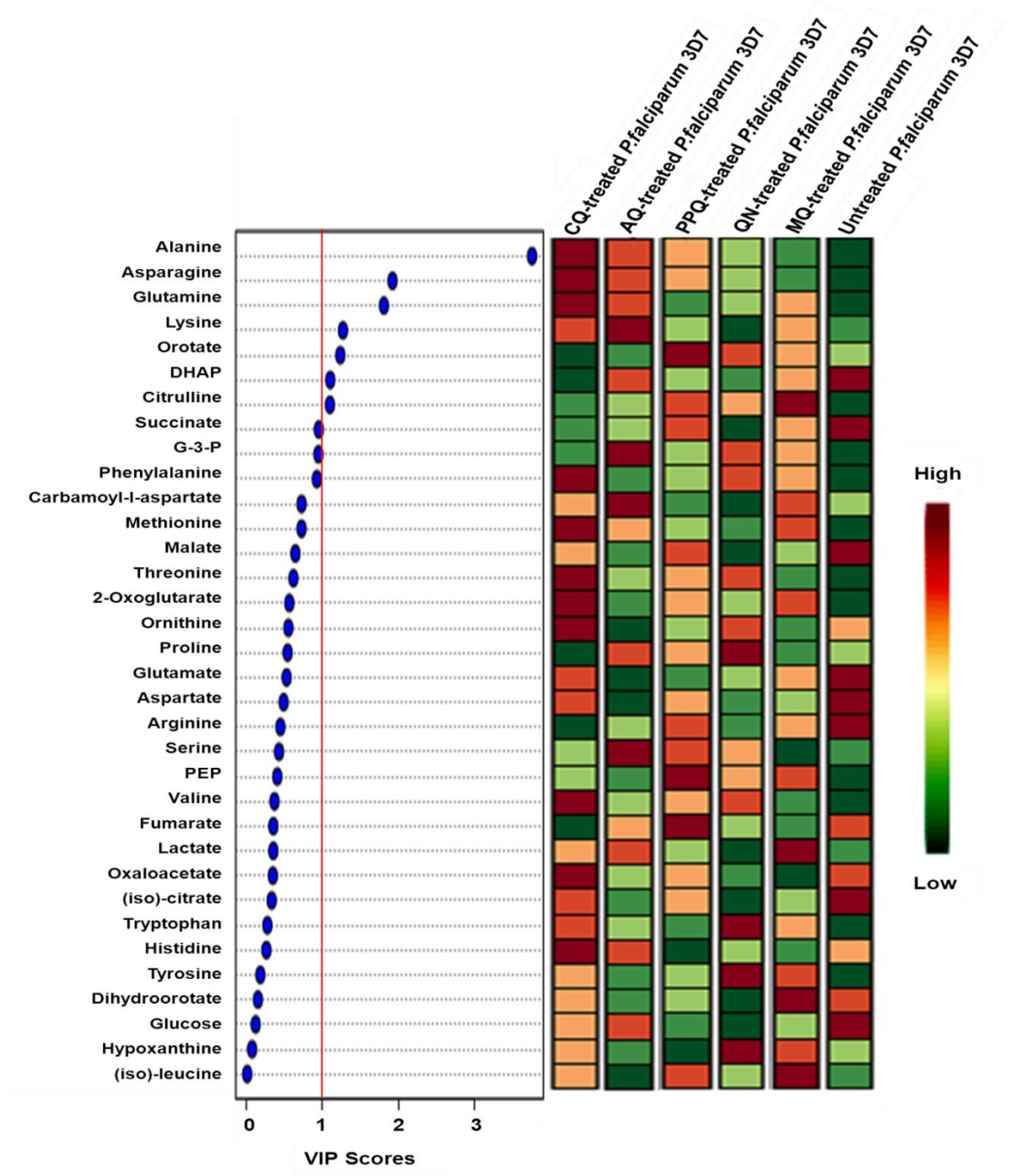

Figure 7.3 Variable Influence on Projection (VIP) score plot for *P. falciparum* 3D7 upon exposure to quinoline-containing antimalarial drugs (QCDs).

Metabolite with VIP score > 1 was considered the most important metabolite responsible for the differentiation among the different members of QCDs used to treat *P. falciparum* parasites. The coloured boxes on the right indicate the relative ratios of the corresponding metabolite in each group under study. Colour scale shows the colours gradient for the VIP score with dark red and dark green being the colours for high and low changed metabolites, respectively. VIP score plot shows that the most important metabolites responsible for differentiation were alanine, asparagine, glutamine, lysine, orotate, DHAP and citrulline.

7.3.1.2. Heat map for *P. falciparum* metabolome profiling

The heat map demonstrated visually the relative difference of the dynamic changes of the *P. falciparum* metabolome upon exposure to different members of QCD including chloroquine, amodiaquine, piperaquine, quinine and mefloquine (Figure 7.4). The metabolomic profiles presented by the heat map showed no major differences between the members of QCD treated parasites and untreated in the glycolysis intermediates (Figure 7.4). However, TCA intermediates showed variable profiles upon the addition of chloroquine, amodiaquine, piperaquine, quinine and mefloquine particularly in (iso)-citrate profile as compared to the untreated parasites (Figure 7.4). In addition, the metabolic profile of pyrimidine intermediates were variable as well following the addition of chloroquine, amodiaquine, piperaquine, quinine and mefloquine particularly in dihydroorotate profile as compared to the untreated parasites (Figure 7.4). Purine intermediate, hypoxanthine, showed no evident changes upon the addition of QCD members to the parasites as compared to untreated (Figure 7.4). Moreover, the metabolic profile observed for amino acids following the addition of chloroquine, amodiaquine, piperaquine, quinine and mefloquine is of particular interest (Figure 7.4). It appears that the changes observed for amino acids metabolic profile is dependent upon the class of drug used. For instance, *P. falciparum* parasite treated with chloroquine showed prominent increasing trends in a number of amino acids as compared to other drugs and untreated as well. These amino acids include valine, ornithine, citrulline, alanine, threonine, asparagine, glutamine, methionine, lysine, phenylalanine, tryptophan and tyrosine (Figure 7.4).

Moreover, the heat map presented in (Figure 7.4) summarized the relative fold changes ratio in *P. falciparum* following the addition of different members of QCD including chloroquine, amodiaquine, piperaquine, quinine and mefloquine. Major and evident metabolite changes were highlighted in the aforementioned paragraphs. However, detailed and specific explanation was presented as time-dependent graphs in the next section (7.3.2).

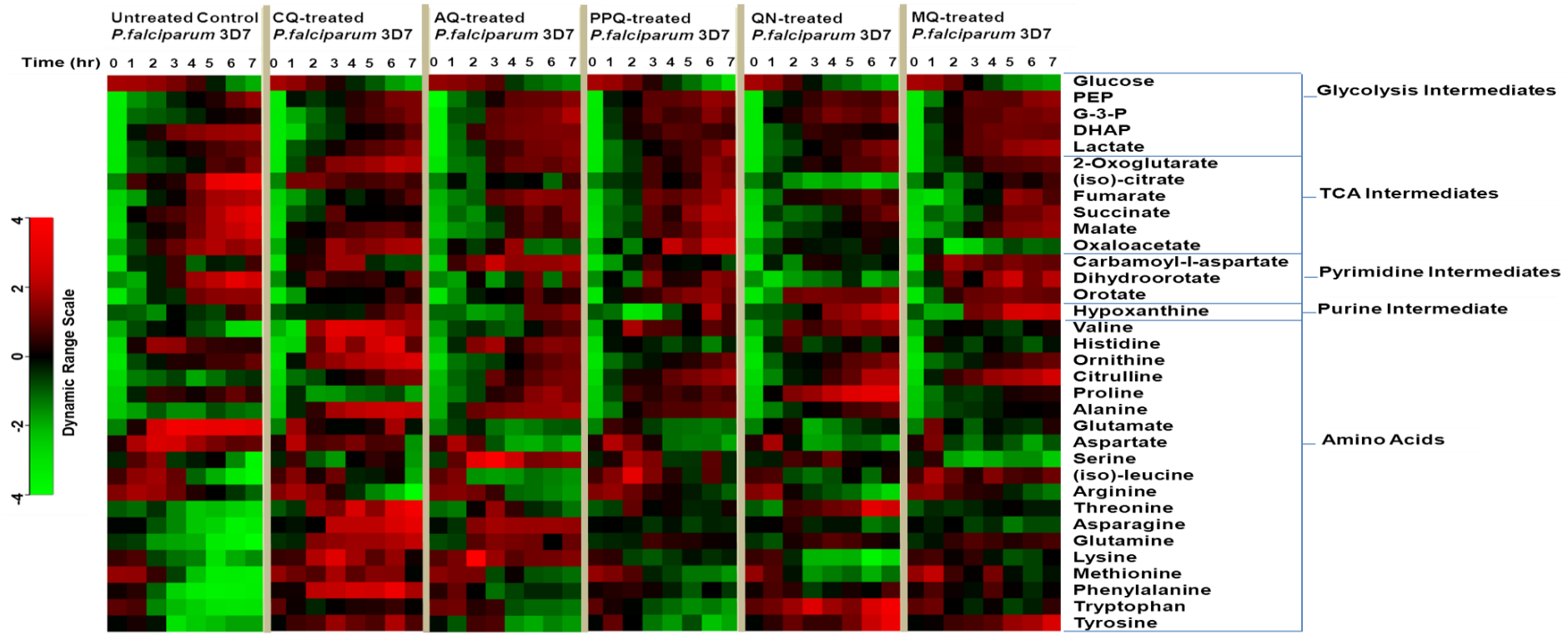

Figure 7.4: Heat map representation of *P. falciparum* 3D7 dynamics metabolome.

Heat map shows a dynamic changes of 34 metabolites in untreated *P. falciparum* control and *P. falciparum* parasites treated after one hour of incubation with chloroquine (CQ), amodiaquine (AQ), piperaquine (PPQ), quinine (QN) and mefloquine (MQ). Average values at each time-point obtained using purified trophozoite-staged from three independent biological replicates were divided by the corresponding average values derived from parasites harvested at time (0hr) to generate the corresponding ratios. Ratios were $\log_2$ transformed and plotted on a colour dynamic range scale. Rows correspond to metabolites measured by LC-MS/MS. Columns correspond to the time course from 0hr to 7hr for each of the six blocks. Green and red colours represent decreases and increases, respectively. Black colour indicates the baseline. Abbreviations: DHAP, dihydroxyaceton phosphate; G-3-P, glycerol-3-phosphate; PEP, phosphoenol pyruvate.

7.3.2. Biochemical time–dependent of metabolites profile in *P. falciparum* parasite

The findings described in the previous metabolomics analysis section (section 7.3.1) were used to distinguish between the MoAs of QCD members used to perturb the biological system of *P. falciparum*. Average concentration values at each time-point obtained using purified trophozoite-stage from biological replicates were divided by the corresponding average values derived from parasites collected prior to the addition of the respective drug to generate the corresponding fold change ratio. Time-dependent graphs for *P. falciparum* untreated control and *P. falciparum* treated with the addition of chloroquine, amodiaquine, piperaquine, quinine and mefloquine were plotted using GraphPad Prism 5.0 (GraphPad Software Inc.).

The data showed that the rate of glucose consumption in *P. falciparum* following the addition of chloroquine, amodiaquine, piperaquine, quinine and mefloquine was slightly higher than that of untreated control particularly in the first few hours of drugs exposure by 0.5 fold at time 3 hr time point (Figure 7.5 A, B, C, D and E). Consequently, the production of phosphoenol pyruvate (PEP) and lactate for parasites treated with chloroquine, amodiaquine, piperaquine, quinine and mefloquine was also marginally higher than that of untreated; with variations in their production rate depending on the drug used (Figure 7.6 and 7.7; A, B, C, D and E). In addition, the level of dihydroxyacetone phosphate (DHAP) was notably decreased upon treating the parasite with chloroquine, amodiaquine, piperaquine, quinine and mefloquine when compared to untreated (Figure 7.8 A, B, C, D and E). The level of glycerol-l-phosphate (G-3-P) was noticeably increased in parasites treated with chloroquine, amodiaquine, piperaquine, quinine and mefloquine as compared to the untreated parasites (Figure 7.9 A, B, C, D and E).

The QCD showed different patterns and trends in Tricarboxylic Acid (TCA) intermediates compared to untreated. Specifically, *P. falciparum* parasites treated with chloroquine showed a noticeable increase in the levels of 2-oxoglutarate but no obvious changes were observed in 2-oxoglutarate for the reminder of QCDs treatment (Figure 7.10 A, B, C, D and E). A distinguished reduction of (iso)-citrate was observed in parasites following the addition of chloroquine, amodiaquine, piperaquine, quinine and mefloquine (Figure 7.11 A, B, C, D and E). With the exception of piperaquine, there

was a notable reduction in the level of succinate in parasites treated with chloroquine, amodiaquine, quinine and mefloquine (Figure 7.12 A, B, D and E). There were no clear changes in the level of fumarate between parasites treated with amodiaquine, piperaquine, quinine and mefloquine and untreated parasites (Figure 7.13 B, C, and E) but a notable reduction was observed in fumarate level in parasites treated with chloroquine and quinine (Figure 7.13 A and D). Moreover, parasites treated with amodiaquine, quinine and mefloquine showed a reduction in the level of oxaloacetate whereas those treated with chloroquine and piperaquine do not (Figure 7.14 A, B, C, D and E). Parasites treated with amodiaquine and quinine showed a notable reduction in malate levels while those treated with chloroquine, piperaquine and mefloquine showed a slight reduction in malate as compared to untreated parasites (Figure 7.15 A, B, C, D and E).

With regards to pyrimidine intermediates, there were no obvious changes noted in the levels of carbamoyl-l-aspartate in parasites treated with chloroquine, amodiaquine, piperaquine, quinine and mefloquine as compared to untreated parasites (Figures 7.16 A, B, C, D and E). However, with the exception of mefloquine, *P. falciaprum* treated with chloroquine, amodiaquine, piperaquine and quinine showed a notable reduction in the levels on dihydroorotate (Figure 7.17 A, B, C, D and E). Orotate level was notably decreased in parasites treated with chloroquine and amodiaquine as compared to untreated parasites but there were no obvious changes in its level in parasites treated with piperaquine, quinine and mefloquine (Figure 7.18 A, B, C, D and E). With regards to purine intermediate, hypoxanthine, parasites treated with chloroquine, amodiaquine and piperaquine showed no clear changes when compared to untreated parasites (Figure 7.19 A, B and C). However, parasites treated with quinine and mefloquine showed a slight increase in the hypoxanthine level as compared to untreated parasites (Figure 7.19 D and E).

Amino acids profile were different upon the addition of QCDs to *P. falciparum* parasites. Following the addition of chloroquine, amodiaquine, piperaquine, quinine and mefloquine to *P. falciparum* parasites, there was a notable accumulation in the level of alanine (Figure 7.20 A, B, C, D and E) and there was a little or no utilization in glutamine and asparagine (Figure 7.21 and 7.23; A, B, C, D and E). In addition, the level of glutamate in parasites treated with all members of QCDs mentioned above

showed a noticeable of invariable changes compared to untreated parasites (Figure 7.22 A, B, C, D and E) whereas there was a notable reduction in the level of aspartate compared to untreated parasites following the addition of QCDs (Figure 7.24 A, B, C, D and E).

Moreover, there were no obvious changes in the levels of arginine and proline upon the addition of chloroquine, amodiaquine, piperaquine, quinine and mefloquine to the *P. falciparum* parasites as compared to the untreated (Figures 7.25 and 7.26; A, B, C, D and E). Interestingly, there was a distinguished accumulation in the level of ornithine in parasites treated with chloroquine (Figure 7.27 A) but no evident changes were observed in ornithine levels in parasites treated with amodiaquine, piperaquine, quinine and mefloquine (Figure 7.27 B, C, D and E). Additionally, there was a little or no utilization in the level of methionine in parasites treated with chloroquine (Figure 7.29 A) but no clear changes were observed in methionine levels in parasites treated with amodiaquine, piperaquine, quinine and mefloquine (Figure 7.29 B, C, D and E). *P. falciparum* parasites treated with chloroquine, amodiaquine, piperaquine, quinine and mefloquine showed a notable accumulation of citrulline as compared to untreated parasite (Figure 7.28 A, B, C, D and E).

There was little or no utilization of lysine upon the addition of chloroquine and amodiaquine to the *P. falciparum* parasites as compared to the untreated (Figure 7.30 A and B). In contrast, parasites treated with piperaquine, quinine and mefloquine showed no obvious changes in the level of lysine compared to untreated parasites (Figure 7.30 C, D and E). Moreover, there were no clear changes in the level of serine and histidine upon the addition of chloroquine, amodiaquine, piperaquine, quinine and mefloquine to the *P. falciparum* parasites as compared to the untreated (Figure 7.31 and 7.32; A, B, C, D and E).

Furthermore, *P. falciparum* parasites treated with chloroquine showed a slight increase in the phenyalanine level whereas those treated with amodiaquine, piperaquine, quinine and mefloquine showed little or no utilization of phenylalanine as compared to untreated parasites (Figure 7.33 A, B, C, D and E). In addition, *P. falciparum* parasites treated with chloroquine, amodiaquine, piperaquine and mefloquine showed little or no utilization of tryptophan (Figure 7.34 A, B, C and E) whereas those treated with quinine

showed a notable increase in tryptophan level as compared to untreated parasites (Figure 7.34 D). Moreover, there was a trend of increase in the level of tyrosine in parasites treated with chloroquine, quinine and mefloquine (Figure 7.35 A, D and E). On the other hand, parasites treated with amodiaquine and piperaquine did not show notable changes in tyrosine level as compared to untreated parasites (Figure 7.35 B and C).

In addition, the *P. falciparum* parasites treated with chloroquine and quinine showed a notable increase in the level of threonine (Figure 7.36 A and D) whereas those treated with amodiaquine, piperaquine and mefloquine showed little or no utilization of threonine as compared to untreated (Figure 7.36 B, C and E). In addition, parasites treated with chloroquine, amodiaquine, piperaquine, quinine and mefloquine showed a notable increase in the valine level by at least 0.5 fold at 7 hr time point as compared to untreated (Figure 7.37 A, B, C, D and E). There was no obviuos changes observed in the level of (iso)-leucine in parasites treated with chloroquine, amodiaquine, piperaquine, quinine and mefloquine as compared to untreated parasites (Figure 7.38 A, B, C, D and E).

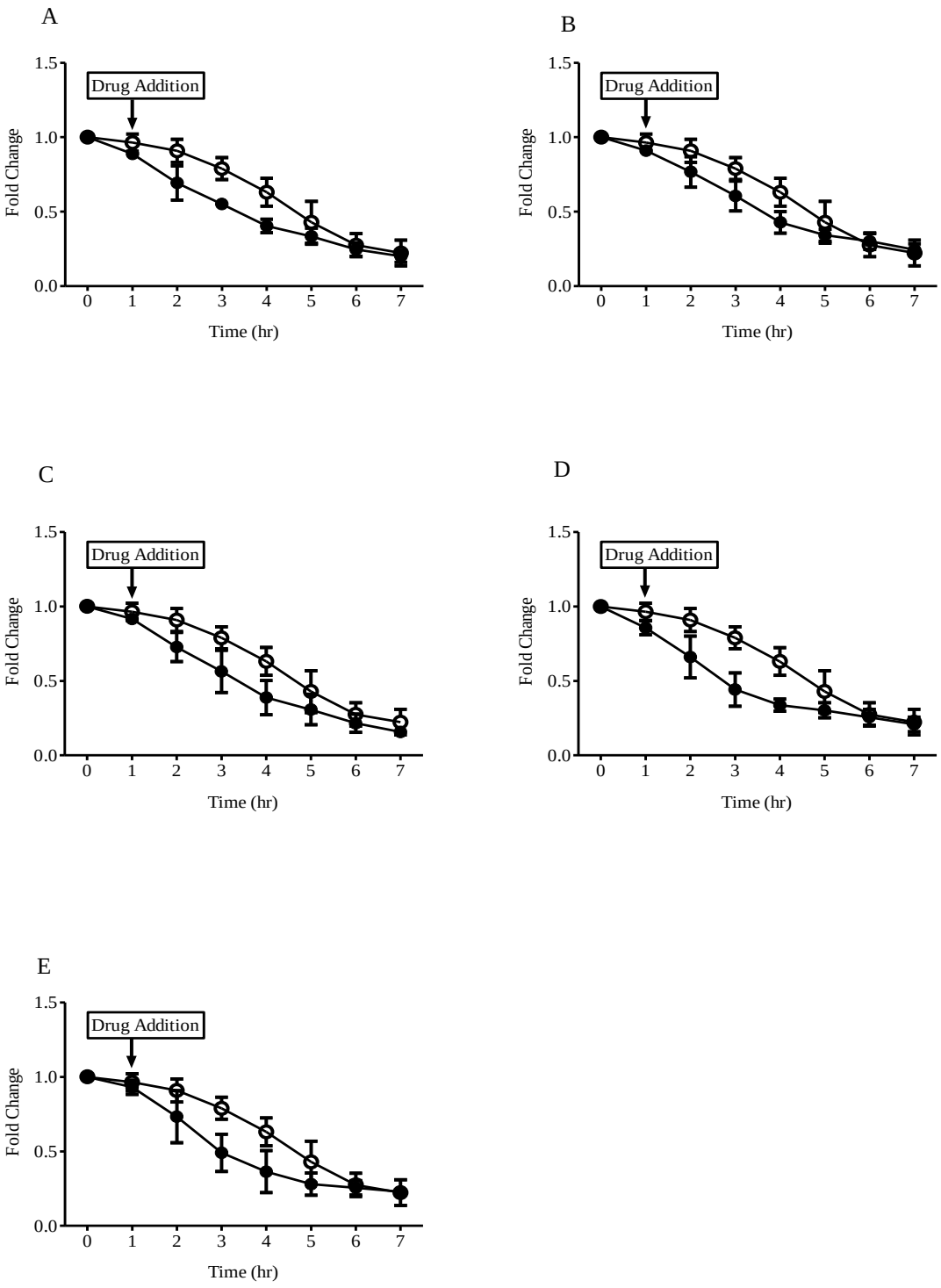

Figure 7.5. Time-dependent of glucose fermentation in drug-treated and untreated *P. falciparum* 3D7 parasites.

Glucose levels were determined in untreated (open circle) and drug-treated (closed circle) *P. falciparum* trophozoite-stage parasites by LC-MS/MS. The following drugs were added to the parasites after one hour of incubation (A) 50 nM chloroquine, (B) 50 nM amodiaquine, (C) 80 nM piperaquine, (D) 100 nM quinine and (E) 50 nM mefloquine. Data showed clearly the utilization of glucose in drugs treated and untreated parasites. The points represent the mean ± SEM of at least duplicate independent experiments.

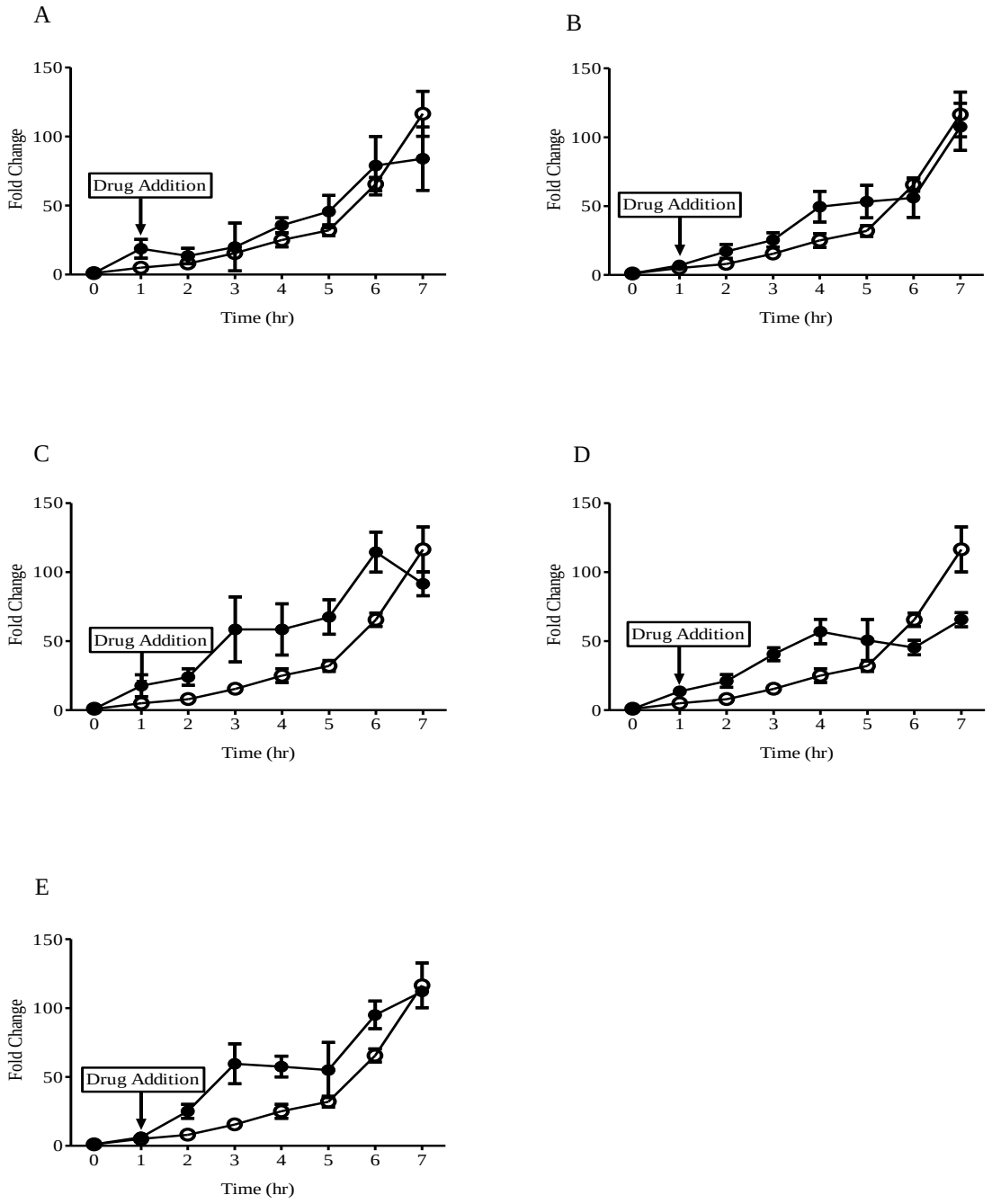

Figure 7.6. Time-dependent curves of phosphoenol pyruvate (PEP) in drug-treated and untreated *P. falciparum* 3D7 parasites.

PEP levels were determined in untreated (open circle) and drug-treated (closed circle) *P. falciparum* trophozoite-stage parasites by LC-MS/MS. The following drugs were added to the parasites after one hour of incubation (A) 50 nM chloroquine, (B) 50 nM amodiaquine, (C) 80 nM piperaquine, (D) 100 nM quinine and (E) 50 nM mefloquine. Data showed slight increase in PEP levels after one hour of incubation in parasites treated with (A) 50 nM chloroquine, (B) 50 nM amodiaquine, (C) 80 nM piperaquine, (D) 100 nM quinine and (E) 50 nM mefloquine as compared to untreated parasites. The points represent the mean ± SEM of at least duplicate independent experiments.

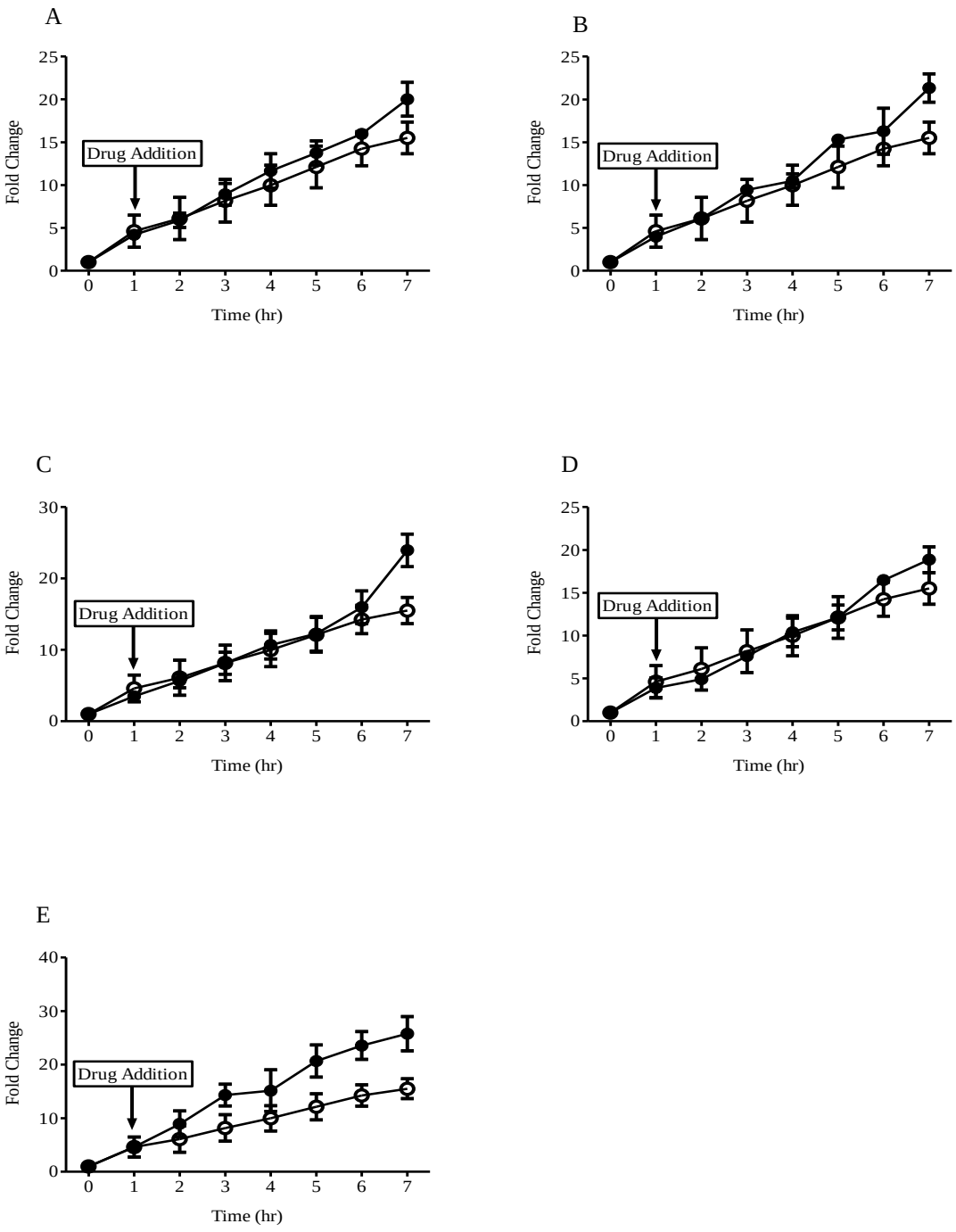

Figure 7.7. Time-dependent curves of lactate production in drug-treated and untreated *P. falciparum* 3D7 parasites.

Lactate levels were measured in untreated (open circle) and drug-treated (closed circle) *P. falciparum* trophozoite-stage parasites by LC-MS/MS. The following drugs were added to the parasites after one hour of incubation (A) 50 nM chloroquine, (B) 50 nM amodiaquine, (C) 80 nM piperaquine, (D) 100 nM quinine and (E) 50 nM mefloquine. Data showed slight increase in lactate levels at 7 hr time point in parasites treated with (A) 50 nM chloroquine, (B) 50 nM amodiaquine, (C) 80 nM piperaquine, (D) 100 nM quinine and (E) 50 nM mefloquine as compared to untreated parasites. The points represent the mean ± SEM of at least duplicate independent experiments.

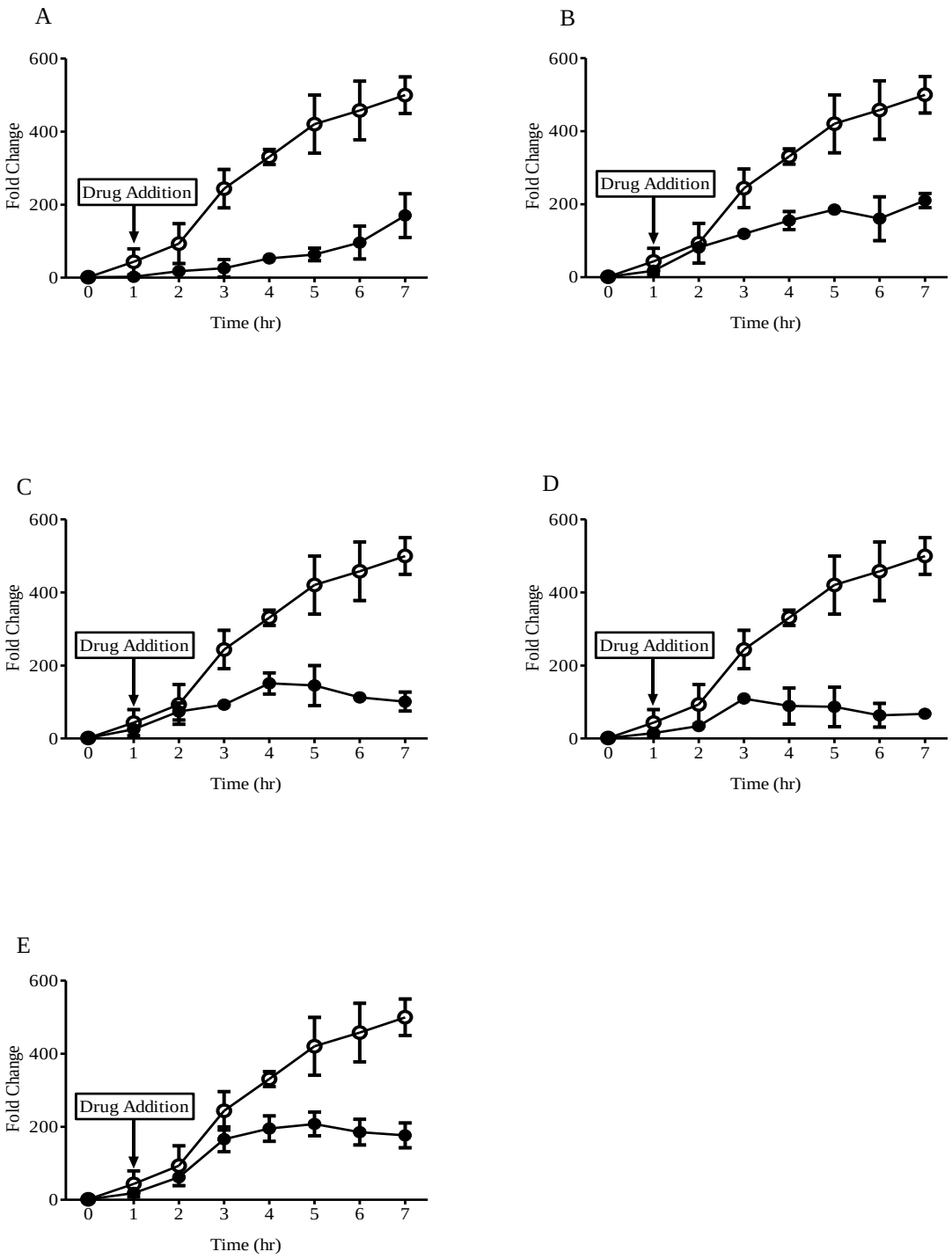

Figure 7.8. Time-dependent curves of dihydroxyaceton phosphate (DHAP) in drug-treated and untreated *P. falciparum* 3D7 parasites.

DHAP levels were measured in untreated (open circle) and drug-treated (closed circle) *P. falciparum* trophozoite-stage parasites by LC-MS/MS. Data showed a notable reduction of DHAP after one hour of incubation in parasites treated with (A) 50 nM chloroquine, (B) 50 nM amodiaquine, (C) 80 nM piperaquine, (D) 100 nM quinine and (E) 50 nM mefloquine. The points represent the mean ± SEM of at least duplicate independent experiments.

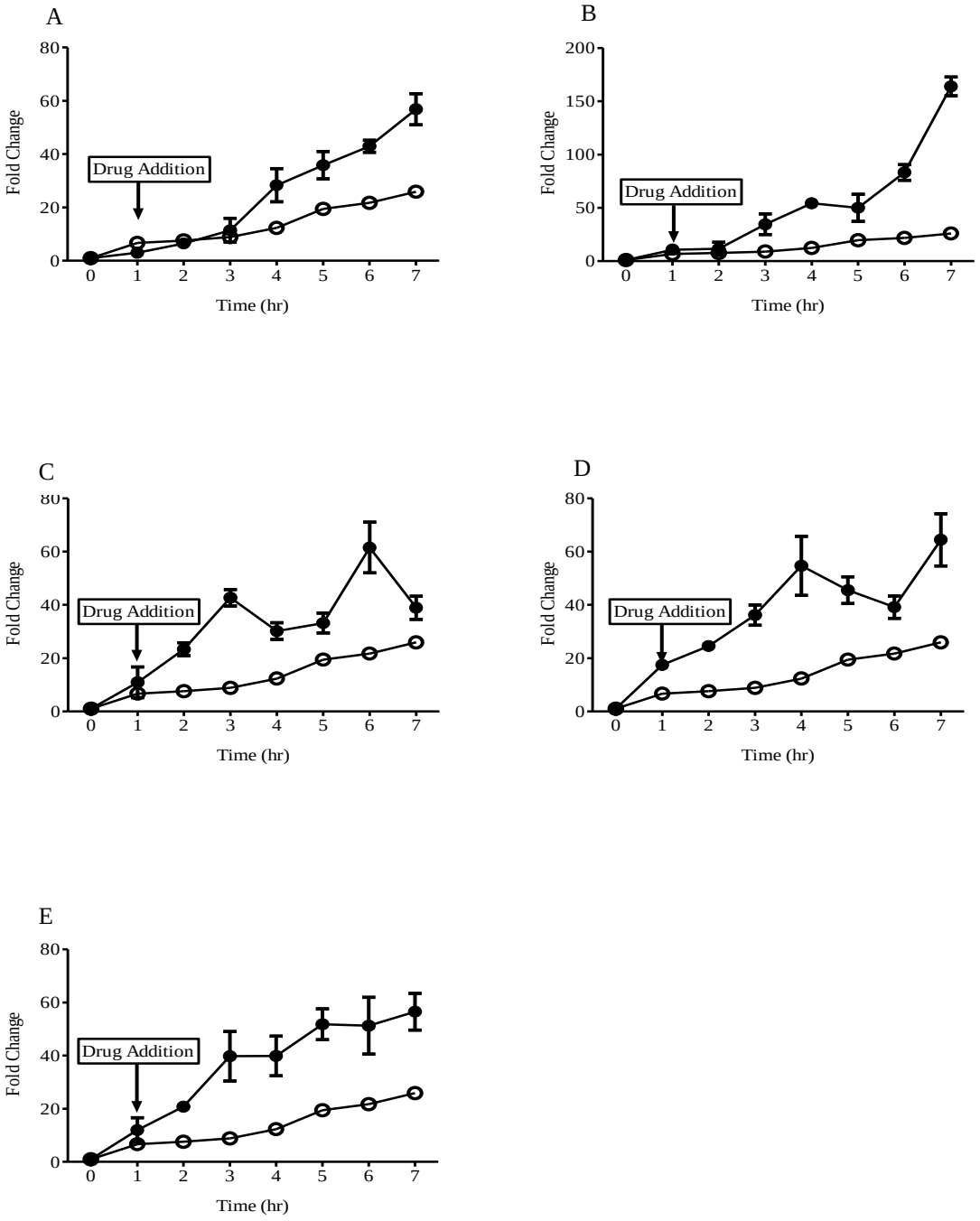

Figure 7.9. Time-dependent curves of glycerol-3-phosphate (G-3-P) in drug-treated and untreated *P. falciparum* 3D7 parasites.

G-3-P levels were determined in untreated (open circle) and drug-treated (closed circle) *P. falciparum* trophozoite-stage parasites by LC-MS/MS. Data showed a notable increase in G-3-P after one hour of incubation in parasites treated with (A) 50 nM chloroquine, (B) 50 nM amodiaquine, (C) 80 nM piperaquine, (D) 100 nM quinine and (E) 50 nM mefloquine. The points represent the mean ± SEM of at least duplicate independent experiments.

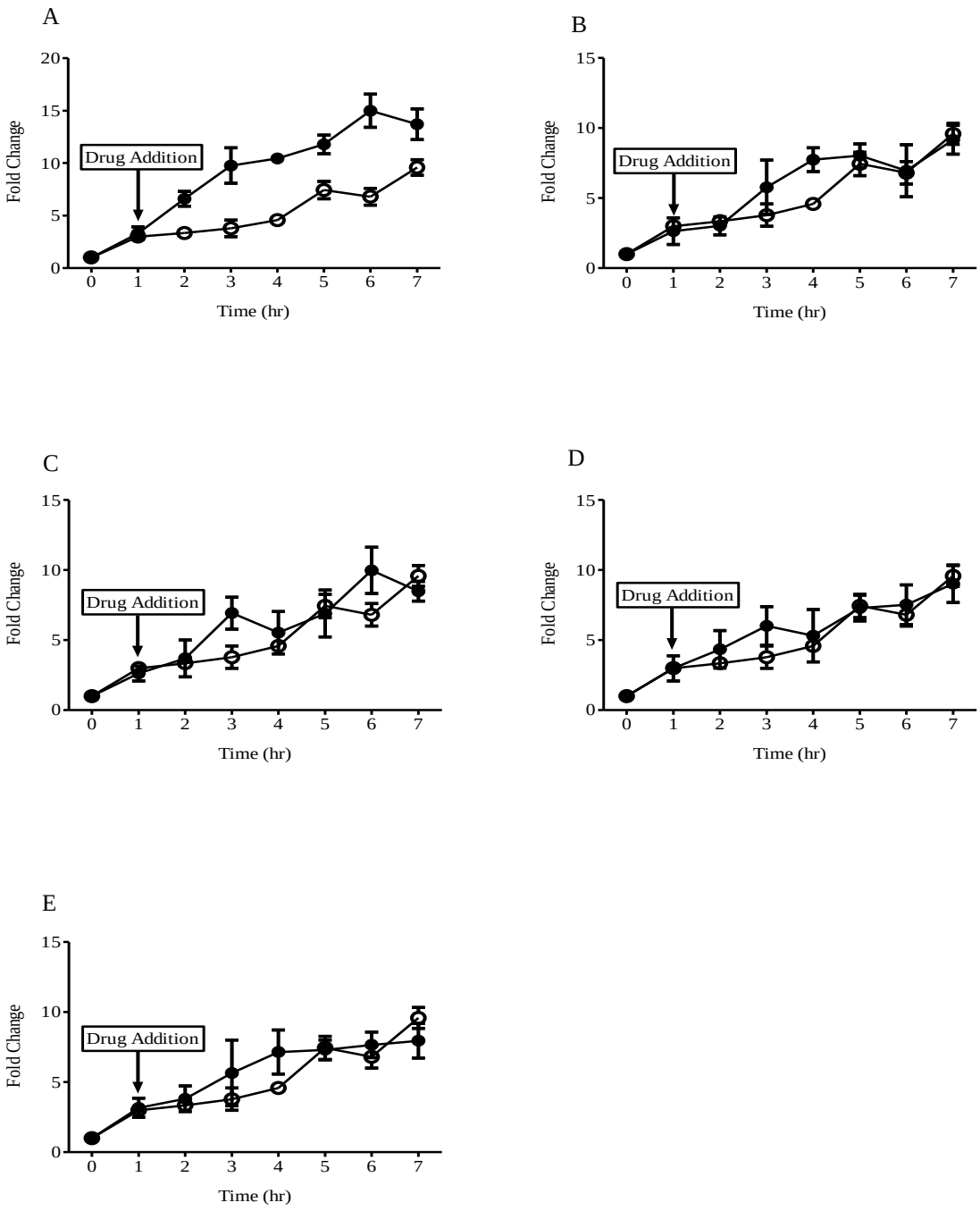

Figure 7.10. Time-dependent curves of 2-oxoglutarate in drug-treated and untreated *P. falciparum* 3D7 parasites.

2-oxoglutarate levels were determined in untreated (open circle) and drug-treated (closed circle) *P. falciparum* trophozoite-stage parasites by LC-MS/MS. The following drugs were added to the parasites after one hour of incubation (A) 50 nM chloroquine, (B) 50 nM amodiaquine, (C) 80 nM piperaquine, (D) 100 nM quinine and (E) 50 nM mefloquine. Data showed a notable increase in 2-oxoglutarate in parasite treated with (A) 50 nM chloroquine compared to untreated. There were no clear changes between others drug-treated and untreated parasites. The points represent the mean ± SEM of at least duplicate independent experiments.

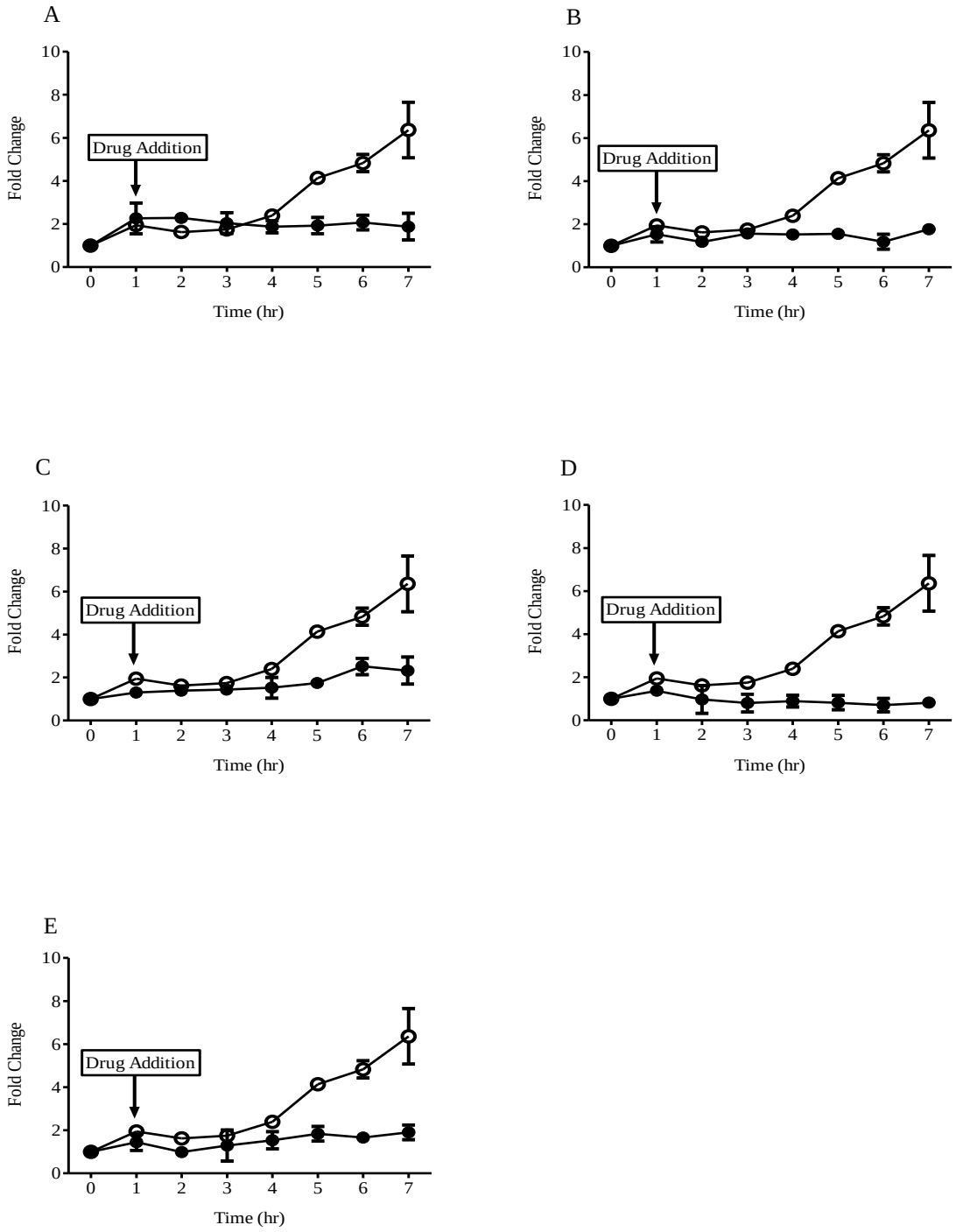

Figure 7.11. Time-dependent curves of (iso)-citrate in drug-treated and untreated *P. falciparum* 3D7 parasites.

The (iso)-citrate levels were determined in untreated (open circle) and drug-treated (closed circle) *P. falciparum* trophozoite-stage parasites by LC-MS/MS. Data showed a distinguished reduction in (iso)-citrate after one hour of incubation in parasites treated with (A) 50 nM chloroquine, (B) 50 nM amodiaquine, (C) 80 nM piperaquine, (D) 100 nM quinine and (E) 50 nM mefloquine. The points represent the mean ± SEM of at least duplicate independent experiments.

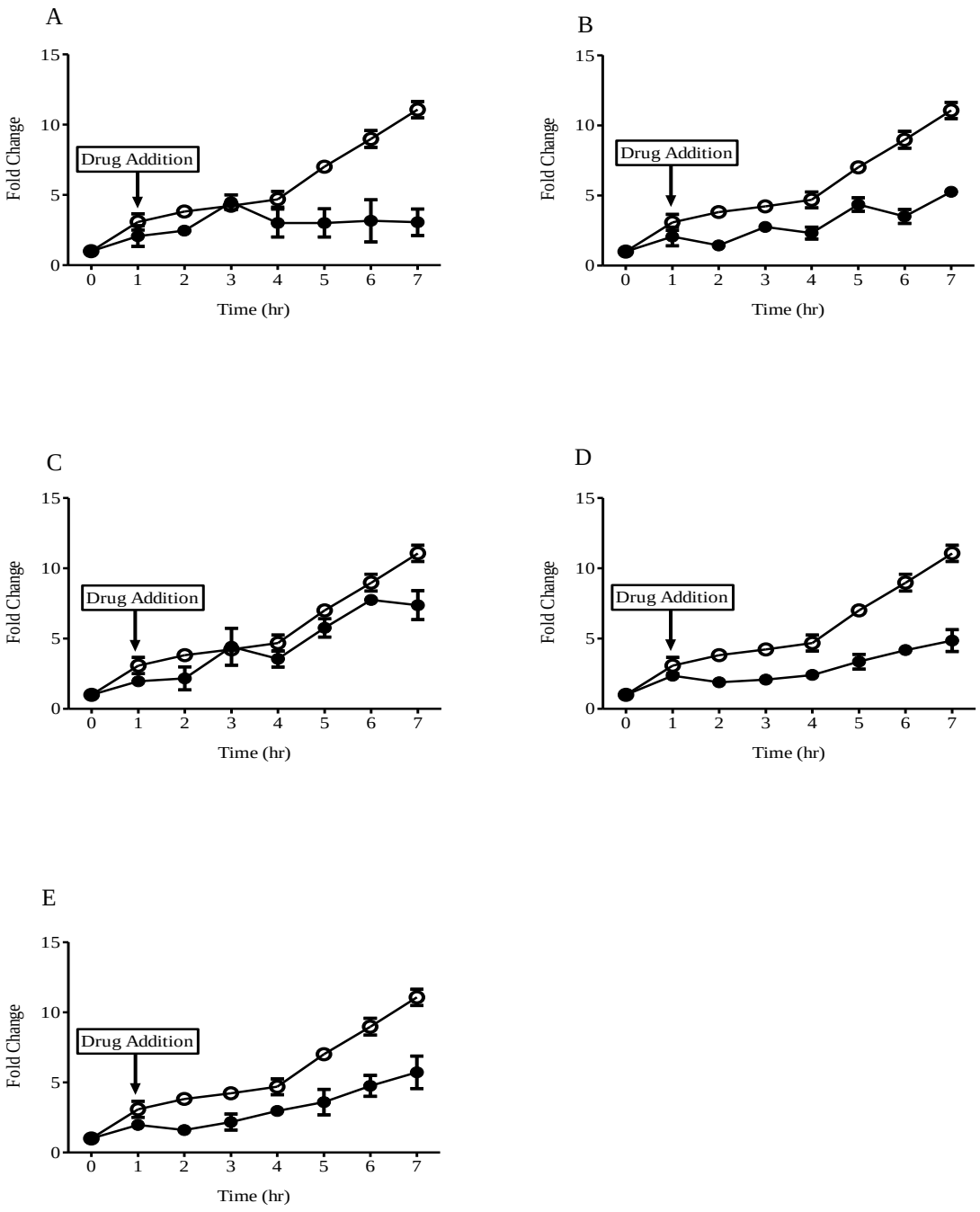

Figure 7.12. Time-dependent curves of succinate in drug-treated and untreated *P. falciparum* 3D7 parasites.

Succinate levels were determined in untreated (open circle) and drug-treated (closed circle) *P. falciparum* trophozoite-staged parasites by LC-MS/MS. The following drugs were added to the parasites after one hour of incubation (A) 50 nM chloroquine, (B) 50 nM amodiaquine, (C) 80 nM piperaquine, (D) 100 nM quinine and (E) 50 nM mefloquine. With the exception of (C) piperaquine, data showed an evident reduction in the level of succinate in parasites treated with (A) 50 nM chloroquine, (B) 50 nM amodiaquine, (D) 100 nM quinine and (E) 50 nM mefloquine. The points represent the mean ± SEM of at least duplicate independent experiments.

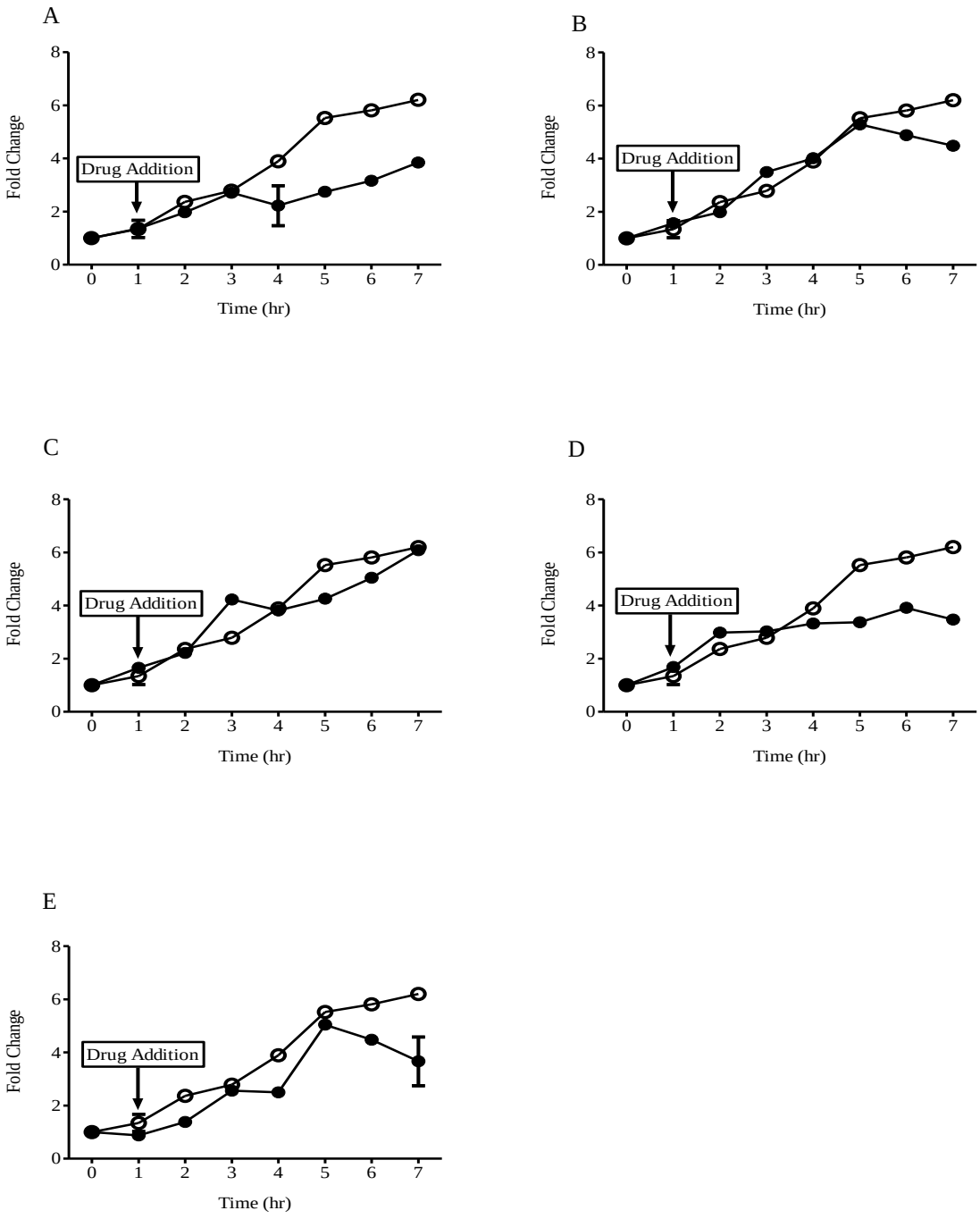

Figure 7.13. Time-dependent curves of fumarate in drug-treated and untreated *P. falciparum* 3D7 parasites.

Fumarate levels were determined in untreated (open circle) and drug-treated (closed circle) *P. falciparum* trophozoite-staged parasites by LC-MS/MS. The following drugs were added to the parasites after one hour of incubation (A) 50 nM chloroquine, (B) 50 nM amodiaquine, (C) 80 nM piperaquine, (D) 100 nM quinine and (E) 50 nM mefloquine. There were no clear changes in the level of fumarate between parasites treated with (B) 50 nM amodiaquine, (C) 80 nM piperaquine, and (E) 50 nM mefloquine but a notable reduction was observed in fumarate level in parasites treated with (A) 50 nM chloroquine and (D) 100 nM quinine. The points represent the mean ± SEM of at least duplicate independent experiments.

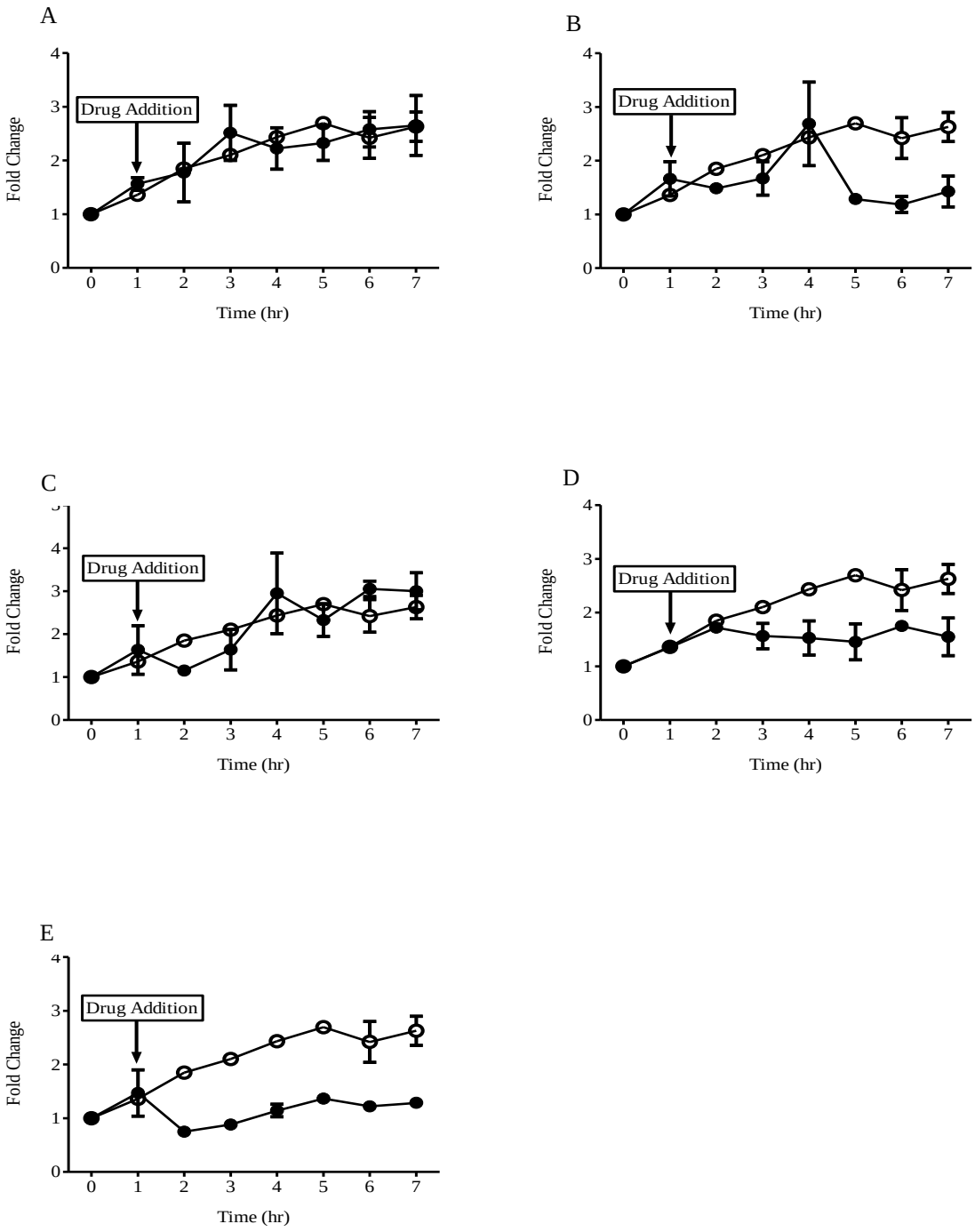

Figure 7.14. Time-dependent curves of oxaloacetate levels in drug-treated and untreated *P. falciparum* 3D7 parasites.

Oxaloacetate levels were determined in untreated (open circle) and drug-treated (closed circle) *P. falciparum* trophozoite-staged parasites by LC-MS/MS. The following drugs were added to the parasites after one hour of incubation (A) 50 nM chloroquine, (B) 50 nM amodiaquine, (C) 80 nM piperaquine, (D) 100 nM quinine and (E) 50 nM mefloquine. Data showed a notable reduction in the level of oxaloacetate in parasites treated with (B) 50 nM amodiaquine, (D) 100 nM quinine and (E) 50 nM mefloquine whereas no clear changes were observed in others drug used. The points represent the mean ± SEM of at least duplicate independent experiments.

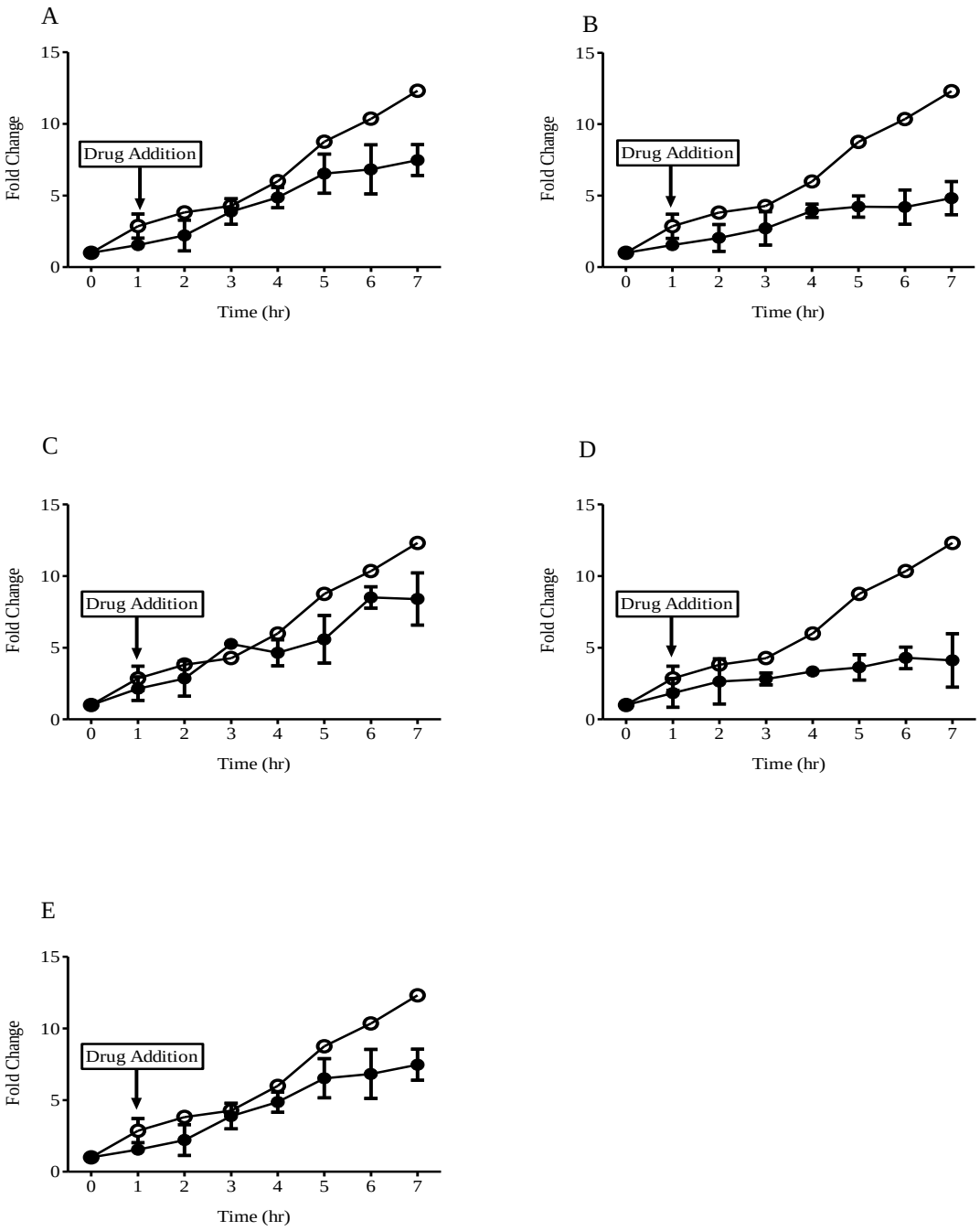

Figure 7.15. Time-dependent curves of malate production in drug-treated and untreated *P. falciparum* 3D7 parasites.

Malate levels were measured in untreated (open circle) and drug-treated (closed circle) *P.falciparum* trophozoite-staged parasites by LC-MS/MS. The following drugs were added to the parasites after one hour of incubation (A) 50 nM chloroquine, (B) 50 nM amodiaquine, (C) 80 nM piperaquine, (D) 100 nM quinine and (E) 50 nM mefloquine. Data showed an evident reduction in the level of malate in parasites treated with (B) 50 nM amodiaquine and (D) 100 nM quinine while those treated (A) 50 nM chloroquine, (C) 80 nM piperaquine and (E) 50 nM mefloquine showed a slight reduction in malate as compared to untreated parasites. The points represent the mean ± SEM of at least duplicate independent experiments.

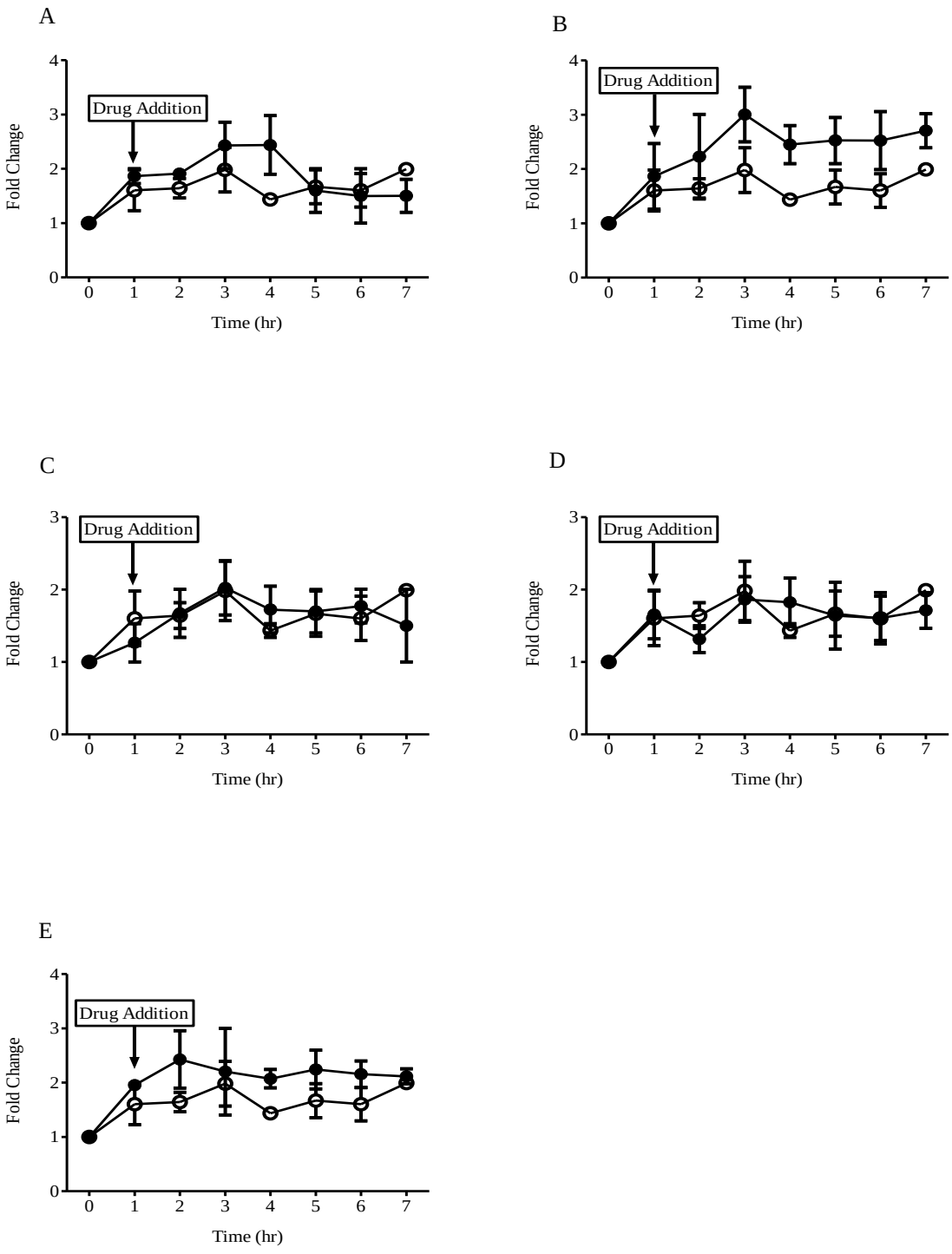

Figure 7.16. Time-dependent curves of carbamoyl-L-aspartate in drug-treated and untreated *P. falciparum* 3D7 parasites.

Carbamoyl-L-aspartate levels were determined in untreated (open circle) and drug-treated (closed circle) *P. falciparum* trophozoite-stage parasites by LC-MS/MS. The following drugs were added to the parasites after one hour of incubation (A) 50 nM chloroquine, (B) 50 nM amodiaquine, (C) 80 nM piperaquine, (D) 100 nM quinine and (E) 50 nM mefloquine. There were no obvious changes between drugs-treated and untreated parasites. The points represent the mean ± SEM of at least duplicate independent experiments.

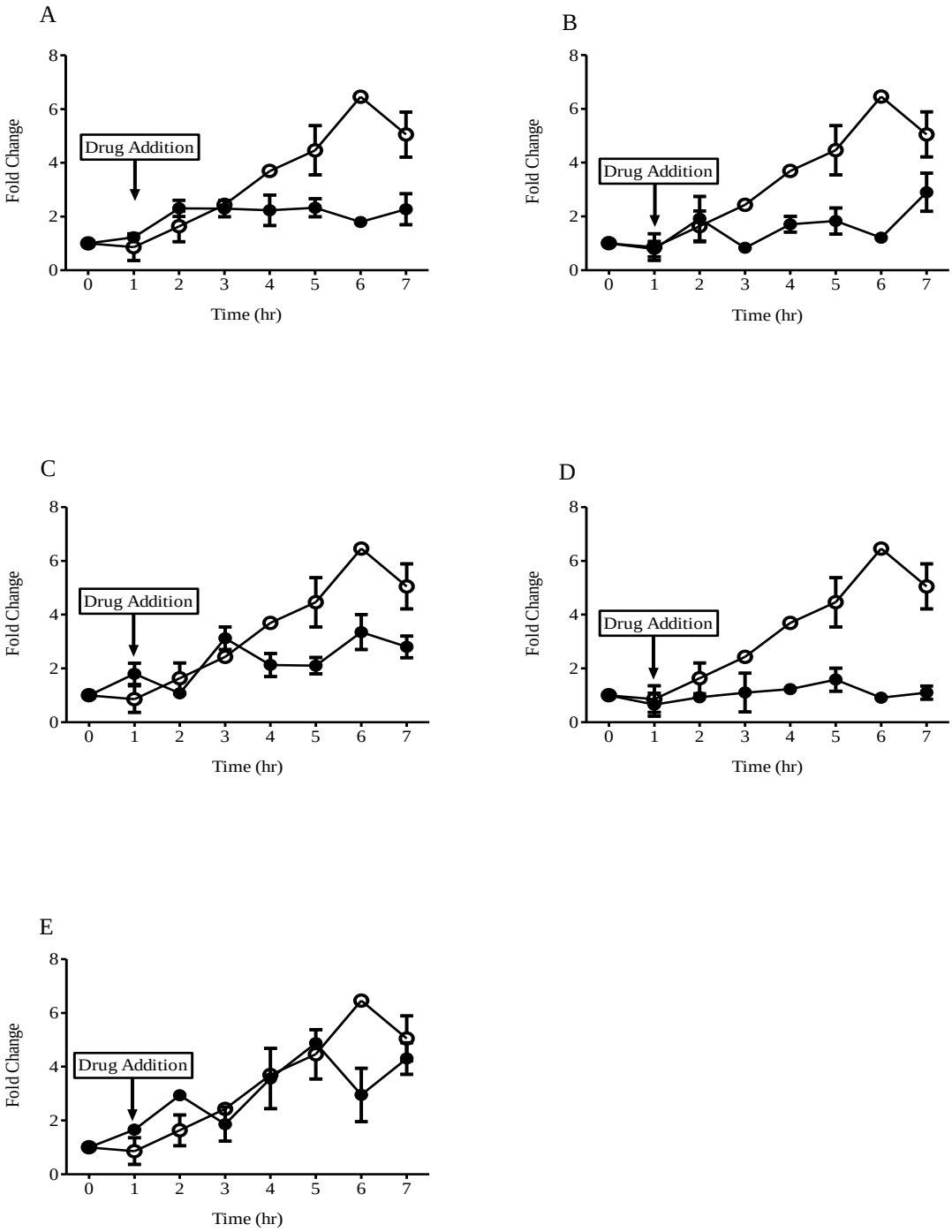

Figure 7.17. Time-dependent curves of dihydroorotate in drug-treated and untreated *P. falciparum* 3D7 parasites.

Dihydroorotate levels were determined in untreated (open circle) and drug-treated (closed circle) *P. falciparum* trophozoite-stage parasites by LC-MS/MS. The following drugs were added to the parasites after one hour of incubation (A) 50 nM chloroquine, (B) 50 nM amodiaquine, (C) 80 nM piperaquine, (D) 100 nM quinine and (E) 50 nM mefloquine. Data showed a notable reduction in dihydroorotate levels in parasites treated with A) 50 nM chloroquine, (B) 50 nM amodiaquine, (C) 80 nM piperaquine and (D) 100 nM quinine. The points represent the mean ± SEM of at least duplicate independent experiments.

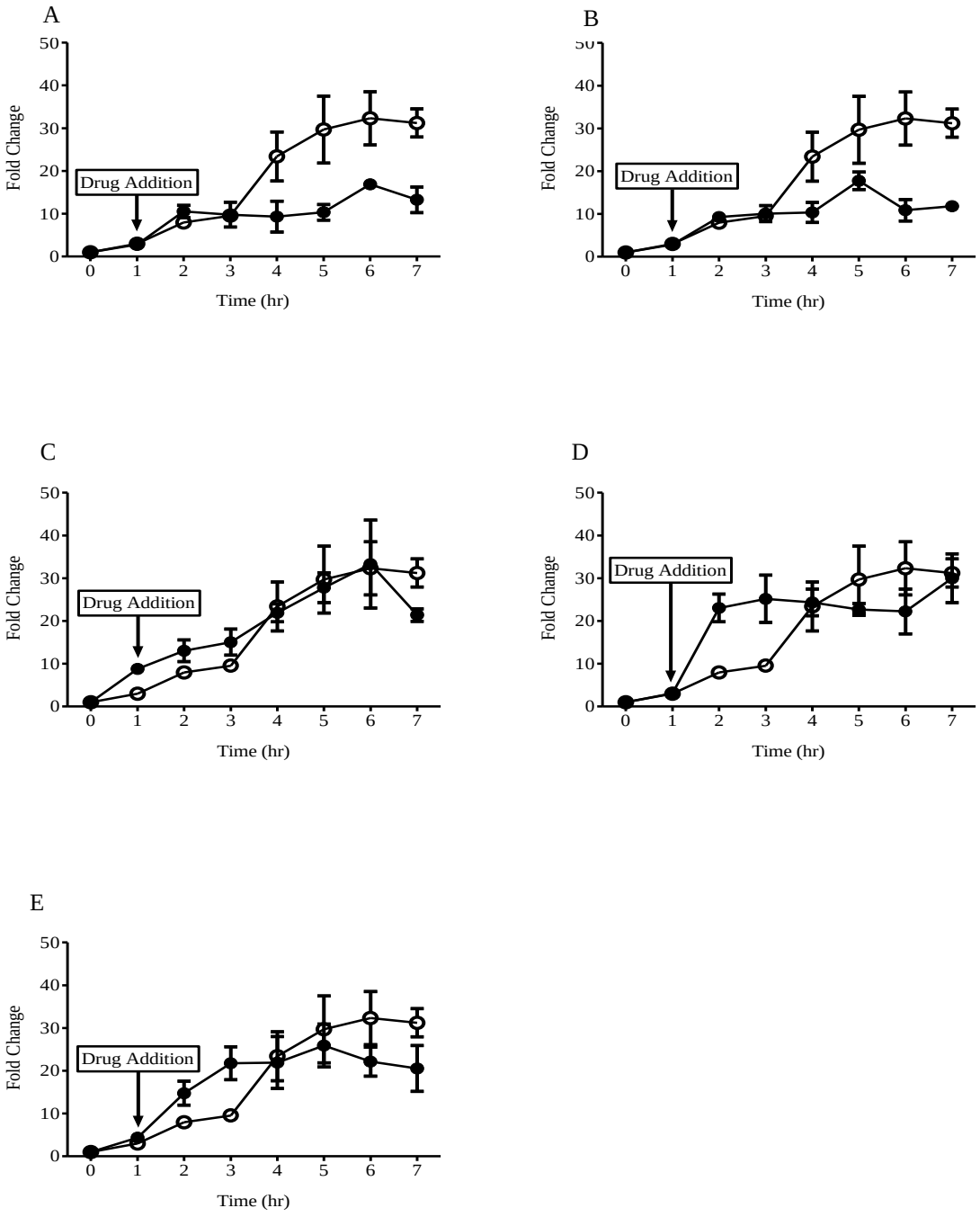

Figure 7.18. Time-dependent curves of orotate in drug-treated and untreated *P. falciparum* 3D7 parasites.

Orotate levels were determined in untreated (opencircle) and drug-treated (closed circle) *P. falciparum* trophozoite-stage parasites by LC-MS/MS. The following drugs were added to the parasites after one hour of incubation (A) 50 nM chloroquine, (B) 50 nM amodiaquine, (C) 80 nM piperaquine, (D) 100 nM quinine and (E) 50 nM mefloquine. Data showed a notable reduction in orotate level in parasites treated with (A) 50 nM chloroquine and (B) 50 nM amodiaquine. There were no obvious changes observed between other drugs-treated and untreated parasites. The points represent the mean ± SEM of at least duplicate independent experiments.

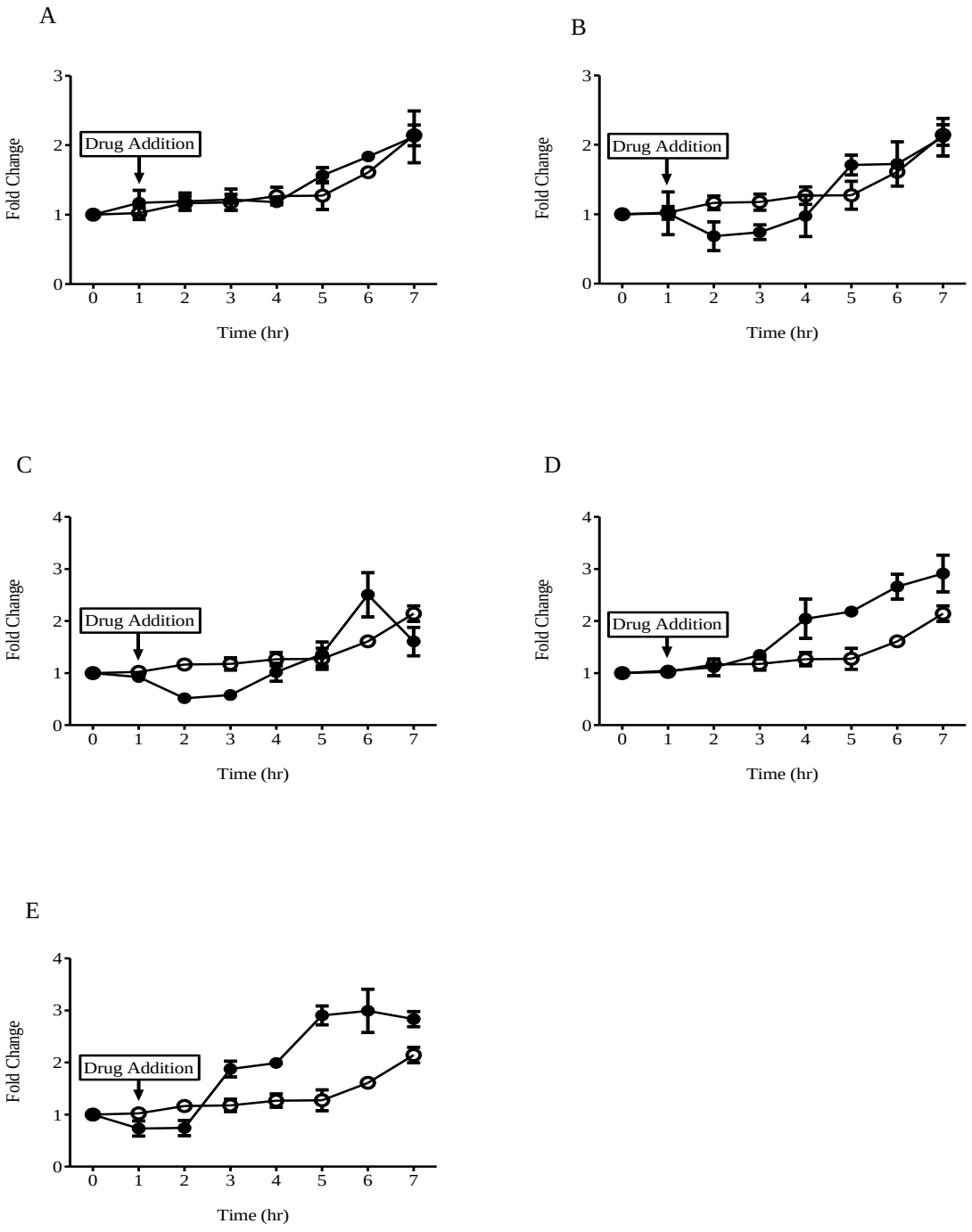

Figure 7.19. Time-dependent curves of hypoxanthine in drug-treated and untreated *P. falciparum* 3D7 parasites.

Hypoxanthine levels were determined in untreated (open circle) and drug-treated (closed circle) *P. falciparum* trophozoite-stage parasites by LC-MS/MS. The following drugs were added to the parasites after one hour of incubation (A) 50 nM chloroquine, (B) 50 nM amodiaquine, (C) 80 nM piperaquine, (D) 100 nM quinine and (E) 50 nM mefloquine. A slight elevation was observed in parasites treated with (D) 100 nM quinine and (E) 50 nM mefloquine. There were no clear changes observed between other drugs-treated and untreated parasites. The points represent the mean ± SEM of at least duplicate independent experiments.

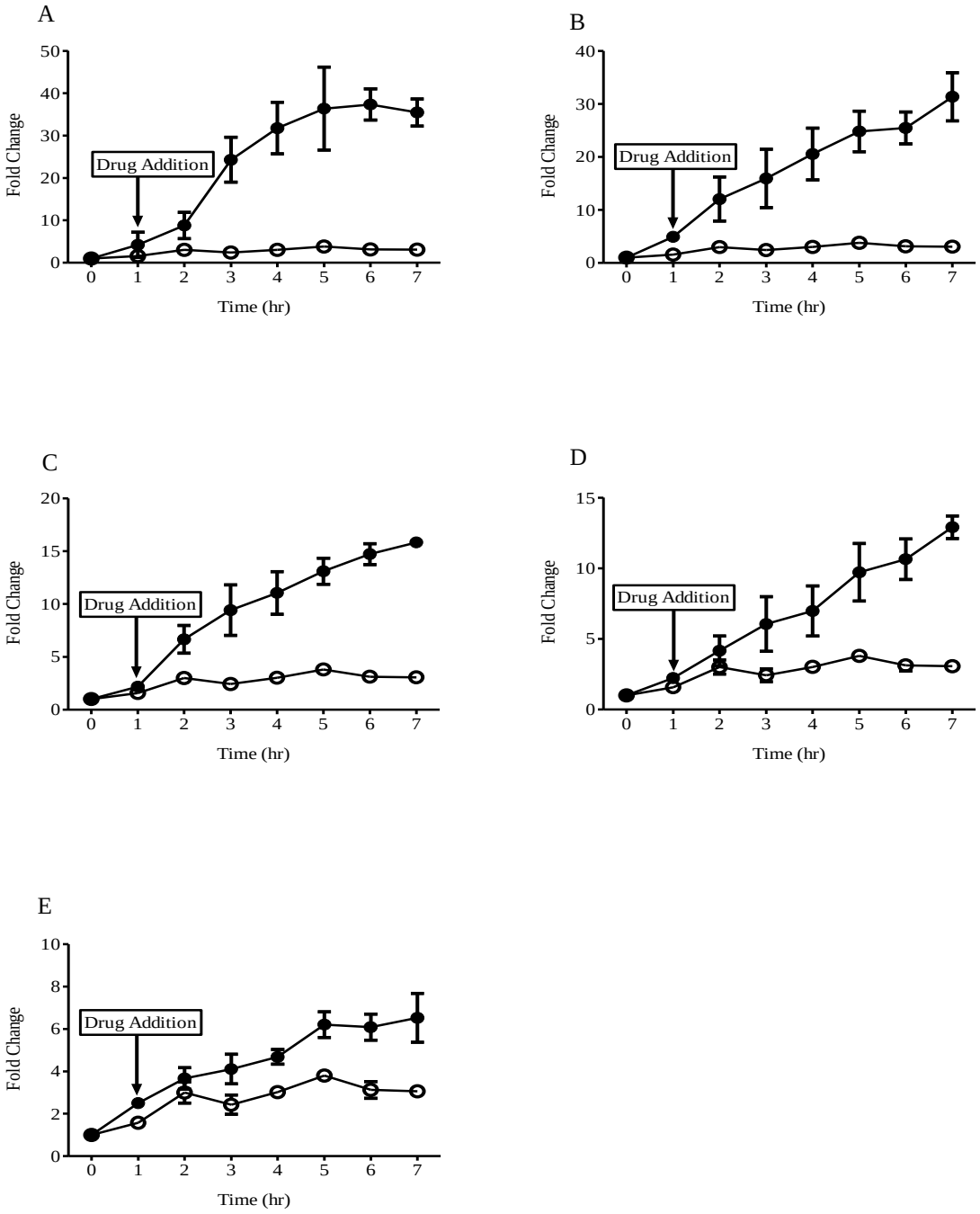

Figure 7.20. Time-dependent curves of alanine accumulation in drug-treated *P. falciparum* 3D7 parasites.

Alanine levels were determined in untreated (open circle) and drug-treated (closed circle) *P.falciparum* trophozoite-stage parasites by LC-MS/MS. Data showed a distinguished accumulation of alanine after one hour of incubation in parasites treated with (A) 50 nM chloroquine, (B) 50 nM amodiaquine, (C) 80 nM piperaquine, (D) 100 nM quinine and (E) 50 nM mefloquine. Data represent the mean ± SEM of at least duplicate independent experiments.

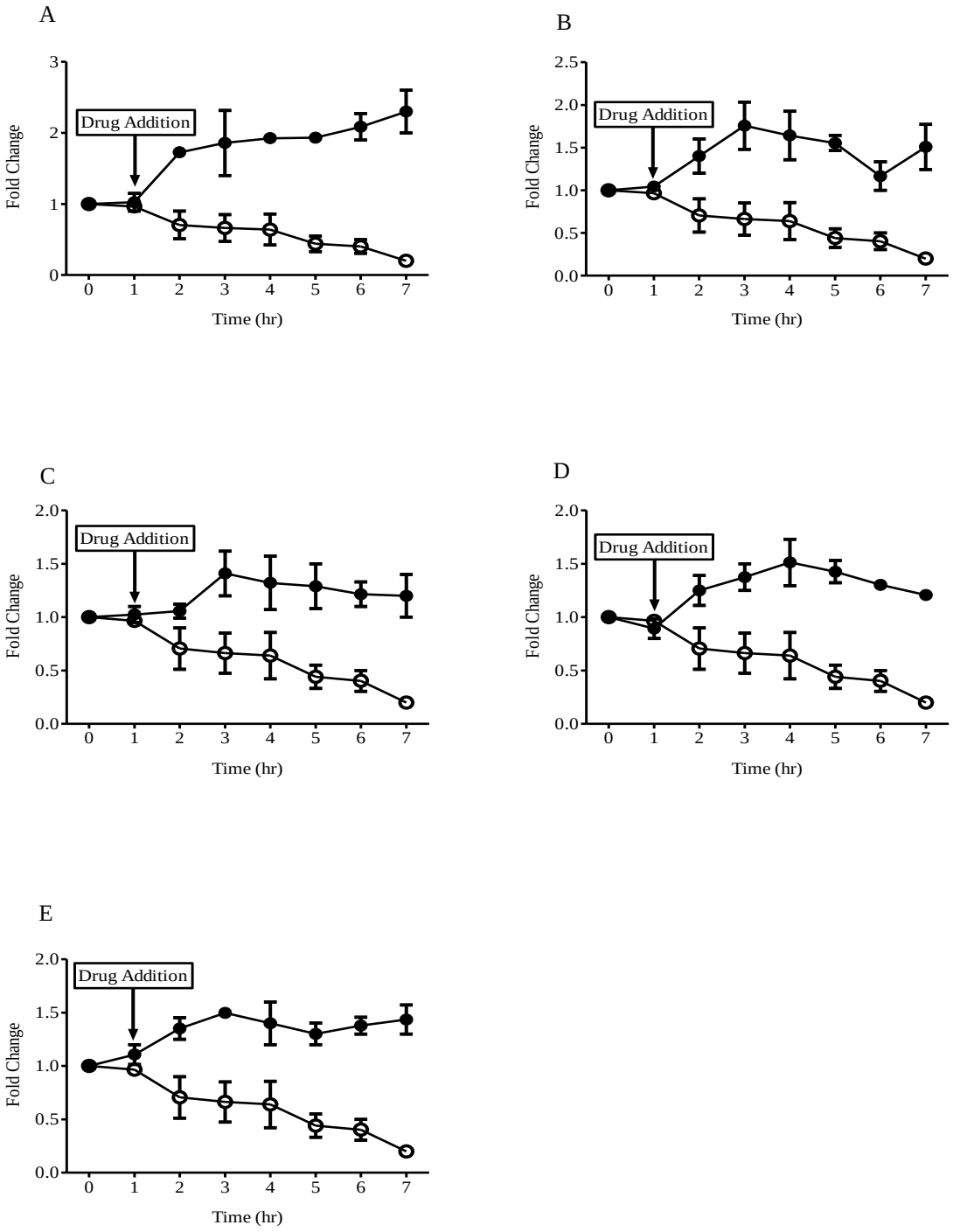

Figure 7.21. Time-dependent curves of glutamine in drug-treated and untreated *P. falciparum* 3D7 parasites.

Glutamine levels were determined in untreated (open circle) and drug-treated (closed circle) *P.falciparum* trophozoite-stage parasites by LC-MS/MS. Data showed a little or no utilization of glutamine after one hour of incubation in parasites treated with (A) 50 nM chloroquine, (B) 50 nM amodiaquine, (C) 80 nM piperaquine, (D) 100 nM quinine and (E) 50 nM mefloquine. Data represent the mean ± SEM of at least duplicate independent experiments.

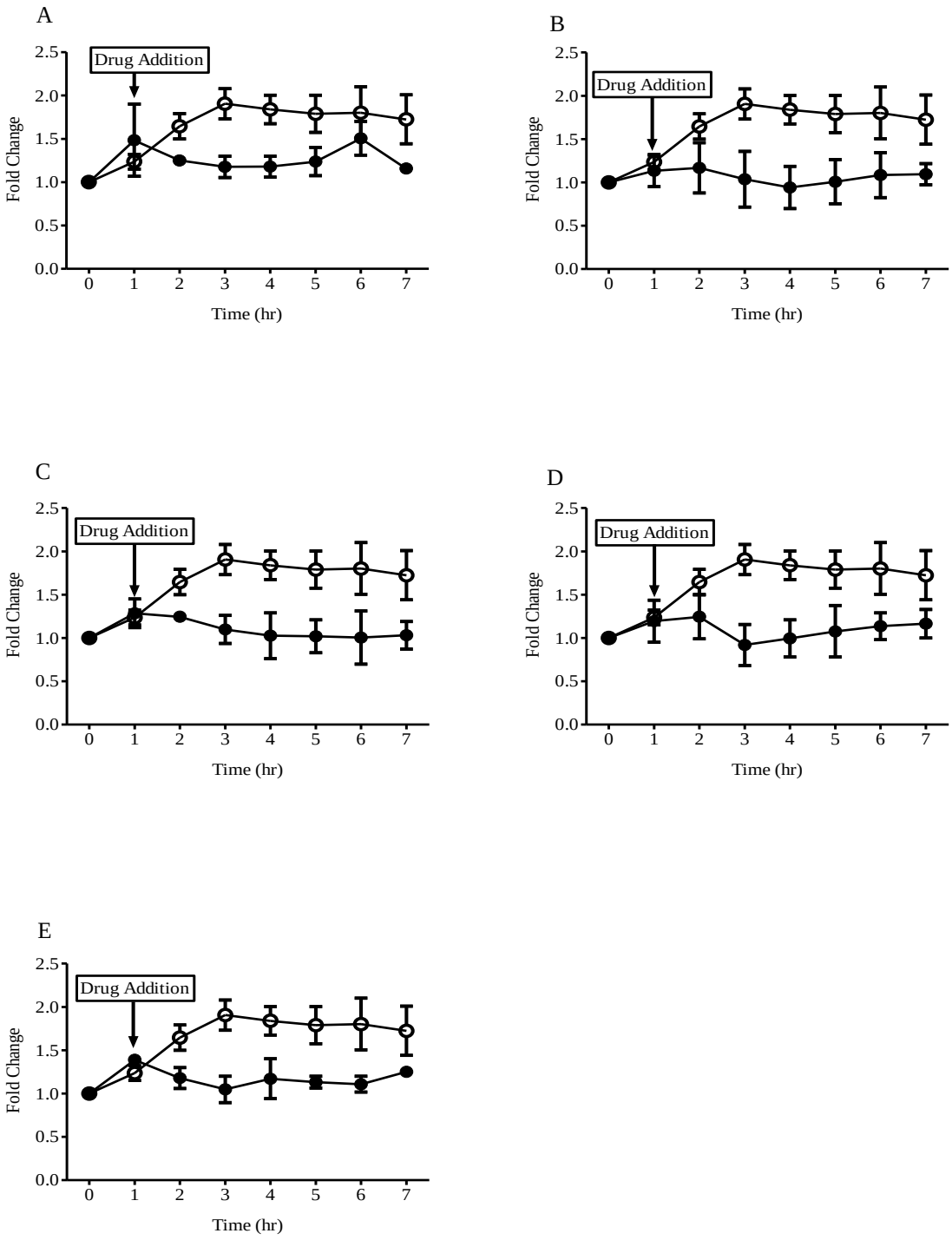

Figure 7.22. Time-dependent curves of glutamate in drug-treated and untreated *P. falciparum* 3D7 parasites.

Glutamate levels were determined in untreated (open circle) and drug-treated (closed circle) *P.falciparum* trophozoite-stage parasites by LC-MS/MS. Notable invariable changes were observed in glutamate after one hour of incubation in parasites treated with (A) 50 nM chloroquine, (B) 50 nM amodiaquine, (C) 80 nM piperaquine, (D) 100 nM quinine and (E) 50 nM mefloquine. Data represent the mean ± SEM of at least duplicate independent experiments.

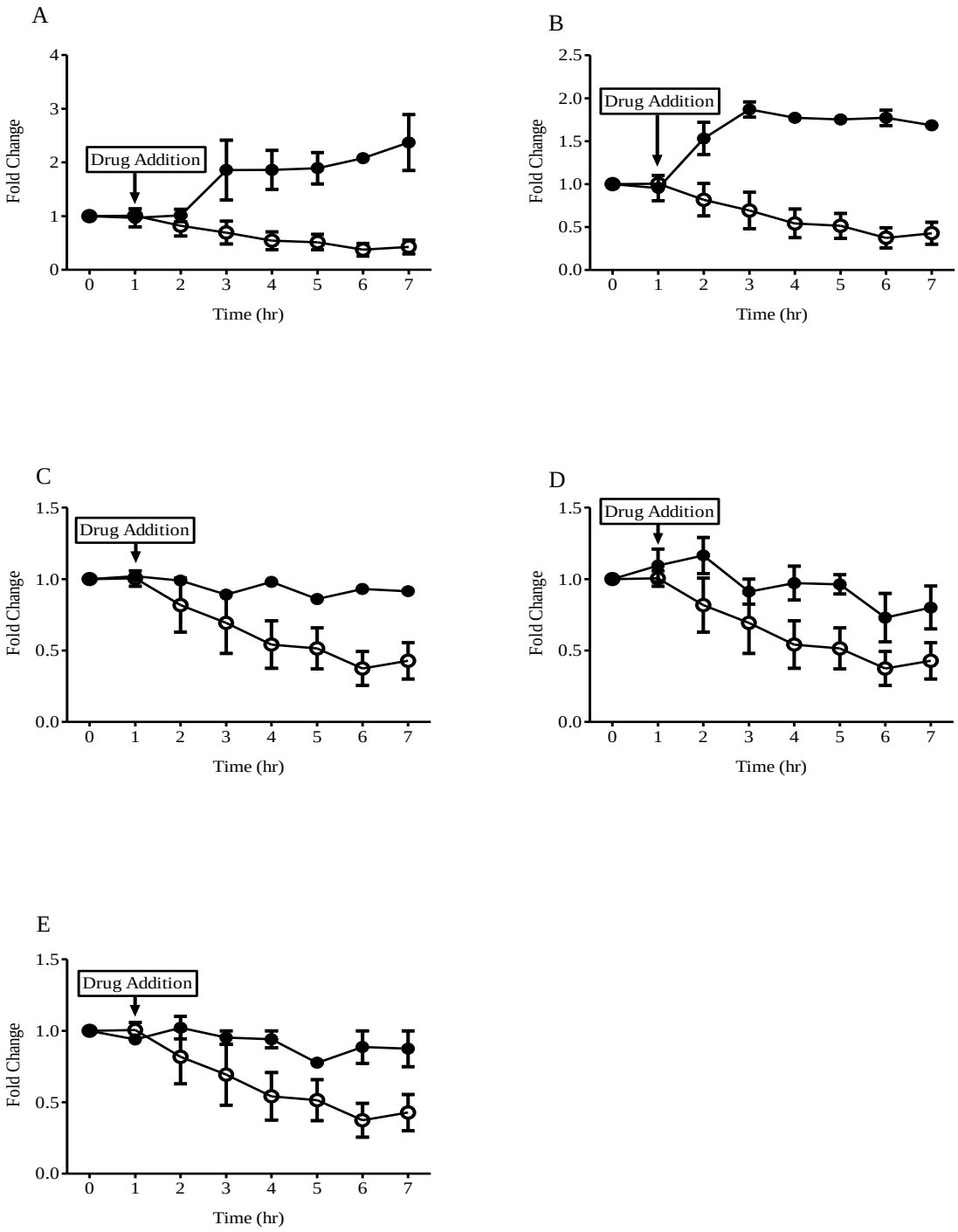

Figure 7.23. Time-dependent curves of asparagine in drug-treated and untreated *P. falciparum* 3D7 parasites.

Asparagine levels were determined in untreated (open circle) and drug-treated (closed circle) *P.falciparum* trophozoite-staged parasites by LC-MS/MS. Data showed little or no utilization of asparagine after one hour of incubation in parasites treated with (A) 50 nM chloroquine and (B) 50 nM amodiaquine. Significant invariable changes was observed in parasites treated with (C) 80 nM piperaquine, (D) 100 nM quinine and (E) 50 nM mefloquine. Data represent the mean ± SEM of at least duplicate independent experiments.

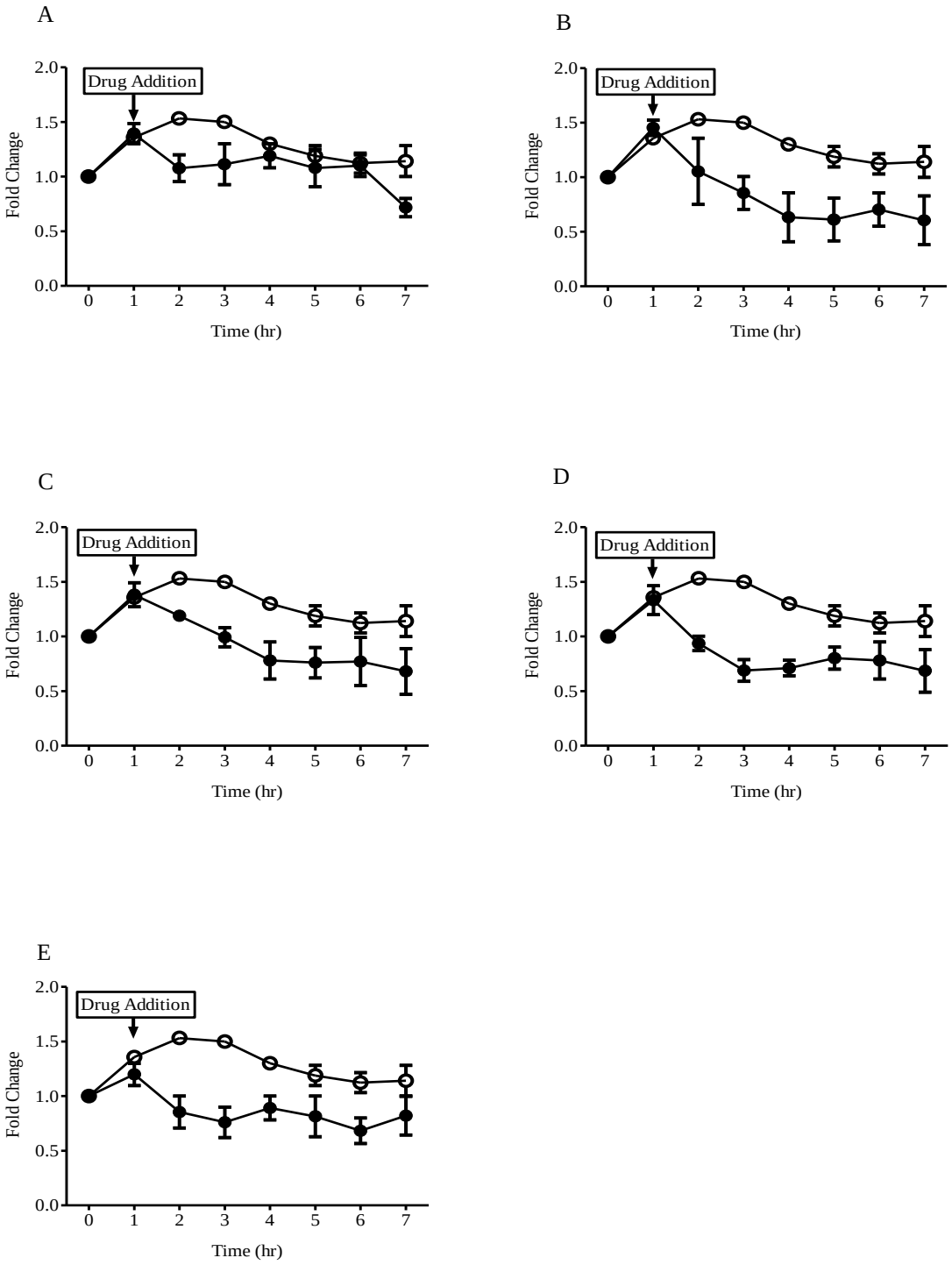

Figure 7.24. Time-dependent curves of aspartate in drug-treated and untreated *P. falciparum* 3D7 parasites.

Aspartate levels were determined in untreated (open circle) and drug-treated (closed circle) *P.falciparum* trophozoite-stage parasites by LC-MS/MS. Data showed a notable reduction of aspartate levels after one hour of incubation in parasites treated with (A) 50 nM chloroquine, (B) 50 nM amodiaquine, (C) 80 nM piperaquine, (D) 100 nM quinine and (E) 50 nM mefloquine. Data represent the mean ± SEM of at least duplicate independent experiments.

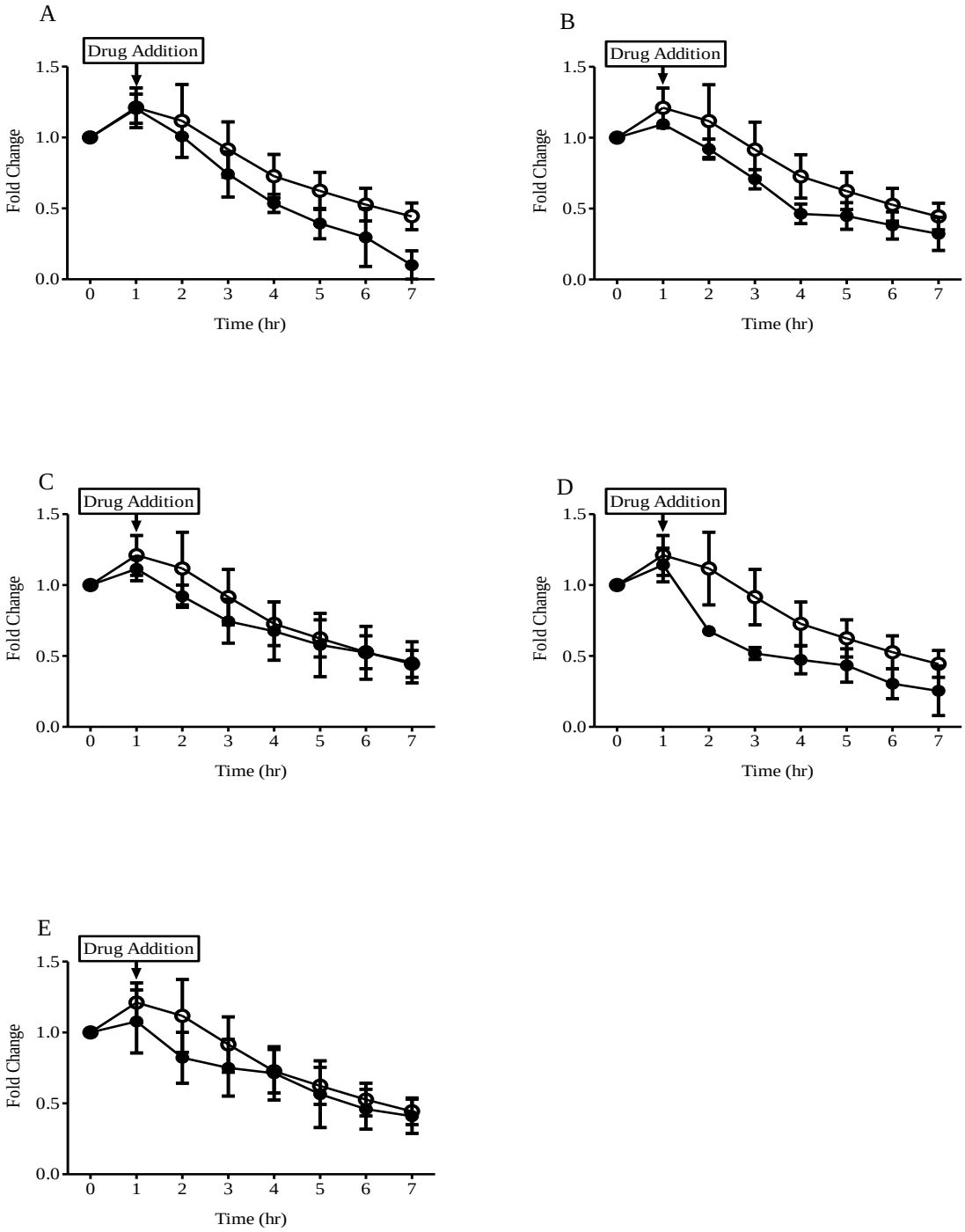

Figure 7.25. Time-dependent curves of arginie degradation in drug-treated and untreated *P. falciparum* 3D7 parasites.

Arginine degradation levels were measured in untreated (open circle) and drug-treated (closed circle) *P. falciparum* trophozoite-stage parasites by LC-MS/MS. The following drugs were added to the parasites after one hour of incubation (A) 50 nM chloroquine, (B) 50 nM amodiaquine, (C) 80 nM piperaquine, (D) 100 nM quinine and (E) 50 nM mefloquine. There were no obvious changes observed between drugs-treated and untreated parasites. The points represent the mean ± SEM of at least duplicate independent experiments.

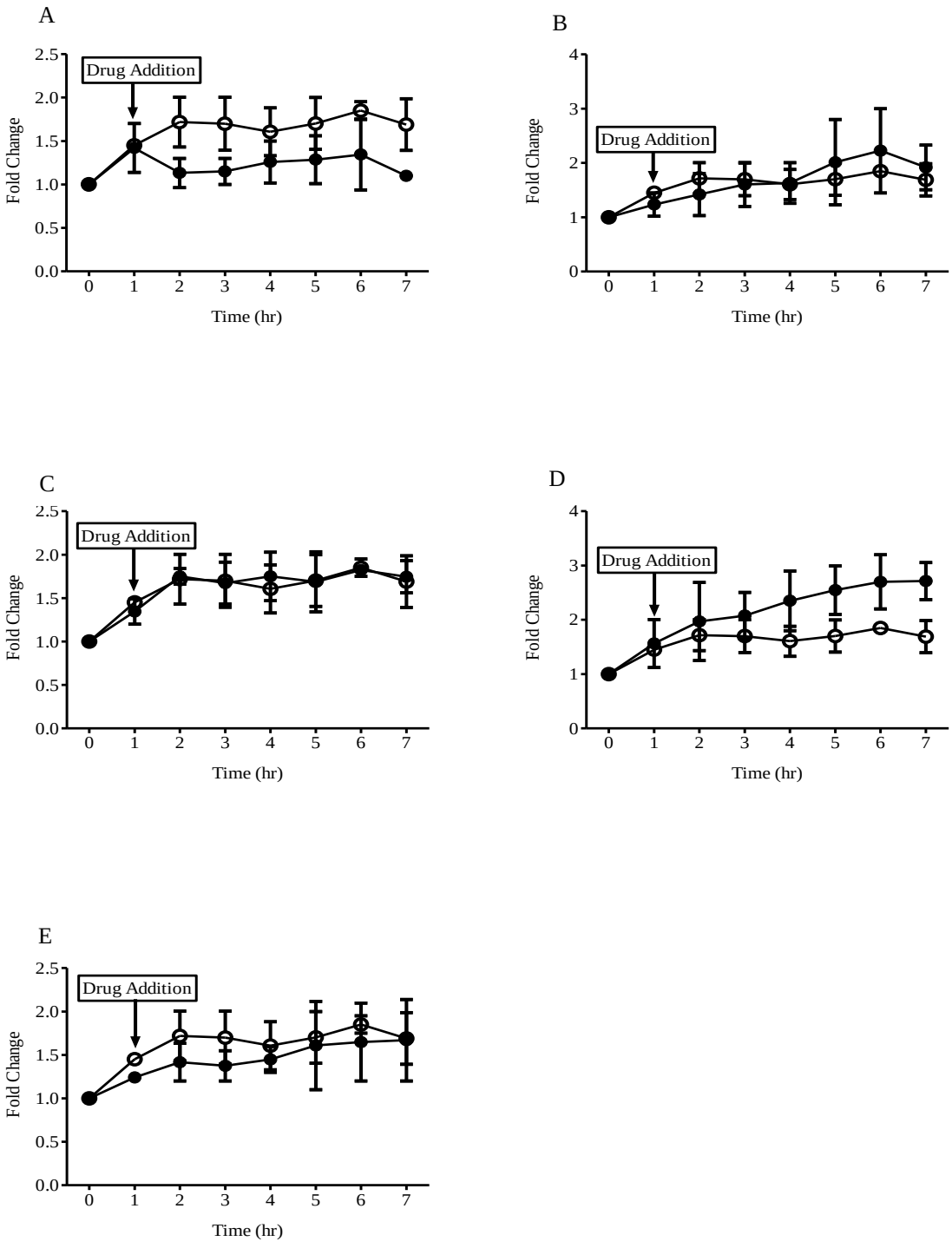

Figure 7.26. Time-dependent curves of proline in drug-treated and untreated *P. falciparum* 3D7 parasites.

Proline levels were determined in untreated (open circle) and drug-treated (closed circle) *P. falciparum* trophozoite-stage parasites by LC-MS/MS. The following drugs were added to the parasites after one hour of incubation (A) 50 nM chloroquine, (B) 50 nM amodiaquine, (C) 80 nM piperaquine, (D) 100 nM quinine and (E) 50 nM mefloquine. There were no obvious changes observed between drugs-treated and untreated parasites. The points represent the mean ± SEM of at least duplicate independent experiments.

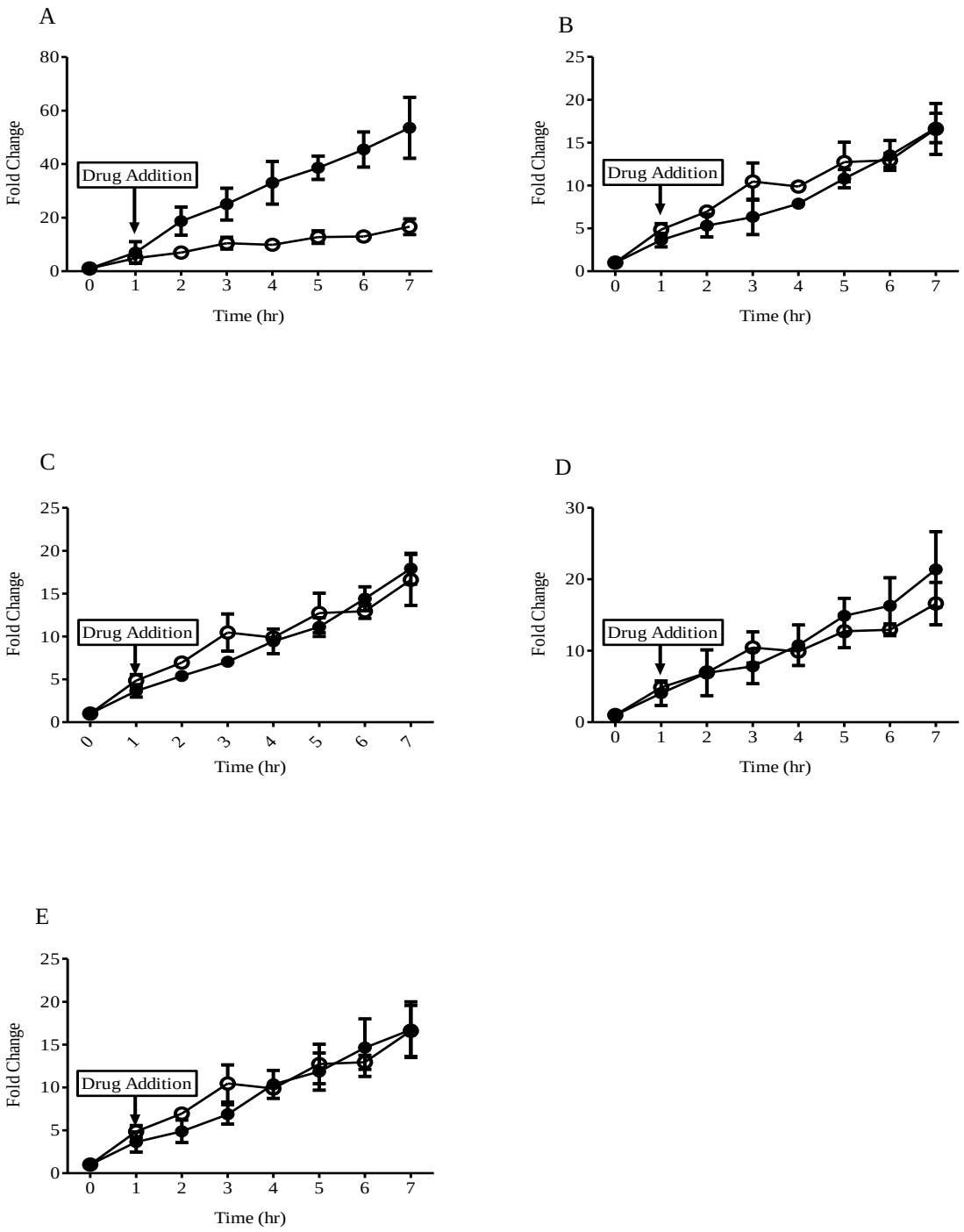

Figure 7.27. Time-dependent curves of ornithine production in drug-treated and untreated *P. falciparum* 3D7 parasites.

Ornithine levels were determined in untreated (open circle) and drug-treated (closed circle) *P. falciparum* trophozoite-stage parasites by LC-MS/MS. The following drugs were added to the parasites after one hour of incubation (A) 50 nM chloroquine, (B) 50 nM amodiaquine, (C) 80 nM piperaquine, (D) 100 nM quinine and (E) 50 nM mefloquine. Data showed a distinguished accumulation of ornithine in parasites treated with (A) 50 nM chloroquine but not with other drugs treated as compared to untreated. The points represent the mean ± SEM of at least duplicate independent experiments.

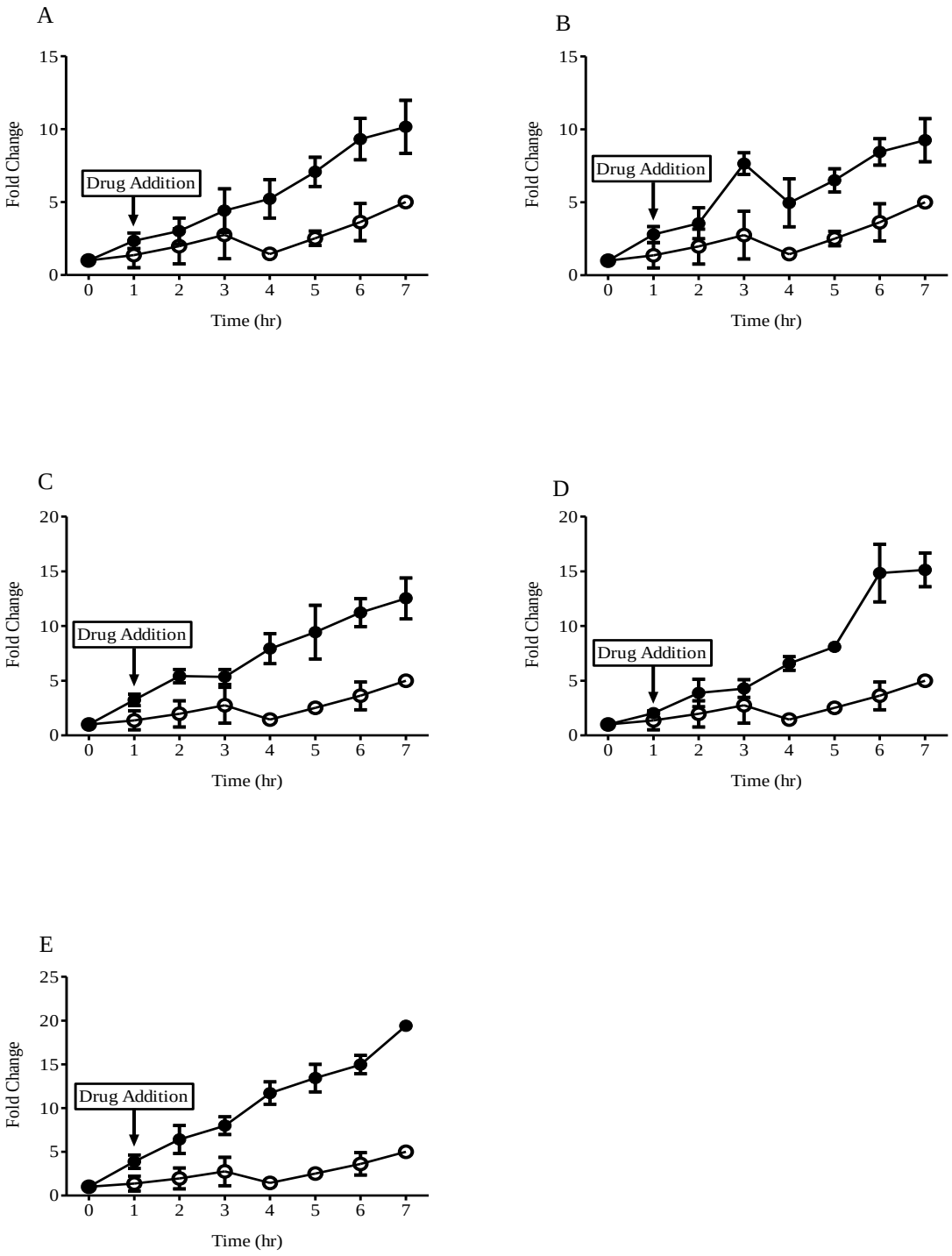

Figure 7.28. Time-dependent curves of citrulline in drug-treated and untreated *P. falciparum* 3D7 parasites.

The citrulline levels were determined in untreated (open circle) and drug-treated (closed circle) *P. falciparum* trophozoite-stage parasites by LC-MS/MS. Data showed a notable accumulation of citrulline after one hour of incubation in parasites treated with (A) 50 nM chloroquine, (B) 50 nM amodiaquine, (C) 80 nM piperaquine, (D) 100 nM quinine and (E) 50 nM mefloquine. Data represent the mean ± SEM of at least duplicate independent experiments.

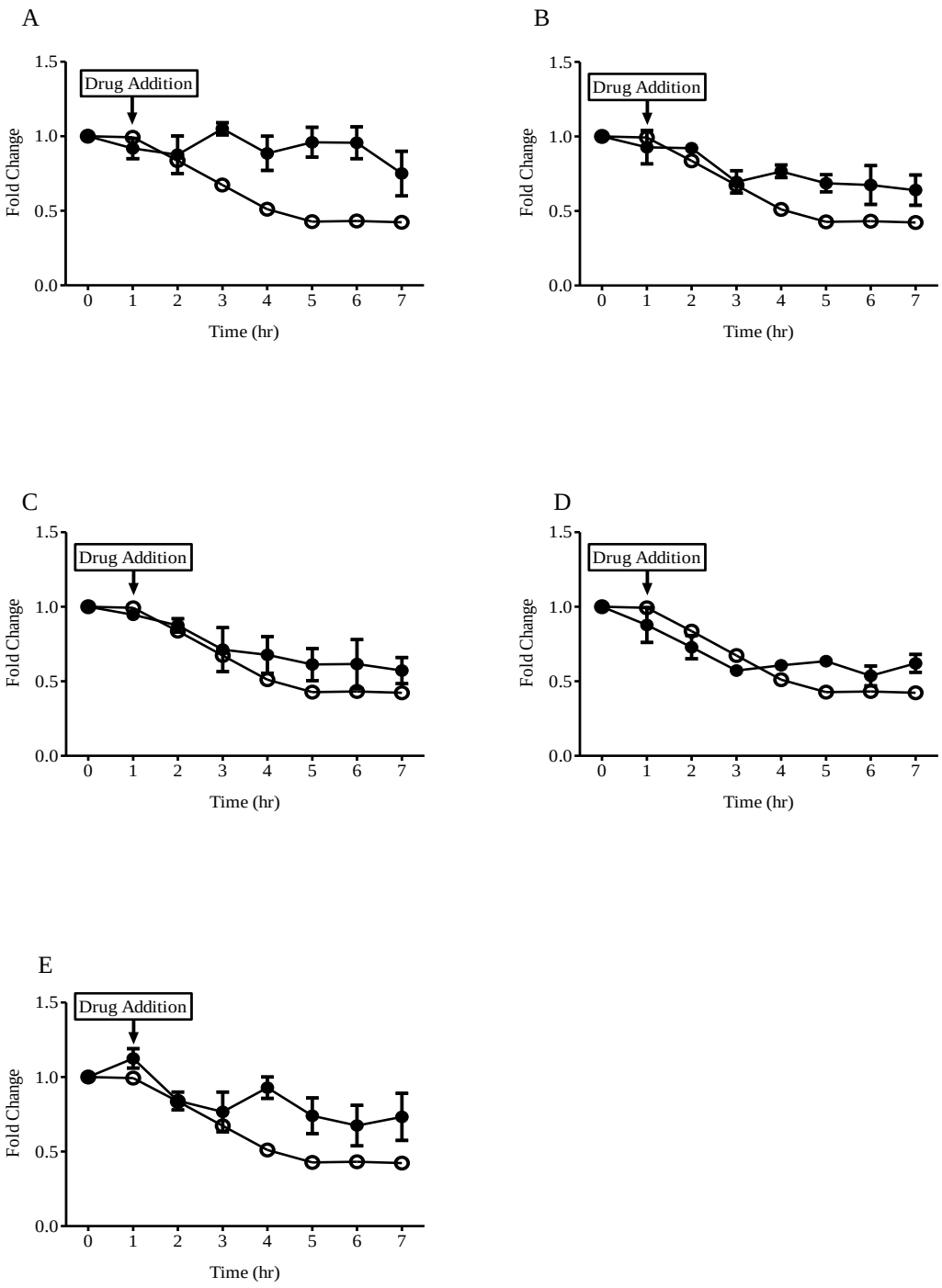

Figure 7.29. Time-dependent curves of methionine in drug-treated and untreated *P. falciparum* 3D7 parasites.

Methionine levels were determined in untreated (open circle) and drug-treated (closed circle) *P.falciparum* trophozoite-stage parasites by LC-MS/MS. Data showed little or no utilization of methionine levels after one hour of incubation in parasites treated with (A) 50 nM chloroquine. No obviuos changes were observed in parasites treated with (B) 50 nM amodiaquine, (C) 80 nM piperaquine, (D) 100 nM quinine and (E) 50 nM mefloquine. Data represent the mean ± SEM of at least duplicate independent experiments.

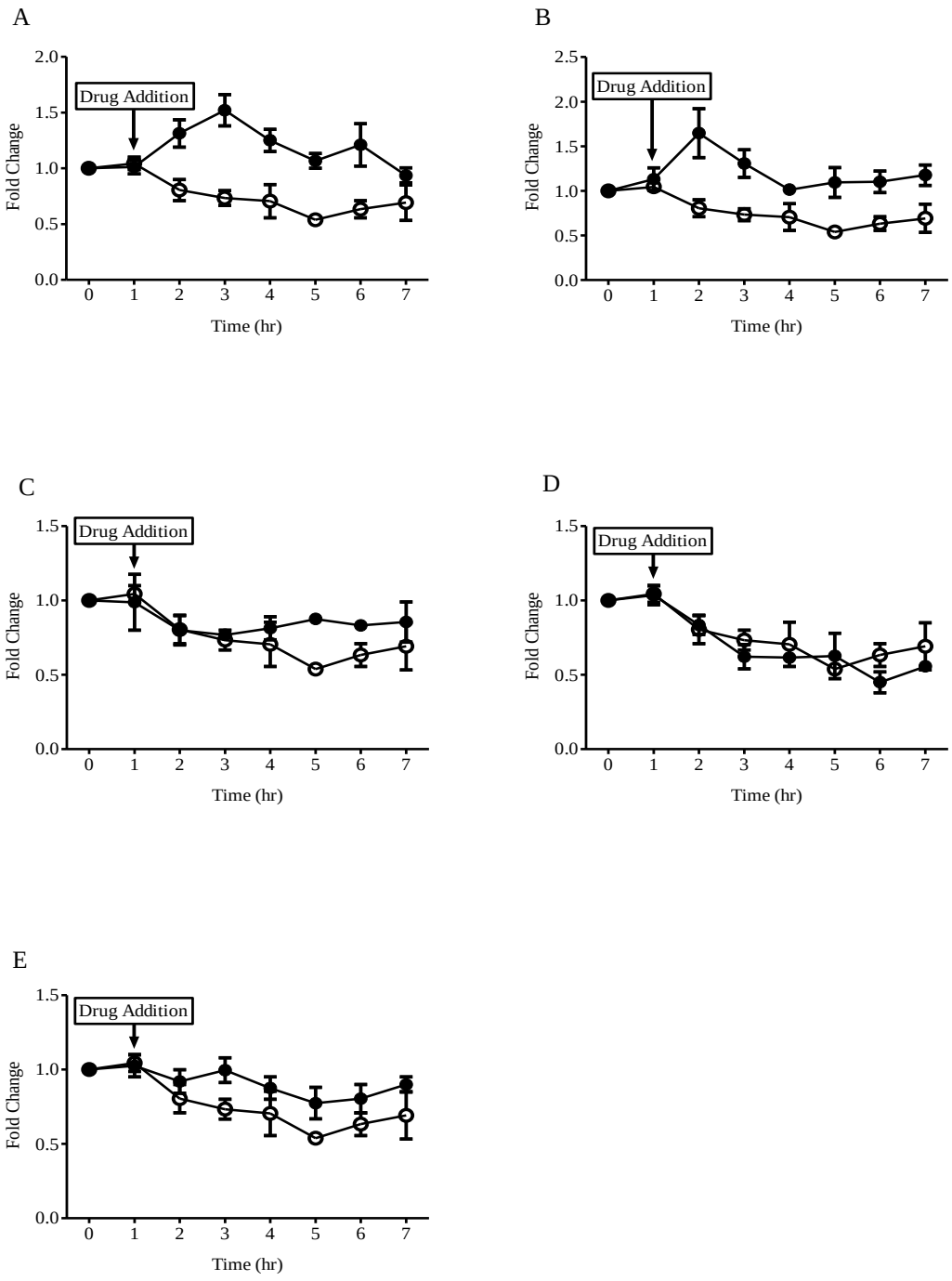

Figure 7.30. Time-dependent curves of lysine degradation in drug-treated and untreated *P. falciparum* 3D7 parasites.

Lysine degredation levels were determined in untreated (open circle) and drug-treated (closed circle) *P. falciparum* trophozoite-stage parasites by LC-MS/MS. Data showed little or no utilization of lysine after one hour of incubation in parasites treated with (A) 50 nM chloroquine and (B) 50 nM amodiaquine. Parasites treated with (C) 80 nM piperaquine, (D) 100 nM quinine and (E) 50 nM mefloquine showed no clear changes. Data represent the mean ± SEM of at least duplicate independent experiments.

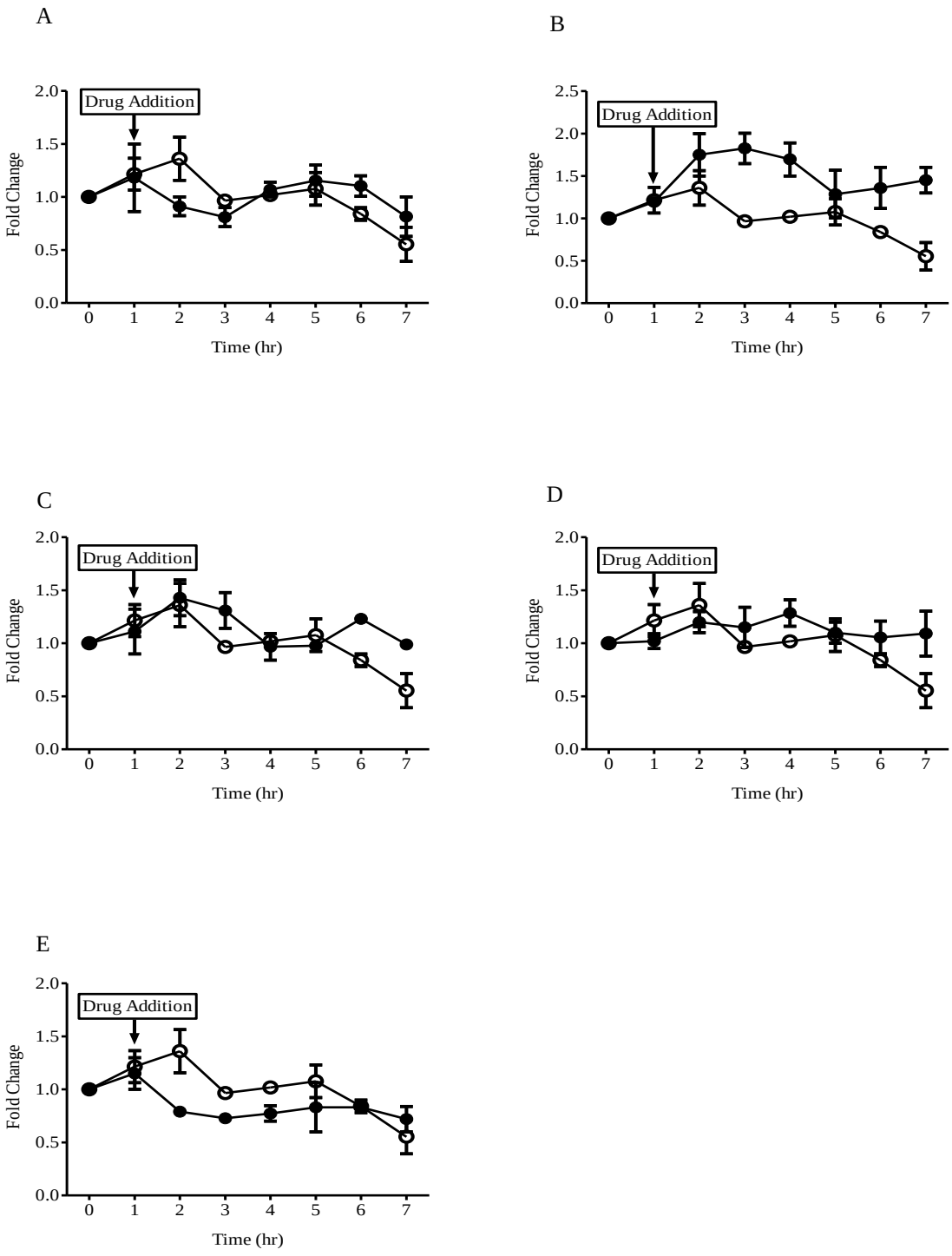

Figure 7.31. Time-dependent curves of serine in drug-treated and untreated *P. falciparum* 3D7 parasites.

Serine levels were determined in untreated (open circle) and drug-treated (closed circle) *P. falciparum* trophozoite-stage parasites by LC-MS/MS. The following drugs were added to the parasites after one hour of incubation (A) 50 nM chloroquine, (B) 50 nM amodiaquine, (C) 80 nM piperaquine, (D) 100 nM quinine and (E) 50 nM mefloquine. There were clear changes observed among drugs-treated parasites as compared to untreated. The points represent the mean ± SEM of at least duplicate independent experiments.

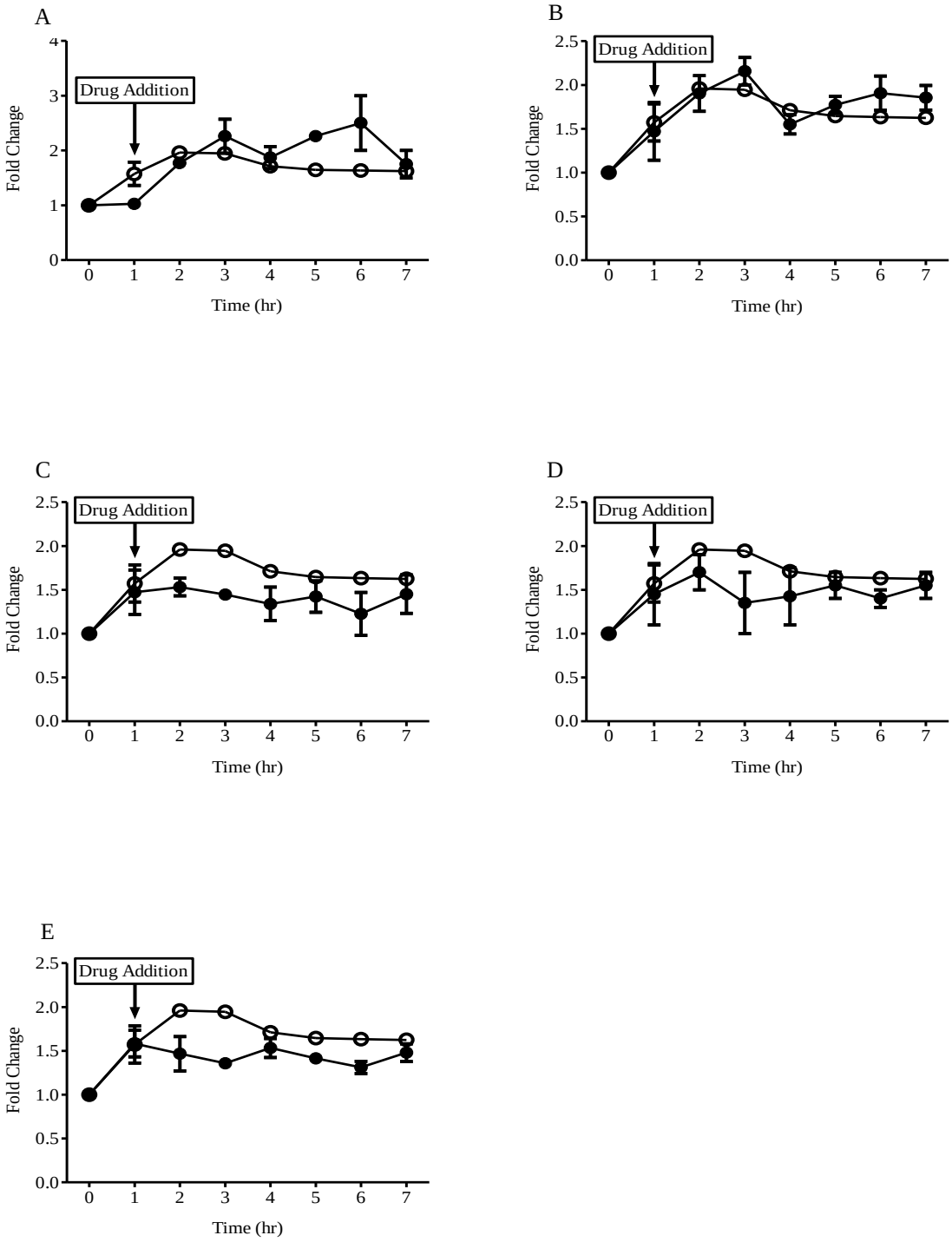

Figure 7.32. Time-dependent curves of histidine in drug-treated and untreated *P. falciparum* 3D7 parasites.

Histidine levels were determined in untreated (open circle) and drug-treated (closed circle) *P. falciparum* trophozoite-stage parasites by LC-MS/MS. The following drugs were added to the parasites after one hour of incubation (A) 50 nM chloroquine, (B) 50 nM amodiaquine, (C) 80 nM piperaquine, (D) 100 nM quinine and (E) 50 nM mefloquine. There were clear changes observed among drugs-treated parasites as compared to untreated. The points represent the mean ± SEM of at least duplicate independent experiments.

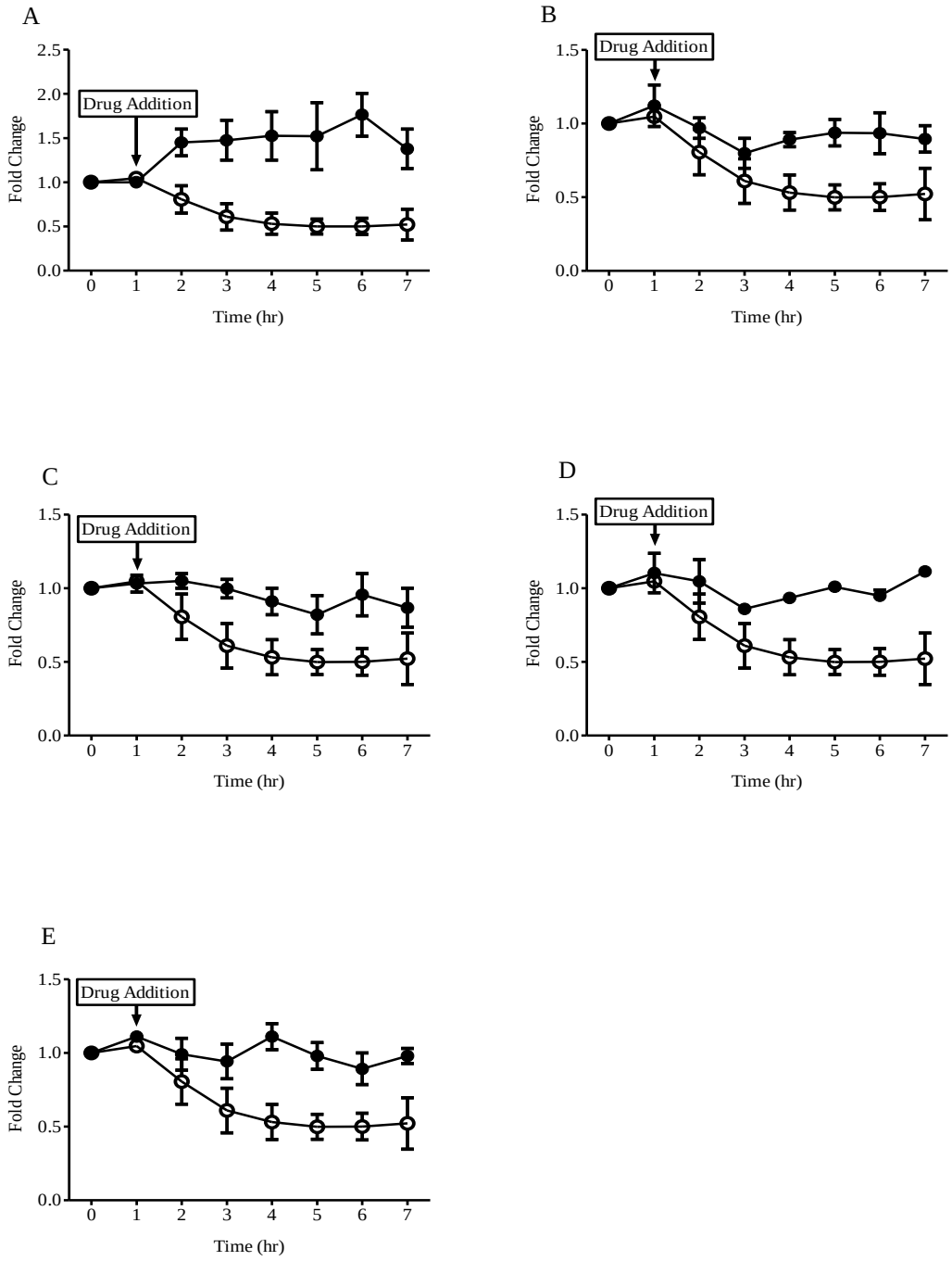

Figure 7.33. Time-dependent curves of phenylalanine in drug-treated and untreated *P. falciparum* 3D7 parasites.

Phenylalanine levels were determined in untreated (open circle) and drug-treated (closed circle) *P.falciparum* trophozoite-stage parasites by LC-MS/MS. Phenylalanine was slightly accumulated after one hour of incubation in parasites treated with (A) 50 nM chloroquine. Parasites treated with (B) 50 nM amodiaquine, (C) 80 nM piperaquine, (D) 100 nM quinine, (E) 50 nM mefloquine showed little or no utilization of phenylalanine as compared to untreated. Data represent the mean ± SEM of at least duplicate independent experiments.

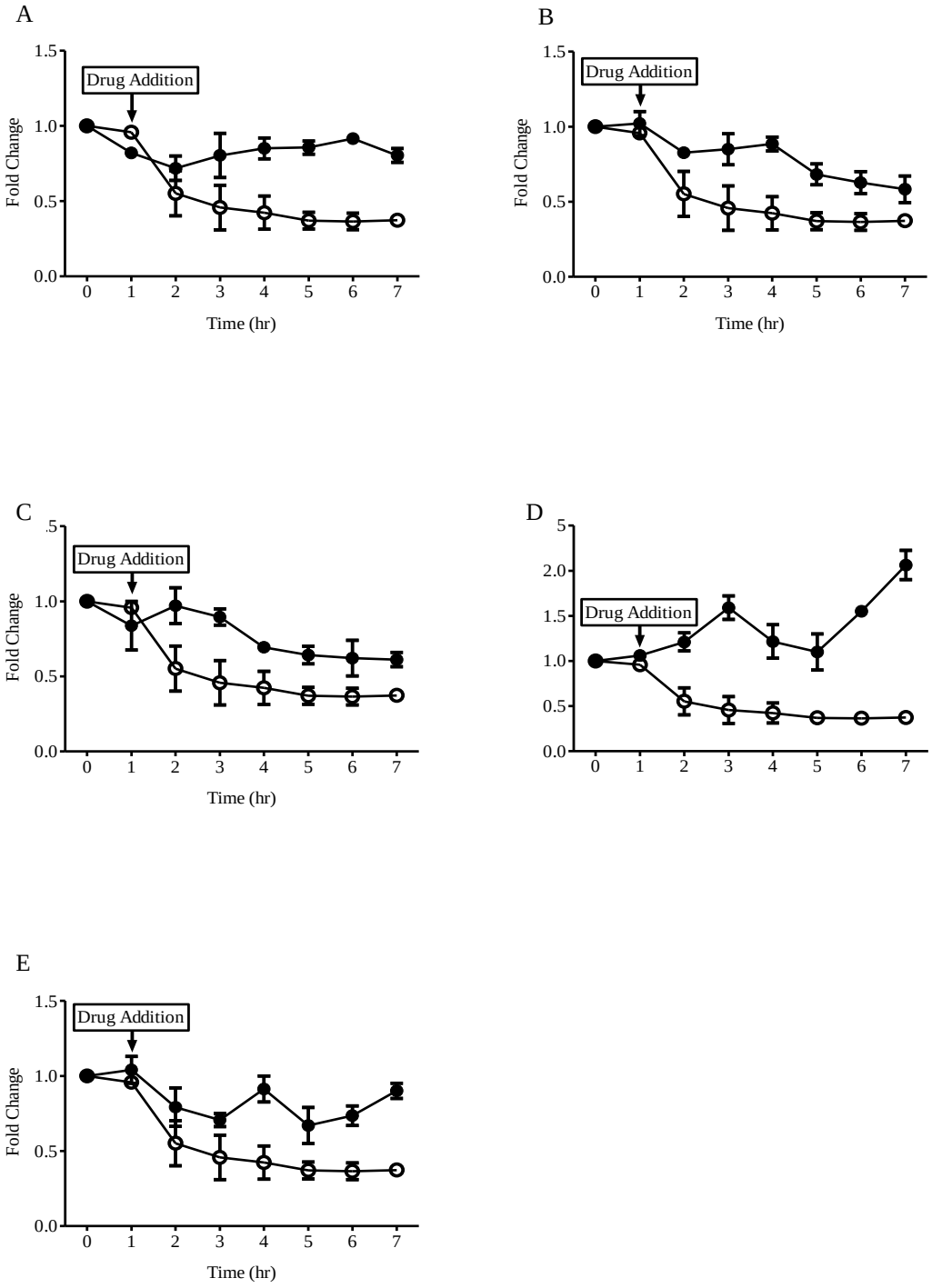

Figure 7.34. Time-dependent curves of tryptophan in drug-treated and untreated *P. falciparum* 3D7 parasites.

Tryptophan levels were determined in untreated (open circle) and drug-treated (closed circle) *P. falciparum* trophozoite-stage parasites by LC-MS/MS. Data showed a notable accumulation of tryptophan levels after one hour of incubation in parasites treated with (D) 100 nM quinine. Parasites treated with (A) 50 nM chloroquine, (B) 50 nM amodiaquine, (C) 80 nM piperaquine and (E) 50 nM mefloquine illustrated little or no utilization of tryptophan as compared to untreated. Data represent the mean ± SEM of at least duplicate independent experiments.

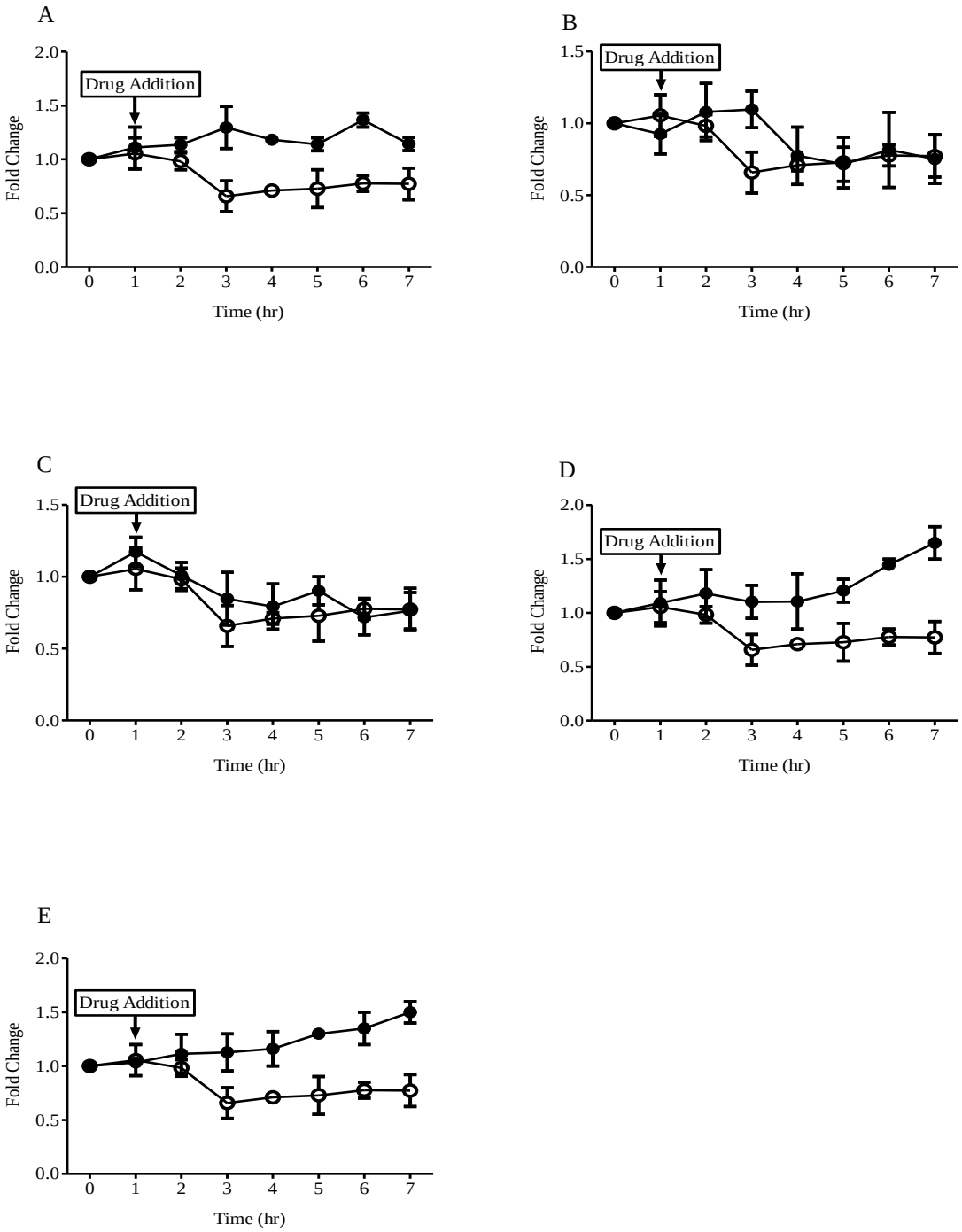

Figure 7.35. Time-dependent curves of tyrosine in drug-treated and untreated *P. falciparum* 3D7 parasites.

Tyrosine levels were determined in untreated (open circle) and drug-treated (closed circle) *P. falciparum* trophozoite-stage parasites by LC-MS/MS. Data showed a notable increasing trend of tyrosine after one hour of incubation in parasites treated with (A) 50 nM chloroquine, (D) 100 nM quinine and (E) 50 nM mefloquine. Parasites treated with (B) 50 nM amodiaquine, (C) 80 nM piperaquine illustrated no obvious changes as compared to untreated. Data represent the mean ± SEM of at least duplicate independent experiments.

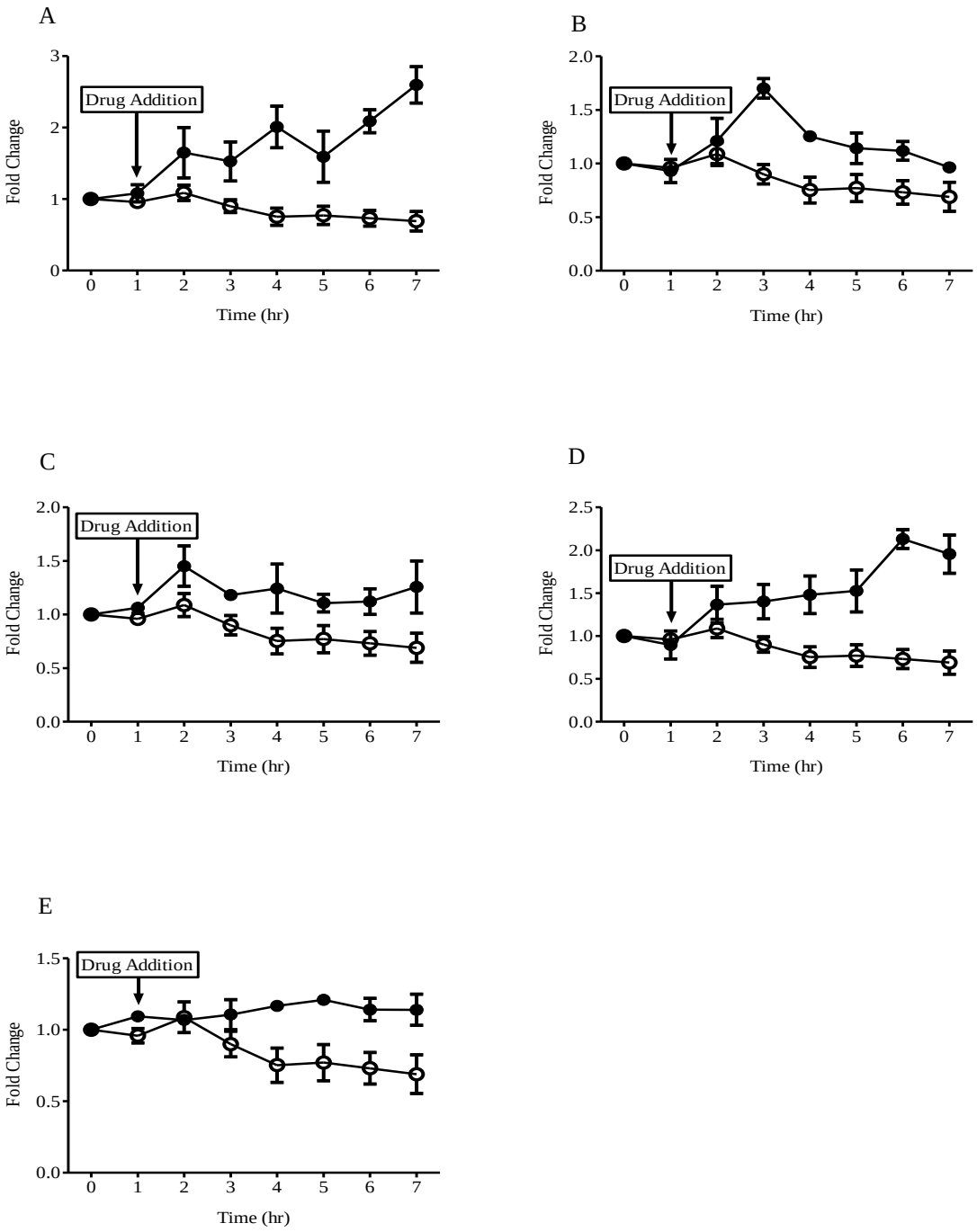

Figure 7.36. Time-dependent curves of threonine in drug-treated and untreated *P. falciparum* 3D7 parasites.

Threonine levels were determined in untreated (open circle) and drug-treated (closed circle) *P.falciparum* trophozoite-staged parasites by LC-MS/MS. Data showed a notable increase in the threonine levels after one hour of incubation in parasites treated with (A) 50 nM chloroquine and (D) 100 nM quinine whereas little or no utilization was observed in parasites treated with (B) 50 nM amodiaquine, (C) 80 nM piperaquine and (E) 50nM mefloquine as compared to untreated. Data represent the mean ± SEM of at least duplicate independent experiments.

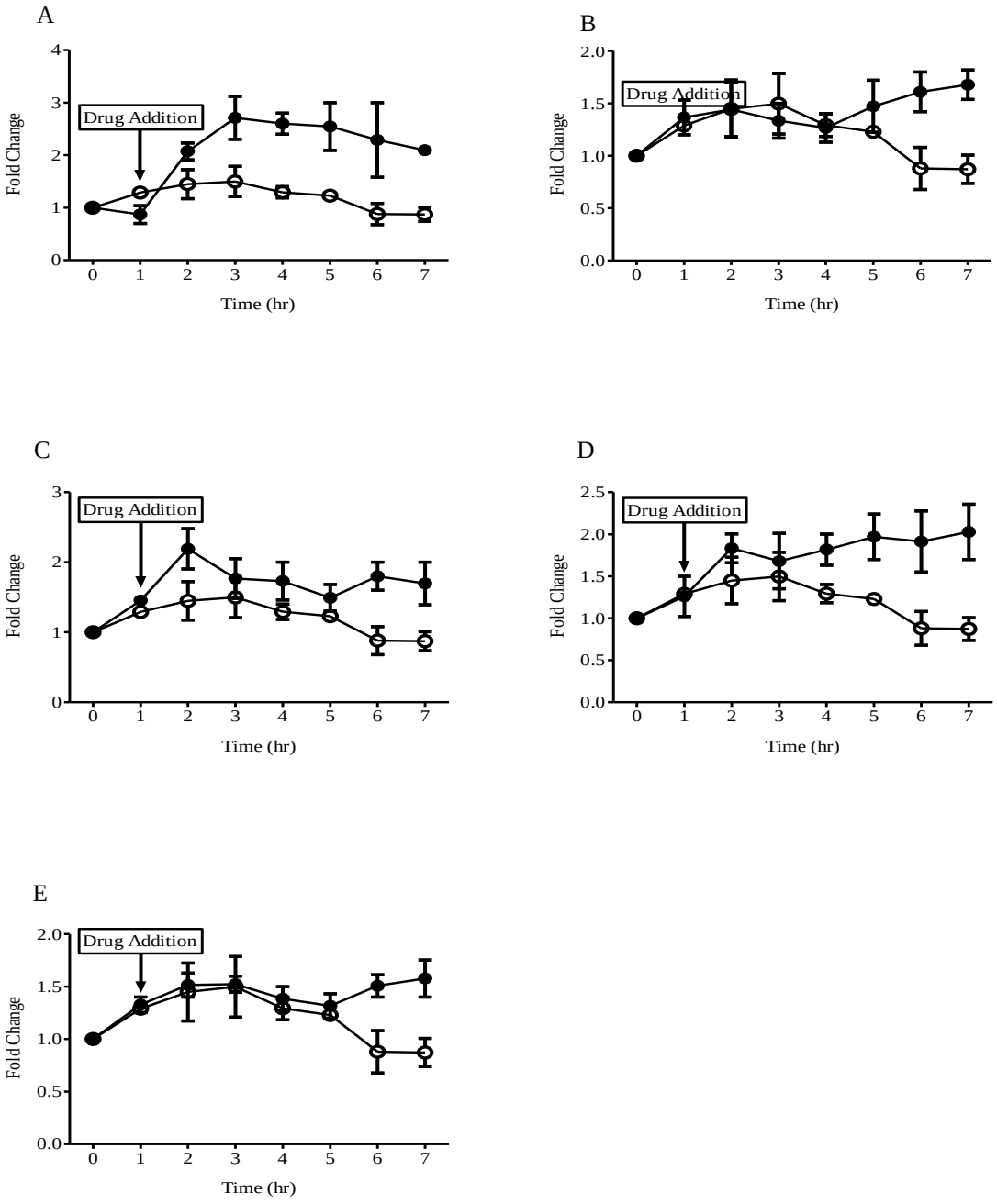

Figure 7.37. Time-dependent curves of valine in drug-treated and untreated *P. falciparum* 3D7 parasites.

Valine levels were determined in untreated (opened circle) and drug-treated (closed circle) *P.falciparum* trophozoite-staged parasites by LC-MS/MS. Data showed a notable increase in the valine level by at least 0.5 fold at 7 hr time point as compared to untreated in parasites treated with (A) 50 nM chloroquine, (B) 50 nM amodiaquine, (C) 80 nM piperaquine (D) 100 nM quinine and (E) 50 nM mefloquine. Data represent the mean ± SEM of at least duplicate independent experiments.

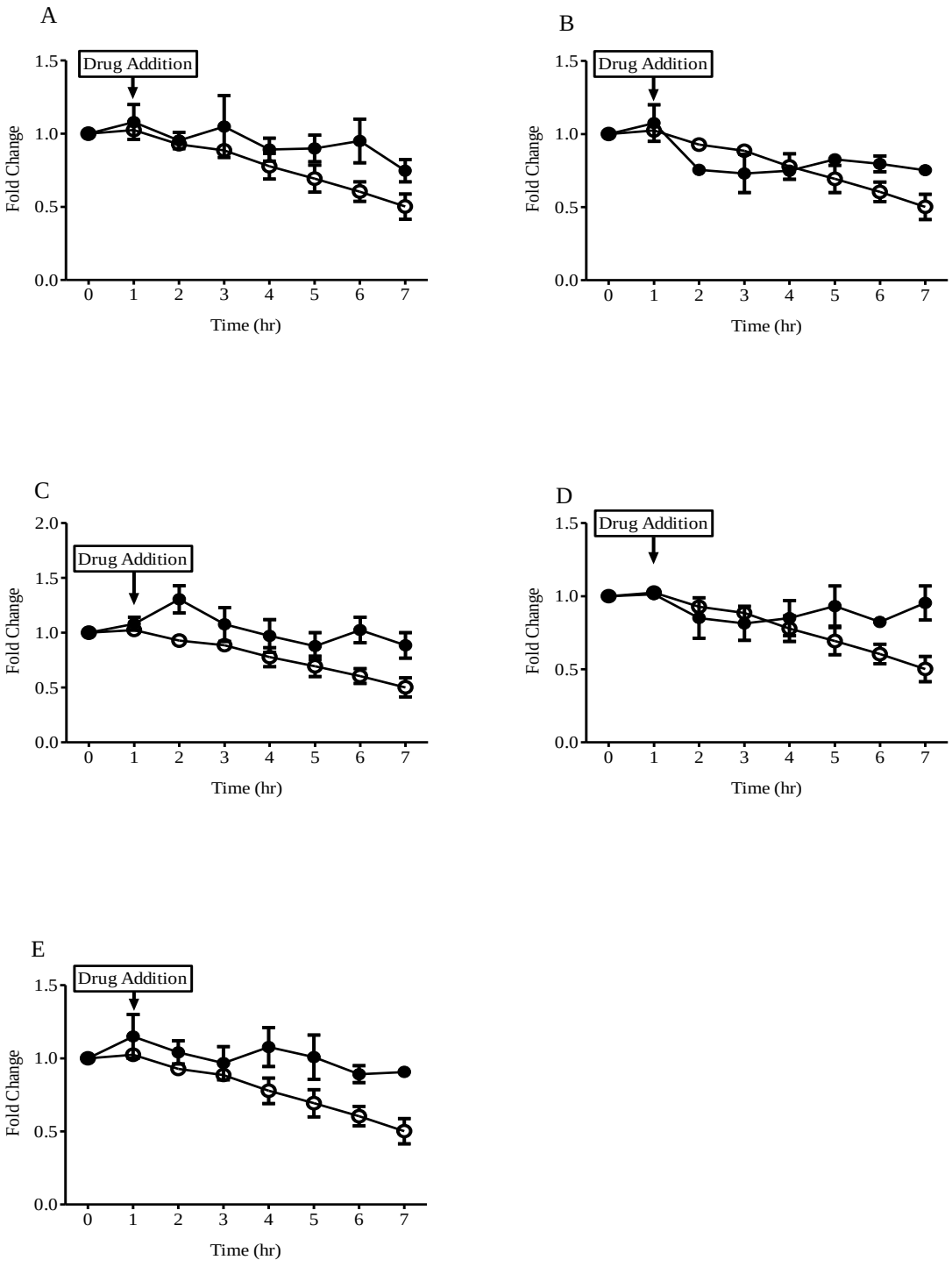

Figure 7.38. Time-dependent curves of (iso)-leucine in drug-treated and untreated *P. falciparum* 3D7 parasites.

The (iso)-leucine levels were determined in untreated (open circle) and drug-treated (closed circle) *P.falciparum* trophozoite-staged parasites by LC-MS/MS. The following drugs were added to the parasites after one hour of incubation (A) 50 nM chloroquine, (B) 50 nM amodiaquine, (C) 80 nM piperaquine, (D) 100 nM quinine and (E) 50 nM mefloquine. There were no obvious changes observed between drugs-treated and untreated parasites. The points represent the mean ± SEM of at least duplicate independent experiments.

7.4. Discussion

In this chapter, a pharmacometabolomics approach was used to determine the MoA of quinoline-containing antimalarial drugs (QCDs) in order to study the role of digestive vacuole in *P. falciparum*. Two classes of QCDs, including type-1 drugs 4-aminoquinolines and type-2 drugs aryl-amino alcohols, were investigated in this study. Type-1 drugs 4-aminoquinolines include chloroquine, amodiaquine and piperaquine while type-2 drugs aryl-amino alcohols include quinine and mefloquine. The metabolomics analysis performed using PCA and PLS-DA demonstrated interesting findings. The 2-D of PCA showed the divergence of two main clusters including one cluster of untreated *P. falciparum* parasite and another cluster of *P. falciparum* parasite treated with chloroquine, amodiaquine, piperaquine, quinine and mefloquine. This finding showed clearly that the parasite metabolism phenotype was altered upon apparently the perturbation caused by the addition of QCD members. The 3-D of PCA showed better representation and positioning of the drugs-treated and untreated parasites points. It demonstrated that the cluster of parasite treated with chloroquine was distinctly separated from the clusters of untreated parasites and parasites treated with amodiaquine, piperaquine, quinine and mefloquine. This finding suggests that the MoA of chloroquine is different from that of amodiaquine, piperaquine, quinine and mefloquine. Nonetheless, further discriminate analysis (PLS-DA) was conducted to investigate whether the MoA of QCD members are similar or at least related. Interestingly, the findings of 2-D and 3-D PLS-DA showed the separation of five main clusters. These include cluster of parasites treated with chloroquine, cluster of parasite treated with amodiaquine, clusters of parasites treated with piperaquine and mefloquine, cluster of parasites treated with quinine and cluster of untreated parasites. These results showed clearly that the MoA of QCD members, including chloroquine, amodiaquine, piperaquine, quinine and mefloquine, is probably drug class dependent. Specifically, it appears that the parasites treated with chloroquine and amodiaquine had their clusters together in the 2-D and 3-D PLS-DA plots. This indicates that chloroquine and amodiaquine had a similar MoA effects on the parasite because they are from the same drug class. In contrast, parasites treated with quinine had its cluster in different direction of those treated with chloroquine and amodiaquine suggesting that quinine had different effects on parasites than other members of QCD. However, it was noteworthy that although parasites treated with two different drugs class; including piperaquine and

mefloquine, of QCDs had their clusters overlapping each other suggesting perhaps the commonality in the MoA of both antimalarial drugs. This finding is of particular interest as it indicates that piperaquine, bisquinolines, and mefloquine shared possibly a common target.

Moreover, the VIP score plot showed that the most important metabolites that had VIP score > 1 were alanine, asparagine, glutamine, lysine, orotate, DHAP and citrulline indicating that the effects of QCD are involved in the disruption of more than one metabolic pathway which may include the haemoglobin digestion, glycolysis pathway, pyrimidine biosynthesis and perhaps exogenously acquired amino acids. The hypothesis of the interaction of chloroquine and perhaps other QCD members with haemoglobin digestion is supported by other studies that have provided evidence of undigested haemoglobin in parasites treated with chloroquine (Krugliak et al., 2002, Roberts et al., 2008, Yayon et al., 1984c). It has been ultra-structurally demonstrated that chloroquine inhibited the last step of the feeding process (i.e. vacuolar degradation) in trophozoite stage of *P. falciparum* manifested by the accumulation of intact vesicles bounded by single membranes within the vacuolar space (Yayon et al., 1984c). In addition, a recent study has shown an increase in free heme and decrease in hemozoin upon quinoline-related antimalarials exposure to *P. falciparum* parasites (Combrinck et al., 2013). However, this increase and decrease in heme and hemozoin, respectively, is significantly less than that for parasites treated with chloroquine (Combrinck et al., 2013). This either indicates the multiple MoA of these drugs and/or differences in the toxicity of heme-drug complexes (Combrinck et al., 2013). This indication is supported by the metabolomic findings obtained for parasites treated with different members of QCD demonstrating clear discrimination and clustering of each drug being used. In addition, it was also demonstrated by the biochemical time-dependent result that following the addition of chloroquine, amodiaquine, piperaquine, quinine and mefloquine to *P. falciparum* parasites, the level of glutamate was noticeably invariable. This finding suggests that the MoA effect of these drugs paralyzed the metabolism of glutamate which might be as well affecting other metabolic pathway linked to glutamate such as TCA cycle, pyrimidine *de novo* synthesis, CO_2 fixation process, protein synthesis, redox metabolism and porphyrin metabolism. Therefore, glutamate is this case could be regarded as a central hub to different metabolic network in the parasite. However, this hypothesis is required to be further analysed and confirmed using

bioinformatic tools for system biology (currently underway in the LSTM). Intriguingly, aspartate levels upon QCDs exposure were notably decreased which could be explained as the presence of high demand needed for making DNA and RNA under drug pressure as well as a transition state from trophozoite to schizont.

As noted in the introduction, amino acids such as glutamine, glutamate, cysteine, proline, tyrosine, (iso)-leucine and methionine are rare or absent in human haemoglobin (Divo et al., 1985a). Cysteine was below the limit of detection for the current metabolomics approach. Glutamine, glutamate, proline, tyrosine, (iso)-leucine and methionine were supplied in the culture media and it appears that the untreated parasite utilized some of these amino acids to conduct several metabolic biosynthetic pathways. In addition, It has been reported that the *P. falciparum* parasite digested up to 65% of the RBC haemoglobin but up to 16% of digested haemoglobin is converted to parasite protein (Krugliak et al., 2002). On the other hand, it has been shown previously that when radiolabelled RBCs were transfused into *P. lophurae*- and *P. berghei*-infected RBC and the parasites were allowed to invade and grow in these tagged RBC, the amino acids in the radioactive haemoglobin became incorporated into the parasite proteins (Sherman and Tanigosh.L, 1970, Theaksto.Rd et al., 1970). Therefore, given that pharmacometabolomic experiments were conducted on *P. falciparum* parasite incubated with culture media, it is probably that the availability of amino acids in the parasite cytosol is governed by a dynamic equilibrium between haemoglobin degradation, efflux of generated amino acids and influx of amino acids from the extracellular media in order to incorporate them into proteins and other metabolic pathways. Therefore, it appears that actions of quinoline-containing antimalarial drugs used in this study were primarily concerted on two main targets: haemoglobin degradation process in digestive vacuole and other amino acids metabolic pathways including amino acids acquisition through new permeability pathway (NPP). Indeed, chloroquine treated parasites showed a distinguished accumulation in ornithine suggesting that the MoA of chloroquine is also extended to the parasite cytosol which may further leads to inhibition of polyamine metabolism. This result is consistent with previous study showing that incubation of *P. falciparum*-iRBC with 1 µM chloroquine inhibited the ornithine decarboxylase activity by 63% as compared to untreated controls (Konigk and Putfarken, 1983). In addition, it has been suggested that free heme escapes from the digestive vacuole and is degraded in the parasite cytosol by reduced

glutathione (GSH) (Ginsburg et al., 1998). Therefore, it has been hypothesized that chloroquine and amodiaquine competes for this process leading to the disruption of parasite plasma membrane as free heme builds up in the cytosol (Ginsburg et al., 1998). This hypothesis was supported by the study showing that manipulation the external concentration of GSH alters the sensitivity of the parasite to chloroquine (Raj et al., 2009). Accordingly, methionine levels were notably not changed in chloroquine treated parasite as compared to untreated parasites indicating perhaps dual-inhibitions which include the blocking of polyamine synthesis by targeting ornithine decarboxylase and targeting the NPP preventing the accesses to the methionine available in the extracellular medium. Interestingly, citrulline levels were noticeably increased upon the addition of chloroquine, amodiaquine, piperaquine, quinine and mefloquine suggesting possibly the extensive production of nitric oxide (NO) via the oxidation of arginine to citrulline as a consequence of instant drug pressure. This was observed as well in the slightly excessive utilization of arginine in QCDs treated parasites particularly in the first few hours of the incubation as compared to untreated.

Furthermore, chloroquine and amodiaquine treated parasites showed little or no utilization of lysine particularly in the first few hours of incubation compared to untreated parasite control. This indicates the commonality in the MoA of chloroquine and amodiaquine possibly in targeting the same route of lysine metabolic pathway. There was also a notable increase in threonine levels following the addition of chloroquine and quinine as compared to untreated. However, parasites treated with chloroquine, amodiaquine, piperaquine, quinine and mefloquine showed a notable increase in the valine as compared to untreated. This indicates probably the direct or indirect involvement of chloroquine and quinine in the interference of metabolism of threonine and valine. However, it is difficult to explain or propose why there was such an effect seen on threonine and valine upon chlolorquine and quinine addition as well as for others QCD effects on valine; which are remained to be explored.

Moreover, the slight increase seen in the level of phenylalanine upon the addition of chloroquine suggesting its interaction with phenylalanine metabolism and/or transport. However, other members of QCDs including amodiaquine, piperaquine, quinine and mefloquine showed little or no utilization of phenylalanine indicating may be the less involvement in the interaction with phenylalanine. In addition, since chloroquine, an amphiphilic compound, is able to gain entry into cells without the assistance of

membrane transporters (Ferrari and Cutler, 1991), this may explains why other members of QCD had not shown a similar effect as chloroquine. Additionally, *P. falciparum* parasites treated with quinine showed remarkable accumulation in the level of tryptophan whereas those treated with chloroquine, amodiaquine, piperaquine and mefloquine showed little or no utilization of tryptophan. This finding suggests that these QCDs commonly interact with tryptophan but with different efficacy or activity. This is consistent with the recent study showing that quinine interferes with tryptophan metabolism in the malaria parasite and yeast model through inhibiting tryptophan uptake competitively (Islahudin et al., 2012, Khozoie et al., 2009). In addition, parasites treated with chloroquine, quinine and mefloquine showed a notable increase in tyrosine level but not with amodiaquine and piperaquine as compared to untreated parasites. As noted above, this may indicates the mode of chloroquine, quinine and mefloquine toxicity to the parasite resulting in the tyrosine starvation. This finding of tyrosine accumulation upon quinine exposure is consistent with the clinical study showing that the level of tyrosine in plasma of malaria patients increased ≥2- fold during quinine therapy (Islahudin et al., 2012).

The notable consumption of glucose, marginal elevation of phosphoenolpyruvate and lactate and the notable decrease and increase in DHAP and glycerol-3-phosphate, respectively, upon treating *P. falciparum* parasites with chloroquine, amodiaquine, piperaquine, quinine and mefloquine indicates that these QCD members may exert indirect MoA effect on glycolysis metabolic pathway and probably on glycerol-3-phosphate shuttle between cytosol and mitochondria. This indirect effect of these drugs might be resulted from the accumulation of free toxic heme leading to imbalance perturbation effect of metabolic system biology of the parasite. These findings are inconsistent with the previous studies carried out on *P. falciparum* (Menting et al., 1997, Read et al., 1999) and yeast (Lenz and Holzer, 1984) showing that chloroquine acts as competitive inhibitor in the NADH binding pocket of *P. falciparum* lactate dehydrogenase (*Pf* LDH) and it causes a rapid and drastic decrease of the ATP content of the yeast by preventing the fermentation of glucose and formation of ethanol, respectively. However, the concentration of chloroquine used in these studies (Lenz and Holzer, 1984, Read et al., 1999, Menting et al., 1997) was in the millimolar range while that of used in this study was in nanomolar range. Moreover, the variable (decrease and/or increase) notable changes seen in a number of TCA intermediates such as 2-

oxoglutarate, (iso)-citrate, succinate, oxaloacetate and malate as well as pyrimidine dihydroorotate intermediate following the QCDs addition to the *P. falciparum* parasite could be explained again as discussed above as an indirect effect of these QCD drugs.

Overall, it appears that *P. falciparum* digestive vacuole plays a pivotal role in maintaining the biological function of the parasite. It provides amino acids for protein synthesis that are responsible for cellular structure and function. However, this pharmacometabolomics study suggests that in addition to this, quinolone-based drugs are acting on the parasite cytosol and membrane which resulting in blocking other vital metabolic pathways leading to parasite death.

With regards to the limitation of this study, it is almost the same as the limitation discussed in the preceding chapters in terms of inability of the current metabolomics method to detect a number of metabolites which the bioenergetics/redox couples, UMP, UDP, UTP, TTP, CTP, and GTP perhaps due to the presence of inadequate parasite materials. With regards to future experiments, it can be underlined that *P. falciparum* digestive vacuole has a vital and essential biological role in the maintenance of amino acids abundance and toxic detoxification. It might be of interest to explore this organelle further by using drugs such as artemisinin as well as specific inhibitors to the digestive vacuole degradation enzyme such as pepstatin for proteases.

CHAPTER 8

Summary, Conclusions, Limitations and Future Perspectives

8.1. Summary and conclusions

The aim of this chapter is to present the main findings of this thesis and place them in the broader context of the current understanding of *P. falciparum* parasite biology, particularly, to provide comprehensive views about the metabolic roles of the *P. falciparum* mitochondria and digestive vacuole using known antimalarial drugs, and some inhibitors.

Malaria remains one of the leading causes of disease and death in the world, particularly in tropical countries. Malaria treatment remains the cornerstone of patient management and, in the absence of a fully effective vaccine, will likely remain so for the foreseeable future. However, in order to introduce an effective antimalarial drug therapy, prior knowledge of malaria parasite biology needs to be thoroughly understood. This can then be translated into identifying the vital and critical functions of malaria parasite biological systems for the development and discovery of effective and potent drugs. Metabolomics offers an attractive modern methodology for fast and comprehensive determination of parasite systems biology metabolites, and for establishing metabolic phenotypes, for instance in drug treated versus untreated parasites.

Therefore, targeted metabolomics platform was set out (as described in Chapter 3) for studying the *P. falciparum* metabolome in order get new insights into the parasite biology, as well as exploring the likely drug MoAs. The development and validation of this was carried out in accordance with a number of criteria that include selectivity and carryover, metabolite recovery and stability, linearity and sensitivity (limit of detection, LOD), and performance reproducibility. Overall, this metabolomics platform was able to detect and quantify accurately ~10% of the *P. falciparum* metabolome with LOD ranging from low nM to µM concentrations. This is an important aspect in the metabolomics field because there are several biosynthetic metabolic pathways, making the biosynthesized metabolites present in low levels, that *P. falciparum* parasite depends on to carry an essential metabolic function such as pyrimidine *de novo* synthesis. As indicated previously in Chapter 3, there are few limitations in the developed targeted metabolomics method which are discussed below.

Moreover, metabolomics data analysis software such as MetaboAnalyst web-based software (http://www.metaboanalyst.ca) (Xia et al., 2012; Xia et al., 2009) has the ability to cluster drug candidates according to their common MoAs. Based on a metabolomic analysis, principal component analysis (PCA), and partial least squares discriminant analysis (PLS-DA) of compound profiles for drug candidates can be performed. The ability to cluster drug candidates according to their common MoAs has been proven for the study in this thesis to be very useful in predicting the mode of unknown drug candidates such as CK-2-68, which has been shown to have similar MoA to potassium cyanide and bongkrekic acid and a different MoA of atovaquone although all these drugs shared general metabolic fingerprints in the upstream intermediates of pyrimidine biosynthesis, carbamoyl-l-aspartate and dihydroorotate (Chapter 6). This interesting finding is an example of the power of this type of analysis, demonstrating the significant benefits and practicality of the pharmacometabolomics approach for prioritizing drug candidates.

Furthermore, the application of the pharmacometabolomics approach in this thesis has enabled the identification and reliable prediction of the physiological functions of *P. falciparum* parasite, particularly the roles of mitochondria and digestive vacuole. *P. falciparum*, like any eukaryotic cell, requires the metabolism of a wide range of metabolites including amino acids, carbohydrates, nucleotides, redox, vitamins and other substances in order to sustain life. It has been shown and discussed (Chapter 4) that *P. falciparum*-iRBC had higher metabolic activity than non-infected RBC, particularly in the glucose fermentation process, and also in other vital metabolic process to the parasite, such as pyrimidine biosynthesis, amino acids metabolism, and in operating TCA cycle metabolic pathway.

It has been shown that the mitochondrion of malaria parasites is highly divergent from its mammalian counterpart, and its physiology has been validated as a target for anti-malarial drugs such as atovaquone (Mather and Vaidya, 2008; Vaidya and Mather, 2005, 2009). In the study of this thesis, *P. falciparum* mitochondria and its electron transport chain (ETC) were biochemically analysed using a number of selective inhibitors and some antimalarial drugs as described previously (Chapters 5 and 6). The primary metabolic fingerprint differences observed between *P. falciparum* sensitive 3D7 and transgenic 3D7-yDHOD·GFP strains following atovaquone and CK-2-68

addition were in the upstream intermediates of pyrimidine biosynthesis, carbamoyl-l-aspartate and dihydroorotate (Chapter 5, and Biagini et al., 2012). This supports the hypothesis that the *P. falciparum* mtETC acts as electron disposal system for the mitochondrially-located dihydroorotate dehydrogenase (DHODH) and thus supporting essential pyrimidine biosynthesis (Painter et al., 2007). Further examination into the *P. falciparum* mtETC components using a selective inhibitor for each one revealed an indirect effect as a consequence of mtETC collapse leading to the disruption of mtETC at the point of DHODH (Chapter 6). Intriguingly, perturbing the *P. falciparum* mitochondrion at the level of the ADP/ATP transporter using bongkrekic acid demonstrated a remarkable effect on mtETC as displayed by the accumulation of two metabolic fingerprints, carbamoyl-l-aspartate and dihydroorotate. This observation, together with the findings obtained for mtETC components, suggests that the *P. falciparum* mitochondrion may serve as a multi-target for drug discovery. In addition, these results suggest that ATP/ADP exchange is a vital bioenergetic process. In the absence of oxidative phosphorylation it has been previously postulated that this exchange is required to allow H+ leak (Fisher et al., 2007). Some potential *P. falciparum* mitochondrion drug targets may include PfNDH2, DHODH, ADP/ATP transporter, cytochrome bc_1 (complex III) and cytochrome *c* oxidase (complex IV). Moreover, it is well known that elongation factor G plays a crucial role in the mitochondrial protein synthesis machinery and it has been shown recently that this factor is a component of malaria parasite mitochondria, as demonstrated by its sensitivity to the action of fusidic acid (Johnson et al., 2011). Interestingly, the addition of fusidic acid to *P. falciparum* had no effect on mtETC as there were no changes observed in the pyrimidine intermediates. In contrast, fusidic acid exerted its action on the mitochondrial protein synthesis machinery as primarily shown in the profile of several amino acids including: (1) the accumulation of glutamine, ornithine, citrulline, phenylalanine, tryptophan, tyrosine, threonine and valine; and (2) blocking the degradation of serine, asparagine and lysine (Chapter 6).

The malaria parasite digestive vacuole is regarded as a headquarters for the parasite's metabolic activities (Olliaro and Goldberg, 1995). A number of heme-binding drugs (quinolone-containing antimalarial drugs, QCDs) were used in order to perturb the metabolic processes in the digestive vacuole and hence assign the similarities and differences in QCDs MoA. It was clear that the metabolic fingerprints generating from

QCDs were distinct from those obtained for mitochondrial inhibitors. Furthermore, it was clearly shown, by using the PCA and PLS-DA metabolomics analysis, that the MoA of QCD members, including chloroquine, amodiaquine, piperaquine, quinine and mefloquine, were probably drug class dependent. The different metabolic profiles observed in amino acids upon the addition of QCDs suggests that these QCD members primarily target the metabolism of amino acids, which could be acquired from the digestion of hemoglobin as well as exogenously through perhaps targeting the new permeability pathway (NPP) (Chapter 7). Therefore, it appears that the digestive vacuole of *P. falciparum* has many possible roles which include: (1) providing amino acids for protein synthesis; (2) heme detoxification processes; (3) prevent RBC lysis by creating a niche for itself during the parasite development; and (4) participate together with other parasite metabolic functions in the control of RBC osmotic stability through a dynamic equilibrium between hemoglobin degradation, efflux of generated amino acids and influx of amino acids from the extracellular media (Chapter 7).

To conclude, it appears that the pharmacometabolomics approach is a useful method in the understanding of malaria parasite physiological functions and identification of drug MoAs. The *P. falciparum* mitochondrion and digestive vacuole appear to be physiologically central to many related metabolic processes in the parasite. The unraveling of the complexities of mitochondrial functions are an immense challenges but these challenges must be met in order to determine whether mitochondrial manipulation can be harnessed therapeutically. Therefore, continued biological approaches, such as pharmacometabolomics in parallel with bioinformatics, genomics and proteomics, are critical and thus scientists can understand known pathways on a molecular level and characterize new pathways and components behaviour and functions that impact on the parasite system biology.

8.2. Limitations and future perspectives

Although the study of this thesis contributes to the understanding of the biological functions of *P. falciparum* parasite and gives new insights into drug MoAs, there were some limitations in the study which need to be considered for the future experiments. These include:

1- The study was primarily carried out using targeted metabolomics approach. Despite its reproducibility, sensitivity and robustness, it is only limited to analysing small portions of the parasite metabolome. Therefore, metabolites that are not included in the list of targeted metabolomics platform will not be analysed by the LC-MS/MS and hence any effects on these metabolites upon drugs addition will not be observed. In this case, untargeted metabolomics approaches well as a combination of different analysers (e.g. NMR, FT-IR and MS); will greatly enhance a comprehensive coverage of parasite metabolome.
2- The targeted metabolomics approach was developed using two internal standards (ISs) namely β-analine for positive mode and DL-arabinose for negative mode. Both ISs become eluted in the first 15 min of the LC run whereas the total LC run is 45 min. This might hide any unseen problems in LC run after 15 min. Therefore, including three ISs with different elution times (preferentially one IS become eluted at beginning of LC run, second IS become eluted at middle of LC run and third IS become eluted at end) will enhance the precision and accuracy of the analytical producer. In addition, absolute metabolite quantification can be carried out using isotopes. However, isotopes are expensive and not always available for each individual metabolite.
3- One problem with LC-MS/MS triple quadrupole mass analyser is an inability to differentiate between isomers. Therefore, a combinational approach is recommended as noted above.
4- The detection of bioenergetics/redox couples, UMP, UDP, UTP, TTP, CTP, and GTP was below the limit of detection (LOD) in the parasite samples, although their LOD were in nanomolar range as described in Chapter 3. This could be justified as the presence of inadequate parasite materials, as these metabolites are required to be biosynthesized by the parasite leading them to be present in very low levels. Therefore, increasing the sensitivity of detection for these metabolites, as well as preparation of adequate parasite materials may help in solving this issue in these metabolite detections.
5- All the experiments carried out in this thesis were performed using high gradient magnetic separation (HGMS) for trophozoite stage *P. falciparum*. In addition to a highly synchronous parasite culture, magnetic isolation of trophozoite stage can concentrate the culture to a parasitemia more than 95%. However, this procedure is hindered by limited column capacity, inconsistent separation

purities and high costs. Therefore, carefully following the magnetic separation protocol is critical to the quality of the experiments.

6- It is noted that all the findings included in this thesis were obtained from trophozoite stage *P. falciparum* parasite. Whilst there is nothing wrong with this, it would be a more comprehensive analysis and a broader picture could be drawn if this was performed on the developmental asexual cycle of the parasite. This could be suggested for the future experiments to examine the temporal metabolic profiles in ring, trophozoite and schizont stages following the addition of drugs.

7- It appears from several recent studies and reviews (Jayaraman et al., 2012, Bulusu et al., 2011, Wrenger et al., 2012) that aspartate bridges a number of metabolic pathways that include pyrimidine biosynthesis, purine salvage, protein synthesis and carbohydrate metabolism and mtETC. It would be of particular interest to investigate the inhibition effect of aspartate aminotransferase, whose biochemical function is the reversible catalysis of aspartate and 2-oxoglutarate to oxaloactetate and glutamate, in the abovementioned metabolic pathways. In addition, aspartate aminotransferase offers a high potential for the development of novel drug to tackle the emergence of drug resistant malaria parasites because it functions in multiple metabolic pathways.

APPENDICES

APPENDIX I

Table 1: Metabolite primary and working stocks concentration for ion path tuning.

Metabolites	Primary Stock Concentration (mg/ml)	Working Stock Concentration (ug/ml)	Solvent	Source
Alanine	1	10	H_2O	Sigma-Aldrich, UK
Asparagine	1	10	H_2O	Sigma-Aldrich, UK
Aspartate	1	10	H_2O	Sigma-Aldrich, UK
Glutamine	1	10	H_2O	Sigma-Aldrich, UK
Glutamate	1	10	H_2O	Sigma-Aldrich, UK
Arginine	1	10	MeOH	Sigma-Aldrich, UK
Proline	1	10	H_2O	Sigma-Aldrich, UK
Serine	1	10	H_2O	Sigma-Aldrich, UK
Valine	1	10	H_2O	Sigma-Aldrich, UK
Threonine	1	10	H_2O	Sigma-Aldrich, UK
Cysteine	1	10	H_2O	Sigma-Aldrich, UK
(Iso)-leucine	1	10	H_2O	Sigma-Aldrich, UK
Lysine	1	10	H_2O	Sigma-Aldrich, UK
Methionine	1	10	H_2O	Sigma-Aldrich, UK
Histidine	1	10	DMSO	Sigma-Aldrich, UK
Phenylalanine	1	10	MeOH	Sigma-Aldrich, UK
Tryptophan	1	10	H_2O	Sigma-Aldrich, UK
Tyrosine	1	10	H_2O	Sigma-Aldrich, UK
Ornithine	1	10	MeOH	Sigma-Aldrich, UK
Citrulline	1	10	H_2O	Sigma-Aldrich, UK
NAD	1	10	H_2O	Sigma-Aldrich, UK
NADH	1	10	DMSO	Sigma-Aldrich, UK
GSH	1	10	H_2O	Sigma-Aldrich, UK
GSSG	1	10	H_2O	Sigma-Aldrich, UK
NADP	1	10	H_2O	Sigma-Aldrich, UK
NADPH	1	10	DMSO	Sigma-Aldrich, UK
FAD	1	10	MeOH	Sigma-Aldrich, UK
UMP	1	10	H_2O	Sigma-Aldrich, UK
UDP	1	10	H_2O	Sigma-Aldrich, UK
UTP	1	10	H_2O	Sigma-Aldrich, UK
CTP	1	10	MeOH	Sigma-Aldrich, UK
TTP	1	10	H_2O	Sigma-Aldrich, UK
AMP	1	10	H_2O	Sigma-Aldrich, UK
ADP	1	10	H_2O	Sigma-Aldrich, UK
ATP	1	10	H_2O	Sigma-Aldrich, UK
GTP	1	10	H_2O	Sigma-Aldrich, UK
Carbamoyl-l-Aspartate	1	10	MeOH	Alfa-Aesar lab, UK
Acetyl-CoA	1	10	MeOH	Sigma-Aldrich, UK
Succinyl-CoA	1	10	H_2O	Sigma-Aldrich, UK
Propionyl-CoA	1	10	H_2O	Sigma-Aldrich, UK
Glucose	1	10	H_2O	Sigma-Aldrich, UK
Fumarate	1	10	H_2O	Sigma-Aldrich, UK

Table 1: (*Continued*)

Metabolites	Primary Stock Concentration (mg/ml)	Working Stock Concentration (ug/ml)	Solvent	Source
Succinate	1	10	H_2O	Sigma-Aldrich, UK
Malate	1	10	H_2O	Sigma-Aldrich, UK
2-oxoglutarate	1	10	MeOH	Sigma-Aldrich, UK
(iso)-Citrate	1	10	MeOH	Sigma-Aldrich, UK
PEP	1	10	H_2O	Sigma-Aldrich, UK
PABA	1	10	H_2O	Sigma-Aldrich, UK
G-3-P	1	10	H_2O	Sigma-Aldrich, UK
Hypoxanthine	1	10	DMSO	Sigma-Aldrich, UK
Orotate	1	10	DMSO	Sigma-Aldrich, UK
Dihydroorotate	1	10	MeOH	Sigma-Aldrich, UK
Lactate	1	10	H_2O	Sigma-Aldrich, UK
DHAP	1	10	H_2O	Sigma-Aldrich, UK
Oxaloacetate	1	10	H_2O	Sigma-Aldrich, UK
Carbamoyl-P	1	10	DMSO	Sigma-Aldrich, UK

Table 2: Metabolite primary stocks concentration for calibration curve standards and QC samples

Metabolites	Primary Stock Concentration (mg/ml)	MW (g/mol)	Primary Stock Concentration (mM)	Solvent
Alanine	2	89.09	22.44	H_2O
Asparagine	2	132.12	15.13	H_2O
Aspartate	2	133.1	15.02	H_2O
Glutamine	2	146.14	13.68	H_2O
Glutamate	2	147.13	13.59	H_2O
Arginine	2	174.2	11.48	MeOH
Proline	2	115.13	17.37	H_2O
Serine	2	105.09	19.03	H_2O
Valine	2	117.15	17.07	H_2O
Threonine	2	119.12	16.78	H_2O
Cysteine	2	121.16	33.02	H_2O
(Iso)-leucine	2	131.17	15.24	H_2O
Lysine	2	146.19	13.68	H_2O
Methionine	2	149.21	13.40	H_2O
Histidine	2	155.15	12.89	DMSO
Phenylalanine	2	165.19	12.10	MeOH
Tryptophan	2	204.23	9.79	H_2O
Tyrosine	2	181.19	11.03	H_2O
Ornithine	2	132.19	15.13	MeOH
Citrulline	2	175.19	11.41	H_2O
NAD	2	663.43	3.01	H_2O
NADH	2	664.43	3.00	DMSO
GSH	2	307.32	6.50	H_2O
GSSG	2	612.63	3.26	H_2O
NADP	2	744.41	2.69	H_2O
NADPH	2	745.41	2.68	DMSO
FAD	2	785.55	2.54	MeOH
UMP	2	324.18	6.16	H_2O
UDP	2	404.16	4.94	H_2O
UTP	2	484.14	4.13	H_2O
CTP	2	483.15	4.13	MeOH
TTP	2	482.16	4.14	H_2O
AMP	2	347.22	5.76	H_2O
ADP	2	427.20	4.68	H_2O
ATP	2	507.18	3.94	H_2O
GTP	2	523.18	3.82	H_2O
Carbamoyl-l-Aspartate	2	176.12	11.35	MeOH
Acetyl-CoA	10	809.57	12.35	MeOH
Succinyl-CoA	5	867.60	5.76	H_2O
Propionyl-CoA	4	823.60	6.07	H_2O
Glucose	2	180.16	11.10	H_2O
Fumarate	2	116.07	17.23	H_2O
Succinate	2	118.09	16.93	H_2O
Malate	2	134.09	14.91	H_2O
2-oxoglutarate	2	146.11	13.68	MeOH

Table 2: (*Continued*)

Metabolites	Primary Stock Concentration (mg/ml)	MW (g/mol)	Primary Stock Concentration (mM)	Solvent
(Iso)-Citrate	2	192.12	10.41	MeOH
PEP	2	168.04	11.90	H_2O
PABA	2	137.14	14.58	H_2O
G-3-P	2	170.05	11.62	H_2O
Hypoxanthine	2	136.12	14.70	DMSO
Orotate	2	156.10	12.81	DMSO
Dihydroorotate	2	158.11	12.64	MeOH
Lactate	4	90.08	44.40	H_2O
DHAP	4	170.06	23.52	H_2O
Oxaloacetate	20	132.07	151.43	H_2O
Carbamoyl-P	30	141.02	212.76	DMSO

Table 3: Mixture of standards concentration levels for plotting calibration standard curves

		Standard mixture conc.(uM)	Sixteen levels of serial dilution of standard mixture solution concentration (uM)															
Metabolite	**Primary Stock Conc. (mM)**	**Mixture of standad stock solution was prepared by adding 100ul of each primary stock solution giving the total volume of 5600ul.**	**LEVEL 1 1:1**	**LEVEL 2 1:2**	**LEVEL 3 1:4**	**LEVEL 4 1:8**	**LEVEL 5 1:16**	**LEVEL 6 1:32**	**LEVEL 7 1:64**	**LEVEL 8 1:128**	**LEVEL 9 1:256**	**LEVEL 10 1:512**	**LEVEL 11 1:1024**	**LEVEL 12 1:2048**	**LEVEL 13 1:4096**	**LEVEL 14 1:8192**	**LEVEL 15 1:16384**	**LEVEL 16 1:32768**
Alanine	22.45		400.9	200.4	100.2	50.1	25.05	12.53	6.26	3.13	1.57	0.78	0.39	0.20	0.098	0.049	0.024	0.012
Asparagine	15.14		270.3	135.2	67.6	33.8	16.90	8.45	4.22	2.11	1.06	0.53	0.26	0.13	0.066	0.033	0.016	0.008
Aspartate	15.03		268.3	134.2	67.1	33.5	16.77	8.39	4.19	2.10	1.05	0.52	0.26	0.13	0.066	0.033	0.016	0.008
Glutamine	13.69		244.4	122.2	61.1	30.5	15.27	7.64	3.82	1.91	0.95	0.48	0.24	0.12	0.060	0.030	0.015	0.007
Glutamate	13.59		242.7	121.4	60.7	30.3	15.17	7.59	3.79	1.90	0.95	0.47	0.24	0.12	0.059	0.030	0.015	0.007
Arginine	11.48		205.0	102.5	51.3	25.6	12.81	6.41	3.20	1.60	0.80	0.40	0.20	0.10	0.050	0.025	0.013	0.006
Proline	17.37		310.2	155.1	77.6	38.8	19.39	9.69	4.85	2.42	1.21	0.61	0.30	0.15	0.076	0.038	0.019	0.009
Serine	19.03		339.8	169.9	85.0	42.5	21.24	10.62	5.31	2.66	1.33	0.66	0.33	0.17	0.083	0.041	0.021	0.010
Valine	17.07		304.9	152.4	76.2	38.1	19.05	9.53	4.76	2.38	1.19	0.60	0.30	0.15	0.074	0.037	0.019	0.009
Threonine	16.79		299.8	149.9	75.0	37.5	18.74	9.37	4.68	2.34	1.17	0.59	0.29	0.15	0.073	0.037	0.018	0.009
Cysteine	33.03		589.7	294.9	147.4	73.7	36.86	18.43	9.21	4.61	2.30	1.15	0.58	0.29	0.144	0.072	0.036	0.018
(Iso)-leucine	15.25		272.3	136.1	68.1	34.0	17.02	8.51	4.25	2.13	1.06	0.53	0.27	0.13	0.066	0.033	0.017	0.008
Lysine	13.68		244.3	122.2	61.1	30.5	15.27	7.63	3.82	1.91	0.95	0.48	0.24	0.12	0.060	0.030	0.015	0.007
Methionine	13.40		239.4	119.7	59.8	29.9	14.96	7.48	3.74	1.87	0.93	0.47	0.23	0.12	0.058	0.029	0.015	0.007
Histidine	12.89		230.2	115.1	57.5	28.8	14.39	7.19	3.60	1.80	0.90	0.45	0.22	0.11	0.056	0.028	0.014	0.007
Phenylalanine	12.11		216.2	108.1	54.1	27.0	13.51	6.76	3.38	1.69	0.84	0.42	0.21	0.11	0.053	0.026	0.013	0.007
Tryptophan	9.79		174.9	87.4	43.7	21.9	10.93	5.46	2.73	1.37	0.68	0.34	0.17	0.09	0.043	0.021	0.011	0.005
Tyrosine	11.04		197.1	98.6	49.3	24.6	12.32	6.16	3.08	1.54	0.77	0.38	0.19	0.10	0.048	0.024	0.012	0.006

Table 3: (*Continued*)

Ornithine	15.13		270.2	135.1	67.6	33.8	16.89	8.44	4.22	2.11	1.06	0.53	0.26	0.13	0.066	0.033	0.016	0.008
Citrulline	11.42		203.9	101.9	51.0	25.5	12.74	6.37	3.19	1.59	0.80	0.40	0.20	0.10	0.050	0.025	0.012	0.006
NAD	3.01		53.8	26.9	13.5	6.7	3.36	1.68	0.84	0.42	0.21	0.11	0.05	0.03	0.013	0.007	0.003	0.002
NADH	3.01		53.7	26.8	13.4	6.7	3.35	1.68	0.84	0.42	0.21	0.10	0.05	0.03	0.013	0.007	0.003	0.002
GSH	6.51		116.2	58.1	29.1	14.5	7.26	3.63	1.82	0.91	0.45	0.23	0.11	0.06	0.028	0.014	0.007	0.004
GSSG	3.26		58.3	29.1	14.6	7.3	3.64	1.82	0.91	0.46	0.23	0.11	0.06	0.03	0.014	0.007	0.004	0.002
NADP	2.69		48.0	24.0	12.0	6.0	3.00	1.50	0.75	0.38	0.19	0.09	0.05	0.02	0.012	0.006	0.003	0.001
NADPH	2.68		47.9	24.0	12.0	6.0	2.99	1.50	0.75	0.37	0.19	0.09	0.05	0.02	0.012	0.006	0.003	0.001
FAD	2.55		45.5	22.7	11.4	5.7	2.84	1.42	0.71	0.36	0.18	0.09	0.04	0.02	0.011	0.006	0.003	0.001
UMP	6.17		110.2	55.1	27.5	13.8	6.89	3.44	1.72	0.86	0.43	0.22	0.11	0.05	0.027	0.013	0.007	0.003
UDP	4.95		88.4	44.2	22.1	11.0	5.52	2.76	1.38	0.69	0.35	0.17	0.09	0.04	0.022	0.011	0.005	0.003
UTP	4.13		73.8	36.9	18.4	9.2	4.61	2.31	1.15	0.58	0.29	0.14	0.07	0.04	0.018	0.009	0.005	0.002
CTP	4.14		73.9	37.0	18.5	9.2	4.62	2.31	1.15	0.58	0.29	0.14	0.07	0.04	0.018	0.009	0.005	0.002
TTP	4.15		74.1	37.0	18.5	9.3	4.63	2.31	1.16	0.58	0.29	0.14	0.07	0.04	0.018	0.009	0.005	0.002
AMP	5.76		102.9	51.4	25.7	12.9	6.43	3.21	1.61	0.80	0.40	0.20	0.10	0.05	0.025	0.013	0.006	0.003
ADP	4.68		83.6	41.8	20.9	10.5	5.23	2.61	1.31	0.65	0.33	0.16	0.08	0.04	0.020	0.010	0.005	0.003
ATP	3.94		70.4	35.2	17.6	8.8	4.40	2.20	1.10	0.55	0.28	0.14	0.07	0.03	0.017	0.009	0.004	0.002
GTP	3.82		68.3	34.1	17.1	8.5	4.27	2.13	1.07	0.53	0.27	0.13	0.07	0.03	0.017	0.008	0.004	0.002
Carbamyl-L-Aspartate	11.36		202.8	101.4	50.7	25.3	12.67	6.34	3.17	1.58	0.79	0.40	0.20	0.10	0.050	0.025	0.012	0.006
Acetyl-CoA	12.35		220.6	110.3	55.1	27.6	13.79	6.89	3.45	1.72	0.86	0.43	0.22	0.11	0.054	0.027	0.013	0.007
Succinyl-CoA	5.76		102.9	51.5	25.7	12.9	6.43	3.22	1.61	0.80	0.40	0.20	0.10	0.05	0.025	0.013	0.006	0.003
Propionyl-CoA	6.07		108.4	54.2	27.1	13.6	6.78	3.39	1.69	0.85	0.42	0.21	0.11	0.05	0.026	0.013	0.007	0.003
D-glucose	11.10		198.2	99.1	49.6	24.8	12.39	6.20	3.10	1.55	0.77	0.39	0.19	0.10	0.048	0.024	0.012	0.006
Fumarate	17.23		307.7	153.8	76.9	38.5	19.23	9.62	4.81	2.40	1.20	0.60	0.30	0.15	0.075	0.038	0.019	0.009

Table 3: (*Continued*)

Succinate	16.94		302.4	151.2	75.6	37.8	18.90	9.45	4.73	2.36	1.18	0.59	0.30	0.15	0.074	0.037	0.018	0.009
Malate	14.92		266.4	133.2	66.6	33.3	16.65	8.32	4.16	2.08	1.04	0.52	0.26	0.13	0.065	0.033	0.016	0.008
2-Oxoglutarate	13.69		244.5	122.2	61.1	30.6	15.28	7.64	3.82	1.91	0.95	0.48	0.24	0.12	0.060	0.030	0.015	0.007
(iso)-Citrate	10.42		186.0	93.0	46.5	23.3	11.63	5.81	2.91	1.45	0.73	0.36	0.18	0.09	0.045	0.023	0.011	0.006
PEP	11.90		212.5	106.3	53.1	26.6	13.28	6.64	3.32	1.66	0.83	0.42	0.21	0.10	0.052	0.026	0.013	0.006
PABA	14.58		260.4	130.2	65.1	32.6	16.28	8.14	4.07	2.03	1.02	0.51	0.25	0.13	0.064	0.032	0.016	0.008
G-3-P	11.62		207.6	103.8	51.9	25.9	12.97	6.49	3.24	1.62	0.81	0.41	0.20	0.10	0.051	0.025	0.013	0.006
Hypoxanthine	14.71		262.6	131.3	65.7	32.8	16.41	8.21	4.10	2.05	1.03	0.51	0.26	0.13	0.064	0.032	0.016	0.008
Orotate	12.81		228.8	114.4	57.2	28.6	14.30	7.15	3.57	1.79	0.89	0.45	0.22	0.11	0.056	0.028	0.014	0.007
Dihydroorotate	12.65		225.9	112.9	56.5	28.2	14.12	7.06	3.53	1.76	0.88	0.44	0.22	0.11	0.055	0.028	0.014	0.007
Lactate	44.41		793.0	396.5	198.3	99.1	49.56	24.78	12.39	6.20	3.10	1.55	0.77	0.39	0.194	0.097	0.048	0.024
DHAP	23.53		420.2	210.1	105.0	52.5	26.26	13.13	6.57	3.28	1.64	0.82	0.41	0.21	0.103	0.051	0.026	0.013
Oxaloacetate	151.43		2704.2	1352.	676.0	338.0	169.0	84.51	42.25	21.13	10.56	5.28	2.64	1.32	0.660	0.330	0.165	0.083
Carbamoyl phosphate	212.77		3799.4	1899.	949.8	474.9	237.4	118.7	59.37	29.68	14.84	7.42	3.71	1.86	0.928	0.464	0.232	0.116

Table 4: Mixture of standards concentration for preparing QC samples

Metabolite	Primary Stock Concentration (mM)	Mixture of standad stock solution was prepared by adding 100ul of each primary stock solution giving the total volume of 5600ul.	Serially diluted standard mixture concentration (uM)		
			HQC 1:1	MQC 1:10	LQC 1:100
Alanine	22.45		400.9	40.09	4.01
Asparagine	15.14		270.3	27.03	2.70
Aspartate	15.03		268.3	26.83	2.68
Glutamine	13.69		244.4	24.44	2.44
Glutamate	13.59		242.7	24.27	2.43
Arginine	11.48		205.0	20.50	2.05
Proline	17.37		310.2	31.02	3.10
Serine	19.03		339.8	33.98	3.40
Valine	17.07		304.9	30.49	3.05
Threonine	16.79		299.8	29.98	3.00
Cysteine	33.03		589.7	58.97	5.90
(Iso)-leucine	15.25		272.3	27.23	2.72
Lysine	13.68		244.3	24.43	2.44
Methionine	13.40		239.4	23.94	2.39
Histidine	12.89		230.2	23.02	2.30
Phenylalanine	12.11		216.2	21.62	2.16
Tryptophan	9.79		174.9	17.49	1.75
Tyrosine	11.04		197.1	19.71	1.97
Ornithine	15.13		270.2	27.02	2.70
Citrulline	11.42		203.9	20.39	2.04
NAD	3.01		53.8	5.38	0.54
NADH	3.01		53.7	5.37	0.54
GSH	6.51		116.2	11.62	1.16
GSSG	3.26		58.3	5.83	0.58
NADP	2.69		48.0	4.80	0.48
NADPH	2.68		47.9	4.79	0.48
FAD	2.55		45.5	4.55	0.45
UMP	6.17		110.2	11.02	1.10
UDP	4.95		88.4	8.84	0.88
UTP	4.13		73.8	7.38	0.74
CTP	4.14		73.9	7.39	0.74
TTP	4.15		74.1	7.41	0.74
AMP	5.76		102.9	10.29	1.03
ADP	4.68		83.6	8.36	0.84
ATP	3.94		70.4	7.04	0.70
GTP	3.82		68.3	6.83	0.68
Carbamoyl-l-Aspartate	11.36		202.8	20.28	2.03

Table 4: (*Contintued*)

Acetyl-CoA	12.35		220.6	22.06	2.21
Succinyl-CoA	5.76		102.9	10.29	1.03
Propionyl-CoA	6.07		108.4	10.84	1.08
Glucose	11.10		198.2	19.82	1.98
Fumarate	17.23		307.7	30.77	3.08
Succinate	16.94		302.4	30.24	3.02
Malate	14.92		266.4	26.64	2.66
2-Oxoglutarate	13.69		244.5	24.45	2.44
(Iso)-Citrate	10.42		186.0	18.60	1.86
PEP	11.90		212.5	21.25	2.13
PABA	14.58		260.4	26.04	2.60
G-3-P	11.62		207.6	20.76	2.08
Hypoxanthine	14.71		262.6	26.26	2.63
Orotate	12.81		228.8	22.88	2.29
Dihydroorotate	12.65		225.9	22.59	2.26
Lactate	44.41		793.0	79.30	7.93
DHAP	23.53		420.2	42.02	4.20
Oxaloacetate	151.43		2704.2	270.42	27.04
Carbamyl-P	212.77		3799.4	379.94	37.99

APPENDIX II

A)

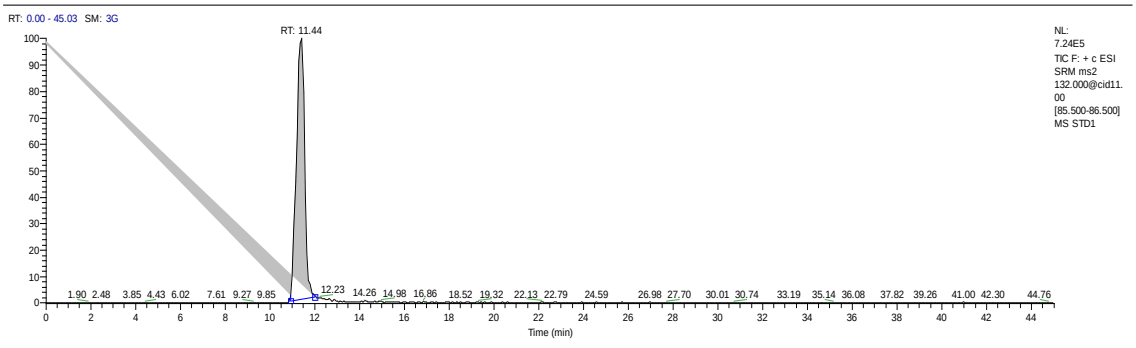

B)

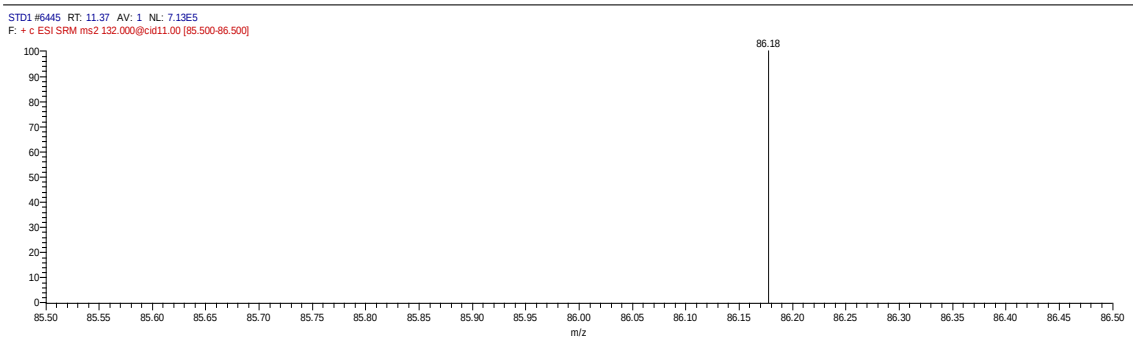

Figure 1: LC-MS/MS chromatogram of (iso)-leucine. A) Chromatographic separation of (iso)-leucine peak shows retention time (RT) at ~11min. B) SRM scan of ionized (iso)-leucine shows the detection of its product ion at mass-to-charge (m/z) of 86.

A)

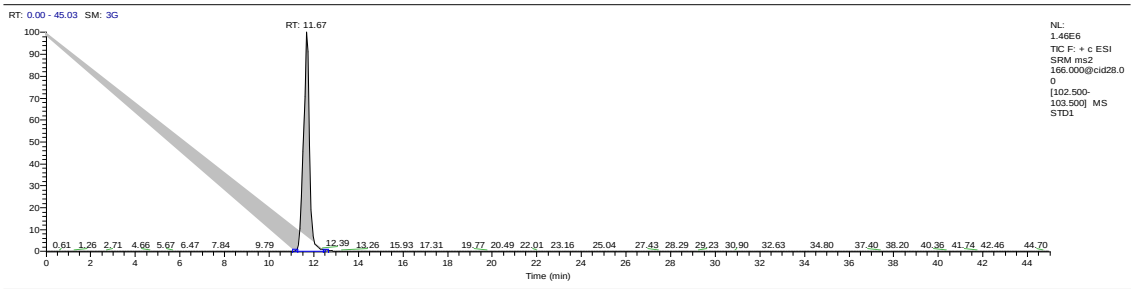

B)

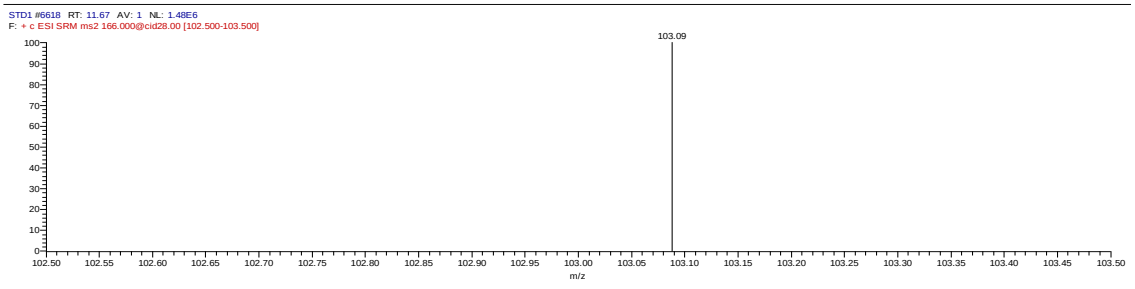

Figure 2: LC-MS/MS chromatogram of phenylalanine. A) Chromatographic separation of phenylalanine peak shows retention time (RT) at ~11.6min. B) SRM scan of ionized phenylalanine shows the detection of its product ion at mass-to-charge (m/z) of 103.

A)

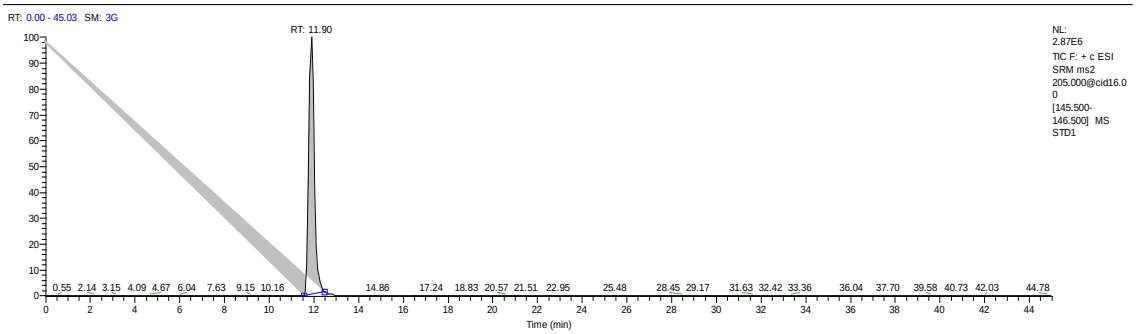

B)

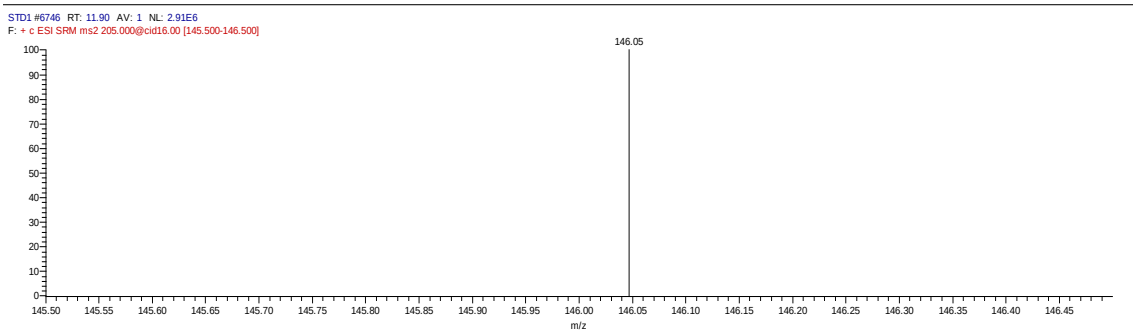

Figure 3: LC-MS/MS chromatogram of tryptophan. A) Chromatographic separation of tryptophan peak shows retention time (RT) at ~11.9min. B) SRM scan of ionized tryptophan shows the detection of its product ion at mass-to-charge (m/z) of 146.

A)

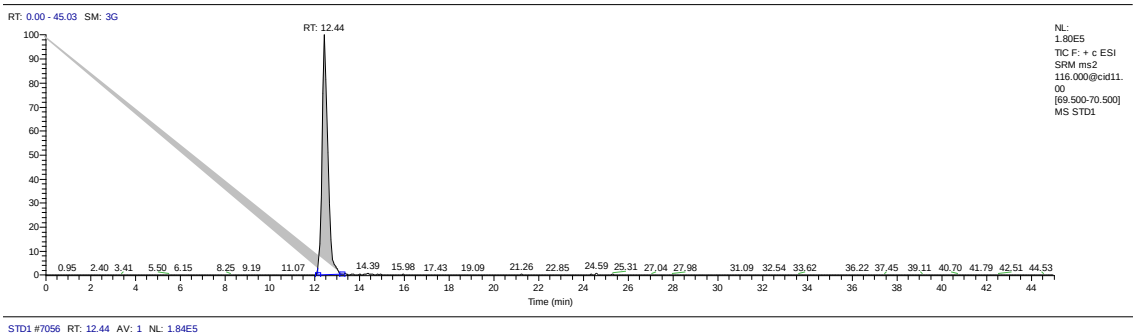

B)

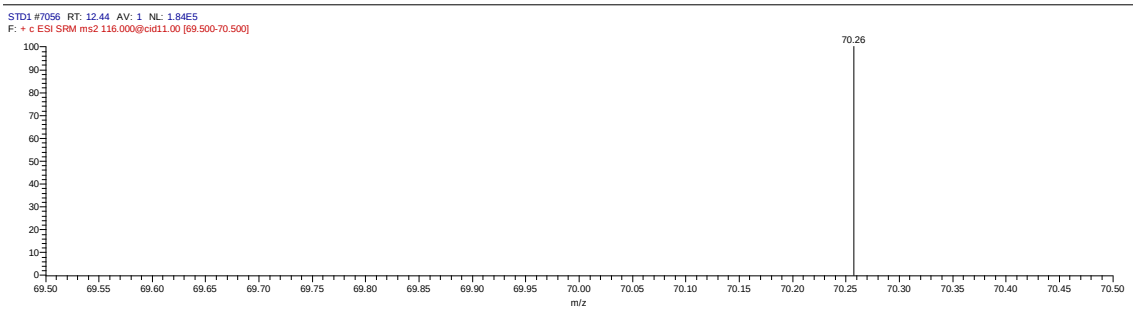

Figure 4: LC-MS/MS chromatogram of proline. A) Chromatographic separation of proline peak shows retention time (RT) at ~12.4min. B) SRM scan of ionized proline shows the detection of its product ion at mass-to-charge (m/z) of 70.

A)

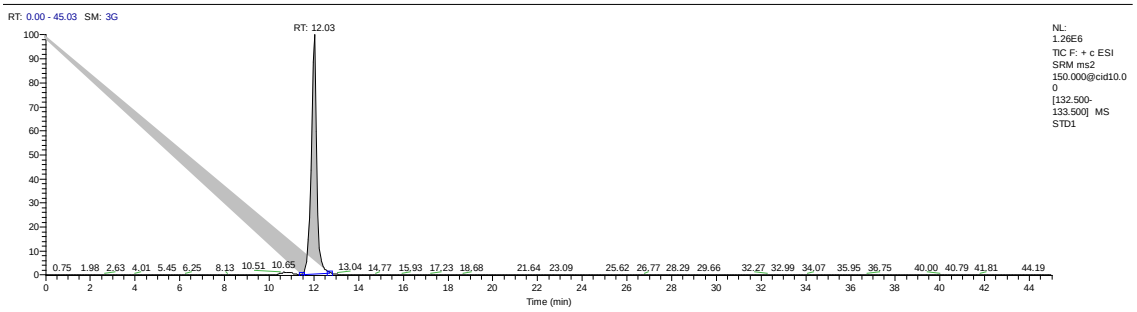

B)

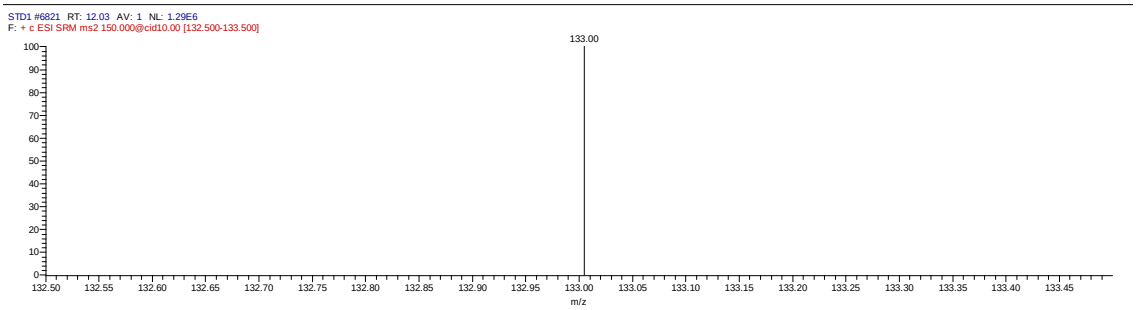

Figure 5: LC-MS/MS chromatogram of methionine. A) Chromatographic separation of methionine peak shows retention time (RT) at ~12min. B) SRM scan of ionized methionine shows the detection of its product ion at mass-to-charge (m/z) of 133.

A)

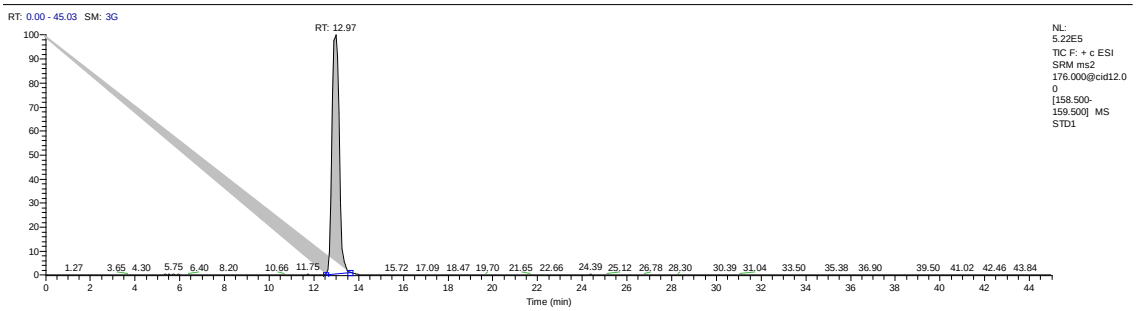

B)

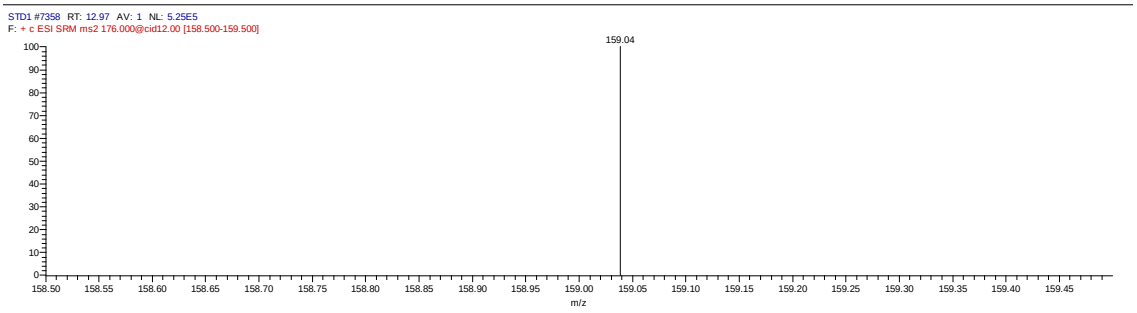

Figure 6: LC-MS/MS chromatogram of citrulline. A) Chromatographic separation of citrulline peak shows retention time (RT) at ~12.9 min. B) SRM scan of ionized citrulline shows the detection of its product ion at mass-to-charge (m/z) of 159.

A)

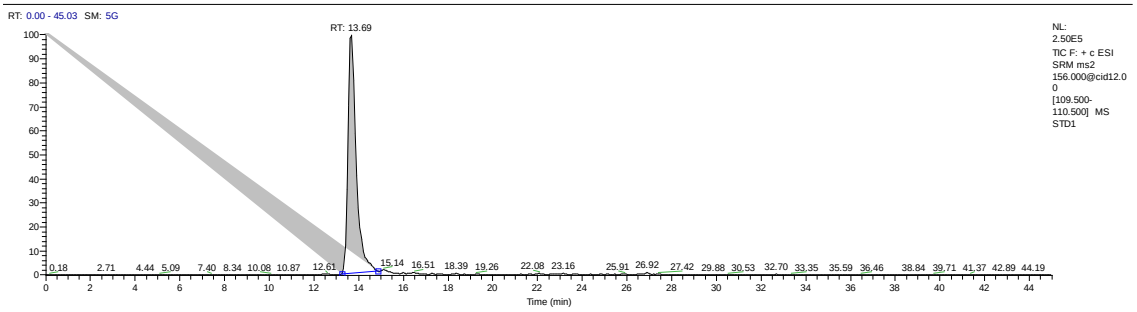

B)

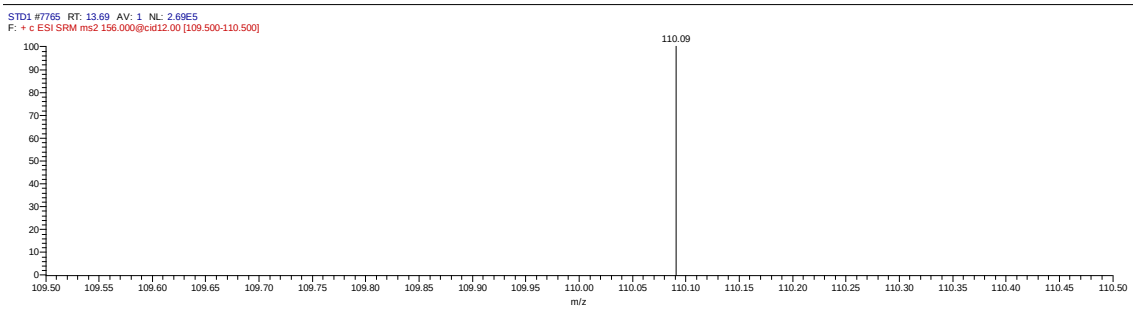

Figure 7: LC-MS/MS chromatogram of histidine. A) Chromatographic separation of histidine peak shows retention time (RT) at ~13.6 min. B) SRM scan of ionized histidine shows the detection of its product ion at mass-to-charge (m/z) of 110.

A)

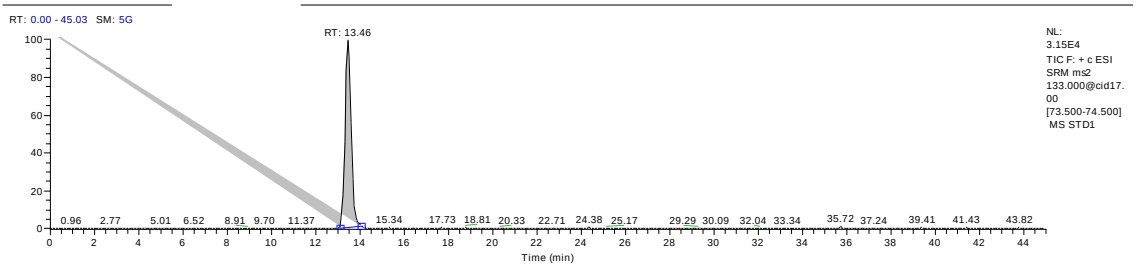

B)

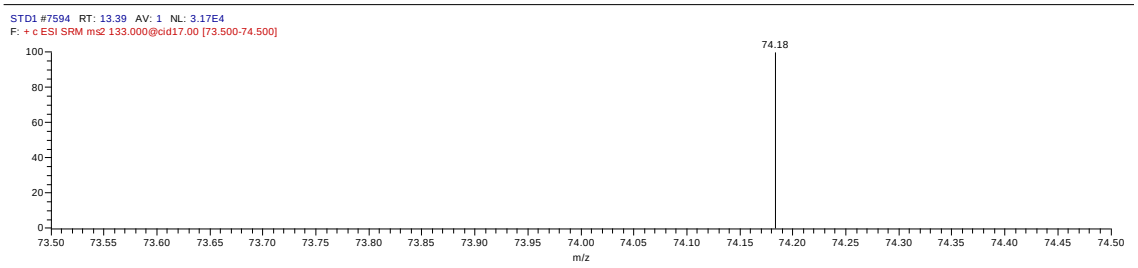

Figure 8: LC-MS/MS chromatogram of asparagine. A) Chromatographic separation of asparagine peak shows retention time (RT) at ~13.4 min. B) SRM scan of ionized asparagine shows the detection of its product ion at mass-to-charge (m/z) of 74.

A)

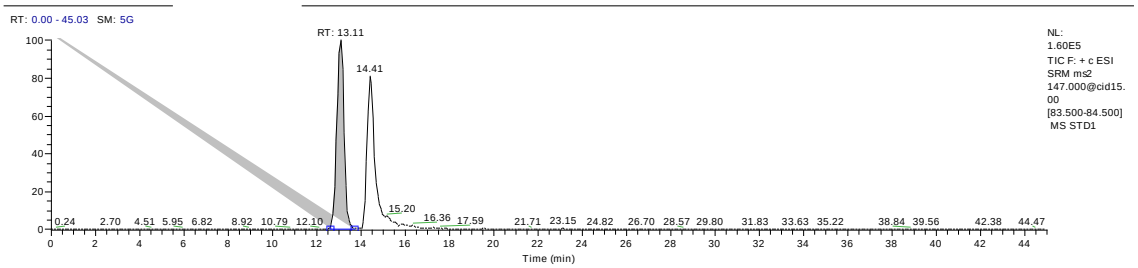

B)

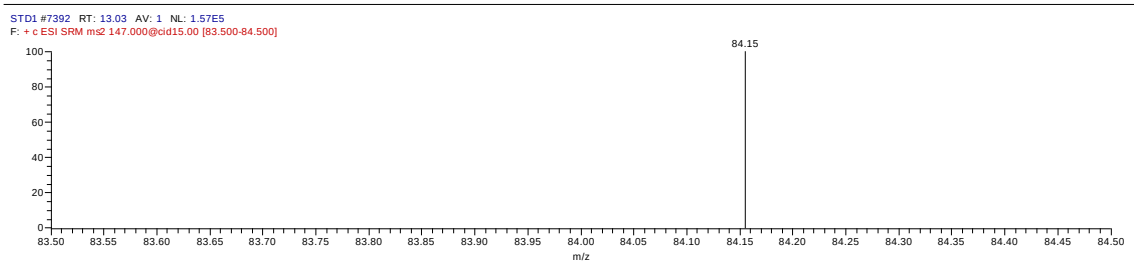

Figure 9: LC-MS/MS chromatogram of glutamine. A) Chromatographic separation of glutamine peak shows retention time (RT) at ~13.1 min. B) SRM scan of ionized glutamine shows the detection of its product ion at mass-to-charge (m/z) of 84.

A)

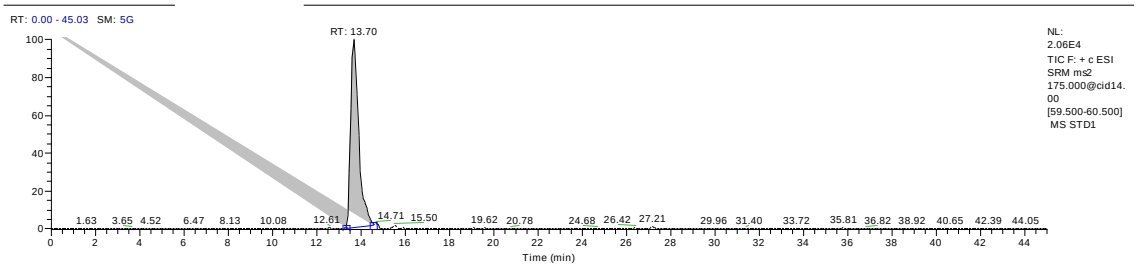

B)

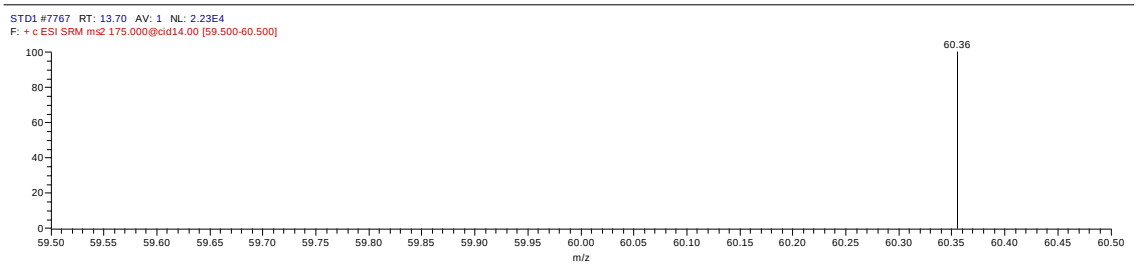

Figure 10: LC-MS/MS chromatogram of arginine. A) Chromatographic separation of arginine peak shows retention time (RT) at ~13.7 min. B) SRM scan of ionized arginine shows the detection of its product ion at mass-to-charge (m/z) of 60.

A)

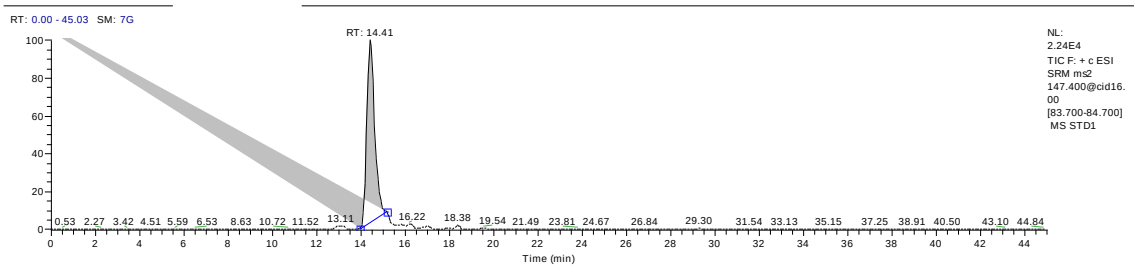

B)

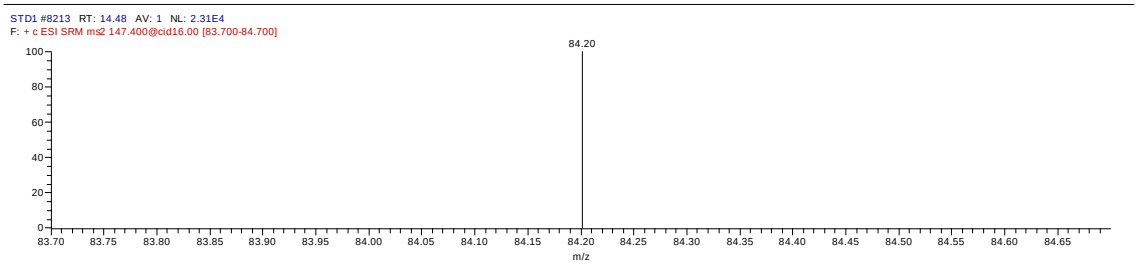

Figure 11: LC-MS/MS chromatogram of lysine. A) Chromatographic separation of lysine peak shows retention time (RT) at ~14.4min. B) SRM scan of ionized lysine shows the detection of its product ion at mass-to-charge (m/z) of 84.

A)

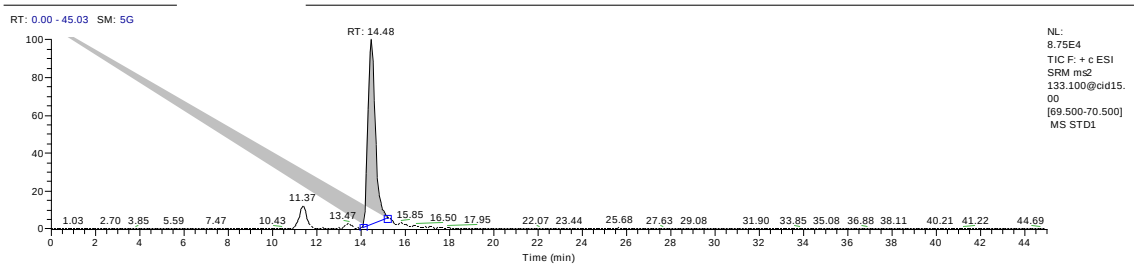

B)

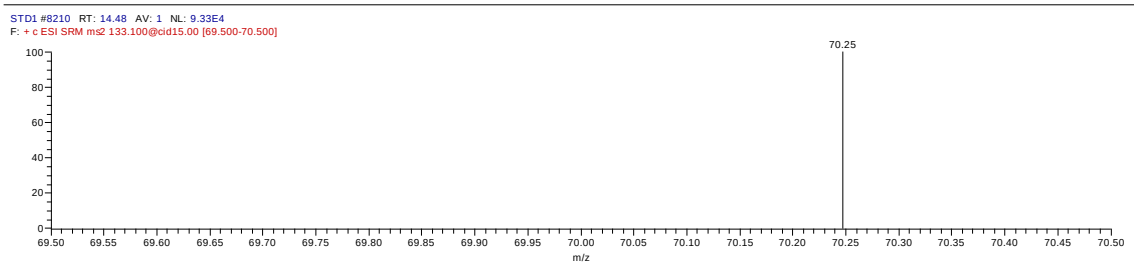

Figure 12: LC-MS/MS chromatogram of ornithine. A) Chromatographic separation of ornithine peak shows retention time (RT) at ~14.4 min. B) SRM scan of ionized ornithine shows the detection of its product ion at mass-to-charge (m/z) of 70.

A)

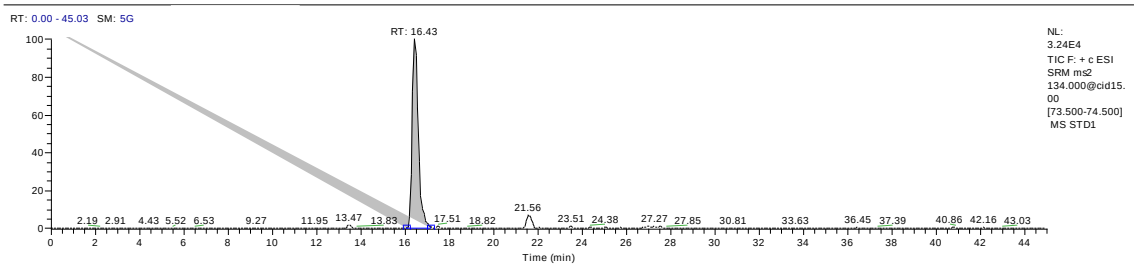

B)

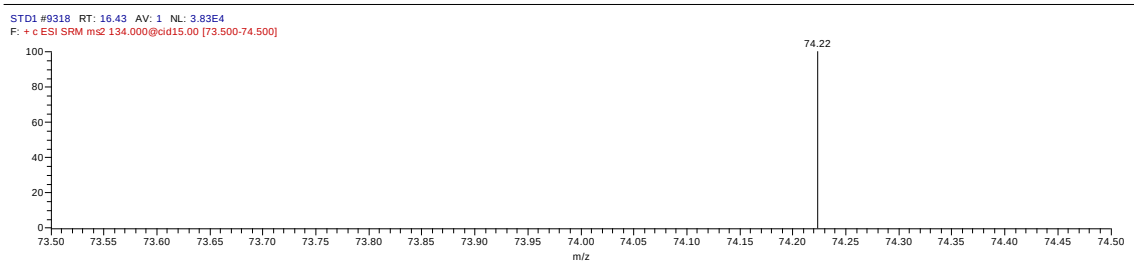

Figure 13: LC-MS/MS chromatogram of aspartate. A) Chromatographic separation of aspartate peak shows retention time (RT) at ~16.4 min. B) SRM scan of ionized aspartate shows the detection of its product ion at mass-to-charge (m/z) of 74.

A)

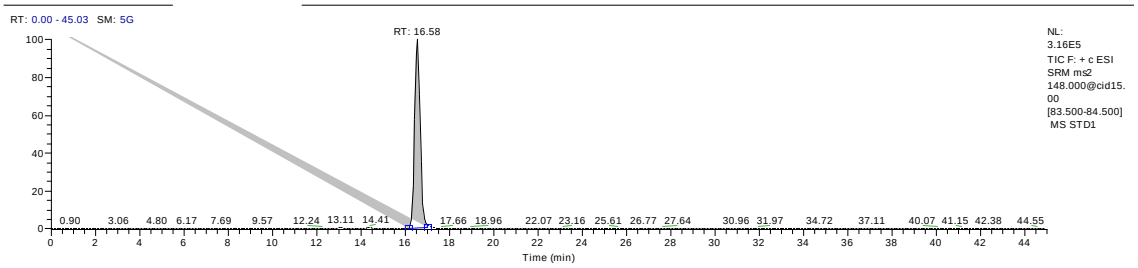

B)

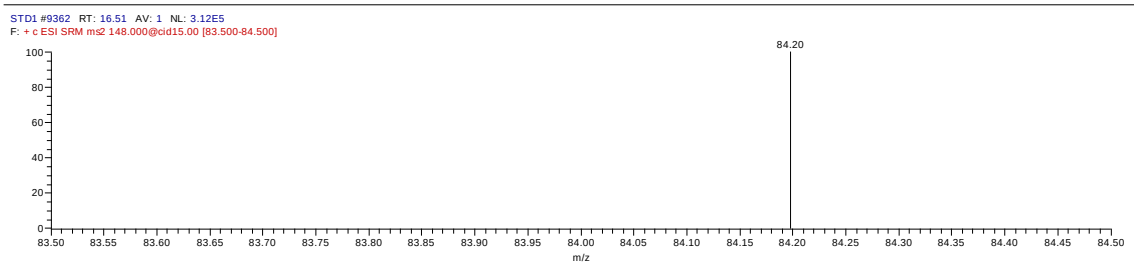

Figure 14: LC-MS/MS chromatogram of glutamate. A) Chromatographic separation of glutamate peak shows retention time (RT) at ~16.5 min. B) SRM scan of ionized glutamate shows the detection of its product ion at mass-to-charge (m/z) of 84.

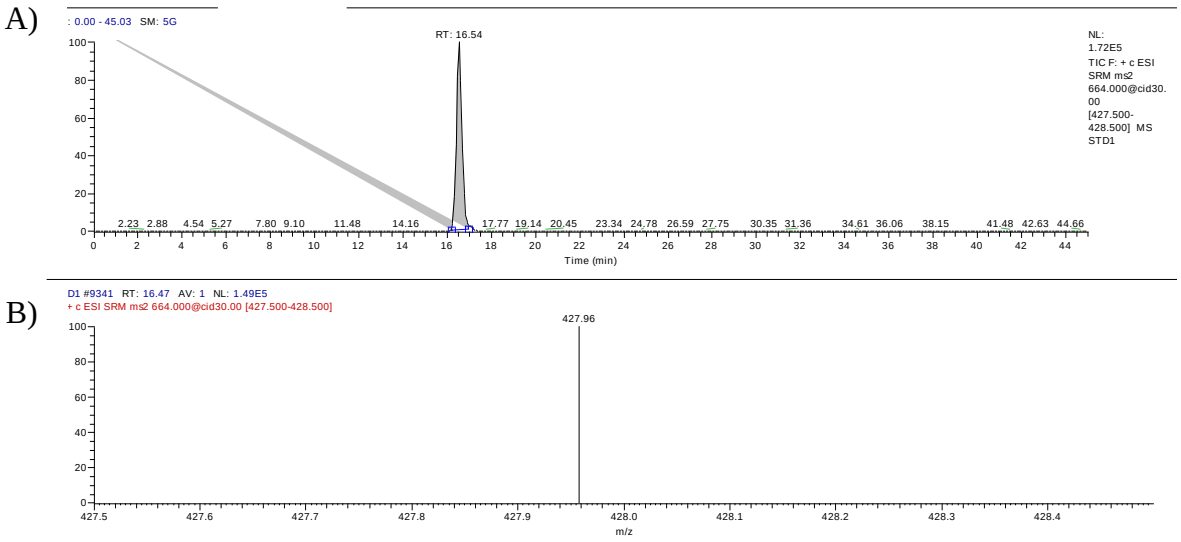

Figure 15: LC-MS/MS chromatogram of NAD. A) Chromatographic separation of NAD peak shows retention time (RT) at ~16.5 min. B) SRM scan of ionized NAD shows the detection of its product ion at mass-to-charge (m/z) of 428.

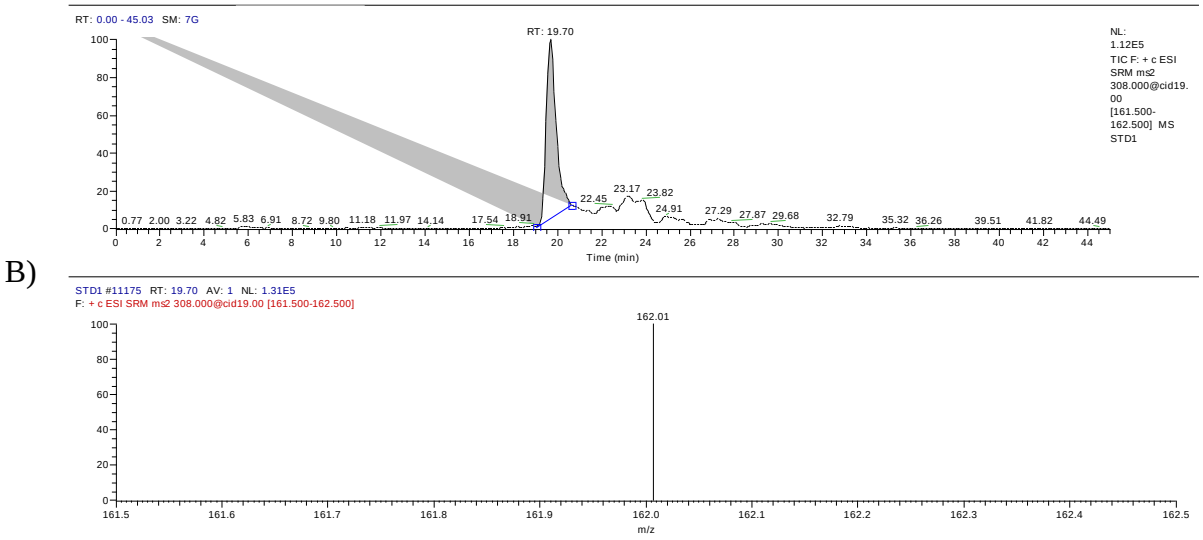

Figure 16: LC-MS/MS chromatogram of GSH. A) Chromatographic separation of GSH peak shows retention time (RT) at ~19.7 min. B) SRM scan of ionized GSH shows the detection of its product ion at mass-to-charge (m/z) of 162.

A)

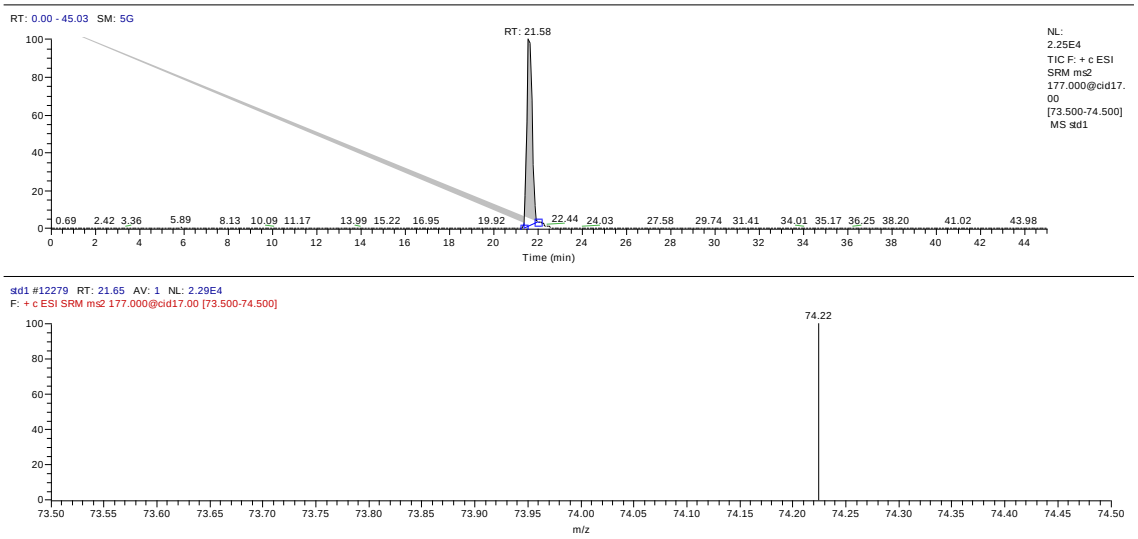

B)

Figure 17: LC-MS/MS chromatogram of carbamoyl-l-aspartate. A) Chromatographic separation of carbamoyl-l-aspartate peak shows retention time (RT) at ~21.5 min. B) SRM scan of ionized carbamoyl-l-aspartate shows the detection of its product ion at mass-to-charge (m/z) of 74.

A)

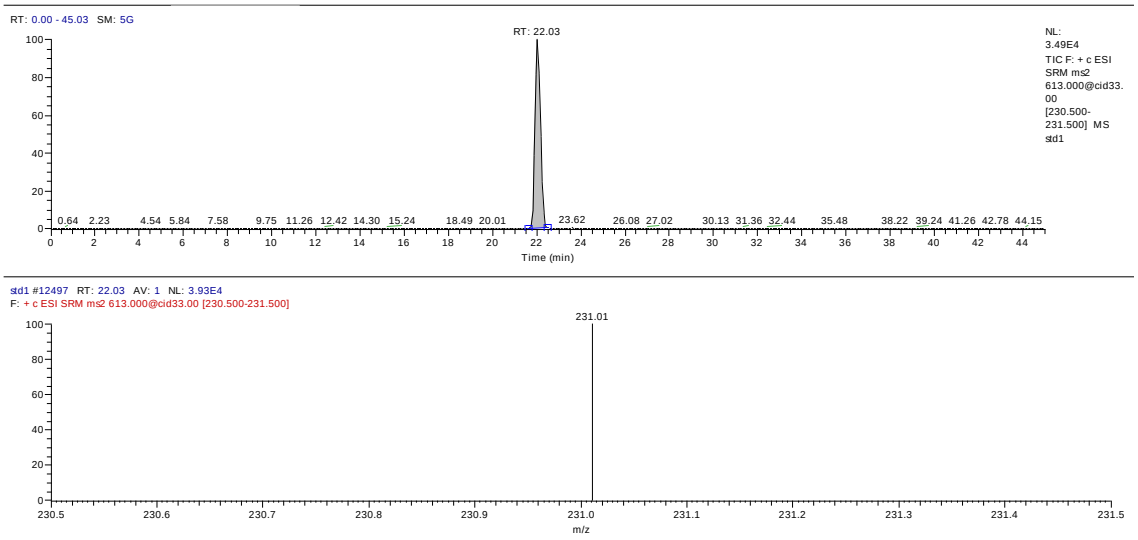

B)

Figure 18: LC-MS/MS chromatogram of GSSG. A) Chromatographic separation of GSSG peak shows retention time (RT) at ~22 min. B) SRM scan of ionized GSSG shows the detection of its product ion at mass-to-charge (m/z) of 231.

A)

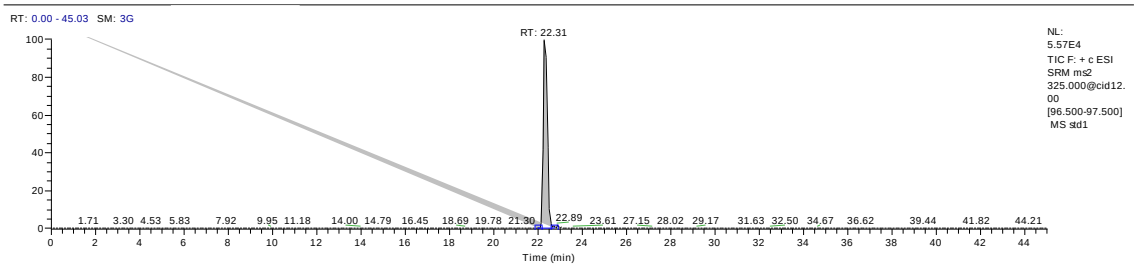

B)

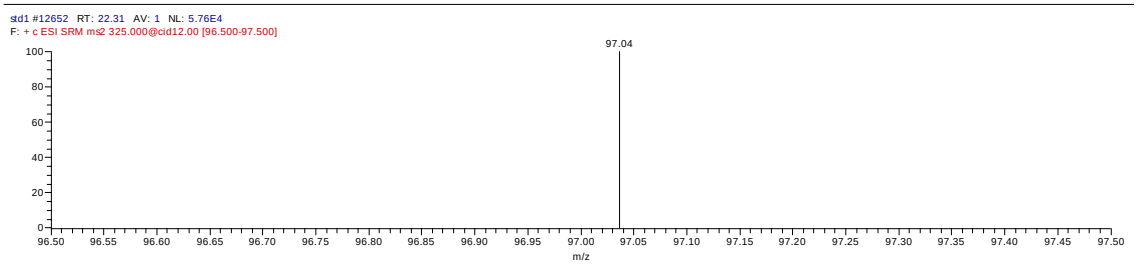

Figure 19: LC-MS/MS chromatogram of UMP. A) Chromatographic separation of UMP peak shows retention time (RT) at ~22.3 min. B) SRM scan of ionized UMP shows the detection of its product ion at mass-to-charge (m/z) of 97.

A)

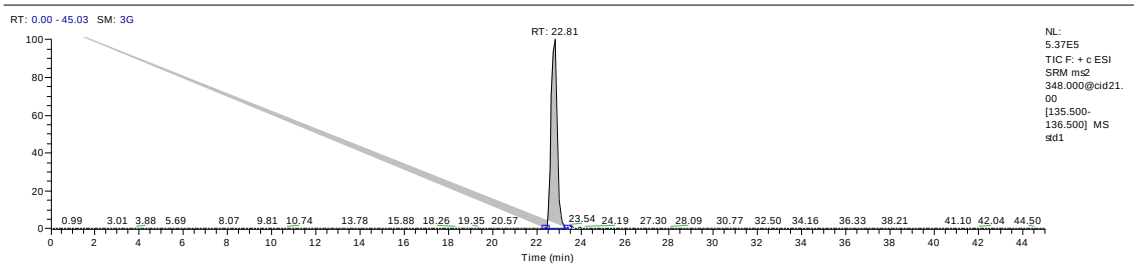

B)

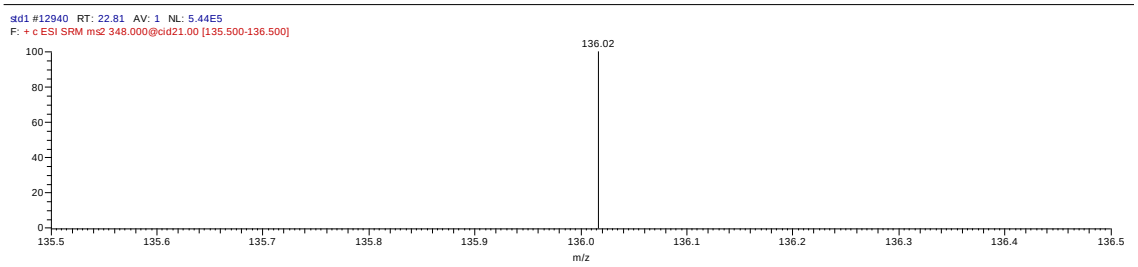

Figure 20: LC-MS/MS chromatogram of AMP. A) Chromatographic separation of AMP peak shows retention time (RT) at ~22.8 min. B) SRM scan of ionized AMP shows the detection of its product ion at mass-to-charge (m/z) of 136.

A)

B)

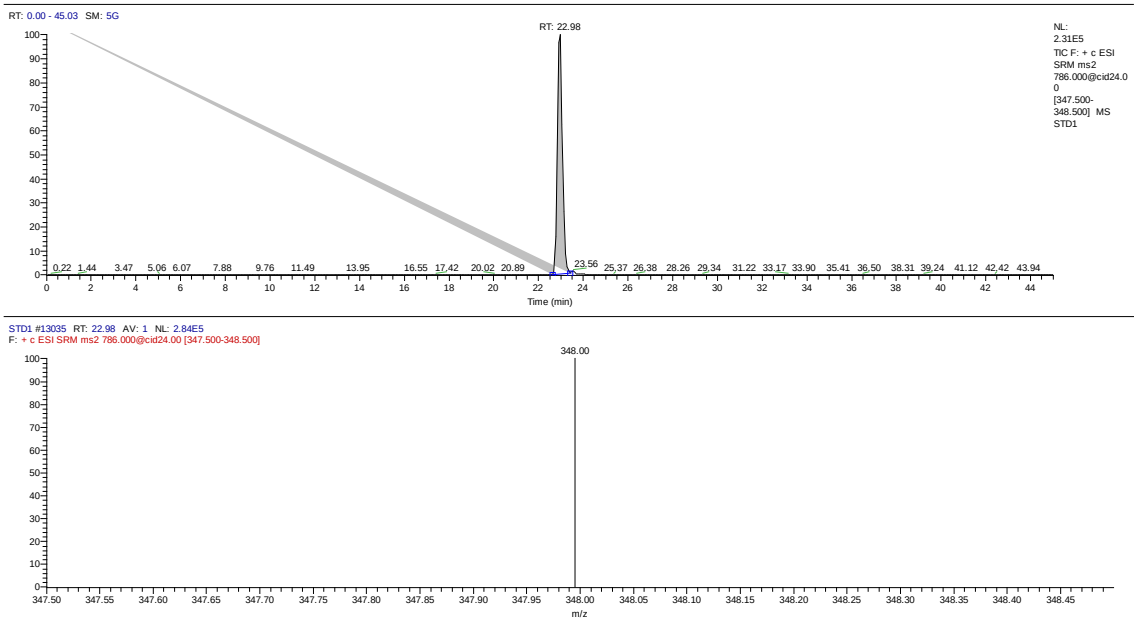

Figure 21: LC-MS/MS chromatogram of FAD. A) Chromatographic separation of FAD peak shows retention time (RT) at ~22.9 min. B) SRM scan of ionized FAD shows the detection of its product ion at mass-to-charge (m/z) of 348.

A)

B)

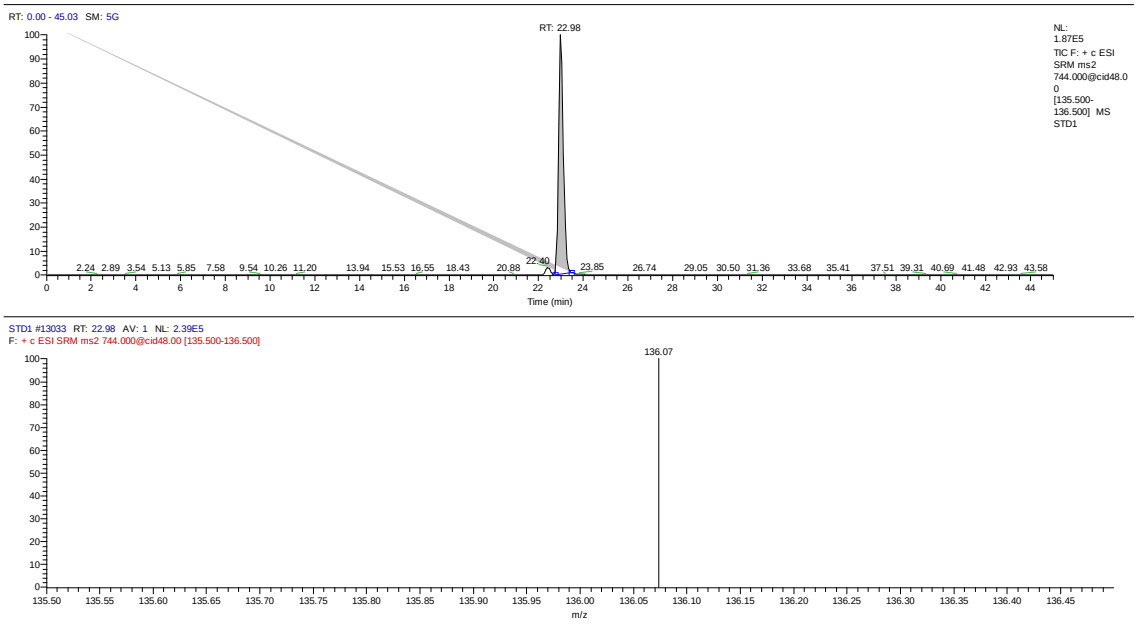

Figure 22: LC-MS/MS chromatogram of NADP. A) Chromatographic separation of NADP peak shows retention time (RT) at ~22.9 min. B) SRM scan of ionized NADP shows the detection of its product ion at mass-to-charge (m/z) of 136.

A)

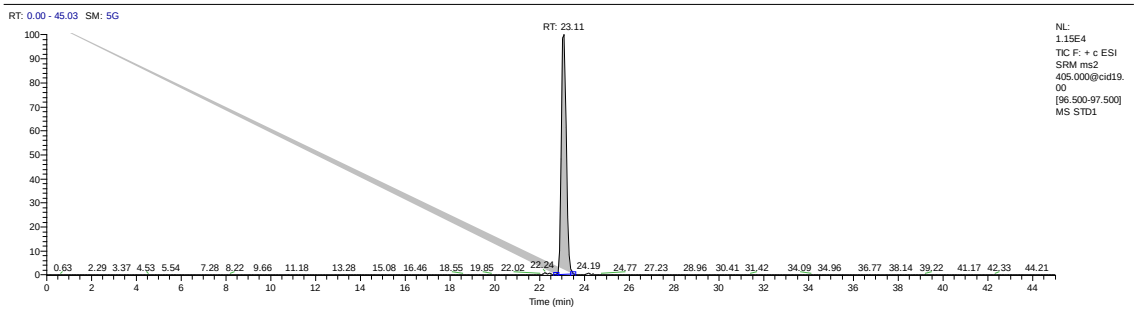

B)

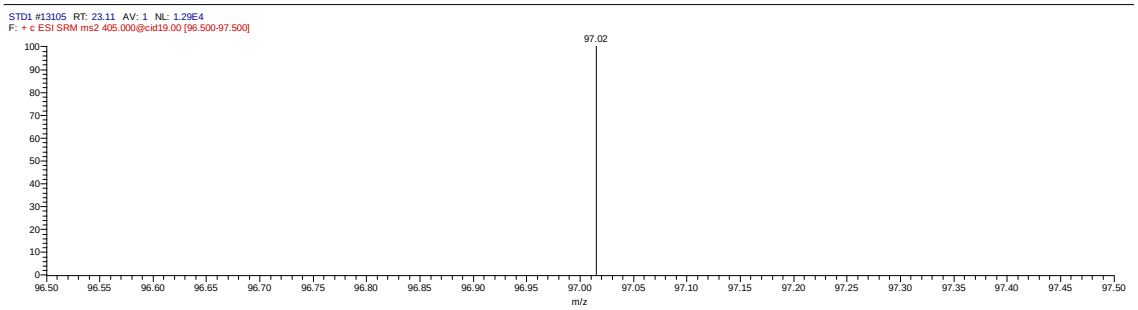

Figure 23: LC-MS/MS chromatogram of UDP. A) Chromatographic separation of UDP peak shows retention time (RT) at ~23.1 min. B) SRM scan of ionized UDP shows the detection of its product ion at mass-to-charge (m/z) of 97.

A)

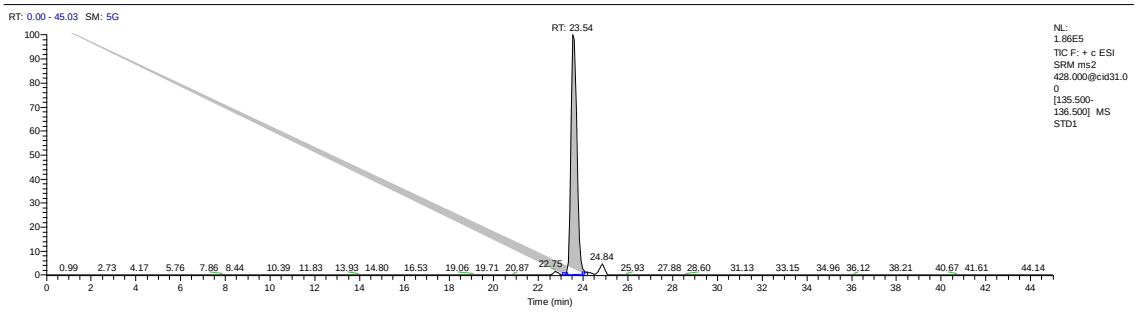

B)

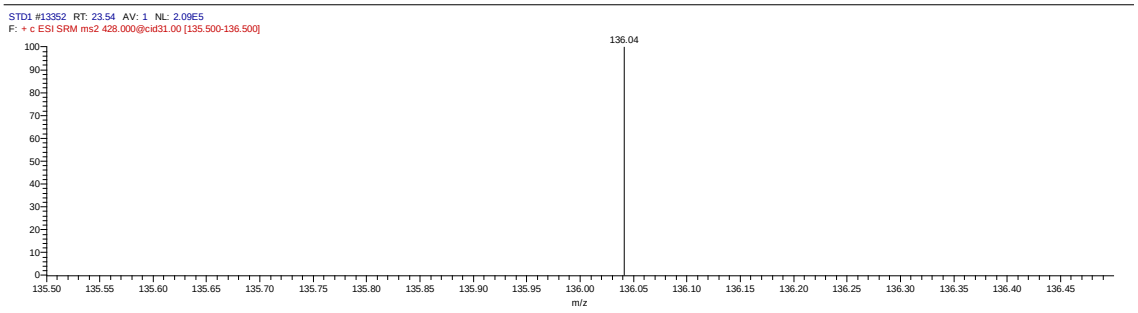

Figure 24: LC-MS/MS chromatogram of ADP. A) Chromatographic separation of ADP peak shows retention time (RT) at ~23.5 min. B) SRM scan of ionized ADP shows the detection of its product ion at mass-to-charge (m/z) of 136.

A)

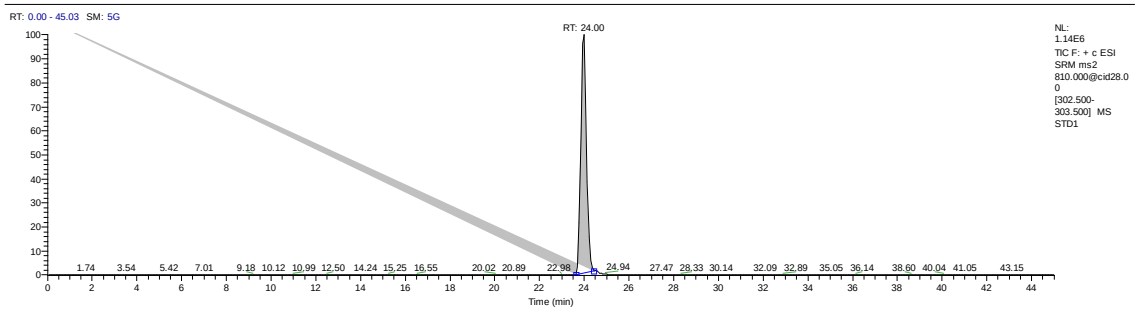

B)

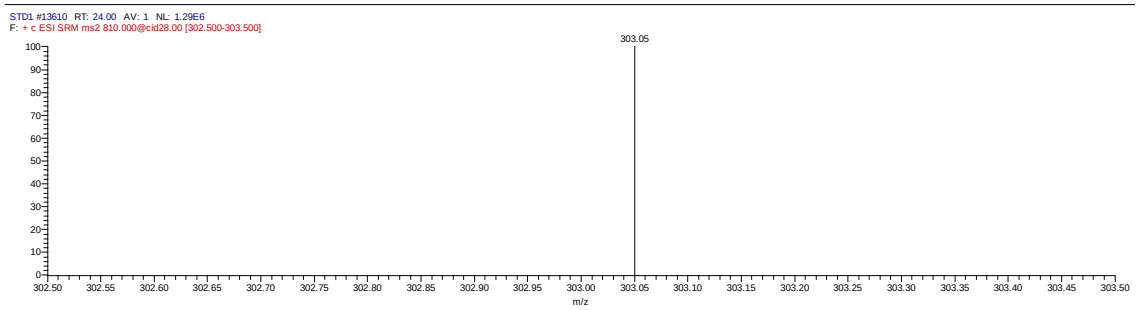

Figure 25: LC-MS/MS chromatogram of acetyl-CoA. A) Chromatographic separation of acetyl-CoA peak shows retention time (RT) at ~24 min. B) SRM scan of ionized acetyl-CoA shows the detection of its product ion at mass-to-charge (m/z) of 303.

A)

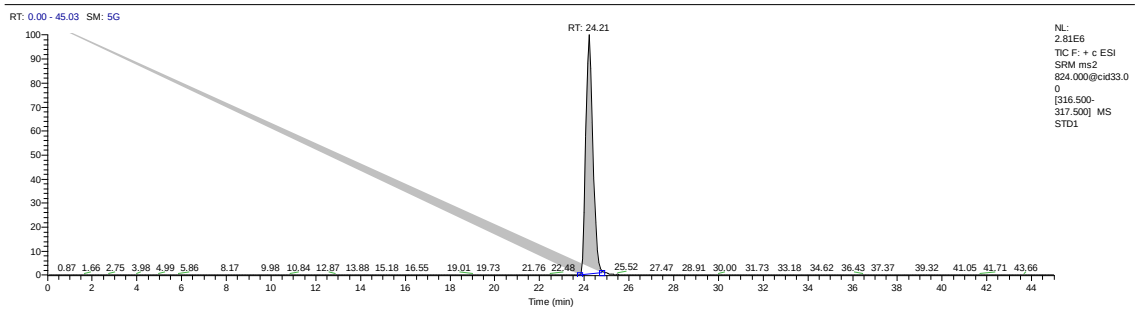

B)

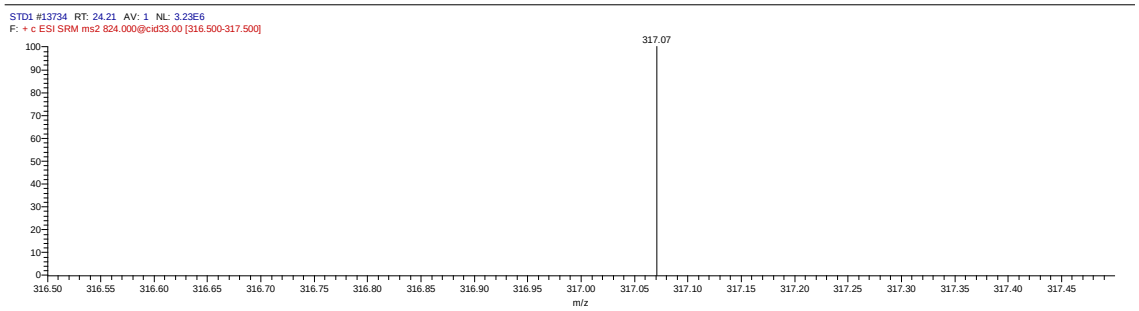

Figure 26: LC-MS/MS chromatogram of propionyl-CoA. A) Chromatographic separation of propionyl-CoA peak shows retention time (RT) at ~24.2 min. B) SRM scan of ionized propionyl-CoA shows the detection of its product ion at mass-to-charge (m/z) of 317.

A)

B)

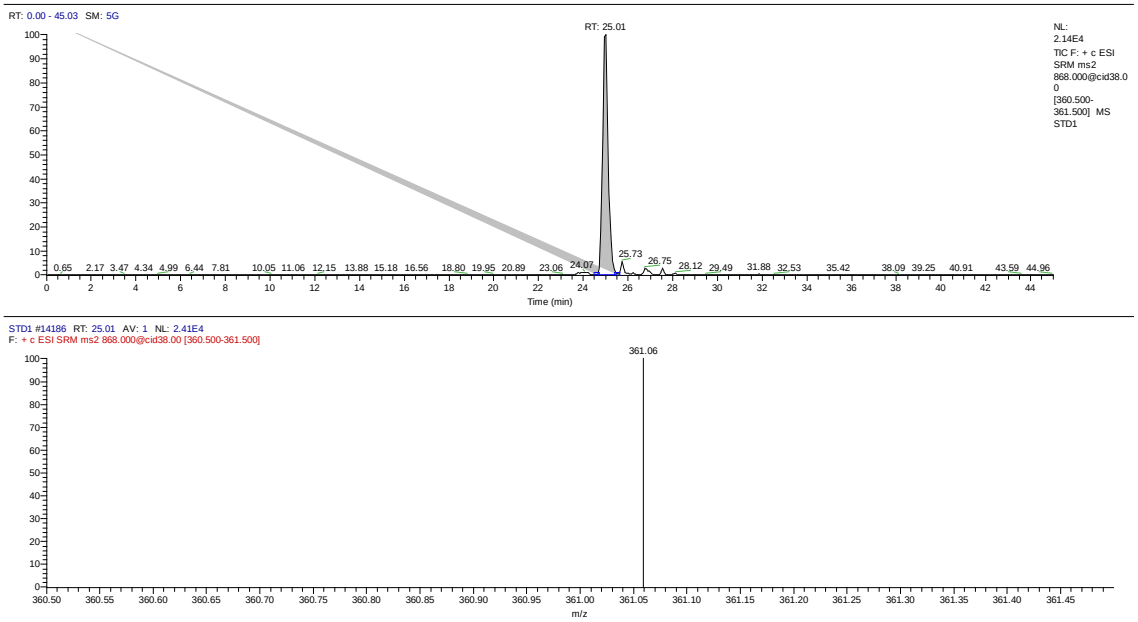

Figure 27: LC-MS/MS chromatogram of succinyl-CoA. A) Chromatographic separation of succinyl-CoA peak shows retention time (RT) at ~25 min. B) SRM scan of ionized succinyl-CoA shows the detection of its product ion at mass-to-charge (m/z) of 361.

A)

B)

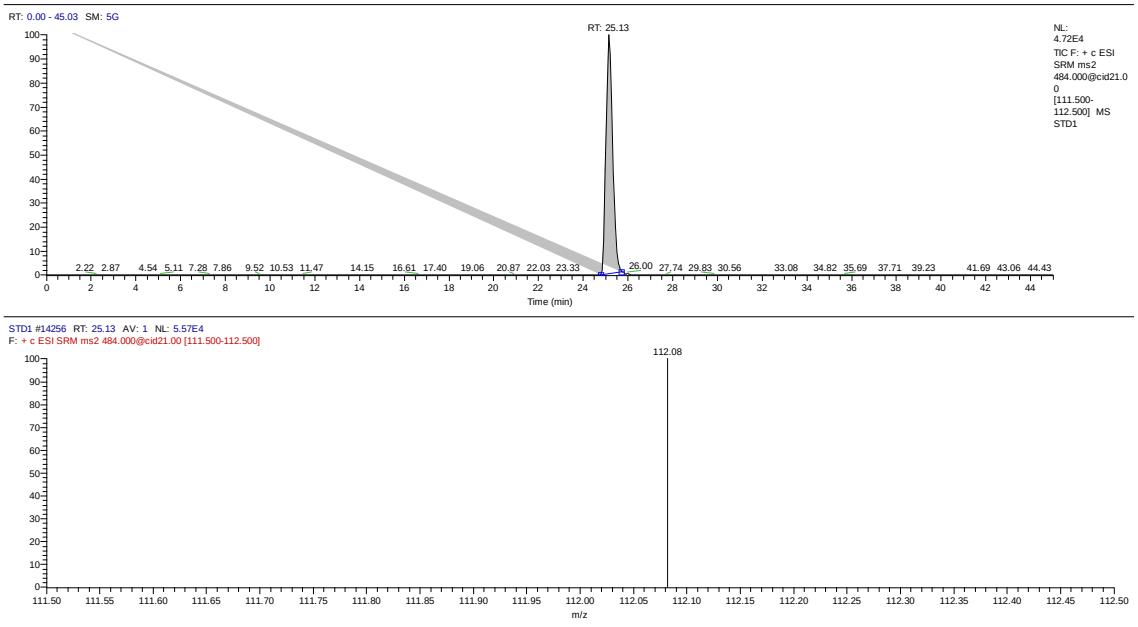

Figure 28: LC-MS/MS chromatogram of CTP. A) Chromatographic separation of CTP peak shows retention time (RT) at ~25.1 min. B) SRM scan of ionized CTP shows the detection of its product ion at mass-to-charge (m/z) of 112.

A)

B)

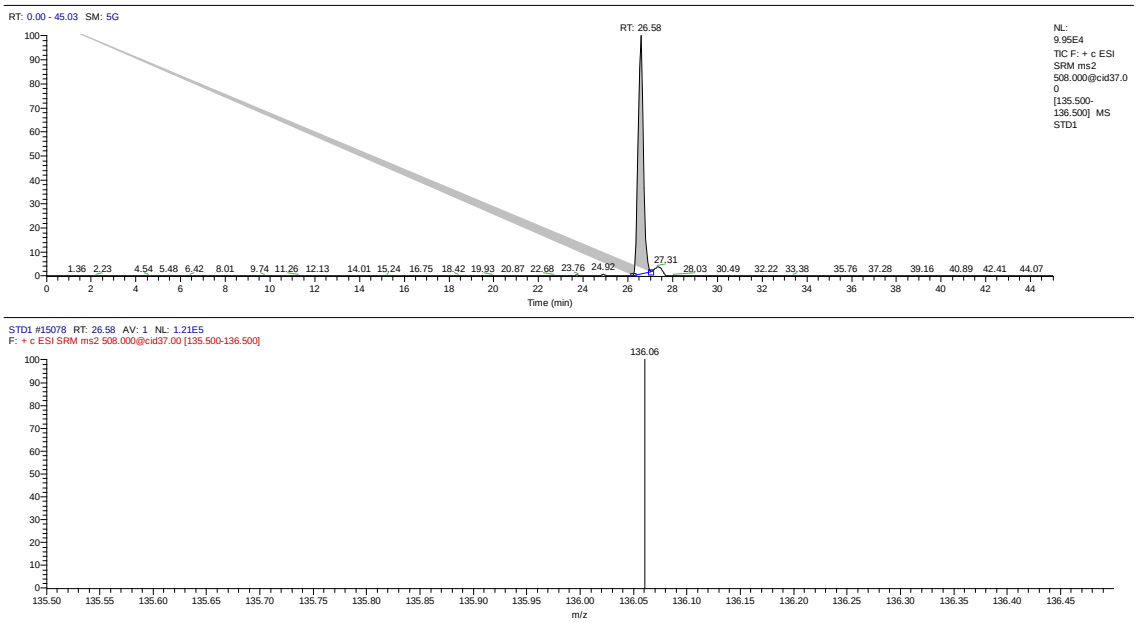

Figure 29: LC-MS/MS chromatogram of ATP. A) Chromatographic separation of ATP peak shows retention time (RT) at ~25.5 min. B) SRM scan of ionized ATP shows the detection of its product ion at mass-to-charge (m/z) of 136.

A)

B)

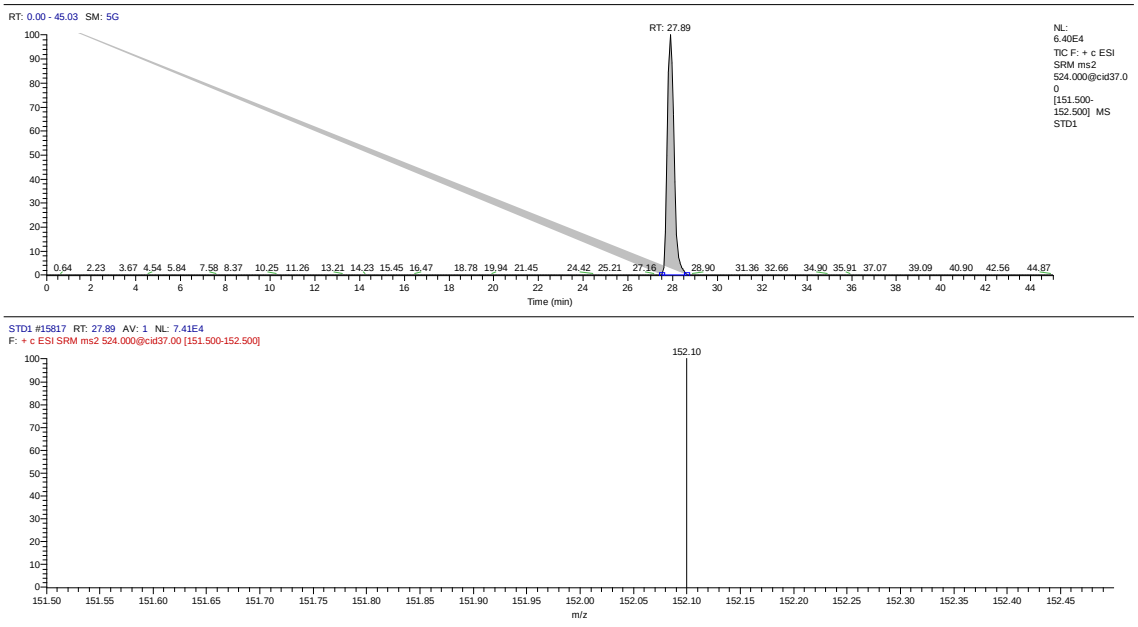

Figure 30: LC-MS/MS chromatogram of GTP. A) Chromatographic separation of GTP peak shows retention time (RT) at ~27.8 min. B) SRM scan of ionized GTP shows the detection of its product ion at mass-to-charge (m/z) of 152.

A)

B)

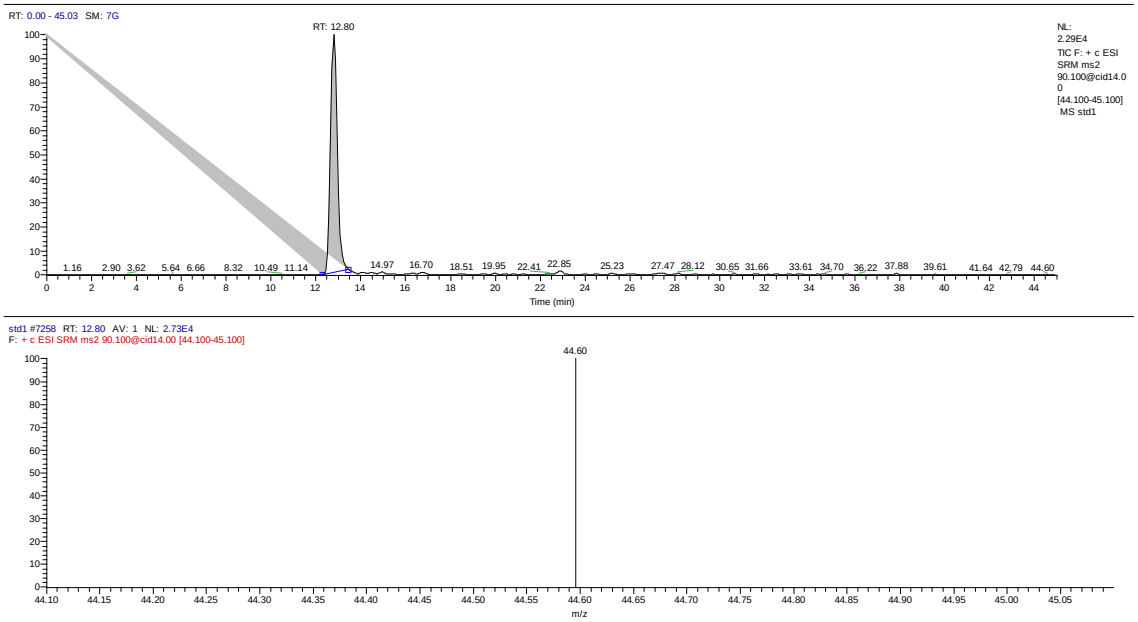

Figure 31: LC-MS/MS chromatogram of alanine. A) Chromatographic separation of alanine peak shows retention time (RT) at ~12.8 min. B) SRM scan of ionized alanine shows the detection of its product ion at mass-to-charge (m/z) of 44.1.

A)

B)

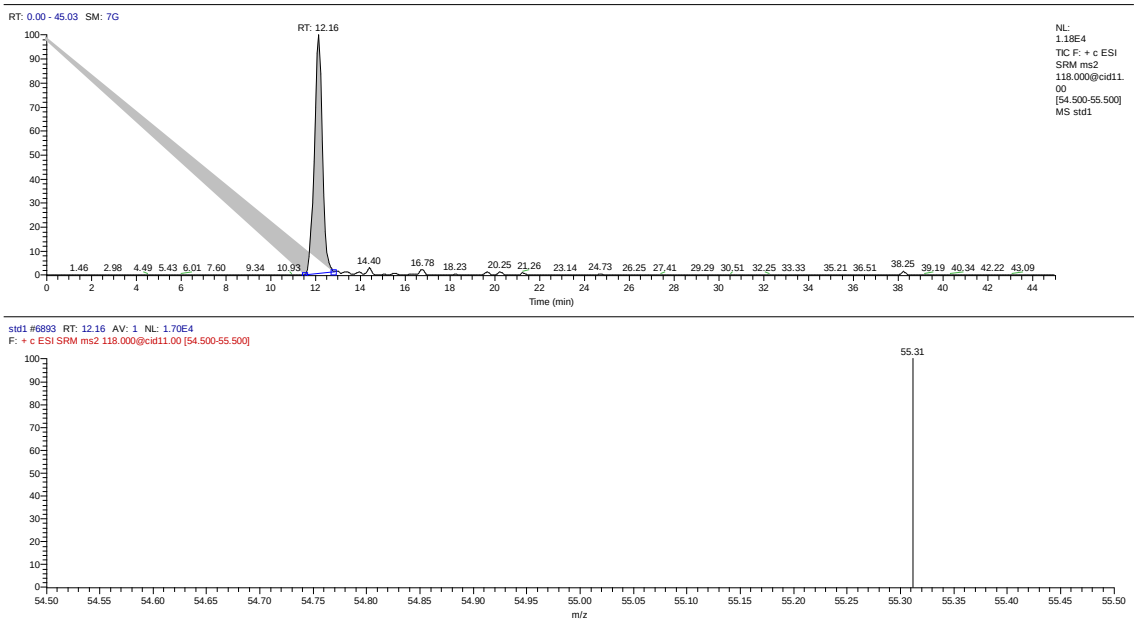

Figure 32: LC-MS/MS chromatogram of valine. A) Chromatographic separation of valine peak shows retention time (RT) at ~12.1 min. B) SRM scan of ionized valine shows the detection of its product ion at mass-to-charge (m/z) of 55.

A)

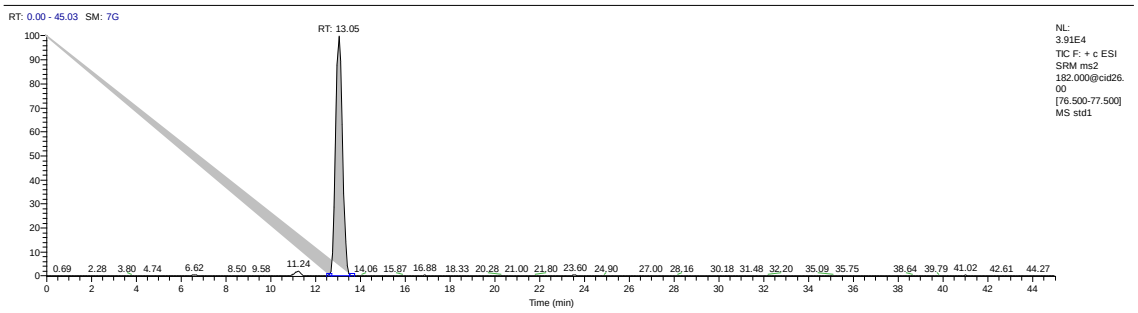

B)

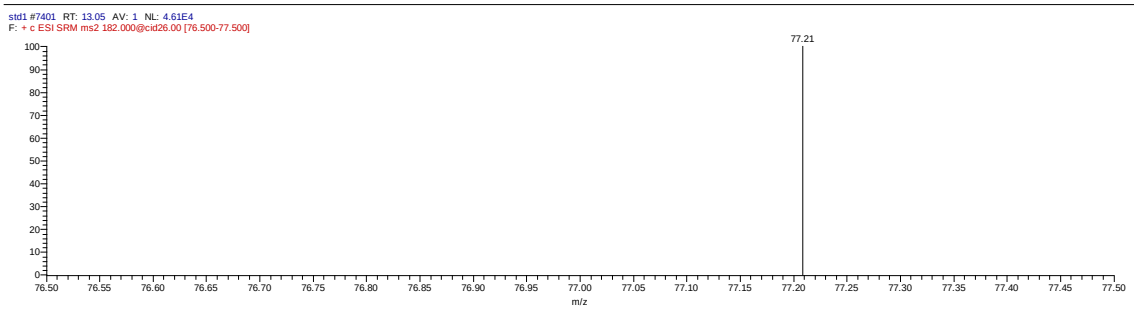

Figure 33: LC-MS/MS chromatogram of tyrosine. A) Chromatographic separation of tyrosine peak shows retention time (RT) at ~13 min. B) SRM scan of ionized tyrosine shows the detection of its product ion at mass-to-charge (m/z) of 77.

A)

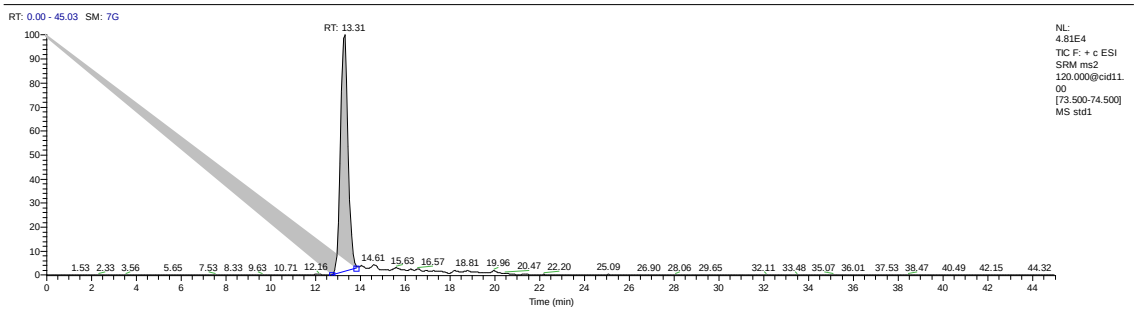

B)

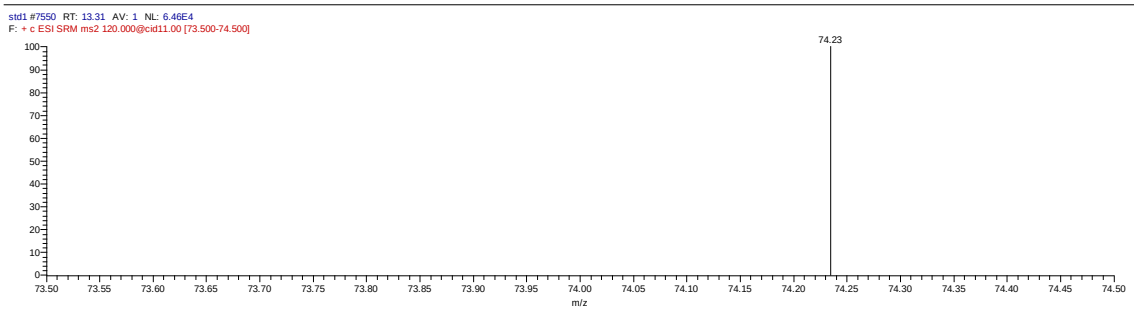

Figure 34: LC-MS/MS chromatogram of threonine. A) Chromatographic separation of threonine peak shows retention time (RT) at ~13.3 min. B) SRM scan of ionized threonine shows the detection of its product ion at mass-to-charge (m/z) of 74.

A)

B)

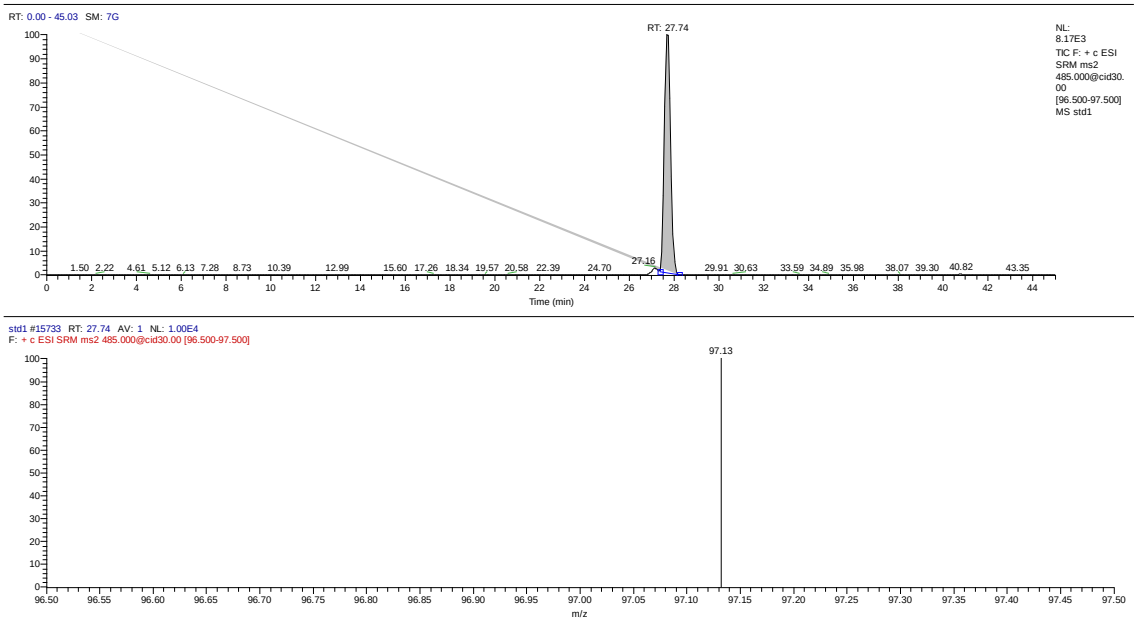

Figure 35: LC-MS/MS chromatogram of UTP. A) Chromatographic separation of UTP peak shows retention time (RT) at ~27.7 min. B) SRM scan of ionized UTP shows the detection of its product ion at mass-to-charge (m/z) of 97.

A)

B)

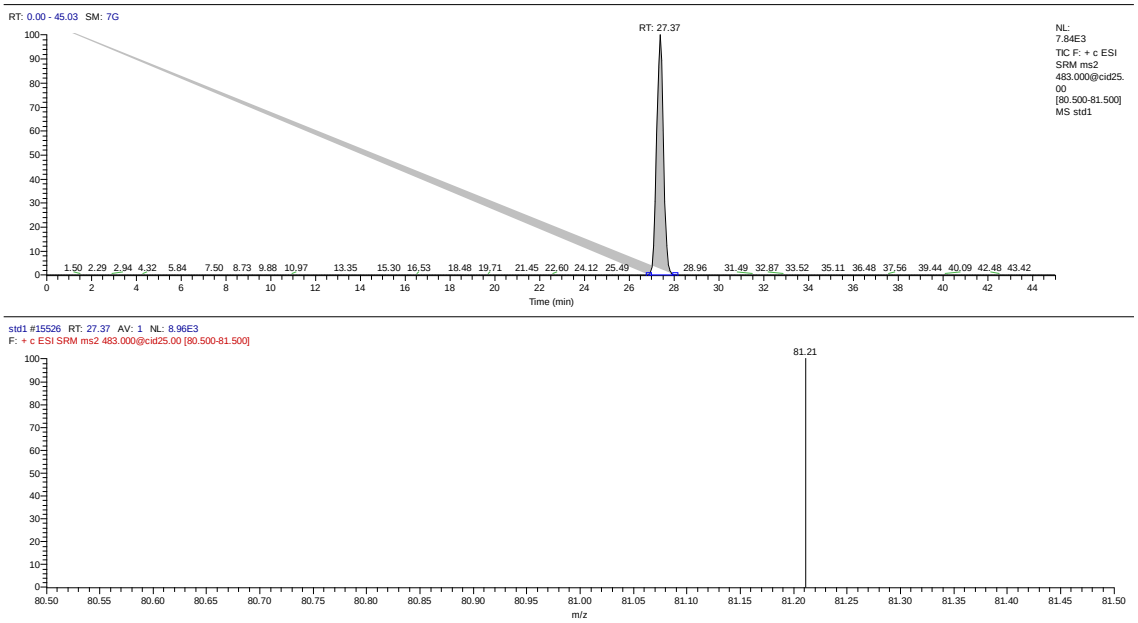

Figure 36: LC-MS/MS chromatogram of TTP. A) Chromatographic separation of TTP peak shows retention time (RT) at ~27.3 min. B) SRM scan of ionized TTP shows the detection of its product ion at mass-to-charge (m/z) of 81.

A)

B)

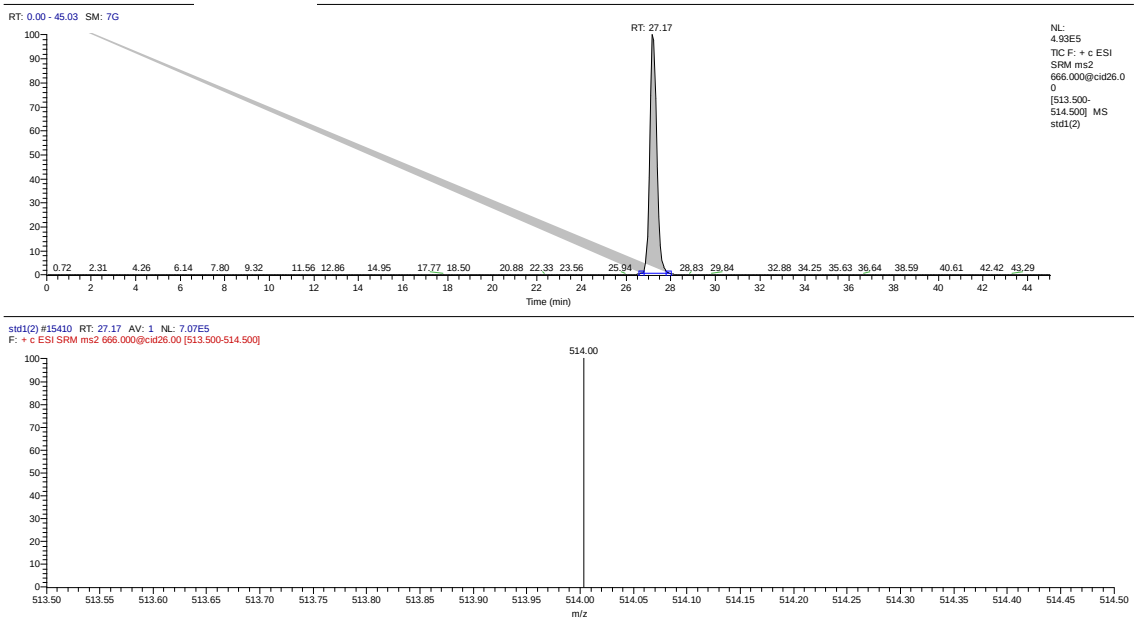

Figure 37: LC-MS/MS chromatogram of NADH. A) Chromatographic separation of NADH peak shows retention time (RT) at ~27.1 min. B) SRM scan of ionized NADH shows the detection of its product ion at mass-to-charge (m/z) of 514.

A)

B)

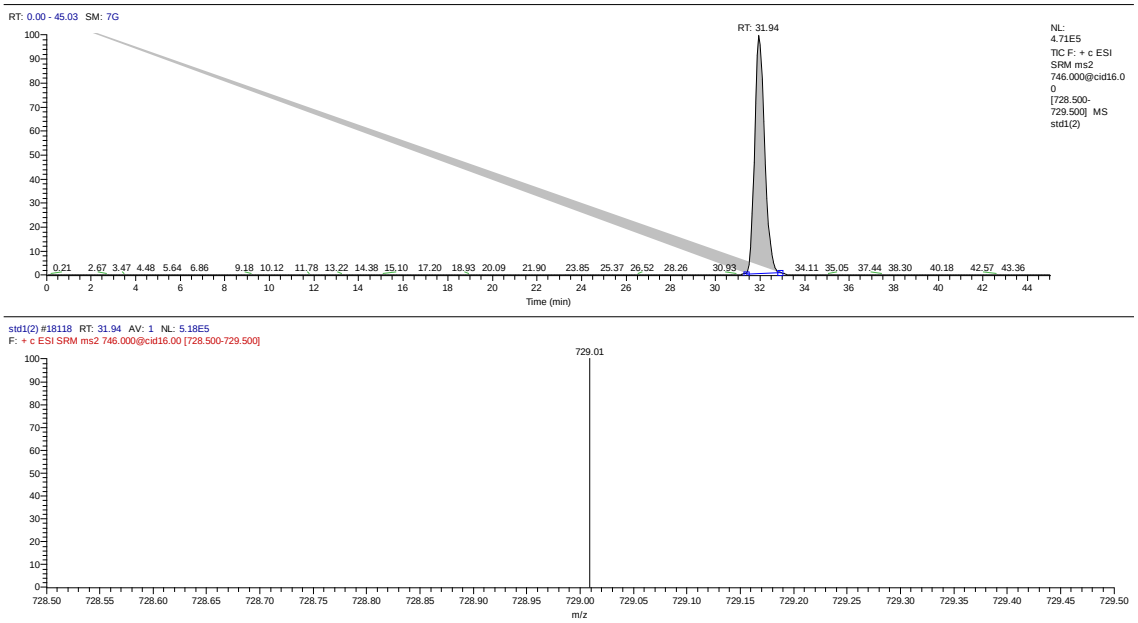

Figure 38: LC-MS/MS chromatogram of NADPH. A) Chromatographic separation of NADPH peak shows retention time (RT) at ~31.9 min. B) SRM scan of ionized NADPH shows the detection of its product ion at mass-to-charge (m/z) of 729.

A)

B)

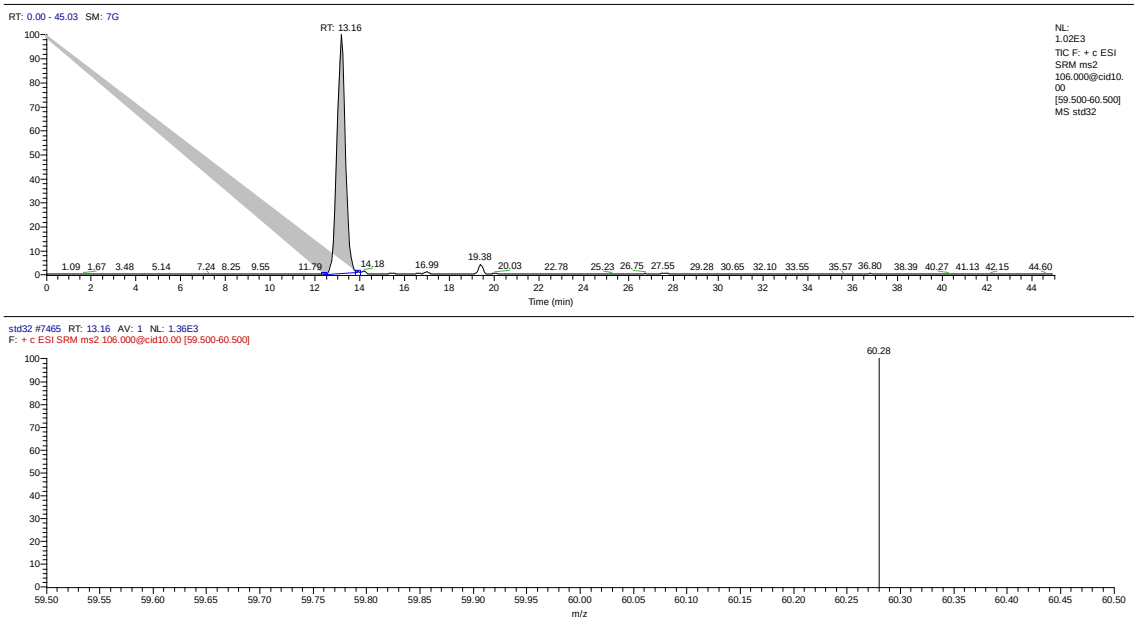

Figure 39: LC-MS/MS chromatogram of serine. A) Chromatographic separation of serine peak shows retention time (RT) at ~13.1 min. B) SRM scan of ionized serine shows the detection of its product ion at mass-to-charge (m/z) of 60.

A)

B)

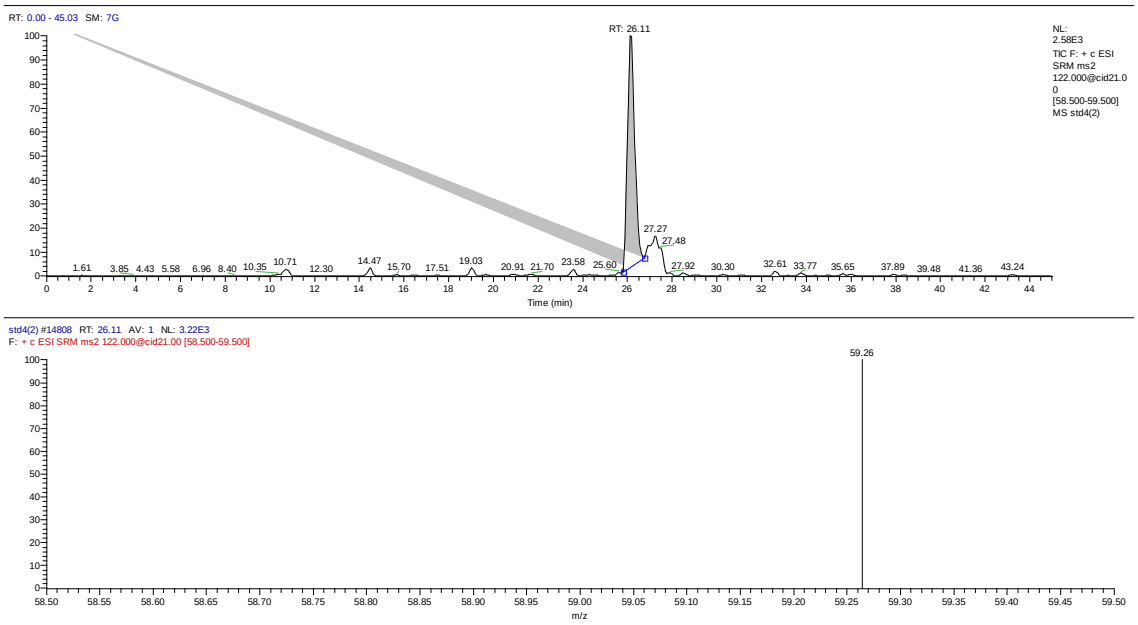

Figure 40: LC-MS/MS chromatogram of cysteine. A) Chromatographic separation of cysteine peak shows retention time (RT) at ~26.1 min. B) SRM scan of ionized cysteine shows the detection of its product ion at mass-to-charge (m/z) of 59.

A)

B)

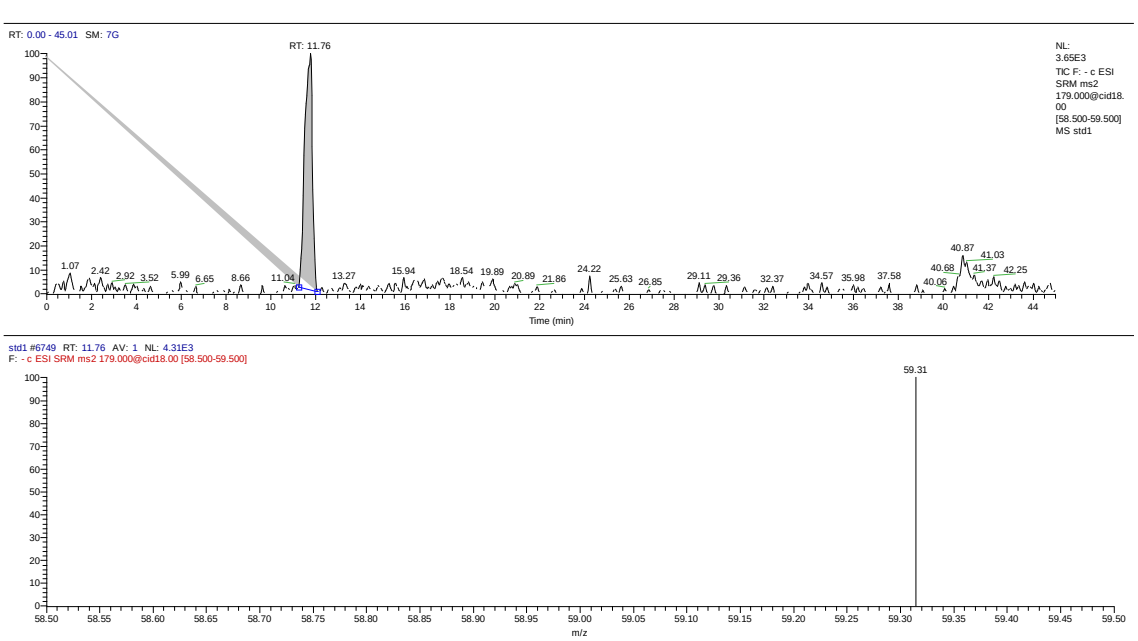

Figure 41: LC-MS/MS chromatogram of glucose. A) Chromatographic separation of glucose peak shows retention time (RT) at ~11.7 min. B) SRM scan of ionized glucose shows the detection of its product ion at mass-to-charge (m/z) of 59.

A)

B)

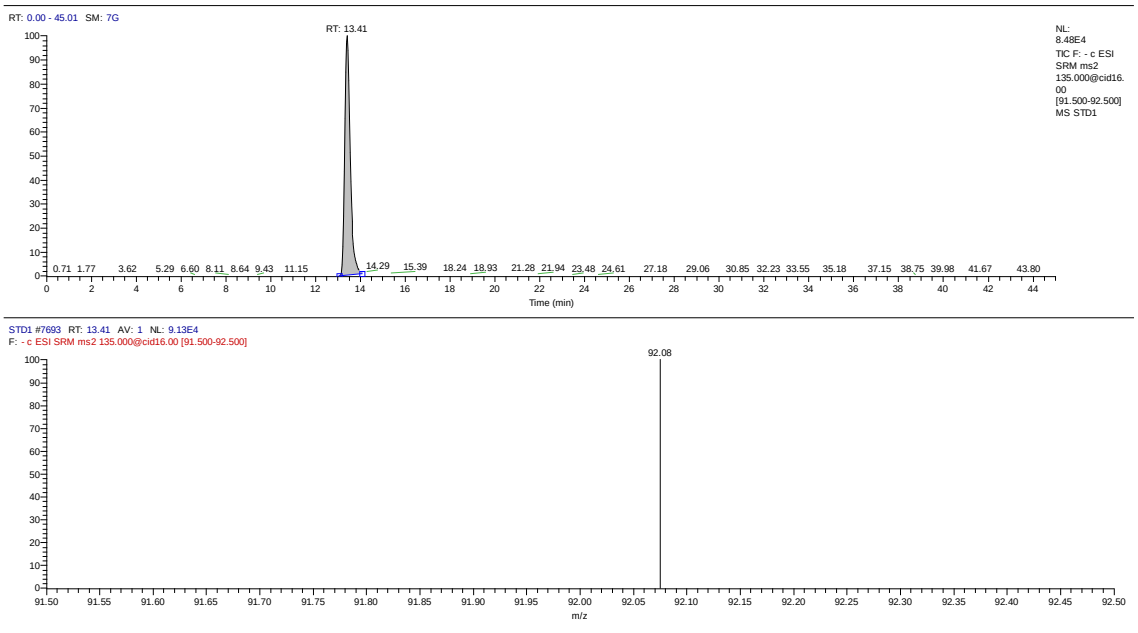

Figure 42: LC-MS/MS chromatogram of hypoxanthine. A) Chromatographic separation of hypoxanthine peak shows retention time (RT) at ~13.4 min. B) SRM scan of ionized hypoxanthine shows the detection of its product ion at mass-to-charge (m/z) of 92.

A)

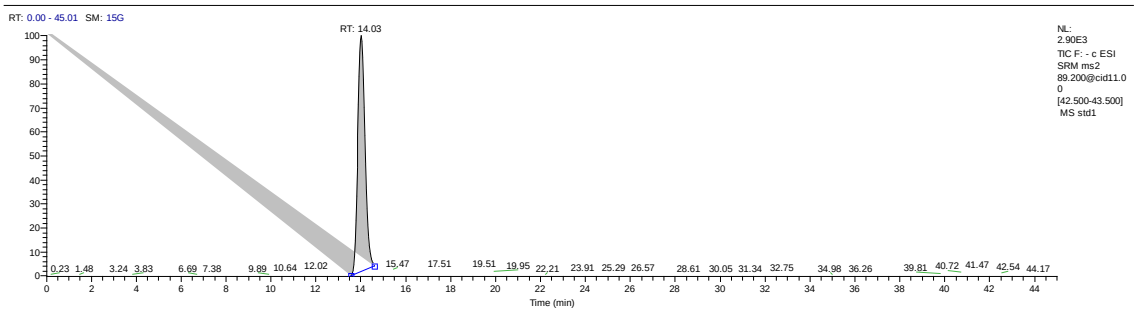

B)

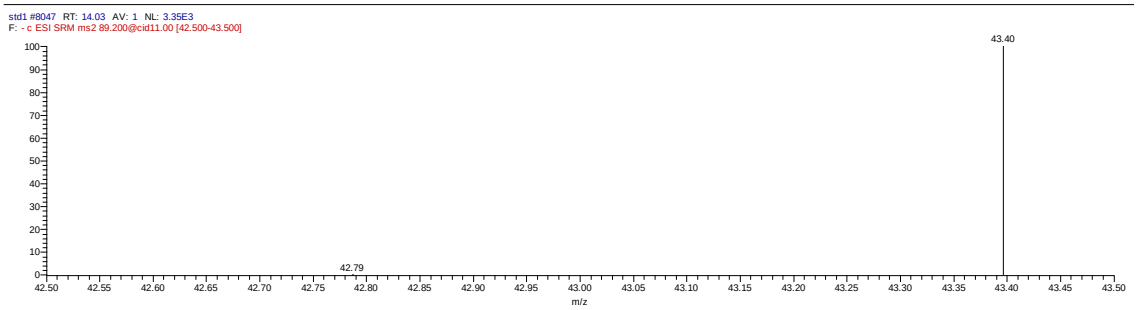

Figure 43: LC-MS/MS chromatogram of lactate. A) Chromatographic separation of lactate peak shows retention time (RT) at ~14 min. B) SRM scan of ionized lactate shows the detection of its product ion at mass-to-charge (m/z) of 43.

A)

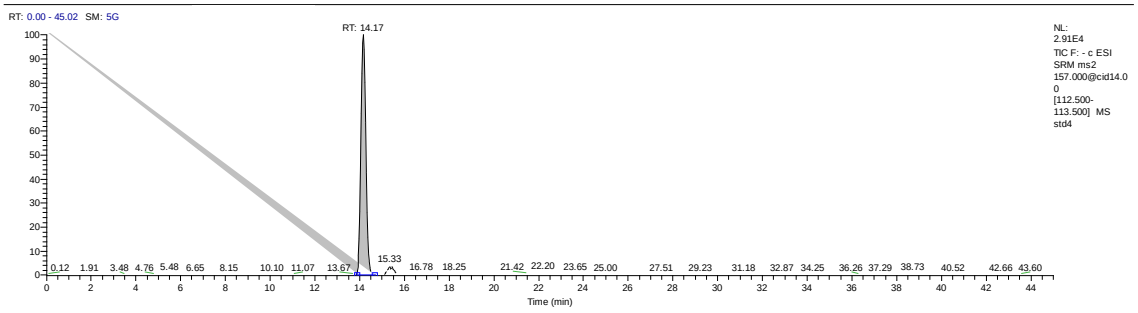

B)

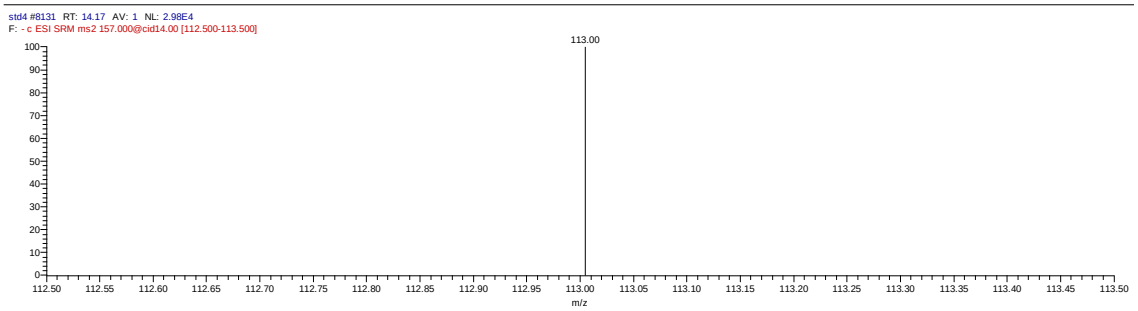

Figure 44: LC-MS/MS chromatogram of dihydroorotate. A) Chromatographic separation of dihydroorotate peak shows retention time (RT) at ~14.1 min. B) SRM scan of ionized dihydroorotate shows the detection of its product ion at mass-to-charge (m/z) of 113.

A)

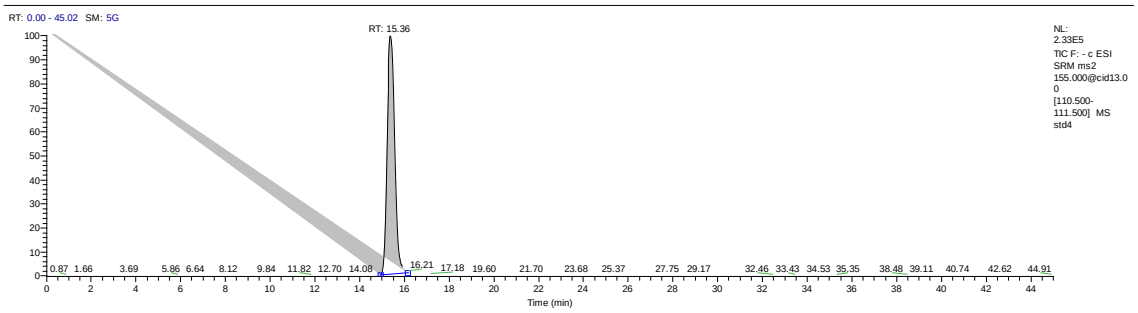

B)

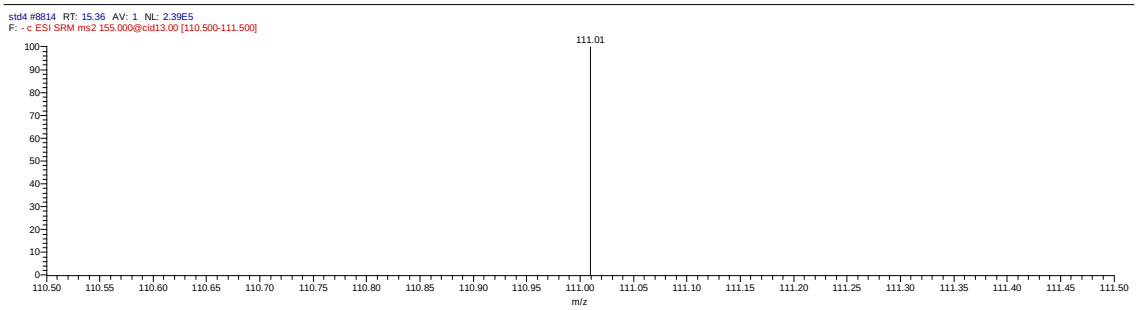

Figure 45: LC-MS/MS chromatogram of orotate. A) Chromatographic separation of orotate peak shows retention time (RT) at ~15.3 min. B) SRM scan of ionized orotate shows the detection of its product ion at mass-to-charge (m/z) of 111.

A)

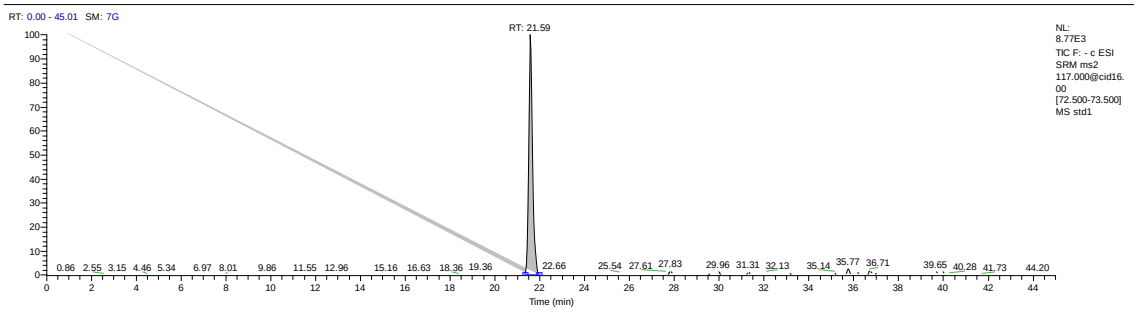

B)

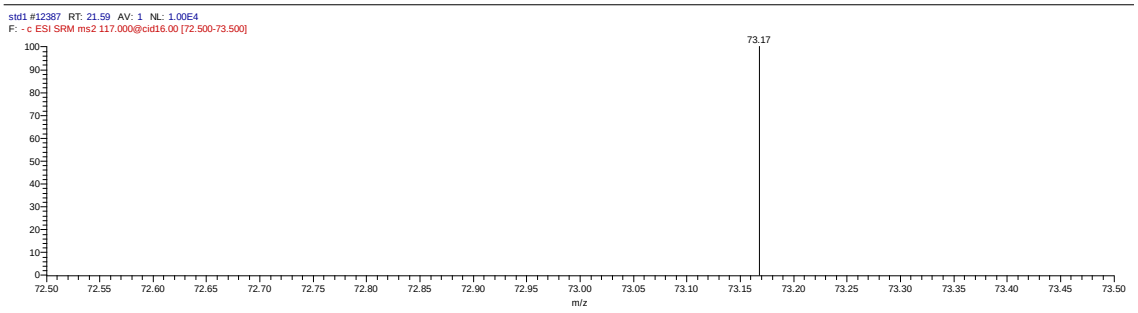

Figure 46: LC-MS/MS chromatogram of succinate. A) Chromatographic separation of succinate peak shows retention time (RT) at ~21.5 min. B) SRM scan of ionized succinate shows the detection of its product ion at mass-to-charge (m/z) of 73.

A)

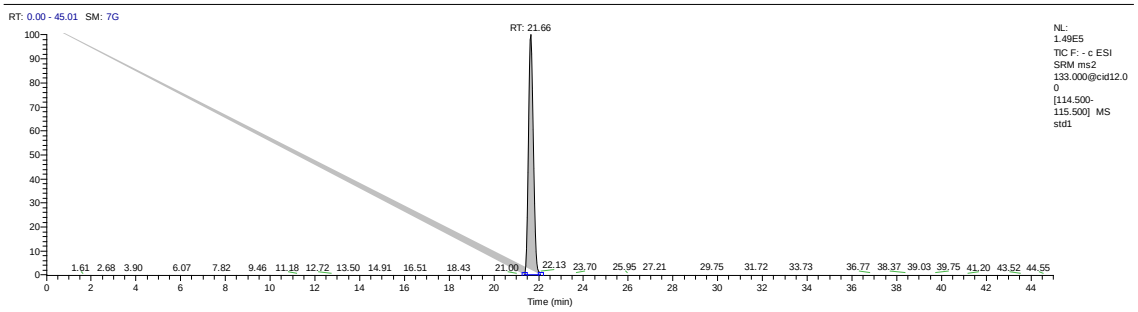

B)

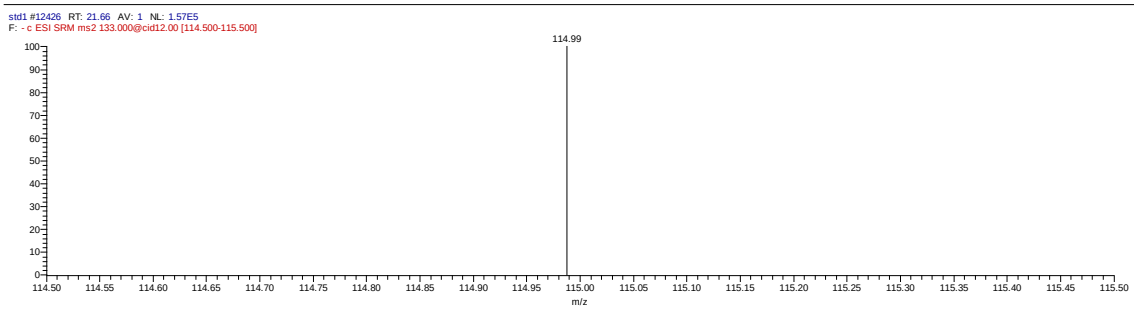

Figure 47: LC-MS/MS chromatogram of malate. A) Chromatographic separation of malate peak shows retention time (RT) at ~21.6 min. B) SRM scan of ionized malate shows the detection of its product ion at mass-to-charge (m/z) of 115.

A)

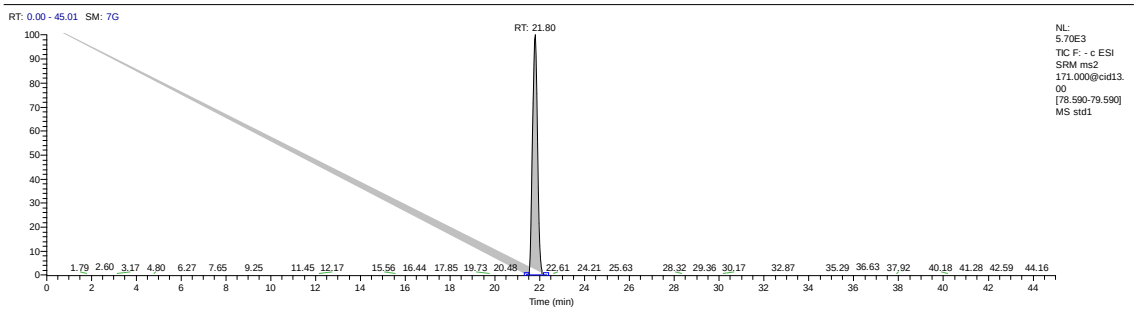

B)

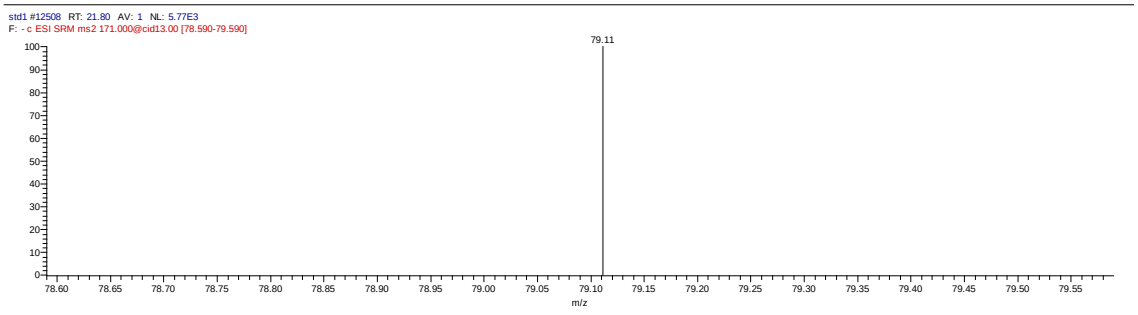

Figure 48: LC-MS/MS chromatogram of glycerol-3-phosphate (G-3-P). A) Chromatographic separation of G-3-P peak shows retention time (RT) at ~21.8 min. B) SRM scan of ionized G-3-P shows the detection of its product ion at mass-to-charge (m/z) of 79.

A)

B)

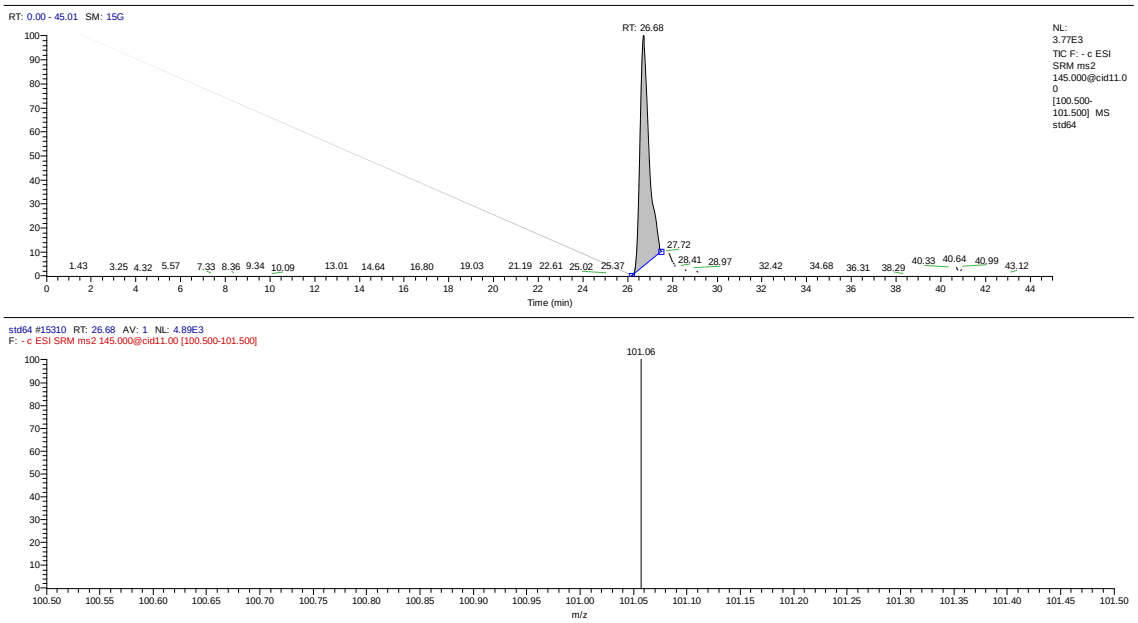

Figure 49: LC-MS/MS chromatogram of 2-oxoglutrate. A) Chromatographic separation of 2-oxoglutrate peak shows retention time (RT) at ~26.6 min. B) SRM scan of ionized 2-oxoglutrate shows the detection of its product ion at mass-to-charge (m/z) of 101.

A)

B)

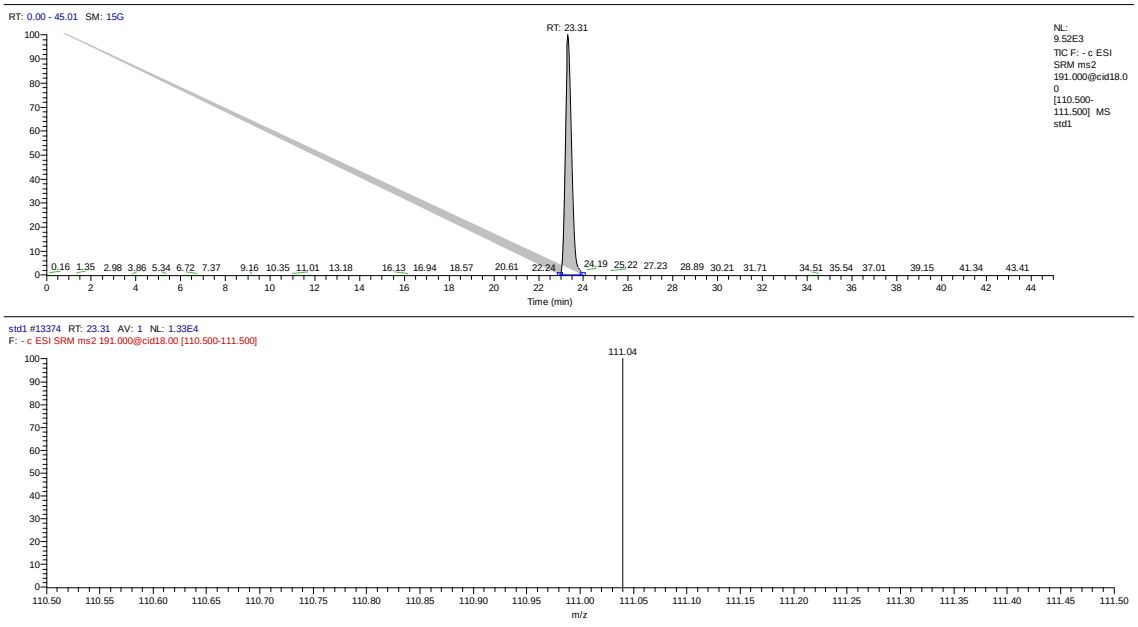

Figure 50: LC-MS/MS chromatogram of (iso)-citrate. A) Chromatographic separation of (iso)-citrate peak shows retention time (RT) at ~23.3 min. B) SRM scan of ionized (iso)-citrate shows the detection of its product ion at mass-to-charge (m/z) of 111.

A)

B)

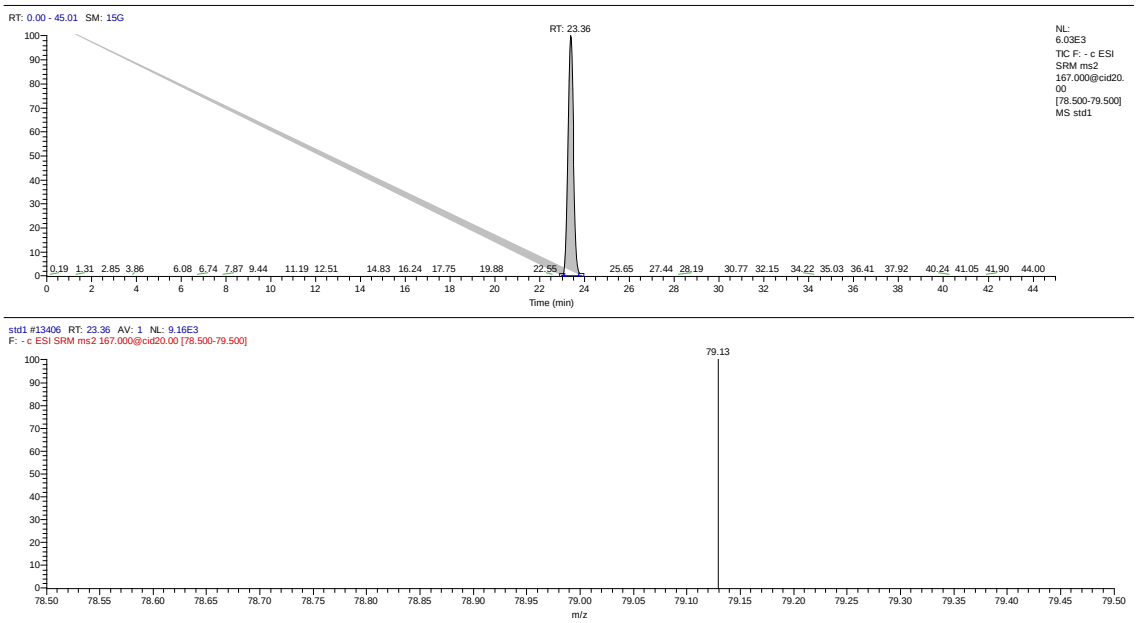

Figure 51: LC-MS/MS chromatogram of phosphoenol pyruvate (PEP). A) Chromatographic separation of PEP peak shows retention time (RT) at ~23.3 min. B) SRM scan of ionized PEP shows the detection of its product ion at mass-to-charge (m/z) of 79.

A)

B)

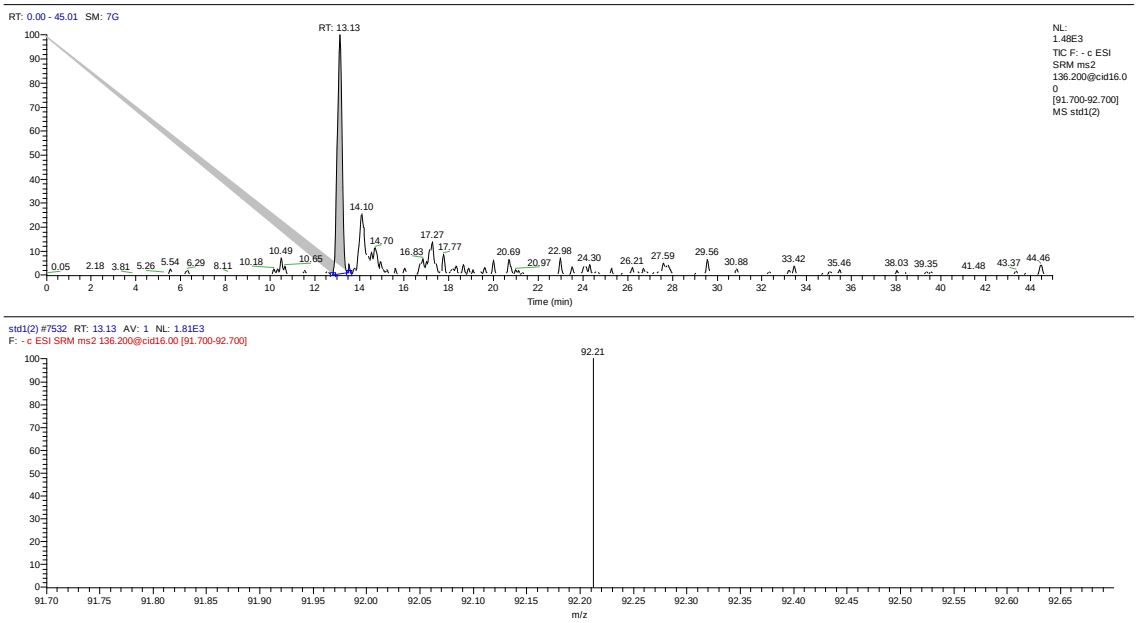

Figure 52: LC-MS/MS chromatogram of *p*-aminobenzoic acid (PABA). A) Chromatographic separation of PABA peak shows retention time (RT) at ~13.1 min. B) SRM scan of ionized PABA shows the detection of its product ion at mass-to-charge (m/z) of 92.

A)

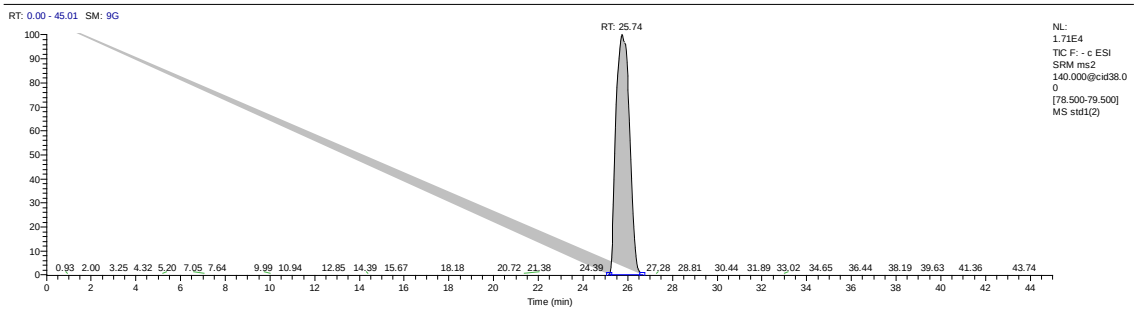

B)

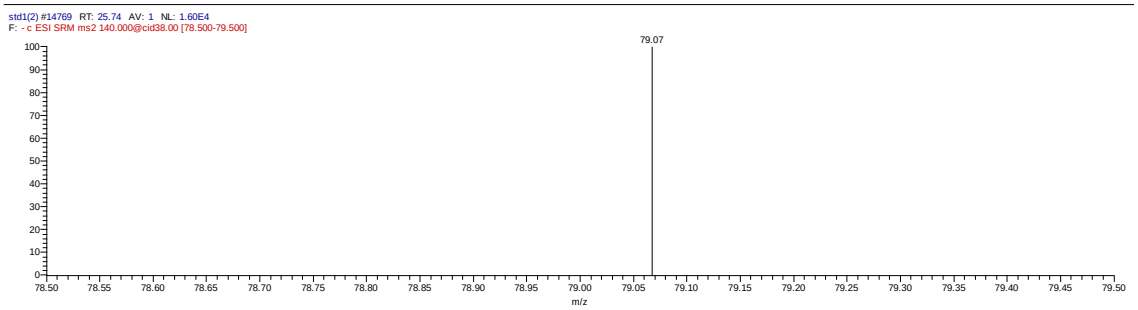

Figure 53: LC-MS/MS chromatogram of carbamoyl-phosphate. A) Chromatographic separation of carbamoyl-phosphate peak shows retention time (RT) at ~25.7 min. B) SRM scan of ionized carbamoyl-phosphate shows the detection of its product ion at mass-to-charge (m/z) of 79.

A)

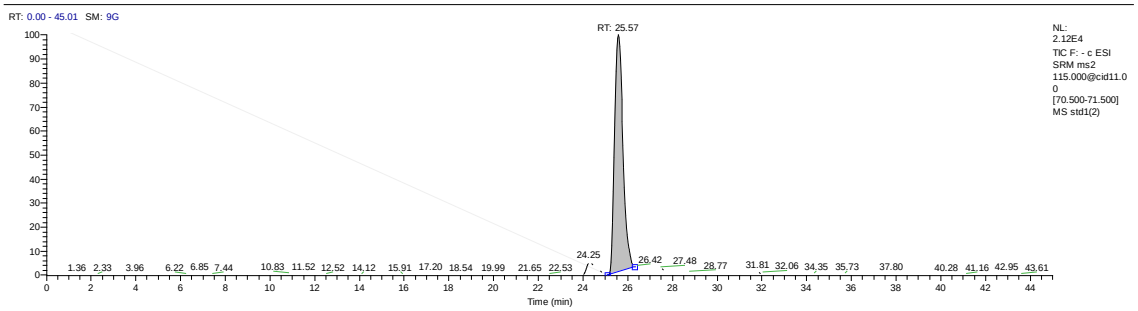

B)

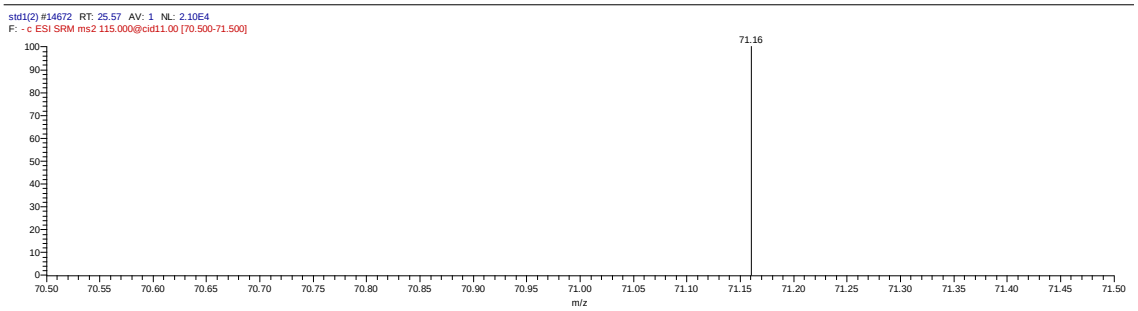

Figure 54: LC-MS/MS chromatogram of fumarate. A) Chromatographic separation of fumarate peak shows retention time (RT) at ~25.5 min. B) SRM scan of ionized fumarate shows the detection of its product ion at mass-to-charge (m/z) of 71.

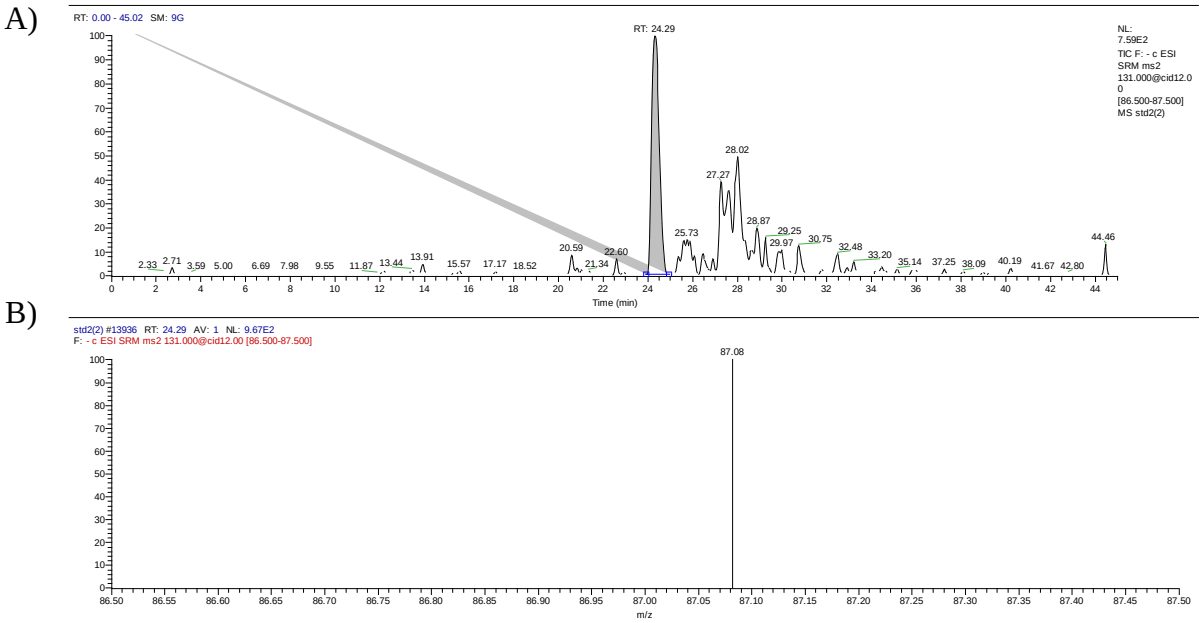

Figure 55: LC-MS/MS chromatogram of oxaloacetate. A) Chromatographic separation of oxaloacetate peak shows retention time (RT) at ~24.2 min. B) SRM scan of ionized oxaloacetate shows the detection of its product ion at mass-to-charge (m/z) of 87.

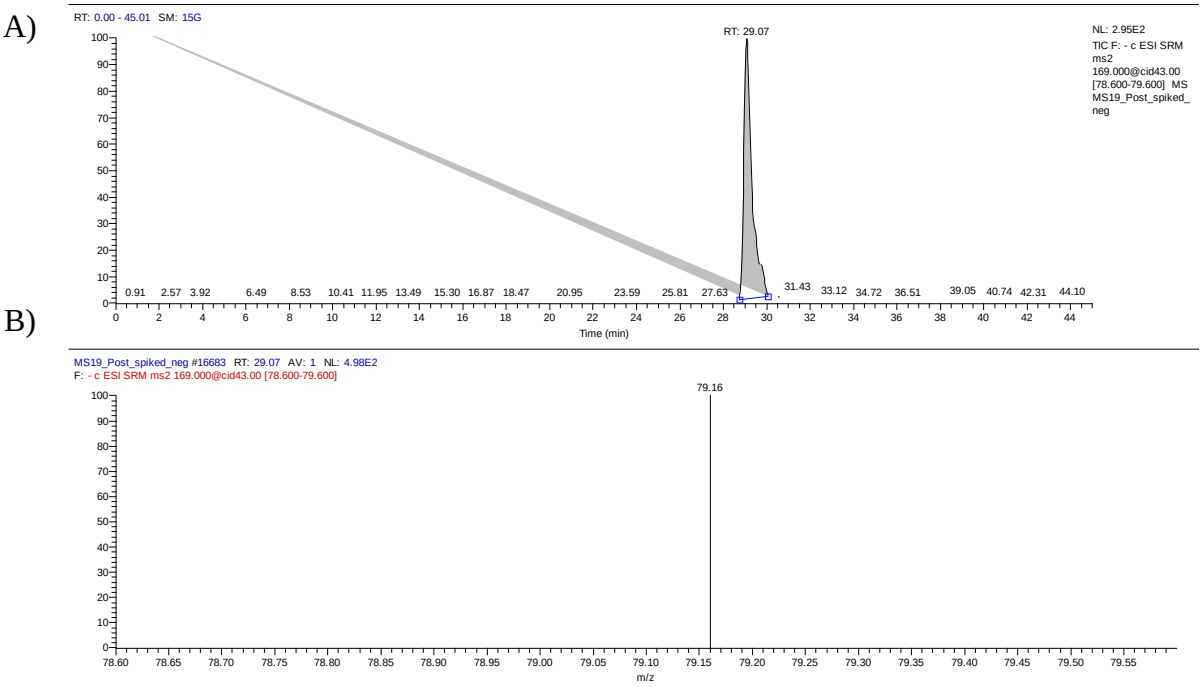

Figure 56: LC-MS/MS chromatogram of dihydroxyaceton phosphate (DHAP). A) Chromatographic separation of DHAP peak shows retention time (RT) at ~29 min. B) SRM scan of ionized DHAP shows the detection of its product ion at mass-to-charge (m/z) of 79.

A)

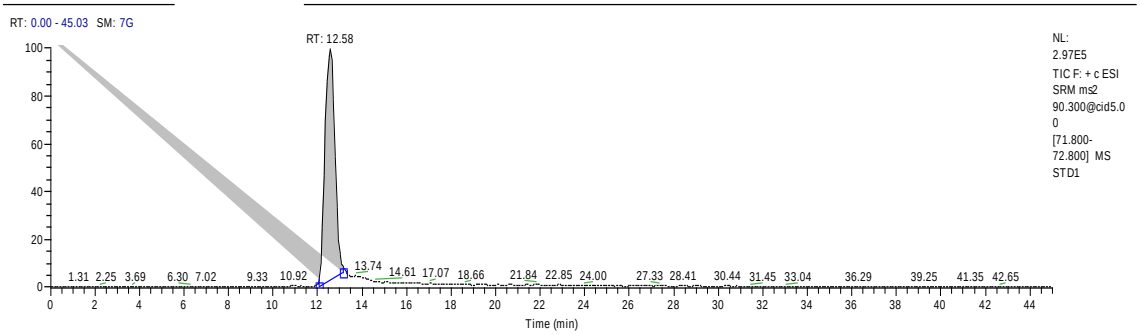

B)

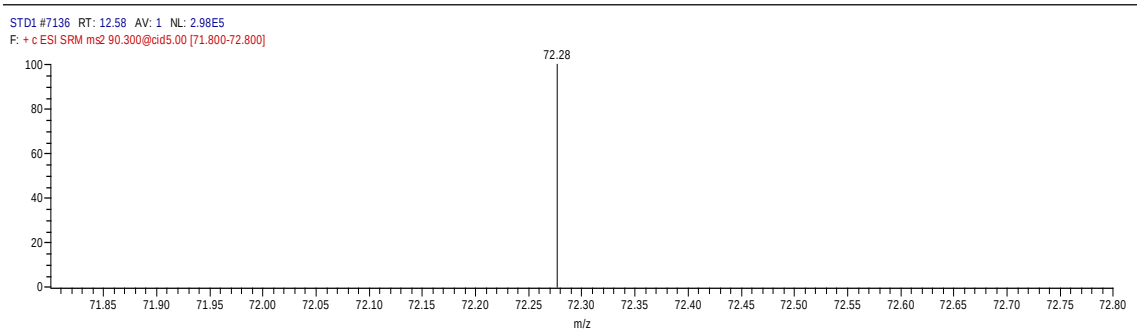

Figure 57: LC-MS/MS chromatogram of β–alanine (Internal Standard). A) Chromatographic separation of β–alanine peak shows retention time (RT) at ~12.5 min. B) SRM scan of ionized β–alanine shows the detection of its product ion at mass-to-charge (m/z) of 71.8.

A)

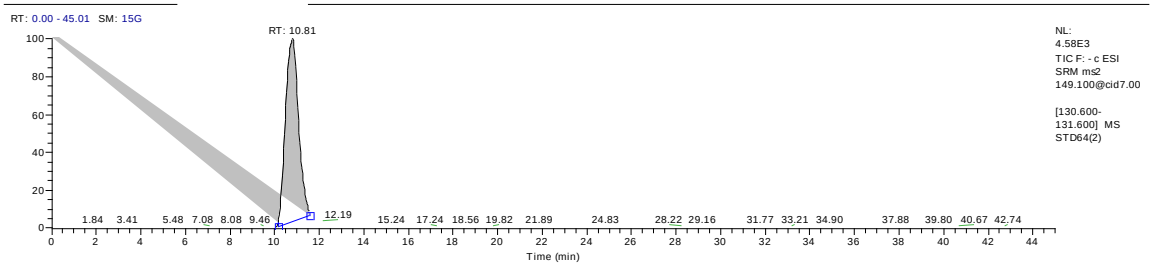

B)

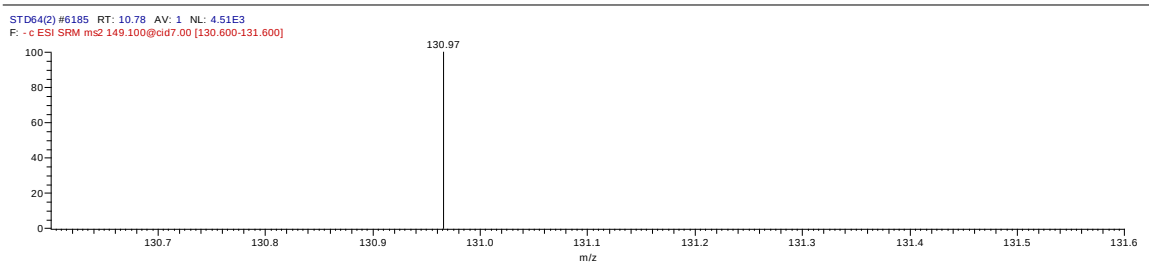

Figure 58: LC-MS/MS chromatogram of DL-arabinose (Internal Standard). A) Chromatographic separation of DL-arabinose peak shows retention time (RT) at ~10.8 min. B) SRM scan of ionized DL-arabinose shows the detection of its product ion at mass-to-charge (m/z) of 130.6.

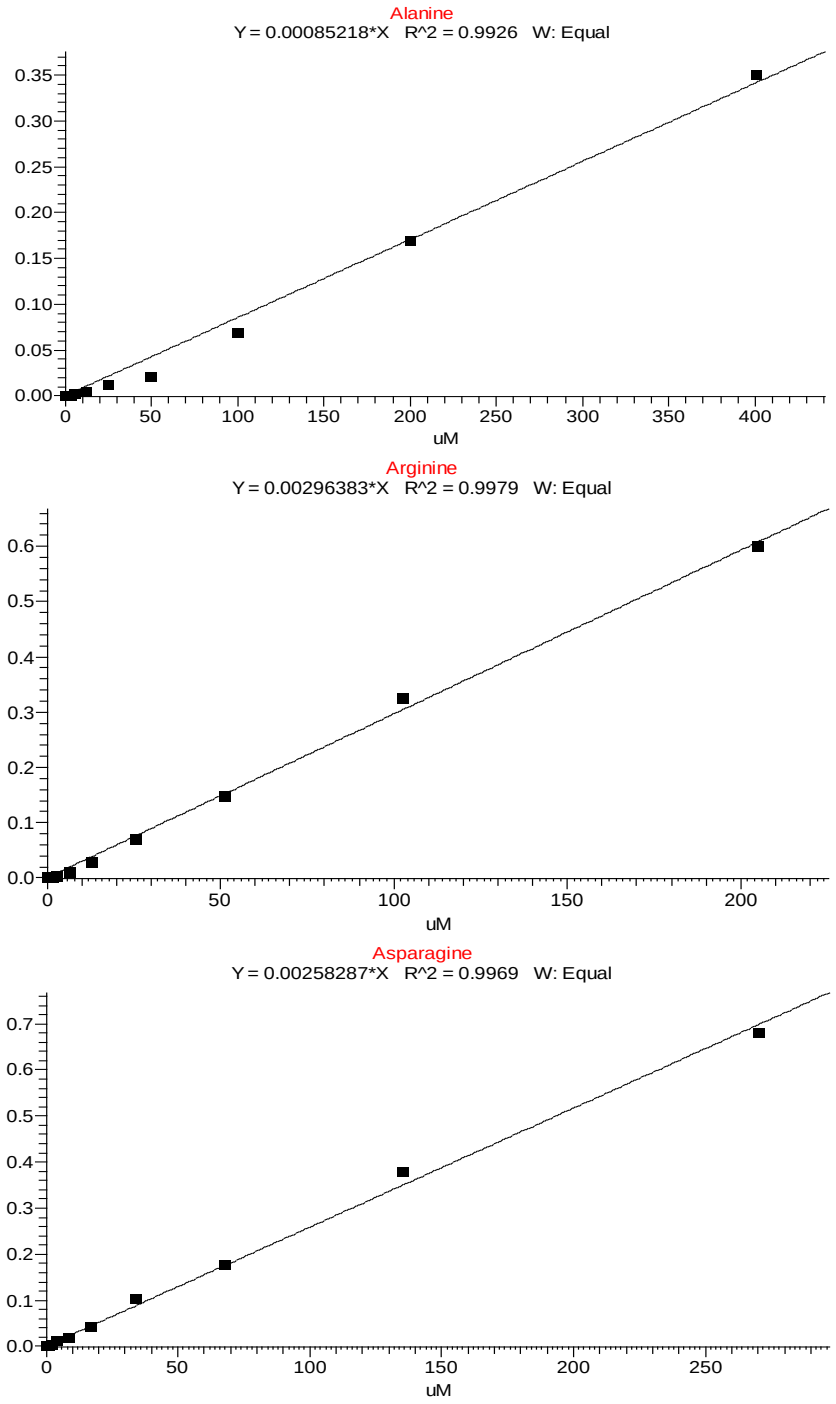

Figure 59. Standard calibration curves for alanine, arginine and asparagine show $R^2 \geq 0.99$. The line of best fit for each calibration curve was generated using equal weighted linear regression as the mathematical model of best fit. Metabolites concentration in QC and parasite samples were calculated from the resulting area ratio and the regression equation of the calibration curve.

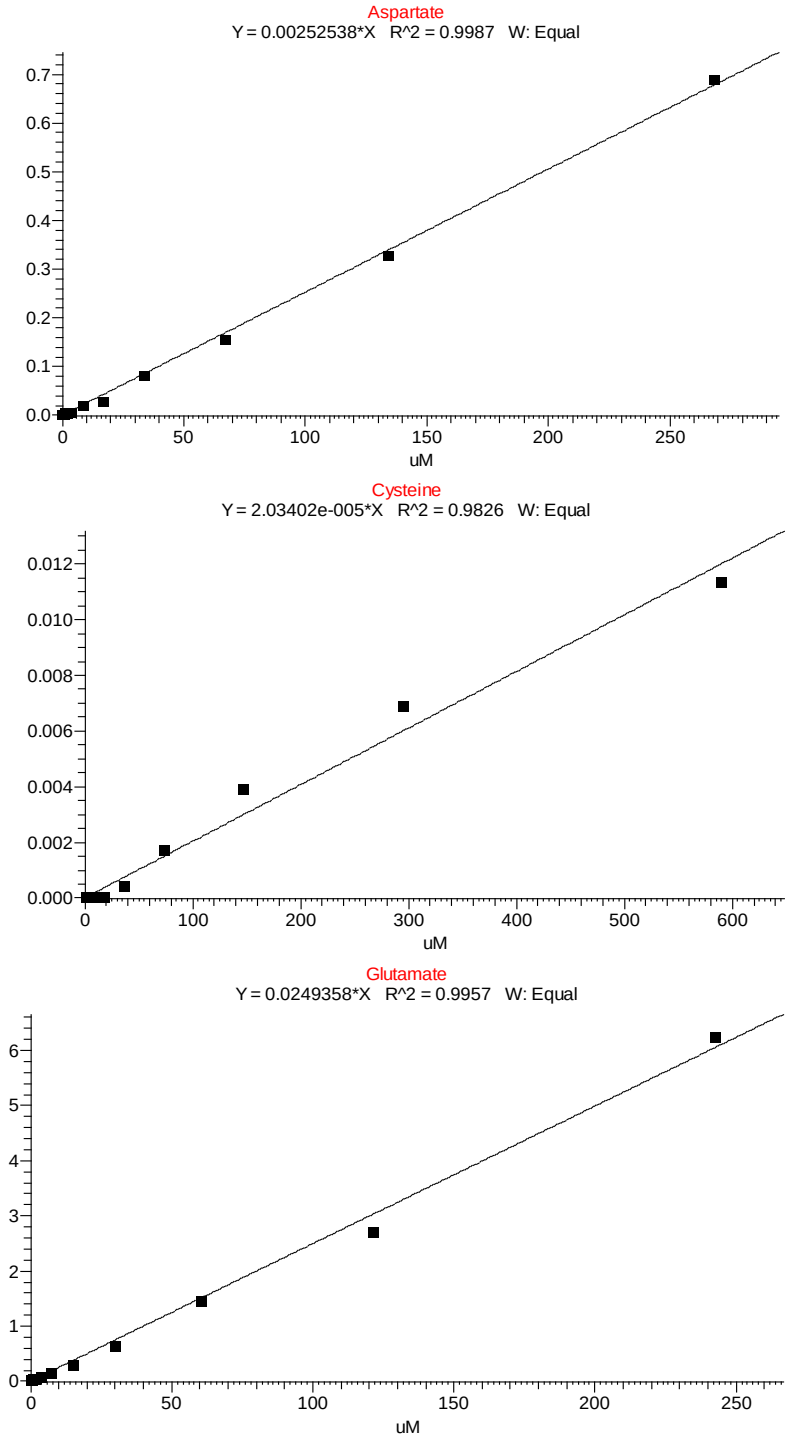

Figure 60. Standard calibration curves for aspartate, cysteine and glutamate show $R^2 \geq 0.98$. The line of best fit for each calibration curve was generated using equal weighted linear regression as the mathematical model of best fit. Metabolites concentration in QC and parasite samples was calculated from the resulting area ratio and the regression equation of the calibration curve.

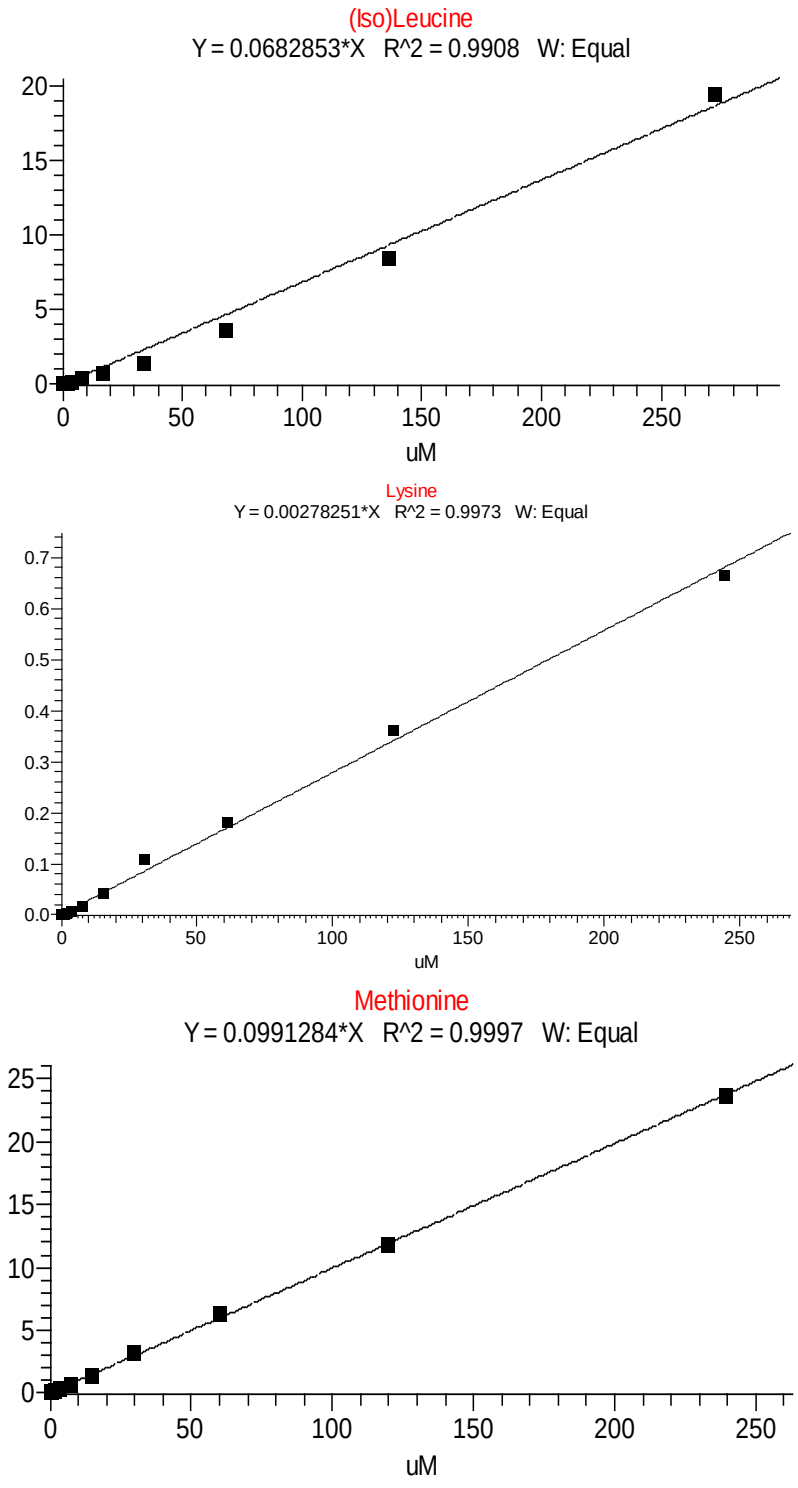

Figure 61. Standard calibration curves for (iso)-leucine, lysine and methionine show $R^2 \geq 0.99$. The line of best fit for each calibration curve was generated using equal weighted linear regression as the mathematical model of best fit. Metabolites concentration in QC and parasite samples was calculated from the resulting area ratio and the regression equation of the calibration curve.

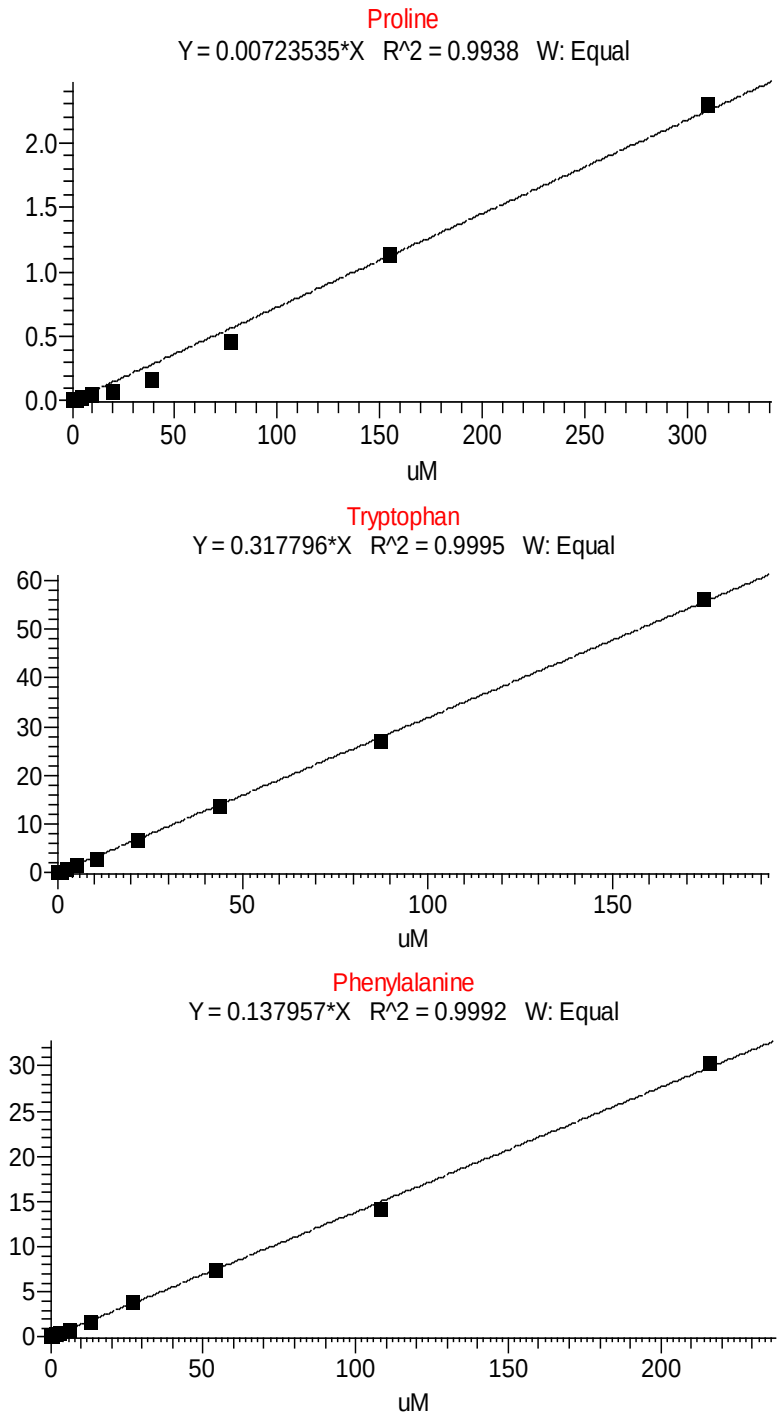

Figure 62. Standard calibration curves for proline, tryptophan and phenyalanine show $R^2 \geq 0.99$. The line of best fit for each calibration curve was generated using equal weighted linear regression as the mathematical model of best fit. Metabolites concentration in QC and parasite samples was calculated from the resulting area ratio and the regression equation of the calibration curve.

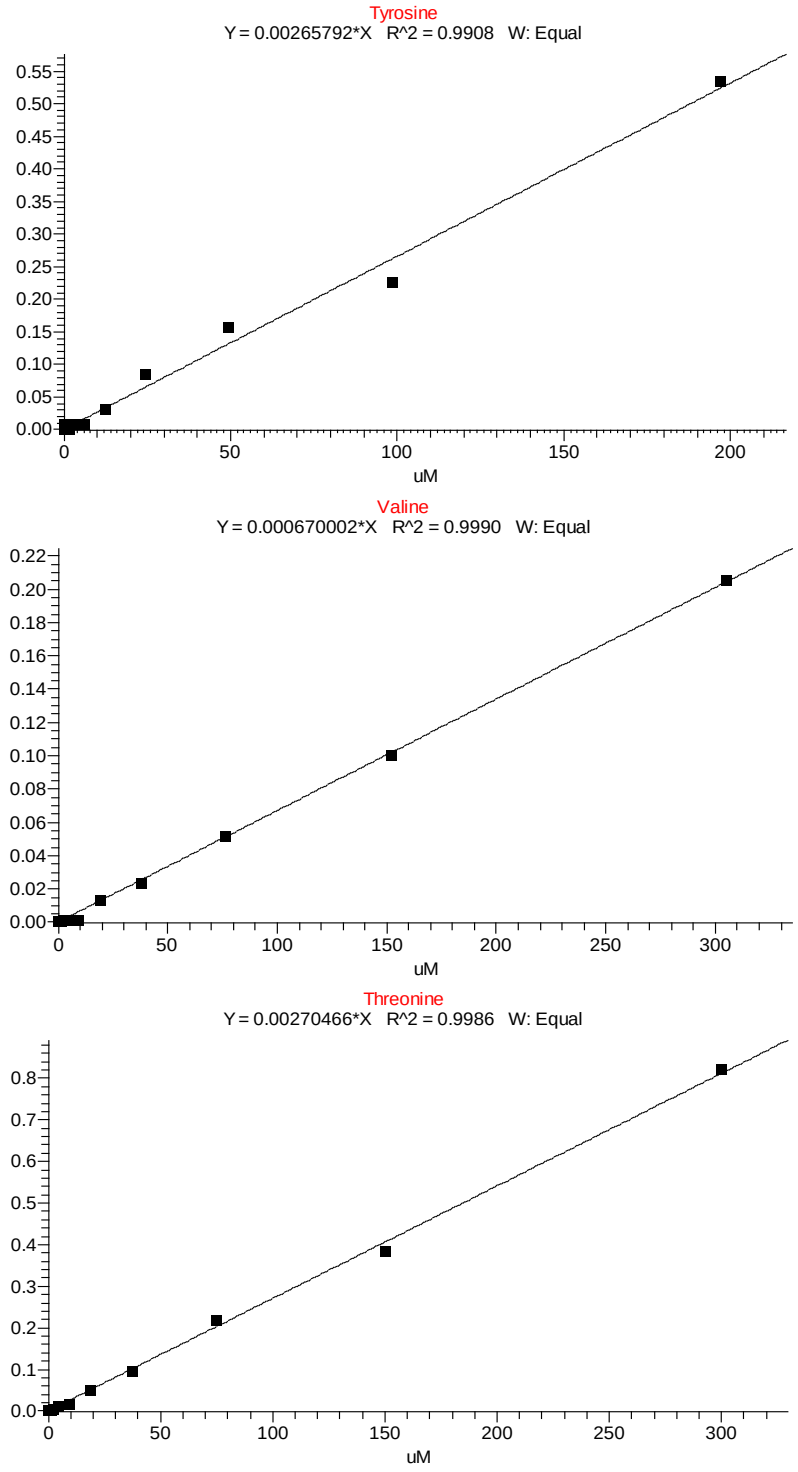

Figure 63. Standard calibration curves for tyrosine, valine and threonine show $R^2 \geq 0.99$. The line of best fit for each calibration curve was generated using equal weighted linear regression as the mathematical model of best fit. Metabolites concentration in QC and parasite samples was calculated from the resulting area ratio and the regression equation of the calibration curve.

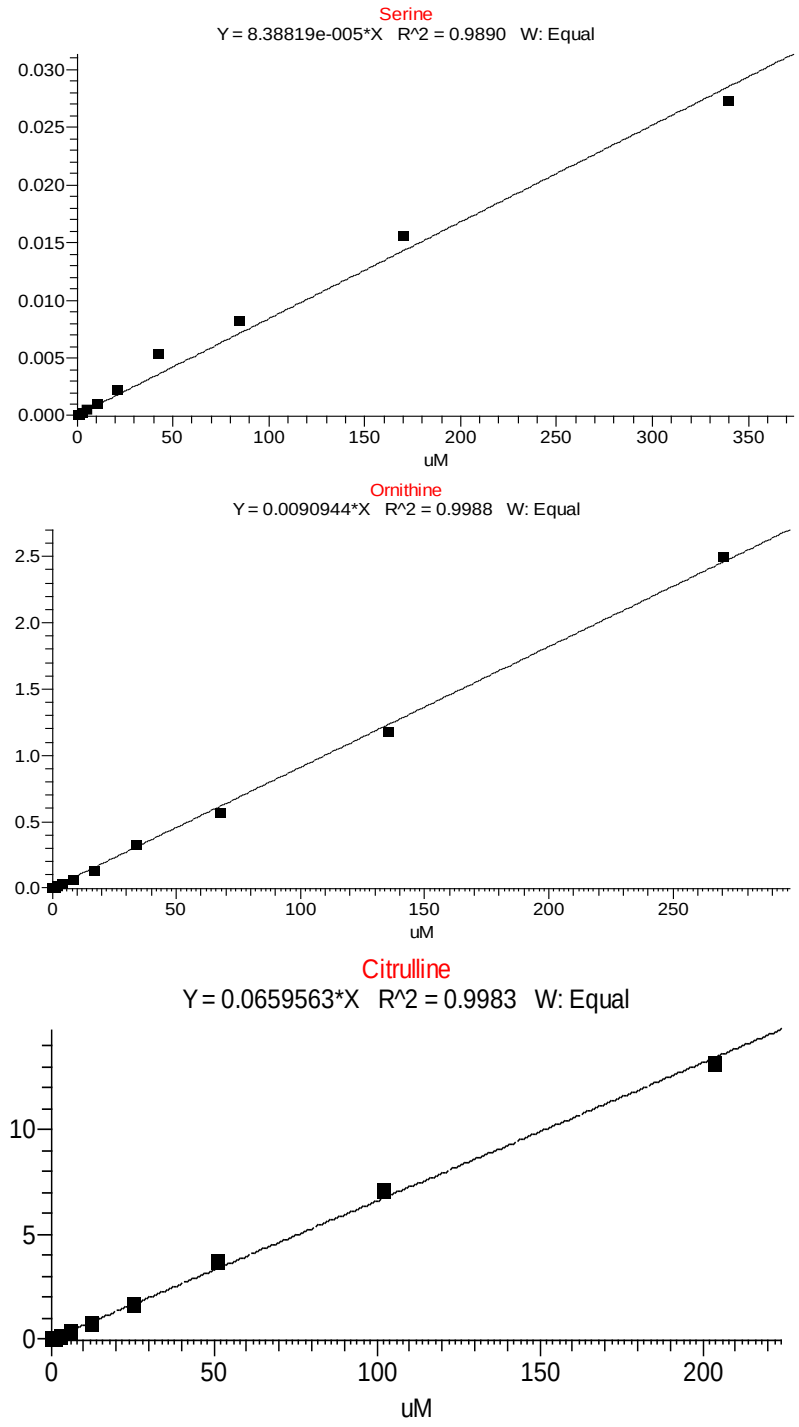

Figure 64. Standard calibration curves for serine, ornithine and citrulline show $R^2 \geq 0.98$. The line of best fit for each calibration curve was generated using equal weighted linear regression as the mathematical model of best fit. Metabolites concentration in QC and parasite samples was calculated from the resulting area ratio and the regression equation of the calibration curve.

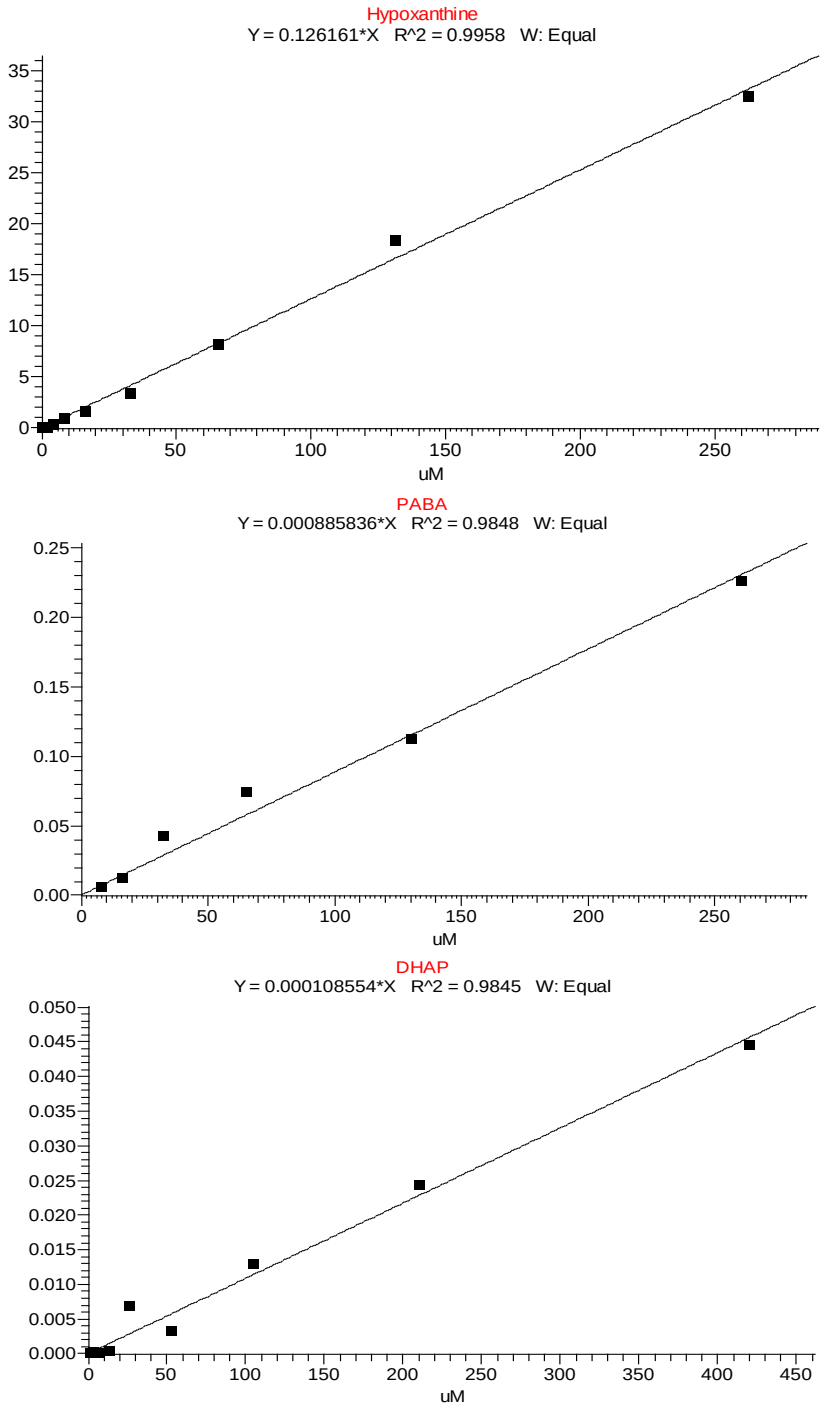

Figure 65. Standard calibration curves for hypoxanthine, PABA and DHAP show $R^2 \geq 0.98$. The line of best fit for each calibration curve was generated using equal weighted linear regression as the mathematical model of best fit. Metabolites concentration in QC and parasite samples was calculated from the resulting area ratio and the regression equation of the calibration curve.

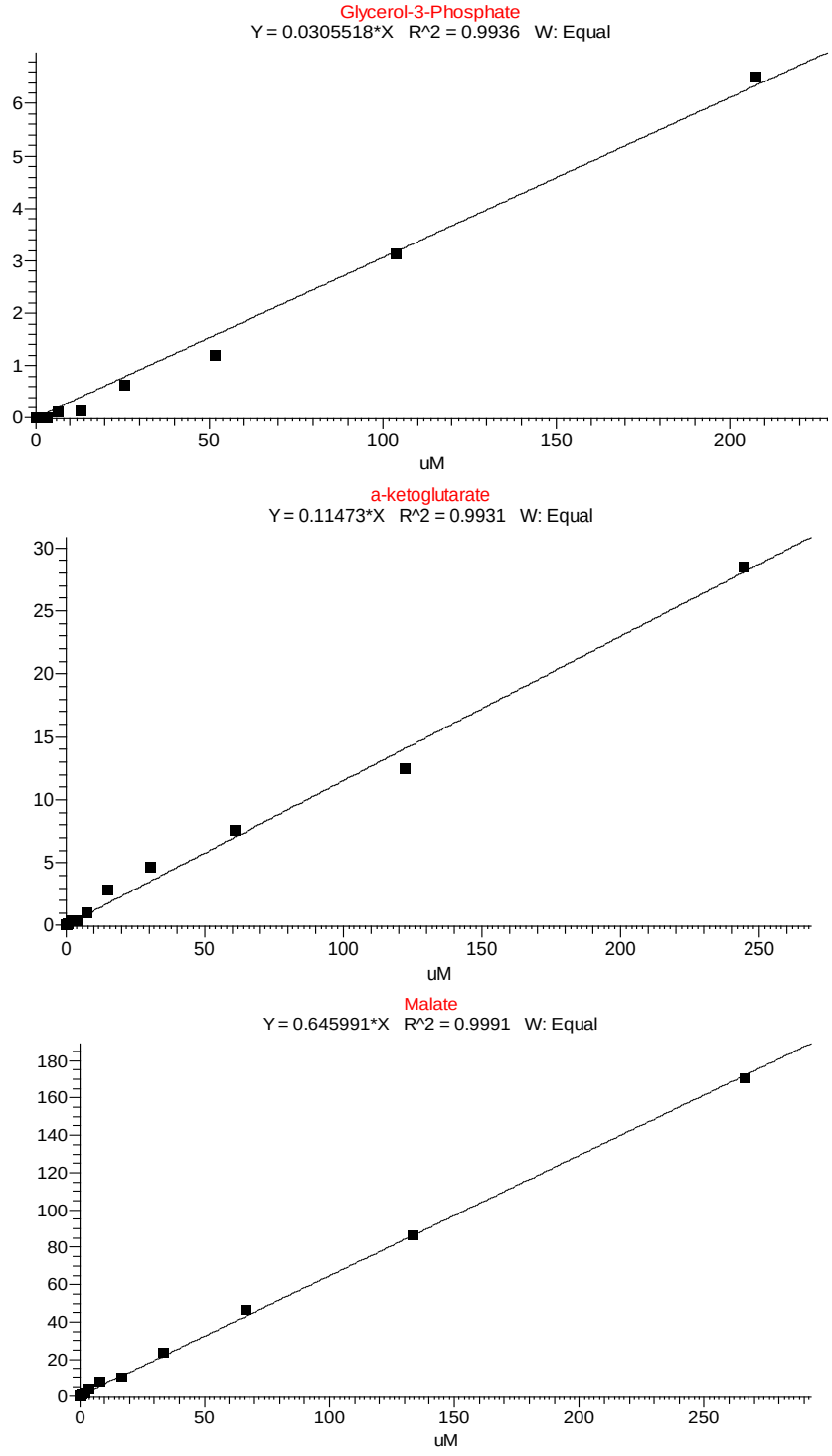

Figure 66. Standard calibration curves for glycerol-3-phosphate, 2-oxoglutarate and malate show R^2 ≥0.99 . The line of best fit for each calibration curve was generated using equal weighted linear regression as the mathematical model of best fit. Metabolites concentration in QC and parasite samples was calculated from the resulting area ratio and the regression equation of the calibration curve.

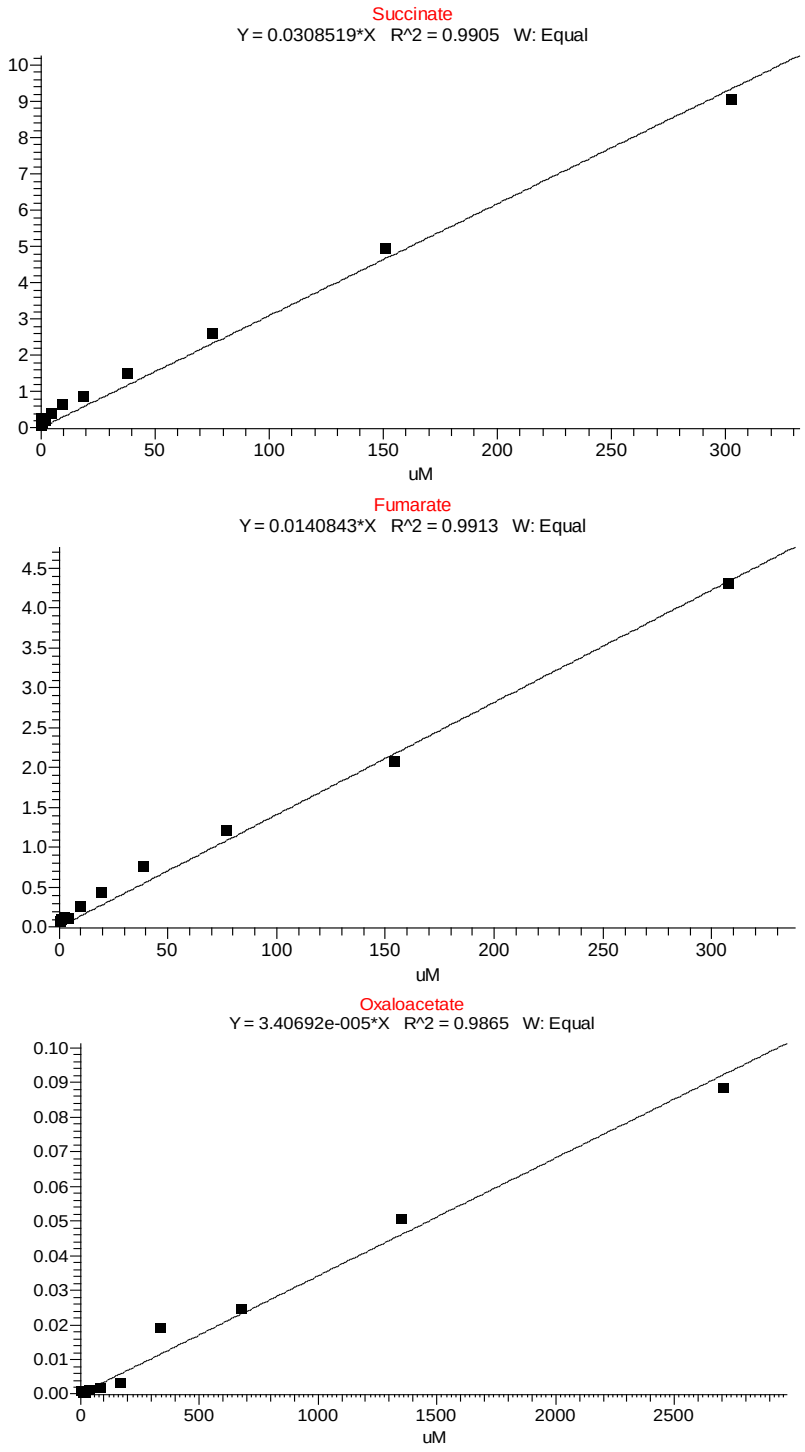

Figure 67. Standard calibration curves for succinate, fumarate and oxaloacetate show $R^2 \geq 0.99$. The line of best fit for each calibration curve was generated using equal weighted linear regression as the mathematical model of best fit. Metabolites concentration in QC and parasite samples was calculated from the resulting area ratio and the regression equation of the calibration curve.

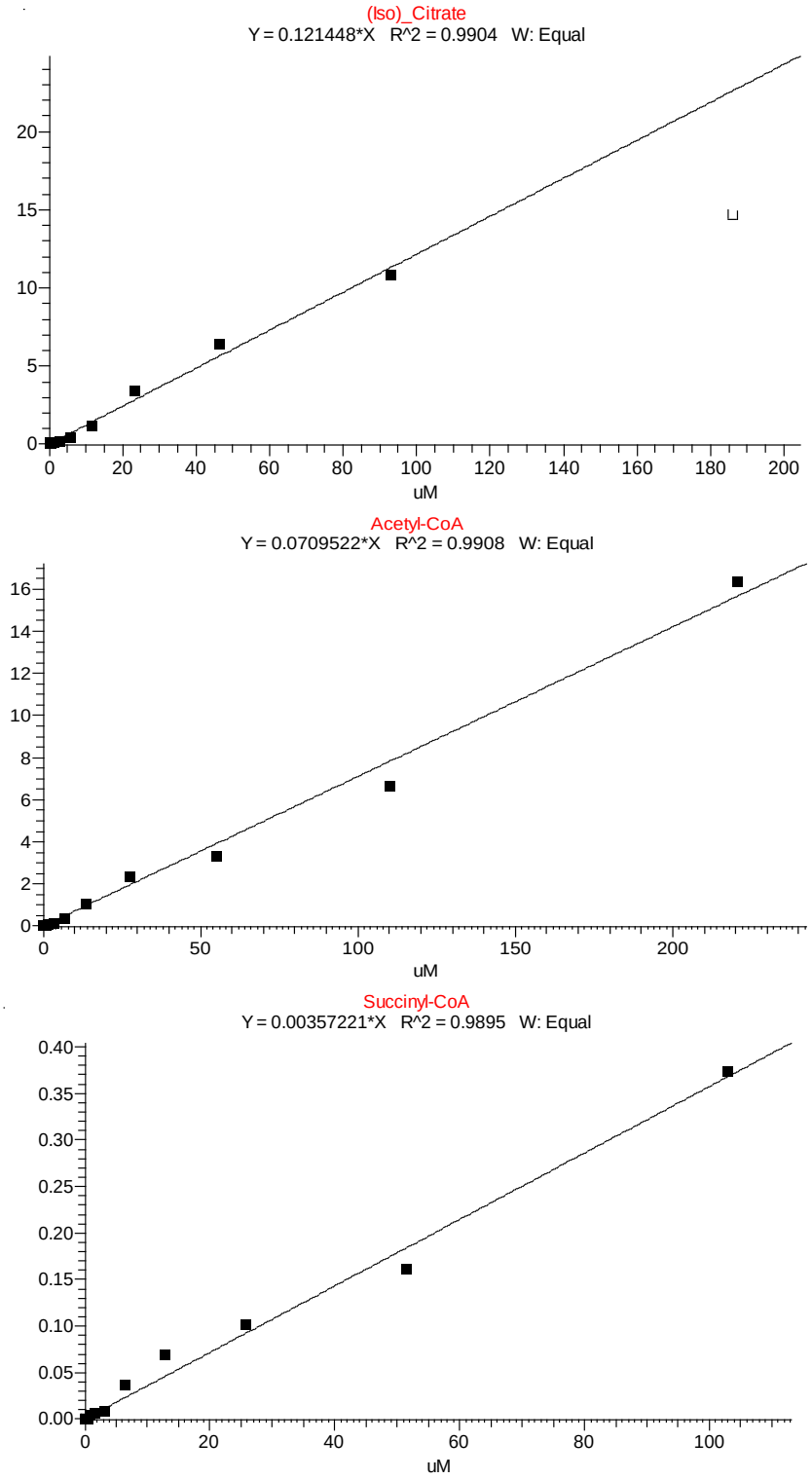

Figure 68. Standard calibration curves for (iso)-citrate, acetyl-CoA and succinyl-CoA show R^2 ≥0.99 . The line of best fit for each calibration curve was generated using equal weighted linear regression as the mathematical model of best fit. Metabolites concentration in QC and parasite samples was calculated from the resulting area ratio and the regression equation of the calibration curve.

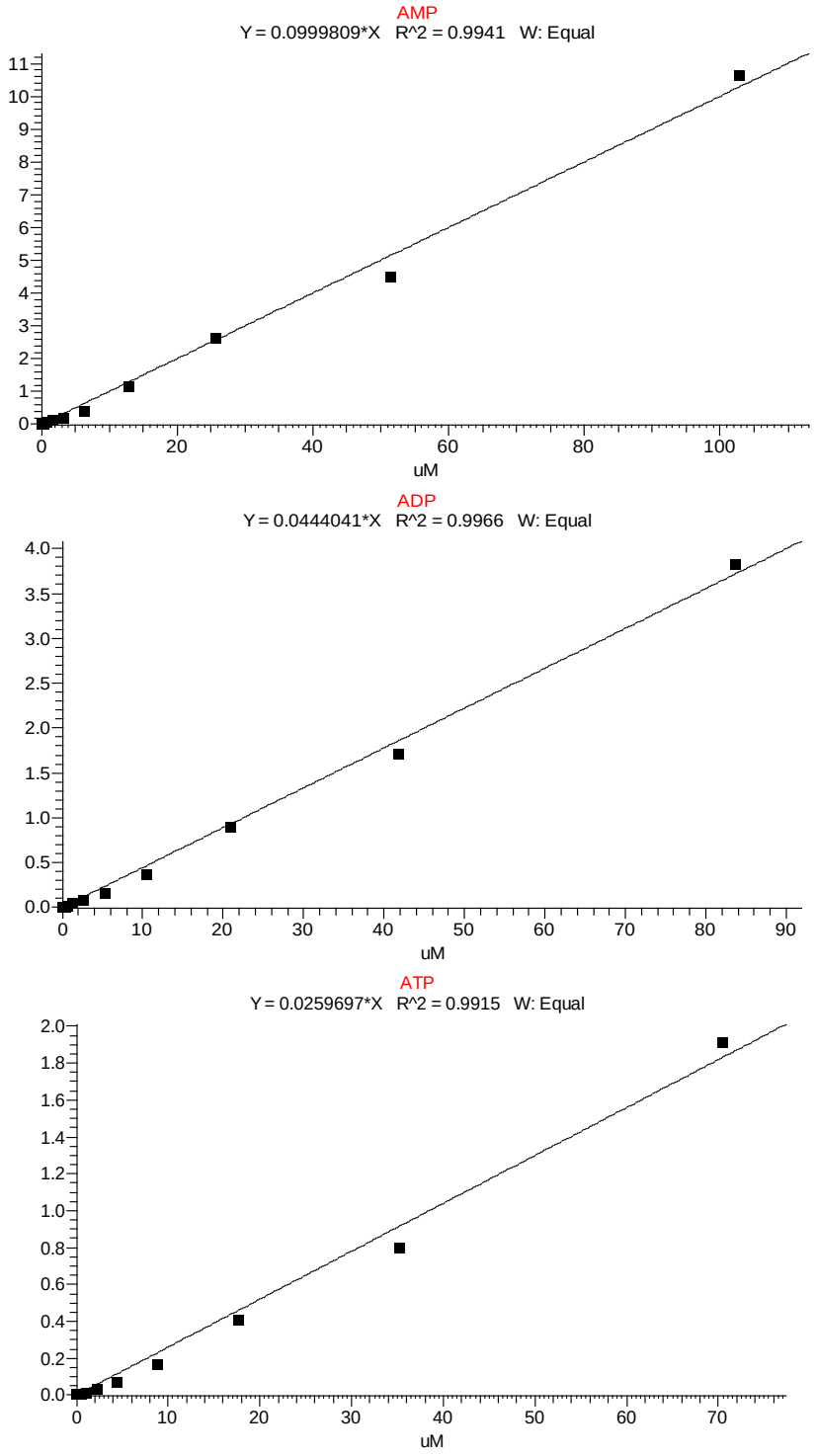

Figure 69. Standard calibration curves for AMP, ADP and ATP show $R^2 \geq 0.99$. The line of best fit for each calibration curve was generated using equal weighted linear regression as the mathematical model of best fit. Metabolites concentration in QC and parasite samples was calculated from the resulting area ratio and the regression equation of the calibration curve.

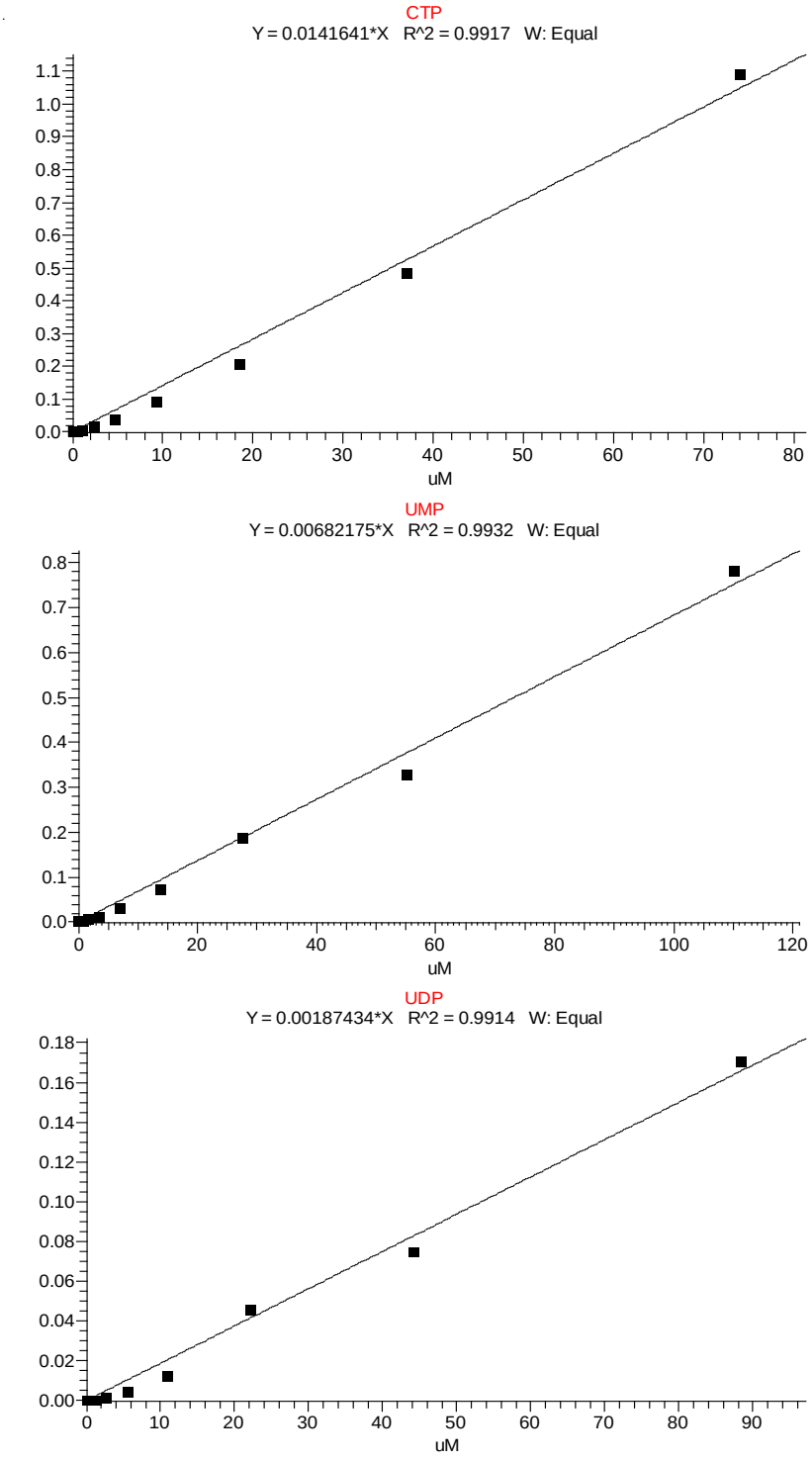

Figure 70. Standard calibration curves for CTP, UMP and UDP show $R^2 \geq 0.99$. The line of best fit for each calibration curve was generated using equal weighted linear regression as the mathematical model of best fit. Metabolites concentration in QC and parasite samples was calculated from the resulting area ratio and the regression equation of the calibration curve.

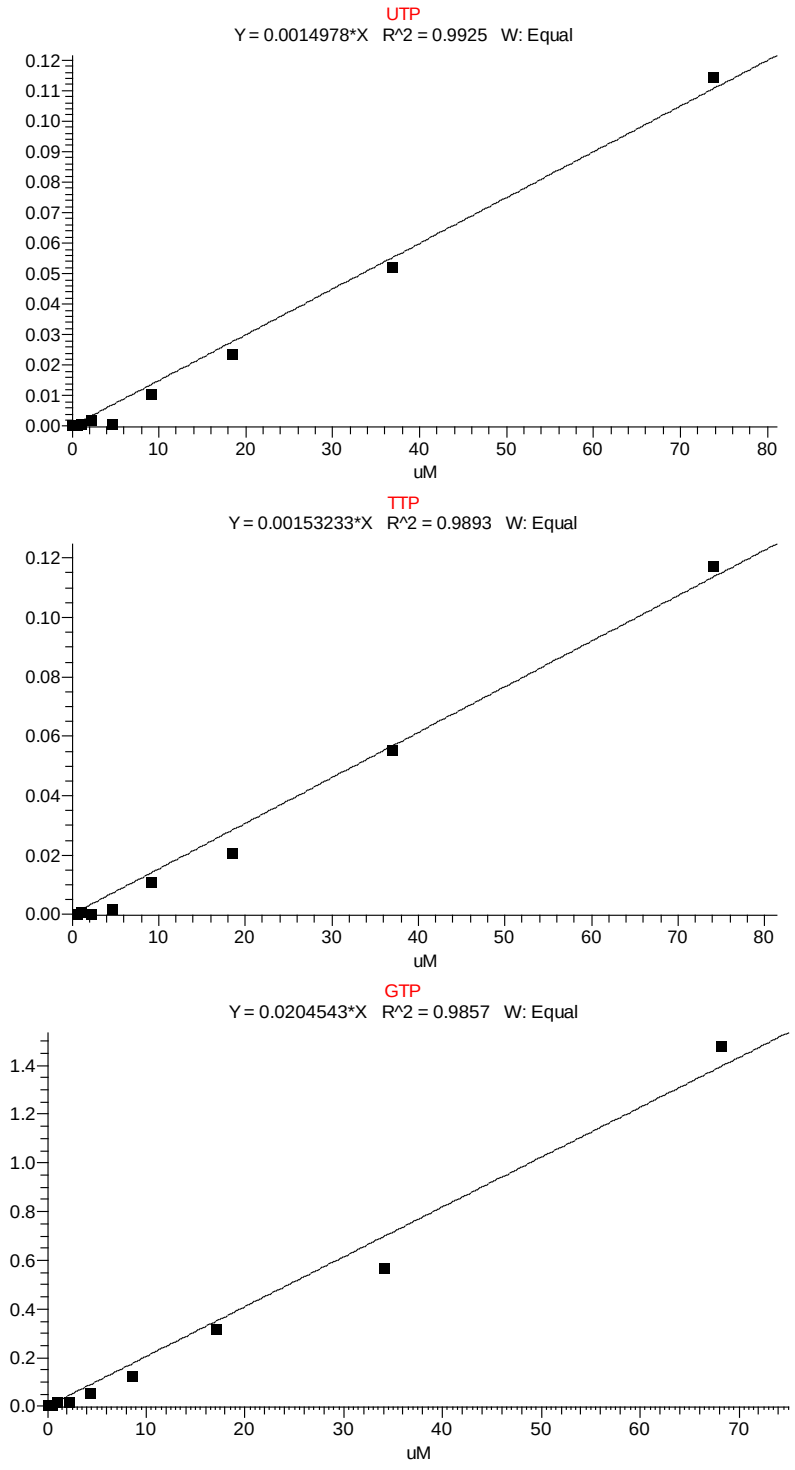

Figure 71. Standard calibration curves for UTP, TTP and GTP show $R^2 \geq 0.98$. The line of best fit for each calibration curve was generated using equal weighted linear regression as the mathematical model of best fit. Metabolites concentration in QC and parasite samples was calculated from the resulting area ratio and the regression equation of the calibration curve.

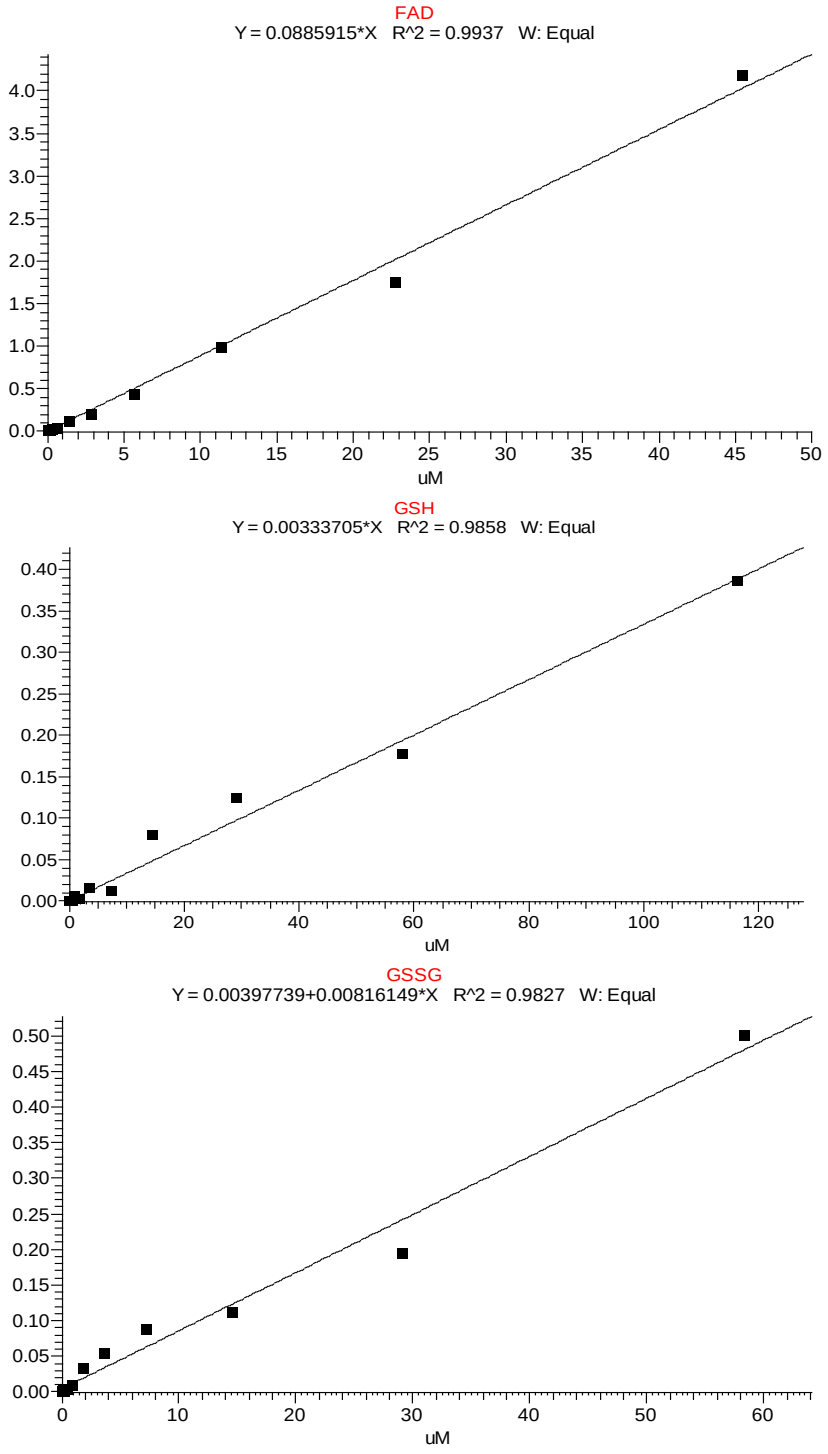

Figure 72. Standard calibration curves for FAD, GSH and GSSG show $R^2 \geq 0.98$. The line of best fit for each calibration curve was generated using equal weighted linear regression as the mathematical model of best fit. Metabolites concentration in QC and parasite samples was calculated from the resulting area ratio and the regression equation of the calibration curve.

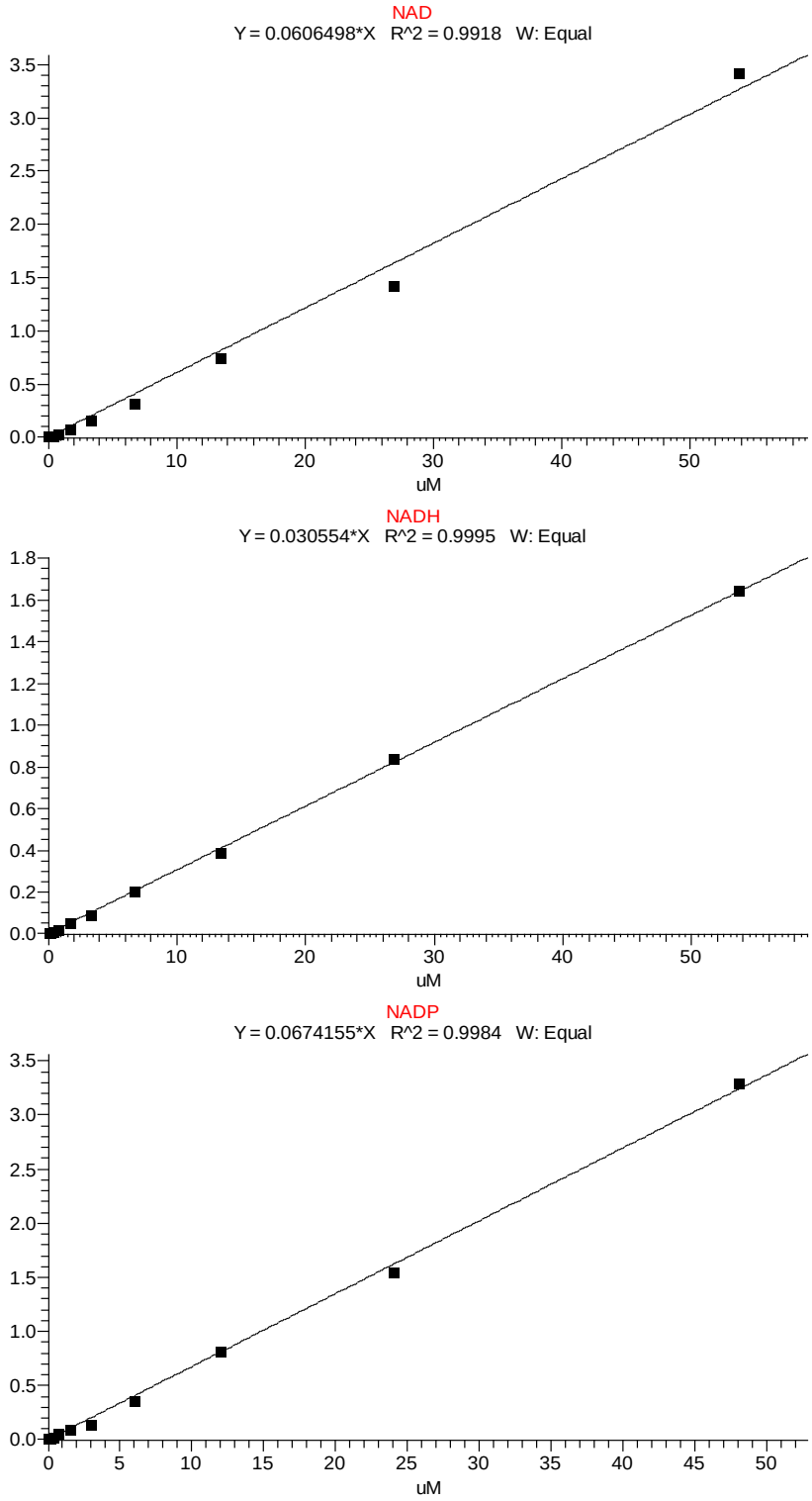

Figure 73. Standard calibration curves for NAD, NADH and NADP show $R^2 \geq 0.99$. The line of best fit for each calibration curve was generated using equal weighted linear regression as the mathematical model of best fit. Metabolites concentration in QC and parasite samples was calculated from the resulting area ratio and the regression equation of the calibration curve.

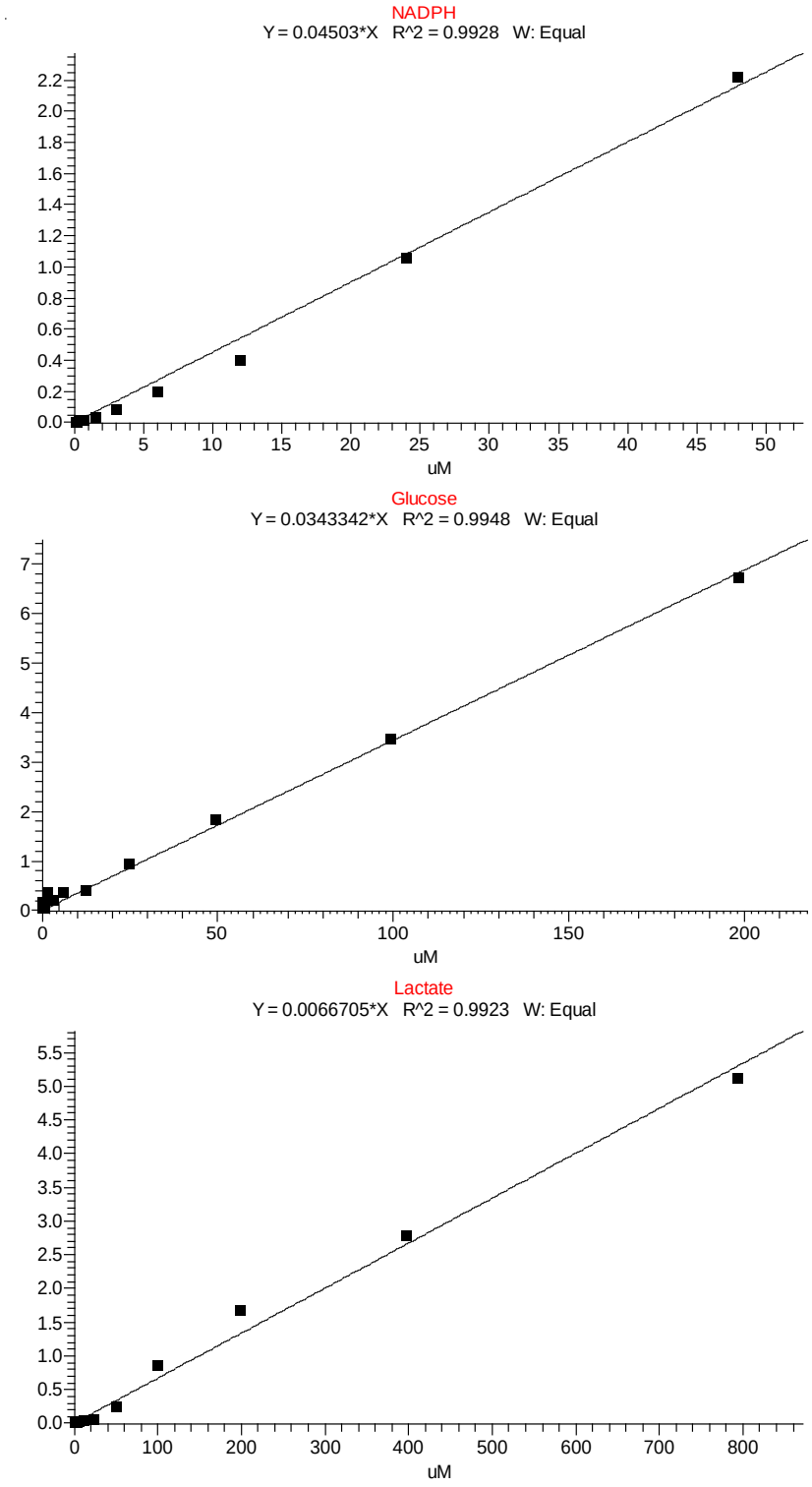

Figure 74. Standard calibration curves for NADPH, glucose and lactate show $R^2 \geq 0.99$. The line of best fit for each calibration curve was generated using equal weighted linear regression as the mathematical model of best fit. Metabolites concentration in QC and parasite samples was calculated from the resulting area ratio and the regression equation of the calibration curve.

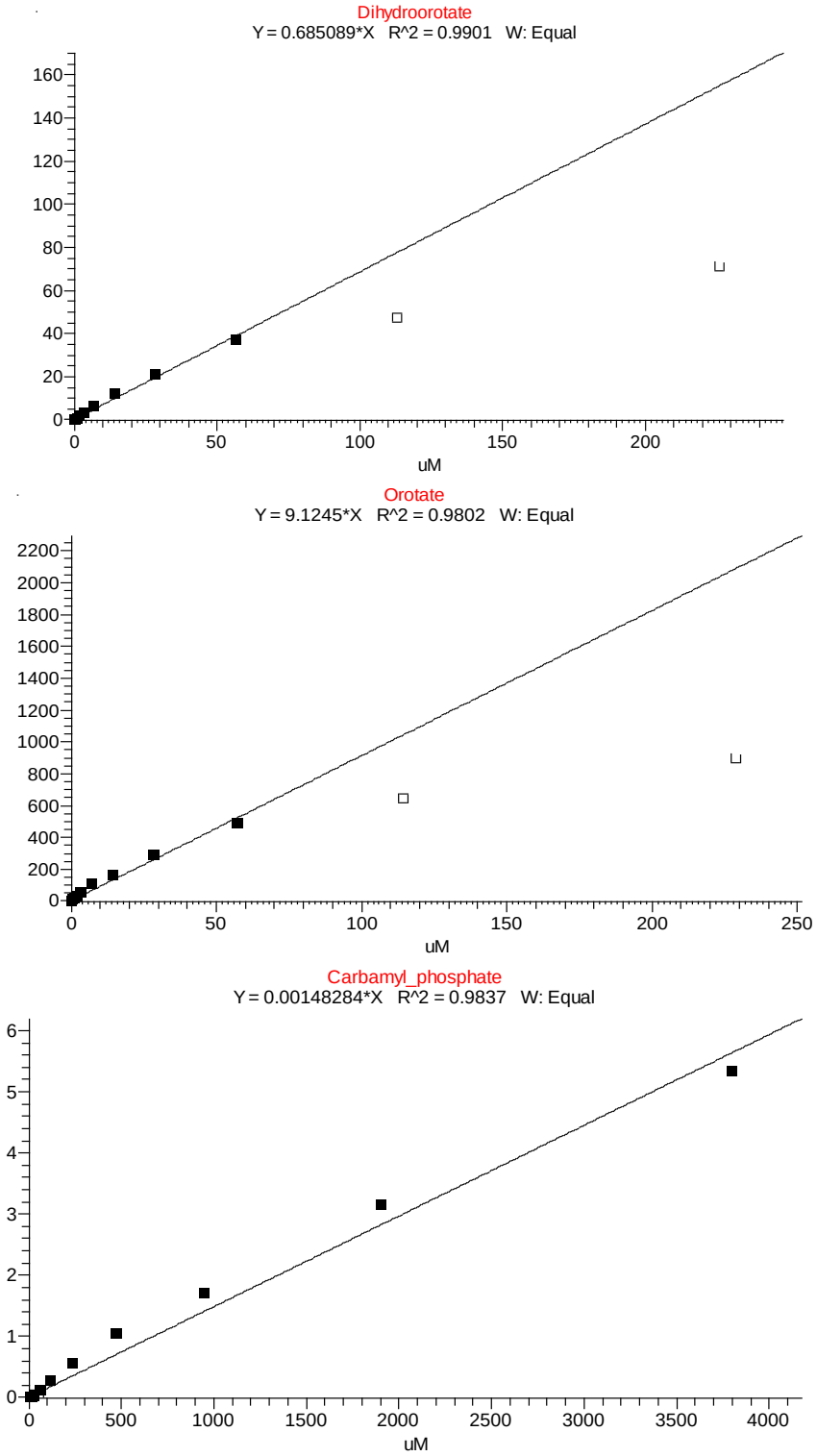

Figure 75. Standard calibration curves for dihydroorotate, orotate and carbamoyl-phosphate show R^2 ≥0.98 . The line of best fit for each calibration curve was generated using equal weighted linear regression as the mathematical model of best fit. Metabolites concentration in QC and parasite samples was calculated from the resulting area ratio and the regression equation of the calibration curve.

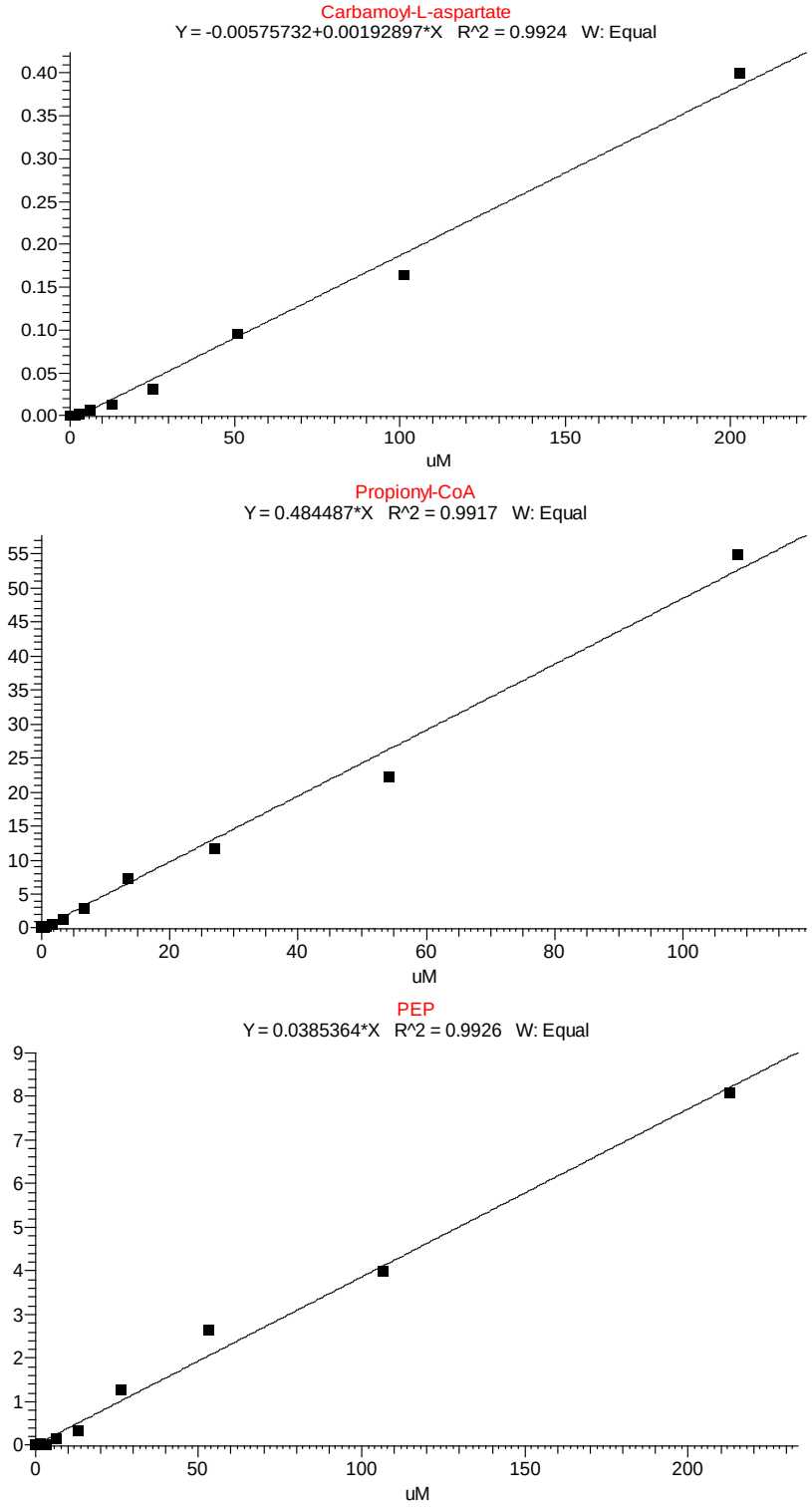

Figure 76. Standard calibration curves for carbamoyl-l-aspartate, propionyl-CoA and PEP show R^2 ≥0.99. The line of best fit for each calibration curve was generated using equal weighted linear regression as the mathematical model of best fit. Metabolites concentration in QC and parasite samples was calculated from the resulting area ratio and the regression equation of the calibration curve.

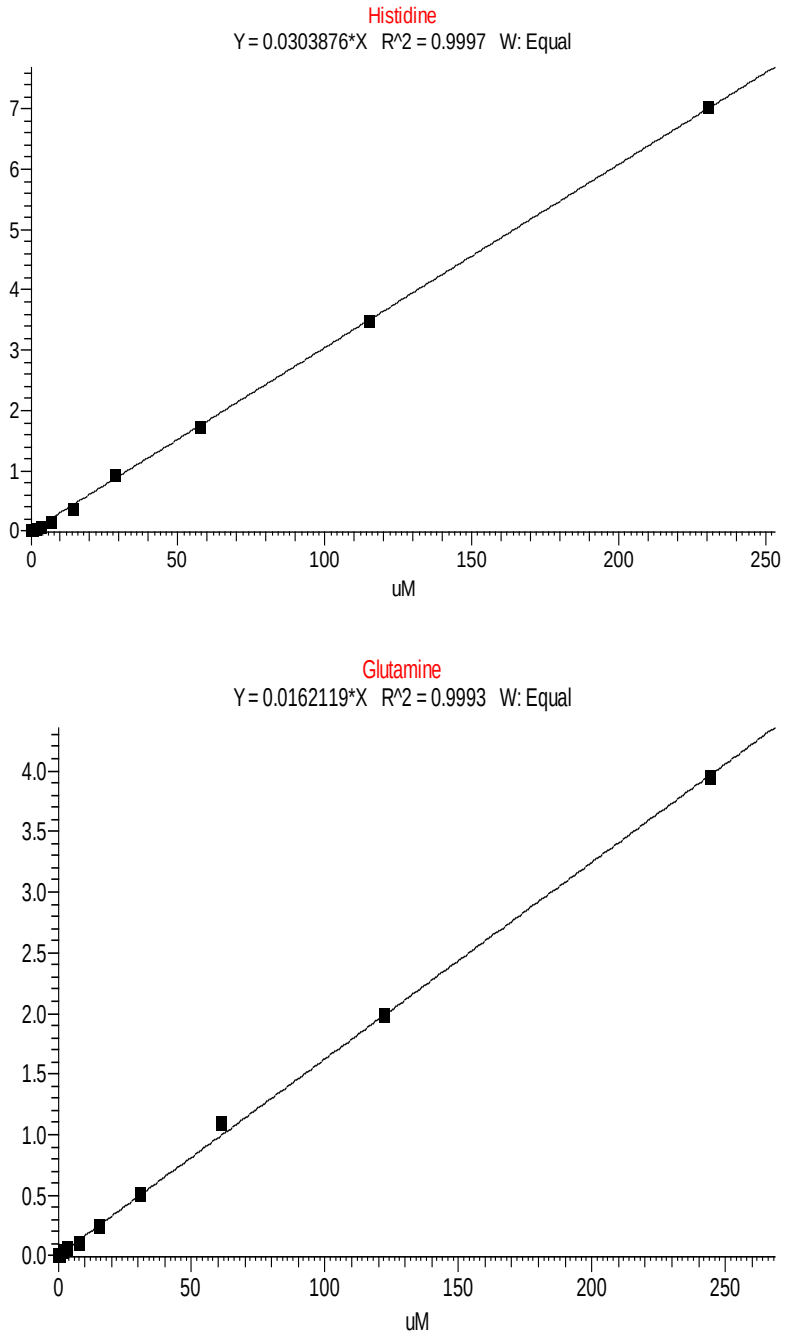

Figure 77. Standard calibration curves for histidine and glutamine show $R^2 \geq 0.99$. The line of best fit for each calibration curve was generated using equal weighted linear regression as the mathematical model of best fit. Metabolites concentration in QC and parasite samples was calculated from the resulting area ratio and the regression equation of the calibration curve.

REFERENCES

ACHAN, J., TALISUNA, A. O., ERHART, A., YEKA, A., TIBENDERANA, J. K., BALIRAINE, F. N., ROSENTHAL, P. J. & D'ALESSANDRO, U. 2011. Quinine, an old anti-malarial drug in a modern world: role in the treatment of malaria. *Malaria Journal,* 10,144.

AHN, S.-Y., SHIN, M.-Y., KIM, Y.-A., YOO, J.-A., KWAK, D.-H., JUNG, Y.-J., JUN, G., RYU, S.-H., YEOM, J.-S., AHN, J.-Y., CHAI, J.-Y. & PARK, J.-W. 2008. Magnetic separation: a highly effective method for synchronization of cultured erythrocytic Plasmodium falciparum. *Parasitology Research,* 102, 1195-1200.

ALDRITT, S. M., JOSEPH, J. T. & WIRTH, D. F. 1989. Sequence identification of cytochrome-b in Plasmodium-gallinaceum. *Molecular and Cellular Biology*, 9, 3614-3620.

ANDRIANTSOANIRINA, V., MENARD, D., RABEARIMANANA, S., HUBERT, V., BOUCHIER, C., TICHIT, M., BRAS, J. L. & DURAND, R. 2010. Association of microsatellite variations of Plasmodium falciparum Na+/H+ exchanger (Pfnhe-1) gene with reduced in vitro susceptibility to quinine: lack of confirmation in clinical isolates from Africa. *Am J Trop Med Hyg*, 82**,** 782-787.

ANNESLEY, T. M. 2003. Ion suppression in mass spectrometry. *Clinical Chemistry,* 49**,** 1041-1044.

ANTOINE, T. 2013. Molecular and biochemical characterisation of the electron transport chain of Plasmodium falciparum. PhD, University of Liverpool.

AOKI, T. T., BRENNAN, M. F., MULLER, W. A., SOELDNER, J. S., ALPERT, J. S., SALTZ, S. B., KAUFMANN, R. L., TAN, M. H. & CAHILL, G. F. 1976. Amino-acid levels across normal forearm muscle and splanchnic bed after a protein meal. *American Journal of Clinical Nutrition,* 29**,** 340-350.

ASAWAMAHASAKDA, W. & YUTHAVONG, Y. 1993. The methionine synthesis cycle and salvage of methyltetrahydrofolate from host red-cells in the malaria parasite (Plasmodium-falciparum). *Parasitology,* 107**,** 1-10.

ASSARAF, Y. G., GOLENSER, J., SPIRA, D. T. & BACHRACH, U. 1984. Polyamine levels and the activity of their biosynthetic-enzymes in human-erythrocytes infected with the malarial parasite, Plasmodium-falciparum. *Biochemical Journal*, 222**,** 815-819.

ATKINSON, C. T. & AIKAWA, M. 1990. Ultrastructure of malaria-infected erythrocytes. *Blood Cells,* 16**,** 351-368.

AYI, I., NONAKA, D., ADJOVU, J., HANAFUSA, S., JIMBA, M., BOSOMPEM, K., MIZOUE, T., TAKEUCHI, T., BOAKYE, D. & KOBAYASHI, J. 2010. School-based participatory health education for malaria control in Ghana: engaging children as health messengers. *Malaria Journal,* 9**,** 98.

BAJAD, S. U., LU, W., KIMBALL, E. H., YUAN, J., PETERSON, C. & RABINOWITZ, J. D. 2006. Separation and quantitation of water soluble cellular metabolites by hydrophilic interaction chromatography-tandem mass spectrometry. *Journal of Chromatography A,* 1125**,** 76-88.

BALDWIN, J., FARAJALLAH, A. M., MALMQUIST, N. A., RATHOD, P. K. & PHILLIPS, M. A. 2002. Malarial dihydroorotate dehydrogenase. *Journal of Biological Chemistry,* 277, 41827-41834.

BALDWIN, J., MICHNOFF, C. H., MALMQUIST, N. A., WHITE, J., ROTH, M. G., RATHOD, P. K. & PHILLIPS, M. A. 2005. High-throughput screening for potent and selective inhibitors of Plasmodium falciparum dihydroorotate dehydrogenase. *Journal of Biological Chemistry,* 280, 21847-21853.

BALL, E. G., MCKEE, R. W., ANFINSEN, C. B., CRUZ, W. O. & GEIMAN, Q. M. 1948. Studies on malarial parasites; chemical and metabolic changes during growth and multiplication invivo and invitro. *Journal of Biological Chemistry,* 175**,** 547-571.

BANNISTER, L. H., HOPKINS, J. M., FOWLER, R. E., KRISHNA, S. & MITCHELL, G. H. 2000. A brief illustrated guide to the ultrastructure of Plasmodium falciparum asexual blood stages. *Parasitology Today,* 16, 427-433.

BARTON, V., FISHER, N., BIAGINI, G. A., WARD, S. A. & O'NEILL, P. M. 2010. Inhibiting Plasmodium cytochrome bc(1): a complex issue. *Current Opinion in Chemical Biology,* 14**,** 440-446.

BASCO, L. K. & LEBRAS, J. 1994. In-vitro activity of mitochondrial atp-synthetase inhibitors against Plasmodium falciparum. *Journal of Eukaryotic Microbiology,* 41, 179-183.

BASS, C. C. & JOHNS, F. M. 1912. The cultivation of malarial plasmodia (Plasmodium vivax and Plasmodium falciparum) in vitro. *Journal of Experimental Medicine,* 16, 567-579.

BEALE, M. H. & SUSSMAN, M. R. 2011. Metabolomics of Arabidopsis Thaliana. *Annual Plant Reviews,*43: Biology of Plant Metabolomics (ed R. D. Hall), Wiley-Blackwell, Oxford, UK.

BENNETT, B. D., KIMBALL, E. H., GAO, M., OSTERHOUT, R., VAN DIEN, S. J. & RABINOWITZ, J. D. 2009. Absolute metabolite concentrations and implied enzyme active site occupancy in Escherichia coli. *Nature Chemical Biology,* 5**,** 593-599.

BENNETT, B. D., YUAN, J., KIMBALL, E. H. & RABINOWITZ, J. D. 2008. Absolute quantitation of intracellular metabolite concentrations by an isotope ratio-based approach. *Nature Protocols,* 3**,** 1299-1311.

BERRY, A., SENESCAU, A., LELIEVRE, J., BENOIT-VICAL, F., FABRE, R., MARCHOU, B. & MAGNAVAL, J. F. 2006. Prevalence of Plasmodium falciparum cytochrome b gene mutations in isolates imported from Africa, and implications for atovaquone resistance. *Transactions of the Royal Society of Tropical Medicine and Hygiene,* 100**,** 986-988.

BESIER, S., LUDWIG, A., BRADE, V. & WICHELHAUS, T. A. 2003. Molecular analysis of fusidic acid resistance in Staphylococcus aureus. *Molecular Microbiology,* 47**,** 463-469.

BESTEIRO, S., DUY, S. V., PERIGAUD, C., LEFEBVRE-TOURNIER, I. & VIAL, H. J. 2010. Exploring metabolomic approaches to analyse phospholipid biosynthetic pathways in Plasmodium. *Parasitology,* 137, 1343-1356.

BIAGINI, G. A., FISHER, N., BERRY, N., STOCKS, P. A., MEUNIER, B., WILLIAMS, D. P., BONAR-LAW, R., BRAY, P. G., OWEN, A., O'NEILL, P. M. & WARD, S. A. 2008. Acridinediones: Selective and potent inhibitors of the malaria parasite mitochondrial bc(1) complex. *Molecular Pharmacology,* 73**,** 1347-1355.

BIAGINI, G. A., FISHER, N., SHONE, A. E., MUBARAKI, M. A., SRIVASTAVA, A., HILL, A., ANTOINE, T., WARMAN, A. J., DAVIES, J., PIDATHALA, C., AMEWU, R. K., LEUNG, S. C., SHARMA, R., GIBBONS, P., HONG, D. W., PACOREL, B., LAWRENSON, A. S., CHAROENSUTTHIVARAKUL, S., TAYLOR, L., BERGER, O., MBEKEANI, A., STOCKS, P. A., NIXON, G. L., CHADWICK, J., HEMINGWAY, J., DELVES, M. J., SINDEN, R. E., ZEEMAN, A.-M., KOCKEN, C. H. M., BERRY, N. G., O'NEILL, P. M. & WARD, S. A. 2012. Generation of quinolone antimalarials targeting the Plasmodium falciparum mitochondrial respiratory chain for the treatment and prophylaxis of malaria. *Proceedings of the National Academy of Sciences of the United States of America,* 109**,** 8298-8303.

BIAGINI, G. A., O'NEILL, P. M., NZILA, A., WARD, S. A. & BRAY, P. G. 2003. Antimalarial chemotherapy: young guns or back to the future? *Trends in Parasitology,* 19**,** 479-487.

BIAGINI, G. A., VIRIYAVEJAKUL, P., O'NEILL, P. M., BRAY, P. G. & WARD, S. A. 2006. Functional characterization and target validation of alternative complex I of Plasmodium falciparum mitochondria. *Antimicrobial Agents and Chemotherapy,* 50**,** 1841-1851.

BISHOP, C. 1960. PURINE METABOLISM IN HUMAN AND CHICKEN BLOOD, INVITRO. *Journal of Biological Chemistry,* 235**,** 3228-3232.

BISHOP, C. 1961. Changes in the Nucleotides of Stored or Incubated Human Blood. *Transfusion,* 1**,** 349-354.

BISHOP, C. 1964. Overall red cell metabolism. *In:* BISHOP, C., AND SUGENOR, D. M., (ed.) *The Red Blood Cell.* New York: Academic Press.

BLACK, F. T., WILDFANG, I. L. & BORGBJERG, K. 1985. Activity of fusidic acid against Plasmodium falciparum invitro. *Lancet,* 1, 578-579.

BLUM, J. J. & GINSBURG, H. 1984. Absence of alpha-ketoglutarate dehydrogenase-activity and presence of CO_2-fixing activity in Plasmodium-falciparum grown-invitro in human-erythrocytes. *Journal of Protozoology,* 31, 167-169.

BLUM, J. J., YAYON, A., FRIEDMAN, S. & GINSBURG, H. 1984. Effects of mitochondrial protein-synthesis inhibitors on the incorporation of isoleucine into Plasmodium-falciparum invitro. *Journal of Protozoology,* 31, 475-479.

BOSIA, A., GHIGO, D., TURRINI, F., NISSANI, E., PESCARMONA, G. P. & GINSBURG, H. 1993. Kinetic characterization of Na+/H+ antiport of Plasmodium falciparum membrane. *J Cell Physiol,* 154**,** 527-34.

BOSSI, D. & GIARDINA, B. 1996. Red cell physiology. *Molecular Aspects of Medicine,* 17**,** 117-128.

BOWMAN, I. B., GRANT, P. T. & KERMACK, W. O. 1960. The metabolism of Plasmodium berghei, the malaria parasite of rodents. I. The preparation of the erythrocytic form of P. berghei separated from the host cell. *Experimental parasitology,* 9, 131-136.

BOWMAN, I. B., KERMACK, W. O., OGSTON, D. & GRANT, P. T. 1961. Metabolism of Plasmodium berghei, malaria parasite of rodents .2. an effect of mepacrine on metabolism of glucose by parasite separated from its host cell. *Biochemical Journal,* 78, 472–478.

BOZDECH, Z., LLINAS, M., PULLIAM, B. L., WONG, E. D., ZHU, J. C. & DERISI, J. L. 2003. The transcriptome of the intraerythrocytic developmental cycle of Plasmodium falciparum. *Plos Biology,* 1, 85-100.

BRAUER, M. J., YUAN, J., BENNETT, B. D., LU, W., KIMBALL, E., BOTSTEIN, D. & RABINOWITZ, J. D. 2006. Conservation of the metabolomic response to starvation across two divergent microbes. *Proceedings of the National Academy of Sciences of the United States of America,* 103**,** 19302-19307.

BRAY, P. G., WARD, S. A. & O'NEILL, P. M. 2005. Quinolines and artemisinin: Chemistry, biology and history. *Malaria: Drugs, Disease and Post-Genomic Biology,* 295, 3-38.

BRIOLANT, S., PELLEAU, S., BOGREAU, H., HOVETTE, P., ZETTOR, A., CASTELLO, J., BARET, E., AMALVICT, R., ROGIER, C. & PRADINES, B. 2011. In vitro susceptibility to quinine and microsatellite variations of the Plasmodium falciparum Na+/H+ exchanger (Pfnhe-1) gene: the absence of association in clinical isolates from the Republic of Congo. *Malar J,* 10**,** 37.

BRUCE-CHWATT, L. J. 1987. Malaria and its control present situation and future prospects. *Annual Review of Public Health,* 8, 75-110.

BRYANT, C., SMITH, M. J. H. & VOLLER, A. 1964. Incorporation of radioactivity from (^{14}C) glucose into soluble metabolic intermediates of malaria parasites. *American Journal of Tropical Medicine and Hygiene,* 13, 515-519.

BULUSU, V., JAYARAMAN, V. & BALARAM, H. 2011. Metabolic Fate of Fumarate, a Side Product of the Purine Salvage Pathway in the Intraerythrocytic Stages of Plasmodium falciparum. *Journal of Biological Chemistry,* 286**,** 9236-9245.

BUNGENER, W. 1967. Adenosine deaminase and nucleoside phosphorylase in malaria parasites. *Zeitschrift Fur Tropenmedizin Und Parasitologie,* 18**,** 48-52.

CANFIELD, C. J., PUDNEY, M. & GUTTERIDGE, W. E. 1995. Interactions of atovaquone with other antimalarial drugs against Plasmodium falciparum in vitro. *Experimental Parasitology,* 80**,** 373-381.

CARRINGTON, H. C., CROWTHER, A. F., DAVEY, D. G., LEVI, A. A. & ROSE, F. L. 1951. A metabolite of paludrine with high antimalarial activity. *Nature,* 168, 1080-1080.

CASSERA, M. B., HAZLETON, K. Z., RIEGELHAUPT, P. M., MERINO, E. F., LUO, M., AKABAS, M. H. & SCHRAMM, V. L. 2008. Erythrocytic Adenosine Monophosphate as an Alternative Purine Source in Plasmodium falciparum. *Journal of Biological Chemistry,* 283**,** 32889-32899.

CASSERA, M. B., ZHANG, Y., HAZLETON, K. Z. & SCHRAMM, V. L. 2011. Purine and Pyrimidine Pathways as Targets in Plasmodium falciparum. *Current Topics in Medicinal Chemistry,* 11**,** 2103-2115.

COHEN, S. N. & YIELDING, K. L. 1965. Inhibition of DNA and RNA polymerase reactions by chloroquine. *Proceedings of the National Academy of Sciences,* 54**,** 521-527.

COLLINS, W. E. & JEFFERY, G. M. 2005. Plasmodium ovale: Parasite and Disease. *Clinical Microbiology Reviews,* 18**,** 570-581.

COLLINS, W. E. & JEFFERY, G. M. 2007. Plasmodium malariae: Parasite and Disease. *Clinical Microbiology Reviews,* 20**,** 579-592.

COMBRINCK, J. M., MABOTHA, T. E., NCOKAZI, K. K., AMBELE, M. A., TAYLOR, D., SMITH, P. J., HOPPE, H. C. & EGAN, T. J. 2013. Insights into the Role of Heme in the Mechanism of Action of Antimalarials. *Acs Chemical Biology,* 8**,** 133-137.

COWMAN, A. F., BERRY, D. & BAUM, J. 2012. The cellular and molecular basis for malaria parasite invasion of the human red blood cell. *Journal of Cell Biology,* 198**,** 961-971.

COWMAN, A. F., KARCZ, S., GALATIS, D. & CULVENOR, J. G. 1991. A P-glycoprotein homolog of Plasmodium falciparum is localized on the digestive vacuole. *Journal of Cell Biology,* 113**,** 1033-1042.

COX, F. E. G. 2002. History of human parasitology. *Clinical Microbiology Reviews,* 15, 595–612.

COX, F. E. G. 2010. History of the discovery of the malaria parasites and their vectors. *Parasites & Vectors,* 3, 5.

COX-SINGH, J., DAVIS, T. M. E., LEE, K.-S., SHAMSUL, S. S. G., MATUSOP, A., RATNAM, S., RAHMAN, H. A., CONWAY, D. J. & SINGH, B. 2008. Plasmodium knowlesi malaria in humans is widely distributed and potentially life threatening. *Clinical Infectious Diseases,* 46, 165-171.

COX-SINGH, J. & SINGH, B. 2008. Knowlesi malaria: newly emergent and of public health importance? *Trends in Parasitology,* 24, 406-410.

CRAWFORD, M. J., FRAUNHOLZ, M.J., AND ROOS, D.S. 2003. Energy metabolism in the Apicomplexa. *In:* MARR, J. J., NILSEN, T.W., KOMUNIECKI, R.W. (ed.) *Molecular Medical Parasitology.* Academic Press, London, UK.

CROWTHER, A. F. & LEVI, A. A. 1953. Proguanil - The isolation of a metabolite with high antimalarial activity. *British Journal of Pharmacology and Chemotherapy,* 8, 93-97.

CUBBON, S., ANTONIO, C., WILSON, J. & THOMAS-OATES, J. 2010. Metabolomic applications of HILIC-LC-MS. *Mass Spectrometry Reviews,* 29**,** 671-684.

DAHL, E. L. & ROSENTHAL, P. J. 2008. Apicoplast translation, transcription and genome replication: targets for antimalarial antibiotics. *Trends in Parasitology,* 24**,** 279-284.

DAHLSTROM, S., VEIGA, M. I., MARTENSSON, A., BJORKMAN, A. & GIL, J. P. 2009. Polymorphism in PfMRP1 (Plasmodium falciparum Multidrug Resistance Protein 1) Amino Acid 1466 Associated with Resistance to Sulfadoxine-Pyrimethamine Treatment. *Antimicrobial Agents and Chemotherapy,* 53**,** 2553-2556.

DANNE, J. C., GORNIK, S. G., MACRAE, J. I., MCCONVILLE, M. J. & WALLER, R. F. 2013. Alveolate Mitochondrial Metabolic Evolution: Dinoflagellates Force Reassessment of the Role of Parasitism as a Driver of Change in Apicomplexans. *Molecular Biology and Evolution,* 30**,** 123-139.

DAVIES, M., HEIKKILA, T., MCCONKEY, G. A., FISHWICK, C. W. G., PARSONS, M. R. & JOHNSON, A. P. 2009. Structure-Based Design, Synthesis, and Characterization of Inhibitors of Human and Plasmodium falciparum Dihydroorotate Dehydrogenases. *Journal of Medicinal Chemistry,* 52, 2683-2693.

DE VOS, R. C. H., MOCO, S., LOMMEN, A., KEURENTJES, J. J. B., BINO, R. J. & HALL, R. D. 2007. Untargeted large-scale plant metabolomics using liquid chromatography coupled to mass spectrometry. *Nature Protocols,* 2**,** 778-791.

DETTMER, K., ARONOV, P. A. & HAMMOCK, B. D. 2007. Mass spectrometry-based metabolomics. *Mass Spectrometry Reviews,* 26**,** 51-78.

DING, X. C., BECK, H.-P. & RASO, G. 2011. Plasmodium sensitivity to artemisinins: magic bullets hit elusive targets. *Trends in Parasitology,* 27**,** 73-81.

DIVO, A. A., GEARY, T. G., DAVIS, N. L. & JENSEN, J. B. 1985a. Nutritional-requirements of Plasmodium falciparum in culture .1. exogenously supplied dialyzable components necessary for continuous growth. *Journal of Protozoology,* 32**,** 59-64.

DIVO, A. A., GEARY, T. G., JENSEN, J. B. & GINSBURG, H. 1985b. The mitochondrion of Plasmodium falciparum visualized by rhodamine-123 fluorescence. *Journal of Protozoology,* 32, 442-446.

DONDORP, A. M., NOSTEN, F., YI, P., DAS, D., PHYO, A. P., TARNING, J., LWIN, K. M., ARIEY, F., HANPITHAKPONG, W., LEE, S. J., RINGWALD, P., SILAMUT, K., IMWONG, M., CHOTIVANICH, K., LIM, P., HERDMAN, T., AN, S. S., YEUNG, S., SINGHASIVANON, P., DAY, N. P. J., LINDEGARDH, N., SOCHEAT, D. & WHITE, N. J. 2009. Artemisinin resistance in Plasmodium falciparum malaria. *New England Journal of Medicine,* 361**,** 455-467.

DONG, C. K., PATEL, V., YANG, J. C., DVORIN, J. D., DURAISINGH, M. T., CLARDY, J. & WIRTH, D. F. 2009. Type II NADH dehydrogenase of the respiratory chain of Plasmodium falciparum and its inhibitors. *Bioorganic & Medicinal Chemistry Letters,* 19**,** 972-975.

DOWNIE, M. J., KIRK, K. & BEN MAMOUN, C. 2008. Purine salvage pathways in the intraerythrocytic malaria parasite Plasmodium falciparum. *Eukaryotic Cell,* 7**,** 1231-1237.

DUDLEY, E., YOUSEF, M., WANG, Y. & GRIFFITHS, W. J. 2010. Targeted metabolomics and mass spectrometry. *Advances in Protein Chemistry and Structural Biology,* 80**,** 45-83.

DUNN, W. B. 2011. Chapter two - Mass Spectrometry in Systems Biology: An Introduction. *In:* DANIEL JAMESON, M. V. A. H. V. W. (ed.) *Methods in Enzymology.* Academic Press.

DUNN, W. B., BROADHURST, D. I., ATHERTON, H. J., GOODACRE, R. & GRIFFIN, J. L. 2011. Systems level studies of mammalian metabolomes: the roles of mass spectrometry and nuclear magnetic resonance spectroscopy. *Chemical Society Reviews,* 40**,** 387-426.

DUNN, W. B. & ELLIS, D. I. 2005. Metabolomics: Current analytical platforms and methodologies. *TrAC Trends in Analytical Chemistry,* 24**,** 285-294.

ECKSTEIN-LUDWIG, U., WEBB, R. J., VAN GOETHEM, I. D. A., EAST, J. M., LEE, A. G., KIMURA, M., O'NEILL, P. M., BRAY, P. G., WARD, S. A. & KRISHNA, S. 2003. Artemisinins target the SERCA of Plasmodium falciparum. *Nature,* 424**,** 957-961.

EGAN, T. J. 2008. Haemozoin formation. *Molecular and Biochemical Parasitology,* 157**,** 127-136.

EGAN, T. J., COMBRINCK, J. M., EGAN, J., HEARNE, G. R., MARQUES, H. M., NTENTENI, S., SEWELL, B. T., SMITH, P. J., TAYLOR, D., VAN SCHALKWYK, D. A. & WALDEN, J. C. 2002. Fate of haem iron in the malaria parasite Plasmodium falciparum. *Biochemical Journal,* 365**,** 343-347.

EJAZ, A., HAQNAWAZ, K., HUSSAIN, Z., BUTT, R., AWAN, Z. I. & BUX, H. 2007. Treatment of uncomplicated plasmodium falciparum malaria with

quinine-doxycycline combination therapy. *JPMA. The Journal of the Pakistan Medical Association,* 57**,** 502-5.

EL-ANEED, A., COHEN, A. & BANOUB, J. 2009. Mass Spectrometry, Review of the Basics: Electrospray, MALDI, and Commonly Used Mass Analyzers. *Applied Spectroscopy Reviews,* 44**,** 210-230.

ELFORD, B. C., COWAN, G. M. & FERGUSON, D. J. P. 1995. Parasite-regulated membrane-transport processes and metabolic control in malaria-infected erythrocytes. *Biochemical Journal,* 308**,** 361-374.

ELLINGER, J. J., LEWIS, I. A. & MARKLEY, J. L. 2011. Role of aminotransferases in glutamate metabolism of human erythrocytes. *Journal of Biomolecular Nmr,* 49**,** 221-229.

ELLIS, D. I. & GOODACRE, R. 2006. Metabolic fingerprinting in disease diagnosis: biomedical applications of infrared and Raman spectroscopy. *Analyst,* 131**,** 875-885.

FAMIN, O. & GINSBURG, H. 2002. Differential effects of 4-aminoquinoline-containing antimalarial drugs on hemoglobin digestion in Plasmodium falciparum-infected erythrocytes. *Biochemical Pharmacology,* 63**,** 393-398.

FEAGIN, J. E. 1992. The 6-kb element of Plasmodium falciparum encodes mitochondrial cytochrome genes. *Molecular and Biochemical Parasitology,* 52, 145-148.

FEAGIN, J. E., MERICLE, B. L., WERNER, E. & MORRIS, M. 1997. Identification of additional rRNA fragments encoded by the Plasmodium falciparum 6 kb element. *Nucleic Acids Research,* 25, 438-446.

FERRARI, V. & CUTLER, D. J. 1991. Kinetics and thermodynamics of chloroquine and hydroxychloroquine transport across the human erythrocyte-membrane. *Biochemical Pharmacology,* 41**,** 23-30.

FIDOCK, D. A., NOMURA, T., TALLEY, A. K., COOPER, R. A., DZEKUNOV, S. M., FERDIG, M. T., URSOS, L. M., SIDHU, A. B., NAUDE, B., DEITSCH, K. W., SU, X. Z., WOOTTON, J. C., ROEPE, P. D. & WELLEMS, T. E. 2000. Mutations in the P. falciparum digestive vacuole transmembrane protein PfCRT and evidence for their role in chloroquine resistance. *Mol Cell,* 6**,** 861-71.

FIEHN, O. 2002. Metabolomics - the link between genotypes and phenotypes. *Plant Molecular Biology,* 48**,** 155-171.

FIEHN, O. 2006. Metabolite profiling in Arabidopsis. *Methods in Molecular Biology,* 323**,** 439-447.

FISHER, N., BRAY, P. G., WARD, S. A. & BIAGINI, G. A. 2007. The malaria parasite type IINADH : quinone oxidoreductase: an alternative enzyme for an alternative lifestyle. *Trends in Parasitology,* 23**,** 305-310.

FISHER, N., BRAY, P. G., WARD, S. A. & BIAGINI, G. A. 2008. Malaria-parasite mitochondrial dehydrogenases as drug targets: too early to write the obituary. *Trends in Parasitology,* 24**,** 9-10.

FISHER, N., WARMAN, A. J., WARD, S. A. & BIAGINI, G. A. 2009. Chapter 17 Type II NADH: Quinone Oxidoreductases of Plasmodium falciparum and Mycobacterium tuberculosis. Kinetic and High-Throughput Assays. *Methods in Enzymology,* 456, 303-320.

FITCH, C. D. 2004. Ferriprotoporphyrin IX, phospholipids, and the antimalarial actions of quinoline drugs. *Life Sciences,* 74**,** 1957-1972.

FITCH, C. D., CHEVLI, R., BANYAL, H. S., PHILLIPS, G., PFALLER, M. A. & KROGSTAD, D. J. 1982. Lysis of Plasmodium falciparum by ferriprotoporphyrin-ix and a chloroquine-ferriprotoporphyrin-ix complex. *Antimicrobial Agents and Chemotherapy,* 21**,** 819-822.

FIVELMAN, Q. L., MCROBERT, L., SHARP, S., TAYLOR, C. J., SAEED, M., SWALES, C. A., SUTHERLAND, C. J. & BAKER, D. A. 2007. Improved synchronous production of Plasmodium falciparum gametocytes in vitro. *Molecular and Biochemical Parasitology,* 154**,** 119-123.

FOLEY, M. & TILLEY, L. 1998. Quinoline antimalarials: Mechanisms of action and resistance and prospects for new agents. *Pharmacology & Therapeutics,* 79**,** 55-87.

FOOTE, S. J., THOMPSON, J. K., COWMAN, A. F. & KEMP, D. J. 1989. Amplification of the multidrug resistance gene in some chloroquine-resistant isolates of P. falciparum. *Cell,* 57**,** 921-930.

FOTH, B. J., STIMMLER, L. M., HANDMAN, E., CRABB, B. S., HODDER, A. N. & MCFADDEN, G. I. 2005. The malaria parasite Plasmodium falciparum has only one pyruvate dehydrogenase complex, which is located in the apicoplast. *Molecular Microbiology,* 55**,** 39-53.

FRANCIS, S. E., GLUZMAN, I. Y., OKSMAN, A., KNICKERBOCKER, A., MUELLER, R., BRYANT, M. L., SHERMAN, D. R., RUSSELL, D. G. & GOLDBERG, D. E. 1994. Molecular characterization and inhibition of a Plasmodium falciparum aspartic hemoglobinase. *Embo Journal,* 13**,** 306-317.

FRANCIS, S. E., SULLIVAN JR, D. J. & GOLDBERG, D. E. 1997. Hemoglobin metabolism in the malaria parasite Plasmodium falciparium. *Annual Review of Microbiology,* 51**,** 97-123.

FRY, M. & BEESLEY, J. E. 1991. Mitochondria of mammalian Plasmodium spp. *Parasitology,* 102 Pt 1**,** 17-26.

FRY, M. & PUDNEY, M. 1992. Site of action of the antimalarial hydroxynaphthoquinone, 2-[trans-4-(4'-chlorophenyl) cyclohexyl]-3- hydroxy-1,4-naphthoquinone (566C80). *Biochemical Pharmacology,* 43**,** 1545-1553.

FRY, M., WEBB, E. & PUDNEY, M. 1990. Effect of mitochondrial inhibitors on adenosine-triphosphate levels in Plasmodium falciparum. *Comparative Biochemistry and Physiology B-Biochemistry & Molecular Biology,* 96, 775-782.

GARCIA-BASTEIRO, A. L., BASSAT, Q. & ALONSO, P. L. 2012. Approaching the target: the path towards an effective malaria vaccine. *Mediterranean journal of hematology and infectious diseases,* 4**,** e2012015-e2012015.

GARDNER, M. J., HALL, N., FUNG, E., WHITE, O., BERRIMAN, M., HYMAN, R. W., CARLTON, J. M., PAIN, A., NELSON, K. E., BOWMAN, S., PAULSEN, I. T., JAMES, K., EISEN, J. A., RUTHERFORD, K., SALZBERG, S. L., CRAIG, A., KYES, S., CHAN, M. S., NENE, V., SHALLOM, S. J., SUH, B., PETERSON, J., ANGIUOLI, S., PERTEA, M., ALLEN, J., SELENGUT, J., HAFT, D., MATHER, M. W., VAIDYA, A. B., MARTIN, D. M. A., FAIRLAMB, A. H., FRAUNHOLZ, M. J., ROOS, D. S., RALPH, S. A., MCFADDEN, G. I., CUMMINGS, L. M., SUBRAMANIAN, G. M., MUNGALL, C., VENTER, J. C., CARUCCI, D. J., HOFFMAN, S. L., NEWBOLD, C., DAVIS, R. W., FRASER, C. M. & BARRELL, B. 2002. Genome sequence of the human malaria parasite Plasmodium falciparum. *Nature,* 419**,** 498-511.

GEARY, T. G. & JENSEN, J. B. 1983. Effects of antibiotics on Plasmodium falciparum invitro. *American Journal of Tropical Medicine and Hygiene,* 32, 221-225.

GENTON, B. & REED, Z. H. 2007. Asexual blood-stage malaria vaccine development: facing the challenges. *Current Opinion in Infectious Diseases,* 20**,** 467-475.

GERO, A. M., BROWN, G. V. & OSULLIVAN, W. J. 1984. Pyrimidine denovo synthesis during the life-cycle of the intraerythrocytic stage of Plasmodium falciparum. *Journal of Parasitology,* 70, 536-541.

GERO, A. M., FINNEY, K. G., BENNETT, J. C. & OSULLIVAN, W. J. 1981a. Comparative studies on dihydroorotate dehydrogenase from P.berghei and the mouse reticulocyte. *Australian Journal of Experimental Biology and Medical Science,* 59, 477-490.

GERO, A. M. & OSULLIVAN, W. J. 1990. Purines and pyrimidines in malarial parasites. *Blood Cells,* 16**,** 467-484.

GERO, A. M., TETLEY, K., COOMBS, G. H. & PHILLIPS, R. S. 1981b. Dihydroorotate dehydrogenase, orotate phosphoribosyltransferase and orotidine-5'-phosphate decarboxylase in Plasmodium falciparum. *Transactions of the Royal Society of Tropical Medicine and Hygiene,* 75, 719-720.

GHIGO, D., TODDE, R., GINSBURG, H., COSTAMAGNA, C., GAUTRET, P., BUSSOLINO, F., ULLIERS, D., GIRIBALDI, G., DEHARO, E., GABRIELLI, G., PESCARMONA, G. & BOSIA, A. 1995. Erythrocyte stages of plasmodium-falciparum exhibit a high nitric-oxide synthase (NOS) activity and release an nos-inducing soluble factor. *Journal of Experimental Medicine,* 182**,** 677-688.

GINSBURG, H. 1990. Some reflections concerning host erythrocyte-malarial parasite interrelationships. *Blood Cells,* 16**,** 225-235.

GINSBURG, H. 2010. Metabolism: Malaria parasite stands out. *Nature,* 466**,** 702-703.

GINSBURG, H., DIVO, A. A., GEARY, T. G., BOLAND, M. T. & JENSEN, J. B. 1986. Effects of mitochondrial inhibitors on intraerythrocytic Plasmodium falciparum in invitro cultures. *Journal of Protozoology,* 33, 121-125.

GINSBURG, H., FAMIN, O., ZHANG, J. M. & KRUGLIAK, M. 1998. Inhibition of glutathione-dependent degradation of heme by chloroquine and amodiaquine as a possible basis for their antimalarial mode of action. *Biochemical Pharmacology,* 56**,** 1305-1313.

GINSBURG, H. & GEARY, T. G. 1987. Current concepts and new ideas on the mechanism of action of quinoline-containing antimalarials. *Biochemical Pharmacology,* 36**,** 1567-1576.

GINSBURG, H. & KRUGLIAK, M. 1992. Quinoline-containing antimalarials - mode of action, drug-resistance and its reversal - an update with unresolved puzzles. *Biochemical Pharmacology,* 43**,** 63-70.

GINSBURG, H., KUTNER, S., KRUGLIAK, M. & CABANTCHIK, Z. I. 1985. Characterization of permeation pathways appearing in the host membrane of Plasmodium falciparum infected red blood-cells. *Molecular and Biochemical Parasitology,* 14**,** 313-322.

GIRARD, M. P., REED, Z. H., FRIEDE, M. & KIENY, M. P. 2007. A review of human vaccine research and development: Malaria. *Vaccine,* 25**,** 1567-1580.

GOLDBERG, D. E. 2005. Hemoglobin degradation. *Malaria: Drugs, Disease and Post-Genomic Biology,* 295**,** 275-291.

GOLDBERG, D. E., SLATER, A. F. G., CERAMI, A. & HENDERSON, G. B. 1990. Hemoglobin degradation in the malaria parasite Plasmodium falciparum - an ordered process in a unique organelle. *Proceedings of the National Academy of Sciences of the United States of America,* 87**,** 2931-2935.

GOMEZ, Z. M. & RATHOD, P. K. 1990. Antimalarial activity of a combination of 5-fluoroorotate and uridine in mice. *Antimicrobial Agents and Chemotherapy,* 34, 1371-1375.

GOODACRE, R. 2005. Metabolomics - the way forward. *Metabolomics,* 1**,** 1-2.

GOODACRE, R., VAIDYANATHAN, S., DUNN, W. B., HARRIGAN, G. G. & KELL, D. B. 2004. Metabolomics by numbers: acquiring and understanding global metabolite data. *Trends in Biotechnology,* 22**,** 245-252.

GOSONIU, L., VOUNATSOU, P., TAMI, A., NATHAN, R., GRUNDMANN, H. & LENGELER, C. 2008. Spatial effects of mosquito bednets on child mortality. *Bmc Public Health,* 8**,** 356.

GRASSI, B. 1900. *Studi di uno zoologo sulla Malaria*.

GREENWOOD, B. M., FIDOCK, D. A., KYLE, D. E., KAPPE, S. H. I., ALONSO, P. L., COLLINS, F. H. & DUFFY, P. E. 2008. Malaria: progress, perils, and prospects for eradication. *Journal of Clinical Investigation,* 118**,** 1266-1276.

GREGSON, A. & PLOWE, C. V. 2005. Mechanisms of resistance of malaria parasites to antifolates. *Pharmacological Reviews,* 57**,** 117-145.

GU, W. & NOVAK, R. J. 2009. Predicting the impact of insecticide-treated bed nets on malaria transmission: the devil is in the detail. *Malaria Journal,* 8, 256.

GUERIN, P. J., OLLIARO, P., NOSTEN, F., DRUILHE, P., LAXMINARAYAN, R., BINKA, F., KILAMA, W. L., FORD, N. & WHITE, N. J. 2002. Malaria: current status of control, diagnosis, treatment, and a proposed agenda for research and development. *Lancet Infectious Diseases,* 2**,** 564-573.

GUNN, A. A. P., S. J. 2012. *Parasitology: An Integrated Approach,* John Wiley & Sons, Ltd., Chichester, UK.

GUNTHER, S., MCMILLAN, P. J., WALLACE, L. J. M. & MULLER, S. 2005. Plasmodium falciparum possesses organelle-specific alpha-keto acid dehydrogenase complexes and lipoylation pathways. *Biochemical Society Transactions,* 33**,** 977-980.

GUTMAN, J., KACHUR, S. P., SLUTSKER, L., NZILA, A. & MUTABINGWA, T. 2012. Combination of probenecid-sulphadoxine-pyrimethamine for intermittent preventive treatment in pregnancy. *Malaria Journal,* 11, 39.

GUTTERIDGE, W.E. & TRIGG, P. I. 1970. Incorporation of radioactive precursors into DNA and RNA of Plasmodium knowlesi in-vitro. *Journal of Protozoology,* 17**,** 89-96.

GUTTERIDGE, W. E., DAVE, D. & RICHARDS, W. H. G. 1979. Conversion of dihydroorotate to orotate in parasitic protozoa. *BBA - General Subjects,* 582**,** 390-401.

HAMMOND, D. J., BURCHELL, J. R. & PUDNEY, M. 1985. Inhibition of pyrimidine biosynthesis de novo in Plasmodium falciparum by 2-(4-t-butylcyclohexyl)-3-hydroxy-1,4-naphthoquinone in vitro. *Molecular and Biochemical Parasitology,* 14**,** 97-109.

HARRIS, J. W., AND KELLERMEYER, R.W., 1979. *The Red Cell,* Harvard University Press, Cambridge.

HARTWIG, C. L., ROSENTHAL, A. S., D'ANGELO, J., GRIFFIN, C. E., POSNER, G. H. & COOPER, R. A. 2009. Accumulation of artemisinin trioxane derivatives within neutral lipids of Plasmodium falciparum malaria parasites is endoperoxide-dependent. *Biochemical Pharmacology,* 77**,** 322-336.

HATIN, I., JAMBOU, R., GINSBURG, H. & JAUREGUIBERRY, G. 1992. Single or multiple localization of ADP ATP transporter in human malarial Plasmodium falciparum. *Biochemical Pharmacology,* 43**,** 71-75.

HAYAKAWA, T., ARISUE, N., UDONO, T., HIRAI, H., SATTABONGKOT, J., TOYAMA, T., TSUBOI, T., HORII, T. & TANABE, K. 2009. Identification of Plasmodium malariae, a Human Malaria Parasite, in Imported Chimpanzees. *Plos One,* 4, e7412.

HEGNER, R. W. & MACDOUGALL, M. S. 1926. Modifying the course of infections with bird malaria by changing the sugar content of the blood (Preliminary report). *American Journal of Hygiene,* 6, 602-609.

HEIKKILA, T., RAMSEY, C., DAVIES, M., GALTIER, C., STEAD, A. M. W., JOHNSON, A. P., FISHWICK, C. W. G., BOA, A. N. & MCCONKEY, G. A. 2007. Design and synthesis of potent inhibitors of the malaria parasite dihydroorotate dehydrogenase. *Journal of Medicinal Chemistry,* 50, 186-191.

HEIKKILA, T., THIRUMALAIRAJAN, S., DAVIES, M., PARSONS, M. R., MCCONKEY, A. G., FISHWICK, C. W. G. & JOHNSON, A. P. 2006. The first de novo designed inhibitors of Plasmodium falciparum dihydroorotate dehydrogenase. *Bioorganic & Medicinal Chemistry Letters,* 16, 88-92.

HEIKKILÄ, T., RAMSEY, C., DAVIES, M., GALTIER, C., STEAD, A. M. W., JOHNSON, A. P., FISHWICK, C. W. G., BOA, A. N. & MCCONKEY, G. A. 2007. Design and synthesis of potent inhibitors of the malaria parasite dihydroorotate dehydrogenase. *Journal of Medicinal Chemistry,* 50**,** 186-191.

HEMINGWAY, J. & RANSON, H. 2000. Insecticide resistance in insect vectors of human disease. *Annual Review of Entomology,* 45**,** 371-391.

HENDERSON, P. J. & LARDY, H. A. 1970. Bongkrekic acid. An inhibitor of the adenine nucleotide translocase of mitochondria. *Journal of Biological Chemistry,* 245**,** 1319-1326.

HENRY, M., BRIOLANT, S., ZETTOR, A., PELLEAU, S., BARAGATTI, M., BARET, E., MOSNIER, J., AMALVICT, R., FUSAI, T., ROGIER, C. & PRADINES, B. 2009. Plasmodium falciparum Na+/H+ exchanger 1 transporter is involved in reduced susceptibility to quinine. *Antimicrob Agents Chemother,* 53**,** 1926-30.

HOMEWOOD, C. A., WARHURST, D. C., PETERS, W. & BAGGALEY, V. C. 1972. Electron-transport in intraerythrocytic Plasmodium berghei. *Proceedings of the Helminthological Society of Washington,* 39, 382-386.

HOMMEL, M., AND GILLS, H.M. 2005. Malaria. *In:* COX, F. E. G., WAKELIN, D., GILLESPIE, S.H., AND DESPOMMIER, D.D. (ed.) *Topley and Wilson's Microbiology and Microbial Infections, Parasitology.* Hodder Arnold, London, UK.

HU, Q. Z., NOLL, R. J., LI, H. Y., MAKAROV, A., HARDMAN, M. & COOKS, R. G. 2005. The Orbitrap: a new mass spectrometer. *Journal of Mass Spectrometry,* 40**,** 430-443.

HUDSON, A. T., DICKINS, M., GINGER, C. D., GUTTERIDGE, W. E., HOLDICH, T., HUTCHINSON, D. B. A., PUDNEY, M., RANDALL, A. W. & LATTER, V. S. 1991. 566C80 - A potent broad-spectrum antiinfective agent with activity against malaria and opportunistic infections in aids patients. *Drugs under Experimental and Clinical Research,* 17, 427-435.

HYDE, J. E. 2007a. Drug-resistant malaria - An insight. *FEBS Journal,* 274**,** 4688-4698.

HYDE, J. E. 2007b. Targeting purine and pyrimidine metabolism in human apicomplexan parasites. *Current Drug Targets,* 8**,** 31-47.

IMWONG, M., DONDORP, A. M., NOSTEN, F., YI, P., MUNGTHIN, M., HANCHANA, S., DAS, D., PHYO, A. P., LWIN, K. M., PUKRITTAYAKAMEE, S., LEE, S. J., SAISUNG, S., KOECHAROEN, K., NGUON, C., DAY, N. P. J., SOCHEAT, D. & WHITE, N. J. 2010. Exploring the Contribution of Candidate Genes to Artemisinin Resistance in Plasmodium falciparum. *Antimicrobial Agents and Chemotherapy,* 54**,** 2886-2892.

ISLAHUDIN, F., PLEASS, R. J., AVERY, S. V. & TING, K.-N. 2012. Quinine interactions with tryptophan and tyrosine in malaria patients, and implications for quinine responses in the clinical setting. *Journal of Antimicrobial Chemotherapy,* 67**,** 2501-2505.

ITTARAT, I., ASAWAMAHASAKDA, W. & MESHNICK, S. R. 1994. The effects of antimalarials on the Plasmodium falciparum dihydroorotate dehydrogenase. *Experimental Parasitology,* 79**,** 50-56.

JACKSON, K. E., HABIB, S., FRUGIER, M., HOEN, R., KHAN, S., PHAM, J. S., RIBAS DE POUPLANA, L., ROYO, M., SANTOS, M. A. S., SHARMA, A. & RALPH, S. A. 2011. Protein translation in Plasmodium parasites. *Trends in Parasitology,* 27**,** 467-476.

JAIKARIA, N. S., ROZARIO, C., RIDLEY, R. G. & PERKINS, M. E. 1993. BIOGENESIS OF RHOPTRY ORGANELLES IN PLASMODIUM-FALCIPARUM. *Molecular and Biochemical Parasitology,* 57**,** 269-280.

JAMSHIDI, N., EDWARDS, J. S., FAHLAND, T., CHURCH, G. M. & PALSSON, B. O. 2001. Dynamic simulation of the human red blood cell metabolic network. *Bioinformatics,* 17, 286-287.

JAYARAMAN, V., BULUSU, V. & BALARAM, H. 2012. Crosstalk between purine nucleotide metabolism and mitochondrial pathways in Plasmodium falciparum. *Current Science,* 102, 757-766.

JENSEN, J. B. & TRAGER, W. 1977. Plasmodium falciparum in culture - use of outdated erythrocytes and description of candle jar method. *Journal of Parasitology,* 63**,** 883-886.

JENSEN, J. B. & TRAGER, W. 1978. Plasmodium falciparum in culture Establishment of additional strains. *American Journal of Tropical Medicine and Hygiene,* 27**,** 743-746.

JENSEN, M. D., CONLEY, M. & HELSTOWSKI, L. D. 1983. Culture of Plasmodium falciparum - the role of pH, glucose, and lactate. *Journal of Parasitology,* 69, 1060-1067.

JOHNS, F. M. 1931. Influence of dextrose and of low temperatures on preservation, transportation and viability of malaria parasites. *Proceedings of the Society for Experimental Biology and Medicine,* 28, 0743-0745.

JOHNSON, R. A., MCFADDEN, G. I. & GOODMAN, C. D. 2011. Characterization of two malaria parasite organelle translation elongation factor G proteins: The likely targets of the anti-malarial fusidic acid. *PLoS ONE,* 6, e20633.

JOSHI, A. & PALSSON, B. O. 1989. Metabolic dynamics in the human red-cell .1. a comprehensive kinetic-model. *Journal of Theoretical Biology,* 141**,** 515-528.

KADDURAH-DAOUK, R., KRISTAL, B. S. & WEINSHILBOUM, R. M. 2008. Metabolomics: A global biochemical approach to drug response and disease. *Annual Review of Pharmacology and Toxicology,* 48**,** 653-683.

KAFSACK, B. F. C. & LLINÁS, M. 2010. Eating at the Table of Another: Metabolomics of Host-Parasite Interactions. *Cell Host and Microbe,* 7**,** 90-99.

KAMLEH, M. A., HOBANI, Y., DOW, J. A. T. & WATSON, D. G. 2008. Metabolomic profiling of Drosophila using liquid chromatography Fourier transform mass spectrometry. *Febs Letters,* 582**,** 2916-2922.

KATAJAMAA, M. & ORESIC, M. 2007. Data processing for mass spectrometry-based metabolomics. *Journal of Chromatography A,* 1158**,** 318-328.

KELL, D. B. 2004. Metabolomics and systems biology: making sense of the soup. *Current Opinion in Microbiology,* 7**,** 296-307.

KELL, D. B. 2006. Systems biology, metabolic modelling and metabolomics in drug discovery and development. *Drug Discovery Today,* 11**,** 1085-1092.

KESSL, J. J., MOSKALEV, N. V., GRIBBLE, G. W., NASR, M., MESHNICK, S. R. & TRUMPOWER, B. L. 2007. Parameters determining the relative efficacy of hydroxy-naphthoquinone inhibitors of the cytochrome bc(1) complex. *Biochimica Et Biophysica Acta-Bioenergetics,* 1767, 319-326.

KHOO, S. H. G. & AL-RUBEAI, M. 2007. Metabolomics as a complementary tool in cell culture. *Biotechnology and Applied Biochemistry,* 47**,** 71-84.

KHOZOIE, C., PLEASS, R. J. & AVERY, S. V. 2009. The Antimalarial Drug Quinine Disrupts Tat2p-mediated Tryptophan Transport and Causes Tryptophan Starvation. *Journal of Biological Chemistry,* 284**,** 17968-17974.

KIMBALL, E. & RABINOWITZ, J. D. 2006. Identifying decomposition products in extracts of cellular metabolites. *Analytical Biochemistry,* 358**,** 273-280.

KIRK, K. 2001. Membrane transport in the malaria-infected erythrocyte. *Physiological Reviews,* 81**,** 495-537.

KIRK, K., HOWITT, S. M., BRÖER, S., SALIBA, K. J. & DOWNIE, M. J. 2009. Purine uptake in Plasmodium: transport versus metabolism. *Trends in Parasitology,* 25**,** 246-249.

KIRK, K., MARTIN, R. E., BROER, S., HOWITT, S. M. & SALIBA, K. J. 2005. Plasmodium permeomics: Membrane transport proteins in the malaria parasite. *Malaria: Drugs, Disease and Post-Genomic Biology,* 295**,** 325-356.

KLEINBONGARD, P., SCHULZ, R., MUENCH, M., RASSAF, T., LAUER, T., GOEDECKE, A. & KELM, M. 2006. Red blood cells express a functional endothelial nitric oxide synthase. *European Heart Journal,* 27**,** 127-127.

KOCHAR, D. K., SAXENA, V., SINGH, N., KOCHAR, S. K., KUMAR, S. V. & DAS, A. 2005. Plasmodium vivax malaria. *Emerging Infectious Diseases,* 11,132–134.

KOEK, M. M., JELLEMA, R. H., VAN DER GREEF, J., TAS, A. C. & HANKEMEIER, T. 2011. Quantitative metabolomics based on gas chromatography mass spectrometry: status and perspectives. *Metabolomics,* 7, 307-328.

KOEK, M. M., MUILWIJK, B., VAN DER WERF, M. J. & HANKEMEIER, T. 2006. Microbial metabolomics with gas chromatography/mass spectrometry. *Analytical Chemistry,* 78**,** 1272-1281.

KOLAKOVICH, K. A., GLUZMAN, I. Y., DUFFIN, K. L. & GOLDBERG, D. E. 1997. Generation of hemoglobin peptides in the acidic digestive vacuole of Plasmodium falciparum implicates peptide transport in amino acid production. *Molecular and Biochemical Parasitology,* 87**,** 123-135.

KONIGK, E. & PUTFARKEN, B. 1983. Inhibition of ornithine decarboxylase of invitro cultured Plasmodium falciparum by chloroquine. *Tropenmedizin Und Parasitologie,* 34**,** 1-3.

KORAM, K. A., BENNETT, S., ADIAMAH, J. H. & GREENWOOD, B. M. 1995. Socio-economic determinants are not major risk factors for severe malaria in Gambian children. *Transactions of the Royal Society of Tropical Medicine and Hygiene,* 89**,** 151-154.

KORSINCZKY, M., CHEN, N. H., KOTECKA, B., SAUL, A., RIECKMANN, K. & CHENG, Q. 2000. Mutations in Plasmodium falciparum cytochrome b that are associated with atovaquone resistance are located at a putative drug-binding site. *Antimicrobial Agents and Chemotherapy,* 44, 2100-2108.

KREMSNER, P. G. & KRISHNA, S. 2004. Antimalarial combinations. *Lancet,* 364**,** 285-294.

KRISHNA, S., BUSTAMANTE, L., HAYNES, R. K. & STAINES, H. M. 2008. Artemisinins: their growing importance in medicine. *Trends in Pharmacological Sciences,* 29**,** 520-527.

KRISHNA, S., UHLEMANN, A. C. & HAYNES, R. K. 2004. Artemisinins: mechanisms of action and potential for resistance. *Drug Resistance Updates,* 7**,** 233-244.

KROEGER, A., MEYER, R., MANCHENO, M. & GONZALEZ, M. 1996. Health education for community-based malaria control: An intervention study in Ecuador, Colombia and Nicaragua. *Tropical Medicine & International Health,* 1**,** 836-846.

KROGSTAD, D. J. & SCHLESINGER, P. H. 1987. Acid-vesicle function, intracellular pathogens, and the action of chloroquine against Plasmodium falciparum. *New England Journal of Medicine,* 317**,** 542-549.

KROTOSKI, W. A. 1985. Discovery of the hypnozoite and a new theory of malarial relapse. *Transactions of the Royal Society of Tropical Medicine and Hygiene,* 79**,** 12-20.

KROTOSKI, W. A., COLLINS, W. E., BRAY, R. S., GARNHAM, P. C., COGSWELL, F. B., GWADZ, R. W., KILLICK-KENDRICK, R., WOLF, R., SINDEN, R., KOONTZ, L. C. & STANFILL, P. S. 1982. Demonstration of hypnozoites in sporozoite-transmitted Plasmodium vivax infection. *Am J Trop Med Hyg,* 31**,** 1291-1293.

KRUGLIAK, M., ZHANG, J. M. & GINSBURG, H. 2002. Intraerythrocytic Plasmodium falciparum utilizes only a fraction of the amino acids derived from the digestion of host cell cytosol for the biosynthesis of its proteins. *Molecular and Biochemical Parasitology,* 119**,** 249-256.

KRUNGKRAI, J. 1995. Purification, characterization and localization of mitochondrial dihydroorotate dehydrogenase in Plasmodium falciparum, human malaria parasite. *Biochimica et Biophysica Acta - General Subjects,* 1243**,** 351-360.

KRUNGKRAI, J. 2004. The multiple roles of the mitochondrion of the malarial parasite. *Parasitology,* 129**,** 511-524.

KRUNGKRAI, J., BURAT, D., KUDAN, S., KRUNGKRAI, S. & PRAPUNWATTANA, P. 1999. Mitochondrial oxygen consumption in asexual and sexual blood stages of the human malarial parasite, Plasmodium falciparum. *Southeast Asian Journal of Tropical Medicine and Public Health,* 30**,** 636-642.

KRUNGKRAI, J., KRUNGKRAI, S. R. & PHAKANONT, K. 1992. Antimalarial activity of orotate analogs that inhibit dihydroorotase and dihydroorotate dehydrogenase. *Biochemical Pharmacology,* 43, 1295-1301.

KRUNGKRAI, J., PRAPUNWATANA, P., WICHITKUL, C., REUNGPRAPAVUT, S., KRUNGKRAI, S. R. & HORII, T. 2003. Molecular biology and biochemistry of malarial parasite pyrimidine biosynthetic pathway. *The*

Southeast Asian journal of tropical medicine and public health, 34 Suppl 2**,** 32-43.

KRUNGKRAI, J., PRAPUNWATTANA, P. & KRUNGKRAI, S. R. 2000. Ultrastructure and function of mitochondria in gametocytic stage of Plasmodium falciparum. *Parasite,* 7**,** 19-26.

KRUNGKRAI, J., WEBSTER, H. K. & YUTHAVONG, Y. 1989. Denovo and salvage biosynthesis of pteroylpentaglutamates in the human malaria parasite, Plasmodium falciparum. *Molecular and Biochemical Parasitology,* 32**,** 25-37.

KUBLIN, J. G., DZINJALAMALA, F. K., KAMWENDO, D. D., MALKIN, E. M., CORTESE, J. F., MARTINO, L. M., MUKADAM, R. A. G., ROGERSON, S. J., LESCANO, A. G., MOLYNEUX, M. E., WINSTANLEY, P. A., CHIMPENI, P., TAYLOR, T. E. & PLOWE, C. V. 2002. Molecular markers for failure of sulfadoxine-pyrimethamine and chlorproguanil-dapsone treatment of Plasmodium falciparum malaria. *Journal of Infectious Diseases,* 185**,** 380-388.

KUROSAWA, Y., DORN, A., KITSUJI-SHIRANE, M., SHIMADA, H., SATOH, T., MATILE, H., HOFHEINZ, W., MASCIADRI, R., KANSY, M. & RIDLEY, R. G. 2000. Hematin polymerization assay as a high-throughput screen for identification of new antimalarial pharmacophores. *Antimicrobial Agents and Chemotherapy,* 44**,** 2638-2644.

LAISHRAM, D. D., SUTTON, P. L., NANDA, N., SHARMA, V. L., SOBTI, R. C., CARLTON, J. M. & JOSHI, H. 2012. The complexities of malaria disease manifestations with a focus on asymptomatic malaria. *Malaria Journal,* 11, 29.

LAKSHMANAN, V., BRAY, P. G., VERDIER-PINARD, D., JOHNSON, D. J., HORROCKS, P., MUHLE, R. A., ALAKPA, G. E., HUGHES, R. H., WARD, S. A., KROGSTAD, D. J., SIDHU, A. B. & FIDOCK, D. A. 2005. A critical role for PfCRT K76T in Plasmodium falciparum verapamil-reversible chloroquine resistance. *EMBO J,* 24**,** 2294-305.

LAKSHMANAN, V., RHEE, K. Y. & DAILY, J. P. 2011. Metabolomics and malaria biology. *Molecular and Biochemical Parasitology,* 175**,** 104-111.

LAMBROS, C. & VANDERBERG, J. P. 1979. Synchronization of plasmodium-falciparum erythrocytic stages in culture. *Journal of Parasitology,* 65**,** 418-420.

LANG-UNNASCH, N. & MURPHY, A. D. 1998. Metabolic changes of the malaria parasite during the transition from the human to the mosquito host. *Annual Review of Microbiology,* 52**,** 561-590.

LANGRETH, S. G., JENSEN, J. B., REESE, R. T. & TRAGER, W. 1978. Fine-structure of human malaria invitro. *Journal of Protozoology,* 25, 443-452.

LAVERAN, A. 1880. A new parasite found in the blood of malarial patients. Parasitic origin of malarial attacks. *Bull. Mem. Soc. Med. Hosp. Paris,* 17**,** 158-164.

LELL, B. & KREMSNER, P. G. 2002. Clindamycin as an antimalarial drug: Review of clinical trials. *Antimicrobial Agents and Chemotherapy,* 46**,** 2315-2320.

LENZ, A. G. & HOLZER, H. 1984. Effects of chloroquine on proteolytic processes and energy-metabolism in yeast. *Archives of Microbiology,* 137**,** 104-108.

LEW, V. L., TIFFERT, T. & GINSBURG, H. 2003. Excess hemoglobin digestion and the osmotic stability of Plasmodium falciparum-infected red blood cells. *Blood,* 101**,** 4189-4194.

LEWIS, I. A., CAMPANELLA, M. E., MARKLEY, J. L. & LOW, P. S. 2009. Role of band 3 in regulating metabolic flux of red blood cells. *Proceedings of the National Academy of Sciences of the United States of America,* 106**,** 18515-18520.

LI, G. Q., GUO, X. B., FU, L. C., JIAN, H. X. & WANG, X. H. 1994. Clinical trials of artemisinin and its derivatives in the treatment of malaria in China. *Transactions of the Royal Society of Tropical Medicine and Hygiene,* 88**,** S5-S6.

LI, W., MO, W. K., SHEN, D., SUN, L. B., WANG, J., LU, S., GITSCHIER, J. M. & ZHOU, B. 2005. Yeast model uncovers dual roles of mitochondria in the action of arternisinin. *Plos Genetics,* 1**,** 329-334.

LIAN, L.-Y., AL-HELAL, M., ROSLAINI, A. M., FISHER, N., BRAY, P. G., WARD, S. A. & BIAGINI, G. A. 2009. Glycerol: An unexpected major metabolite of energy metabolism by the human malaria parasite. *Malaria Journal,* 8, 38.

LIM, L. & MCFADDEN, G. I. 2010. The evolution, metabolism and functions of the apicoplast. *Philosophical Transactions of the Royal Society B-Biological Sciences,* 365**,** 749-763.

LISEC, J., MEYER, R. C., STEINFATH, M., REDESTIG, H., BECHER, M., WITUCKA-WALL, H., FIEHN, O., TOERJEK, O., SELBIG, J., ALTMANN, T. & WILLMITZER, L. 2008. Identification of metabolic and biomass QTL in Arabidopsis thaliana in a parallel analysis of RIL and IL populations. *Plant Journal,* 53**,** 960-972.

LIU, J., ISTVAN, E. S., GLUZMAN, I. Y., GROSS, J. & GOLDBERG, D. E. 2006. Plasmodium falciparum ensures its amino acid supply with multiple acquisition pathways and redundant proteolytic enzyme systems. *Proceedings of the National Academy of Sciences of the United States of America,* 103, 8840-8845.

LOOAREESUWAN, S., CHULAY, J. D., CANFIELD, C. J., HUTCHINSON, D. B. A. & MALARONE CLINICAL TRIALS STUDY, G. 1999a. Malarone (R) (atovaquone and proguanil hydrochloride): A review of its clinical development for treatment of malaria. *American Journal of Tropical Medicine and Hygiene,* 60**,** 533-541.

LOOAREESUWAN, S., VIRAVAN, C., WEBSTER, H. K., KYLE, D. E. & CANFIELD, C. J. 1996. Clinical studies of atovaquone, alone or in combination with other antimalarial drugs, for treatment of acute uncomplicated malaria in Thailand. *American Journal of Tropical Medicine and Hygiene,* 54, 62-66.

LOOAREESUWAN, S., WILAIRATANA, P., CHALERMARUT, K., RATTANAPONG, Y., CANFIELD, C. J. & HUTCHINSON, D. B. A. 1999b.

Efficacy and safety of atovaquone/proguanil compared with mefloquine for treatment of acute Plasmodium falciparum malaria in Thailand. *American Journal of Tropical Medicine and Hygiene,* 60**,** 526-532.

LU, W., BENNETT, B. D. & RABINOWITZ, J. D. 2008. Analytical strategies for LC-MS-based targeted metabolomics. *Journal of Chromatography B: Analytical Technologies in the Biomedical and Life Sciences,* 871**,** 236-242.

LU, W., CLASQUIN, M. F., MELAMUD, E., AMADOR-NOGUEZ, D., CAUDY, A. A. & RABINOWITZ, J. D. 2010. Metabolomic Analysis via Reversed-Phase Ion-Pairing Liquid Chromatography Coupled to a Stand Alone Orbitrap Mass Spectrometer. *Analytical Chemistry,* 82, 3212-3221.

LU, W. Y., KIMBALL, E. & RABINOWITZ, J. D. 2006. A high-performance liquid chromatography-tandem mass spectrometry method for quantitation of nitrogen-containing intracellular metabolites. *Journal of the American Society for Mass Spectrometry,* 17, 37-50.

MAIER, A. G., COOKE, B. M., COWMAN, A. F. & TILLEY, L. 2009. Malaria parasite proteins that remodel the host erythrocyte. *Nature Reviews Microbiology,* 7**,** 341-354.

MALMQUIST, N. A., GUJJAR, R., RATHOD, P. K. & PHILLIPS, M. A. 2008. Analysis of flavin oxidation and electron-transfer inhibition in Plasmodium falciparum dihydroorotate dehydrogenase. *Biochemistry,* 47**,** 2466-75.

MARSHALL, A. G., HENDRICKSON, C. L. & JACKSON, G. S. 1998. Fourier transform ion cyclotron resonance mass spectrometry: A primer. *Mass Spectrometry Reviews,* 17**,** 1-35.

MARTIN, R. E. & KIRK, K. 2004. The malaria parasite's chloroquine resistance transporter is a member of the drug/metabolite transporter superfamily. *Mol Biol Evol,* 21**,** 1938-49.

MARTIN, R. E. & KIRK, K. 2007. Transport of the essential nutrient isoleucine in human erythrocytes infected with the malaria parasite Plasmodium falciparum. *Blood,* 109**,** 2217-2224.

MARTIN, R. E., MARCHETTI, R. V., COWAN, A. I., HOWITT, S. M., BROER, S. & KIRK, K. 2009. Chloroquine transport via the malaria parasite's chloroquine resistance transporter. *Science,* 325**,** 1680-1682.

MARTINEZ-TORRES, D., CHANDRE, F., WILLIAMSON, M. S., DARRIET, F., BERGE, J. B., DEVONSHIRE, A. L., GUILLET, P., PASTEUR, N. & PAURON, D. 1998. Molecular characterization of pyrethroid knockdown resistance (kdr) in the major malaria vector Anopheles gambiae S.S. *Insect Molecular Biology,* 7**,** 179-184.

MCCORMIC.GJ 1970. Amino acid transport and incorporation in red blood cells of normal and Plasmodium knowlesi-infected rhesus monkeys. *Experimental Parasitology,* 27**,** 143-149.

MCFADDEN, G. I. & ROOS, D. S. 1999. Apicomplexan plastids as drug targets. *Trends in Microbiology,* 7**,** 328-333.

MEHTA, M., SONAWAT, H. M. & SHARMA, S. 2006. Glycolysis in Plasmodium falciparum results in modulation of host enzyme activities. *Journal of Vector Borne Diseases,* 43, 95-103.

MENTING, J. G., TILLEY, L., DEADY, L. W., NG, K., SIMPSON, R. J., COWMAN, A. F. & FOLEY, M. 1997. The antimalarial drug, chloroquine, interacts with lactate dehydrogenase from Plasmodium falciparum. *Molecular and Biochemical Parasitology,* 88**,** 215-224.

MERYMAN, H. T. & HORNBLOW.M 1968. A membrane-stabilizing effect of sugars in red cell-suspending media and its effect in reducing freezing hemolysis. *Cryobiology,* 4**,** 255-256.

MESHNICK, S. R. 1990. Chloroquine as intercalator: a hypothesis revived. *Parasitology Today,* 6**,** 77-79.

MESHNICK, S. R., TAYLOR, T. E. & KAMCHONWONGPAISAN, S. 1996. Artemisinin and the antimalarial endoperoxides: From herbal remedy to targeted chemotherapy. *Microbiological Reviews,* 60**,** 301-315.

MIAN-MCCARTHY, S., AGNANDJI, S. T., LELL, B., FERNANDES, J. F., ABOSSOLO, B. P., METHOGO, B. G. N. O., KABWENDE, A. L., ADEGNIKA, A. A., MORDMUELLER, B., ISSIFOU, S., KREMSNER, P. G., SACARLAL, J., AIDE, P., LANASPA, M., APONTE, J. J., MACHEVO, S., ACACIO, S., BULO, H., SIGAUQUE, B., MACETE, E., ALONSO, P., ABDULLA, S., SALIM, N., MINJA, R., MPINA, M., AHMED, S., ALI, A. M., MTORO, A. T., HAMAD, A. S., MUTANI, P., TANNER, M., TINTO, H., D'ALESSANDRO, U., SORGHO, H., VALEA, I., BIHOUN, B., GUIRAUD, I., KABORE, B., SOMBIE, O., GUIGUEMDE, R. T., OUEDRAOGO, J. B., HAMEL, M. J., KARIUKI, S., ONEKO, M., ODERO, C., OTIENO, K., AWINO, N., MCMORROW, M., MUTURI-KIOI, V., LASERSON, K. F., SLUTSKER, L., OTIENO, W., OTIENO, L., OTSYULA, N., GONDI, S., OTIENO, A., OWIRA, V., OGUK, E., ODONGO, G., BEN WOODS, J., OGUTU, B., NJUGUNA, P., CHILENGI, R., AKOO, P., KERUBO, C., MAINGI, C., LANG, T., OLOTU, A., BEJON, P., MARSH, K., MWANBINGU, G., OWUSU-AGYEI, S., ASANTE, K. P., OSEI-KWAKYE, K., BOAHEN, O., DOSOO, D., ASANTE, I., ADJEI, G., KWARA, E., CHANDRAMOHAN, D., GREENWOOD, B., LUSINGU, J., GESASE, S., MALABEJA, A., ABDUL, O., MAHENDE, C., LIHELUKA, E., MALLE, L., LEMNGE, M., THEANDER, T. G., DRAKELEY, C., ANSONG, D., AGBENYEGA, T., ADJEI, S., BOATENG, H. O., RETTIG, T., BAWA, J., SYLVERKEN, J., SAMBIAN, D., SARFO, A., et al. 2012. A Phase 3 Trial of RTS,S/AS01 Malaria Vaccine in African Infants. *New England Journal of Medicine,* 367**,** 2284-2295.

MILLER, L. H., BARUCH, D. I., MARSH, K. & DOUMBO, O. K. 2002. The pathogenic basis of malaria. *Nature,* 415**,** 673-679.

MILLER, R. L., IKRAM, S., ARMELAGOS, G. J., WALKER, R., HARER, W. B., SHIFF, C. J., BAGGETT, D., CARRIGAN, M. & MARET, S. M. 1994. Diagnosis of plasmodium-falciparum infections in mummies using the rapid manual parasight(TM)-F test. *Transactions of the Royal Society of Tropical Medicine and Hygiene,* 88, 31-32.

MITA, T., TANABE, K. & KITA, K. 2009. Spread and evolution of Plasmodium falciparum drug resistance. *Parasitology International,* 58**,** 201-209.

MOCO, S., BINO, R. J., DE VOS, R. C. H. & VERVOORT, J. 2007. Metabolomics technologies and metabolite identification. *Trac-Trends in Analytical Chemistry,* 26**,** 855-866.

MOK, S., IMWONG, M., MACKINNON, M. J., SIM, J., RAMADOSS, R., YI, P., MAYXAY, M., CHOTIVANICH, K., LIONG, K. Y., RUSSELL, B., SOCHEAT, D., NEWTON, P. N., DAY, N. P. J., WHITE, N. J., PREISER, P. R., NOSTEN, F., DONDORP, A. M. & BOZDECH, Z. 2011. Artemisinin resistance in Plasmodium falciparum is associated with an altered temporal pattern of transcription. *BMC Genomics,* 12, 391.

MONZOTE, L. & GILLE, L. 2010. Mitochondria as a promising antiparasitic target. *Current Clinical Pharmacology,* 5**,** 55-66.

MORRISON, D. B. & JESKEY, H. A. 1948. Alterations in some constituents of the monkey erythrocyte infected with Plasmodium knowlesi as related to pigment formation. *Journal. National Malaria Society,* 7**,** 259-64.

MOULDER, J. W. 1948. The metabolism of malarial parasites. *Annual Review of Microbiology,* 2**,** 101-120.

MOURA, P. A., DAME, J. B. & FIDOCK, D. A. 2009. Role of Plasmodium falciparum Digestive Vacuole Plasmepsins in the Specificity and Antimalarial Mode of Action of Cysteine and Aspartic Protease Inhibitors. *Antimicrobial Agents and Chemotherapy,* 53**,** 4968-4978.

MULLER, I. B. & HYDE, J. E. 2010. Antimalarial drugs: Modes of action and mechanisms of parasite resistance. *Future Microbiology,* 5**,** 1857-1873.

MUNGTHIN, M., BRAY, P. G., RIDLEY, R. G. & WARD, S. A. 1998. Central role of hemoglobin degradation in mechanisms of action of 4-aminoquinolines, quinoline methanols, and phenanthrene methanols. *Antimicrobial Agents and Chemotherapy,* 42**,** 2973-2977.

MURPHY, A. D., DOELLER, J. E., HEARN, B. & LANGUNNASCH, N. 1997. Plasmodium falciparum: Cyanide-resistant oxygen consumption. *Experimental Parasitology,* 87, 112-120.

MURPHY, A. D. & LANG-UNNASCH, N. 1999. Alternative oxidase inhibitors potentiate the activity of atovaquone against Plasmodium falciparum. *Antimicrobial Agents and Chemotherapy,* 43, 651-654.

MURRAY, C. J. L., ROSENFELD, L. C., LIM, S. S., ANDREWS, K. G., FOREMAN, K. J., HARING, D., FULLMAN, N., NAGHAVI, M., LOZANO, R. & LOPEZ, A. D. 2012. Global malaria mortality between 1980 and 2010: a systematic analysis. *Lancet,* 379, 413-431.

MUSSET, L., BOUCHAUD, O., MATHERON, S., MASSIAS, L. & LE BRAS, J. 2006. Clinical atovaquone-proguanil resistance of Plasmodium falciparum associated with cytochrome b codon 268 mutations. *Microbes and Infection,* 8, 2599-2604.

MUTURI, E. J., BURGESS, P. & NOVAK, R. J. 2008. Malaria vector management: Where have we come from and where are we headed? *American Journal of Tropical Medicine and Hygiene,* 78**,** 536-537.

NAGARAJA.K 1968. Metabolism of Plasmodium berghei .3. carbon dioxide fixation and role of pyruvate and dicarboxylic acids. *Experimental Parasitology,* 22, 33-42.

NAJERA, J. A., GONZALEZ-SILVA, M. & ALONSO, P. L. 2011. Some Lessons for the Future from the Global Malaria Eradication Programme (1955-1969). *Plos Medicine,* 8, e1000412.

NICHOLSON, J. K., CONNELLY, J., LINDON, J. C. & HOLMES, E. 2002. Metabonomics: a platform for studying drug toxicity and gene function. *Nature Reviews Drug Discovery,* 1**,** 153-161.

NIKINMAA, M. 1990. *Vertebrate Red Blood Cells. Adaptations of Function to Respiratory Requirements,* Berlin, Springer-Verlag.

NINA, P. B., MORRISEY, J. M., GANESAN, S. M., KE, H., PERSHING, A. M., MATHER, M. W. & VAIDYA, A. B. 2011. ATP Synthase Complex of Plasmodium falciparum dimeric assembly in mitochondrial membranes and resistance to genetic disruption. *Journal of Biological Chemistry,* 286, 41312-41322.

NOSTEN, F. & WHITE, N. J. 2007. Artemisinin-based combination treatment of falciparum malaria. *The American journal of tropical medicine and hygiene,* 77**,** 181-192.

NOVOTNY, M. V., SOINI, H. A. & MECHREF, Y. 2008. Biochemical individuality reflected in chromatographic, electrophoretic and mass-spectrometric profiles. *Journal of Chromatography B-Analytical Technologies in the Biomedical and Life Sciences,* 866**,** 26-47.

O'MEARA, W. P., NOOR, A., GATAKAA, H., TSOFA, B., MCKENZIE, F. E. & MARSH, K. 2009. The impact of primary health care on malaria morbidity - defining access by disease burden. *Tropical Medicine & International Health,* 14**,** 29-35.

O'NEILL, P. M., BRAY, P. G., HAWLEY, S. R., WARD, S. A. & PARK, B. K. 1998. 4-Aminoquinolines—Past, present, and future; A chemical perspective. *Pharmacology & Therapeutics,* 77**,** 29-58.

O'NEILL, P. M. & POSNER, G. H. 2004. A medicinal chemistry perspective on artemisinin and related endoperoxides. *Journal of Medicinal Chemistry,* 47**,** 2945-2964.

OAKS JR, S. C., MITCHELL, V. S., PEARSON, G. W., AND CARPENTER, C. C. J. 1991. *Malaria: Obstacles and opportunities,* National Academy Press, Washington, DC.

OKOMBO, J., KIARA, S. M., RONO, J., MWAI, L., POLE, L., OHUMA, E., BORRMANN, S., OCHOLA, L. I. & NZILA, A. 2010. In vitro activities of quinine and other antimalarials and pfnhe polymorphisms in Plasmodium isolates from Kenya. *Antimicrob Agents Chemother,* 54**,** 3302-3307.

OLLIARO, P. 2001. Mode of action and mechanisms of resistance for antimalarial drugs. *Pharmacology & Therapeutics,* 89**,** 207-219.

OLLIARO, P. L. & GOLDBERG, D. E. 1995. The Plasmodium digestive vacuole - metabolic headquarters and choice drug target. *Parasitology Today,* 11**,** 294-297.

OLLIARO, P. L., HAYNES, R. K., MEUNIER, B. & YUTHAVONG, Y. 2001. Possible modes of action of the artemisinin-type compounds. *Trends in Parasitology,* 17**,** 122-126.

OLLIARO, P. L. & YUTHAVONG, Y. 1999. An Overview of Chemotherapeutic Targets for Antimalarial Drug Discovery. *Pharmacology & Therapeutics,* 81**,** 91-110.

OLSZEWSKI, K. L. & LLINAS, M. 2011. Central carbon metabolism of Plasmodium parasites. *Molecular and Biochemical Parasitology,* 175**,** 95-103.

OLSZEWSKI, K. L., MATHER, M. W., MORRISEY, J. M., GARCIA, B. A., VAIDYA, A. B., RABINOWITZ, J. D. & LLINÁS, M. 2011. Erratum: Branched tricarboxylic acid metabolism in Plasmodium falciparum (Nature (2010) 466 (774-778)). *Nature,* 469**,** 432.

OLSZEWSKI, K. L., MATHER, M. W., MORRISEY, J. M., GARCIA, B. A., VAIDYA, A. B., RABINOWITZ, J. D. & LLINÁS, M. 2013. Retraction: Branched tricarboxylic acid metabolism in Plasmodium falciparum. *Nature,* 497**,** 652.

OLSZEWSKI, K. L., MORRISEY, J. M., WILINSKI, D., BURNS, J. M., VAIDYA, A. B., RABINOWITZ, J. D. & LINAS, M. 2009. Host-Parasite Interactions Revealed by Plasmodium falciparum Metabolomics. *Cell Host & Microbe,* 5, 191-199.

O'NEILL, P., BARTON, V., WARD, S. & CHADWICK, J. 2012. 4-Aminoquinolines: Chloroquine, Amodiaquine and Next-Generation Analogues. *In:* STAINES, H. M. & KRISHNA, S. (eds.) *Treatment and Prevention of Malaria.* Springer Basel.

PAINTER, H. J., MORRISEY, J. M., MATHER, M. W. & VAIDYA, A. B. 2007. Specific role of mitochondrial electron transport in blood-stage Plasmodium falciparum. *Nature,* 446**,** 88-91.

PANDEY, A. V., TEKWANI, B. L., SINGH, R. L. & CHAUHAN, V. S. 1999. Artemisinin, an endoperoxide antimalarial, disrupts the hemoglobin catabolism and heme detoxification systems in malarial parasite. *Journal of Biological Chemistry,* 274**,** 19383-19388.

PATEL, V., BOOKER, M., KRAMER, M., ROSS, L., CELATKA, C. A., KENNEDY, L. M., DVORIN, J. D., DURAISINGH, M. T., SLIZ, P., WIRTH, D. F. & CLARDY, J. 2008. Identification and Characterization of Small Molecule Inhibitors of Plasmodium falciparum Dihydroorotate Dehydrogenase. *Journal of Biological Chemistry,* 283**,** 35078-35085.

PATTI, G. J., YANES, O. & SIUZDAK, G. 2012. Metabolomics: the apogee of the omics trilogy. *Nature Reviews Molecular Cell Biology,* 13**,** 263-269.

PAUL, F., ROATH, S., MELVILLE, D., WARHURST, D. C. & OSISANYA, J. O. S. 1981. Separation of malaria-infected erythrocytes from whole-blood - use of a selective high-gradient magnetic separation technique. *Lancet,* 2, 70-71.

PAYNE, D. 1987. Spread of chloroquine resistance in Plasmodium falciparum. *Parasitology Today,* 3**,** 241-246.

PEDERSEN, K. S., KRISTENSEN, T. N., LOESCHCKE, V., PETERSEN, B. O., DUUS, J. O., NIELSEN, N. C. & MALMENDAL, A. 2008. Metabolomic Signatures of Inbreeding at Benign and Stressful Temperatures in Drosophila melanogaster. *Genetics,* 180**,** 1233-1243.

PERKINS, S. L. & AUSTIN, C. C. 2009. Four new species of Plasmodium from new guinea lizards: integrating morphology and molecules. *Journal of Parasitology,* 95**,** 424-433.

PETERSEN, I., EASTMAN, R. & LANZER, M. 2011. Drug-resistant malaria: Molecular mechanisms and implications for public health. *FEBS Letters,* 585**,** 1551-1562.

PHANG, J. M., VALLE, D. & KOWALOFF, E. M. 1975. Proline biosynthesis and degradation in mammalian cells and tissue. *Annals of Clinical and Laboratory Science,* 5**,** 298-302.

PHILLIPS, M. A., GUJJAR, R., MALMQUIST, N. A., WHITE, J., EL MAZOUNI, F., BALDWIN, J. & RATHOD, P. K. 2008. Triazolopyrimidine-based dihydroorotate dehydrogenase inhibitors with potent and selective activity against the malaria parasite Plasmodium falciparum. *J Med Chem,* 51**,** 3649-53.

PHILLIPS-HOWARD, P. A., NAHLEN, B. L., KOLCZAK, M. S., HIGHTOWER, A. W., TER KUILE, F. O., ALAII, J. A., GIMNIG, J. E., ARUDO, J., VULULE, J. M., ODHACHA, A., KACHUR, S. P., SCHOUTE, E., ROSEN, D. H., SEXTON, J. D., OLOO, A. J. & HAWLEY, W. A. 2003. Efficacy of permethrin-treated bed nets in the prevention of mortality in young children in

an area of high perennial malaria transmission in western Kenya. *American Journal of Tropical Medicine and Hygiene,* 68**,** 23-29.

PIDATHALA, C., AMEWU, R., PACOREL, B., NIXON, G. L., GIBBONS, P., HONG, W. D., LEUNG, S. C., BERRY, N. G., SHARMA, R., STOCKS, P. A., SRIVASTAVA, A., SHONE, A. E., CHAROENSUTTHIVARAKUL, S., TAYLOR, L., BERGER, O., MBEKEANI, A., HILL, A., FISHER, N. E., WARMAN, A. J., BIAGINI, G. A., WARD, S. A. & O'NEILL, P. M. 2012. Identification, Design and Biological Evaluation of Bisaryl Quinolones Targeting Plasmodium falciparum Type II NADH:Quinone Oxidoreductase (PfNDH2). *Journal of Medicinal Chemistry,* 55**,** 1831-1843.

PLATA, G., HSIAO, T. L., OLSZEWSKI, K. L., LLINÁS, M. & VITKUP, D. 2010. Reconstruction and flux-balance analysis of the Plasmodium falciparum metabolic network. *Molecular Systems Biology,* 6, 408.

PLOWE, C. V., KUBLIN, J. G. & DOUMBO, O. K. 1998. P. falciparum dihydrofolate reductase and dihydropteroate synthase mutations: epidemiology and role in clinical resistance to antifolates. *Drug Resistance Updates,* 1**,** 389-396.

POZEFSKY, T., FELIG, P., TOBIN, J. D., SOELDNER, J. S. & CAHILL, G. F. 1969. Amino acid balance across tissues of forearm in postabsorptive man . effects of insulin at 2 dose levels. *Journal of Clinical Investigation,* 48**,** 2273-2282.

PRANKERD, T. A. J. 1955. The metabolism of the human erythrocyte - a review. *British Journal of Haematology,* 1**,** 131-145.

PRAPUNWATTANA, P., OSULLIVAN, W. J. & YUTHAVONG, Y. 1988. Depression of Plasmodium falciparum dihydroorotate dehydrogenase-activity in invitro culture by tetracycline. *Molecular and Biochemical Parasitology,* 27, 119-124.

QUASTEL, J. H. 1931. The action of dyestuffs on enzymes. II. Fumarase. *Biochemical Journal,* 25**,** 898-913.

QUEEN, S. A., VANDERJAGT, D. L. & REYES, P. 1990. Invitro susceptibilities of Plasmodium falciparum to compounds which inhibit nucleotide-metabolism. *Antimicrobial Agents and Chemotherapy,* 34, 1393-1398.

RABINOWITZ, J. D. 2007. Cellular metabolomics of Escherchia coli. *Expert Review of Proteomics,* 4**,** 187-198.

RABINOWITZ, J. D. & KIMBALL, E. 2007. Acidic acetonitrile for cellular metabolome extraction from Escherichia coli. *Analytical Chemistry,* 79**,** 6167-6173.

RACCURT, C. P. 1997. Malaria, anopheles, the anti-malaria campaign in French Guyana: between dogmatism and judgment. *Medecine tropicale : revue du Corps de sante colonial,* 57**,** 401-406.

RAJ, D. K., MU, J., JIANG, H., KABAT, J., SINGH, S., SULLIVAN, M., FAY, M. P., MCCUTCHAN, T. F. & SU, X.-Z. 2009. Disruption of a Plasmodium

falciparum Multidrug Resistance-associated Protein (PfMRP) Alters Its Fitness and Transport of Antimalarial Drugs and Glutathione. *Journal of Biological Chemistry,* 284**,** 7687-7696.

RALPH, S. A., VAN DOOREN, G. G., WALLER, R. F., CRAWFORD, M. J., FRAUNHOLZ, M. J., FOTH, B. J., TONKIN, C. J., ROOS, D. S. & MCFADDEN, G. I. 2004. Metabolic maps and functions of the Plasmodium falciparum apicoplast. *Nature Reviews Microbiology,* 2**,** 203-216.

RAMYA, T. N. C., MISHRA, S., KARMODIYA, K., SUROLIA, N. & SUROLIA, A. 2007. Inhibitors of nonhousekeeping functions of the apicoplast defy delayed death in Plasmodium falciparum. *Antimicrobial Agents and Chemotherapy,* 51**,** 307-316.

RATHOD, P. K., KHATRI, A., HUBBERT, T. & MILHOUS, W. K. 1989. Selective activity of 5-fluoroorotic acid against Plasmodium falciparum in vitro. *Antimicrobial Agents and Chemotherapy,* 33**,** 1090-1094.

RATHOD, P. K. & REYES, P. 1983. Orotidylate-metabolizing enzymes of the human malarial parasite, Plasmodium falciparum, differ from host-cell enzymes. *Journal of Biological Chemistry,* 258, 2852-2855.

READ, J. A., WILKINSON, K. W., TRANTER, R., SESSIONS, R. B. & BRADY, R. L. 1999. Chloroquine binds in the cofactor binding site of Plasmodium falciparum lactate dehydrogenase. *Journal of Biological Chemistry,* 274**,** 10213-10218.

REAVES, M. L. & RABINOWITZ, J. D. 2011. Metabolomics in systems microbiology. *Current Opinion in Biotechnology,* 22**,** 17-25.

REYES, P., RATHOD, P. K., SANCHEZ, D. J., MREMA, J. E. K., RIECKMANN, K. H. & HEIDRICH, H. G. 1982. Enzymes of purine and pyrimidine metabolism from the human malaria, Plasmodium falciparum. *Molecular and Biochemical Parasitology,* 5**,** 275-290.

RIBAUT, C., BERRY, A., CHEVALLEY, S., REYBIER, K., MORLAIS, I., PARZY, D., NEPVEU, F., BENOIT-VICAL, F. & VALENTIN, A. 2008. Concentration and purification by magnetic separation of the erythrocytic stages of all human Plasmodium species. *Malaria Journal,* 7, 45.

ROBERTS, L., EGAN, T. J., JOINER, K. A. & HOPPE, H. C. 2008. Differential effects of quinoline antimalarials on endocytosis in Plasmodium falciparum. *Antimicrobial Agents and Chemotherapy,* 52**,** 1840-1842.

ROSENTHAL, P. J. 1998. Proteases of malaria parasites: New targets for chemotherapy. *Emerging Infectious Diseases,* 4**,** 49-57.

ROSS, R. 1898. *The Lancet,* 2**,** 488-489.

ROTH, E. F. 1987. Malarial parasite hexokinase and hexokinase-dependent glutathione reduction in the Plasmodium falciparum-infected human erythrocyte. *Journal of Biological Chemistry,* 262**,** 15678-15682.

ROTH, E. F., CALVIN, M. C., MAXAUDIT, I., ROSA, J. & ROSA, R. 1988. The enzymes of the glycolytic pathway in erythrocytes infected with Plasmodium falciparum malaria parasites. *Blood,* 72, 1922-1925.

ROTH JR, E. 1990. Plasmodium falciparum carbohydrate metabolism: A connection between host cell and parasite. *Blood Cells,* 16**,** 453-460.

ROWE, A. W., EYSTER, E. & KELLNER, A. 1968. Liquid nitrogen preservation of red blood cells for transfusion - a low glycerol-rapid freeze procedure. *Cryobiology,* 5**,** 119-1228.

RYAN, D. & ROBARDS, K. 2006. Metabolomics: The greatest omics of them all? *Analytical Chemistry,* 78**,** 7954-7958.

SAUL, A. 2007. Mosquito stage, transmission blocking vaccines for malaria. *Current Opinion in Infectious Diseases,* 20**,** 476-481.

SCHEIBEL, L. W., ASHTON, S. H. & TRAGER, W. 1979. Plasmodium falciparum microaerophilic requirements in human red blood-cells. *Experimental Parasitology,* 47**,** 410-418.

SCHEIBEL, L. W. & MILLER, J. 1969. Glycolytic and cytochrome oxidase activity in plasmodia. *Military Medicine,* 134, 1074-1080.

SCHEIBEL, L. W. & PFLAUM, W. K. 1970. Carbohydrate metabolism in Plasmodium knowlesi. *Comparative Biochemistry and Physiology,* 37, 543-553.

SCHLITZER, M. 2008. Antimalarial drugs - What is in use and what is in the pipeline. *Archiv Der Pharmazie,* 341, 149-63.

SCHWEIGER, H. G. 1962. Pathways of metabolism in nucleate and anucleate erythrocytes. *International Review of Cytology-a Survey of Cell Biology,* 13**,** 135-201.

SCOTT, H. V., GERO, A. M. & OSULLIVAN, W. J. 1986. Invitro inhibition of Plasmodium falciparum by pyrazofurin, an inhibitor of pyrimidine biosynthesis de novo. *Molecular and Biochemical Parasitology,* 18, 3-15.

SEEBER, F., LIMENITAKIS, J. & SOLDATI-FAVRE, D. 2008. Apicomplexan mitochondrial metabolism: a story of gains, losses and retentions. *Trends in Parasitology,* 24**,** 468-478.

SEEBER, F. & SOLDATI-FAVRE, D. 2010. Metabolic pathways in the apicoplast of apicomplexa. *International Review of Cell and Molecular Biology,* 281, 161-228.

SEEMAN, J. I. 2007. The Woodward-Doering/Rabe-Kindler total synthesis of quinine: Setting the record straight. *Angewandte Chemie-International Edition,* 46**,** 1378-1413.

SEYMOUR, K. K., LYONS, S. D., PHILLIPS, L., RIECKMANN, K. H. & CHRISTOPHERSON, R. I. 1994. Cytotoxic effects of inhibitors of de-novo

pyrimidine biosynthesis upon Plasmodium falciparum. *Biochemistry,* 33, 5268-5274.

SEYMOUR, K. K., YEO, A. E. T., RIECKMANN, K. H. & CHRISTOPHERSON, R. I. 1997. dCTP levels are maintained in Plasmodium falciparum subjected to pyrimidine deficiency or excess. *Annals of Tropical Medicine and Parasitology,* 91**,** 603-609.

SHERMAN, I. W. 1977. Amino acid metabolism and protein-synthesis in malarial parasites. *Bulletin of the World Health Organization,* 55**,** 265-276.

SHERMAN, I. W. 1979. Biochemistry of Plasmodium (malarial parasites). *Microbiological Reviews,* 43**,** 453-495.

SHERMAN, I. W. 1998. *Malaria: parasite biology, pathogenesis, and protection,* ASM Press, Washington, D.C.

SHERMAN, I. W. & TANIGOSH.L 1970. Incorporation of ^{14}C-amino-acids by malaria (Plasmodium-lophurae) .4. in-vivo utilization of host cell haemoglobin. *International Journal of Biochemistry,* 1**,** 635-637.

SHERMAN, I. W. & TING, I. P. 1966. Carbon dioxide fixation in malaria (Plasmodium iophurae). *Nature,* 212**,** 1387-1388.

SHERMAN, I. W. & TING, I. P. 1968. Carbon dioxide fixation in malaria .2. Plasmodium knowlesi (monkey malaria). *Comparative Biochemistry and Physiology,* 24**,** 639-642.

SHORTT, H. E. & GARNHAM, P. C. C. 1948. Pre-erythrocytic stage in mammalian malaria parasites. *Nature,* 161**,** 126-126.

SHRAGO, E. 1965. Cytoplasmic characteristics of human erythrocyte malic dehydrogenase. *Archives of Biochemistry and Biophysics,* 109**,** 57-61.

SINDEN, R. E. & BILLINGSLEY, P. F. 2001. Plasmodium invasion of mosquito cells: hawk or dove? *Trends in Parasitology,* 17**,** 209-211.

SINGH, B., SUNG, L. K., MATUSOP, A., RADHAKRISHNAN, A., SHAMSUL, S. S. G., COX-SINGH, J., THOMAS, A. & CONWAY, D. J. 2004. A large focus of naturally acquired Plasmodium knowlesi infections in human beings. *Lancet,* 363, 1017-1024.

SKINNER-ADAMS, T. S., STACK, C. M., TRENHOLME, K. R., BROWN, C. L., GREMBECKA, J., LOWTHER, J., MUCHA, A., DRAG, M., KAFARSKI, P., MCGOWAN, S., WHISSTOCK, J. C., GARDINER, D. L. & DALTON, J. P. 2010. Plasmodium falciparum neutral aminopeptidases: new targets for anti-malarials. *Trends in Biochemical Sciences,* 35**,** 53-61.

SLATER, A. F. G. & CERAMI, A. 1992. Inhibition by chloroquine of a novel heme polymerase enzyme-activity in malaria trophozoites. *Nature,* 355**,** 167-169.

SLOMIANNY, C. 1990. 3-Dimensional reconstruction of the feeding process of the malaria parasite - commentary. *Blood Cells,* 16**,** 369-378.

SLOMIANNY, C. & PRENSIER, G. 1986. Application of the serial sectioning and tridimensional reconstruction techniques to the morphological-study of the Plasmodium falciparum mitochondrion. *Journal of Parasitology,* 72, 595-598.

SMITH, D. C. & SANFORD, L. B. 1985. Laveran germ - the reception and use of a medical discovery. *American Journal of Tropical Medicine and Hygiene,* 34, 2-20.

SMITH, R. J. & PHANG, J. M. 1978. Proline metabolism in cartilage - importance of proline biosynthesis. *Metabolism-Clinical and Experimental,* 27**,** 685-694.

SNOW, R. W., GUERRA, C. A., NOOR, A. M., MYINT, H. Y. & HAY, S. I. 2005. The global distribution of clinical episodes of Plasmodium falciparum malaria. *Nature,* 434**,** 214-217.

SRIVASTAVA, I. K., ROTTENBERG, H. & VAIDYA, A. B. 1997. Atovaquone, a broad spectrum antiparasitic drug, collapses mitochondrial membrane potential in a malarial parasite. *Journal of Biological Chemistry,* 272**,** 3961-3966.

SRIVASTAVA, I. K. & VAIDYA, A. B. 1999. A mechanism for the synergistic antimalarial action of atovaquone and proguanil. *Antimicrobial Agents and Chemotherapy,* 43**,** 1334-1339.

STAINES, H. M., DERBYSHIRE, E. T., SLAVIC, K., TATTERSALL, A., VIAL, H. & KRISHNA, S. 2010. Exploiting the therapeutic potential of Plasmodium falciparum solute transporters. *Trends in Parasitology,* 26**,** 284-296.

STERLING, P. 1978. Mosquitos, malaria and man - Harrison, G. *New Republic,* 179, 23-25.

STORM, J. & MUELLER, S. 2012. Lipoic Acid Metabolism of Plasmodium - A Suitable Drug Target. *Current Pharmaceutical Design,* 18**,** 3480-3489.

SULLIVAN, D. J. 2002. Theories on malarial pigment formation and quinoline action. *International Journal for Parasitology,* 32**,** 1645-1653.

SUN, F., HUO, X., ZHAI, Y. J., WANG, A. J., XU, J. X., SU, D., BARTLAM, M. & RAO, Z. H. 2005. Crystal structure of mitochondrial respiratory membrane protein complex II. *Cell,* 121**,** 1043-1057.

SUN, G., YANG, K., ZHAO, Z., GUAN, S., HAN, X. & GROSS, R. W. 2007. Shotgun metabolomics approach for the analysis of negatively charged water-soluble cellular metabolites from mouse heart tissue. *Analytical Chemistry,* 79**,** 6629-6640.

SURGENOR, D. M. 1974. *The Red Blood Cell,* Academic Press, New York.

SUROLIA, N. & PADMANABAN, G. 1991. Chloroquine inhibits heme-dependent protein synthesis in Plasmodium falciparum. *Proceedings of the National Academy of Sciences of the United States of America,* 88**,** 4786-4790.

TAKKEN, W. & KNOLS, B. G. J. 2009. Malaria vector control: current and future strategies. *Trends in Parasitology,* 25**,** 101-104.

TANAKA, T. Q., HIRAI, M., WATANABE, Y.-I. & KITA, K. 2012. Toward understanding the role of mitochondrial complex II in the intraerythrocytic stages of Plasmodium falciparum: Gene targeting of the Fp subunit. *Parasitology International,* 61**,** 726-728.

TAX, W. J. M., PETERS, G. J. & VEERKAMP, J. H. 1979. Pyrimidine metabolism in lymphocytes and erythrocytes of man, horse and cattle. *International Journal of Biochemistry,* 10**,** 7-10.

TENG, R., JUNANKAR, P. R., BUBB, W. A., RAE, C., MERCIER, P. & KIRK, K. 2009. Metabolite profiling of the intraerythrocytic malaria parasite Plasmodium falciparum by ^{1}H-NMR spectroscopy. *Nmr in Biomedicine,* 22, 292-302.

TER KUILE, F. O., TERLOUW, D. J., PHILLIPS-HOWARD, P. A., HAWLEY, W. A., FRIEDMAN, J. F., KOLCZAK, M. S., KARIUKI, S. K., SHI, Y. P., KWENA, A. M., VULULE, J. M. & NAHLEN, B. L. 2003. Impact of permethrin-treated bed nets on malaria and all-cause morbidity in young children in an area of intense perennial malaria transmission in western Kenya: Cross-sectional survey. *American Journal of Tropical Medicine and Hygiene,* 68**,** 100-107.

THEAKSTON, R.D., FLETCHER, K. A. & MAEGRAITH, B. G. 1970. Use of electron microscope autoradiography for examining uptake and degradation of haemoglobin by Plasmodium berghei. *Annals of Tropical Medicine and Parasitology,* 64**,** 63-71.

TILLEY, L., DIXON, M. W. A. & KIRK, K. 2011. The Plasmodium falciparum-infected red blood cell. *International Journal of Biochemistry and Cell Biology,* 43**,** 839-842.

TIZIANI, S., LODI, A., KHANIM, F. L., VIANT, M. R., BUNCE, C. M. & GUENTHER, U. L. 2009. Metabolomic Profiling of Drug Responses in Acute Myeloid Leukaemia Cell Lines. *Plos One,* 4, e4251.

TRAGER, W. & JENSEN, J. B. 1976. Human malaria parasites in continuous culture. *Science,* 193**,** 673-675.

TRANG, D. T. X., HUY, N. T., KARIU, T., TAJIMA, K. & KAMEI, K. 2004. One-step concentration of malarial parasite-infected red blood cells and removal of contaminating white blood cells. *Malaria Journal,* 3, 7.

TRAUGER, S. A., KALISAK, E., KALISIAK, J., MORITA, H., WEINBERG, M. V., MENON, A. L., POOLE, F. L., II, ADAMS, M. W. W. & SIUZDAK, G. 2008. Correlating the transcriptome, proteome, and metabolome in the environmental adaptation of a hyperthermophile. *Journal of Proteome Research,* 7**,** 1027-1035.

ULKER, P., SATI, L., CELIK-OZENCI, C., MEISELMAN, H. J. & BASKURT, O. K. 2009. Mechanical stimulation of nitric oxide synthesizing mechanisms in erythrocytes. *Biorheology,* 46**,** 121-132.

UYEMURA, S. A., LUO, S., VIEIRA, M., MORENO, S. N. & DOCAMPO, R. 2004. Oxidative phosphorylation and rotenone-insensitive malate- and NADH-quinone oxidoreductases in Plasmodium yoelii yoelii mitochondria in situ. *J Biol Chem,* 279**,** 385-393.

VAIDYA, A. B. 2004. Mitochondrial and plastid functions as antimalarial drug targets. *Current Drug Targets - Infectious Disorders,* 4, 11-23.

VAIDYA, A. B., AKELLA, R. & SUPLICK, K. 1989. Sequences similar to genes for two mitochondrial proteins and portions of ribosomal RNA in tandemly arrayed 6-kilobase-pair DNA of a malarial parasite. *Molecular and Biochemical Parasitology,* 35**,** 97-108.

VAIDYA, A. B. & MATHER, M. W. 2005. A post-genomic view of the mitochondrion in malaria parasites. *Current Topics in Microbiology and Immunology,* 295, 233-250.

VAIDYA, A. B. & MATHER, M. W. 2009. Mitochondrial evolution and functions in malaria parasites. *Annual Review of Microbiology,* 63, 249-267.

VAIDYA, A. B., PAINTER, H. J., MORRISEY, J. M. & MATHER, M. W. 2008. The validity of mitochondrial dehydrogenases as antimalarial drug targets. *Trends in Parasitology,* 24**,** 8-9.

VAN BRUMMELEN, A. C., OLSZEWSKI, K. L., WILINSKI, D., LLINAS, M., LOUW, A. I. & BIRKHOLTZ, L.-M. 2009. Co-inhibition of Plasmodium falciparum S-Adenosylmethionine Decarboxylase/Ornithine Decarboxylase Reveals Perturbation-specific Compensatory Mechanisms by Transcriptome, Proteome, and Metabolome Analyses. *Journal of Biological Chemistry,* 284, 4635-46.

VAN DEN BERG, H. 2009. Global Status of DDT and Its Alternatives for Use in Vector Control to Prevent Disease. *Environmental Health Perspectives,* 117**,** 1656-1663.

VAN DOOREN, G. G., MARTI, M., TONKIN, C. J., STIMMLER, L. M., COWMAN, A. F. & MCFADDEN, G. I. 2005. Development of the endoplasmic reticulum, mitochondrion and apicoplast during the asexual life cycle of Plasmodium falciparum. *Molecular Microbiology,* 57, 405-419.

VAN DOOREN, G. G., STIMMLER, L. M. & MCFADDEN, G. I. 2006. Metabolic maps and functions of the Plasmodium mitochondrion. *Fems Microbiology Reviews,* 30**,** 596-630.

VANCER JAGT, D. L., HUNSAKER, L. A. & CAMPOS, N. M. 1986. Characterization of a hemoglobin-degrading, low molecular weight protease from Plasmodium falciparum. *Molecular and Biochemical Parasitology,* 18**,** 389-400.

VANDERJAGT, D. L., HUNSAKER, L. A., CAMPOS, N. M. & BAACK, B. R. 1990. D-Lactate production in erythrocytes infected with Plasmodium falciparum. *Molecular and Biochemical Parasitology,* 42**,** 277-284.

VAZQUEZ, D. 1966. Antibiotics affecting chloramphenicol uptake by bacteria - their effect on amino acid incorporation in a cell-free system. *Biochimica Et Biophysica Acta,* 114, 289-95.

VILLAS-BOAS, S. G., MAS, S., AKESSON, M., SMEDSGAARD, J. & NIELSEN, J. 2005. Mass spectrometry in metabolome analysis. *Mass Spectrometry Reviews,* 24**,** 613-646.

VINAYAVEKHIN, N. & SAGHATELIAN, A. 2010. Untargeted metabolomics. *Current protocols in molecular biology,* Chapter 30**,** Unit 30.1,1-24.

WALKER, K. & LYNCH, M. 2007. Contributions of Anopheles larval control to malaria suppression in tropical Africa: review of achievements and potential. *Medical and Veterinary Entomology,* 21**,** 2-21.

WALSH, C. J. & SHERMAN, I. W. 1968a. Isolation characterization and synthesis of DNA from a malaria parasite. *Journal of Protozoology,* 15**,** 503-508.

WALSH, C. J. & SHERMAN, I. W. 1968b. Purine and pyrimidine synthesis by avian malaria parasite Plasmodium lophurae. *Journal of Protozoology,* 15**,** 763-770.

WALSH, P. J., WOOD, C. M., AND MOON,T. W., 1998. Red Blood Cell Metabolism. *In:* PERRY, S. F., AND TUFTS, B., (ed.) *Fish Respiration.* Academic Press, New York.

WANG, J., HUANG, L., LI, J., FAN, Q., LONG, Y., LI, Y. & ZHOU, B. 2010. Artemisinin Directly Targets Malarial Mitochondria through Its Specific Mitochondrial Activation. *Plos One,* 5**,** A158-A169.

WARD, S. A. & BRAY, P. G. 2000. Definitive proof for a role of pfmdr 1 in quinoline resistance in Plasmodium falciparum. *Drug Resistance Updates,* 3**,** 80-81.

WARRELL, D. A. 1997. Cerebral malaria: clinical features, pathophysiology and treatment. *Annals of Tropical Medicine and Parasitology,* 91**,** 875-884.

WAY, J. L. 1984. CYANIDE INTOXICATION AND ITS MECHANISM OF AND ITS MECHANISM OF ANTAGONISM. *Annual Review of Pharmacology and Toxicology,* 24**,** 451-481.

WEATHERALL, D. J., MILLER, L. H., BARUCH, D. I., MARSH, K., DOUMBO, O. K., CASALS-PASCUAL, C. & ROBERTS, D. J. 2002. Malaria and the Red Cell. *ASH Education Program Book,* 2002**,** 35-57.

WECKWERTH, W. 2003. Metabolomics in systems biology. *Annual Review of Plant Biology,* 54, 669-689.

WELLEMS, T. E. & PLOWE, C. V. 2001. Chloroquine-resistant malaria. *Journal of Infectious Diseases,* 184**,** 770-776.

WHITE, J. H. & KILBEY, B. J. 1996. DNA replication in the malaria parasite. *Parasitology Today,* 12**,** 151-155.

WHITE, N. J. 2004. Antimalarial drug resistance. *Journal of Clinical Investigation,* 113**,** 1084-1092.

WHITE, N. J. 2008a. Plasmodium knowlesi: The fifth human malaria parasite. *Clinical Infectious Diseases,* 46, 172-173.

WHITE, N. J. 2008b. Qinghaosu (artemisinin): The price of success. *Science,* 320**,** 330-334.

WHO 2012. World Health Organization, World malaria report: 2012. Geneva: World Health Organization.

WIBACK, S. J. & PALSSON, B. O. 2002. Extreme pathway analysis of human red blood cell metabolism. *Biophysical Journal,* 83**,** 808-818.

WILLIAMS, J. A. & PHANG, J. M. 1982. Production of ornithine by intact human-erythrocytes. *American Journal of Physiology,* 242**,** C393-C397.

WILSON, R. J. M., FARRANT, J. & WALTER, C. A. 1977. Preservation of intraerythrocytic forms of malarial parasites by one-step and 2-step cooling procedures. *Bulletin of the World Health Organization,* 55**,** 309-315.

WINSTANLEY, P. & WARD, S. 2006. Malaria chemotherapy. *Advances in Parasitology, Vol 61: Control of Human Parasitic Diseases,* 61**,** 47-76.

WINSTANLEY, P. A. 2000. Chemotherapy for Falciparum Malaria: The Armoury, the Problems and the Prospects. *Parasitology Today,* 16**,** 146-153.

WISHART, D. S. 2010. Computational Approaches to Metabolomics. *Bioinformatics Methods in Clinical Research,* 593**,** 283-313.

WOODROW, C. J., BURCHMORE, R. J. & KRISHNA, S. 2000. Hexose permeation pathways in Plasmodium falciparum-infected erythrocytes. *Proceedings of the National Academy of Sciences of the United States of America,* 97**,** 9931-9936.

WOODWARD, R. B. & DOERING, W. E. 1944. The total synthesis of quinine. *Journal of the American Chemical Society,* 66**,** 849-849.

WRENGER, C., MUELLER, I. B., SILBER, A. M., JORDANOVA, R., LAMZIN, V. S. & GROVES, M. R. 2012. Aspartate Aminotransferase - Bridging Carbohydrate and Energy Metabolism in Plasmodium Falciparum. *Current Drug Metabolism,* 13**,** 332-336.

WU, Y., ELLIS, R. D., SHAFFER, D., FONTES, E., MALKIN, E. M., MAHANTY, S., FAY, M. P., NARUM, D., RAUSCH, K., MILES, A. P., AEBIG, J., ORCUTT, A., MURATOVA, O., SONG, G., LAMBERT, L., ZHU, D., MIURA, K., LONG, C., SAUL, A., MILLER, L. H. & DURBIN, A. P. 2008. Phase 1 Trial of Malaria Transmission Blocking Vaccine Candidates Pfs25 and Pvs25 Formulated with Montanide ISA 51. *Plos One,* 3, e2636.

XIA, J., MANDAL, R., SINELNIKOV, I. V., BROADHURST, D. & WISHART, D. S. 2012. MetaboAnalyst 2.0-a comprehensive server for metabolomic data analysis. *Nucleic Acids Research,* 40, W127-133.

XIA, J., PSYCHOGIOS, N., YOUNG, N. & WISHART, D. S. 2009. MetaboAnalyst: a web server for metabolomic data analysis and interpretation. *Nucleic Acids Research,* 37, W652-660.

XIAYAN, L. & LEGIDO-QUIGLEY, C. 2008. Advances in separation science applied to metabonomics. *Electrophoresis,* 29, 3724-3736.

YAYON, A., CABANTCHIK, Z. I. & GINSBURG, H. 1984a. Identification of the acidic compartment of Plasmodium falciparum-infected human-erythrocytes as the target of the antimalarial drug chloroquine. *Embo Journal,* 3**,** 2695-2700.

YAYON, A., CABANTCHIK, Z. I. & GINSBURG, H. 1984b. PH-dependent sensitivity of human malaria parasites to chloroquine. *Journal of Protozoology,* 31**,** A82-A83.

YAYON, A., TIMBERG, R., FRIEDMAN, S. & GINSBURG, H. 1984c. Effects of chloroquine on the feeding mechanism of the intraerythrocytic human malarial parasite Plasmodium falciparum. *Journal of Protozoology,* 31**,** 367-372.

YUAN, J., BENNETT, B. D. & RABINOWITZ, J. D. 2008. Kinetic flux profiling for quantitation of cellular metabolic fluxes. *Nature Protocols,* 3**,** 1328-1340.

ZARCHIN, S., KRUGLIAK, M. & GINSBURG, H. 1986. Digestion of the host erythrocyte by malaria parasites is the primary target for quinoline-containing antimalarials. *Biochemical Pharmacology,* 35**,** 2435-2442.

ZEREZ, C. R., LACHANT, N. A. & TANAKA, K. R. 1990. Impaired erythrocyte methemoglobin reduction in sickle-cell disease - dependence of methemoglobin reduction on reduced nicotinamide adenine-dinucleotide content. *Blood,* 76**,** 1008-1014.

ZHANG, A., SUN, H., WANG, P., HAN, Y. & WANG, X. 2012. Modern analytical techniques in metabolomics analysis. *Analyst,* 137**,** 293-300.

ČUPERLOVIĆ-CULF, M., BARNETT, D. A., CULF, A. S. & CHUTE, I. 2010. Cell culture metabolomics: applications and future directions. *Drug Discovery Today,* 15**,** 610-621.